Nonlinear Finite Element Analysis of Punching Shear of Reinforced Concrete Slabs Supported on Rectangular Columns

by

Graeme Milligan

A thesis
presented to the University of Waterloo
in fulfillment of the
thesis requirement for the degree of
Master of Applied Science
in
Civil Engineering

Waterloo, Ontario, Canada, 2018

Author's Declaration

This thesis consists of material all of which I authored or co-authored: see Statement of Contributions included in the thesis. This is a true copy of the thesis, including any required final revisions, as accepted by my examiners.

I understand that my thesis may be made electronically available to the public.

Statement of Contributions

Portions of the material contained in Section 4.3.3, 4.4, and 4.5.2 of this thesis are part of a publication which has been accepted for publication in American Concrete Institute (ACI) Special Publication 328. The paper submitted and accepted for this special publication was co-authored by Dr. Aikaterini Genikomsou (a former Ph.D. student of Professor Polak), Professor Maria Anna Polak (my MASc supervisor) and myself. In this special publication the calibration of the finite element model used in this thesis and experimental setups of the AM series (Section 4.3.3) and PT series slabs (Section 4.5.2) are discussed. In this paper the results of the boundary condition study, dilation angle study, fracture energy study, and combined dilation angle and fracture energy study for slab AM04 were presented. This information has been paraphrased and expanded on in this thesis (Section 4.3.3 and 4.4), and ACI provides copyright permission to the authors to reproduce figures from their published papers. The load-rotation curves predicted for the PT series slabs (Section 4.5.2) were also presented in this paper. However, this work is entirely my own as the paper was separated into numerous parts. In the first paper of the paper, Dr. Genikomsou's calibrated model for analyzing punching shear in ABAQUS was presented. In the second part of the paper, my calibrated finite element model, which was also implemented in ABAQUS, but focused on slabs supported on rectangular columns, was presented. In the final part of the paper parametric studies using Dr. Genikomsou's model were presented. My calibrated model was developed entirely by me during my MASc studies under the supervision of Professor Polak. I also conducted the numerical simulations, extracted the results and created the figures. However, Dr. Genikomsou provided guidance in regards to the figure formatting. Dr. Genikomsou's calibrated model is also discussed in this thesis (Section 4.2), but the information contained in this thesis is based on information contained in Dr. Genikomsou's thesis and previous publications and was not based on the information co-authored in the special publication.

Some of this same information has been submitted for publication as a conference paper for the 2018 *fib* (International Federation for Structural Concrete) conference in Melbourne, Australia. This paper is co-authored with my supervisor, Professor Maria Anna Polak, only. In this paper, the calibration of the finite element model discussed in Sections 4.3.3 and 4.4 of this thesis is briefly summarized. A brief discussion of the code reduction factors, which are presented in greater detail in Section 5.1.1 of this thesis, were also included in this paper. Finally, this paper also included some initial results of the parametric study discussed in Section 5.2 of this thesis. In particular, the load-displacement results for

c_{min}/d ratios of 0.792 and 1.287, crack patterns for a c_{min}/d ratio of 1.287, the shear stress distributions around the support plate perimeter for a c_{min}/d ratio of 1.287 and the normalized nominal shear stress computed from the finite element results and design codes (ACI 318M-14, Eurocode 2 (2004) and Model Code 2010 (LoA IV)) for c_{min}/d ratios of 0.792 and 1.287 were presented in this paper. This material, which was entirely authored by myself, has been paraphrased and expanded on in this thesis.

In the publication with Dr. Genikomsou and Dr. Polak, I wrote the section of the paper related to my work. Dr. Genikomsou and Dr. Polak assisted with editing this portion of this paper. I wrote the *fib* conference paper and Dr. Polak assisted me with editing.

Known bibliographic information for each paper at the time this thesis was published is as follows:

Documents currently awaiting publication (accepted):
Title: Modeling Parameters in Punching Shear Finite Element Analysis of Concrete Slabs
Authors: Aikaterini S. Genikomsou, **Graeme J. Milligan** and Maria Anna Polak
Publication: ACI Special Publication 328
Paper originally presented during Shear in Structural Concrete, Part 2 of 2, Sunday, March 25, 2018 at ACI Spring 2018 Conference (Salt Lake City, Utah, United States of America)

Documents submitted (provisionally accepted):
Title: Finite Element Investigation on the Effect of Column Rectangularity on Punching Shear Strength of Concrete Slabs
Authors: **Graeme J. Milligan** and Maria Anna Polak
Conference: International Federation for Structural Concrete 5th International *fib* Congress, October 7-11, 2018, Melbourne, Australia
Paper ID: 163

Abstract

Historical and current design code provisions for the punching shear of reinforced concrete slabs supported on rectangular columns vary greatly and are primarily based on empirical results. Additionally, the existing database for slabs supported on rectangular columns is quite small compared to the empirical database for reinforced concrete slabs supported on square columns. Conducting experimental tests of slabs supported on rectangular columns can be quite expensive and time consuming due to the required specimen size. As such, properly calibrated finite element simulations can be useful to expand the existing database and verify the accuracy of code provisions.

In this thesis a three-dimensional nonlinear finite element analysis (FEA) of interior slab-column connections subjected to concentric vertical loading, in the commercial FEA software ABAQUS, is presented. The finite element model was calibrated following the calibration procedure described in Genikomsou (2015), which was focused on the FEA of punching shear of slabs supported on square columns. Slab AM04, which was a slab tested by Sagaseta et al. (2014), and which represents an interior slab-column connection with a column rectangularity (aspect ratio) of three is considered as the control specimen in the calibration. The calibration was then verified by modelling the three remaining slabs in the AM series and three additional slabs tested by Sagaseta et al. (2011). These additional slabs were supported on square columns and had different concrete strengths and flexural reinforcing ratios than the AM series slabs. The calibrated finite element model (FEM) was found to be able to accurately predict the load deflection response and crack patterns of the tested slabs.

The calibrated FEM was then used to conduct a parametric study on the impact of column rectangularity on the punching shear behaviour of interior slab-column connections. Based on a comparison of current and historical code provisions two parameters, the column aspect ratio, and the ratio of the length of the minimum column dimension, c_{min}, to the effective flexural depth of the slab, d, were considered in the parametric study. In total 77 simulations spanning 8 c_{min}/d ratios were conducted. The results of these 77 simulations demonstrated that the impact of column rectangularity is not independent of the c_{min}/d ratio. As the c_{min}/d ratio increased the impact of column rectangularity predicted by the FEM, Eurocode 2 (2004), Model Code 2010 and the Critical Shear Crack Theory (CSCT) became more severe. Predictions according to ACI318M-14 were nearly independent of the ratio of c_{min}/d and were typically unconservative compared to the FEM results for c_{min}/d ratios greater than approximately 1.3. Additionally, the FEM, Eurocode 2 (2004), Model Code 2010 and the CSCT

predicted an impact of rectangularity for column aspect ratios between 1 and 2, which differs from the current ACI 318 provisions. The shear stress distributions in the slab along the support perimeter were also analyzed. Shear stresses were found to concentrate near the corner of the supported area and along the short side of the supported area. As the c_{min}/d ratio increased these concentrations became more focused at the column corner.

Acknowledgements

Firstly, I would like to thank those who made my Master's degree possible. Specifically, Dr. Katerina Genikomsou, Professor Maria Anna Polak and Dr. Cory Zurell. Dr. Katerina Genikomsou for recommending I talk to Professor Polak about pursuing a graduate degree. Professor Polak for accepting me as a student, for always trusting my judgement and for providing guidance when I was struggling with my research. Dr. Zurell for providing me with a practical research problem and for providing me with the time I needed to answer this problem.

I would like to acknowledge the funding I received from the QEII-GSST Scholarship and provided by the Natural Sciences and Engineering Research Council (NSERC) of Canada.

I would also like to thank my reviewers Professor Maria Anna Polak, Professor Stanislav Potapenko and Professor James Craig for the time they spent reviewing my thesis.

I also wish to extend my gratitude to all the professors at the University of Waterloo who have helped me during my studies. Professor Jeffrey West, Professor Giovanni Cascante, Professor Scott Walbridge and Professor Mahesh Pandey for providing me with reference letters for my numerous scholarship applications and my Ph.D. application. Professor Adil Al-Mayah and Professor Lei Xu for giving me the opportunity to assist in teaching courses. Professor Brush for always being there to help me sort through problems or decisions throughout my undergraduate or graduate studies. Professor Martin Pei, who has spent countless hours helping me understand concepts from numerous fields of study including applied mathematics and statistics.

Many thanks also need to be extended to my friends and colleagues for all the help and support throughout my graduate studies. Colin Van Niejenhuis, Stan Fong and Matt Sjaarda for helping me develop my teaching skills. Ryan Barrage and Mickey Laguta for discussing ABAQUS issues and helping me create or debug numerous Python scripts. James St. Onge for teaching me helpful tricks in AutoCAD over the years and for sharing his knowledge of ABAQUS. Peter Loudfoot for the assistance with using SAP2000 and for keeping me properly fed for the last two years. Adam Felinczak, Nader Sleiman, Kyle Balkos and Piotr Wiciak for providing me an opportunity to get some time away from my computer and work in the lab. Tim Tedford for taking the time to discuss numerous engineering problems and for sharing his design knowledge from previous co-op terms. Ania Polak for brainstorming how to solve various issues in my finite element model. And Casey Vanderwerff for always supporting me when I was struggling with research or course work.

Finally, I would like to thank my parents for their financial and emotional support and for always understanding when I missed family events due to working on my research or coursework. Without their support the successful completion of my Master's degree would not have been possible.

Dedication

I would like to dedicate this thesis to my parents, John and Paula Milligan, my grandmother, Angela Milligan, and my late uncle, Bernard Osbaldeston.

Table of Contents

List of Figures

List of Tables

Chapter 1: Introduction

1.1 Research Significance and Objectives

Reinforced concrete flat slabs are a commonly used structural system due to the many advantages they offer such as simple formwork, reduced floor height and lower construction costs. However, high stresses are developed at the connection between the slab and the supporting columns due to the lack of horizontal supporting members such as beams and girders. These stresses can result in a brittle failure mode known as punching shear. Due to its brittle nature a punching shear failure of a single slab-column connection can lead to the progressive collapse of a portion or an entire structure if the slab reinforcement is not properly designed or detailed. Punching shear failures typically occur before a building is complete, due to the partially cured concrete having insufficient strength when the temporary supports are removed (Gardner N. J., 2011). However, punching failures have also occurred in occupied structures, such as the Sampoong department store collapse in Seoul, South Korea in 1995, which resulted in the deaths of approximately 500 people. The collapse of the north wing of this five-story commercial building was attributed to the punching shear failure of a slab-column connection on the fifth floor (Gardner, Huh, & Chung, 2002; Gardner N. J., 2011). A designer has many options to increase the punching capacity of a slab-column including using a higher concrete compressive strength, increasing the effective flexural depth of the slab, increasing the flexural reinforcement ratio (not accounted for in North American codes), or designing and detailing shear reinforcement. Another popular option to increase the punching capacity of a slab-column connection, especially in parking garages or multi-story office or residential buildings, is to use a larger column size, or to use a rectangular column. The use of rectangular columns also has many additional benefits such as reducing the slab clean span between the columns in the direction of the elongated column dimension and providing lateral stiffness to the structure (Sagaseta, Tassinari, Fernández Ruiz, & Muttoni, 2014). Based on a linear elastic analysis of a continuous slab Simmonds (1970) also found that the use of slightly rectangular columns resulted in reduced slab deflections and bending moments.

Due to its brittle nature, and possibility of progressive collapse if punching failures do occur, many researchers have investigated the punching shear behaviour of reinforced concrete flat slabs. To date, most of this research has been focused on experimental tests which have formed the basis of many historical and current design code provisions. Due to the high cost and space requirements of testing full multi-bay slab systems, most of the reported tests are for isolated slab-column connections.

Isolated slab-column connections are sized to represent the extent of the negative moment region around the column, which is commonly referred to as the radius of contraflexure. Testing isolated specimens is still quite expensive and time consuming, and as such, the existing experimental database cannot cover all aspects which affect punching shear failures. For example, most of the previous research has been focused on slabs supported on square or circular columns, even though the use of rectangular columns with flat slabs is quite common. Properly calibrated finite element analysis (FEA) can be a cost-effective way to expand the existing experimental database and verify the accuracy of current design code provisions. Nonlinear finite element analysis (NLFEA) can be used to predict the punching capacity, deflected shape, reinforcement stresses, crack patterns and stresses at any point in the slab. However, the finite element model must first be calibrated based on experimental results before it can be used to conduct parametric studies.

In this thesis the NLFEA of reinforced concrete slabs supported on square and rectangular columns selected from published literature, using the commercial finite element software ABAQUS, are presented. Based on previous work conducted at the University of Waterloo by Stoner (2015), Barrage (2017) and Genikomsou (2015), the "Concrete Damaged Plasticity" (CDP) model is used for the constitutive modelling of concrete. The CDP has also been successfully applied by other researchers to model many applications in reinforced concrete structures including damage estimation of reinforced concrete beams (Hanif, Ibrahim, Jameel, Ghaedi, & Aslam, 2016), and FRP confined concrete (Yu, Teng, Wong, & Dong, 2010; Hany, Hantouche, & Harajli, 2016).

The simulated punching shear specimens are taken from four experimental programs. The first specimen analyzed, slab SB1, was tested at the University of Waterloo by Adetifa and Polak (2005), and represented an interior slab-column connection without shear reinforcement supported on a square column subjected to concentric vertical loading. Slab SB1 was also analyzed by Genikomsou (2015) in order to calibrate a nonlinear finite element model in ABAQUS using the CDP. Genikomsou's calibrated model was then used to study the punching shear behavior of slabs supported on square columns (2015). Next, to verify ABAQUS' capability to capture the impact of the column rectangularity nine slabs tested by Hawkins, Fallsen and Hinojosa (1971) were analyzed. These tests, which represented interior slab-column connections with column aspect ratios between 1 and 4.33 with similar critical perimeter lengths, formed the basis of the American Concrete Institute (ACI) 318 provisions for punching shear of rectangular columns (ACI Committee 318, 2014; ASCE-ACI Committee 426, 1974; Al-Yousif & Regan, 2003; Mitchell, Cook, & Dilger, 2005). Hawkins et

al. (1971) found that increasing the column aspect ratio (rectangularity) lead to a decrease in the nominal punching capacity around the critical the critical perimeter located at d/2 from the column face, where d is the average effective depth of the slab. The next four specimens analyzed were from a study conducted by Sagaseta, Tassinari, Fernández Ruiz and Muttoni (2014) in which the effect of loading pattern (one-way or two-way) on the punching behaviour of an isolated slab-column connection with a rectangularity of 3 was analyzed. Based on the experimental results and numerical studies, they found that the concentration of shear stresses and forces around a rectangular column with an aspect ratio of three is dependent on both the column geometry and the slab deflections due to bending. The authors also concluded that the failure mode, capacity and rotations (deflections) are strongly dependent on the column orientation with respect to the primary slab span, especially in cases of one-way loading (Sagaseta, Tassinari, Fernández Ruiz, & Muttoni, 2014). The final three slabs studied were from an experimental program by Sagaseta, Muttoni, Fernández Ruiz and Tassinari (2011) which was focused on the impact of non-axis symmetric conditions on punching behaviour of isolated slab-column connections. The experimental setup in the 2014 experimental program by Sagaseta et al. was similar to the setup used in this experimental program. The slabs in the 2011 study were supported on square plates, had different reinforcing ratios and concrete compressive strengths than those in the 2014 program, and were tested under two-way loading conditions. Based on the test results, it was observed that slabs subjected to symmetric loading, with a large reinforcing ratio in one direction and with a shear capacity lower than the shear force corresponding to a yield line failure, had nearly symmetrical responses, even for slabs where the ratio of the reinforcing ratios in both orthogonal directions was equal to two. Specimens with a low flexural reinforcing ratio in one direction (0.3%) demonstrated an asymmetrical punching failure due to the formation of a plastic hinge (Sagaseta, Muttoni, Fernández Ruiz, & Tassinari, 2011).

The experimental specimens discussed above were modelled in ABAQUS to examine the impact of column rectangularity on the punching shear behaviour of reinforced concrete flat slabs supported on columns. The primary objective of this thesis was to create a calibrated finite element model which could be used to study the impact of column rectangularity on punching shear since the database for slabs supported on rectangular columns is much smaller than that for square columns. The FEA results can also be used to verify the accuracy of current code provisions which vary greatly in their treatment of column rectangularity.

The specific objectives of this research are as follows:

1. Summarize the historical and current code provisions related to the impact of column rectangularity on punching shear;
2. Develop a calibrated three-dimensional finite element model which can be used to investigate the impact of column rectangularity on the punching shear capacity of isolated slab-column connections in reinforced concrete flat slabs;
3. Use the calibrated model to conduct a parametric study of column rectangularity and analyze the effect of column rectangularity on the load-deflection behaviour, and shear stress distributions around the column perimeter or any selected critical perimeter and;
4. Compare the impact of column rectangularity on punching capacity predicted by the FEA with that predicted by current reinforced concrete design codes including ACI 318M-14, Eurocode 2 (2004), *fib* Model Code 2010 and predictions based on the Critical Shear Crack Theory (CSCT).

1.2 Outline

The outline of this thesis is as follows:

The introduction of this thesis (Chapter 1) provides a brief introduction of the research problem, advantages of using finite element analysis and outlines the research objectives. Next, a description of the phenomenon of punching shear is provided in Chapter 2. A literature review of previous experimental, analytical and finite element studies of reinforced concrete slabs focused on punching shear is also provided in Chapter 2. This literature review is primarily focused on interior slab-column connections subjected to static concentric loading without shear reinforcement. Furthermore, an overview of current and historical design code provisions for punching shear focused on the impact of column rectangularity is provided. Chapter 3 provides a brief overview of the mechanical behaviour of concrete. Chapter 4 presents a summary of the previous finite element work conducted at the University of Waterloo and the development of the calibrated finite element model used to conduct the parametric analysis of the impact of column rectangularity. In Chapter 4, an overview of the considered experimental specimens, the methodology used to create the finite element model and a comparison of the experimental results, code predictions and FEA results is provided. Based on these comparisons it is concluded that ABAQUS is capable of capturing the impact of column rectangularity and the predicted behaviour matches experimental observations by other researchers

and code predictions. Chapter 5 presents the overview of the parametric study based on the calibrated model and provides a detailed discussion of the results. As expected, ABAQUS predicts a negative impact on nominal punching capacity as column rectangularity is increased. Finally, Chapter 6 presents a summary of the research, conclusions and provides guidance for future work.

Chapter 2: Punching Shear in Reinforced Concrete Slabs

2.1 Introduction

Today, reinforced concrete flat slabs are one of the most commonly used structural systems, especially for buildings where open floor plans are critical such as warehouses, parking garages and office buildings. According to Sozen and Siess (1963) the flat slab was invented rather than developed, since an accepted theory of their structural behaviour was not available until 1921. George M. Hill is credited with constructing the first flat slab in the United States of America in 1901. He had originally introduced the concept of a reinforced concrete flat slab supported on monolithic concrete columns in the American Society of Civil Engineers (ASCE) Transactions in 1900. Following the work of Hill, Orlando W. Norcross patented a flat slab system which used four-way reinforcement in 1902, with the goal of removing the need for horizontal supports such as beams and girders for slabs. However, it appears that the use of Norcross' patented system was rather limited (Gasparini, 2002).

The two people considered to have the largest influence on popularizing the flat slab system are American engineer C.A.P. Turner and Swiss engineer Robert Maillart, both of whom were credited with inventing their flat slab systems independently. In 1906, Turner built his first flat slab building, the Johnson Bovey Building, in Minneapolis. Turner's designs, which used much less reinforcing steel than other flat slab systems built later, used four-way flexural reinforcing, and large steel shear heads with a diameter equal to approximately half the slab span above the columns and column capitals. The capitals and steel shear heads, which Turner referred to as mushrooms, were included to provide additional shear strength, as Turner realized the weakness of concrete in tension and in shear in its uncured state (Gasparini, 2002). An example of Turner's design for the column capital and shearhead is shown in Figure 2-1. On the other hand, Maillart's designs only used reinforcement in two orthogonal directions, and did not account for the negative moment near the slab-column connection. Even though Maillart neglected negative moments he successfully designed and built many flat slabs buildings and bridges (Fürst & Marti, 1997).

The success of the designs by Turner and Maillart were a key development in structural engineering as the flat slab represented a new structural form (Fürst & Marti, 1997) compared to the typical systems seen in steel and timber construction (Gasparini, 2002). Between 1906 and 1910, Turner constructed at least 34 flat slab buildings throughout the United States (Gasparini, 2002) and by 1913 over 1000 flat slab buildings had been built worldwide (Sozen & Siess, 1963). The rapid development of the flat slab system was likely due to the many economic advantages this system

offered, such as minimized formwork, reduced floor framing depths and easier installation of finishes and lighting.

In this chapter, a discussion of the phenomenon of punching shear and its consequences are discussed first. Then a review of the testing background, focused on slabs without shear reinforcement supported on square or rectangular columns and primarily subjected to concentric punching, is provided. Next, a summary of some historical and current mechanical models and design code provisions for punching shear with a focus on column rectangularity is provided. Finally, a review of the previous finite element modelling of reinforced concrete flat slabs is presented.

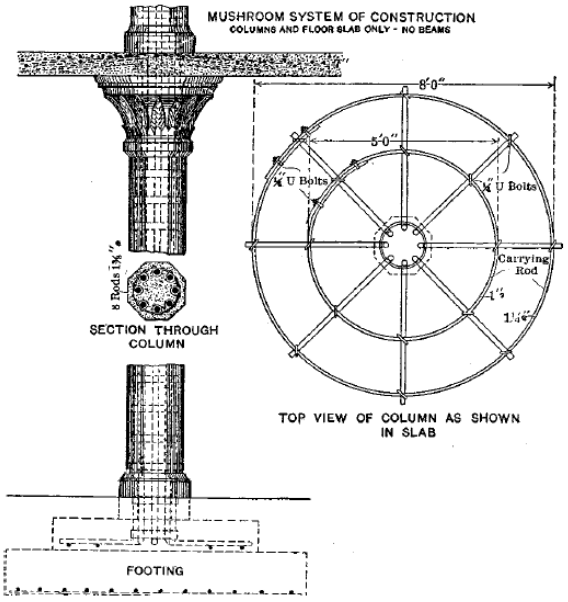

Figure 2-1: Turner's Design for Column Capital and Steel Shearhead (Turner, C.A.P., 1905) (taken from (Gasparini, 2002))

2.2 Phenomenon of Punching Shear

Reinforced concrete flat slabs supported on columns are currently one of the most commonly used structural systems for buildings such as warehouses, parking garages and residential or commercial high rises due to the many advantages they offer. These advantages include simplified formwork, reduced floor height, reduced material requirements and simplified installation of finishes. Throughout their history reinforced concrete flat slabs, which typically are simple in appearance, have taken numerous forms as shown in Figure 2-2, due to the complexity of their loading carrying behaviour in flexure and shear (FIB, 2001). As the understanding of the behaviour of reinforced

concrete flat slabs has developed, the flat slab supported on columns without capitals or beams has become increasing popular. However, the removal of the beams and girders results in a statical discontinuity at the intersection of the slab and column. This intersection is a D region which is subjected to a complex three-dimensional state of stress due to flexural and shear stresses (FIB, 2001). When the shear stresses near the slab-column connection exceed the shear strength of the connection, the column and a portion of the slab, which has a truncated cone shape, push through the slab resulting in a failure of the connection, and potentially the progressive collapse of an entire structure. A typical punching surface is shown in Figure 2-3. The action of the column and the truncated cone of concrete pushing through the slab is a brittle failure mode, known as punching shear, which has been studied extensively since the 1950s as the popularity of slabs supported on columns without capitals has grown (Muttoni, 2008).

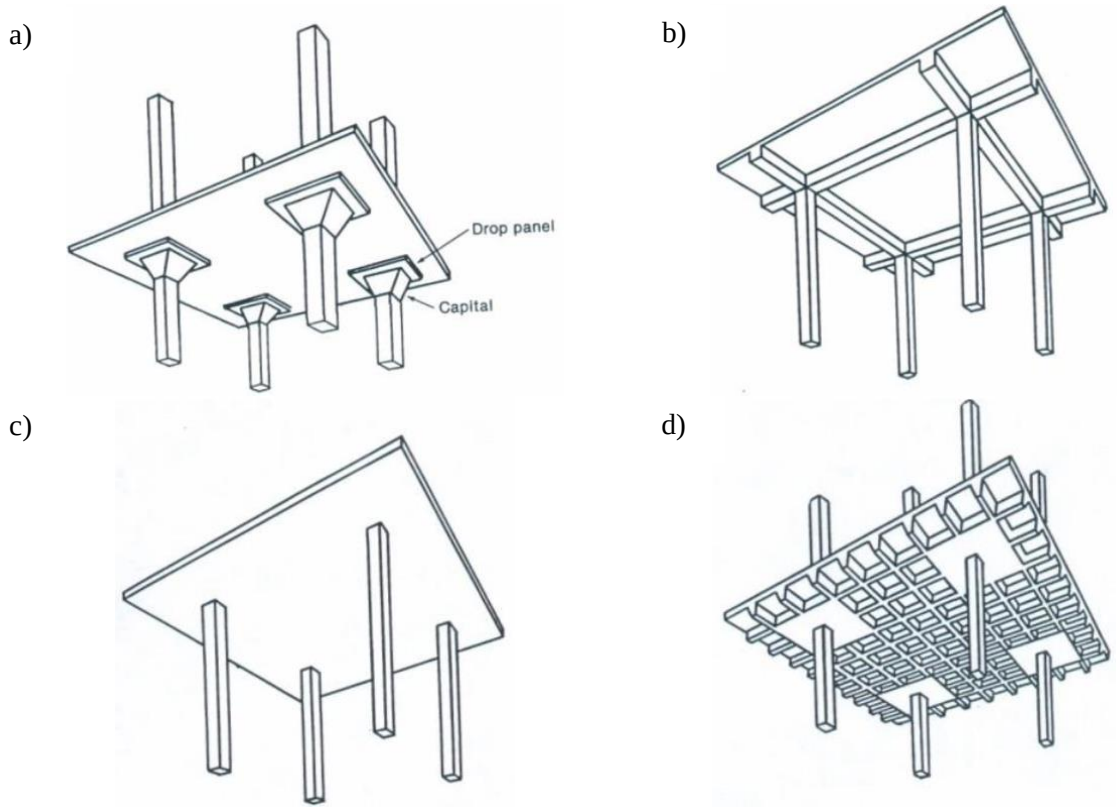

Figure 2-2: Typical Flat Slab Systems, a) Flat Slab with Column Capitals and Drop Panels, b) Two-way slab on beams and girders, c) Flat Slab, d) Waffle Slab, Acknowledgement: Reinforced Concrete Mechanics and Design, MacGregor and Bartlett (2000), ©2000 Pearson Education Canada Inc.

Previous research has shown that punching shear failures are preceded by radial cracking of the slab concrete around the slab-column connection due to the moment carried by the slab (FIB, 2010; MacGregor & Bartlett, 2000). As additional load is applied after this initial radial cracking a crack pattern which is similar to that assumed in the yield-line analysis of a two-way slab is formed (MacGregor & Bartlett, 2000). Simultaneously, inclined internal cracks begin forming in the slab due to the large increase in vertical strains in the vicinity of the slab-column connection (FIB, 2010; MacGregor & Bartlett, 2000; Regan & Braestrup, 1985). As the magnitude of the load is further increased, these inclined cracks, which typically have an angle of 25-30 degrees, extend towards the compression surface of the slab at a distance away from the column face (Alexander & Simmonds, 1987; Regan & Braestrup, 1985). A punching shear failure occurs when the strength of the connection, which can be attributed to the shear carried by the compression zone, aggregate interlock along the crack, and dowel action of the reinforcing bars (Theodorakopoulos & Swamy, 2002), is exceeded. Once the shear strength of the connection is exceeded, a truncated cone of concrete and the column punch through the slab, resulting in the failure surface shown in Figure 2-3. Examples of punching shear crack patterns are shown in Figure 2-4 and Figure 2-5. Even though punching failures have typically been found to be associated with yielding of the flexural reinforcement in the vicinity of the slab-column connection the failure mode is brittle (Alexander & Simmonds, 1987; Park & Gamble, 1980; Theodorakopoulos & Swamy, 2002).

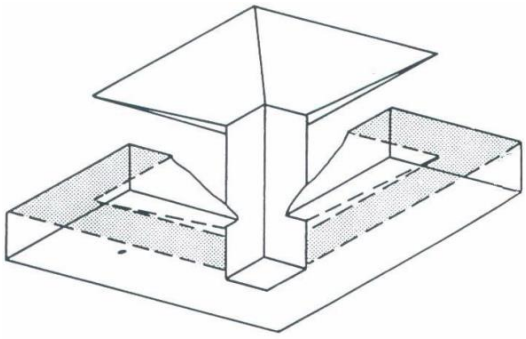

Figure 2-3: Punching Shear Failure Surface, Acknowledgement: Reinforced Concrete Mechanics and Design, MacGregor and Bartlett (2000), ©2000 Pearson Education Canada Inc.

The punching shear capacity of a slab-column connection may govern numerous design parameters such as the column size, column capital size or slab thickness (Park & Gamble, 1980). In cases where the overall capacity of a flat slab system is governed by the punching shear capacity, designers should be aware that the level of safety, or chance of warning of failure, between the majority of the slab and

the area of the slab around the column, are not the same due to the brittle nature of punching shear failures compared to a ductile flexural slab failure (FIB, 2001).

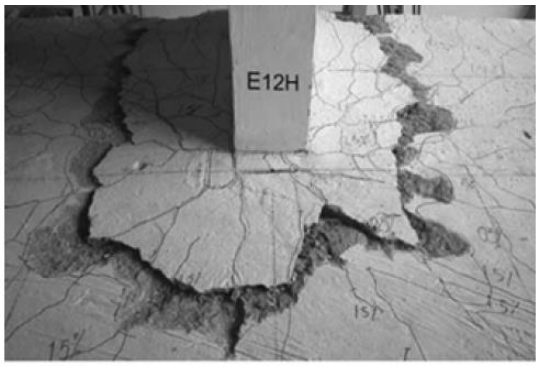

Figure 2-4: Tension Surface Cracks (Anggadjaja & Teng, 2008), authorized reprint from ACI Structural Journal, Volume 84, Issue 3, 2008

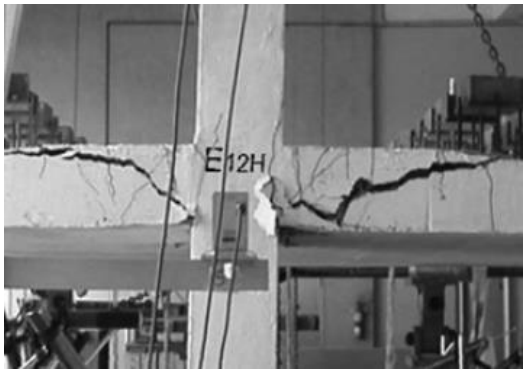

Figure 2-5: Inclined Shear Cracks in Slab After Punching Failure (Anggadjaja & Teng, 2008), authorized reprint from ACI Structural Journal, Volume 84, Issue 3, 2008

2.3 Review of Punching Shear Tests

2.3.1 Introduction

According to Moe (1961), some of the first contributors to punching shear research were Talbot (1913), Bach and Graf (1915), Graf (1933 and 1938) and Richart (1948). Talbot tested 114 wall footings and 83 column footings, of which 20 failed in shear. Based on his results, Talbot proposed an equation to estimate the shear capacity of reinforced concrete footings. Bach and Graf (1915) conducted an extensive program to investigate the flexural behaviour of reinforced concrete slabs. Most of their slabs were loaded at eight or more discrete points, while others were loaded at the slab

center. Some of the slabs which were subjected to central loads experienced shear failures. Graf (1933) studied the shear capacity of reinforced concrete slabs subjected to concentrated loads near their supports. Based on the results of three tests, it was observed that the shear capacity of the slabs decreased as the distance between the load and support was increased. Graf hypothesized that flexural cracking impacted the shear strength of the slabs. In 1938, Graf presented the experimental results of 8 slab tests, 6 of which included shear reinforcement. Richart (1948) published the results of an extensive testing program of reinforced concrete footings. Based on the results, he concluded that shear stresses may govern footing design instead of bond stresses (Moe, 1961).

In the time since these initial studies, many researchers have conducted experiments to investigate the punching shear behaviour of reinforced concrete slabs. Many of these experimental programs are summarized in databases which are curated by organizations, such as the American Concrete Institute (ACI) or the International Federation for Structural Concrete (*fib*), or by independent researchers. However, many of these databases are primarily focused on slabs supported on square or circular columns. For example, the *fib* database, which is contained in *fib* Bulletin 12, "Punching of Structural Concrete Slabs," contains information on 400 experimental tests of concentrically loaded reinforced concrete slabs cast from normal density concrete conducted between 1954 and 1999. The vast majority of the 400 experimental results are for slabs supported on square or circular columns, and 150 are for slabs with shear reinforcement (FIB, 2001). The ACI database, which is curated by ACI-ASCE Committee 445 Shear and Torsion, currently contains the results of 519 experimental tests of reinforced concrete slabs since 1938. Of the 519 tests only 27 are for slabs supported on rectangular columns (Ospina, et al., 2015). One of the largest databases for slabs supported on rectangular columns was curated by Paiva, Ferreira, Oliveira, Lima Neto and Teixeira (2015) and contains the experimental results for 131 slab tests. However, many of reported tests are for slabs supported on square columns or are for one-way slabs subjected to concentrated loads.

In this section, some of the previous experimental research of reinforced concrete flat slabs supported on square or circular and rectangular columns will be summarized. Since the experimental database for slabs supported on square or circular columns is quite large, only select experimental programs will be presented.

2.3.2 Square or Circular Columns

As seen in the current punching shear databases, many researchers have investigated the punching shear behaviour of reinforced concrete flat slabs supported on square or circular columns. Some of

the largest of these programs were conducted by Elstner and Hognestad (Elstner & Hognestad, 1956), Moe (1961), Mowrer and Vanderbilt (1967) and Regan (Regan P. E., 1986).

Elstner and Hognestad (1956) published experimental results for 39 slab-column connection tests. Most of the tested slabs were simply supported on four sides and were subjected to concentric loading applied through the column stub. The remaining slabs were either supported on two sides only or were subjected to eccentric loading to introduce unbalanced moment on the connection. 34 of the slabs failed in shear. The testing program was focused on determining the impact of multiple parameters on the punching shear behaviour of slab-column connections including concrete compressive strength, tensile reinforcing ratio, compressive reinforcing ratio, column size, support and load conditions, tensile reinforcement layout and use of shear reinforcement. The experimental results were quite important since many of the previous American punching shear studies were conducted on footings, which are typically much thicker than floor slabs. At the time, the provisions for punching shear of floor slabs were extrapolated from the footing test results which was questionable due to the lower thickness to span ratios and higher shear to moment ratios typically used in slabs compared to footings (Elstner & Hognestad, 1956).

Following the work of Elstner and Hognestad (1956), Moe (1961) tested 43 slab-column connections, which were six feet square, six inches thick and simply supported along all four edges with corners free to lift. Moe investigated the impact of openings in the slab, concentrations of tensile reinforcement near the column, the use of shear reinforcement, column size and eccentric loading on the punching shear behaviour of slab-column connections. Of his 43 tests, one was supported on a rectangular column with side lengths of six and eighteen inches. Based on the test results, Moe recommended that the column perimeter should be used as the critical perimeter assumed in punching shear design and proposed an equation to estimate the punching capacity of slab-column connections. Moe also concluded that the flexural strength of the slab effects the punching capacity and that the shear capacity per unit length is largest when the ratio of the column dimension to the slab thickness is small. It was also observed that shear reinforcement could be used to increase the punching capacity of slab-column connections if properly anchored. Openings in the slab were also found to significantly reduce the punching capacity. Moe also proposed a modified version of his equation to estimate the punching capacity of slabs supported on rectangular columns (Moe, 1961). Moe's work formed the basis of the ACI 318 provisions (ASCE-ACI Committee 426, 1974).

Mowrer and Vanderbilt (1967) tested 51 isolated slab-column specimens representing interior slab-column connections. 43 of the 51 slabs were cast from lightweight concrete made from expanded shale. Nine of the slabs were tested with two or four edges clamped and the remaining slabs were tested under simply supported conditions. Mowrer and Vanderbilt investigated the impact of lightweight concrete, opening pattern, flexural reinforcing ratio, concrete compressive strength, column size and edge fixity. Based on the test results, they proposed a modified version of Moe's equation, which accounted for lightweight concrete. They also presented a modified version of the typical isolated slab-column specimen with clamped edges that they believed better represented the behaviour of a continuous slab (Mowrer & Vanderbilt, 1967). Using this modified isolated slab-column specimen, Vanderbilt (1972) tested 15 slabs to investigate the impact of column size and shape. The slabs were cast with square or circular columns and were subjected to a uniformly distributed load. Vanderbilt observed shear stress concentrations around the corners of the square columns and a decrease in the nominal shear stress as the ratio of the column size to the slab depth increased (Vanderbilt, 1972).

Regan (1986) tested 28 reinforced slabs simply supported on four sides and subjected to concentrated loads at their centers. The tests were conducted to investigate many parameters including the arrangement of the flexural reinforcement, slab size, slab depth, concrete compressive strength, reinforcing ratio, boundary restraint and size of the loaded area. In many of the tests, the slabs were supported near the slab edges with corners free to lift. In the remaining tests, the supports were moved closer to the load application area. Regan found the British punching shear design provisions used at the time to be unconservative in many cases. The Model Code 1978 provisions were found to be overly conservative and the ACI 318-83 provisions, which are similar to those in ACI 318M-14, were found to be conservative in most cases. It was also concluded that boundary restraint increased the punching capacity of slab-column connections, but this effect was not quantifiable based on the tested slabs. (Regan P. E., 1986).

In addition to the major studies discussed above, numerous other studies have been conducted by various researchers. Some researchers tested isolated slab-column connections which were centrally supported at loaded at the slab edges (Einpaul, Bujnak, Fenández Ruiz, & Muttoni, 2016; Lips, Fernández Ruiz, & Muttoni, 2012; Guandalini, Burdet, & Muttoni, 2009; Yamada, Nanni, & Endo, 1992; Sagaseta, Muttoni, Fernández Ruiz, & Tassinari, 2011). Other researchers tested slabs which were supported at the edges or corners and loaded centrally, typically through a column stub (Adetifa

& Polak, 2005; Alam, Amanat, & Seraj, 2009; Birkle & Dilger, 2008; Marzouk & Hussein, 1991; Inácio, Almeida, Faria, Lúcio, & Ramos, 2015; Moreno & Sarmento, 2013). A much smaller portion of the experimental database has been focused on cantilever slabs subjected to concentrated loads (Vaz Rodrigues, Fernández Ruiz, & Muttoni, 2008) or on the punching shear behaviour of multi-bay slab specimens (Gardner & Shao, 1996).

Yamanda, Nanni and Endo (1992) tested thirteen isolated-slab column specimens which represented interior columns. The specimens were loaded monotonically at 8 discrete points located at a distance of 0.75m from the column center and supported on a central column stub. Two types of shear reinforcement, hat shaped reinforcement, which did not intercept the slab's flexural reinforcement, and double hooked bars, which intercepted the flexural reinforcement, were investigated. The test results showed that shear reinforcement needs to be anchored to the flexural reinforcement, and the spacing between subsequent rows should be less than d/2, where d is the effective slab depth, to be effective and increase the punching capacity and ductility of the connection (Yamada, Nanni, & Endo, 1992).

Guandalini, Burdet and Muttoni (2009) studied the impact of low flexural reinforcement ratios on the punching capacity of slab-column connections since most experimental specimens are constructed with flexural reinforcing ratios much higher than those used in practice to avoid flexural failures. The impact of aggregate size and specimen size was also investigated. Eleven isolated slab-column specimens, representing interior columns, were tested. The slabs had reinforcing ratios between 0.22% and 1.5%. Six of the eleven specimens were constructed at full scale and were 250mm thick. Four specimens were constructed at half scale and were 125mm thick, and the last specimen was constructed at double scale and was 500mm thick. Punching capacity was found to decrease as the slab thickness increased, and slabs with low flexural reinforcing ratios were found to fail in punching after excessive yielding of the slab reinforcement (Guandalini, Burdet, & Muttoni, 2009).

Sagaseta, Muttoni, Fernández Ruiz and Tassinari (2011) also investigated the impact of flexural reinforcement ratio on the punching capacity of interior slab-column connections. Their investigation was primarily focussed on investigating the behaviour of slabs with different flexural reinforcing ratios in both orthogonal directions. Seven square isolated interior slab-column connections, supported on a central steel plate with side lengths of 260mmm, without shear reinforcement were tested. Three of the tested slabs had equal reinforcing ratios in both orthogonal directions, whereas the remaining four slabs had non-axis symmetric reinforcing layouts, where the reinforcing ratio in one

direction was approximately half of that in the other direction. All flexural reinforcing ratios were between 0.32% and 1.64%. Based on the test results, and results from linear elastic finite element analyses, which are briefly discussed in Section 2.6.2, it was found that slabs with non-axis symmetric reinforcing ratios did not have symmetric deflection responses in both orthogonal directions. It was also found that slabs with reinforcing ratios exceeding 0.75% failed brittlely in punching shear (Sagaseta, Muttoni, Fernández Ruiz, & Tassinari, 2011). Some of the slabs from this test series were considered during the calibration of the finite element model used in this thesis. As such, this experimental program will be discussed in more detail in Section 4.5.2.

Lips, Fernández Ruiz and Muttoni (2012) tested sixteen isolated interior slab-column connections loaded at eight discrete points around the column and supported on a central square steel plate to investigate the impact of column size, slab thickness, shear reinforcement type and amount of shear reinforcement on punching shear behaviour. The square steel plates supporting the slab had side lengths between 130mm and 520mm and the slab thicknesses ranged from 250mm to 400mm. Two types of shear reinforcement, shear studs and continuous stirrup cages, were considered. As the column size was increased the punching capacity and rotation at failure were found to increase. Slab slenderness and size were also found to impact the punching capacity, especially for slabs which failed due to crushing of concrete struts. Both types of shear reinforcement were found to increase the punching and rotational capacity of the connection, though shear studs were found to be more effective due to the improved anchorage compared to continuous stirrup cages (Lips, Fernández Ruiz, & Muttoni, 2012).

Einpaul, Bujnak, Fernández Ruiz and Muttoni (2016) tested thirteen symmetric isolated interior slab-column connections subjected to punching shear. Similar to the study by Lips, Fernández Ruiz and Muttoni the primary parameters investigated included the column size and slab slenderness. The impact of the slab's flexural reinforcing ratio and the use of shear reinforcement were also investigated. The slabs were loaded at eight discrete points and supported on central steel plates. Eight of the thirteen slabs had octagonal shapes and were supported on circular steel plates with diameters between 83mm and 660mm. The remaining five slabs were square in shape, with side lengths between 1.7 and 3.9m, and were supported on square steel plates with side lengths between 197mm and 211mm. All thirteen slabs were 250mm thick. The octagonal and square slab series were tested to investigate the influence of column size and slab slenderness respectively. Based on the results, it was found that the shear capacity and flexural stiffness of the slabs decreased as the slab

slenderness was increased. The nominal shear stresses along a critical perimeter loacated at d/2 from the column face were also found to decrease as the column diameter was increased (Einpaul, Bujnak, Fenández Ruiz, & Muttoni, 2016).

Marzouk and Hussein (1991) examined the influence of high strength concrete on the punching capacity of slab-column connections by testing seventeen isolated interior slab-column connections loaded through the column stub and supported on four edges. Fifteen of the slabs were cast from high strength concrete with compressive strengths between 66MPa and 80MPa. The punching capacity was found to increase as the compressive strength was increased but at a rate lower than the square root of compressive strength, which is assumed in many codes. They also developed a modified version of the Kinnunen and Nylander model, which accounted for the use of high strength concrete (Marzouk & Hussein, 1991).

Morento and Sarmento (2013) also investigated the impact of high compressive strengths on the punching capacity of slab-column connections with and without shear reinforcement. Six slabs, which were supported at eight discrete points along a 2165mm diameter circle whose center was coincident with the column center, and loaded through a 250x250mm central square column, were tested. Half of the slabs were tested under concentric punching and the other half were tested with a load eccentricity of 200mm. The slabs were cast from normal and steel fibre reinforced self-compacting concretes with compressive strengths ranging from 36.9MPa to 66.2MPa. The use of steel fibres and double headed shear studs as shear reinforcement was also investigated (Moreno & Sarmento, 2013). The experimental results were used to calibrate a nonlinear finite element model which is discussed in Section 2.6.2.

Inácio, Almeida, Faria, Lúcio and Pinho Ramos (2015) also investigated the impact of high strength concretes on punching capacity. Three slabs cast from high strength concrete, with compressive strengths ranging from 125.6MPa to 130.1MPa, and one slab cast from normal strength concrete, with a compressive strength of 35.9MPa were tested. The slabs were loaded through central square steel plates with side lengths of 200mm and were supported at eight discrete points located near the radius of contraflexure (Inácio, Almeida, Faria, Lúcio, & Ramos, 2015), which is similar to the test setup used by Marzouk and Hussein (1991). The use of high strength concrete compared to normal strength concrete was found to result in a substantial increase in punching capacity. The punching capacity was also found to increase as the flexural reinforcing ratio increased (Inácio, Almeida, Faria, Lúcio, & Ramos, 2015). Both results match those of Marzouk and Hussein (1991).

Adetifa and Polak (2005) tested six isolated interior slab-column connections to investigate the use of post installed shear bolts for shear reinforcement. One slab contained no shear reinforcement, and the second, third and fourth slabs contained two, three and four rows of shear bolts respectively. The rows of shear bolts were arranged in an orthogonal pattern around a 150x150mm square column stub. The final two slabs tested had four rows of shear bolts and two or four openings in the slab around the column. The slabs were 120mm thick, simply supported along their edges and concentrically loaded through the monolithic column stub. Post-installed shear bolts were found to be a viable shear reinforcing method, as they increased the punching and ductility capacity of the slab. The use of shear bolts resulted in flexural failures for all five reinforced slabs, compared to a brittle punching failure for the unreinforced slab. The connection ductility was found to increase with the number of shear bolts. Lower punching strengths were observed for connections with openings in the slab due to the loss of shear resisting perimeter (Adetifa & Polak, 2005).

Birkle and Dilger (2008) also investigated the influence of shear reinforcement on the punching capacity of reinforced concrete slab-column connections. Nine octagonal slabs, six of which were reinforced with steel shear studs, were tested. The slabs were supported at eight discrete points near the slab edges and load was applied through a monolithic square column stub. The three slabs in each of the test series were 250mm, 300mm and 350mm thick respectively. The slabs with shear reinforcement were designed to fail either inside or outside the shear reinforced zone. A severe decrease in nominal shear stress capacity at the critical perimeter located at d/2 from the column face was found as the slab thickness increased for the unreinforced slabs. A similar trend was observed for the slabs with shear reinforcement, although the decrease was not as severe. The use of shear studs was also found to greatly increase the punching and ductility capacity of the slab-column connection compared to the unreinforced specimens (Birkle & Dilger, 2008).

Alam, Amanat and Seraj (2009) tested fifteen isolated interior slab-column connections to investigate the influence of boundary restraint, flexural reinforcing ratio and slab thickness on punching shear behaviour. Twelve of the fifteen slabs were cast with edge beams of varying widths to provide edge restraint. The slabs were supported on steel blocks at each corner of the slab, and concentrated loading was applied through a central square steel plate with side lengths of 120mm. The punching capacity was found to increase as the width of the edge beams increased. Additionally, as the flexural reinforcing ratio was increased from 0.5% to 1%, and the slab thickness was increased

from 60mm to 80mm, the nominal shear capacity along the critical perimeter located at d/2 from the column face was found to increase (Alam, Amanat, & Seraj, 2009).

Unlike other researchers who tested slabs isolated slab-column connections with square columns, Vaz Rodrigues, Fernández Ruiz and Muttoni (2008) tested cantilever slabs subjected to concentrated loads. The tested specimens were ¾ scale typical box-girder deck slabs and concentrated loads were applied through 30mm thick square steel plates with side lengths of 300mm. Each slab was tested to failure three times under different load layouts. The thickness of the cantilever deck varied from 380mm at the supported end to 190mm at the free end. All slabs were found to fail in punching shear, and for tests with the same loading layout but different reinforcing ratios the punching shear capacity was found to decrease as the reinforcing ratio decreased. A linear elastic FEA using shell elements was also conducted to estimate the effective critical perimeter length around the concentrated loads (Vaz Rodrigues, Fernández Ruiz, & Muttoni, 2008).

All of the studies outlined above were conducted on isolated slab-column specimens or isolated cantilever spans. The use of isolated specimens is common due to their lower space and material requirements compared to continuous slabs. However, the use of isolated slab-column specimens neglects the impact of compressive membrane forces present in continuous slabs (Alam, Amanat, & Seraj, 2009; Mowrer & Vanderbilt, 1967; Genikomsou & Polak, 2017a), which can improve the punching capacity (Alam, Amanat, & Seraj, 2009; Genikomsou & Polak, 2017a).

One of the few experimental studies of punching shear using a continuous slab specimen was conducted by Gardner and Shao (1996). In this study, a half-scale two bay by two bay slab system with four edge columns, four corner columns and one interior column was loaded to failure to study the behaviour of reinforced concrete flat slabs with temporary construction shores installed around the columns. The slab span between the column centerlines was equal to 2743mm and the slab was 140mm thick. Of the nine columns, seven were square, with side lengths of 254mm, and two were circular, with diameters of 254mm. To simulate a uniformly distributed load, forty concentrated loads, whose magnitudes were dependent on their tributary area, were applied to the slab surface. To avoid premature failure the load was applied in increments with the temporary shores in place. The slab was then unloaded, and the shores were removed. The slab was then loaded and unloaded again with the shores removed. The shores were reinstalled before the start of the next load increment. Punching shear failure around the interior column was the first failure to occur during testing. To continue testing, this portion of the slab was shored permanently and loading was applied until two

edge columns, one circular and one square failed. These areas were then shored, and the slab was loaded until a corner column and another edge column failed. The use of temporary shoring was found to increase the punching capacity of the connections by taking a portion of the applied load (Gardner & Shao, 1996).

2.3.3 Rectangular Columns

One of the first experimental programs focused on investigating the impact of column rectangularity on punching shear behaviour was conducted by Hawkins, Fallsen and Hinojosa (1971). In this experimental program, nine isolated interior slab-column connections were tested. The slabs were supported on a central column stub with an aspect ratio between 1 and 4.33. Loading was applied at discrete points along the slab edges. In six of the nine tests only two slab edges were loaded, and in the remaining three tests all four slab edges were loaded (Hawkins, Fallsen, & Hinojosa, 1971). Based on the results of this testing program, the ACI 318 provisions were modified to account for column rectangularity based on a simple relationship dependent on the column aspect ratio (Al-Yousif & Regan, 2003). The nine slabs tested by Hawkins, Fallsen and Hinojosa were modelled during the calibration of the finite element model used in this thesis, and as such, this experimental program is discussed in more detail in Section 4.3.2.

Since the study by Hawkins, Fallsen and Hinojosa (1971), many researchers have investigated the impact of column rectangularity on the punching shear behaviour of slab-column connections. Most of the experimental research has been conducted using isolated slab-column connections which are supported on the slab edges or a central column. Other researchers have focused on the punching shear behaviour of one-way slabs subjected to concentrated loads, while some have tested multi-bay continuous slab systems.

Al-Yousif and Regan (2003) tested four isolated interior slab-column connections to investigate the impact of column aspect ratio and flexural loading conditions on punching shear behaviour. The tested slabs were 100mm thick and concentric loads were applied through a column stub. Three of the tested slabs had a 500x100mm column stub and the fourth had a 300mm square column stub. Two of the four tests were supported on all four sides and the remaining two were supported on two sides only. The slabs supported on two sides only were supported on the slab sides parallel to long side of the column or parallel to the short side of the column. All four slabs failed in punching shear. Shear force concentrations near the column corners were observed in the three tests with the 500x100mm columns. It was noted that the concentration of shear forces at the column corners is dependent on the

ratio of the column side dimensions to the effective slab depth and flexural deformations of the slab. When the slab is predominately bent in one direction, the impact of the ratio of the column dimension to the effective slab depth is more severe (Al-Yousif & Regan, 2003).

Filatov and Bubnov (2016) tested three isolated interior slab-column specimens which were loaded through a central column stub and supported at 8 discrete points along the radius of contraflexure to study the impact of column rectangularity on punching shear behaviour. Three column sizes, 200x200mm, 200x500mm and 200x800mm, were investigated. All three slabs were 140mm thick (Filatov & Bubnov, 2016). Filatov (2017) added a fourth specimen to the study, which was loaded through a circular column with a diameter of 210mm. All four slabs failed brittlely due to punching shear. For the slabs loaded through rectangular columns the maximum concrete strains were observed near the column corners. The measured tangential concrete strains along the long side of the column decreased from a maximum at the corners to a minimum near the center of the column. Similar trends were observed in the measured flexural reinforcing strains. The strains in the flexural reinforcement were also found to be highest along the column perimeter and deceased in magnitude as the distance from the column perimeter was increased (Filatov, 2017). The largest deflections for the slabs supported on rectangular columns were measured perpendicular to the short side of the column and along a diagonal line whose origin is the column corner (Filatov & Bubnov, 2016).

Tan and Teng (2005) tested five ¾ scale interior slab-column connections with rectangular columns subjected to combined gravity and biaxial lateral loads. The study was focussed on investigating the impact of biaxial lateral load and the use of shear stud reinforcement on the performance of slab-column connections with column aspect ratios of five. The slabs, which had a thickness of 150mm, were supported along their edges and loaded through a 180x900mm column stub. Tan and Teng concluded that slab-column connections with a column aspect ratio of five may not be able to sustain a 1.5% lateral drift even when the ratio between gravity and lateral loads is small. They recommended that the gravity to shear force ratio be limited to a value of 0.28 to ensure that the connections have sufficient drift capacity. The stiffness of the slab-column connection was found to be influenced by column rectangularity, and the connection strength was higher in the direction perpendicular to the short side of the column (Tan & Teng, 2005).

Erdogan, Binici and Ozcebe (2011) tested seven ¾ scale isolated specimens representing interior slab-column connections supported on rectangular columns with aspect ratios between one and three. The column sizes were chosen so that each column had a similar critical perimeter length. Three of

the tested slabs did not include any shear reinforcement and four were reinforced with carbon fibre reinforced polymer (CFRP) dowels. The slabs were simply supported, and the load was applied through the column stub. All seven slabs failed in punching shear. In both the unreinforced and shear reinforced specimens, the punching capacity decreased as the column rectangularity increased. Since the critical perimeter length was kept approximately constant between the specimens, an increase in column rectangularity corresponds to a reduced column area. The energy absorption capacity of each connection, which was defined as the area under the load deflection curve, was also found to decrease as the column rectangularity was increased (Erdogan, Binici, & Ozcebe, 2011).

Borges, Melo and Gomes (2013) tested thirteen isolated slab-column connections with and without openings and stud rail shear reinforcement supported on 200x600mm steel plates. Loads were applied to the slab through the steel plate and the slabs were supported along their edges by a series of plates and rods tied to the laboratory floor. For the tests with openings, one or two openings with widths equal to the minimum dimension of the steel plate were located adjacent to the short side of the steel plate. The experimental results were compared to predictions from ACI 318-11 and Model Code 1990. Both codes were found to be generally conservative although the authors recommended using straight projections instead of radial projections, which are specified in ACI 318, when reducing the effective critical perimeter length (Borges, Melo, & Gomes, 2013).

Eom, Song, Song, Kang, Yoon and Kang (2017) studied the influence of uneven shear transfer caused by unequal span lengths and the use of pre-assembled bar trusses as shear reinforcement on punching shear behaviour of slab-column connections. Four isolated slab-column connections representing interior columns were tested. One slab included no shear reinforcement, one was reinforced with conventional stirrups, and two were reinforced with pre-assembled bar trusses. The trusses did not intercept the flexural reinforcement and both orthogonal and radial layouts around the column were investigated. The slabs were loaded through a precast column with an aspect ratio of 2.67 and were supported along their edges. The use of pre-assembled bar trusses in the orthogonal and radial layouts was found to increase the punching capacity by 42% and 49% respectively compared to the unreinforced specimen. This capacity increase was much higher than the 13% increase observed in the slab reinforced with stirrups. The use of a radial truss layout was determined to be more beneficial compared to the orthogonal layout when uneven shear transfer is anticipated (Eom, et al., 2017).

Sherif, Emara, Ibrahim and Magd (2005) tested five half scale slab-edge column connections to investigate the impact of column rectangularity and the ratio of the critical perimeter length, b_o, to the effective slab depth, d, on punching shear behaviour. The column aspect ratio was varied from 1 to 2.5 and the ratio of the critical perimeter length to the effective slab depth ranged from 6.5 to 11. The slabs were 120mm thick and supported on three sides. The load was applied with an eccentricity of 300mm with regards to the column center to simulate the behaviour of a continuous slab system under gravity loads. All five specimens failed in punching shear and shear stress concentrations near the column corners were observed. It was concluded that the punching capacity decreases as the b_o/d ratio increases due to a decreased level of confinement on the failure surface provided by the in-plane stresses in the slab. The ductility of the slab-edge column connections was found to decrease as the b_o/d ratio was decreased and increased as the column rectangularity was increased. No clear trends in deflection were observed in regards to varying column aspect ratios (Sherif, Emara, Ibrahim, & Magd, 2005).

Anggadjaja and Teng (2008) tested fifteen 135mm thick slabs loaded through 180x900mm columns to investigate the impact of column rectangularity, gravity load level and cyclic biaxial loading on the connection strength, stiffness, ductility and drift capacity of slab-edge column connections. One slab was tested under gravity load only, two were tested under combined gravity and uniaxial lateral load, and two were tested under combined gravity and biaxial lateral load. It was observed that shear stresses concentrated around the short side of the column, and the shear stress magnitude decreased as the distance from the short side increased. The slab-edge column connections were found to behave more brittlely when the lateral load was applied perpendicular to the short side of the column. The use of rectangular columns was found to allow a larger moment to be transferred along the strong-axis of the column. However, it was observed that the stiffness in the weak column direction was lower than in the strong direction.

Himawan and Teng (2014) studied the behaviour of post-tensioned slab-rectangular column connections under cyclic loading. Three slab specimens, loaded through a 180x900mm rectangular column, were tested. One slab was subjected to concentric punching only, whereas the remaining two specimens were subjected to lateral load in one or two directions respectively. The increase in shear strength due to prestressing for slabs supported on rectangular columns was found to be lower than that observed for slabs supported on square or circular columns (Himawan & Teng, 2014). As was observed by Anggadjaja and Teng (2008) the stiffness of the slab-column connections along the

strong direction, which is perpendicular to the short side of the column, was found to be higher than that perpendicular to the short side (Himawan & Teng, 2014).

Oliveira, Regan and Melo (2004) tested fifteen reinforced concrete slabs cast from high strength concrete, which were supported on rectangular steel plates, with aspect ratios ranging from one to five, under different loading conditions. In five of the tests, loading was applied on all four slab edges and in the other ten tests, the loading was applied on two edges only. All fifteen slabs failed in punching shear, but the shape of the failure surface was found to be dependent on the load conditions. For slabs supported on a steel plate with an aspect ratio greater than or equal to three and loaded along the two slab edges perpendicular to the short side of the supported area, the failure surface did not extend around the longer side of the steel plate. Based on the experimental results, and a finite element analysis in SAP 2000, which is discussed in Section 2.6.3, it was concluded that the effective critical perimeter length is dependent on the column rectangularity and flexural loading conditions of the slab (Oliveira, Regan, & Melo, 2004).

Sagaseta, Tassinari, Fernández Ruiz and Muttoni (2014) tested four slabs supported on 260x780mm steel plates to investigate the influence of loading conditions on the punching shear capacity of reinforced concrete slabs supported on rectangular columns. All slabs except for one, in which the loading was applied on the two slab edges perpendicular to the long side of the steel plate, failed in punching. The load layout was found to have a significant impact on the punching capacity and overall behaviour of the slabs. During testing, the measured reaction forces were found to concentrate around the short sides of the steel plate (Sagaseta, Tassinari, Fernández Ruiz, & Muttoni, 2014). The four slabs in this test series were used to calibrate the finite element model used in the parametric study presented in Chapter 5, and as such, a detailed discussion of this experimental program is provided in Sections 4.3.3.1 and 4.5.1.1.

Teng, Cheong, Kuang and Geng (2004) investigated the punching shear behaviour of slab-column connections with rectangular columns and openings in the slab. Twenty isolated slab-column connections representing interior columns were tested. The slabs were loaded along the slab edges and supported on central column stubs. Three column sizes, 200x200mm, 200x600mm and 200x1000mm, were investigated. The impact of different loading ratios in the two orthogonal directions was also studied. All twenty slabs failed in punching shear. It was observed that the punching capacity was reduced due to the presence of openings in the slab or if the load in the orthogonal direction perpendicular to the short side of the column was larger than the load

perpendicular to the long side. It was concluded that the assumption of uniform stress on the critical perimeter at d/2 from the column face is reasonable for slabs supported on square columns, but is unreasonable for slabs supported on rectangular columns (Teng, Cheong, Kuang, & Geng, 2004).

Oliveira, Gomes and Melo (2014) also investigated the impact of openings on the punching shear capacity of slabs supported on rectangular columns in addition to the impact of unbalanced moments. Seven slabs supported on 200x500mm prestressed concrete columns were tested to failure. The slabs were loaded at discrete points along the slab edges and unbalanced moments were imposed by increasing the load magnitude on one side of the connection. All seven slabs failing in punching shear. It was concluded that the use of two 300x200mm openings along the long side of the column was less detrimental to the punching capacity than the use of one 400x400mm opening adjacent to the shorter column side when the moment was applied to the shorter column side. The inclusion of unbalanced moments in addition to gravity loads resulted in a 38% capacity loss for the slabs without openings compared to the slab subjected to concentric punching only. (Oliveira, Gomes, & Melo, 2014).

Habibi, Redl, Egberts, Cook and Mitchell (2012) evaluated the adequacy of the punching shear integrity reinforcement provisions in CSA A23.3-04. Seven specimens were tested to investigate the influence of slab thickness, integrity reinforcement length, integrity reinforcement distribution in slabs supported on rectangular columns and integrity reinforcement placement in slabs with drop panels. The slabs were loaded at eight discrete points along the radius of contraflexure and supported on a central column. Two of the seven specimens were supported on rectangular columns with dimensions of 200x300mm and 180x270mm respectively. Column rectangularity and the use of three times the amount of integrity reinforcement in one direction compared to the other was found to have an insignificant impact on the post-punching strength. However, the ultimate displacements of the slab column connections reinforced in this way, and supported on rectangular columns, were found to have lower ultimate deflections compared to the other specimens (Habibi, Redl, Egberts, Cook, & Mitchell, 2012).

Teng, Chanthabouala, Lim and Hidayat (2018) investigated the punching shear behaviour of slabs cast from concrete with compressive strengths around 100MPa and with reinforcing ratios between 0.28% and 1.43%. The slabs were loaded at eight discrete points and supported on column stubs which had sizes of 200x200mm, 200x600mm or 200x1000mm. The ACI 318-14 provisions were found to be unconservative for slabs with low reinforcement ratios (i.e. <0.7%). During the tests,

these slabs failed in punching after an initial flexural failure (Teng, Chanthabouala, Lim, & Hidayat, 2018). Based on the results of this test program, and previous results from the authors and other researchers, a modified version of the empirical equation to estimate punching capacity proposed by Teng, Cheong, Kuang and Geng (2004) was proposed (Teng, Chanthabouala, Lim, & Hidayat, 2018).

Regan and Rezai-Jorabi (1988) studied the punching shear behaviour of one-way slabs subjected to concentrated loads. Twenty-nine 100mm thick slabs were tested. Twenty-three of the slabs were supported at their ends and subjected to two central concentrated loads applied through plates. The aspect ratio of these load plates varied from one (75x75mm) to ten (1000x100mm). Most of the tests failed in one-way shear, but three failed in punching around one or both loads, or in a combination of one-way and punching shear. The final six tests reused some of the original twenty-three slabs. The location of one support was moved closer to the other and the slabs were subjected to one central concentrated load. The aspect ratio of the load plates in these six tests ranged from 1.33 (100x75mm) to 6 (600x100mm). Four of the six slabs failed in punching shear. The orientation of the load plates was found to affect the observed capacity. In cases where the longer plate dimension was parallel to the slab span a higher capacity was observed compared to when the longer plate dimension was perpendicular to the slab span. For small loaded areas the failure surface was similar to those observed in pure punching and the slab capacity was found to increase as the distance between the loads was increased. The one-way shear capacity of a reinforced concrete slab subjected to concentrated loads was found to be different than when the slab is subjected to a uniformly distributed load (Regan & Rezai-Jorabi, 1988).

Simmonds (1970) conducted an in-depth analysis of the structural behaviour of flat slabs supported on rectangular columns using a combination of linear elastic analysis, which is discussed in Section 2.6.3, and an experimental test of a one-third scale three bay by three bay continuous flat slab. The slab was supported on rectangular columns with a maximum column dimension equal to 40% of the distance between the column centerlines. This maximum column dimension was chosen since it marked the transition point from two-way to one-way slab action based on the results of the linear elastic analysis. In total, eight separate tests with different load magnitudes and locations were completed. Testing was stopped when one of the corner columns connections failed in punching. The structure was found to be stiffer in the direction of the maximum column dimension. The crack patterns of the slab confirmed that the behaviour of the slab was predominantly one-way. Based on the results of the analytical and experimental study, Simmonds concluded that the maximum

deflection and bending moments in a flat slab are reduced as the column cross-section is elongated in one direction (1970).

2.4 Mechanical Models

In addition to the numerous experimental and finite element studies of punching shear behaviour, many researchers have presented mechanical models to estimate the punching capacity of slab-column connections. In this section, some of the most popular mechanical models will be briefly summarized. Many additional models such as the model by Bazant and Cao (1987), which is based on fracture mechanics, and many modified versions of the Kinnunen and Nylander model, such as those proposed by Georgopoulos (1988, 1989) and Broms (1990) exist, but are not presented here. Many of these additional models, and the models discussed in this section are summarized in CEB Bulletin 168 (1985) and *fib* Bulletin 12 (FIB, 2001).

2.4.1 Kinnunen and Nylander

The model presented by Kinnunen and Nylander is a plasticity-based model which was derived from tests of circular isolated slab-column specimens with slab ring reinforcement. The original model was proposed in 1960, and later modified in 1963 to account for flexural reinforcement installed in two orthogonal directions, and to account for dowel action. The model, which is shown in Figure 2-6, assumes that a truncated cone of concrete is bounded by a shear crack. Beyond this shear crack, the slab is divided into segments which are assumed to rotate rigidly. These slab segments are assumed to be supported by a fictitious conical shell, which is subjected to compressive stresses, between the column face and base of the shear crack. To estimate the ultimate capacity of the slab-column connection the equilibrium of the internal forces, which are dependent on the slab rotation, and a failure criterion are used (Regan & Braestrup, 1985). The failure criterion is based on two conditions, a maximum value of the inclined compressive stress and a maximum value of the tangential compressive strain at the shear crack (FIB, 2001; Menétrey P. , 1996). The assumed failure mode is a compression failure of the conical shell. The assumed failure mode does not match experimental observations since punching capacity has been shown to be related to the concrete's tensile capacity (Menétrey P. , 1996).

However, the model presented by Kinnunen and Nylander was the first mechanical model for punching shear which resulted in capacity predictions that agreed well with available experimental results and allowed for visualization of the flow of forces in the vicinity of the slab-column

connection (FIB, 2001). Additionally, the model allowed the failure mode, either flexural or punching, to be determined, and allowed the slab deformations to be approximated (Regan & Braestrup, 1985).

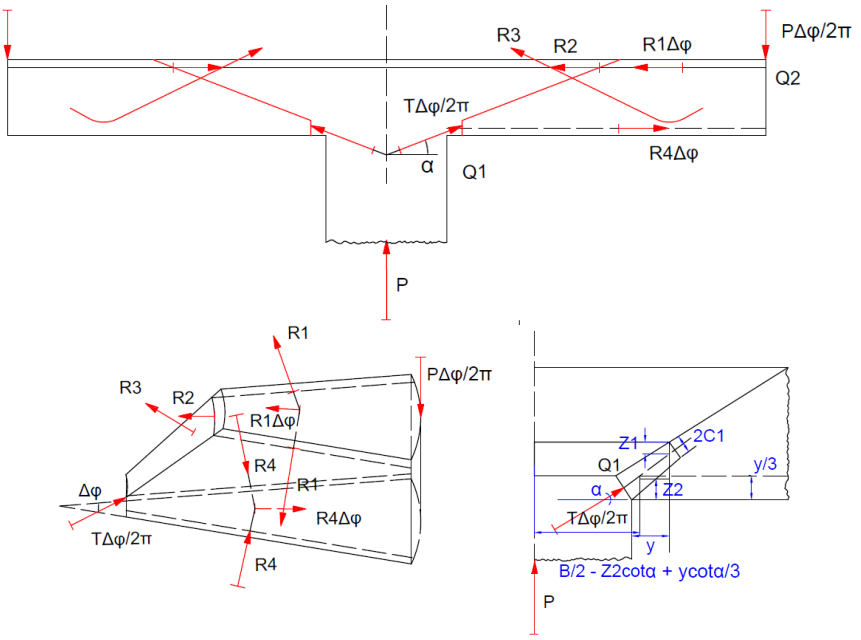

Figure 2-6: Punching Shear Model by Kinnunen and Nylander (1960), Adapted from (Kinnunen & Nylander, 1960), Reproduced with Permission

2.4.2 Upper Bound Plasticity Approach

Braestrup, Nielsen, Jensen and Bach proposed an upper bound plasticity solution to estimate the punching capacity of reinforced concrete slabs in 1976. The punching capacity was calculated by equating the rate of external work due to the applied load to the internal work dissipated to create the failure surface shown in Figure 2-7. To derive the equations used in the model, it was assumed that all deformation occurred within the rotation symmetric failure surface around the slab-column connection (Menétrey P. , 1996). The concrete contained within the failure surface was assumed to punch out of the slab while the remaining concrete was assumed to remain rigid. The yield criterion used in the model was based on the modified Coulomb failure criterion and the associated flow rule. The concrete was also assumed to be a rigid, perfectly plastic material. The impact of dowel action was neglected resulting in the flexural reinforcing ratio having no impact on the predicted punching strength. The predicted punching capacity was found to be strongly dependent on the assumed concrete tensile strength (Regan & Braestrup, 1985).

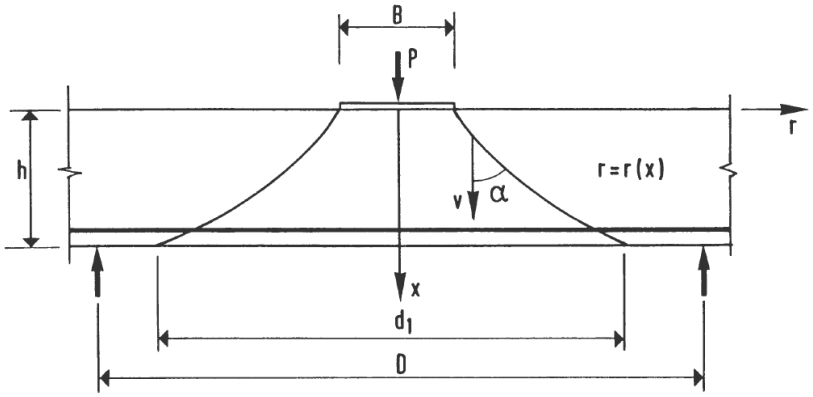

Figure 2-7: Failure Surface Considered by Braestrup et al. Reproduced from CEB Bulletin 168:- Punching Shear in Reinforced Concrete a state of art report by P.E. Regan and M.W. Braestrup (January 1985) with permission from the International Federation for Structural Concrete (*fib*)

2.4.3 Nölting Model

In 1984, Nölting proposed a method for estimating the punching shear capacity of flat slabs, one-way slabs, footings and slabs with eccentrically loaded columns based on an inclined compression approach. In the model, all inclined cracks near the location of concentrated loads or supports were assumed to be due to punching shear regardless of the slab reinforcement. Failure was assumed to occur when the compressive diagonal strain in the concrete reached a value of -4.5%. The magnitude of this diagonal strain was dependent on the applied load level and considered the relationship between the load and the critical moment at the column or loaded area, the moment and the horizontal strain in the concrete, and the horizontal and inclined strains in the concrete. Due to the difficulty of using the model, Nölting provided tabulated moments for certain typical slab types and for all others numerical coefficients derived from FEA were provided (Regan & Braestrup, 1985).

2.4.4 Models by Alexander and Simmonds

In 1987, Alexander and Simmonds proposed the first of their two models to estimate the punching capacity of slab-column connections. The first model they proposed, shown in Figure 2-8, was based on a three-dimensional truss which was made up of linear concrete compressive struts and steel tension ties. The model was an expansion of the truss model for edge slab-column connections conceptualized, but never fully developed, by Van Dusen in 1985. Two types of compression struts were assumed, those parallel to the plane of the slab, referred to as anchoring struts, and those

inclined with regard to the plane of the slab, referred to as shear struts. Both types of struts were tied to the column by the strut steel (Alexander & Simmonds, 1987).

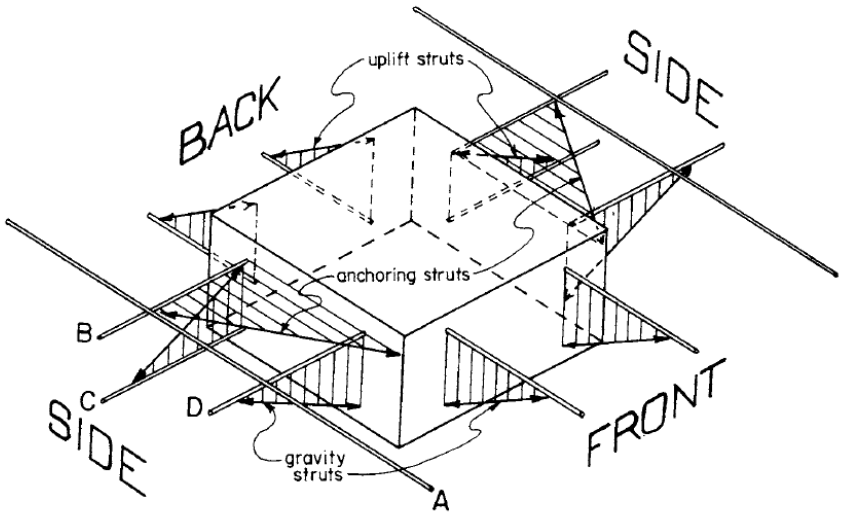

Figure 2-8: Alexander and Simmonds Truss Model, (Alexander & Simmonds, 1987) Authorized Reprint from ACI Structural Journal, Volume 84, Issue 3 (1987)

To estimate the punching capacity, it was assumed that the strut steel yielded. Based on this assumption, it was then assumed that the compressive capacity of the concrete struts in plane would never be exceeded. Therefore, failure of the slab-column connection was assumed to occur when the concrete could no longer resist the out of plane force component in the compression strut. This out of plane force is a measure of the slab's ability to confine the flexural reinforcing bars, and is a function of the tributary width of each bar, the reinforcing cover and the tensile strength of the concrete. The advantages of the truss model were that it explained the load path around a slab-column connection, it explained the role of the flexural reinforcement on the punching capacity, and the model was capable of accounting for column rectangularity if modification factors were applied and each face of the column was considered individually (Alexander & Simmonds, 1987).

Based on the results of experimental tests conducted after the truss model was published, Alexander and Simmonds determined that the radial compression struts were curved, as shown in Figure 2-9, instead of linear as originally assumed. To account for the struts being curved, modifications to the mechanics used in the truss model were required. In 1992, Alexander and Simmonds proposed an improved version of the truss model based on the shear stress on a critical

section and radial arching action, which was referred to as the bond model (Alexander & Simmonds, 1992; Lantsoght, van der Veen, Walraven, & de Boer, 2015).

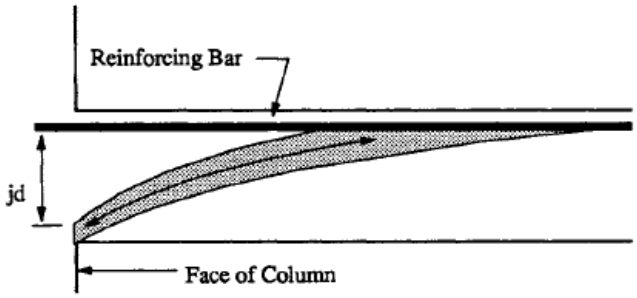

Figure 2-9: Curved Compression Strut Used in Bond Model (Alexander & Simmonds, 1992), Authorized reprint from ACI Structural Journal, Volume 89, Issue 3 (1992)

The bond model is only applicable for slabs with orthogonal reinforcing layouts and assumes that all load is carried from the slab to the column by radial strips. The shear forces are assumed to be transferred from the slab to the column by the radial compression arches. The minimum force in each arch occurs where the arch intersects the flexural reinforcing and the maximum force occurs at the column face. Equilibrium of the radial strips is considered in the bond model and the model considers both the flexural capacity of the radial strips and the shear capacity of the slab quadrants adjacent to the radial strips. Punching failure is assumed to occur due to the slab's inability to sustain the force gradients present in the flexural reinforcement in the area near the slab-column connection. These force gradients are assumed to be limited by either the bond between the reinforcing bars and the concrete or the extent of yielding along the reinforcement length. Unlike the truss model, which was capable of accounting for column rectangularity, the bond model does not properly account for column rectangularity as the model assumes all force is carried by arching action. As the column width increases, there is a transition from two-way to one-way shear action which results in the force being carried by a combination of arching and beam action. However, Alexander and Simmonds stated that the bond model should be conservative if the effect of rectangularity is neglected for slabs which were commonly used in practice at the time of its derivation (Alexander & Simmonds, 1992).

2.4.5 Rankin and Long Yield Line Model

In 1987, Rankin and Long presented a model to estimate the punching capacity of slab-column connections based on three failure modes, yielding of reinforcement, crushing of concrete or internal

diagonal cracking. Failures due to reinforcement yielding or concrete crushing were defined as flexural failures and failures due to internal inclined cracking were defined as shear failures. The model related the punching capacity of the slab to the flexural behaviour of the slab. For lightly reinforced slabs the final failure mode approaches that assumed in the yield line method as the reinforcing ratio is reduced since failure occurs after extensive yielding of the flexural reinforcement. In heavily reinforced slabs, the extent of yielding becomes localized, and the failure mode becomes similar to that of a localized concrete compression failure near the column. As such, the punching capacity should lie somewhere between the extremes of localized compression failure and the full yield line pattern, shown in Figure 2-10 (Rankin & Long, 1987).

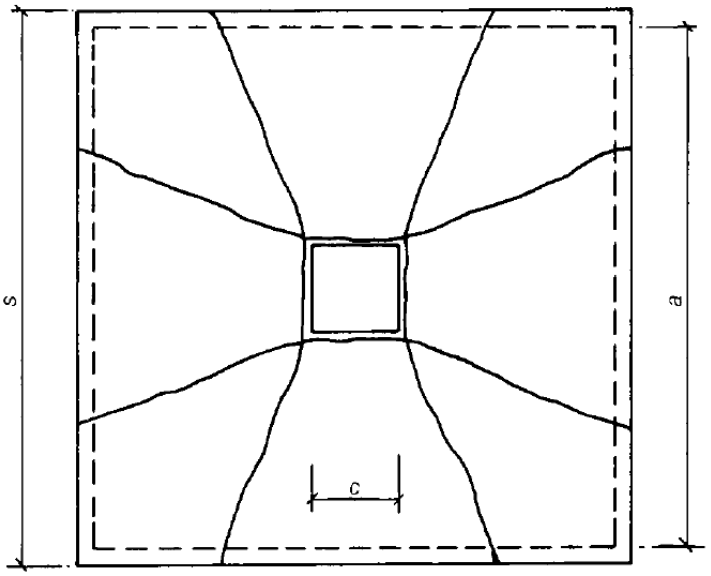

Figure 2-10: Yield Line Pattern for Isolated Slab-Column Specimen (taken from Rankin & Long, 1987), Reproduced with Permission from Institution of Civil Engineers

The shear capacity of the slab at flexural failure, P_{flex} (N), assuming the full yield line pattern shown in Figure 2-10 can be calculated using equation 2.1.

$$P_{flex} = 8\left(\frac{s}{a-c} - 0.172\right)M_b \qquad (2.1)$$

where s is the side length of a conventional isolated slab-column specimen (mm), c is the length of the column dimension (mm), and a is the distance between supports in a conventional isolated slab-column specimen (mm, typically assumed as 0.4L) (Rankin & Long, 1987).

The shear capacity of a slab failing due to localized compression at the column face can be calculated using equation 2.2

$$P = \left(\frac{25}{(\ln(2.5a/c))^{1.5}}\right) 0.333 f_c' d^2 \quad (2.2)$$

where $0.333 f_c' d^2$ represents the balanced moment of resistance and is taken from an empirical equation by Whitney (1937) (Rankin & Long, 1987).

The punching capacity of the slab is calculated as the minimum of two equations. One equation is used to estimate the capacity of a slab-column connection failing in flexural punching, which is characterized as a punching failure where partial yielding of the slab reinforcement has occurred. The second equation is used to estimate the "shear" punching capacity of slabs which fail before the reinforcement yields, or the concrete crushes (Rankin & Long, 1987).

The flexural punching capacity of a slab-column connection, P_{vf} (N), is calculated using equation 2.3 and must be less than a maximum value computed with equation 2.4.

$$P_{vf} = \left(8\left(\frac{s}{a-c} - 0.172\right) - \left(8\left(\frac{s}{a-c} - 0.172\right) - \frac{\frac{25}{(ln(2.5a/c))^{1.5}}}{r_f}\right)\frac{M_b}{0.333 f_c' d^2}\right) M_b \quad (2.3)$$

$$P_{vf,max} = \left(\frac{\frac{25}{(\ln(2.5a/c))^{1.5}}}{r_f}\right) 0.333 f_c' d^2 \quad (2.4)$$

where r_f is a column shape factor to account for stress concentrations, f_c' is the concrete compressive strength, and M_b is the flexural capacity of the slab (Nmm). The column shape factor is equal to 1 for circular columns and 1.15 for square columns (Rankin & Long, 1987).

The "shear" punching capacity, P_{vs} (N), is calculated using equation 2.5

$$P_{vs} = 1.66\sqrt{f_c'}(c+d)\, d\, (100\rho)^{0.25} \quad (2.5)$$

where d is the effective slab depth, and ρ is the flexural reinforcement ratio (Rankin & Long, 1987).

2.4.6 Shehata and Regan Model

Shehata and Regan proposed an improved version of the Kinnunen and Nylander model in 1989. As with the model proposed by Kinnunen and Nylander (1960), the slab was assumed to be divided into

rigid segments which rotate about a point, denoted the center of rotation, located at the neutral axis of the slab at the column face. Before failure, it was assumed that a rigid wedge element, which is bounded by the inclined cracks in the slab, and the initial circumferential crack around the column on the slab surface, breaks away from reach rigid segment and rotates independently about the center of rotation. Three equilibrium states in the radial plane are used to relate the slab rotation, neutral axis depth and inclination of the compressive force at the column face to the applied load. Failure is defined as one of three states:

1. When the inclination of the compressive force reaches 20 degrees the front portion of the radial segment, which is in compression, fails due to tensile splitting.
2. Radial crushing of the concrete is assumed to occur if the average radial strain on the compressed face equals 0.0035.
3. Tangential crushing of concrete is assumed to occur if at a distance x from the column face, where x is equivalent to the neutral axis depth, the tangential strain reaches 0.0035 (Shehata & Regan, 1989).

The model proposed by Shehata and Regan is an improvement over that proposed by Kinnunen and Nylander since the dowel action forces are calculated from equilibrium instead of assumed, the slab deformation on top of the column and bounded by the shear crack is accounted for, and a more complete failure definition is used (Shehata & Regan, 1989).

2.4.7 Critical Shear Crack Theory (CSCT)

The Critical Shear Crack Theory (CSCT) is a more recent mechanical model for punching shear proposed by Muttoni (2008). Like the model developed by Kinnunen and Nylander, the CSCT relates punching capacity to slab rotation. The CSCT assumes that the punching capacity of a slab-column connection decreases as the slab rotation increases. The CSCT assumes that the shear strength of a slab-column connection is decreased due to the existence of a critical shear crack which propagates through the slab and intersects the inclined compression strut transferring shear forces from the slab to the column. As this critical shear crack opens the strength of the inclined compression strut is decreased until punching failure occurs. Muttoni and Schwartz (1991) assumed that the width of this critical shear crack is proportional to the product of the slab rotation, ψ, and the effective slab depth, d, as shown in Figure 2-11.

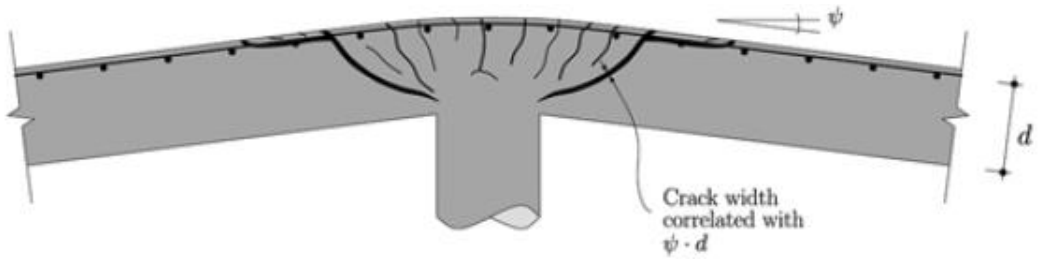

Figure 2-11: Relationship between the critical shear crack width and slab thickness and rotation (Muttoni, 2008), Authorized reprint from ACI Structural Journal, Volume 105, Number 4, 2008)

The amount of shear which can be transferred across the critical crack is assumed to be dependent on the crack roughness, which is estimated using as a function of the maximum aggregate size. Based on research by Walraven (1981) and Vecchio and Collins (1986) the capacity of the critical shear crack to transfer shear force is approximated by dividing the nominal crack width, ψd, by $d_{g0} + d_g$, where d_g is the maximum aggregate size (mm), and d_{g0} is the reference aggregate size of 16mm. Multiplying the slab rotation, ψ, by $d/(d_{g0} + d_g)$ has the additional benefit of cancelling out the effects of slab thickness and aggregate size in the model formulation. Using the assumptions and factors discussed above an improved version of the CSCT failure criterion was published in 2003 by Muttoni (Muttoni, 2008). The improved version of the CSCT failure criterion is discussed in Subsection 2.5.5.

To apply the CSCT, the designer must estimate the load-rotation response of the slab. When evaluating experimental tests, the rotations can be directly measured or can be calculated from measured deflections by assuming a conical deformation pattern of the slab beyond the column region. In design, the load rotation relationship can be estimated using nonlinear finite element analysis or simplified design equations. If different reinforcing ratios are used in each orthogonal direction, the maximum rotation of the slab should be used to estimate the punching capacity of the slab-column connection (Muttoni, 2008).

The CSCT is used as the basis of the current punching provisions in Model Code 2010 (Muttoni, Fernández Ruiz, Bentz, Foster, & Sigrist, 2013). Earlier versions of the CSCT were also adopted in the Swiss concrete design codes SIA 262 (2003) (Muttoni, Fernández Ruiz, Bentz, Foster, & Sigrist, 2013) and SIA 162 (1993) (Muttoni & Fernández Ruiz, 2008). The CSCT has also proven to be applicable to other reinforced concrete members without shear reinforcement with minor modifications. For example, it can be used to estimate the shear capacity of one-way slabs and beams

without transverse reinforcement by assuming the crack width is proportional to the product of the effective slab depth, d , and the longitudinal strain at a depth of 0.6d from the compression surface, ε (Muttoni & Fernández Ruiz, 2008). The CSCT has also been expanded to estimate the punching capacity of slabs which have transverse (shear) reinforcement (Fernández Ruiz & Muttoni, 2009).

2.5 Code Provisions

In this section a detailed discussion of the current punching shear design code provisions from ACI 318M-14, Eurocode 2 (EC2) 2004 and Model Code 2010 will be provided. The historical development of each of the above codes is also briefly discussed. Finally, a discussion of the design equations derived from the Critical Shear Crack Theory (CSCT) presented in Subsection 2.4.7 is provided. Most of the provisions discussed will be focused on interior slab-column connections subjected to concentric punching shear without shear reinforcement.

Many parameters such as the concrete compressive strength, slab flexural reinforcement ratio, slab effective depth, ratio of column perimeter length to slab depth, and shear span ratio to effective depth have been found to influence the punching capacity of slab-column connections (Kueres, Siburg, Herbrand, Classen, & Hegger, 2017). Other research has shown that additional factors such as restraint forces due to frame action and column shape also have a significant impact on the punching capacity of slab-connections (ASCE-ACI Committee 426, 1974). However, current codes of practice differ in their treatment of many of these parameters or do not account for them at all.

2.5.1 Critical Perimeter Concept

Current and historical design codes have many fundamental differences in their treatment of punching shear of reinforced concrete flat slabs. For example, some codes, such as Eurocode 2 (2004), account for the impact of the flexural reinforcing ratio on the impact of punching capacity, whereas others, such as ACI 318M-14, do not. However, all current major design codes for punching shear of reinforced concrete slabs are based on the same fundamental concept, which is the critical perimeter concept. Each code uses a critical perimeter where the shear stresses are typically assumed to be uniform, and these stresses, along with an effective critical perimeter length, are used to estimate the punching capacity of the slab-column connection being designed.

When designing a reinforced concrete beam the nominal shear stresses on a cross-section are used to arrive at a shear design for the beam. The punching shear design of two-way slabs can be completed using a similar methodology if the total punching load is divided by the area of an assumed

control surface or critical perimeter. The critical perimeter assumed in current design codes are typically vertical rectangular or cylindrical surfaces around the slab-column connection. These perimeters are assumed at a set distance from the face of the column or loaded area based on experimental observations or the chosen mechanical model from which the code provisions are derived. The critical perimeter concept was introduced in 1913 by Talbot, based on his observations from tests of square footings loaded through square columns. Talbot found that the shear capacity of the footings could be accurately predicted by considering the nominal shear stresses on a critical perimeter located at a distance of d from the column face, where d is the effective flexural depth of the footing (Regan & Braestrup, 1985).

To make use of the critical perimeter concept in design, the nominal shear stress on the assumed critical perimeter is compared to a fraction of the concrete tensile strength, since the tensile strength of concrete has been found to be related to the shear strength of concrete. The critical perimeter concept is a helpful assumption to simplify design codes but does not necessarily represent the mechanical behaviour of a reinforced concrete flat slab failing in punching shear. Even though it does not represent the complex mechanics of a slab-column connection, the critical perimeter concept has been found by many researchers to lead to reasonable predictions of punching capacity if proper factors are applied (Regan & Braestrup, 1985). Due to its simplicity, the critical perimeter concept is used in all major design codes, through the shape and assumed location of the perimeter varies between codes.

2.5.2 ACI 318M-14

The current version of the ACI 318 code, ACI 318M-14, is the result of over 100 years of research and practical engineering experience regarding the behaviour of concrete. The first official American concrete code was published in 1908 by the National Association of Cement Users (NACU), who by 1920 were known as the American Concrete Institute (ACI) (Committee of Laws and Ordinances, 1908). The first punching shear design provisions were included in ACI Standard Specification Number 23, which was released in 1920. The punching provisions were based on a working stress design methodology considering two critical sections, one vertical surface at the edge of the column capital, and one surface inclined at 45 degrees from the edge of the column capital carrying shear via diagonal tension. The stresses on these two surfaces were compared to maximum values which were fractions of the concrete compressive strength (American Concrete Institute, 1920). In the 1927 edition of the code only one critical section was used instead of two. The new critical section was

assumed to be vertical and located at a distance d from the face of the column capital or drop panel (ACI Committee E-1, 1927). Between 1936 and 1956, the punching provisions were largely unchanged, as only minor modifications were made to maximum allowable stresses and the detailing requirements (ACI Committee 501, 1936; ACI Committee 318, 1956).

The 1963 edition of ACI 318 represented a large change from the previous codes. The 1963 edition of ACI 318 was the first ACI code to include punching provisions for both working stress and ultimate stress design methods. The biggest changes in this code compared to previous versions were in regard to the assumed critical perimeter and maximum allowable stresses. Based on research completed before 1962, ASCE-ACI Committee 326, which is now known as ASCE-ACI Committee 426, recommended the critical perimeter be located at a distance of d/2 from the face of the column or drop panel, which differed from Moe's recommendations. The committee made this recommendation since most of the experimental punching shear test results available at the time displayed a pyramid shaped failure surface with an angle of approximately 45 degrees. This failure surface is under a complex state of stress due to combined bending and shear stresses and starts at the neutral axis of the slab. The committee believed that the use of the failure surface located at d/2 from the face of the column was simpler than using a failure surface at the column perimeter, as recommended by Moe. The design equation presented by Moe, which was derived assuming the critical perimeter to be the column perimeter, required a parameter that accounted for the ratio of the column size, c, to the effective depth of the slab, d (Moe, 1961; ACI Committee 318, 1965). The committee believed that the impact of c/d could be accounted for by using a vertical critical perimeter located at d/2 from the column face. It was assumed that the use of the perimeter at d/2 resulted in a shear stress distribution which was independent of the c/d ratio since the assumed critical surface shared a point with the actual failure surface, and had an area which was proportional to that of the actual failure surface (ACI Committee 318, 1965). The ultimate stress on the chosen failure surface was assumed equal to $4\sqrt{f_c'}$ (imperial units, where f_c' is in psi) or $0.33\sqrt{f_c'}$ (SI units, where f_c' is in MPa) even for irregularly shaped columns (ACI Committee 318, 1965). The use of $\sqrt{f_c'}$ to estimate shear capacity of reinforced concrete was a change from the previous versions of the code which is still used in the current ACI provisions. Finally, ACI 318-63 also added provisions requiring designers to check both one-way and two-way shear capacity, provisions for shear reinforced slabs, provisions for the design of slabs with openings near the slab-column connection and mentioned that the negative impact of

unbalanced moments on punching capacity needed to be accounted for, although no specific provisions were provided (ACI Committee 318, 1963; ACI Committee 318, 1965).

The assumption that the use of a critical perimeter located at d/2 resulted in uniform shear stress distributions for any size column was later found to be invalid, but researchers have shown that the use of a critical perimeter at d/2 leads to the most accurate estimation of punching capacity. Many current codes other than ACI 318M-14 including Model Code 2010, and SIA 232:2013 (Switzerland) and many historical codes such as Model Code 1978 and DIN 1045 (Germany) have used a critical perimeter located at d/2 from the column face (Kueres, Siburg, Herbrand, Classen, & Hegger, 2017). The critical perimeter assumed in ACI 318M-14 is shown in Figure 2-12.

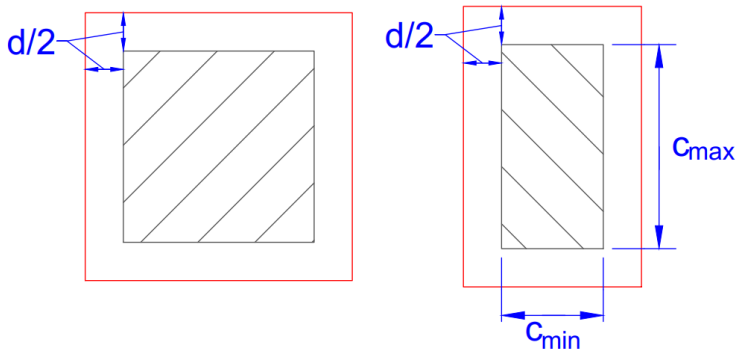

Figure 2-12: Critical Perimeter Assumed in ACI 318M-14 (ACI Committee 318, 2014)

The current ACI 318M-14 provisions for punching shear are very similar to those in ACI 318-63 for concentric punching around square columns. However, the assumption of the shear stress on the critical perimeter being independent of column size was incorrect and as such two additional equations for the shear capacity along the critical perimeter were added. The two-way shear capacity for a slab without shear reinforcement along the critical perimeter, v_c (MPa), is the minimum of equations 2.6, 2.7 and 2.8,

$$0.33\lambda\sqrt{f_c'} \tag{2.6}$$

$$0.17\left(1 + {}^{2}/_{\beta}\right)\lambda\sqrt{f_c'} \tag{2.7}$$

$$0.083\left(2 + \alpha_s\, {}^{d}/_{b_o}\right)\lambda\sqrt{f_c'} \tag{2.8}$$

where λ is a term to account for the density of concrete, f_c' is the concrete compressive strength (MPa), β is the ratio of the length of the long and short sides of the column, α_s is a constant

dependent on the column location (which equals 40 for interior columns (SI units)), d is the average effective depth (mm), and b_o is the length of the critical perimeter (mm). Equations 2.7 and 2.8 were added in 1977 and 1989 respectively to account for cases where the assumption of uniform stress on the critical perimeter for all column sizes and shapes (equation 2.6) was found to be unconservative. Equation 2.7 is largely derived from experimental results published in 1971 by Hawkins, Fallsen and Hinojosa and accounts for stress concentrations at the corners of rectangular or oddly shaped columns (ACI Committee 318, 2014; ASCE-ACI Committee 426, 1974; Al-Yousif & Regan, 2003; Mitchell, Cook, & Dilger, 2005). As discussed in Subsection 2.3.3, many other researchers have also observed a negative impact of column rectangularity on punching capacity (Oliveira, Regan, & Melo, 2004; Himawan & Teng, 2014; Paiva, Ferreira, Oliveira, Lima Neto, & Teixeira, 2015; Filatov, 2017; Shu, Belletti, Muttoni, Scolari, & Plos, 2017). Equation 2.8 was added based on tests by Vanderbilt (1972) that indicated that the maximum nominal shear stress on the critical perimeter at d/2 from the column face decreased as the ratio of the critical perimeter length, b_o, to the effective slab depth, d, increased (ACI Committee 318, 2014)

After determining the governing shear stress along the critical perimeter, the punching capacity of the slab-column connection, V (kN), is calculated according to equation 2.9.

$$V = v_{c,min} b_o d \div 1000 \tag{2.9}$$

where v_{cmin} is the governing shear stress along the critical perimeter which is the minimum of equation 2.6, 2.7, and 2.8 (MPa) and b_o and d are as previously defined (mm).

2.5.3 Eurocode 2 (2004)

The primary reason for the development of the Eurocodes was to harmonize the multiple national design codes used in the different European nations. The adoption of the Eurocodes allowed the same design code framework to be used throughout Europe, while allowing the individual nations to retain control of certain parameters, such as load levels (Johnson, 2009).

As with the 2004 edition of Eurocode 2 (EC2), which was primarily based on Model Code 1990 (European Concrete Platform ASBL, 2008), the original draft of Eurocode 2, released in 1991, ENV1992-1-1, was greatly influenced by the most recent Model Code available at the time. In addition to Model Code 1978, ENV1992-1-1 was also influenced by four British Standards, BS 8110 – Structural Use of Concrete: Parts 1-3 (1985) and BS 5400-4 – Steel, Concrete and Composite Bridges: Part 4 (1984) (The Concrete Centre, part of the MPA, n.d.). Unlike EC2 (2004), which does

not account for column rectangularity when calculating the punching resistance of concentrically loaded slab-column connections, ENV 1992-1-1 accounted for column rectangularity by reducing the effective critical perimeter length if the column dimensions exceeded specific values (Al-Yousif & Regan, 2003; Teng, Cheong, Kuang, & Geng, 2004). The lengths of the straight portions of the effective critical perimeter in ENV 1992-1-1 matched the lengths of the straight portions of the critical perimeter assumed to carry two-way shear in Model Code 1978. However, the critical perimeter assumed in ENV 1992-1-1 had two major differences compared to that used in Model Code 1978. Firstly, the portion of the critical perimeter assumed to carry one-way shear in Model Code 1978 was neglected in the ENV 1992-1-1. Secondly, even though the same lengths for the straight portions were assumed in both codes the critical perimeters were located at different distances. The critical perimeter was located at a distance of d/2 from the column face in Model Code 1978, and at a distance of 1.5d from the column face in ENV 1992-1-1, which matched the critical perimeter assumed in the British design standards. Examples of the critical perimeters assumed in ENV 1992-1-1 around typical columns and large rectangular columns are shown in Figure 2-13.

a) Typical Columns

b) Large Rectangular Columns

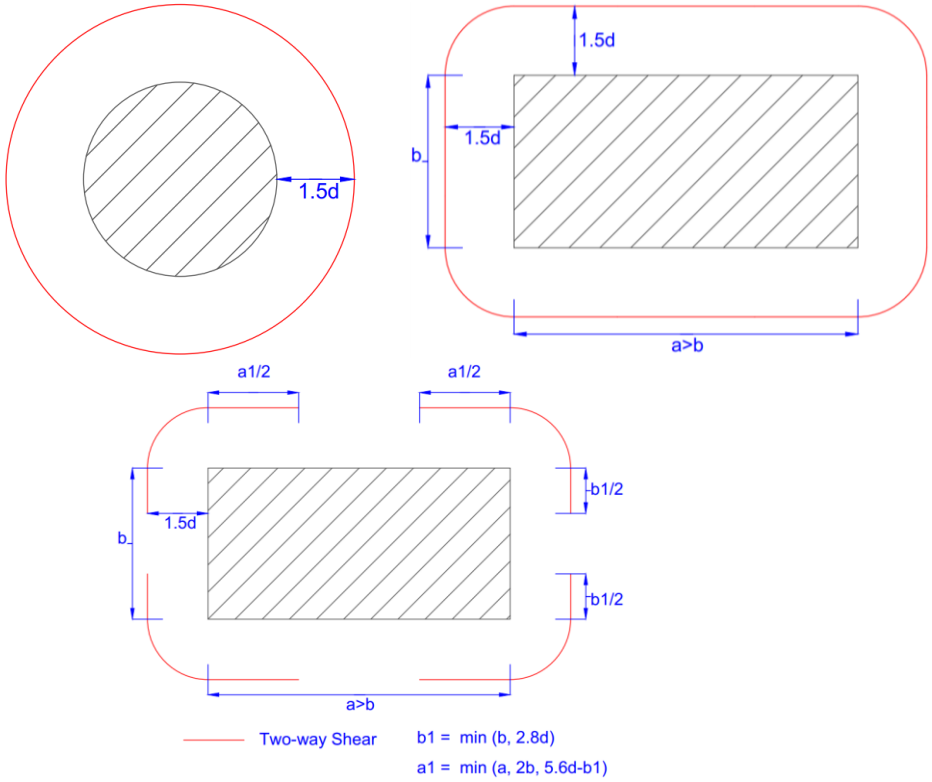

Figure 2-13: Critical Perimeters Assumed in ENV 1992-1-1 (European Comittee for Standardization (CEN), 1993)

EC2 (2004), also known as EN 1992-1-1 (2004) was primarily based of Model Code 1990, and included many changes compared to its draft form, ENV 1992-1-1 (European Concrete Platform ASBL, 2008; Ricker & Siburg, 2016; Walraven & Bigaj, 2011; Gardner N. J., 2011). Firstly, the critical perimeter location was moved from a distance of 1.5d to 2d from the column face to match the critical perimeter used in Model Code 1990. Secondly, the reductions in the effective critical perimeter length to account for column rectangularity were removed (European Commitee For Standardization, 2004; European Concrete Platform ASBL, 2008). The assumed critical perimeter was modified from 1.5d to 2d since the further perimeter was found to result in a more uniform shear stress distribution even for different column sizes. The use of the critical perimeter at 2d also allowed the same methodology used to calculate shear in members without shear reinforcement to be used for slabs (European Concrete Platform ASBL, 2008; FIB, 2010). Secondly, the punching capacity equation was modified to resemble that used in Model Code 1990, since an error was found in the derivation of the ENV 1992-1-1 equation which resulted in unconservative predictions for high strength concretes (European Concrete Platform ASBL, 2008).

According to EC2 (2004), the nominal punching capacity along the critical perimeter, $v_{Rd,c}$ (MPa), can be calculated according to equation 2.10

$$v_{Rd,c} = C_{Rd,c}\, k\, (100\, \rho_l\, f_{ck})^{\frac{1}{3}} \tag{2.10}$$

where f_{ck} is the characteristic concrete strength (MPa), k is a size effect factor which is equal to $1 + \sqrt{200/d} \leq 2.0$ where d is the average effective depth (mm), ρ_l is a term based on the flexural reinforcement ratio in each orthogonal direction which is equal to $\sqrt{p_{ly}\, \rho_{lz}} \leq 0.02$ where ρ_{ly} and ρ_{lz} are the reinforcement ratios for a slab width equal to the column width plus $3d$ on each column side in each orthogonal direction, and $C_{Rd,c}$ is a constant equal to $0.18/\gamma_c$, where γ_c is a safety factor found in the national annexes that typically equals 1.5 (European Commitee For Standardization, 2004). Since equation 2.10 tends to 0 as the reinforcing ratio approaches 0, which was also the case in Model Code 1990, an equation was added to calculate a minimum punching resistance around the critical perimeter (European Concrete Platform ASBL, 2008). The minimum punching resistance around the critical perimeter, v_{min} (MPa), is calculated using equation 2.11 (European Commitee For Standardization, 2004).

$$v_{min} = 0.035\, k^{\frac{3}{2}}\, f_{ck}^{\frac{1}{2}} \tag{2.11}$$

EC2 (2004) also requires the designer to check the punching capacity based on a maximum stress around the column perimeter. The resistance of the slab-column connection along the column perimeter, $v_{Rd,max}$ (MPa), is calculated according to equation 2.12.

$$v_{Rd,max} = 0.4\,[0.6\,(1 - f_{ck}/250)]\,f_{cd} \qquad (2.12)$$

where f_{cd} is the design concrete strength (MPa) which is calculated as $\alpha_{cc} f_{ck}/\gamma_c$ where α_{cc} is a factor to account for long term effects with a recommended value of 1 (European Commitee For Standardization, 2004). In equation 2.12 the $(1 - f_{ck}/250)$ term accounts for reduced strength of the compression struts in cracked concrete due to lateral tensile stresses (Kueres, Siburg, Herbrand, Classen, & Hegger, 2017; Ricker & Siburg, 2016).

The punching capacity of the slab-column connection according to EC2 (2004) is determined as the minimum of the capacity based on the shear stress along the critical perimeter at 2d and along the column perimeter. To compute the punching capacity based on the column perimeter $v_{Rd,max}$ is multiplied by the column perimeter and the average effective depth. The punching capacity based on the shear stress at the critical perimeter is calculated using equation 2.13

$$V_{2d} = v\,u_1\,d \qquad (2.13)$$

where V_{2d} is the punching capacity (N), v is maximum of the shear stresses calculated from equations 2.10 and 2.11 (MPa), d is the average effective slab depth (mm) and u_1 is the length of the critical perimeter located at 2d from the column face. The critical perimeter assumed in EC2-2004 is shown in Figure 2-14.

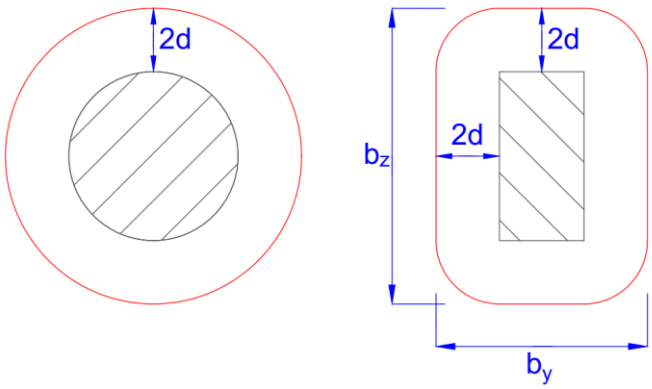

Figure 2-14: EC2 (2004) Critical Perimeter (European Commitee For Standardization, 2004)

As previously mentioned EC2 (2004) does not account for column rectangularity when calculating the punching resistance of slabs subjected to concentric loading. However, EC2 does account for column rectangularity in cases where unbalanced moments are transferred to the column.

In cases where the support reaction is eccentric with regards to the critical perimeter or column perimeter, the shear stress due to the applied loading, v_{Ed} (MPa), is calculated using equation (2.14)

$$v_{Ed} = \beta \frac{V_{Ed}}{u_1 d} \tag{2.14}$$

where V_{Ed} is the applied shear force (N) and β is calculated using equation 2.15 (European Commitee For Standardization, 2004)

$$\beta = 1 + k \frac{M_{Ed}}{V_{Ed}} \frac{u_1}{W_1} \tag{2.15}$$

where k is a coefficient which depends on the ratio of the minimum column dimension to the maximum column dimension, M_{Ed} is the design value of the applied internal bending moment (Nmm) and W_1 is a term to account for the distribution of shear on the critical perimeter (European Commitee For Standardization, 2004). For a rectangular column W_1 is calculated according to equation 2.16.

$$W_1 = \frac{c_1^2}{2} + c_1 c_2 + 4 c_2 d + 16 d^2 + 2\pi d c_1 \tag{2.16}$$

where c_1 is the column dimension parallel to the load eccentricity and c_2 is the column dimension perpendicular to the load eccentricity (European Commitee For Standardization, 2004).

For interior columns with rectangular cross-sections where the reaction is eccentric about both axes an approximate expression for β, shown in equation 2.17, is provided.

$$\beta = 1 + 1.8 \sqrt{\left(\frac{e_y}{b_z}\right)^2 + \left(\frac{e_z}{b_y}\right)^2} \tag{2.17}$$

where e_y and e_z are the eccentricities along the y and z axes respectively and b_y and b_z are the dimensions of the control perimeter as shown in Figure 2-14 (European Commitee For Standardization, 2004).

In the case of edge columns, alternative definitions for β and W_1 are provided, but are not discussed in detail here, as the work in this thesis is focused on interior slab-column connections.

2.5.4 Model Code 2010

Model Code 2010 is the most recent model code published by the International Federation for Structural Concrete (*fib*). It is not a legally binding code but instead is intended to serve as a starting point from which other nations and code committees can create a design code for structural concrete. Model Code 2010 is meant to provide code creators with state-of-the-art knowledge in terms of the material behaviour and analysis/design of concrete structures (fédération internationale du béton (fib), 2013; Walraven & Bigaj, 2011).

Model Code 2010 differs from the two previous Model Codes, Model Code 1978 and Model Code 1990, in two significant areas. Firstly, Model Code 2010 introduced the Level of Approximation (LoA) approach. This approach is meant to provide designers with simplified design procedures that can be used in preliminary design stages, or for the design of non-critical elements while allowing them to use state-of-the-art approaches to assess existing structures or design critical members. Four levels of approximation are provided for punching shear. As the level of approximation is increased more time is required to perform the analysis, but the final results should be more accurate and less conservative. The use of the LoA approach requires the code provisions to be based on sound physical models so that designers can see the relation between the simplified and complicated models through simple assumptions (Belletti, Pimentel, Scolari, & Walraven, 2015). The second fundamental difference between the two previous Model Codes and Model Code 2010 is that the punching provisions for Model Code 2010 are based on the Critical Shear Crack Theory (CSCT), which is a mechanical model, whereas the two previous Model Codes were empirically based (Muttoni & Fernández Ruiz, 2012; Muttoni, Fernández Ruiz, Bentz, Foster, & Sigrist, 2013; Ricker & Siburg, 2016; Soares & Vollum, 2015).

The punching shear capacity of slab-column connection without shear reinforcement is calculated according to equation 2.18.

$$V_{R,c} = k_{\psi}\sqrt{f_{ck}}b_o d \qquad (2.18)$$

where b_o is the length of the effective control perimeter at located at 0.5d from the column face (mm), d is the effective depth of the slab (mm), f_{ck} is the characteristic compressive strength of concrete (MPa) and k_{ψ} is a parameter that is related to the slab rotation and calculated using equation 2.19.

$$k_\psi = \frac{1}{1.5 + 0.9\psi d k_{dg}} \leq 0.6 \quad (2.19)$$

where ψ is the slab rotation and k_{dg} is a factor depending on the maximum aggregate size calculated according to equation 2.20

$$k_{dg} = \frac{32}{16 + d_g} \geq 0.75 \quad (2.20)$$

where d_g is the maximum aggregate size (mm).

Four levels of approximation are provided to estimate the slab rotation, ψ. LoA I is meant to be used for preliminary design and is based on the assumption that all flexural reinforcement in the support strip width yields at failure. This assumption results in very large crack widths, which decreases the predicted punching capacity according to the CSCT. LoA I is a very safe estimation technique since if the finalized design meets this criteria the strength of the slab will be governed by bending and no further punching checks are required. Designs according to LoA I will have very ductile failures (Muttoni & Fernández Ruiz, 2012) and will be very conservative. According to LoA I, the slab rotation can be calculated according to equation 2.21.

$$\psi = 1.5 \frac{r_s f_{yd}}{d E_s} \quad (2.21)$$

where r_s is the location where the radial bending is equal to zero (mm, typically 0.22 times the clear span), f_{yd} is the yield strength of the reinforcement (MPa), and E_s is the elastic modulus of the reinforcement (MPa) (fédération internationale du béton (fib), 2013).

LoA II, which is recommended for the design of new structures (Genikomsou A. , 2015; Paiva, Ferreira, Oliveira, Lima Neto, & Teixeira, 2015), uses a simplified estimate of the moment capacity per unit length of support strip. The moment capacity of the support strip is calculated using an analytical equation which relates the moment in the support strip to the shear force acting in this strip and the moment transferred from the slab to the support region accounting for eccentricity (Muttoni & Fernández Ruiz, 2012). Predictions according to LoA II have been found to be fairly accurate by numerous researchers (Muttoni & Fernández Ruiz, 2012; Muttoni, 2008; Muttoni, Fernández Ruiz, Bentz, Foster, & Sigrist, 2013). According to LoA II, the slab rotation can be calculated according to equation 2.22.

$$\psi = 1.5\,\frac{r_s\,f_{yd}}{d\,E_s}\left(\frac{m_{Ed}}{m_{Rd}}\right)^{1.5} \qquad (2.22)$$

where m_{Ed} is the average moment per unit length for calculation of the flexural reinforcement in the support strip (Nmm/mm) and m_{Rd} is the design average flexural strength per unit length in the support strip (Nmm/mm). To apply LoA II, the rotation must be calculated in both orthogonal directions (fédération internationale du béton (fib), 2013).

LoA III is recommended for use in special cases or to analyze existing structures (Genikomsou A. , 2015; Paiva, Ferreira, Oliveira, Lima Neto, & Teixeira, 2015). Like LoA II, LoA III uses an analytical equation to estimate the slab rotation. However, LoA III allows the designer to improve the estimate of the slab rotation, and the estimate of punching capacity, by using linear elastic FEA to estimate the moment field in the slab. Since a more accurate method is used to estimate the moment, the coefficient of 1.5 in equation 2.22 is reduced to 1.2 (Muttoni & Fernández Ruiz, 2012; fédération internationale du béton (fib), 2013). Reducing this coefficient is equivalent to assuming a stiffer slab response since the calculated slab rotation is lower. Based on the assumptions in the CSCT, the critical crack width is reduced (since rotations are reduced) leading to a higher estimated punching capacity (Muttoni & Fernández Ruiz, 2012).

LoA IV represents the highest level of approximation and is recommended for special cases and for accurate assessments of existing structural capacity (Genikomsou A. , 2015). LoA IV allows the designer to use NLFEA to estimate the slab rotation to be used in equation 2.19 (fédération internationale du béton (fib), 2013). Typically, analyses according to LoA IV are very time consuming and in most cases the increase in capacity between LoA III and LoA IV will be small. Only in cases with low reinforcing ratios, or where significant moment redistribution is expected, will predictions from LoA IV differ greatly compared to those from LoA III. LoA IV also requires an experienced designer as NLFEA is greatly affected by modelling choices. The model used to estimate slab rotations should be verified or calibrated based on experimental results (Muttoni & Fernández Ruiz, 2012).

The basic critical perimeter in Model Code 2010 is located at a distance of d/2 from the column face and has curved corners as shown in Figure 2-15. However, before the punching capacity can be estimated using equation 2.18 the effective critical perimeter length must be calculated. The first reduction in critical perimeter length accounts for large columns. For columns with side lengths greater than 3d the effective length of the critical perimeter is reduced to a length of 3d on each

respective side where the length exceeds 3d, as shown in Figure 2-15. Additional reductions in effective critical perimeter length account for accidental eccentricities and the impact of unbalanced moments. However, all slabs in this thesis were concentrically loaded and were based on carefully tested experimental specimens. Therefore, the additional reductions were neglected when evaluating the adequacy of the Model Code 2010 provisions.

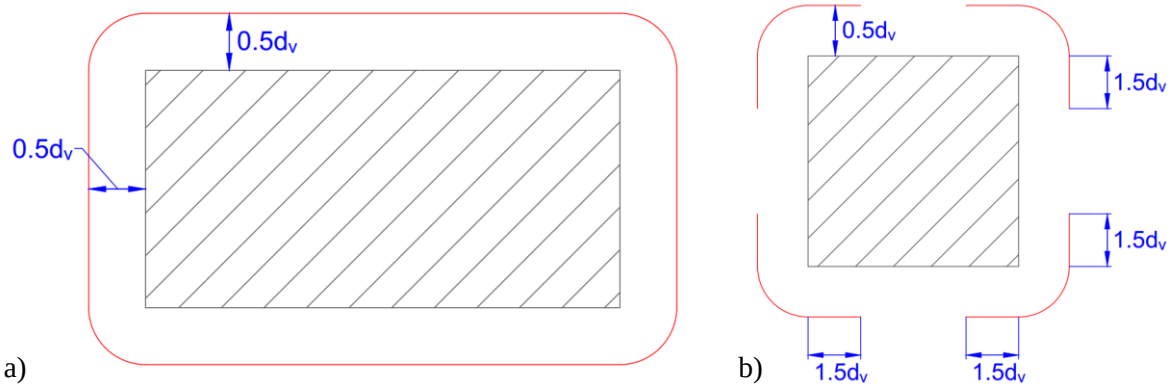

Figure 2-15: Critical Perimeters Assumed in MC 2010, a) Unreduced b) Reduced effective perimeter length (3d method) (fédération internationale du béton (*fib*), 2013)

It is interesting to note that a similar reduction in the critical perimeter length to account for large or rectangular columns was included in Model Code 1978. The commentary to Model Code 1978, contained in CEB Bulletin 137 (Comite Euro-International Du Beton, 1980), states that the use of a critical perimeter at a distance of d/2 from the column face leads to unconservative punching estimates for large columns. Unlike Model Code 2010, where portions of the critical perimeter are assumed to have zero capacity, the critical perimeter in Model Code 1978 was divided into two portions if the column side lengths exceeded certain dimensions as shown in Figure 2-16, one which carried shear through two-way (punching) shear, and one which carried shear through one-way shear. The nominal capacity in one-way shear was assumed to be lower than that in two-way shear in Model Code 1978 (Comité Euro-International Du Béton, 1978).

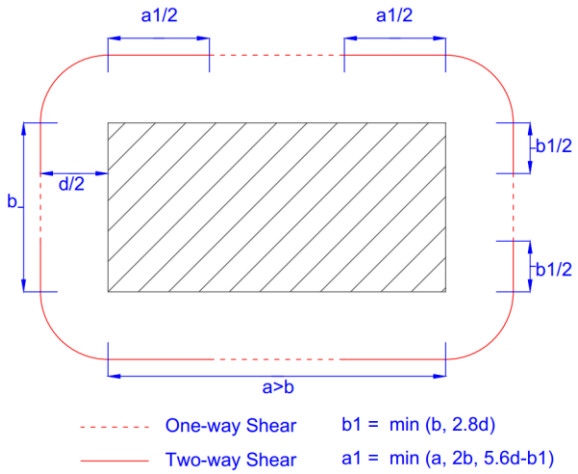

Figure 2-16: Critical Perimeter Around Large or Rectangular Columns Assumed in Model Code 1978 (Comité Euro-International Du Béton, 1978)

The punching shear provisions in Model Code 1990 are extremely similar to those in Eurocode 2 (2004) since Eurocode 2 was derived from Model Code 1990 (European Concrete Platform ASBL, 2008). As such, the punching provisions from Model Code 1990 will not be discussed in detail. However, it is interesting to note that unlike the other two Model Codes, Model Code 1990 did not directly account for column rectangularity in concentric punching. As with Eurocode 2 (2004), the critical perimeter was assumed to be located at a distance of 2d from the column face as it was found to result in a more uniform stress distribution around columns of any size (Comité Euro-International du Béton, 1993).

2.5.5 Critical Shear Crack Theory (CSCT)

Based on the CSCT, the punching shear capacity of a slab-column connection without shear reinforcement, V_R, can be calculated using equation 2.23.

$$V_R = \frac{3}{4} \frac{b_o d \sqrt{f_c'}}{1 + 15 \left(\frac{\psi\, d}{d_{g0} + d_g} \right)} \qquad (2.23)$$

where b_o is the critical perimeter length (mm), d is the effective slab depth (mm), f_c' is the concrete compressive strength (MPa), d_{g0} is a reference aggregate size (16mm), d_g is the maximum aggregate size (mm) and ψ is the slab rotation (Muttoni, 2008). The slab rotation can be estimated through the

use of FEA or can be calculated using a simplified equation proposed by Muttoni, which is provided in equation 2.24.

$$\psi = 1.5\,\frac{r_s\,f_y}{d\,E_s}\left(\frac{V}{V_{flex}}\right)^{3/2} \tag{2.24}$$

where r_s is the distance to the radius of contraflexure (mm, typically taken as 0.22L), f_y is the yield strength of the flexural reinforcement (MPa), E_s is the modulus of elasticity of the flexural reinforcement (MPa), V is the applied shear force (N) and V_{flex} is the shear force associated with the flexural capacity of the slab (N) (Muttoni, 2008). Muttoni (2008) states that the slab's flexural strength is reached when the radius of the zone where the flexural reinforcement has yielded (r_y) equals the radius of an isolated-slab column connection (r_s). Based on this definition V_{flex} can be calculated using equation 2.25.

$$V_{flex} = 2\pi m_R\left(\frac{r_s}{r_q - r_c}\right) \tag{2.25}$$

where m_R is the nominal moment capacity per unit width (Nmm/mm), r_q is the radius of the load introduction at the perimeter (mm), and r_c is the radius of the circular column (mm) (Muttoni, 2008).

In the case of rectangular columns, the punching capacity can be calculated using one of two methods. The first method involves using one maximum rotation to calculate a nominal stress assumed to act over the effective critical perimeter length. The second method, presented by Sagaseta et al. (2014), accounts for the redistribution of shear around the critical perimeter and involves dividing the effective critical perimeter into X and Y components as shown in Figure 2-17. In order to apply this method, the maximum slab rotation in each orthogonal direction is used. Using both maximum rotations the total capacity of the slab-column connection is calculated using equation 2.26

$$V_R = v_{Rx}b_x + v_{Ry}b_y = \frac{V_{Rx}}{b_o}b_x + \frac{V_{Ry}}{b_o}b_y \tag{2.26}$$

where V_{Rx} and V_{Ry} are the punching capacities calculated using equation 2.23 based on the entire effective critical perimeter length and the maximum rotation in the X and Y-directions respectively (N), and b_x and b_y are the lengths of the critical perimeter in the X and Y-directions respectively (Sagaseta, Tassinari, Fernández Ruiz, & Muttoni, 2014).

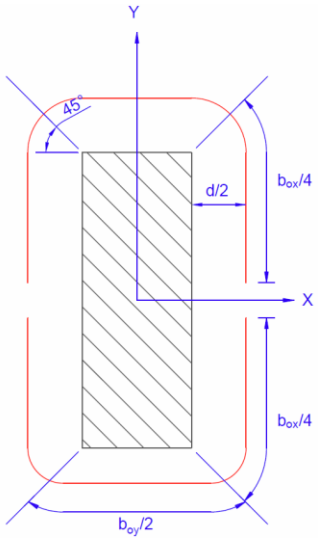

Figure 2-17: Breakdown of Critical Perimeter into X and Y Components

2.6 Review of Previous Finite Element Analysis

2.6.1 Introduction

Similar to the experimental database for punching shear, the majority of previous finite element studies have focused on slabs supported on square or circular columns. The finite element studies for slabs supported on square or circular columns are typically nonlinear and focus on predicting the full response of isolated slab-column connections or continuous slab systems. Finite element studies for slabs supported on rectangular columns are typically linear elastic and focused on estimating the elastic shear stress distribution around the column or critical perimeter. These elastic shear stress distributions are typically used to estimate the effective critical perimeter length which can be combined with code provisions to estimate the punching capacity of slabs supported on rectangular columns.

Some early attempts to use FEA to analyze slab-column connections were conducted by Hawkins, Fallsen and Hinojosa (1971) and Masterson and Long (1974). As part of their detailed study of column rectangularity Hawkins, Fallsen and Hinojosa (1971) conducted two-dimensional finite element analysis to estimate the deflection of the tested isolated slab-column specimens. Masterson and Long (1974) proposed equations to estimate the capacity of slab-column connections, including those with rectangular columns, based on the results of a linear two-dimensional finite element

analysis based on elastic thin plate theory. Since these early attempts to use FEA to analyze the punching shear behaviour of slab-column connections the use of NLFEA has grown in popularity.

The popularity of NLFEA has grown due to the desire of engineers to realistically model structural behaviour under various loading conditions. Nonlinear numerical analyses based on the finite element method have proven to be capable of providing a virtual testing scheme which can be used to simulate structural behaviour and determine the impact of parameters which are difficult to investigate experimentally (Alam & Amanat, 2012). However, simulating the phenomenon of punching shear in reinforced concrete slabs using NLFEA is not trivial due to the interaction between shear and flexure and the development of localized fracture zones as the load is applied to the slab (Wosatko, Pamin, & Polak, 2015; Shu, Belletti, Muttoni, Scolari, & Plos, 2017).

As previously mentioned, early finite element research of reinforced concrete slabs supported on columns was done using two-dimensional elements. As time has passed, the use of three-dimensional models based on shell or continuum (solid) elements has become more popular. Three-dimensional models offer increased flexibility and accuracy in capturing the out-of-plane behaviour of reinforced concrete structures compared to their two-dimensional counterparts (Shu, Plos, Zandi, Johansson, & Nilenius, 2016). Models based on shell elements are typically less detailed than those based on continuum elements since they are based on a smeared cracking approach and consider the reinforcement as a layer within the concrete or account for the reinforcement by modifying the concrete stiffness. Shell element-based models are typically used to conduct a global analysis of a structure, as they use less degrees of freedom and require less computational time compared to models using three-dimensional continuum elements. Three-dimensional solid elements are the ideal choice when a detailed analysis of a small portion of a structure is required (Polak, 1998). Models based on three-dimensional solid elements can be used to conduct detailed studies of cracking and damage in small portions of a structure (Guan & Polak, 2007), such as a slab-column connection. However, skilled practitioners are required to conduct meaningful FEA based on three-dimensional solid elements due to the large impact modelling choices can have on the predicted response (Shu, Fall, Plos, Zandi, & Lundgren, 2015).

In this section, previous finite element studies of slabs supported on square or circular columns and rectangular columns using two-dimensional elements, or three-dimensional shell and solid elements will be discussed.

2.6.2 Square or Circular Columns

2.6.2.1 Two-dimensional Finite Element Analyses

González-Vidosa, Kotsovos and Pavlovic (1988) conducted a NLFEA of axisymmetric slabs based on a two-dimensional plane stress model by Bédard and Kotsovos (Bédard & Kotsovos, 1985). Two series of isolated slab-column connections were modelled. The first series of slabs were four circular slabs tested by Kinnunen, Nylander and Tolf (1978). The second series of slabs, chosen since the reinforcing ratios range between 0.5% and 3%, were five square slabs tested by Elstner and Hognestad (1956). Due to the formulation of the model, the square slabs were approximated through equivalent circular slabs. Eight node and three node isoparametric elements were used to model the concrete and the flexural/shear reinforcement respectively. Concrete cracking was accounted for by using a modified Newton-Raphson method and the residual force concept. The finite element model was found to accurately predict the load deflection curve of the circular slabs and predicted the punching capacity within 10%. The predicted capacities for the square slabs were within 20% of the experimental values, but the predicted stiffness was much higher, likely due to the use of the equivalent circular slab (González-Vidosa, Kotsovos, & Pavlovic, 1988).

Menétrey, Zimmerman, Willam and Regan (1997) modelled isolated slab-circular column connections with four node quadrilateral axisymmetric elements. Concrete cracking was accounted for using a smeared crack model and a strain-softening formulation. The crack width was related to the concrete tensile stress through the fictitious crack model developed by Hillerborg et al. (1976). To overcome mesh locking the mean dilation formulation proposed by Hughes (1980) was used. The model was used to investigate the impact of concrete tensile strength, concrete compressive strength, orthogonal reinforcing layouts, reinforcing ratio and size effect on punching shear behaviour. It was concluded that punching failures are related to the concrete tensile strength and that increasing the flexural reinforcement ratio reduces cracking and increases the punching capacity. The numerical model also predicted a size effect similar to that observed experimentally by others (Menétrey, Walther, Zimmermann, Willam, & Regan, 1997).

Hallgren and Bjerke (2002) simulated experimental tests of two circular column footings in SBETAX 1.2, which is two-dimensional nonlinear analysis program for reinforced concrete structures. The model was based on nonlinear fracture mechanics and used a smeared rotated crack model. Two-dimensional four node isoparametric elements with additional degrees of freedom in the out-of-plane direction were used. Reinforcement was included in a band of elements through a

smeared method. The impact of slab slenderness, concrete compressive strength, concrete tensile strength and assumed concrete fracture energy on the finite element predictions were investigated. The punching capacity of footings was found to be greatly influenced by the slenderness and concrete compressive strength (Hallgren & Bjerke, 2002).

2.6.2.2 Three-dimensional Finite Element Analyses – Shell Elements

Polak (1998) demonstrated the capability of the finite element method for global analyses of reinforced concrete slabs subjected to large concentrated transverse loads using three-dimensional layered shell element formulations based on quadratic, degenerate isoparametric elements which allowed the out-of-plane shear response of the slab to be approximated. The model was formulated based on the Modified Compression Field Theory (MCFT) by Vecchio and Collins (1986). In plane reinforcement was modelled as a layer within each element whereas transverse reinforcement was accounted for by modifying the concrete properties in each layer. A smeared rotating crack approach where the crack direction is assumed to be perpendicular to the direction of the principal tensile strain was used. The model was able to accurately capture transverse shear behaviour and predict the location of flexural or punching failures in structures (Polak, 1998).

Guan and Polak (2007) also used layered shell elements to model punching shear behavior, but their study was focused on slab-edge column connections with openings and the impact of shear reinforcing. Twelve specimens, ten of which were tested experimentally by El-Salakawy, Polak and Soliman (1999, 2000), were modelled using layered shell elements and the layered finite element method (LFEM) presented by Guan and Loo (1997). The use of LFEM allowed the model to account for both flexural and transverse shear cracking until failure. The presented model accurately predicted the slab deflections at failure, load capacity and crack patterns of the experimental specimens. The inclusion of openings was found to reduce both the punching capacity and stiffness of the connection. In cases where the connection was subjected to unbalanced moments, a smaller reduction of punching capacity was observed when the opening was not located in the same direction as the unbalanced moment (Guan & Polak, 2007).

Plos, Shu, Zandi and Lundgren (2017) proposed a multi-level assessment strategy based on successively improved analysis techniques that could be used to evaluate existing reinforced concrete bridge deck slabs. The second and third levels of the assessment strategy use linear elastic and nonlinear three-dimensional shell element models respectively. Level II analyses are based on shell or plate bending theory and the impact of different load cases is analyzed using superposition. A level III

analysis involves a nonlinear finite element study using shell elements where the loads are increased until structural failure is predicted. Level III analyses include reinforcing based on the assumption of perfect bond. Models meeting level III requirements are not capable of capturing out-of-plane shear failures such as punching, and these failure modes must be checked through other methods. Three-dimensional NLFEA based on continuum elements are used for the highest analysis levels, level IV and V respectively. (Plos, Shu, Zandi, & Lundgren, 2017). The assumptions for levels IV and V are discussed in Section 2.6.2.3

2.6.2.3 Three-dimensional Finite Element Analyses – Solid Elements

Alam and Amanat (2012) calibrated a three-dimensional finite element model based on a total strain crack approach based on the experimental results of fifteen slab-column tests conducted by Alam, Amanat and Seraj (2009). The finite element model was implemented in TNO DIANA and was based on the MCFT by Vecchio and Collins (1986) and the three-dimensional extension proposed by Selby and Vecchio (1993). Twenty node isoparametric solid brick elements were used to model the concrete. The flexural reinforcement was assumed to be perfectly bonded to the concrete and was embedded in the concrete elements. The calibrated model was found to accurately predict the load deflection response and crack pattern of the tested slabs (Alam & Amanat, 2012).

Alam and Amanat (2014; 2015) used the model calibrated by Alam and Amanat (2012) to investigate the punching shear behaviour of slab-column connections in continuous multi-panel specimens. The continuous model was a two bay by two bay flat slab system with a thickness of 200mm and with columns spaced at 6000mm on center in both directions. To simulate continuous action the slab was extended 1500mm beyond the column centerlines in all directions. In the 2014 study a total of thirty simulations were completed. In these simulations a constant column size of 400x400mm was used and the concrete compressive strength and reinforcing ratio ranged between 24-60MPa and 0.15-2% respectively (Alam & Amanat, 2014). In the 2015 study a total of seventy-five simulations were presented considering three column sizes, 400x400mm, 600x600mm and 800x800mm. In these seventy-five simulations the concrete strength and flexural reinforcing ratio were varied between 24-60MPa and 0.25-2% respectively for each column size (Alam & Amanat, 2015). In both studies, the punching capacity was found to increase with increasing flexural reinforcing ratio and concrete compressive strength (Alam & Amanat, 2014; Alam & Amanat, 2015). In the 2015 study the nominal shear capacity around the critical perimeter at d/2 from the column face

was found to decrease as the column size, and ratio of column size to slab depth, was increased (Alam & Amanat, 2015).

Eder, Vollum, Elghazouli and Abdel-Fattah (2010) also conducted NLFEA of reinforced concrete flat slabs in DIANA using a total strain crack approach. As with the studies by Alam and Amanat (2012; 2014; 2015), the model was based on MCFT (Vecchio and Collins, 1986) and the three-dimensional extension by Selby and Vecchio (1993). The numerical model was calibrated based on the test of an isolated slab-column connections without shear reinforcement published by the authors (2009). The slab and loading plates were modelled with twenty node isoparametric brick elements and the reinforcement was modelled with three node three-dimensional truss elements, which were assumed to be perfectly bonded to the concrete. To improve the numerical efficiency, a fine mesh was used near the slab-column connection and a coarse mesh was used towards the slab edges. The calibrated model was also used to analyze four slabs, three of which were reinforced with steel shearheads. To accurately predict the structural behaviour of the slab-column connections, it was found that a fine mesh should be used for the portion of the slab extending a distance of twice the slab depth from the end of the shearheads (Eder, Vollum, Elghazouli, & Abdel-Fattah, 2010).

In addition to their experimental study of punching shear of connections with high strength concretes, which was discussed in Section 2.3.2, Moreno and Sarmento (2013) also conducted a three-dimensional NLFEA of isolated slab-column connections in DIANA. The investigated slabs were modelled with 1600 twenty node isoparametric solid elements. The flexural and shear reinforcement was modelled using distributed finite elements, which were embedded in the concrete elements, and bar elements respectively. The finite element model used a smeared crack model based on a strain decomposition concept and a total strain concept. Fixed orthogonal cracks were assumed in the total strain concept, and as such, the decrease in elastic strains that occurs with decreased orthogonal strains was not accounted for. This strain reduction was approximated by setting the Poisson ratio to 0. Good agreement between the experimental results and finite element predictions was observed. However, the finite element results were found to be strongly dependent on the value assumed for the shear retention factor (Moreno & Sarmento, 2013).

Mahmoud (2015) developed a three-dimensional nonlinear finite element model in ANSYS 10 to investigate the impact of shear reinforcement on punching shear behaviour. Sixteen slabs, which were tested by Lips et al (2012), and discussed in Section 2.3.2, were modelled. Eight node elements with three translational degrees of freedom at each node were used to model the concrete. A two node

element with three translational degrees of freedom and a beam element were used to model the steel reinforcing, which consisted of rebar and continuous stirrup cages, and steel shear studs respectively. The model was found capable of predicting the punching capacity within approximately 20% of the experimental values, but greatly underpredicted the observed rotations. The maximum error in the predicted rotations was 65% (Mahmoud, 2015).

Winkler and Stangenberg (2008) presented a preliminary finite element model of slabs failing in punching shear in the commercial finite element software ABAQUS. They stated that the "Concrete Damaged Plasticity" (CDP) model available in ABAQUS must be used when simulating the complex three-dimensional stress state corresponding to punching shear failures of a slab-column connection. The uniaxial tensile stress-strain curve for the concrete was assumed to be linear elastic until the maximum tensile capacity was reached. The post peak response was based on a tensile stress crack opening relationship proposed by Hordijk (1992), which was based on the fictitious crack model by Hillerborg (1983). Eight node or twenty node solid elements were used to model the concrete and eight node three-dimensional truss elements were used to model the reinforcement. The preliminary model was used to simulate previously tested square slabs supported on square columns. The model was found to accurately predict the ultimate load capacity and crack pattern, but the predicted stiffness and overall load deflection response were different than that observed experimentally (Winkler & Stangenberg, 2008).

Bompa and Onet (2016) conducted a three-dimensional NLFEA of isolated slab-column connections in ABAQUS 6.10 to investigate the effect of slab thickness on the angle of the compressive stress field. The triaxial behaviour of concrete was modelled using the CDP model available in ABAQUS. Eight node brick elements were used to model the slab and loading plates and three-dimensional wire elements were used for the flexural reinforcement. The best correlation with the test results was observed for a mesh size of 19mm and a dilation angle of 40 degrees. The other parameters used in the CDP, which control the shape of the deviatoric plane and the eccentricity of the yield surface, were set to the default values of 2/3 and 0.1. The angle of the compressive stress field was found to increase proportionally as the slab thickness was increased from 150mm to 500mm (Bompa & Onet, 2016).

Wosatko, Pamin and Polak (2015) presented two preliminary finite element models of an isolated slab-column connection without shear reinforcement tested by Adetifa and Polak (2005). The first model, implemented in FEAP, was based on a gradient-enhanced damaged plasticity model. The

second model, implemented in ABAQUS was based on the CDP model, which is a rate dependent damaged plasticity model. Both models were nonlinear and used three-dimensional elements to discretize the slab geometry. Perfect bond between the rebar and concrete was assumed. Both models were found to be very sensitive to the assumed concrete tensile behaviour. Premature failures were also predicted due to localized deformation caused by extensive flexural and shear cracking. To avoid these zones of localized deformation regularization was used, which effects the predicted crack pattern (Wosatko, Pamin, & Polak, 2015).

Genikomsou and Polak (2015) proposed an alternate version of the finite element model in ABAQUS proposed by Wosatko, Pamin and Polak (2015). The alternate model was still based on the CDP model, and was calibrated based on the same specimen analyzed by Wosatko, Pamin and Polak (2015). The model was later extended to account for slabs reinforced with shear bolts by Genikomsou and Polak (2016). The calibrated model was also used to investigate numerous other parameters such as the impact of compressive membrane action (Genikomsou & Polak, 2017a), openings around the slab-column connection (Genikomsou & Polak, 2017b), and shear bolt layout and quantity (Genikomsou & Polak, 2017c). Genikomsou and Polak's model (2015), described in more detail in Section 4.2, forms the basis of the model used in this thesis.

Navarro, Ivorra and Varona (2016) also used ABAQUS to simulate the punching shear behaviour of the slab-column connection without shear reinforcement tested by Adetifa and Polak (2005). The ABAQUS model was calibrated following a procedure similar to that presented by Genikomsou and Polak (2015). The flexural reinforcing was modelled using four node reduced integration shell elements instead of the two node truss elements used by Genikomsou and Polak (2015). Good agreement with the experimental results was found and the calibrated model was used to investigate the impact of concrete compressive strength, flexural reinforcement yield strength, reinforcing ratio, ratio of column width to slab width and ratio of column width to slab thickness (c/d). The finite element model predicted a decrease in the nominal shear capacity along the critical perimeter at d/2 as the c/d ratio increased (Navarro, Ivorra, & Varona, 2016).

Shu, Fall, Plos, Zandi and Lundgren (2015) developed a nonlinear finite element model based on three-dimensional continuum elements in DIANA to analyze the structural behaviour of reinforced concrete slabs in bending. The model used a total strain rotating crack model and was based on the MCFT (Vecchio and Collins, 1986) and the three-dimensional extension by Selby and Vecchio (1993). An isotropic damage constitutive law was used to describe the concrete compressive

behaviour and the flexural rebar was assumed to be fully bonded to the concrete. Large displacement theory was used since the expected displacements exceeded the slab thickness. A convergence study showed that at least eight elements were required through the slab depth to avoid shear locking effects. The predicted load capacity and deflection were found to not be affected by modelling the rebar as a grid or with discrete bar elements (Shu, Fall, Plos, Zandi, & Lundgren, 2015).

As previously discussed, Plos, Shu, Zandi and Lundgren (2017) developed a multi-level structural assessment strategy for reinforced concrete bridge deck slabs. Level II and III of this assessment strategy were based on linear elastic and nonlinear FEA conducted using three-dimensional shell elements. Level IV and V, which represent the highest assessment levels, are based on three-dimensional NLFEA using continuum elements. In level IV, the flexural rebar is assumed to be fully bonded to the concrete, whereas in level V, bond slip models between the rebar and concrete are used. Models implemented according to level IV and V have the advantage of capturing shear type failures without the need for additional analysis, as was required for levels II and III (Plos, Shu, Zandi, & Lundgren, 2017).

Shu, Plos, Zandi, Johanssson and Nulenius (2016) modelled eleven isolated slab-column connections with square columns and without shear reinforcement, which were tested by Guandalini and Muttoni (2009), to analyze the impact of slab dimensions, concrete compressive strength and flexural reinforcement ratio on punching capacity. The slabs were modelled in DIANA and discretized using three-dimensional four node tetrahedron elements. Models using first order brick elements were found to result in similar predictions to models using first order tetrahedron elements. The use of second order brick elements resulted in a softer predicted behaviour and lower load capacity. The reinforcement was assumed to be fully bonded to the concrete, which is in line with the level IV analysis later proposed by Plos, Shu, Zandi and Lundgren (2017). The steel plates used to load the slab in the experiments were included in the finite element model and interface elements, based on a Mohr-Coulomb friction model, were used to model the interaction between the plate base and top of the slab. The model was found to accurately predict the experimentally observed structural response. (Shu, Plos, Zandi, Johansson, & Nilenius, 2016).

2.6.3 Rectangular Columns

The purpose of this section is to briefly summarize the previous finite element work for slabs supported on rectangular columns. Most of the previous studies have been focused on isolated slab-

column connections and use three-dimensional elements. The remaining studies have been conducted on multi-bay continuous slabs.

2.6.3.1 Isolated Slab-Column Connections

In addition to their experimental study of column rectangularity, Oliveira, Regan and Melo (2004) also conducted a linear elastic finite element analysis of slabs supported on rectangular columns under different loading conditions using four node shell elements in SAP2000. Their analysis was focused on analyzing the shear force distribution around the column and critical perimeters. Shear force concentrations along the column perimeter near the column corners for columns with aspect ratios exceeding one were predicted. Shear force concentrations were not visible along the control perimeter used in Model Code 1990, which is located at a distance of 2d from the column face. Based on the experimental and finite element results, modification factors to be used in conjunction with the Model Code 1990 punching provision to account for column rectangularity and one-way or two-way shear behaviour were proposed. The modification factors were functions of the ratio of the maximum column dimension, c_{max}, to the effective slab depth, d (Oliveira, Regan, & Melo, 2004).

Sagaseta, Tassinari, Fernández Ruiz and Muttoni (2014) also conducted a linear elastic finite element analysis of slabs supported on rectangular columns in addition to their experimental work. Like Oliveira, Regan and Melo (2004), the finite element analysis used shell elements and was used to investigate the shear stress distribution along the critical perimeter located at d/2 from the column face. Sagaseta et al. (2014) used a methodology proposed by Vaz Rodrigues, Fernández Ruiz and Muttoni (2008) to estimate the effective critical perimeter length. Based on their finite element results, they proposed an alternative method to estimate the effective critical perimeter length based on the predicted contact pressures on the support plate under the slab. Good correlation between the alternative method, the Vaz Rodrigues et al. method and the simplified critical perimeter reduction using in Model Code 2010 was found (Sagaseta, Tassinari, Fernández Ruiz, & Muttoni, 2014).

Shu, Belletti, Muttoni, Scolari and Plos (2017) conducted a detailed study of the punching shear behaviour of reinforced concrete slabs using the finite element method. Their study was focussed on the impact of support geometry, slab geometry, and rebar layout on the shear stress distribution around the critical perimeter. Like Sagaseta et al. (2014), the authors applied the methodology and equation proposed by Vaz Rodrigues et al. (2008) to estimate the effective critical perimeter length. Unlike Sagaseta et al. (2014) and Vaz Rodrigues et al. (2008), they applied the methodology to both the linear elastic and non-linear portion of the predicted slab response. Four slabs, which were tested

between 2004 and 2015 were modelled in Diana (Shu, Belletti, Muttoni, Scolari, & Plos, 2017). Slab PG1 was supported on a square column and tested by Guandalini et al. (2009). Slab PT32 was tested by Sagaseta, Muttoni, Fernández Ruiz, and Tassinari (2011) and was supported on a square steel plate and had a different reinforcing ratio in each orthogonal direction. An octagonal slab tested by Einpaul et al. (2016), PE7, was the third slab modelled. Finally, slab AM04, which was supported on a steel plate with an aspect ratio of three and subjected to two-way loading, was the final slab modelled. Slab AM04 was tested by Sagaseta et al. (2014) and was also modelled in this thesis. Shu et al. (2017) found that the experimentally observed behaviour of all four slabs could be accurately predicted using three-dimensional models based on shell or continuum elements, which correspond to level III and IV analyses in the multi-level assessement strategy proposed by Plos et al. (2017) respectively. Shu et al. (2017) undertook a detailed study of the support conditions assumed in the finite element model and analyzed the shear strress distributions around the critical perimeter. The findings of their support condition study are similar to those described in Section 4.4.

Megally and Ghali (2000) investigated the punching shear behaviour of slab-column connections subjected to unbalanced moments using NLFEA in ANACAP. Their model was based on the incremental theory of plasticity and a cracking criterion based on principal stresses and strains was used. Three-dimensional solid elements were used to model the concrete. The slabs were simply supported along their edges and loads were applied through the column stub. The model was verified based on the experimental results of interior and edge-column connections. Some of the specimens used to verify the finite element model also included column capitals or drop panels. Most of the modelled slabs were found to fail in punching shear, and different crack patterns were in observed in each direction due to the unbalanced moment. The predicted shear stress distribution around the column did not match that assumed in the ACI or CSA codes, but the code assumed distributions were found to be reasonable. The finite element model was used to conduct studies to calibrate the γ_v term used in the ACI or CSA codes. This γ_v term is used in conjunction with the assumed linear shear stress distribution when unbalanced moments are present. The FEA results showed that the amount of unbalanced moment transferred to the column through shear is dependent on the aspect ratio of the column (Megally & Ghali, 2000).

Erdogan, Binici and Ozcebe (2011) conducted a three-dimensional NLFEA of their experimental specimens which were supported on rectangular columns and reinforced with CFRP dowels in DIANA. The model was based on the total strain fixed crack concept by Selby and Vecchio (1993).

Eight node isoparametric elements were used to model the concrete and the reinforcement was assumed to be perfectly bonded to the concrete. Two additional slabs, tested by Binici and Bayrak (2003), were also modelled to verify the applicability of the FEA results for different slab dimensions, reinforcing ratios and shear reinforcing methods. The proposed model was found to accurately predict the experimental load-deflection behaviour and measured stress and strain values in the concrete and shear reinforcement (Erdogan, Binici, & Ozcebe, 2011).

2.6.3.2 Multi-panel Continuous Slab Systems

In addition to the experimental test of a one-third scale three bay by three bay multi-panel system, Simmonds (1970) also conducted a linear elastic finite difference analysis of a typical interior panel supported on rectangular columns assuming the slab to be an elastic medium thick plate. It was also assumed that the columns did not deflect over their cross-section and the slope of the slab at the column face was zero. The analytical study was focusing on analyzing the impact of column elongation, the slab bay aspect ratio and the assumed Poisson ratio. The slab bay aspect ratio was varied between one and five with the longer span parallel to the direction of the longer column dimension. The minimum column dimension was fixed at a width corresponding to a c/L ratio of 0.05, where c is the column width (mm) and L is the centerline distance between the columns (mm). The maximum column dimensions studied corresponded to c/L ratios of 0.05, 0.2, 0.4, 0.6 and 0.8. Solutions for a c/L ratio of 1.0 were derived from beam theory, as this condition was assumed to be a one-way slab supported on continuous walls. Poisson's ratio of 0 and 0.2 were considered. The magnitude of the negative moments in both directions greatly decreased as the column elongation increased. Additionally, as the column aspect ratio was increased the maximum positive moment in the slab in the direction parallel to the elongated column dimension were found to decrease, while the maximum positive moment in the other orthogonal direction slightly increased. This behaviour can be understood as a transition from two-way to one-way behaviour and was found to occur at a c/L ratio of 0.4. (Simmonds, 1970). Simmonds also analyzed the shear stress distribution around the column perimeter, but the assumption of zero deflection over the column cross-section increased the shear stress concentrations at the column corners. Based on the finite difference results, it was found that most of the shear was carried within a distance equal to the column width from the corners for c/L ratios less than 0.3 (Simmonds, 1970).

Hartley and El Kafrawy (1984) simulated a single floor of a flat slab building using a linear elastic finite element model based on eighteen degree of freedom bending elements. The model was used to

study the impact of column elongation and column offsets on the bending moments and punching shear behaviour of reinforced concrete flat slabs. Similar to Simmonds (1970), the minimum column dimension was maintained at a constant value, in this case corresponding to a c/L ratio of 0.06, while the maximum column dimension was varied corresponding to c/L ratios between 0.06 and 0.5. As was observed by Simmonds (1970), one-way behaviour was found to become more prevalent as the maximum column dimension was increased. Hartley and El Kafrawy found that the impact of column elongation on the total positive and negative moments in the direction perpendicular to the maximum column dimension was minimal but was quite significant in the direction parallel to the longer column dimension. The punching shear portion of their study was limited to analyzing the impact of column offset for slabs supported on square columns. As the column offset was increased, the shear forces around the adjacent columns was found to increase, however this effect was found to decrease with increasing column size (Hartley & El Kafrawy, 1984).

Chapter 3: Overview of Mechanical Behaviour of Concrete

In this section, a brief discussion of the short term behaviour of concrete subjected to compressive and tensile loads is discussed. For discussion of the long-term behaviour of concrete, including shrinkage and creep, the reader is referred to Reinforced Concrete: Mechanics and Design (1st Canadian Edition) by MacGregor and Bartlett (2000).

3.1 Uniaxial Compressive Behaviour

Concrete is a mix of cement paste and aggregate, both of which are essentially linear elastic brittle materials in compression. In brittle materials, fractures typically occur perpendicular to the direction of the principal tensile strain. Since concrete's primary constituents are brittle materials, cracks are formed parallel to the direction of the applied load in a uniaxial compression test. Even though its two primary constituents are approximately linear elastic brittle materials, the uniaxial compressive stress-strain curve of concrete is nonlinear and displays some ductility. This ductility and nonlinearity is due to the development of microcracks in the concrete and the stress redistribution to uncracked regions after cracking. There are two primary types of microcracks, those which occur along the interface of the aggregate and cement paste (bond cracks), and those which occur in the mortar between aggregates (mortar cracks) (MacGregor & Bartlett, 2000). The four main stages of microcracking for concrete subjected to uniaxial compression are summarized below.

During curing of the concrete, shrinkage of the cement paste is restrained by the aggregates. This restraint creates internal tensile stresses which cause cracks, referred to as no-load bond cracks, before the concrete is loaded. No-load bond cracks have minimal impact on the uniaxial compressive behaviour of the concrete at low load levels. The initial portion of the uniaxial compressive stress-strain response is still approximately linear until the stress reaches approximately 30% of the uniaxial compressive strength, f_c' (MacGregor & Bartlett, 2000).

When the applied loading results in stress magnitudes which exceed 30-40% of f_c' bond cracks begin to develop. Bond cracks occur when the tensile and shear stresses on inclined planes along the interface of the aggregate and cement paste exceed the tensile and shear stress capacity of the interface. At this load level, the crack propagation is stable, and the crack size only increases when the load is increased. The formation of these bond cracks coincides with the stress-strain response becoming nonlinear as stresses are redistributed to the uncracked portions of the concrete (MacGregor & Bartlett, 2000).

Localized mortar cracks parallel to the applied compressive load develop between the previously formed bond cracks due to transverse tensile strains as the magnitude of the applied load reaches 50-60% of the ultimate compressive capacity of the concrete. The crack propagation during this stage of cracking is still stable and the cracks do not grow in size unless the load is increased. This stage of concrete cracking is referred to as the discontinuity limit (MacGregor & Bartlett, 2000).

When the applied load reaches 75-80% of the ultimate load capacity, which is referred to as the critical stress, the nonlinearity of the uniaxial compressive stress-strain curve increases as the number of mortar cracks increases and a continuous microcracking pattern is formed. At this point, the amount of cracking and lateral tensile strains experienced by the concrete increase rapidly. At the same time, the volumetric strains, which are a function of the compressive axial strain and the tensile lateral strain, also increase rapidly. For confined concrete, these increased volumetric strains cause outward pressures on the confining reinforcement, which resist the lateral expansion of the concrete, delaying failure. At the critical stress level, the crack propagation becomes unstable, and cracks continue to grow in size even when the magnitude of the applied load is not increased. The ultimate compressive capacity of the concrete is reached when the uncracked portions of the concrete can no longer carry additional load. Further loading beyond this point coincides with a reduced stress capacity for an increased strain. For concrete which is subjected to a compressive stress gradient instead of a uniform compressive strain, such as the concrete in the compressed zone of a beam, the onset of unstable crack propagation is delayed because as the portion of the concrete under the highest strain cracks, load is redistributed to the portions subjected to a lower strain.

Some general notes on the uniaxial compressive behaviour of concrete are as follows:

1. The initial modulus of elasticity has been found to increase as the compressive strength, f_c', is increased.
2. The ascending portion of the uniaxial compressive stress-strain curve can be approximated using a parabola. However, as f_c' increases the ascending branch becomes more linear.
3. The strain at the maximum stress, ε_c', increases as f_c' increases, but the maximum strain at failure, ε_u, decreases as f_c' increases.
4. The slope of the descending portion of the stress-strain curve increases as f_c' increases. If f_c' is less than or equal to approximately 40MPa, the slope of the descending portion is

flatter than the ascending portion. If f_c' exceeds 70MPa, the descending branch is nearly vertical (MacGregor & Bartlett, 2000), which denotes a very brittle failure.

3.2 Uniaxial Tensile Behaviour

The uniaxial tensile strength of concrete is typically only 8-15% of its compressive strength. The stress-strain behaviour of concrete subjected to uniaxial tension is slightly curved but typically approximated as linear elastic until the tensile capacity (MacGregor & Bartlett, 2000). According to MacGregor and Bartlett (2000), "After the tensile capacity is reached microcracks are formed in a fracture process zone adjacent to the point of the highest tensile stress, and the tensile capacity of the concrete drops very rapidly with increasing [crack] elongation" (p. 64). At the same time, the concrete beyond the fracture process zone unloads elasticity and the elongations are concentrated in the fracture process zone. The tensile response of concrete is typically modelled with a tensile stress-crack opening relationship as discussed in Section 4.2.2.2, and the tensile capacity is equal to zero when a crack is fully formed (MacGregor & Bartlett, 2000).

3.3 Behaviour Under Biaxial or Triaxial Loads

The behaviour of concrete under biaxial and triaxial loading in compression or tension is typically different than the uniaxial loading case. Detailed investigations focused on the mechanical behaviour of concrete under biaxial loading have been completed by many researchers including Kupfer, Hilsdorf and Rüsch (1969) (MacGregor & Bartlett, 2000). A summary of the findings of these studies based on information presented in MacGregor and Bartlett (2000) is presented below.

For concrete specimens subjected to biaxial tension, the biaxial tensile strength is similar to the uniaxial tensile strength. In this case, failure occurs perpendicular to the direction of maximum tensile stress. Concrete which is subjected to compression in one direction and tension in the other typically fails on planes perpendicular to the maximum tensile stress at a compressive or tensile strength lower the respective uniaxial strength (MacGregor & Bartlett, 2000).

As discussed in Section 3.1, the failure of concrete in uniaxial compression is caused by tensile cracks which form parallel to the direction of the applied load. Under biaxial or triaxial compression, the onset of unstable crack propagation takes longer as the compressive loads delay the formation of cracking, leading to a stronger and more ductile response compared to the uniaxial case (MacGregor & Bartlett, 2000).

Chapter 4: Finite Element Model Calibration

4.1 Introduction

The purpose of this chapter is to outline the process used to calibrate the finite element model used in the parametric study presented in Chapter 5. First, an overview of the previous finite element research focused on the punching shear behaviour of reinforced concrete flat slabs completed at the University of Waterloo is presented. The calibrated model from this previous research by Genikomsou (2015) served as the starting point for the research summarized in this thesis. Next, the results of three preliminary finite element studies created using slightly modified versions of the model calibrated by Genikomsou (2015) are presented. These preliminary studies were completed to verify ABAQUS' capability to predict the impact of column rectangularity on the punching shear behaviour of reinforced concrete slabs. The first preliminary study was a hypothetical extension of the experimental program by Adetifa and Polak (2005). Five slabs supported on rectangular columns were modelled and the predictions were compared to the results for slab SB1, which was a slab without shear reinforcement and supported on a 150mm square column (Adetifa & Polak, 2005). Next, the nine slabs tested by Hawkins, Fallsen and Hinojosa (1971) to study the impact of column rectangularity were modelled. Finally, slab AM04, tested by Sagaseta et al. (2014) was modelled. In all three studies the finite element predictions were compared to available experimental results and code predictions. The results of the capability study confirmed that ABAQUS can be used to accurately estimate the punching shear behaviour of slabs supported on square or rectangular columns. However, a recalibration of the parameters used in the finite element model is required to account for the differences between the experimental setups compared to the SB specimens.

The recalibration of the finite element model considered slab AM04 instead of the Hawkins' slabs due to the level of detail about the experimental program and results provided by Sagaseta et al. (2014). The calibration methodology was similar to that used by Genikomsou (2015). The calibration was verified by modelling six additional slabs from literature. Firstly, the other three slabs in the AM test series by Sagaseta et al. (2014), which were geometrically similar to slab AM04, but loaded along two slab edges only instead of all four, were modelled. Then, three slabs supported on square steel plates, and tested by Sagaseta et al. (2011), were modelled. These three slabs were also geometrically similar to AM04, and were loaded along all four slab edges, but had different concrete strengths and reinforcing ratios than the slabs in the AM series. One of the selected slabs also had different reinforcing ratios in the two orthogonal directions. Based on the results of these analyses, it was

concluded that the calibrated finite element model is capable of accurately predicting the punching shear behaviour of slabs supported on square or rectangular columns and with different reinforcing layouts.

4.2 Overview of Previous Work at the University of Waterloo

Genikomsou (2015) conducted an extensive finite element analysis of punching shear of reinforced concrete slabs supported on square columns in ABAQUS using the "Concrete Damaged Plasticity" (CDP) model. The CDP model available in ABAQUS was chosen for the simulations due to its ability to model concrete under arbitrary loading states, including cyclic loading, and because it has been successfully applied to numerous applications by other researchers, some examples of which were discussed in Sections 1.1 and 2.6. The CDP is a continuum, plasticity, damage-based model that considers tensile cracking and compressive crushing of the concrete (Genikomsou A. , 2015). The finite element model, and the CDP parameters, were calibrated based on published experimental results from numerous testing programs. A brief summary of the work completed by Genikomsou is provided in this section. For a detailed discussion of the mechanics of the CDP, and the finite element models discussed in this section, the reader is referred to the dissertation by Genikomsou (2015).

4.2.1 Calibration of the "Concrete Damaged Plasticity" Model

Before using the CDP to model the punching shear behaviour of reinforced concrete slabs in ABAQUS, Genikomsou verified the ability of the CDP to model concrete behaviour under different loading conditions.

The first specimens considered in the calibration of the CDP were plain concrete specimens tested under combinations of uniaxial/biaxial compression, uniaxial/biaxial tension and combinations of tension and compression by Kupfer et al. (1969). Based on the simulations of the specimens subjected to uniaxial or biaxial compression, Genikomsou concluded that the assumed dilation angle has no impact on the predicted response in the loaded direction, but has a significant impact on the predicted response in the unloaded directions. The dilation angle in the CDP is used to measure the dilatancy of the concrete. Dilatancy is a measure of the volume change caused by the inelastic strains experienced by the concrete due to its brittle nature. As the dilation angle was increased, the ductility of the predicted response was found to increase. The impact of dilation angle observed for specimens subjected to uniaxial or biaxial tension were found to be consistent with those subjected to uniaxial or biaxial compression. However, unlike the specimens loaded in compression, the predicted stiffness of

the specimens loaded in tension was found to increase as the dilation angle was increased. For the specimens subjected to combination of compressive and tensile loads, the chosen dilation angle was found to impact the predicted response in all directions. As the assumed dilation angle was increased, the ultimate stress capacity predicted by the FEM increased (Genikomsou A. , 2015).

The next specimen modelled by Genikomsou was a reinforced concrete shear panel tested by Vecchio (1999) under monotonically increasing biaxial compression and shear loads in proportions of (-0.4:-0.4:1) to analyze the accuracy of the CDP when simulating shear stresses and strains. The predicted crack pattern and shear strain versus shear stress response were found to correlate well with the experimental results verifying the capability of the CDP to accurately model the behaviour of concrete in shear (Genikomsou A. , 2015).

Next, a simply supported beam subjected to four point bending without transverse reinforcement tested by Leonhardt and Walther (1962), which failed in shear, was modelled to determine the impact of dilation angle on a reinforced concrete member. Three dilation angles, 20°, 30° and 40° were investigated with the best correlation to the experimental load-displacement response and crack pattern found for a dilation angle of 30° (Genikomsou A. , 2015).

Finally, two reinforced concrete beams, one with transverse reinforcement, and one without transverse reinforcement, tested by Aoude et al. (2012) were analyzed by Genikomsou using the CDP. The use of dilation angles of 30° and 42° were found to lead to the best correlation between the experimental results and finite element predictions for the beams without and with transverse reinforcement respectively. From this final study, Genikomsou concluded that an increased dilation angle is required when modelling confined concrete members or members with large amounts of reinforcement (Genikomsou A. , 2015).

After verifying the ability of the CDP to accurately capture the behaviour of different plain and reinforced concrete specimens under different loading conditions, Genikomsou conducted an extensive study of punching shear of reinforced concrete slabs supported on square columns. The model calibrated by Genikomsou, which is summarized in the following section, formed the basis of the finite element model used in this thesis.

4.2.2 Discussion of Calibrated Finite Element Model for Studying Punching Shear by Genikomsou

The calibrated model by Genikomsou (2015) was used to analyze the impact of numerous parameters related to punching shear behaviour including unbalanced moments (Genikomsou & Polak, 2015), compressive membrane action (Genikomsou & Polak, 2017a), openings in the slab (Genikomsou & Polak, 2017b) and shear reinforcement (Genikomsou & Polak, 2016; 2017c). However, in this thesis the discussion will focus on the model calibration and results for slab SB1 only. The reader is referred to the papers referenced above or the dissertation by Genikomsou (2015) for details of these additional analyses.

4.2.2.1 Experimental Program

Slab SB1 was one of the six isolated slab-column connections tested by Adetifa and Polak (2005) to study the impact of shear bolt reinforcing on punching shear behaviour and was used by Genikomsou to calibrate the ABAQUS model. Specimen SB1 represented an interior slab-column connection without shear reinforcement and was 1800mm square in plan and was simply supported along lines located at 1500mm. The slab was 120mm thick and had an average effective flexural depth of 90mm. SB1 was loaded through a square column stub, with 150mm long sides, which extended 150mm above and below the slab faces. The concrete used in slab SB1 had an average compressive strength of 44MPa and a maximum aggregate size of 10mm. The flexural reinforcement, which consisted of 10M bars spaced at 100mm and 200mm on the tension and compression sides respectively, had a yield strength of 455MPa (Genikomsou A. , 2015; Adetifa & Polak, 2005).

4.2.2.2 Material Modelling

As discussed in Chapter 3, the uniaxial compressive stress-strain relationship for concrete is nonlinear. In Genikomsou's model the uniaxial behaviour of concrete in compression was modelled using the Hognestad parabola shown in Figure 4-1. The linear elastic portion of the compressive stress-strain response was assumed to have an initial modulus of elasticity, E_o, equal to $5500\sqrt{f_c'}$ (MPa) and was assumed to end at a stress equal to 40% of the concrete compressive strength, f_c'. The second region of the stress-strain curve represents the ascending portion up to the peak strain, ε_o, which is equal to $2f_c'/E_{sec}$, where E_{sec} is equal to $5000\sqrt{f_c'}$ (MPa). The third region represents the post peak response and extends until the ultimate compressive strain, ε_u. As shown in Figure 4-1 the equation for regions 2 and 3 is the same (Genikomsou A. , 2015).

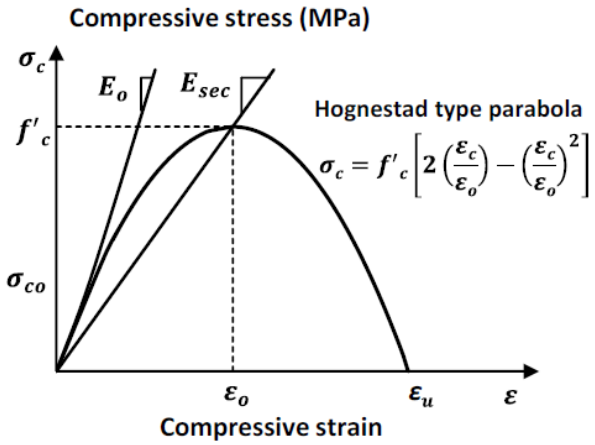

Figure 4-1: Hognestad Parabola (reproduced with permission, (Genikomsou A. , 2015))

Genikomsou (2015) assumed that concrete in tension is linear elastic until the tensile strength, f_t', was reached. As discussed in Chapter 3, the actual uniaxial tensile stress-strain relationship is slightly curved (MacGregor & Bartlett, 2000), but the error introduced by using a linear elastic relationship is minimal in many applications. Due to the inclusion of flexural reinforcement in the model and specimen, the concrete's tensile capacity does not go immediately to zero after cracking, and the post peak response is modelled using a softening process which ends at an ultimate tensile strain where zero residual tensile capacity exists. Due to the brittle nature of concrete in tension, and to limit the mesh sensitivity of the finite element model, the uniaxial tensile behaviour of concrete was characterized through a tensile stress-crack width response instead of a tensile stress-strain response (Dassault Systemes Simulia Corp., 2012; Genikomsou A. , 2015). Genikomsou found that the bilinear tensile stress-crack width relationship proposed by Petersson (1981), shown in Figure 4-2, led to sufficiently accurate results and was more computationally efficient than the exponential tensile stress-crack width relationship proposed by Cornelissen et al (1986).

The bilinear response proposed by Petersson (1981) is dependent on the concrete tensile strength, f_t', which was approximated as $0.33\sqrt{f_c'}$, and the concrete fracture energy, G_f (N/mm), which was calculated according to Model Code 1990 using equation 4.1

$$G_f = G_{f0}(f_{cm}/f_{cmo})^{0.7} \quad (4.1)$$

where G_{f0} is the base fracture energy which is dependent on the maximum aggregate size (N/mm), f_{cm} is the mean value of the concrete compressive strength calculated using equation 4.2 (MPa) and f_{cmo} equals 10MPa according to Model Code 1990 (Comité Euro-International du Béton, 1993).

$$f_{cm} = f_{ck} + 8MPa \tag{4.2}$$

where f_{ck} is the characteristic compressive strength (MPa). According to Model Code 1990, G_{f0} is equal to 0.026N/mm for a maximum aggregate size of 10mm (Comité Euro-International du Béton, 1993).

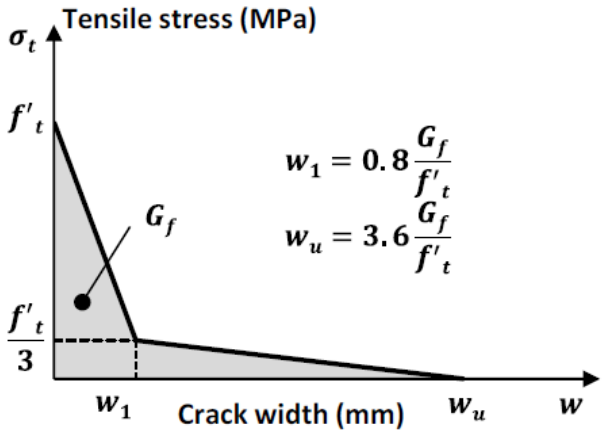

Figure 4-2: Bilinear Tensile Stress-Crack Width Relationship Proposed by Petersson (1981), (reproduced with permission, Genikomsou (2015))

The tensile stress-crack width relationship is then converted to a tensile stress-strain relationship by dividing the cracking displacement by the characteristic element length, which is equal to the cubic root of the element volume for 3D first order solid elements. This conversion results in the uniaxial tensile stress-strain relationship is shown in Figure 4-3.

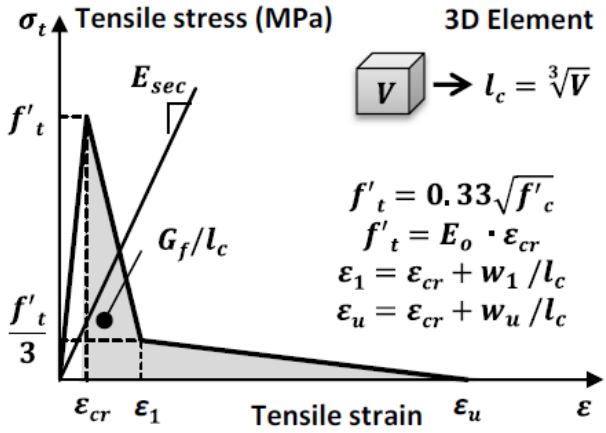

Figure 4-3: Uniaxial Tensile Stress-Strain Curve (reproduced with permission Genikomsou (2015))

An isotropic elasticity definition was used to define the linear elastic portion of the concrete response in tension and compression. This material definition requires two parameters, the elastic modulus and Poisson's ratio. The elastic modulus was inputted as $5500\sqrt{f_c'}$ to match the assumed Hognestad parabola. Since the CDP only allows the user to define one value for Poisson's ratio, even for cracked concrete, a value of 0 was used (Genikomsou & Polak, 2015). For the reinforcing steel a simplified linear elastic perfectly plastic stress-strain response in tension and compression was used. The elastic modulus and Poisson ratio of the flexural reinforcement were inputted as 200000MPa and 0.3 respectively (Genikomsou A. , 2015).

4.2.2.3 Summary of Calibrated Model Parameters

In the analysis of SB1, Genikomsou considered the impact of numerous parameters including the boundary conditions, analysis type, element type, element (mesh) size, use of damage parameters, concrete fracture energy, yield surface shape and dilation angle.

The mesh sensitivity study was of particular importance since the CDP is based on a smeared cracked model which makes the results mesh dependent. In a smeared crack model, cracking is modelled by reducing the concrete stiffness in the direction of the principal stresses. The concrete is assumed to remain a continuum but becomes orthotropic or transversely isotropic (Genikomsou A. , 2015; Chen W. , 1982). The advantage of a smeared crack model is that a new mesh is not required after cracks form. However, the main disadvantage is that cracking can localize into a single row of elements, leading to mesh sensitivity and potentially incorrect results. Genikomsou noted that the chosen mesh size should be larger than the maximum aggregate size. Since reduced integration elements were used in Genikomsou's calibrated model, an upper limit on the chosen mesh size was also imposed. In order to avoid numerical effects such as hourglassing, and distortion of the three-dimensional solid reduced integration elements, at least 5 elements through the specimen depth are needed. Based on a comparison of the experimental and predicted load-displacement response and crack patterns, a 20mm mesh size was found to be adequate (Genikomsou A. , 2015).

Genikomsou also conducted a detailed study investigating the ideal element type to be used when analyzing punching shear in ABAQUS. Since a quasi-static analysis in ABAQUS/Explicit was used for all simulations to maximize computational efficiency, three element types were considered, three-dimensional linear eight node hexahedral reduced integration elements (C3D8R), three-dimensional four node linear tetrahedral elements (C3D4) and three-dimensional ten node quadratic tetrahedral

modified elements (C3D10M). Both C3D8R and C3D10M elements were found to accurately capture the experimental results, but C3D8R elements were much more computationally efficient and were used for all analyses (Genikomsou A. , 2015).

A summary of calibrated model by Genikomsou (2015) is provided in Table 4-1 and the boundary conditions and displacement measurement location used by Genikomsou (2015) are shown in Figure 4-4. The boundary conditions used by Genikomsou (2015) are similar to those used in the SB1 rectangularity study discussed in Section 4.3.1.

Table 4-1: Summary of Calibrated Model by Genikomsou (2015)

Concrete	
ABAQUS Material Model	Concrete Damaged Plasticity
Compression Model	Hognestad Parabola (see Figure 4-1 for general equations)
Tension Model	Bilinear tensile stress-crack width (Petersson, 1981)
Fracture Energy (G_f)	0.082N/mm (Calculated from Model Code 199)
Dilation Angle	40°
Eccentricity (ε)	0.1 (ABAQUS Default)
Viscosity (μ)*	1.0×10^{-5} (not used in ABAQUS/Explicit)
σ_{bo}/σ_{co}	1.16 (ABAQUS Default)
Damage Parameters	Not Included
Element Type	C3D8R
Approximate Element Size	20mm
Modulus of Elasticity (E_c)	36483MPa, Calculated as ($5500\sqrt{f_c'}$)
Poisson's Ratio (ν)	0
Steel – Flexural Rebar	
Material Model	Linear elastic, perfectly plastic (see Figure 4-24)
Modulus of Elasticity	200000MPa
Poisson's Ratio (ν)	0.3
Yield Strength (f_y)	455MPa
Element Type	T3D2 (embedded into concrete elements)
Approximate Element Size	20mm

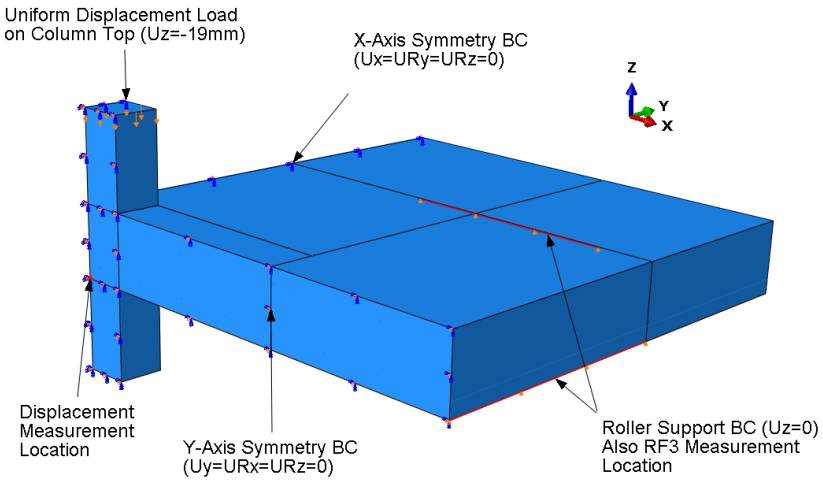

Figure 4-4: Boundary Conditions and Measurement Locations in Genikomsou Model (2015)

4.3 Capability Study

4.3.1 SB1 Rectangularity Study

4.3.1.1 Investigated Specimens

The first column rectangularity investigation was a hypothetical extension of the testing program by Adetifa and Polak (2005). The hypothetical program included slab SB1, tested by Adetifa and Polak (2005), and five hypothetical specimens supported on increasingly rectangular columns with constant critical perimeter lengths according to ACI 318M-14. The column dimensions, column aspect ratios and ratio of the minimum column dimension to the effective slab depth (c_{min}/d) are summarized in Table 4-2. Other than the column dimensions and longitudinal column reinforcement, the slabs were identical to SB1.

Table 4-2: Summary of Column Sizes Considered in SB1 Rectangularity Study

Slab	c_{min} (mm)	c_{max} (mm)	β (c_{max}/c_{min})	c_{min}/d
SB1 (Control)	150	150	1.0	1.7
C1	125	175	1.4	1.4
C2	100	200	2.0	1.1
C3	75	225	3.0	0.8
C4	50	250	5.0	0.6
C5	25	275	11.0	0.3

4.3.1.2 Finite Element Model

The ABAQUS model used to analyze the six slabs was based on the calibrated finite element model by Genikomsou (2015) with one minor change. To reduce computational time in some of the analyses, Genikomsou used a bilinear compressive stress-strain relationship for the concrete instead of the complete Hognestad Parabola, since the punching capacity of slabs is known to be primarily related to the tensile strength of concrete. In this thesis, the full Hognestad parabola introduced in Section 4.2 is used, which resulted in a slightly higher capacity and deflection at failure compared to the results from the Genikomsou model. A comparison of the predicted load-deflection response using the bilinear stress-strain relationship used by Genikomsou (2015) and the Hognestad parabola is provided in Figure 4-5. As expected, the predicted response for both models correlated well with the experimental results, though the initial stiffness predicted by the FEM is much higher than that observed experimentally. The discrepancy in predicted stiffness likely occurs because the FEM does not account for cracking due to temperature, shrinkage and specimen transportation in the laboratory.

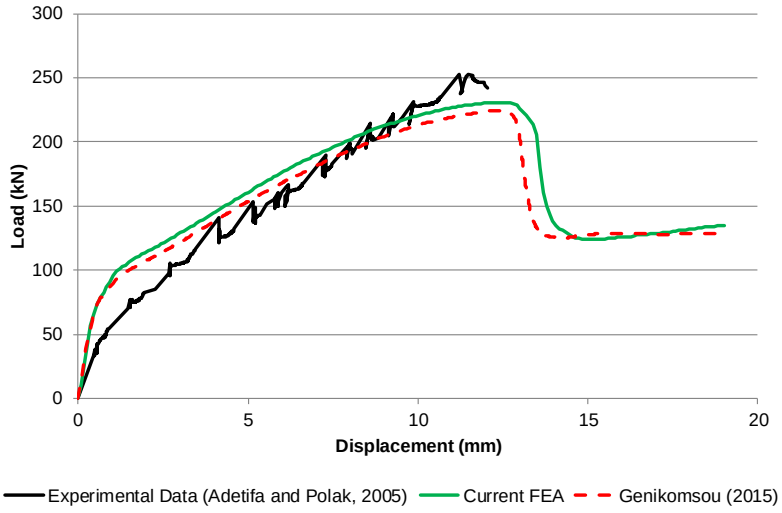

Figure 4-5: Comparison of FEA Results of SB1 With Different Concrete Stress-Strain Curves

4.3.1.3 Finite Element Analysis Results

The predicted load-displacement response for the six slabs is provided in Figure 4-6. Increasing the column rectangularity was found to have a minimal impact on the predicted punching capacity and stiffness of the slab-column connection. As will be discussed in Section 5.1.1, this was expected since the c_{min}/d ratio decreased as the column rectangularity was increased. According to Model Code 2010, the impact of column rectangularity is very small when the c_{min}/d ratio is small.

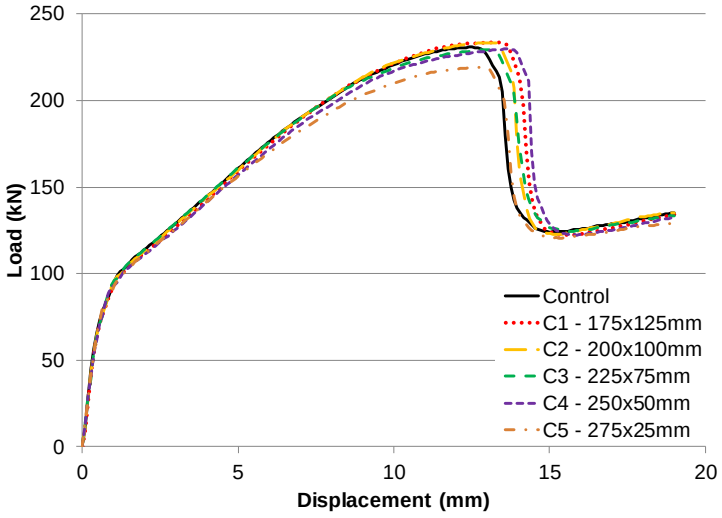

Figure 4-6: Load-Displacement Response Predicted by ABAQUS

A comparison of the predicted crack patterns for slabs SB1 (β=1), C2 (β=2), C4 (β=5) and C5 (β=11), visualized through the contours of maximum principal plastic strain, are shown in Figure 4-7. As expected, the crack pattern for slab SB1, which was loaded through a square column, is approximately uniform in both orthogonal directions. The crack patterns for the other analyzed slabs, except for slab C5, which has a column aspect ratio of 11, are also approximately uniform. For slab C5, the cracks perpendicular to the long side of the column are slightly longer than those perpendicular to the short side of the column. The lack of non-uniformity in the crack patterns supports the conclusion that column rectangularity does not have a large effect on punching shear behaviour when the c_{min}/d ratio is small.

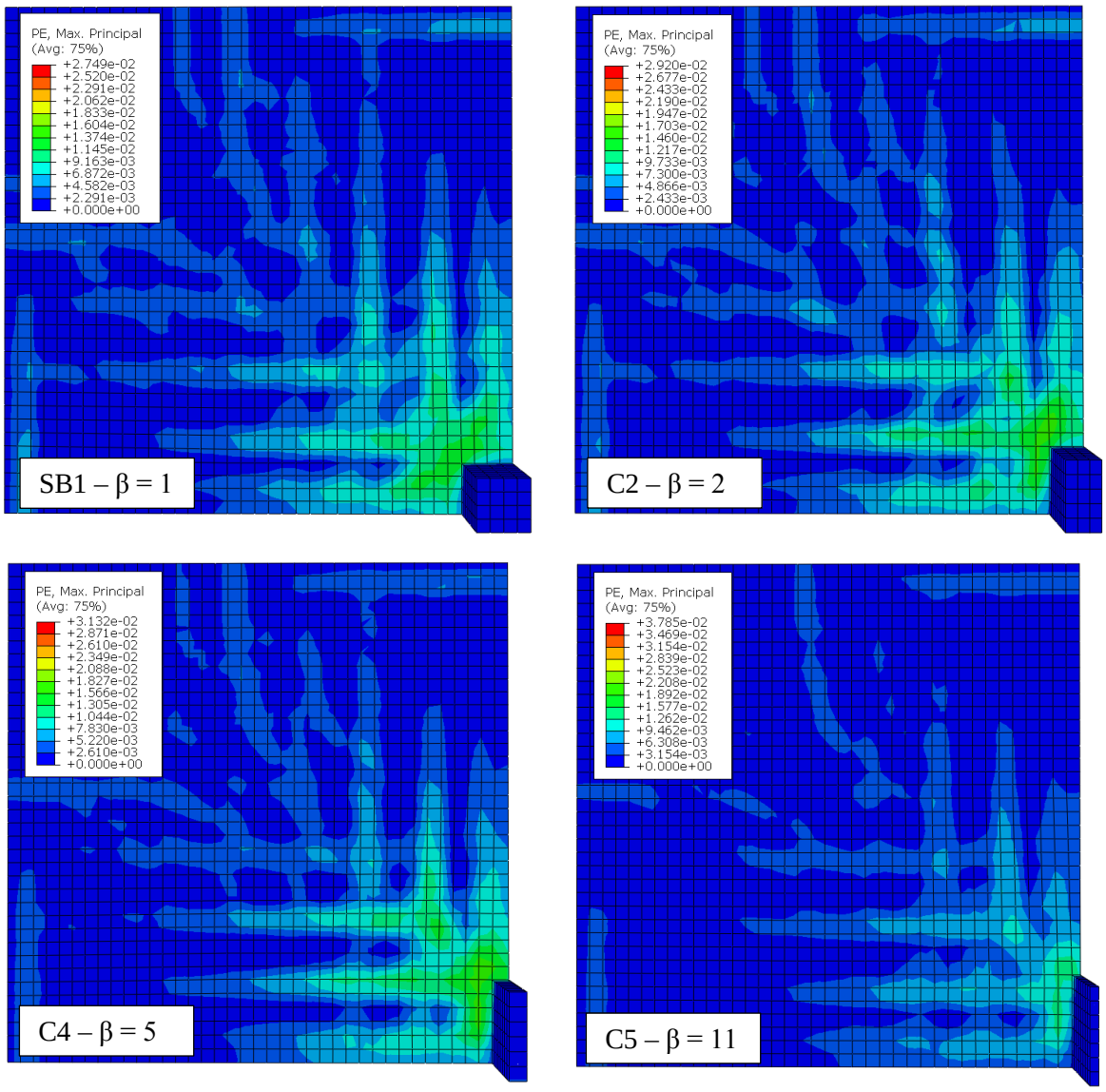

Figure 4-7: Tension Surface Crack Patterns Predicted by ABAQUS

A comparison of the punching capacity predicted by the FEA, ACI 318M-14, Eurocode 2 (2004) (EC2) and Model Code 2010 (MC 2010) LoA I is provided in Table 4-3. The simplest level of approximation was used for MC 2010 since the primary objective of this study was to confirm that ABAQUS was properly predicting the impact of column rectangularity for the modelled slabs. As such, the overall trend predicted by MC 2010 is more important than accurate punching capacity estimates. Comparing the predicted capacities, it was found that ACI 318M-14 predicts a much more significant impact of column rectangularity compared to the other two design codes and the finite

element results. Both Model Code 2010 and EC2 (2004) predict a constant capacity as the column rectangularity was increased since the critical perimeter length was constant for the investigated slab-column connections. Only for slab-column connection C5, which had a rectangularity of 11, did Model Code 2010 predict a slightly lower capacity (112kN vs 114kN). Model Code 2010 predicted a slightly lower capacity for column C5 because the maximum column dimension of 275mm is 5mm greater than 3 times the average effective slab depth (90mm), and so the effective critical perimeter length is lower than the total critical perimeter length for this connection only. It should be noted that a constant flexural reinforcing ratio of 1.2%, which is the average reinforcing ratio of SB1, was assumed in the EC2 (2004) calculations, instead of calculating the reinforcing ratio in each direction over a slab width equal to the column width plus three times the effective slab depth on each side of the column. This assumption simplified the EC2 calculations and removed the influence of slight changes in the reinforcing ratio on the final results. The use of a constant reinforcing ratio resulted in an approximately 4% increase in the predicted capacities for both the control and C4 specimens and a less than 1% increase in capacity for the remaining four specimens.

Table 4-3: Comparison of Punching Capacity Predicted by Codes and FEA

Slab	Column Aspect Ratio (β)	Predicted Punching Shear Capacity (kN)			
		FEA	ACI 318M-14	EC2 (2004)	MC 2010 (LoA I)
Control	1	230.8	189.1	207.8	114.1
C1	1.4	233.7	189.1	207.8	114.1
C2	2	233.6	189.1	207.8	114.1
C3	3	229.2	162.4	207.8	114.1
C4	5	229.7	136.4	207.8	114.1
C5	11	219.2	115.1	207.8	112.8

A comparison of the normalized nominal shear stress capacity per unit length along the ACI 318M-14 critical perimeter, v_{norm}, calculated according to equation 4.3 is provided in Figure 4-8.

$$v_{norm} = \frac{V}{b_{o,ACI} d \sqrt{f_c'}} \quad (4.3)$$

where V is the punching shear capacity predicted by the FEA or the design code (N), $b_{o,ACI}$ is the length of the critical perimeter according to ACI 318M-14 ($2 \times (c_{max} + d) + 2 \times (c_{min} + d)$, mm), d is the average effective slab depth (mm) and f_c' is the concrete compressive strength (MPa)

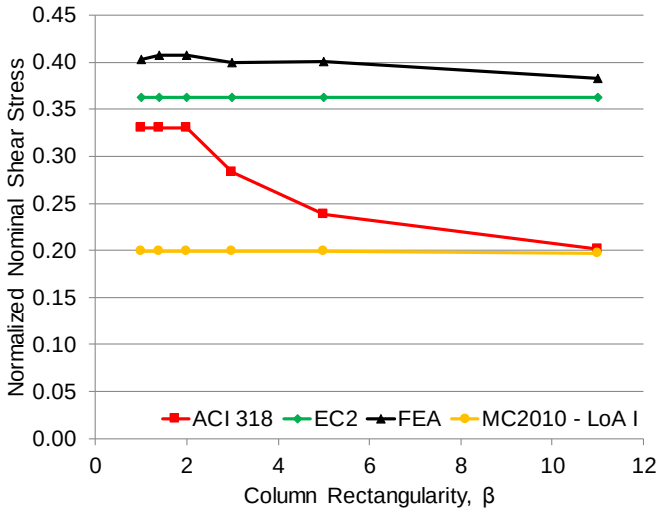

Figure 4-8: Comparison of Nominal Shear Capacity Along the ACI 318 Critical Perimeter Predicted by the FEA and Various Design Codes

Again, the ACI 318 provisions predicted a much more substantial impact of column rectangularity compared to the other design codes and the FEA. As previously discussed, MC 2010 LoA I is very conservative (Muttoni & Fernández Ruiz, 2012) so the nominal stresses predicted using this level of approximation are very low, but the minimal change in nominal stress as the column rectangularity is increased is the important factor, and not the actual magnitude. The EC2 (2004) provisions predict a nominal shear stress close to that predicted by the FEA which validates the predicted behaviour.

4.3.2 Hawkins Slabs

Since five of the six specimens in the SB1 rectangularity analysis were hypothetical it was desired to model slabs which were experimentally tested and supported on rectangular columns to further study the capability of ABAQUS to capture the impact of column rectangularity. The slabs tested by Hawkins, Fallsen and Hinojosa (1971) were selected since the experimental results and findings directly led to modifications to the ACI 318 provisions (ACI Committee 318, 2014; ASCE-ACI Committee 426, 1974; Al-Yousif & Regan, 2003; Mitchell, Cook, & Dilger, 2005).

4.3.2.1 Experimental Program

Hawkins, Fallsen and Hinojosa (1971) tested nine slabs to study the impact of column rectangularity on the shear strength and structural behaviour of reinforced concrete slabs supported on columns. The specimens were isolated slab-column connections sized to represent an interior column in a flat slab system with columns spaced at 4.5m (15') on center. The isolated slabs were 2.1m (7') square, 152mm (6") thick and supported on a 104cm (41") tall central rectangular column stub with an aspect ratio between 1 and 4.33. Slabs 1-8 had a column perimeter of 122cm (48") and slab 9 had a column perimeter of 91cm (36") (Hawkins, Fallsen, & Hinojosa, 1971). The column dimensions, flexural reinforcing details, effective depth and concrete compressive strengths are summarized in Table 4-4 and a schematic of the experimental setup is provided in Figure 4-9. It should be noted that the concrete compressive strengths listed in Table 4-4 correspond to the strength of the concrete used to cast the portion of the slab around the slab-column connection and the average strength of the four batches used to cast each slab respectively.

Table 4-4: Summary of Material Properties of Slabs Tested by Hawkins et al. (1971)

Slab	c_{min} (mm)	c_{max} (mm)	β	f_c' (MPa)	ρ_{avg}	d_{avg} (mm)	c_{min}/d
1	304.8	304.8	1.0	30.3/29.6	1.12	117.3	2.60
2	203.2	406.4	2	26.3/28.1	1.12	117.3	1.73
3	152.4	457.2	3	32.0/29.9	1.12	117.3	1.30
4	114.3	495.3	4.33	31.0/29.3	1.12	117.3	0.97
5*	152.4	457.2	3	26.9/27.4	*	117.3	1.30
6**	152.4	457.2	3	22.7/24.8	1.12	117.3	1.30
7	152.4	457.2	3	25.9/26.1	0.87	117.3	1.30
8	114.3	495.3	4.33	26.1/24.7	0.81	120.65	0.95
9	152.4	304.8	2	29.5/27.1	0.77	120.65	1.26

*4 additional #5 bars added to top reinforcing layer in central 45.7cm (18") of slab

** Column rotated 90 degrees compared to other slabs

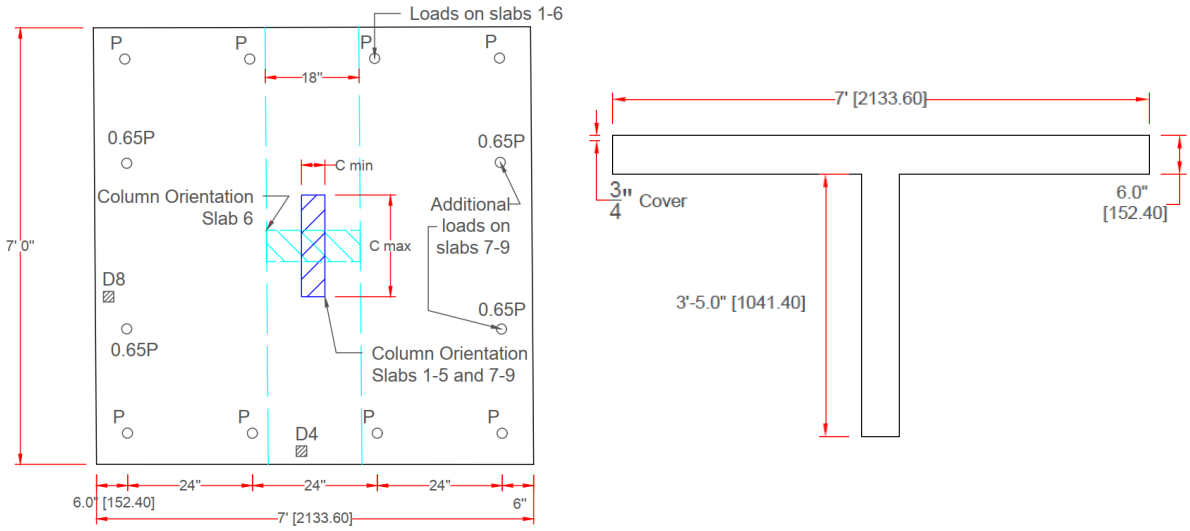

Figure 4-9: Hawkins et al. (1971) Experimental Setup

Slabs 1 through 6 were loaded in one-way action and had column aspect ratios between 1 and 4.33. For slabs 1 through 5 the load was applied on the slab edges parallel to the short side of the column. The column in slab 6 was rotated 90 degrees compared to the other eight slabs, as shown in Figure 4-9, and the load was applied parallel to the long side of the column. Slabs 7 to 9 had column aspect ratios between 2 and 4.33 and were loaded in two-way action. In addition to the loads parallel to the short side of the column, loads with a magnitude equal to 65% of the loads applied parallel to the short side were applied on the slab edges parallel to the long side of the column (Hawkins, Fallsen, & Hinojosa, 1971).

The slabs were reinforced with #4 or #5 deformed steel bars manufactured according to ASTM A432. The yield strengths of the #4 and #5 bars were approximately 412MPa (59700psi) and 414MPa (60000psi) respectively. The reinforcement was symmetric about the slab centerline with the top reinforcement parallel to the long side of the column (Hawkins, Fallsen, & Hinojosa, 1971).

All nine specimens failed due to punching shear. As the column aspect ratio was increased, the punching capacity of the slab-column connections decreased (Hawkins, Fallsen, & Hinojosa, 1971). Reduced capacity with increasing rectangularity is logical because as the column aspect ratio was increased the overall area of the column cross-section was decreased since the column perimeter length was fixed at 122cm in eight of the nine tests. Additionally, the size of the punching cone decreased, and the failure became more abrupt as the aspect ratio increased. It was also found that the

punching capacity of the slabs loaded on all four edges were only slightly lower than those of the slabs loaded on two edges only (Hawkins, Fallsen, & Hinojosa, 1971).

4.3.2.2 Finite Element Model

To take advantage of symmetry, quarter models were used to model the slabs tested by Hawkins et al. However, the boundary conditions assumed in the Hawkins' slab analysis, shown in Figure 4-10, differ from those used in the analysis of the SB1 slabs due to the different experimental setups used by Hawkins et al. (1971) and Adetifa and Polak (2005). As discussed in the previous section, the slabs were supported on 104cm tall column stubs and loaded through discrete points near the slab edges. In ABAQUS, the column support was assumed to act as a roller since exact support details were not provided by Hawkins et al. (1971). Therefore, the vertical displacement along the column base were set to 0. The use of a pinned or fixed condition at the column base was also investigated and found to have no effect on the predicted capacity or behaviour since lateral support was supplied by the symmetry boundary conditions. To ensure uniform load application, a pressure load was applied over each load application area instead of a displacement boundary condition. The magnitude of the P1 loads was set at 7.0MPa and the magnitude of the P2 loads was set at 4.55MPa, which is 65% of the P1 loads. Since the size of the loading plates was not provided, a load application area of 80x80mm was assumed. This size was chosen to ensure that the concrete would not crush under the pressure load and to limit the likelihood of localized element failures in ABAQUS. A pressure-based load in ABAQUS remains perpendicular to the surface throughout the analysis and is a force driven load type. As such, the total force in the model will continually ramp up even after the slab has failed in punching. Therefore, a static analysis cannot be used since a peak in the predicted load-deflection response would never be observed. A quasi-static analysis in ABAQUS/Explicit was used to predict the capacity of the slabs. In addition to the computational benefits of using a quasi-static analysis reported by Genikomsou (2015), the use of ABAQUS/Explicit allows for a peak in the load-deflection curve to be observed even when force driven loads are specified. When punching occurs, the model becomes unstable due to the brittle nature of the failure mode, leading to a noticeable drop in the predicted load carrying capacity.

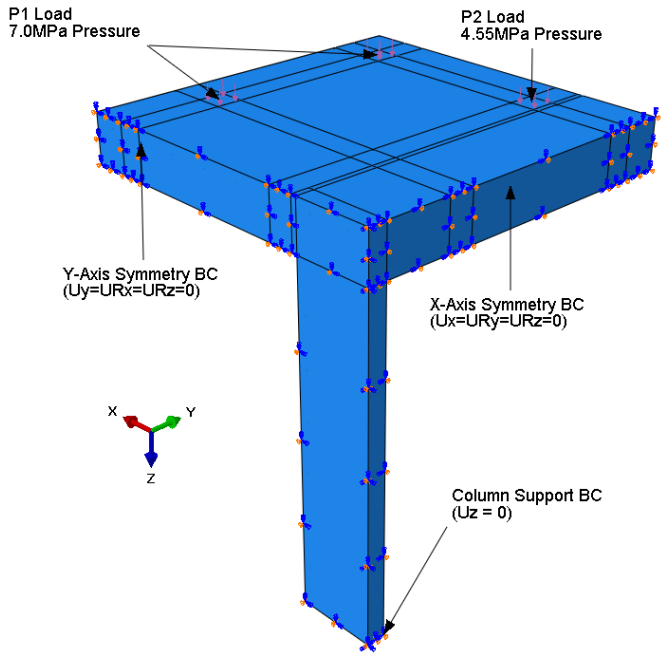

Figure 4-10: Boundary Conditions in Hawkins' Slab Analysis (Slab 8 Shown)

The calibrated SB1 model by Genikomsou was used to model the Hawkins' slabs with minor modifications. Firstly, two different concrete strengths were used in the model. Secondly, a different Hognestad parabola than that used by Genikomsou (2015) was used in the analysis of the Hawkins' slabs, and all subsequent analyses in this thesis, where the concrete compressive strength was less than 60MPa. Thirdly a different steel stress-strain curve, which was based on experimental results by Pfister and Hognestad (1964) was used.

As discussed in the previous section, Hawkins et al. (1971) listed two concrete strengths for each slab. The first of these strengths, referred to as the "shear" concrete strength in the publication, corresponded to the average compressive strength of the concrete batch used to cast the portion of the slab near the column, though the exact location of this batch was not provided. The second strength, referred to as the "flexure" concrete strength, corresponded to the average strength of the four batches used to cast each slab. In the FEM, the first concrete strength listed in Table 4-4 was used for the highlighted region shown in Figure 4-11 and the second concrete strength was used for the remainder of the slab.

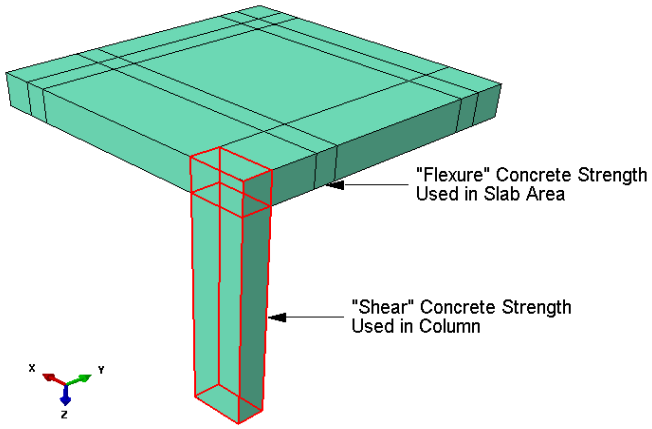

Figure 4-11: Assumed Concrete Strength Locations in FEM

The Hogestad parabola used in the Hawkins' analysis, shown in Figure 4-12, is similar to that used by Stoner (2015) and Barrage (2017) in their analysis of concrete beams reinforced with glass fiber reinforced polymer, and has a smoother transition between the linear and non-linear regions than that used by Genikomsou (2015).

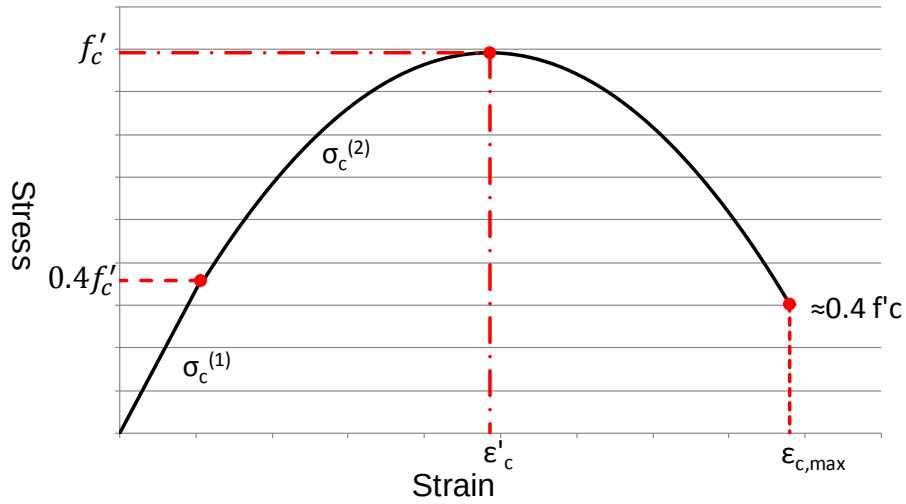

Figure 4-12: Hognestad Parabola used in Hawkins' Analysis

The linear elastic region of the compressive stress-strain curve was assumed to end at a stress equal to 40% of the concrete compressive strength, which has been used by other researchers (Winkler & Stangenberg, 2008; Genikomsou A. , 2015; Stoner, 2015; Barrage, 2017). The initial modulus of elasticity, E_{co}, in region 1 ($\sigma_c^{(1)}$), and the modified modulus of elasticity, E_{ct}, in region 2, ($\sigma_c^{(2)}$), were calculated using equations 4.4 and 4.5 respectively (Stoner, 2015).

$$E_{co} = 5000 \times \sqrt{f_c'}\ (MPa) \tag{4.4}$$

$$E_{ct} = 5500 \times \sqrt{f_c'}\ (MPa) \tag{4.5}$$

The strain at peak stress, ε_c', was calculated using equation 4.6 (Stoner, 2015).

$$\varepsilon_c' = 2f_c'/E_{ct} \tag{4.6}$$

The stress in the linear elastic region, denoted as ($\sigma_c^{(1)}$) in Figure 4-12, and in the non-linear region, denoted as ($\sigma_c^{(2)}$), were calculated using equation 4.7 and 4.8.

$$\sigma_c^{(1)} = E_{co}\varepsilon_c \qquad if\ \varepsilon_c \leq 0.4f_c'/E_{co} \tag{4.7}$$

$$\sigma_c^{(2)} = f_c'\left[2\left(\frac{\varepsilon_c}{\varepsilon_c'}\right) - \left(\frac{\varepsilon_c}{\varepsilon_c'}\right)^2\right] \qquad if\ \varepsilon_c > 0.4f_c'/E_{co} \tag{4.8}$$

where ε_c is the concrete strain (Stoner, 2015). To avoid numerical issues caused by extending the post peak behaviour to a stress of zero the nonlinear region of the stress strain curve was assumed to end at a post peak stress equal to 40% of the concrete compressive strength.

Only the yield strength and the fact that the flexural reinforcement was manufactured according to ASTM A432 was provided by Hawkins et al. (1971). Therefore, the stress-strain curve for the flexural reinforcement had to be assumed. The minimum yield and ultimate tensile strengths of rebar manufactured according to ASTM A432 are 60000psi (413.6MPa) and 90000psi (620.5MPa) respectively (ASTM International, 1965). The minimum yield strength is slightly higher than the value for the #4 bars provided by Hawkins et al. (59700psi) and matches the value provided for the #5 bars. However, no stress-strain curve is provided in ASTM A432.

Pfister and Hognestad (1964) conducted extensive experimental testing of reinforced concrete members reinforced with high strength deformed bars. In part 6 of their study, they focused on the fatigue behaviour of reinforced concrete members. Included in their study was a stress-strain curve bars manufactured according to ASTM A432, which is shown in Figure 4-13.

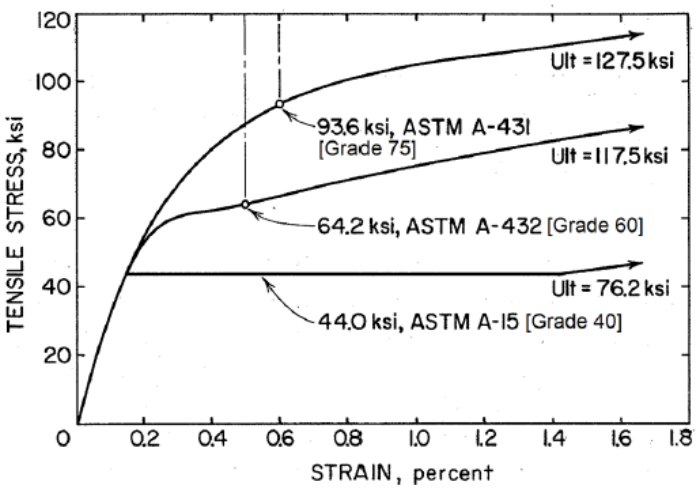

Figure 4-13: Tensile Stress-Strain Curve for Reinforcing Bars Manufactured to Various ASTM Standards (Pfister & Hognestad, 1964), Adapted from the Journal of the PCA Research and Development Laboratories, Volume 6, No. 1 (1964), Reproduced with Permission

The yield strength (64.2ksi) and ultimate strength (117.5ksi) (Pfister & Hognestad, 1964) are greater than those specified in ASTM A432 by 7% and 30.5% respectively. However, the values are similar to those published by Ali Mirza and MacGregor (1979) in their report focused on quantifying the variability in mechanical properties for multiple grades of steel reinforcing bars. Ali Mirza and MacGregor summarized the yield and ultimate strengths from numerous published and unpublished experimental studies. The collected data showed that the mean value of the ultimate tensile strength of bars manufactured to ASTM A432 regularly exceeded 105ksi (724MPa) (Ali Mirza & MacGregor, 1979). The data collected by Ali Mirza and MacGregor suggests that the ultimate strength of deformed steel bars manufactured according to ASTM A432 greatly exceeds the required minimum and may be closer to the value of 117.5ksi (810MPa) observed by Pfister and Hognestad (1964).

Therefore, the stress-strain curve published by Pfister and Hognestad was assumed in the FEM for both the #4 and #5 bars. However, the curve provided by Pfister and Hognestad (1964) does not show the relationship between 80ksi and 117.5ksi, and so a linear relationship was assumed as shown in Figure 4-14. Since strain hardening was accounted for the engineering stress-strain curve, shown in Figure 4-14, was converted to a true stress-true strain curve, which is also shown in Figure 4-14, True strain was calculated using equation 4.9

$$\varepsilon_o = \ln(1 + \varepsilon) \tag{4.9}$$

where ε_o is the true strain and ε is the engineering strain (Ugural & Fenster, 2012). True stress was calculated using equation 4.10.

$$\sigma_t = \sigma \times (1 + \varepsilon) \tag{4.10}$$

where σ_t is the true stress (MPa) and σ is the engineering stress (MPa) (Ugural & Fenster, 2012).

The inputted values for the elastic modulus and Poisson's ratio were 200000MPa and 0.3 respectively. The sharp decrease in tensile capacity after the peak stress, shown in Figure 4-14, was included to assist with identifying flexural failures in the model and to avoid ABAQUS extrapolating the linear relationship.

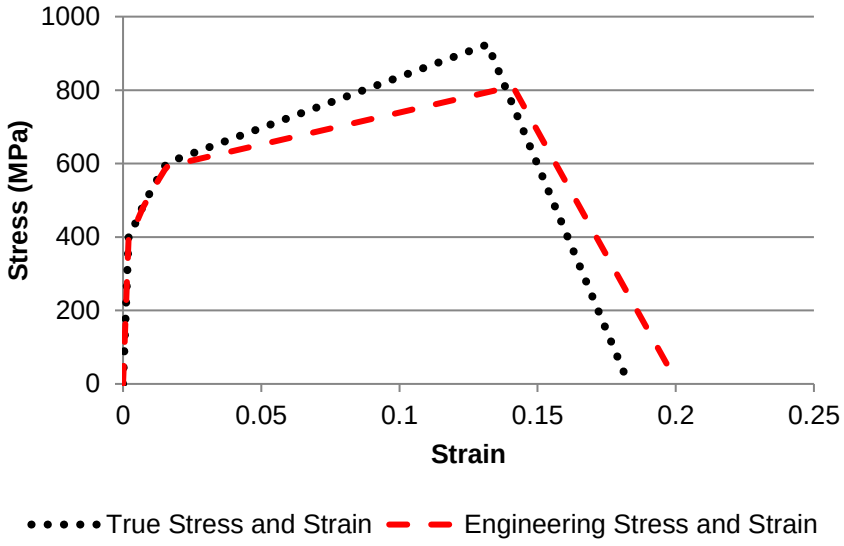

Figure 4-14: Engineering and True Stress-Strain Relationship Assumed in Hawkins' Analysis

4.3.2.3 Finite Element Analysis Results

The experimental capacity, finite element predicted capacity and deflection for the nine Hawkins' slabs are presented in Table 4-5. The FEM underpredicted the punching capacity of all nine slabs, with a maximum error of 24% for slabs 6 and 9. For slabs 1-5 and 7-9 the predicted deflection perpendicular to the short side of the column, D4, is larger than the predicted deflection perpendicular to the long side of the column, D8. For slab 6 the opposite is true, since the column was rotated 90 degrees with respect to the other 8 specimens. This was expected since the larger load is applied in the D4 direction for all nine slabs. The FEM predicted a nearly symmetric response for slabs 7-9 which were loaded in two-way action.

Table 4-5: Summary of Finite Element Results and Experimental Capacities

Slab	β	Shear Capacity		FEA Predicted Displacement (mm)	
		V_{test} (kN)	V_{FEA} (kN)	Perp. To column short side	Perp. To column long side
1	1	383.9	334.8	19.2	11.8
2	2	351.4	313.1	15.8	10.5
3	3	333.2	283.1	13.8	9.4
4	4.33	330.5	287.4	13.9	9.8
5	3	355.0	292.5	14.0	8.4
6	3	335.8	270.1	9.5	14.9
7	3	319.8	268.7	15.1	14.5
8	4.33	314.5	273.1	13.8	13.5
9	2	315.4	253.3	14.2	13.0

A comparison of the experimental and predicted load-deflection curves for slab 1 (β=1), slab 3 (β=3) and slab 7 (β=3) are provided in Figure 4-15, Figure 4-16 and Figure 4-17 respectively. It should be noted that the load-deflection curves provided by Hawkins et al. (1971) are incomplete and do not include measurements up to the peak load. As such, a horizontal line has been added to each plot at the peak load. From all three figures, it is clear that the capacity and stiffness predicted by the FEM does not match the experimental results.

For slab 1, which was loaded in one-way action, the FEM predicted a capacity of 334.8kN, which is approximately 12% lower than the experimental capacity of 383.9kN. Both the finite element predictions and the experimental measurements displayed a different stiffness in both directions. The stiffness in the D4 direction, which is the direction of maximum deflection and load application, was lower than the stiffness in the other direction in both the experiment and in the FEM. However, the FEM predicted a higher stiffness in both directions compared to the experimental results.

For slab 3, which was also loaded in one-way action, the FEM predicted a capacity of 283.1kN, which is approximately 17.7% lower than the experimental capacity of 332.1kN. The finite element results show a much lower stiffness in the direction perpendicular to the short side of the column compared to the direction perpendicular to the long side of the column. The experimental stiffness on the other hand was similar in both directions.

For slab 7, which was loaded in two-way action, the FEM predicted a capacity of 268.7kN, which is approximately 16% lower than the experimental capacity of 319.8kN. Again, the finite element model does not accurately predict the experimentally observed stiffness. In the case of slab 7, the FEM underpredicted the stiffness in both directions, which is the opposite of the results for slabs 1 and 3. The FEM also predicted a similar stiffness in both directions, which differs from the experimental results, which displayed a different stiffness in each direction.

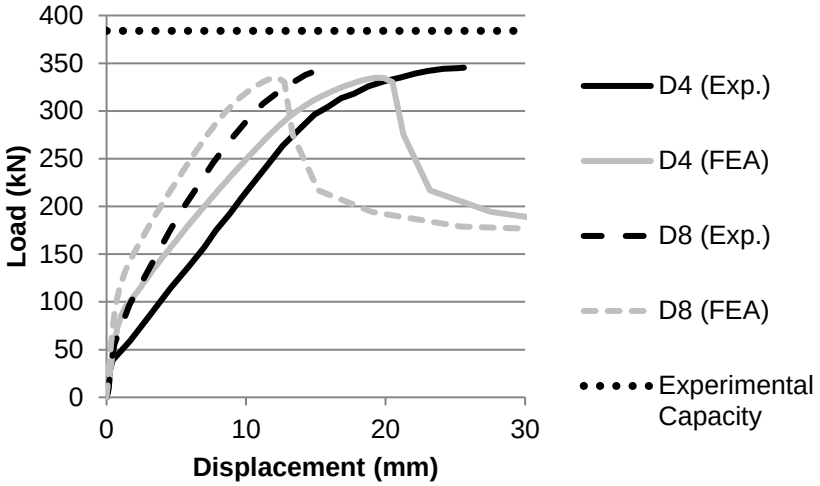

Figure 4-15: Comparison of Predicted and Measured Load Deflection Plots – Slab 1, β = 1

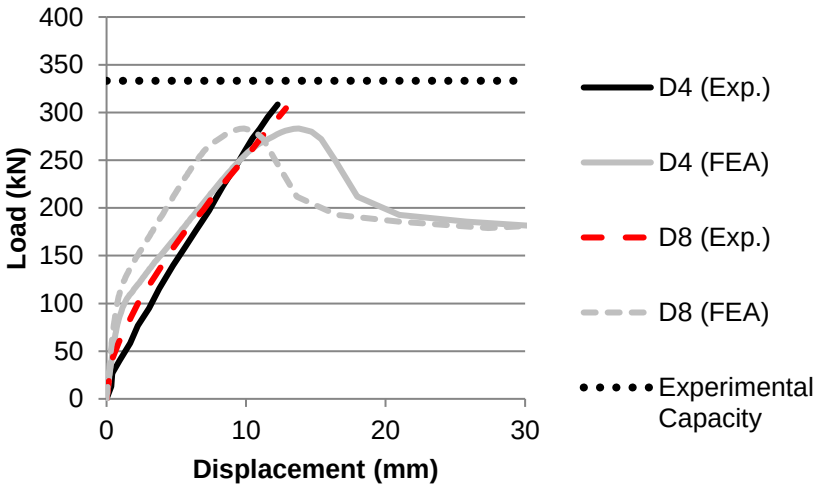

Figure 4-16: Comparison of Predicted and Measured Load Deflection Plots – Slab 3, β = 3

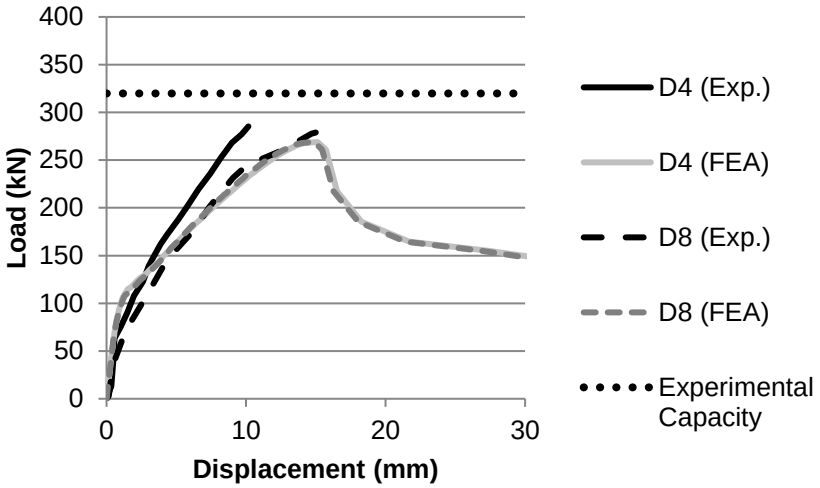

Figure 4-17: Comparison of Predicted and Measured Load Deflection Plots – Slab 7, β = 3

Based on the predicted capacities and comparison of the predicted load-deflection response to the experimental measurements, it is clear that a recalibration of the FEM model is required to account for the different experimental setups of Adetifa and Polak (2005) and Hawkins et al. (1971). However, the objective of the Hawkins's analysis was to verify that ABAQUS is capable of capturing the effect of column rectangularity on punching shear behaviour. To verify ABAQUS' capability of estimating the impact the column rectangularity accurate capacity and deflection measurements are not required, but the overall trends should match those observed experimentally by Hawkins et al. (1971) or by other researchers. Therefore, the predicted load-deflection response and crack patterns for all nine slabs and a comparison of the nominal capacity around the critical perimeter at d/2 predicted by the FEA and various design codes are analyzed.

The load-deflection response predicted by the FEM for slabs 1-6, which were loaded in one-way action, are provided in Figure 4-18. For slabs 1-5, where the load was applied on the slab edges parallel to the short side of the column, the FEM predicted a higher stiffness in the unloaded direction, which is perpendicular to the long side of the column. For slab 6, where the load was applied on the slab edges parallel to the long side of the column, the predicted stiffness in the unloaded direction, which is perpendicular to the short side of the column was higher. Therefore, for all 6 slabs loaded in one-way action the stiffness in the unloaded direction was higher than the loaded direction. These predictions match experimental results from Sagaseta et al. (2014) which are

discussed in Section 4.3.3 and 4.4. The effect of rectangularity on total punching capacity is hard to identify since the predicted capacity for slab 4 (β=4.33) is similar to slabs 3 and 5 (β=3).

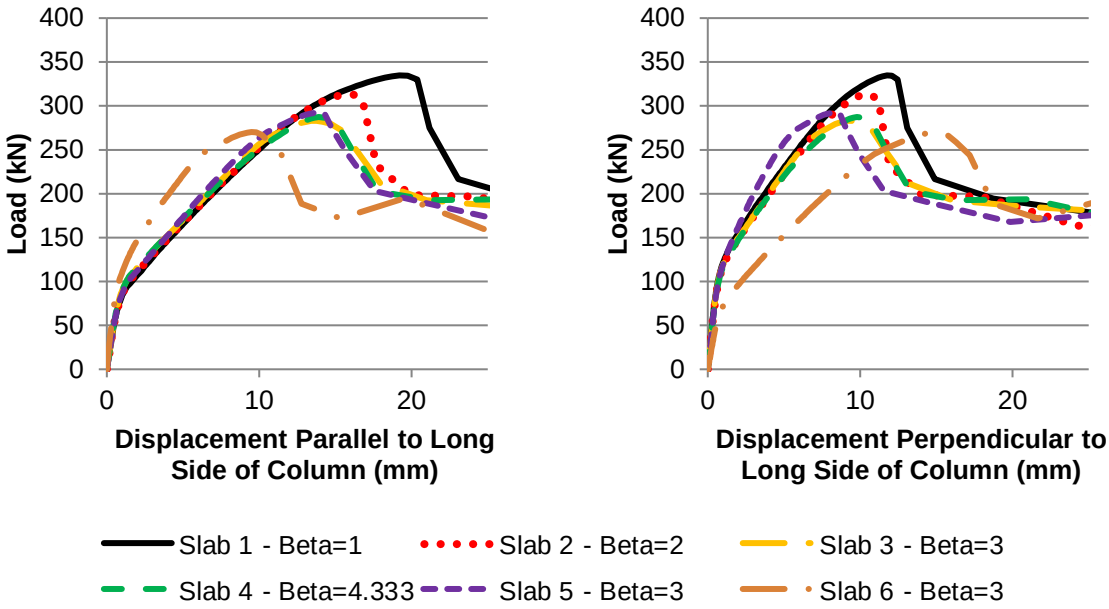

Figure 4-18: Load Deflection Plots for Slabs Loaded in One-Way Action (Slabs 1-6)

The load-deflection response predicted by the FEM for slabs 7-9, which were loaded in two-way action, are provided in Figure 4-19. As was observed for slab 7, the FEM predicted a similar stiffness and maximum deflection in both directions for slabs 8 and 9. This nearly symmetric behaviour matches observations by Sagaseta et al. (2014) for slab AM04, which was supported on a rectangular steel plate with an aspect ratio of three and loaded in two-way action. Additionally, the finite element model predicts a similar capacity for all three slabs even though the column aspect ratio was varied between 2 and 4.33.

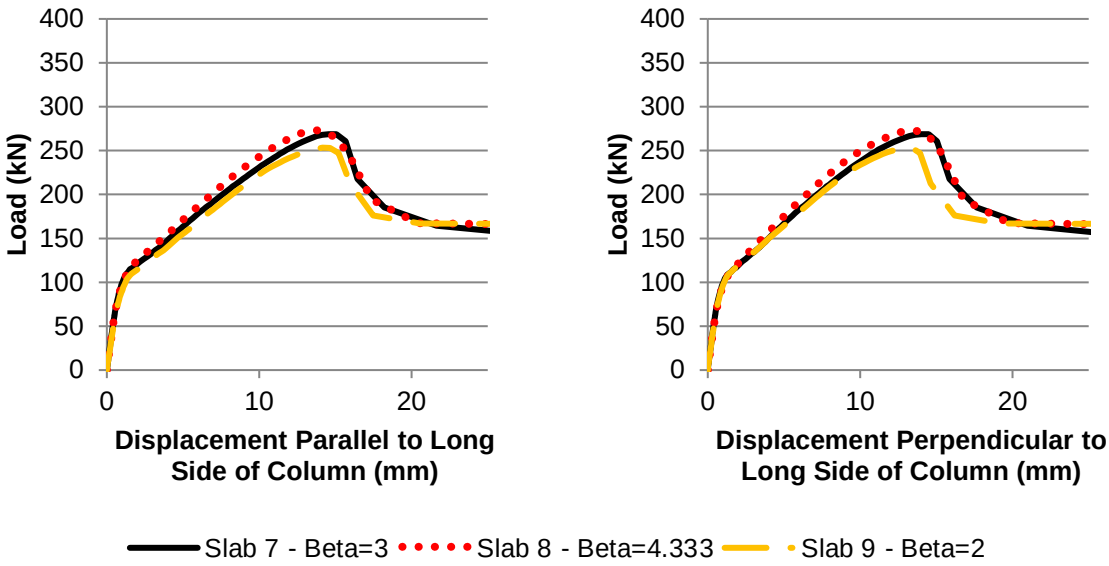

Figure 4-19: Load Deflection Plots for Slabs Loaded in Two-Way Action (Slabs 7-9)

A comparison of the predicted crack patterns for slabs 7, 8 and 9, in order of increasing column aspect ratio, is provided in Figure 4-20. Unlike the crack patterns in the SB1 study, the crack patterns on the tension surface of the slab become increasingly nonsymmetric as the column rectangularity is increased showing that the column rectangularity is having an effect on the overall behaviour of the slab. Additionally, the size of the failure cones on the slab sides decreased as the column aspect was increased which matches the experimental results (Hawkins, Fallsen, & Hinojosa, 1971). Similar behaviour was observed for the slabs loaded in one-way action.

Due to the differences in concrete strengths for the nine slabs, the impact of column rectangularity is hard to identify from Figure 4-18 and Figure 4-19 or the experimental capacities. To estimate the impact of column rectangularity, the normalized nominal shear stress along the critical perimeter, calculated according to equation 4.3 for each slab, was compared.

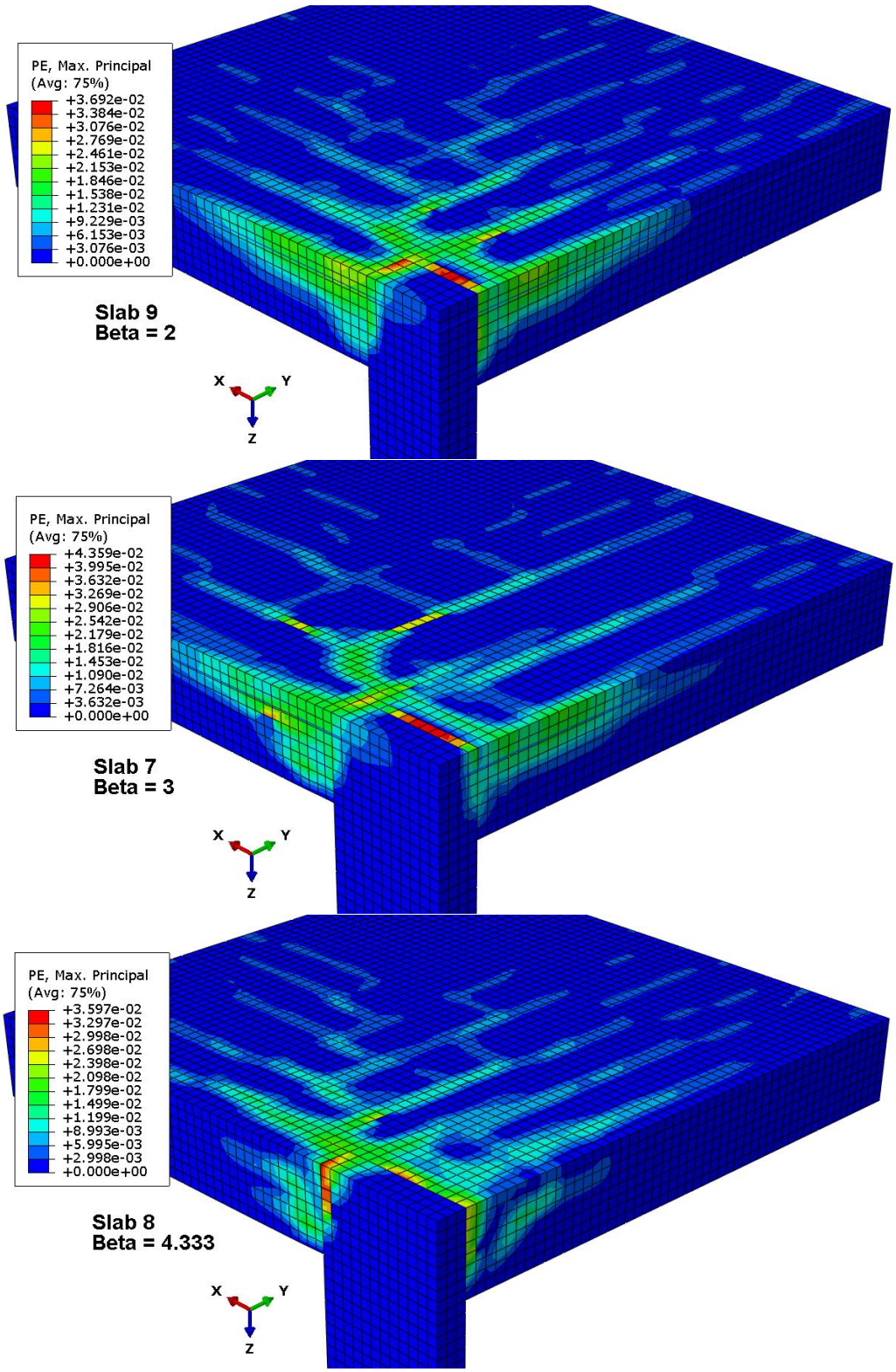

Figure 4-20: Predicted Crack Patterns for Slabs Loaded in Two-Way Action

The normalized nominal shear stress along the ACI 318 critical perimeter based on the experimental results and code predictions for slabs 1-6 and slabs 7-9 are provided in Figure 4-21 and Figure 4-22 respectively. In both figures, both the experimental results, and a trendline of the experimental data are plotted. For all code equations other than ACI 318, which includes the column aspect ratio in the calculation directly, the plotted results correspond to the trendline of the code predictions for the specific column aspect ratios considered in the experimental program.

The trendline of the nominal shear stress predicted by the FEM is much lower than the trendline based on both experimental data sets. This underprediction was expected since the FEM was underpredicting the total capacity by approximately 20%. However, the slope of the trendline for the experimental data and the finite element predictions are similar. Therefore, based on the changes in the predicted crack patterns and the trend of the nominal shear stresses along the critical perimeter predicted by the FEM, it can be concluded that ABAQUS is capable of capturing the impact of column rectangularity, although further calibration of the Hawkins' model is required.

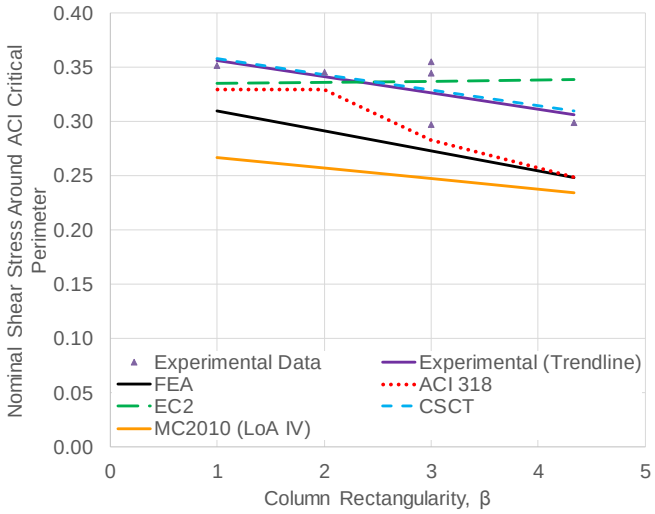

Figure 4-21: Normalized Nominal Shear Stress Around ACI Critical Perimeter, Slabs 1-6

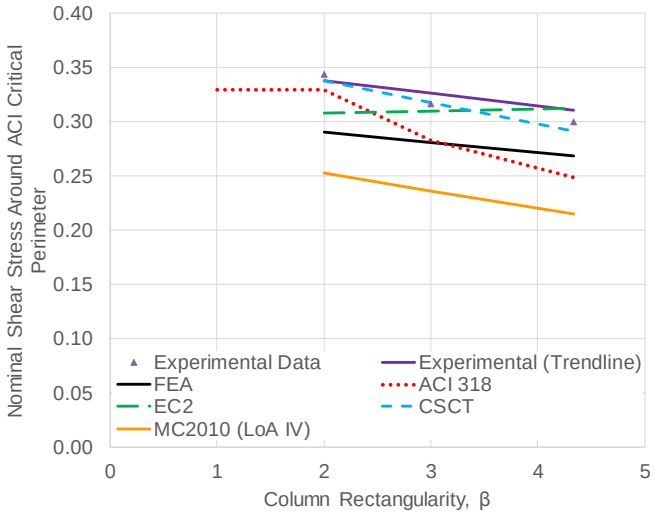

Figure 4-22: Normalized Nominal Shear Stress Around ACI Critical Perimeter, Slabs 7-9

Analyzing the trendlines for the investigated design codes, it is clear that current codes of practice account for column rectangularity differently. ACI 318M-14 is very conservative compared to the experimental results especially for the slabs loaded in two-way action. EC2 (2004) predicts a very minimal impact of column rectangularity due to the fact that all eight of the nine slabs had the same critical perimeter length. The MC 2010 predictions are the most conservative of the codes investigated. The MC 2010 provisions were conducted using LoA IV, which is the highest level of approximation, and therefore, should be the least conservative of the four levels of approximation available (Genikomsou A. , 2015). LoA IV specifies that NLFEA can be used to estimate the slab rotations. To estimate the Hawkins' slab rotations, the slab deflection profile was assumed to be approximately linear. Linear deflection profiles under concentrated loading have been observed or predicted by various researchers (Oliveira, Regan, & Melo, 2004; Teng, Cheong, Kuang, & Geng, 2004; Oliveira, Gomes, & Melo, 2014), and were found to be a reasonable assumption for the finite element predictions, as shown in Appendix A. The overall trend of the MC 2010 provisions correlates well with the experimental results for both one-way and two-way loading, but the estimates are extremely conservative. The CSCT predictions, which form the basis of the MC 2010 design procedures (Muttoni & Fernández Ruiz, 2012; Muttoni, Fernández Ruiz, Bentz, Foster, & Sigrist, 2013; Ricker & Siburg, 2016; Soares & Vollum, 2015), predict the trend of the experimental data quite well, especially for the slabs loaded in one-way action. For the slabs loaded in one-way action, the trendline for nominal stress along the critical perimeter predicted by the CSCT is almost identical to that from the experimental results, though it is slightly unconservative. For the slabs loaded in two-

way action, the CSCT predictions are conservative and predict a slightly more severe impact of column rectangularity compared to the experimental results.

A comparison of the capacity predicted by the FEM and the investigated design codes for each individual slab is provided in Table 4-6. The results for each individual slab support the conclusions of the nominal stress trendline analysis. Both the FEA predictions and the ACI 318 provisions are conservative for all nine slabs. The EC2 (2004) provisions show good correlation with the experimental results and are generally conservative, except for slabs 3 and 4, where the experimental capacity is overpredicted by 19% and 11% respectively. The MC 2010 provisions, using rotations determined in accordance with LoA IV, are the most conservative, and on average underpredict the experimental capacities by 25%. The CSCT capacity estimates, which were also based on the slab rotations estimated from the FEA, best capture the trend of the experimental data with an average ratio of the predicted strength to the experimental strength of 1. The minimum and maximum ratios of the strength predicted by CSCT and experimental strength are 0.94 and 1.16 respectively. It should be noted that the 3d method specified in Model Code 2010 was used to estimate the effective critical perimeter length, and the critical perimeter was divided into X and Y components, as discussed in Section 2.5.5, for both the MC 2010 and CSCT calculations.

Table 4-6: Comparison of Predicted Punching Capacity from FEA and Various Design Codes to Experimental Capacity

					$V_{predicted}/V_{exp}$				
Slab	c_{min}	c_{max}	β	V_{exp} (kN)	FEA	ACI	EC2	MC 2010	CSCT
1	304.8	304.8	1	383.9	0.87	0.94	0.94	0.75	1.01
2	203.2	406.4	2	351.4	0.89	0.95	0.98	0.74	0.99
3	152.4	457.2	3	315.4	0.80	0.96	1.19	0.87	1.16
4	114.3	495.3	4.33	333.2	0.85	0.95	1.11	0.75	1.00
5	152.4	457.2	3	355.0	0.82	0.82	0.98	0.73	0.96
6	152.4	457.2	3	335.8	0.80	0.80	0.97	0.72	0.96
7	152.4	457.2	3	319.8	0.84	0.89	0.98	0.69	0.94
8	114.3	495.3	4.33	330.5	0.87	0.83	0.99	0.71	0.95
9	152.4	304.8	2	314.5	0.87	0.83	0.89	0.76	1.02
				Average	0.85	0.89	1.00	0.75	1.00
				Minimum	0.80	0.80	0.89	0.69	0.94
				Maximum	0.89	0.96	1.19	0.87	1.16

4.3.3 Slab AM04

4.3.3.1 Experimental Program

As previously stated, Sagaseta et al. (2014) tested four reinforced concrete slabs supported on steel plates with an aspect ratio of three to investigate the impact of column rectangularity and loading conditions on punching shear behaviour of interior slab-column connections. These tests, which were conducted at École Polytechnique Féderale de Lausanne (EPFL), were similar to previous tests of slabs supported on square columns or steel plates conducted at EPFL. All four slabs were 3000mm square in plan, 250mm thick and supported on rectangular steel plates with a minimum and maximum dimension of 260mm and 780mm respectively. One of the four slabs, slab AM04, was loaded in two-way action, as shown in Figure 4-23. The slab was loaded through 200x200mm steel plates whose centers were located along the radius of contraflexure. 36mm diameter Dydiwag rods installed through holes drilled in the slab were used to attach the steel plates to a hydraulic jack in the laboratory floor (Sagaseta, Tassinari, Fernández Ruiz, & Muttoni, 2014).

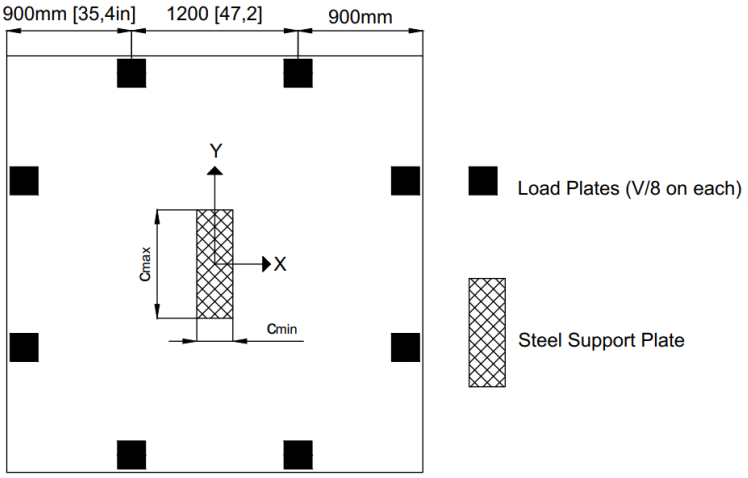

Figure 4-23: Slab AM04 Experimental Setup (Sagaseta, Tassinari, Fernández Ruiz, & Muttoni, 2014)

Slab AM04 had an average effective depth of 202mm and a concrete compressive strength of 44.6MPa. The tensile reinforcement consisted of 16mm diameter steel bars, with a yield strength of 516MPa, spaced at 125mm on center in both directions. Compression reinforcement was also provided, and consisted of 12mm diameter bars with a yield strength of 526MPa, spaced at 125mm in

both directions. The tensile and compressive reinforcing ratios were 0.75% and 0.42% respectively (Sagaseta, Tassinari, Fernández Ruiz, & Muttoni, 2014).

4.3.3.2 Finite Element Model

The initial finite element model of slab AM04 was identical to the finite element model used to analyze the slabs tested by Hawkins et al. (1971) except for the stress-strain curve of the reinforcing steel. Sagaseta et al. (2014) did not provide a complete stress-strain curve of the reinforcing steel. The only information provided was the yield strength of the steel and the fact that the steel used had a well-defined yield plateau and a strain hardening branch. As such, the stress-strain curve for the reinforcing steel had to be assumed. Due to the lack of a clear plateau in the experimental load-rotation curve for slab AM04, and because Sagaseta et al. (2014) calculated that the punching load was approximately 80% of the flexural capacity of the slab, the simplified stress-strain curve shown in Figure 4-24 was used for the reinforcing steel. A sharp drop in stress to 10MPa was also included to help identify flexural failures and ensure ABAQUS did not extrapolate the provided data. As with the other models in this thesis, an elastic modulus of 200000MPa and a Poisson's ratio of 0.3 were assumed.

Based on the experimental results provided by Sagaseta et al. (2014), it was assumed the only minor yielding of the flexural steel would occur, and therefore, the use of a simplified stress-strain relationship compared to one which included for strain hardening was not required. The assumption of minimal yielding was found to be correct as the predicted axial stresses in most of the truss elements used to model flexural reinforcement in ABAQUS were well below the yield strength until after punching occurred in the model. Some yielding did occur, but was primarily restricted to the tensile reinforcement near or crossing the column perimeter, which has been observed by other researchers studying punching shear (Park & Gamble, 1980; Rankin & Long, 1987; Alexander & Simmonds, 1987; Theodorakopoulos & Swamy, 2002).

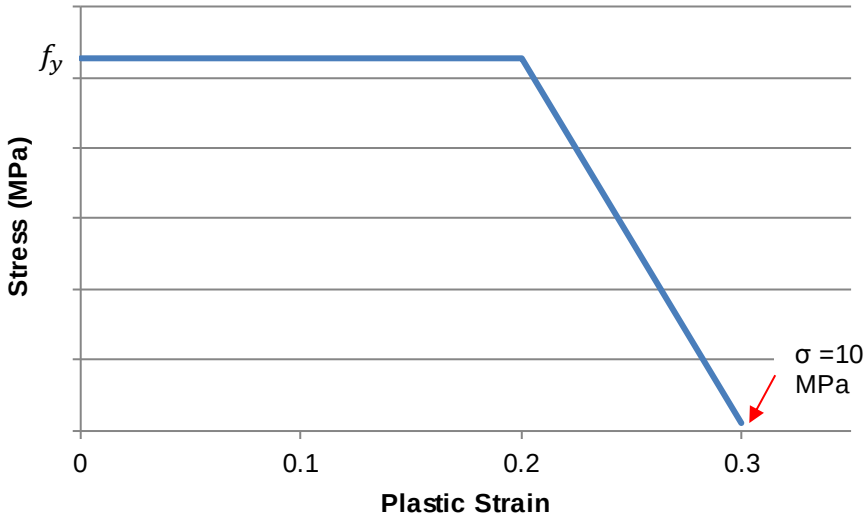

Figure 4-24: Uniaxial stress-plastic strain curve inputted into ABAQUS

For simplicity, the steel load and support plates were not included in the initial finite element model of slab AM04. Instead, the boundary conditions were applied directly to the slab geometry as shown in Figure 4-25. Similar to the Hawkins' analysis, a roller support was used to model the support provided by the steel plate and pressure loads with magnitude of 3.5MPa were applied on the slab top over 200x200mm areas.

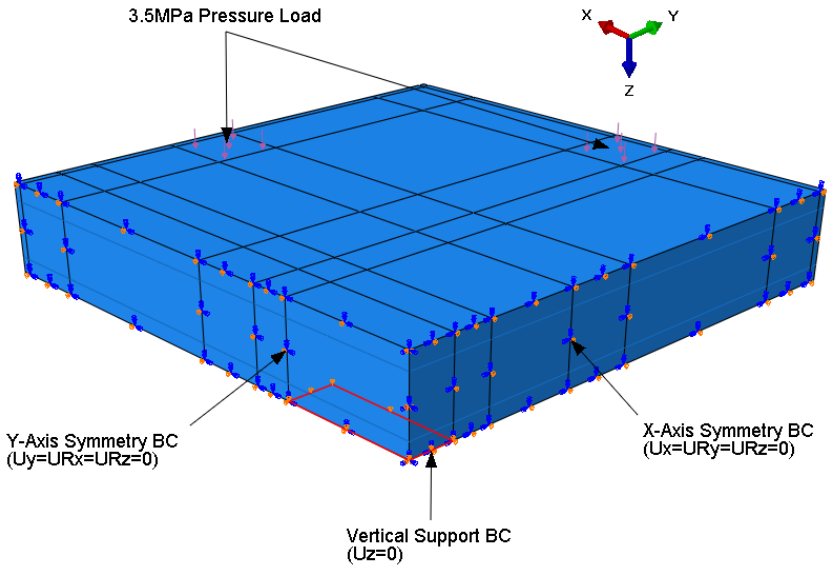

Figure 4-25: Preliminary AM04 Model – Boundary Conditions

4.3.3.3 Finite Element Analysis Results

A comparison of the load-rotation response predicted by ABAQUS and measured experimentally in the X-direction, which is perpendicular to the long side of the supported area, and in the Y-direction, which is perpendicular to the short side of the supported area, are provided in Figure 4-26a and Figure 4-26b respectively. The calibrated model by Genikomsou (2015), with the modifications outlined in Section 4.3.3.2, underpredicted the load and rotation capacity in both orthogonal directions. The initial stiffness predicted by ABAQUS was also much higher than that observed experimentally, but this was expected since the ABAQUS model does not account for any cracking due to temperature, shrinkage or specimen transportation. The model did predict a nearly symmetrical load-rotation response in both orthogonal directions which matches the experimental results (Sagaseta, Tassinari, Fernández Ruiz, & Muttoni, 2014). A comparison of the predicted load and rotation capacity compared to the experimental results is provided in Table 4-7. It should be noted that experimental rotations at failure and the experimental load-rotation curves are approximated based on the plots provided by Sagaseta et al. (2014).

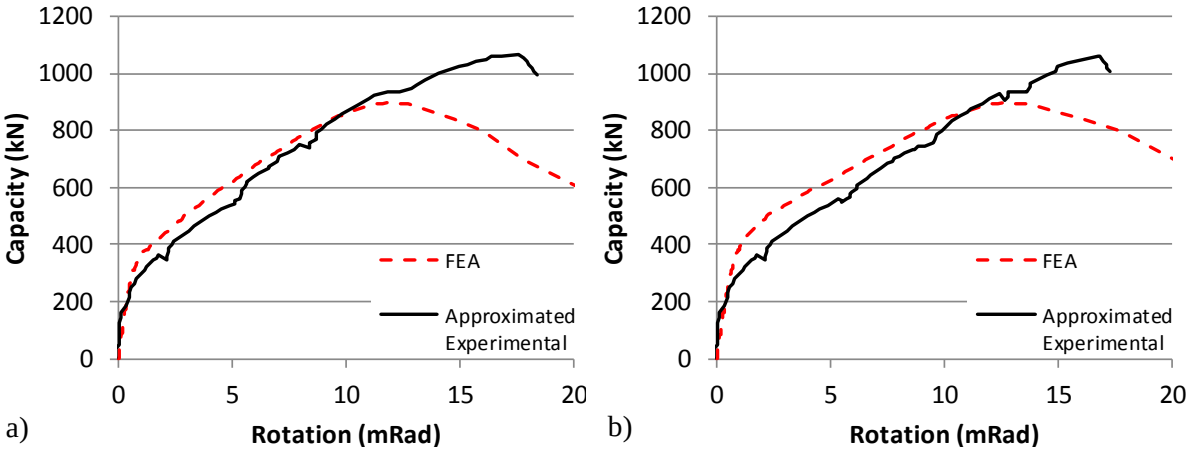

Figure 4-26: Comparison of Predicted Load-Rotation Response and Experimental Results, a) X-rotation, b) Y-rotation

Table 4-7: Comparison of Initial FEA Results and Experimental Results

Slab	Experimental			Finite Element Analysis			% Difference		
	Capacity, kN	ψ_x, mRad	ψ_y, mRad	Capacity kN	ψ_x, mRad	ψ_y, mRad	Capacity	ψ_x	ψ_y
AM04	1067	17.6	16.8	896.4	11.9	12.7	-16.0	-29.1	-24.4

The crack pattern predicted by ABAQUS, visualized through the maximum principal tensile strains in the concrete, and the experimental crack pattern are shown in Figure 4-27. The crack pattern predicted by the finite element model is similar to the experimental crack pattern except for the fact that the finite element model predicted a large concentration of cracking at the slab base above the supported area. This cracking was not observed experimentally since this region is in the compressed zone of the slab. It is predicted numerically since the boundary conditions were applied directly to the concrete nodes at the slab base. Since the displacement of these nodes is set to 0 throughout the analysis, these nodes and the connecting elements are resisting the rotation of the slab due to loading. As such, large tensile stresses are developed which were not observed experimentally since the test setup used by Sagaseta et al. allowed the slabs to lift off the steel support plates (Sagaseta, Tassinari, Fernández Ruiz, & Muttoni, 2014; Shu, 2017).

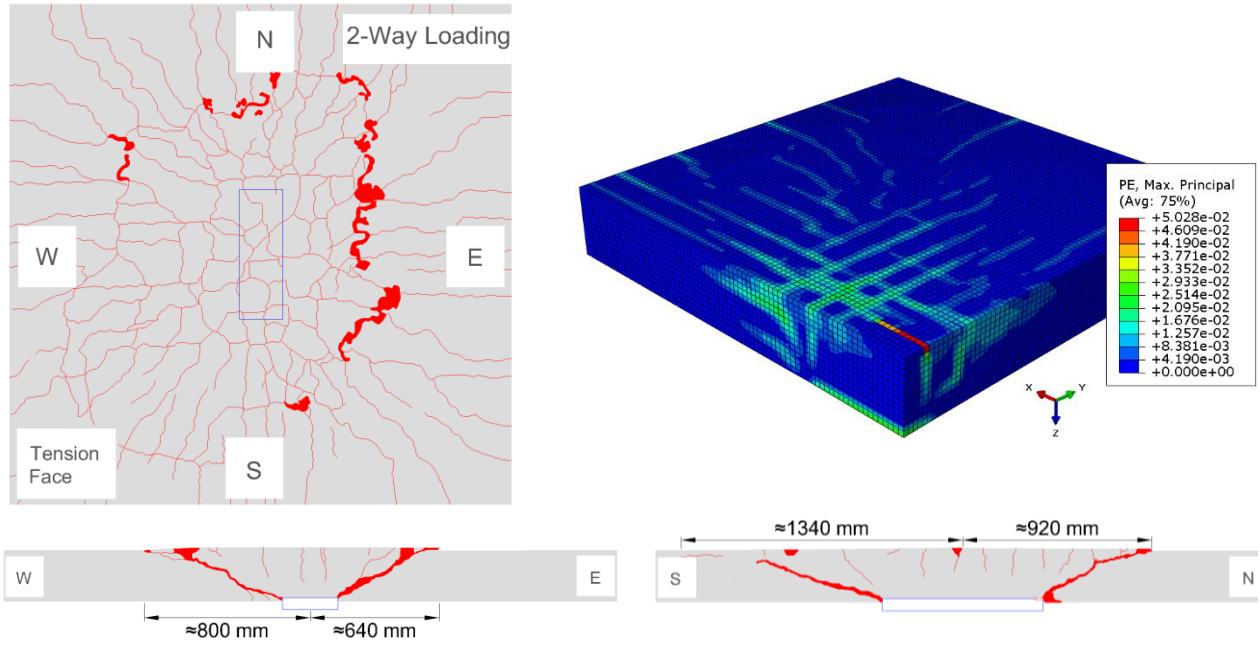

Figure 4-27: Comparison of Experimental and FEM Predicted Crack Pattern (Simple Model)

The shear stress distribution in the slab around the support plate perimeter in the AM04 quarter model is shown in Figure 4-28 and the methodology used to create these distributions from the FEA results is discussed in Appendix B. As expected, the FEM predicts a large shear stress concentration near the corner of the supported area, and the stresses along the short side of the supported area are also high relative to the shear stresses predicted along the long side of the supported area as the distance from the corner increases. The observed shear stress concentrations match experimental and

finite element results of previous research studies (Al-Yousif & Regan, 2003; Teng, Cheong, Kuang, & Geng, 2004; Oliveira, Regan, & Melo, 2004; Anggadjaja & Teng, 2008; Borges, Melo, & Gomes, 2013; Himawan & Teng, 2014; Shu, Belletti, Muttoni, Scolari, & Plos, 2017).

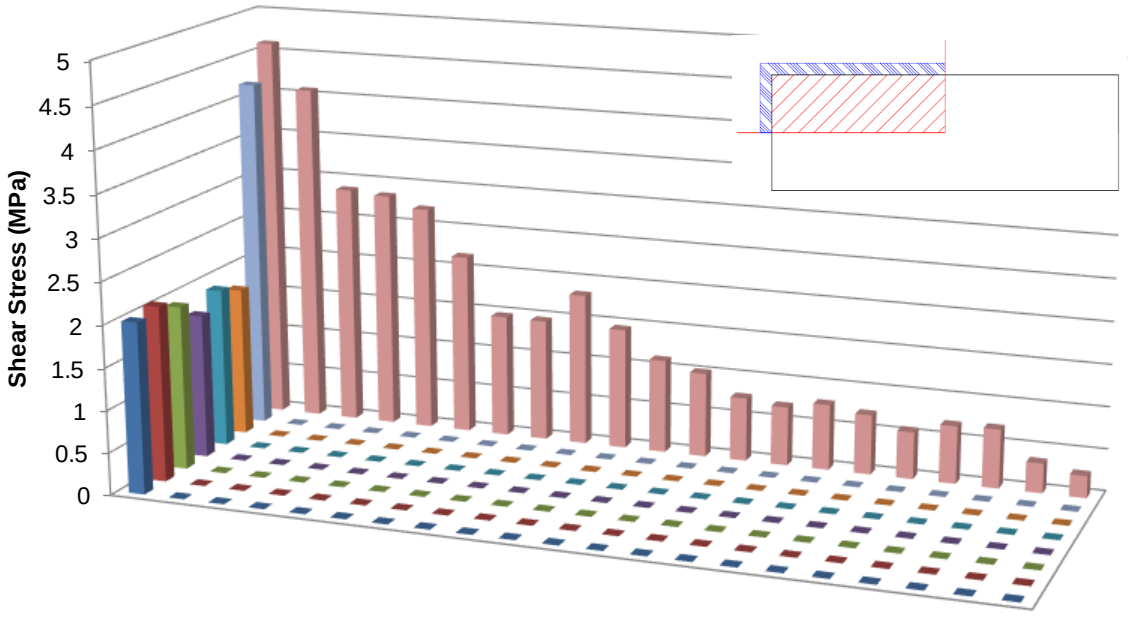

Figure 4-28: Predicted Shear Stress Distribution Around Column Perimeter– Simply Supported AM04 Model

4.4 FEM Calibration – Slab AM04

Based on the results of the capability study, it is clear that ABAQUS is capable of capturing the negative impact of column rectangularity on punching shear capacity and predicts behaviour which is in line with experimental observations and code provisions. However, a recalibration of the finite element model is needed to account for the differences in experimental setups compared to the SB1 tests by Adetifa and Polak (2005). The need to recalibrate finite element models for different experimental setups was also noted by Eder, Vollum, Elghazouli and Abdel-Fattah (2010).

The four slabs tested by Sagaseta et al. (2014) were selected for the finite element calibration since the load-rotation curves and crack patterns were provided for each load arrangement. Additionally, the experimental measurement locations and experimental methodology was more clearly stated in the Sagaseta et al. (2014) study compared to the study by Hawkins et al. (1971). Since the primary objective of this research was to investigate the punching shear behaviour of reinforced concrete slabs

supported on rectangular columns, slab AM04, which was loaded in two-way action, was selected for the calibration.

The calibration process was similar to that of Genikomsou (2015), but certain parameters including the element type and use of damage parameters were not investigated. Following the work of Genikomsou, eight node reduced integration hexahedral elements (C3D8R) were used to model the concrete and two node three-dimensional truss elements (T3D2) embedded in the concrete elements were used to model the flexural reinforcement. Parameters that were considered in the calibration included the boundary conditions, assumed thickness of the steel load and support plates, analysis type, mesh size, assumed concrete dilation angle and assumed concrete fracture energy.

As discussed in the previous section, the initial analysis of slab AM04 was completed using a modified version of the model calibrated by Genikomsou and Polak (2015), based on the SB slab series tested by Adetifa and Polak (2005). In this initial analysis, the boundary conditions were applied directly to the slab geometry. This simplified way of applying the boundary conditions in the model did not include the steel load and support plates used in the experimental setup of slab AM04. The predicted crack pattern also did not accurately capture the experimental behaviour as the FEM predicted extensive cracking in the compressed zone of the slab.

Therefore, the first study conducted in the calibration of the AM04 model was focused on determining the appropriate boundary conditions for use in the FEM. This analysis was conducted using the modified Genikomsou and Polak (2015) model and as such accurate predictions of load capacity and rotations at failure were not expected.

Three methods of modelling the experimental boundary conditions were investigated. The first model, denoted the simple model, matches that discussed in Section 4.3.3.2, and did not include steel load or support plates, and the boundary conditions were applied directly to the slab geometry. The second model, denoted the elastic plate model, included linear elastic load and support plates, which were extruded from the slab geometry. The support and loading boundary conditions were applied directly to these extruded portions of the slab. The third model, denoted the contact model, involved creating separate parts in ABAQUS for the slab, load plates and support plate. Contact interactions between the different parts were assigned using the General Contact Algorithm in ABAQUS/Explicit. As with the elastic plate model, load and support boundary conditions were applied on the load and support plates, as shown in Figure 4-29.

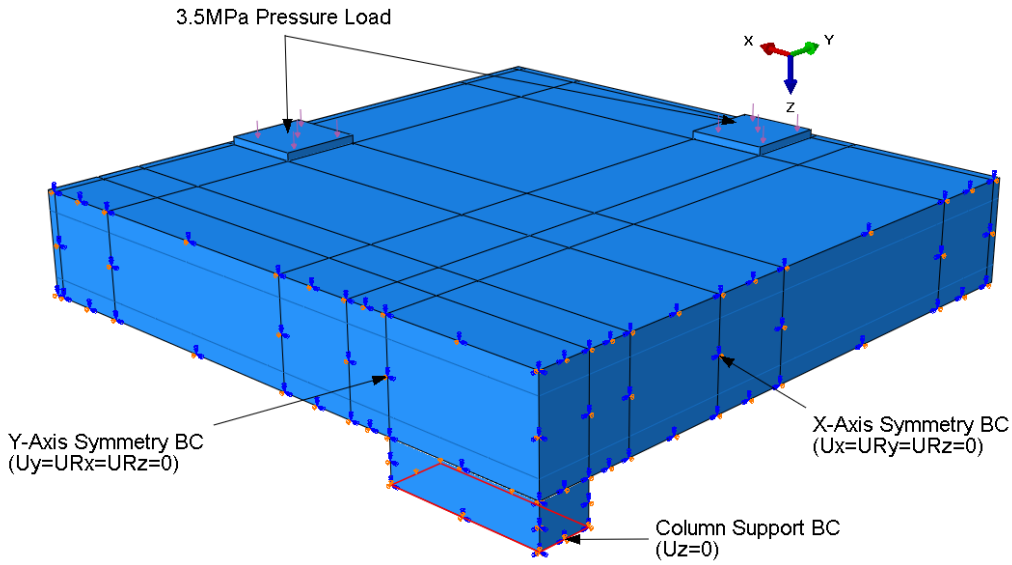

Figure 4-29: Boundary Conditions in Elastic Plate and Contact Models

In the elastic plate and contact models, the load plates were assumed to be 20mm thick and the support plate was assumed to be 100mm thick as this information was not provided by Sagaseta et al. (2014). C3D8R elements with a mesh size of 20mm were used to mesh both plates. An isotropic elasticity definition was used for both the load and support plates with an elastic modulus of 200000MPa and a Poisson's ratio of 0.3.

The predicted load-rotation response in each orthogonal direction and a comparison of the predicted capacity and rotation at failure for all three models are provided in Figure 4-30 and Table 4-8 respectively. The predicted capacity for all three models is similar, and an approximately symmetric response was predicted in both orthogonal directions which matches the experimental observations of Sagaseta et al. (2014). The fundamental difference between the models involves the interaction between the steel support plate and slab. In both the simple and elastic plate models, the slab cannot lift from the supported area, as the supporting nodes are either directly constrained (simple model) or attached to the same mesh as the slab (elastic plate model). The ability of the FEM to capture the slab lifting from the top of the support plate is important because this was observed during the test of slab AM02 (Sagaseta, Tassinari, Fernández Ruiz, & Muttoni, 2014). Therefore, the boundary conditions used in the FEM should be capable of capturing this behaviour to be an accurate representation of the experimental setup.

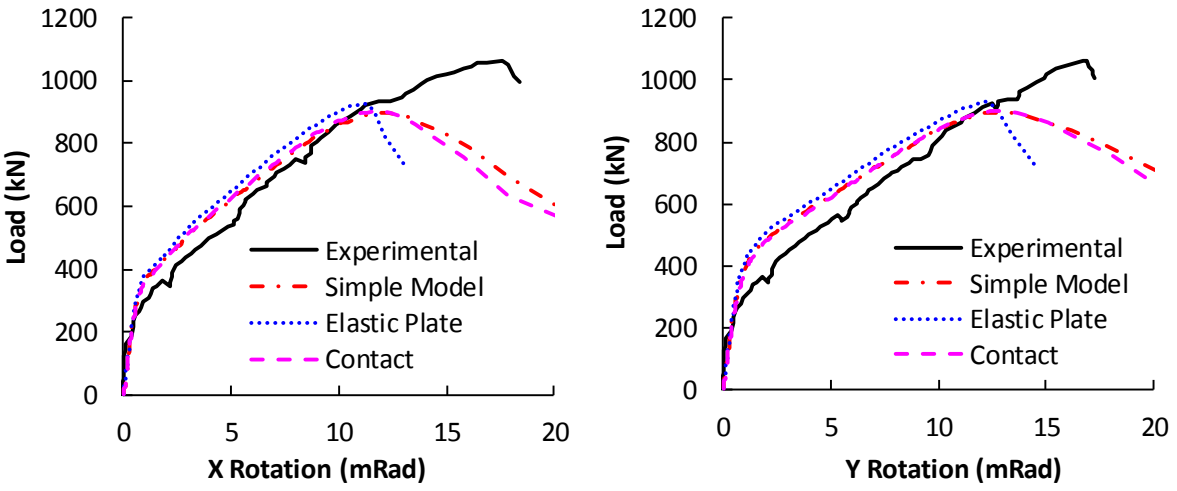

Figure 4-30: Comparison of Load-Rotation Response of Slab AM04 (boundary condition investigation)

Table 4-8: Summary of Results for Boundary Condition Investigation, Slab AM04

Model	Failure Load (kN)	ψ_x (mRad)	ψ_y (mRad)
Simple	896.4	11.94	12.73
Elastic Plate	928.4	10.07	11.08
Contact	903.0	11.32	12.42

Lifting of the slab from the top of the steel support plate was possible in the contact model due to the contact definitions used. Between the base of the slab and top of the support a "hard" contact definition was used. This contact definition attempts to limit penetration of the slab elements into the support plate elements, but allows the two surfaces to separate after initial contact depending on the loading conditions. The use of this hard contact allows the model to predict similar behaviour to that observed experimentally and modelled by Shu, Belletti, Muttoni, Scolari and Plos (2017), through the use of interface elements or non-tension spring elements, in their analysis of AM04 in DIANA. To model the interaction between the base of the load plates and the top of the slab, a separate "cohesive" definition with the default parameters in ABAQUS was used. This cohesive contact also limits element penetration for the surfaces in contact but does not allow the surfaces to separate after initial contact.

The crack patterns predicted from the elastic plate model and contact models are shown in Figure 4-31. Unlike the crack pattern predicted from the simple model, shown in Figure 4-27 on page 101, no cracking is predicting in the compression zone of the slab above the steel support plate, which matches the experimental results. The crack patterns from the elastic plate and contact models both displayed good correlation with the experimental crack patterns.

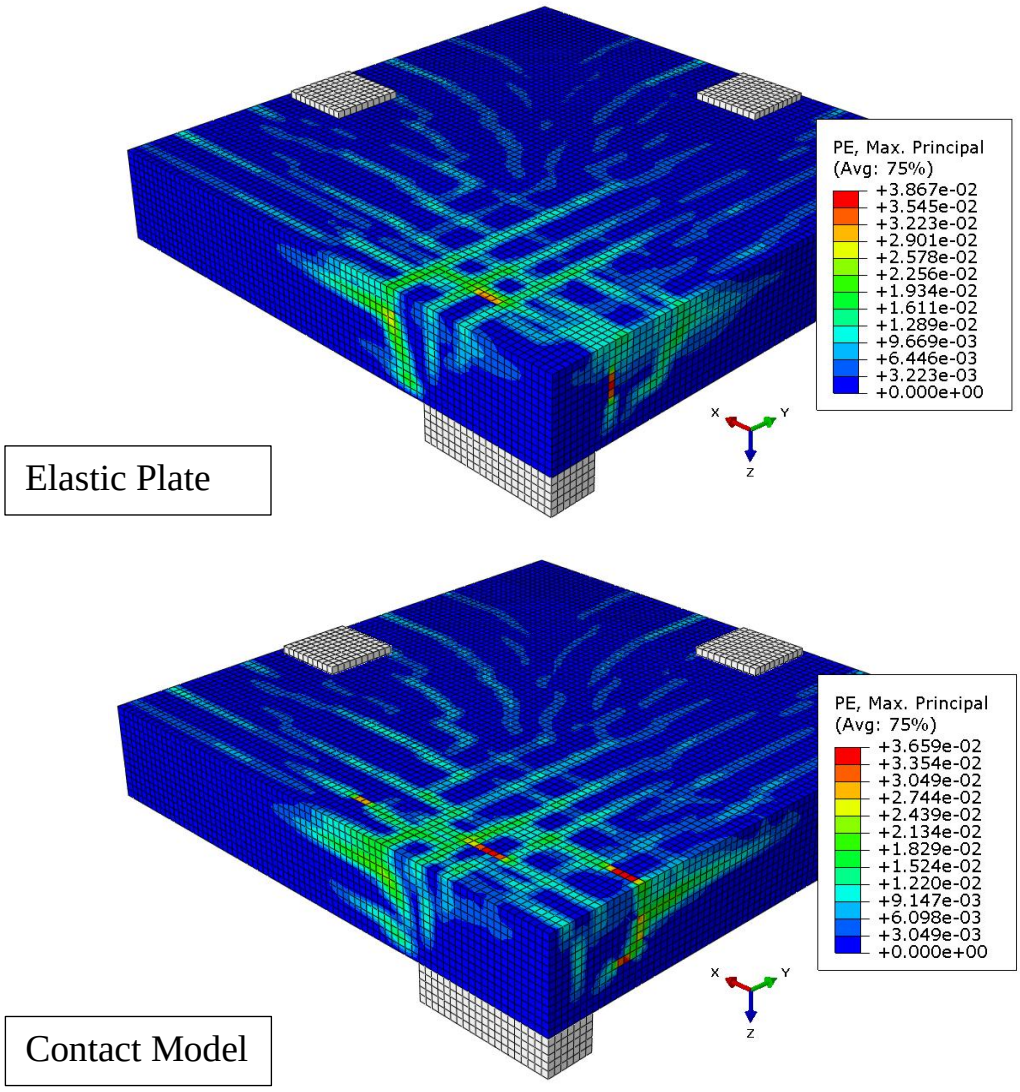

Figure 4-31: Predicted Crack Patterns for Elastic Plate and Contact Model

Finally, the predicted shear stress distribution in the slab around the perimeter of the steel support plate, shown in Figure 4-32, was analyzed. The predicted distributions for the three models are

similar in shape, and all display a shear stress concentration near the corner and along the short side of the steel support plate.

Considering the predicted load-rotation responses, crack patterns and shear stress distributions the contact model was used to analyze AM04, and all subsequent slabs in this thesis, because it more accurately captures the experimental setup and results in similar predictions to the other two models studied.

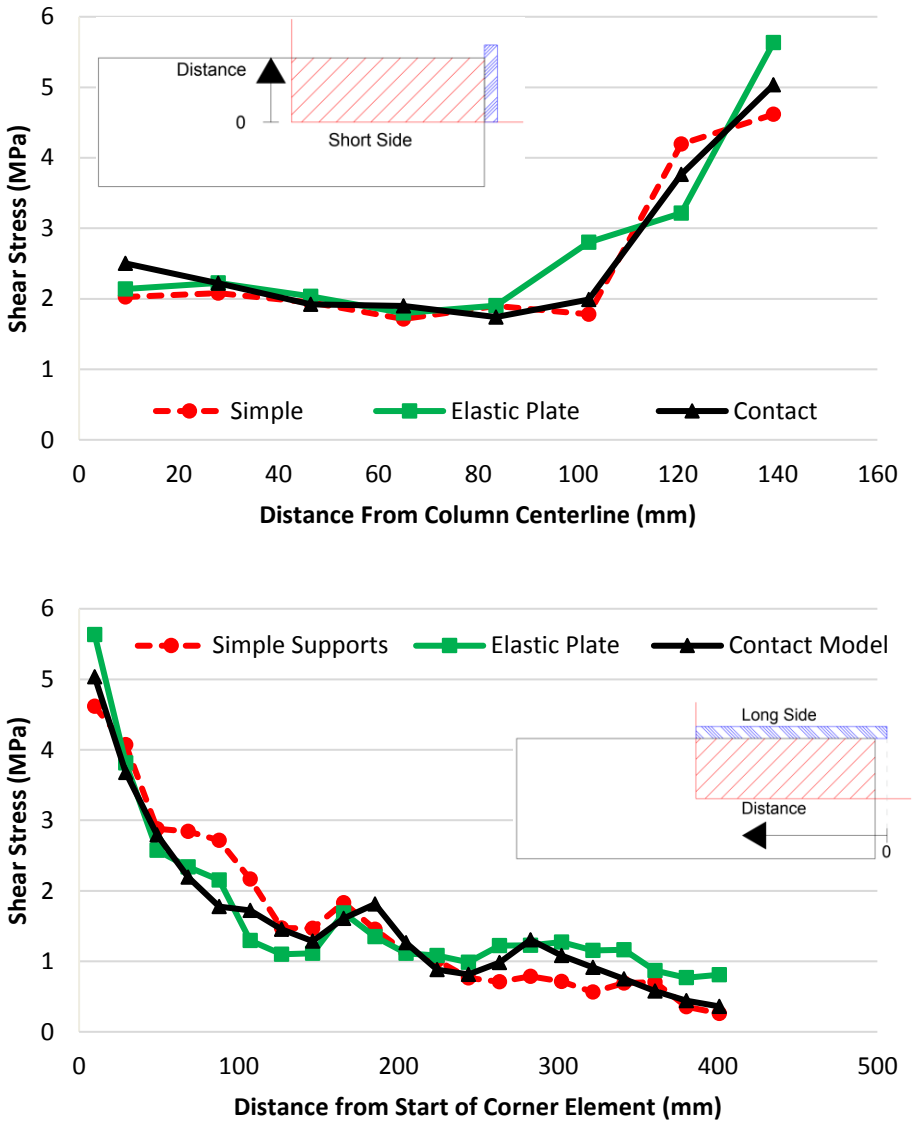

Figure 4-32: Predicted Shear Stress Distribution Around Perimeter of Steel Support Plate, Top: Parallel to Short Side, Bottom: Parallel to Long Side

As previously stated, Sagaseta et al. (2014) did not provide the thickness of the steel load and support plates. Therefore, in the initial model of slab AM04 the thicknesses of the load and support plates were assumed to be 20mm and 100mm respectively. To study the impact of the assumed plate thicknesses, six additional models with varying load and support plate thicknesses were studied. The considered combinations of load and support plate figures are summarized in Table 4-9. The naming convention for the investigated models is XXL YYS where XX and YY are the thickness of the load and support plates in millimeters respectively. The geometry of the slab with a 140mm thick load and support plates is shown in Figure 4-33. Also shown in Figure 4-33 is the displacement location considered in the plate thickness study, which is approximately located on the radius of contraflexure.

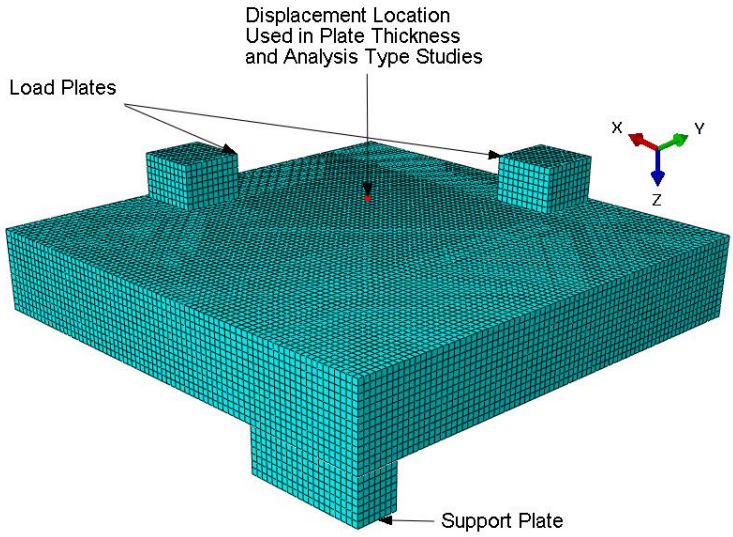

Figure 4-33: Example of Model Used in Plate Thickness Study

Table 4-9: Summary of Models Considered in Plate Thickness Study

Model	Load Plate Thickness (mm)	Support Plate Thickness (mm)
20L 100S (Baseline)	20	100
60L 100S	60	100
100L 100S	100	100
60L 60S	60	60
20L 60S	20	60
20L 140S	20	140
140L 140S	140	140

The predicted load-displacement responses for the models in the plate thickness study, shown in Figure 4-34, are similar, with a maximum difference in estimated capacity and deflection of 1% and 4% respectively. Based on the predicted load-displacement response, the assumed load and support plate thicknesses was found to have a very minimal impact on the finite element predictions. Therefore, 20mm thick load plates and 100mm support plates were used in all subsequent analyses.

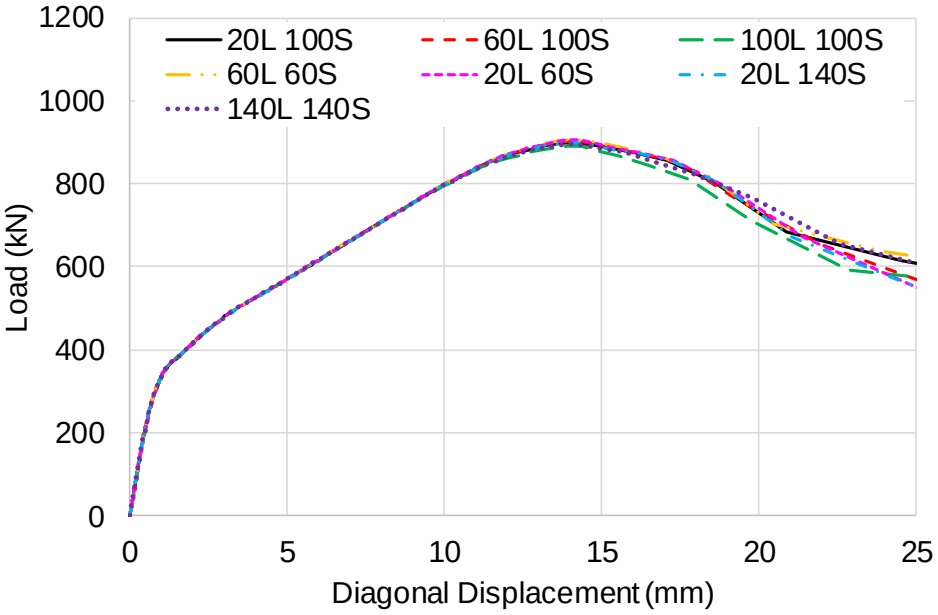

Figure 4-34: Predicted Load-Displacement Response for Various Load and Support Plate Thicknesses, Slab AM04

Genikomsou (2015) studied the impact of the chosen analysis type on the finite element results. Two analyses were performed, a static analysis in ABAQUS/Standard with viscoplastic regularization and a quasi-static analysis in ABAQUS/Explicit. Genikomsou (2015) found that both the static analysis, which included a viscosity parameter of 0.00001, and the quasi-static analysis, predicted a similar load-displacement response. However, the static analysis was found to be less computationally efficient, and as such, all analyses were conducted using a quasi-static analysis in ABAQUS/Explicit.

Since the AM04 model used contact definitions to model interactions between the load and support plates and the slab, and a force driven method was used to load the slab, instead of a displacement boundary condition as used by Genikomsou (2015), the impact of the using a static or quasi-static analysis was analyzed. Following the work of Genikomsou (2015), slab AM04 was analyzed using a

static procedure in ABAQUS/Standard with a viscosity parameter of 0.00001 and a quasi-static analysis procedure in ABAQUS/Explicit. The predicted load-displacement response for both analysis types, where the displacement is measured at the same location as used in the plate thickness study, is shown in Figure 4-35.

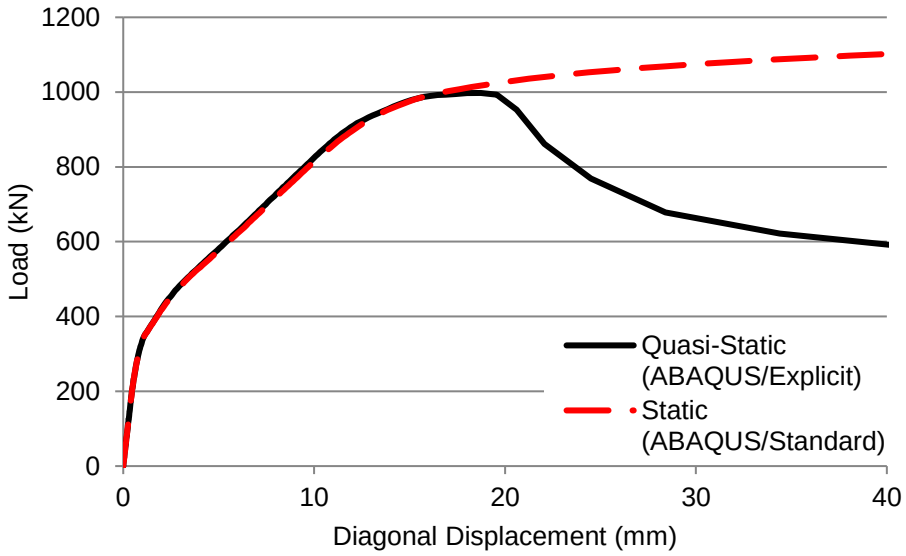

Figure 4-35: Predicted Load-Displacement Response for Static and Quasi-Static Analyses, AM04

The predicted load-displacement response for both analysis types are similar for most of the analysis. However, as discussed in Section 4.3.2, the static analysis did not display a sharp peak in the load-displacement diagram, which is typically associated with punching, since a force driven load was used in the model. Since a force driven load was used, the static procedure predicted a continually increasing force until the end of the analysis time. The quasi-static analysis on the other hand was able to capture the brittle punching failure and associated peak in the load-displacement curve. The peak in the load-displacement curve is observed because the quasi-static model becomes unstable when punching occurs, leading to a significant drop in the predicted reaction force. Since the predicted response from both analyses prior to failure is similar, it can be concluded that the dynamic effects in the ABAQUS/Explicit model are negligible, and as such, the analysis can be assumed to be quasi-static. A force driven load is required to ensure uniform load application on each load plate and so a quasi-static analysis in ABAQUS/Explicit was used for all subsequent analyses in this thesis.

As noted by Genikomsou (2015), the use of a smeared crack approach in the "Concrete Damaged Plasticity" model in ABAQUS can cause strain localization due to the strain softening behaviour of

concrete. This strain softening behaviour is mesh size dependent in numerical models, and can lead to strains accumulating in a narrow band of elements causing premature failure of the model. This effect is more severe for fine meshes and is why most plasticity-based models are mesh size dependent. The mesh size dependency can be limited by introducing viscoplastic regularization in static analyses or a characteristic internal crack length (Genikomsou A. , 2015).

To study the mesh sensitivity of the AM04 model, three different mesh sizes, 16mm, 20mm and 24mm, were used in the analysis. All three investigated mesh sizes were greater than or equal to the maximum aggregate size (16mm) and resulted in more than four elements through the slab depth, which is the minimum number of reduced integration elements that should be used through the slab thickness. If less than four elements are used through the thickness, numerical effects such as hourglassing and distortion of the C3D8R elements may occur, possibly leading to convergence issues or inaccurate results (Genikomsou A. , 2015; Dassault Systemes Simulia Corp., 2012) . 15, 13 and 10 elements through the slab thickness were used for the 16mm, 20mm and 25mm meshes respectively.

Since quasi-static analyses in ABAQUS/Explicit were used, the tensile strains in the uniaxial tensile stress-strain response for the concrete were calculated by dividing the crack widths by the characteristic element length. In the case of eight node brick elements, the characteristic length is equal to the cubic root of the element volume (Dassault Systemes Simulia Corp., 2012; Genikomsou A. , 2015). Even with the introduction of the characteristic element length, the results for the three mesh sizes, shown in Figure 4-36, were mesh size dependent. The predicted failure loads, displacements and rotations at failure are summarized in Table 4-10. When the load-rotation response in both orthogonal directions is considered, the 20mm mesh was found to give the most accurate results compared to the experimental results.

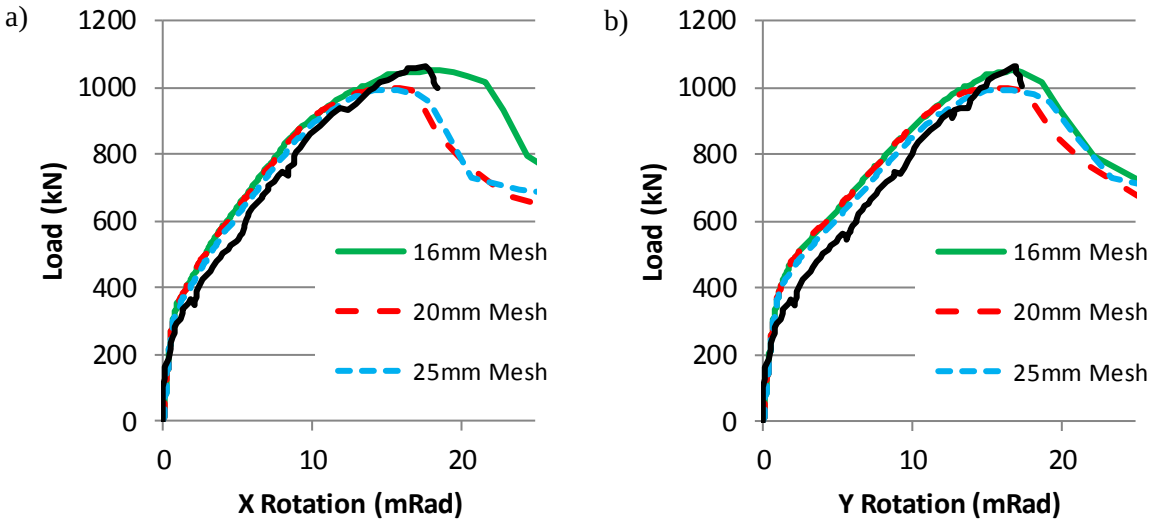

Figure 4-36: Predicted Load-Rotation Responses – AM04 Mesh Study, a) X Rotation, b) Y Rotation

Table 4-10: Summary of Results for Mesh Study – AM04

Mesh Size (mm)	Load (kN)	Displacement (mm)		Rotation (mRad)	
		X-Axis	Y-Axis	X-Axis	Y-Axis
16	1050.1	25.43	18.77	18.56	16.91
20	997.7	21.80	18.20	15.91	16.39
25	994.4	20.26	17.33	14.79	15.62

The shear stress distribution in the slab around the perimeter of the steel support plate for each investigated mesh size is shown in Figure 4-37. For all three meshes, the FEM predicted a concentration of shear stress along the short side of the steel plate and near the corner. The shear stress distribution for the 25mm mesh is different than the distribution for the 16mm and 20mm mesh in two ways. Firstly, the peak stress for the 25mm mesh did not occur at the corner of the support plate but occurred at the next column of elements on the short side. Secondly, a peak in shear stress at an approximate distance of 160mm from the support plate corner was not observed for the 25mm mesh. This peak in shear stress in the 16mm and 20mm mesh models occurs due to a rebar element being located near the integration point of the concrete elements. Since the rebar is stiffer than the concrete, the rebar attracts more load which effects the predicted shear stress distribution.

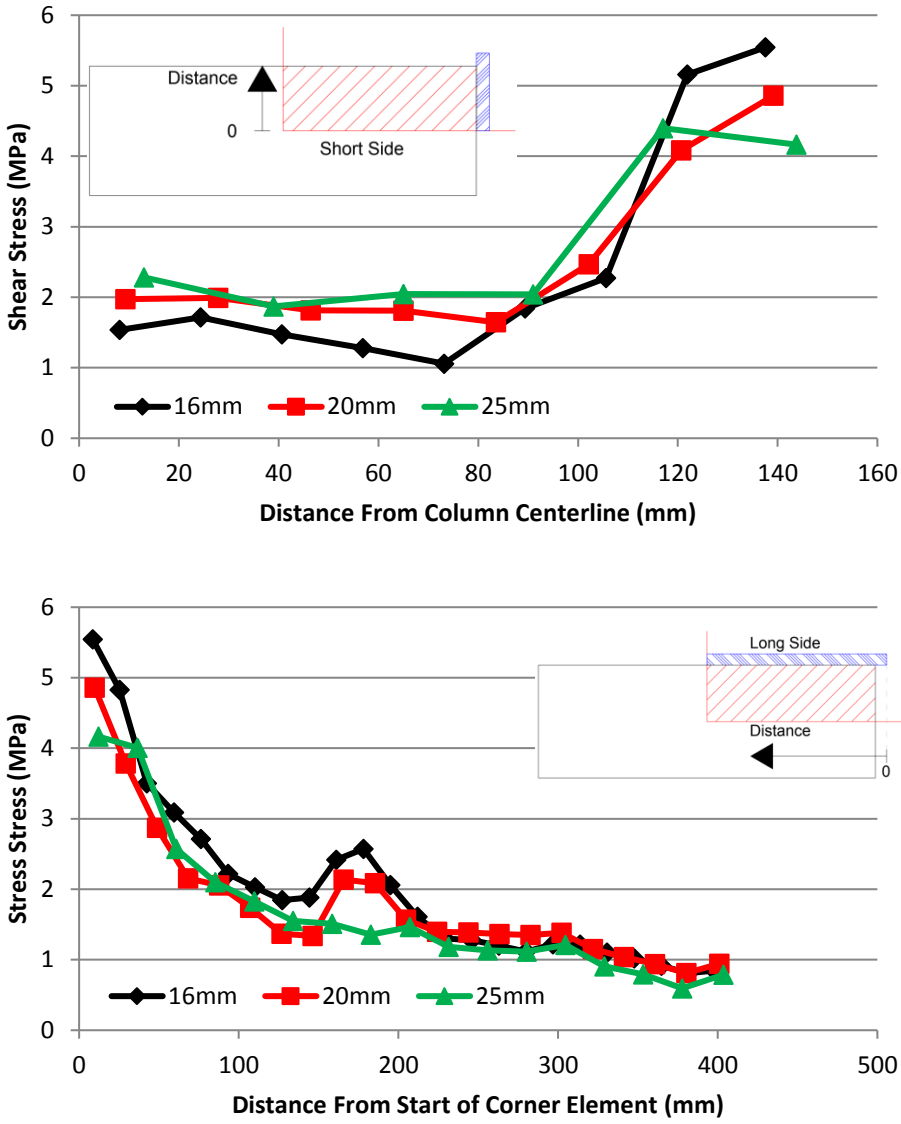

Figure 4-37: Predicted Shear Stress Distribution Around Steel Support Plate in Slab, AM04

The crack patterns for each mesh, provided in Figure 4-38, were also analyzed when selecting a mesh size. As can be seen in Figure 4-38, ABAQUS predicted a large principal plastic strain value, and therefore, a high concentration of cracking, in the slab above and around the support plate for all three mesh sizes. The predicted cracks agreed well with the experimental crack patterns shown in Figure 4-27. However, the 16mm mesh results demonstrated strain localization, as the strain values adjacent to the long side of the support plate are an order of magnitude higher than the strains in the rest of the model. The models with 20mm and 25mm meshes also displayed a higher strain magnitude

adjacent to the long side of the supported area, but the difference in magnitude between this area and the rest of the model is not as large as observed in the 16mm mesh model. The crack patterns for the 20mm and 25mm meshes correlated well with the experimentally recorded cracks.

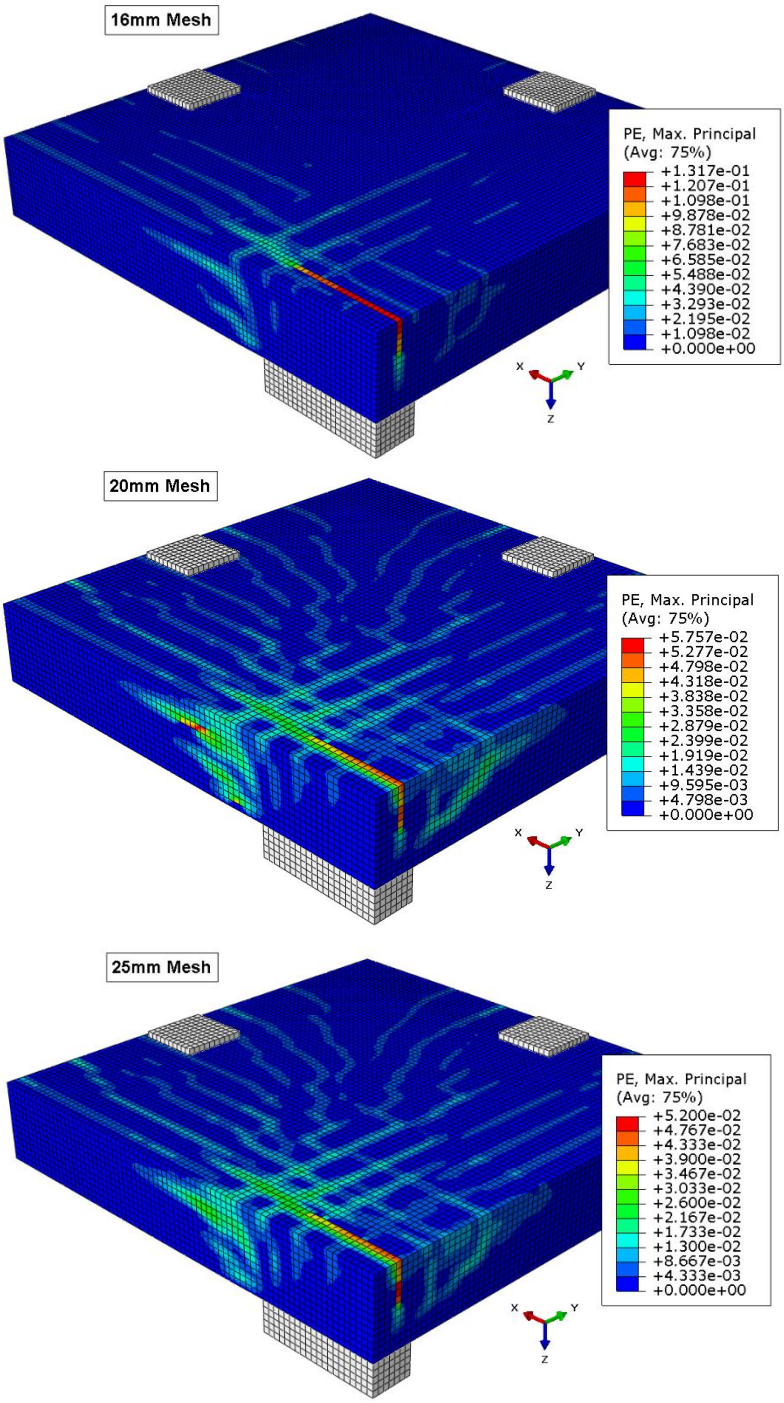

Figure 4-38: Predicted Crack Patterns for 16mm, 20mm and 25mm Meshes, AM04

Based on the analysis of the predicted load-rotation response, crack patterns and shear stress distribution around the column perimeter the 20mm mesh was used in all subsequent analyses in this thesis. The use of the 20mm mesh over the 25mm mesh does require additional computational effort, but increases the number of elements along the perimeter of the supported area and the ACI critical perimeter. Therefore, a more detailed estimation of the shear stress distribution around these two perimeters is possible with the 20mm mesh compared to the 25mm mesh. The chosen mesh size also matches that used by Genikomsou (2015).

Genikomsou and Polak (2015) found the CDP model in ABAQUS to be sensitive to the inputted concrete dilation angle. Since concrete is a brittle material, it undergoes large volume changes, which are caused by inelastic strains. This volume change is termed dilatancy, and is defined in the CDP through the inputted dilation angle. Chen and Han (1988) concluded that the non-associated flow rule should control dilatancy, especially for materials such as concrete, where friction is important. This definition allows the dilation angle to be a material parameter of the concrete. The dilatancy parameter, α_p, in the Drucker-Prager plastic potential function, shown in equation 4.11, has been defined to range between 0.2 and 0.3 (Lee & Fenves, 1998a; Lee & Fenves, 1998b; Wu, Li, & Faria, 2006)

$$G = \sqrt{2J_2} + \alpha_p I_1 \tag{4.11}$$

where G is the plastic potential function, and I_1 and J_2 are the stress invariants (Genikomsou A. , 2015). The flow potential function, $G(\sigma)$ used in the CDP in ABAQUS, provided in equation 4.12, is derived from 4.11.

$$G(\sigma) = \sqrt{(\varepsilon\sigma_{t0}\tan(\psi))^2 + \bar{q}^2} + \frac{1}{3} I_1 \tan(\psi) \tag{4.12}$$

where ε is the eccentricity that determines the rate at which the plastic potential function approaches the asymptote, σ_{t0} is the uniaxial tensile strength, ψ is the dilation angle measured in the p-q plane at a high confining pressure, and $\bar{q}$ is the Mises equivalent effective stress (Genikomsou A. , 2015). Considering the asymptote line to the potential function, Genikomsou derived equation 4.13 which can be used to verify the value used for dilation angle in ABAQUS.

$$\tan(\psi) = 3.67 a_p \tag{4.13}$$

Using equation 4.13, the dilation angle is calculated to be equal to 36.3° or 47.8° degrees for a_p values of 0.2 and 0.3 respectively. Both of these values are less than the maximum value of 56.31° allowed in ABAQUS (Dassault Systemes Simulia Corp., 2012).

In the analysis of AM04, five values for dilation angle were investigated, 35°, 40°, 42°, 45° and 50°. The predicted load-rotation response in each orthogonal direction is shown in Figure 4-39. As observed by Genikomsou (2015), the predicted capacity and deflection (rotation) at failure increased as the dilation angle was increased. Additionally, as the dilation angle was increased towards 50° the predicted response becomes more ductile. The best correlation with the experimental results was found for a dilation angle of 42° or 45° degrees.

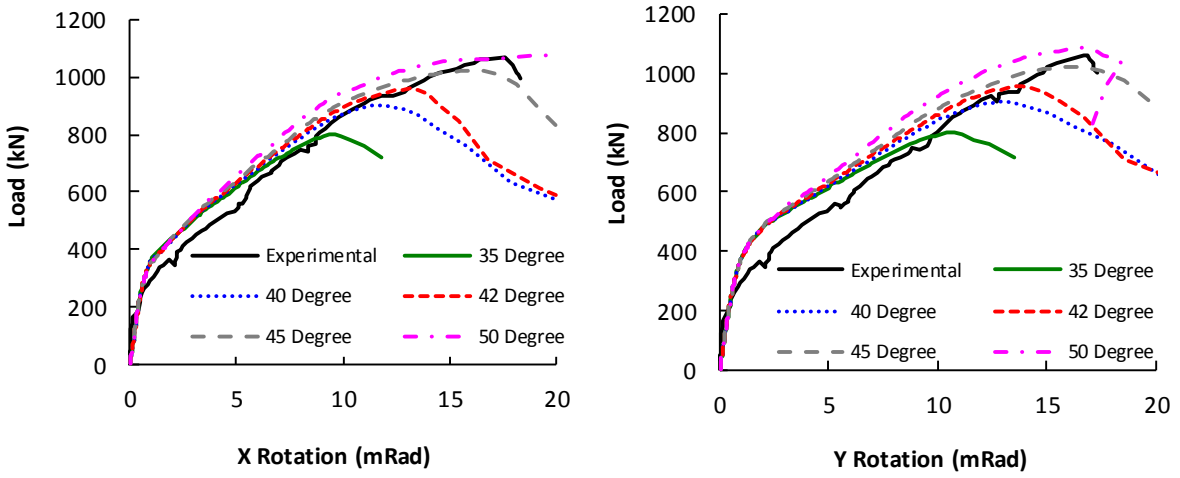

Figure 4-39: Predicted Load-rotation response of Slab AM04 (dilation angle investigation, Gf = 0.093N/mm)

As previously discussed, the fracture energy, which is related to the concrete compressive strength and maximum aggregate size (Comité Euro-International du Béton, 1993), was used when modelling the tensile behaviour of concrete. As outlined in Section 4.2, Model Code 1990 accounts for both of these factors and has been used to estimate the concrete fracture energy in many previous finite element studies (Menétrey, Walther, Zimmermann, Willam, & Regan, 1997; Hallgren & Bjerke, 2002; Genikomsou & Polak, 2015; Shu, Plos, Zandi, Johansson, & Nilenius, 2016; Shu, 2017; Stoner, 2015; Barrage, 2017). According to Model Code 2010, the concrete fracture energy can be calculated using equation 4.14, which neglects the impact of aggregate size

$$G_f = 73 f_{cm}^{0.18} \qquad (4.14)$$

where f_{cm} is the mean compressive strength (MPa) (fédération internationale du béton (fib), 2013).

For slab AM04, which has a concrete compressive strength of 44.6MPa and a maximum aggregate size of 16mm, the fracture energy is estimated as 0.093N/mm or 0.148N/mm based on Model Code 1990 and Model Code 2010 respectively.

Six different values for fracture energy were investigated for slab AM04, 0.093N/mm, 0.10N/mm, 0.11N/mm, 0.12N/mm, 0.13N/mm and 0.148N/mm. The predicted load-rotation response for four of the six values are shown in Figure 4-40. The remaining two values were removed for clarity.

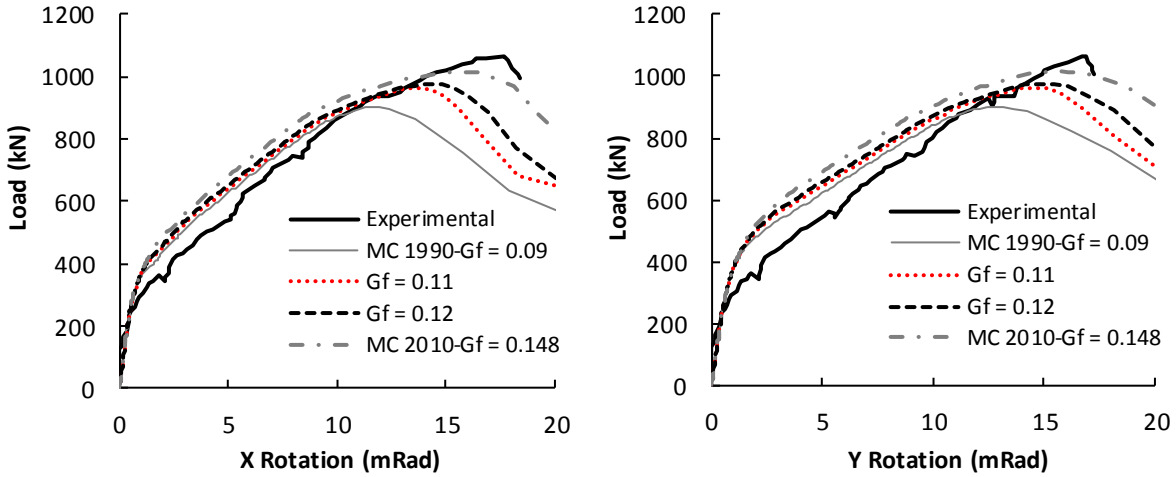

Figure 4-40: Load-rotation Response of Slab AM04 (fracture energy investigation, Dilation Angle = 40°)

As observed by Genikomsou and Polak (2015), the predicted punching capacity and deflection (rotation) at failure increased as the fracture energy increased. Increased load and rotation capacity is predicted since increasing the fracture energy modifies the post-peak tensile stress-crack width relationship. As the fracture energy was increased, the corresponding crack widths increased, leading to the concrete being able to sustain higher tensile strains after cracking. Punching shear failures are initiated due to the formation and opening of inclined cracks near the slab-column connection, and as such, increasing the maximum tensile strain increases the punching capacity.

Finally, the impact of fracture energy and increased dilation angle was investigated. The impact of fracture energy was investigated using dilation angles of 42° and 45° since these two dilation angles showed the best correlation with the experimental results in the dilation angle study. The six fracture energies used with a dilation angle of 40° were studied. The predicted load-rotation response in both

directions for a subset of the considered combinations found to best correlate with the experimental results are shown in Figure 4-41.

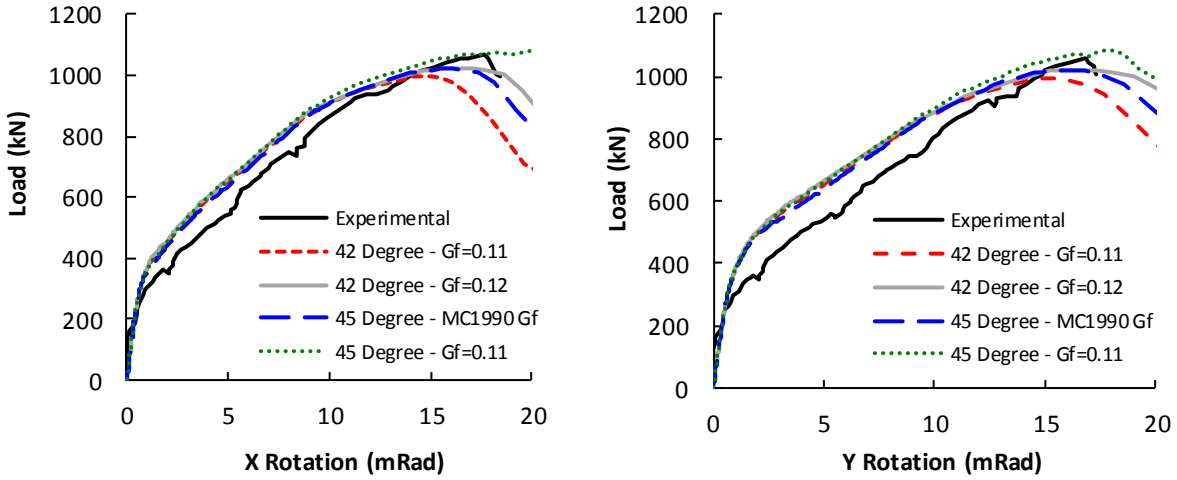

Figure 4-41: Load-Rotation Response of Slab AM04 (Fracture Energy and Dilation Angle Investigation)

Based on the above analyses, a dilation angle of 45 degrees and a fracture energy of 0.093N/mm, which was calculated from Model Code 1990, were found to lead to finite element predictions that best correlated with the experimental data in terms of load-rotation response and predicted crack pattern. A summary of the predicted load capacity and rotations at failure for this model compared to the experimental results is provided in Table 4-11. The crack pattern predicted from this model, which match those for the 20mm mesh in Figure 4-38 on page 114, also correlated well with the experimental crack pattern previously provided in Figure 4-27 on page 101.

Table 4-11: Comparison of FEM Predictions and Experimental Results, AM04

Slab	Experimental			Finite Element Analysis			% Difference		
	Capacity, kN	ψ_x, mRad	ψ_y, mRad	Capacity, kN	ψ_x, mRad	ψ_y, mRad	Capacity	ψ_x	ψ_y
AM04	1067	17.6	16.8	1020.1	16.0	16.1	-4.4	-9.01	-3.8

4.5 Calibration Verification

4.5.1 Remaining AM Series Slabs

4.5.1.1 Experimental Program

The loading layouts for slabs AM01, AM02 and AM03 are shown in Figure 4-42. These three slabs were geometrically similar to slab AM04 but were tested under one-way loading conditions to study the influence of loading layout on the structural behaviour of reinforced concrete slabs supported on rectangular columns. The concrete compressive strength, effective flexural depth and experimental failure load of all four slabs in the AM series are summarized in Table 4-12. Other than the average effective depth, the reinforcing layouts are identical for all four slabs.

Table 4-12: Summary of AM Series Experimental Data (Sagaseta, Tassinari, Fernández Ruiz, & Muttoni, 2014)

Slab	f_c' (MPa)	d_{avg} (mm)	Failure Load (kN)
AM01	44.0	214	950
AM02	39.7	208	919
AM03	42.2	203	883
AM04	44.6	202	1067

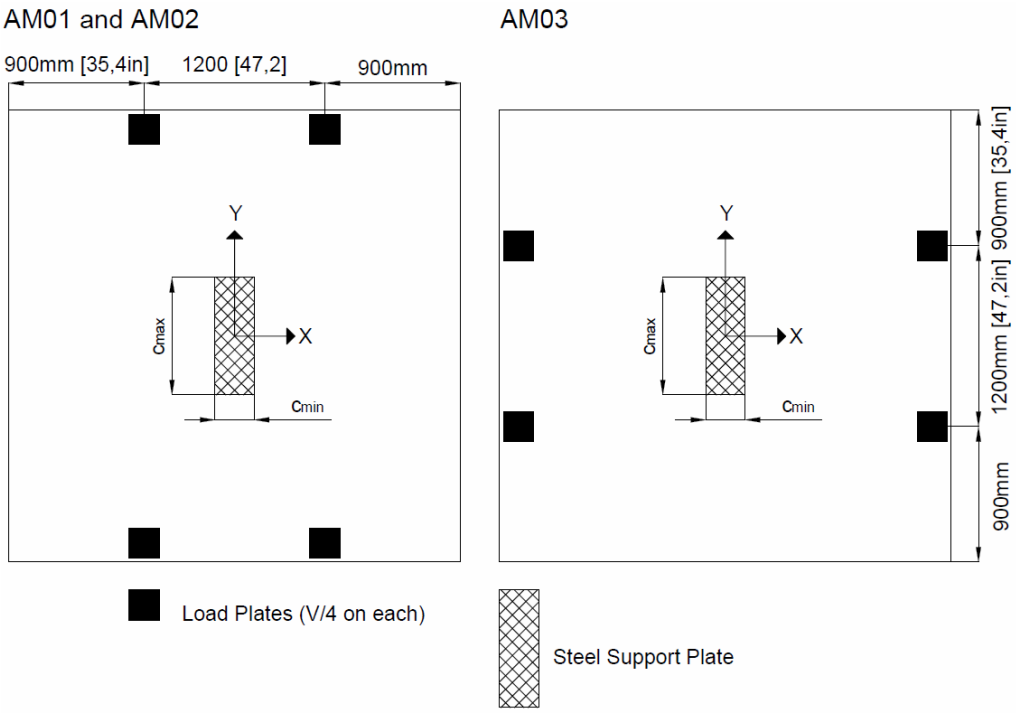

Figure 4-42: Experimental Setups AM01-AM03 (Sagaseta, Tassinari, Fernández Ruiz, & Muttoni, 2014)

4.5.1.2 Finite Element Model

The finite element model of slabs AM01, AM02 and AM03 was identical to that for slab AM04 other than the required modifications to the concrete compressive strength and average effective depth for each slab. Only the tensile reinforcement depth was modified as the depth of reinforcement on the compression side of the slab was not provided. As such, the depth to the compression side reinforcement assumed for slab AM04 was used for all four slabs. The same total load was applied in all four models. Since only one load plate is included in each quarter model the pressure magnitude was increased to 7.0MPa, instead of the 3.5MPa load used on each of the two plates in the AM04 quarter model.

4.5.1.3 Finite Element Analysis Results

A comparison of the experimental and ABAQUS predicted load-rotation response in both orthogonal directions for slab AM01 is shown in Figure 4-43. The punching capacity of slab AM01 predicted by the FEM was 963.6kN, which is approximately 1.4% higher than the experimental capacity of 950kN.

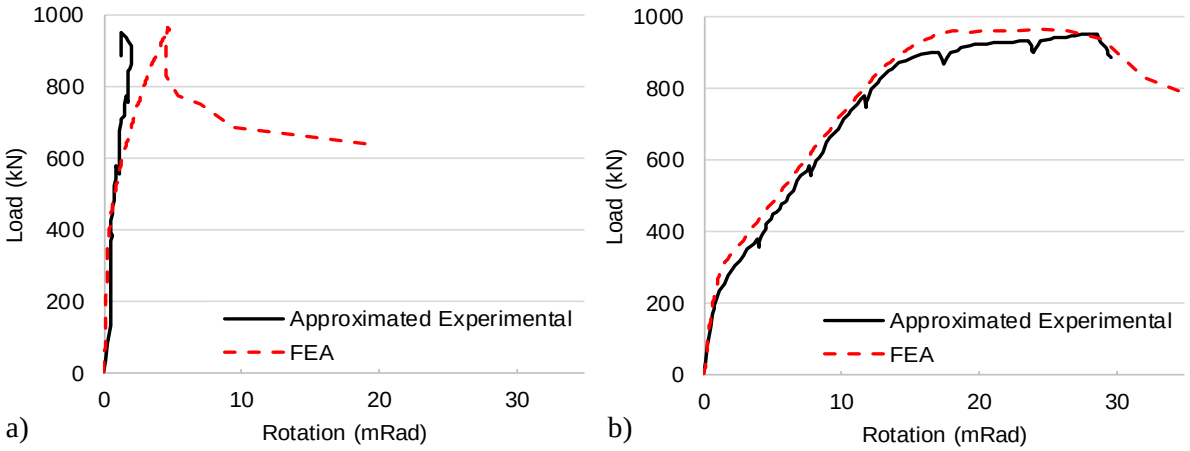

Figure 4-43: Comparison of Predicted Load-Rotation Response and Experimental Data Slab AM01, a) X-direction, b) Y-direction

The predicted load-rotation response of slab AM01 in the Y-direction, which is parallel to the long side of the steel support plate, correlated very well with the experimental results in terms of load capacity, rotation at failure and stiffness. In the X-direction, which is parallel to the short side of the supported area, the finite element predictions deviated from the experimental measurements. It is assumed that the measurement instrumentation in the X-direction malfunctioned during the testing because the predicted load-rotation response for slab AM01 in the X-direction did not display the same trends as that observed for slab AM02. Slab AM01 and AM02 are identical except for small differences in concrete compressive strength and average effective flexural depth. Therefore, the trends in the experimental results should be similar.

A comparison of the load-rotation response of slab AM02 predicted by ABAQUS to the experimental measurements is provided in Figure 4-44. The punching capacity of slab AM02 predicted by the FEM was 926kN, which is only 0.76% higher than the experimental capacity of 919kN. As with the results for slab AM01, the predicted load-rotation response of slab AM02 in the Y-direction was very similar to that measured during the test. However, unlike the results for slab AM01, the predicted response in the X-direction was similar to the experimental measurements, which supports the assumption that there is an error in the X-direction measurements for slab AM01.

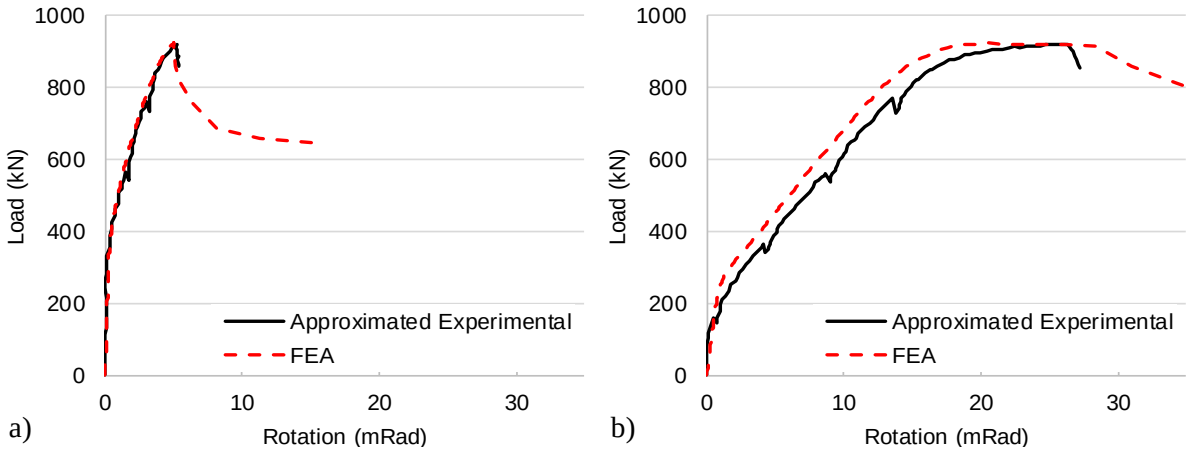

Figure 4-44: Comparison of Predicted Load-Rotation Response and Experimental Data Slab AM02, a) X-direction, b) Y-direction

Both AM01 and AM02 were predicted to fail in punching by the finite element model, which matches the experimental observations. Looking at the predicted deflected shape and crack patterns for both slabs it was observed that the model predicted an initial punching failure, as evidenced by the formation of punching cones on the slab sides and the slab deflections about both sides of the supported region. The predicted deflected shape of the slab AM01 near the support plate is shown in Figure 4-45. After this initial punching failure, the model predicted a secondary one-way shear failure along a plane parallel to the short side of the supported area.

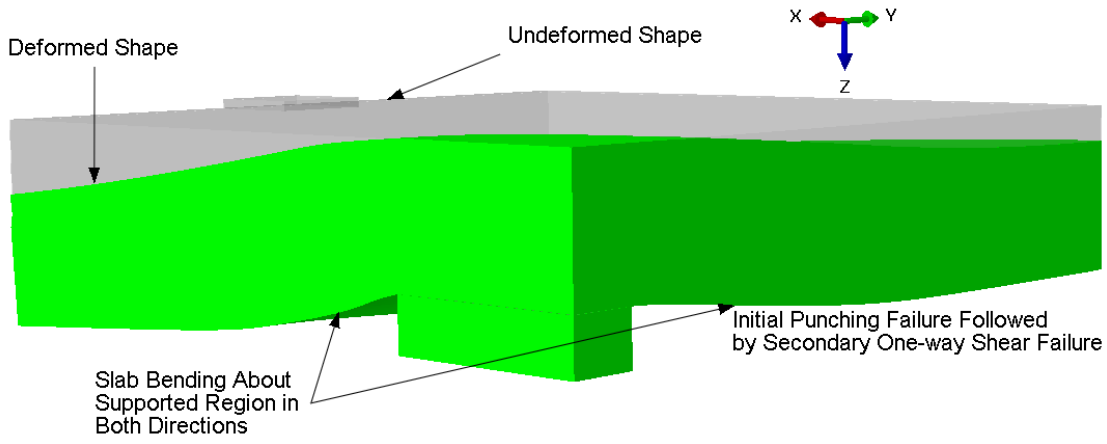

Figure 4-45: Predicted Deflected Shape of Slab AM01 Near the Supported Area

A comparison of the crack pattern predicted by the FEA, visualized through the maximum principal plastic strain contours, and the experimentally observed crack pattern for slab AM02, is

shown in Figure 4-46. The predicted crack pattern agreed well with the experimental crack pattern. On the tension surface of the slab the FEM predicted a large number of horizontal cracks perpendicular to the long side of the supported area, which matches the experimental results. Some diagonal cracks which extend from the corner of the supported area are also present in both crack patterns. As observed experimentally, some of the cracks which are near the end of the supported area extend across the entire slab width. The crack pattern on the slab sides also agreed with those observed experimentally. On the slab side parallel to the long side of the supported area a clear punching cone is predicted. On the slab side parallel to the short side of the supported area the punching cone is not as clear at the onset of punching. If the predicted crack patterns at a later stage of the analysis are analyzed, a clearer punching cone similar to that observed experimentally is predicted, as shown in Figure 4-47.

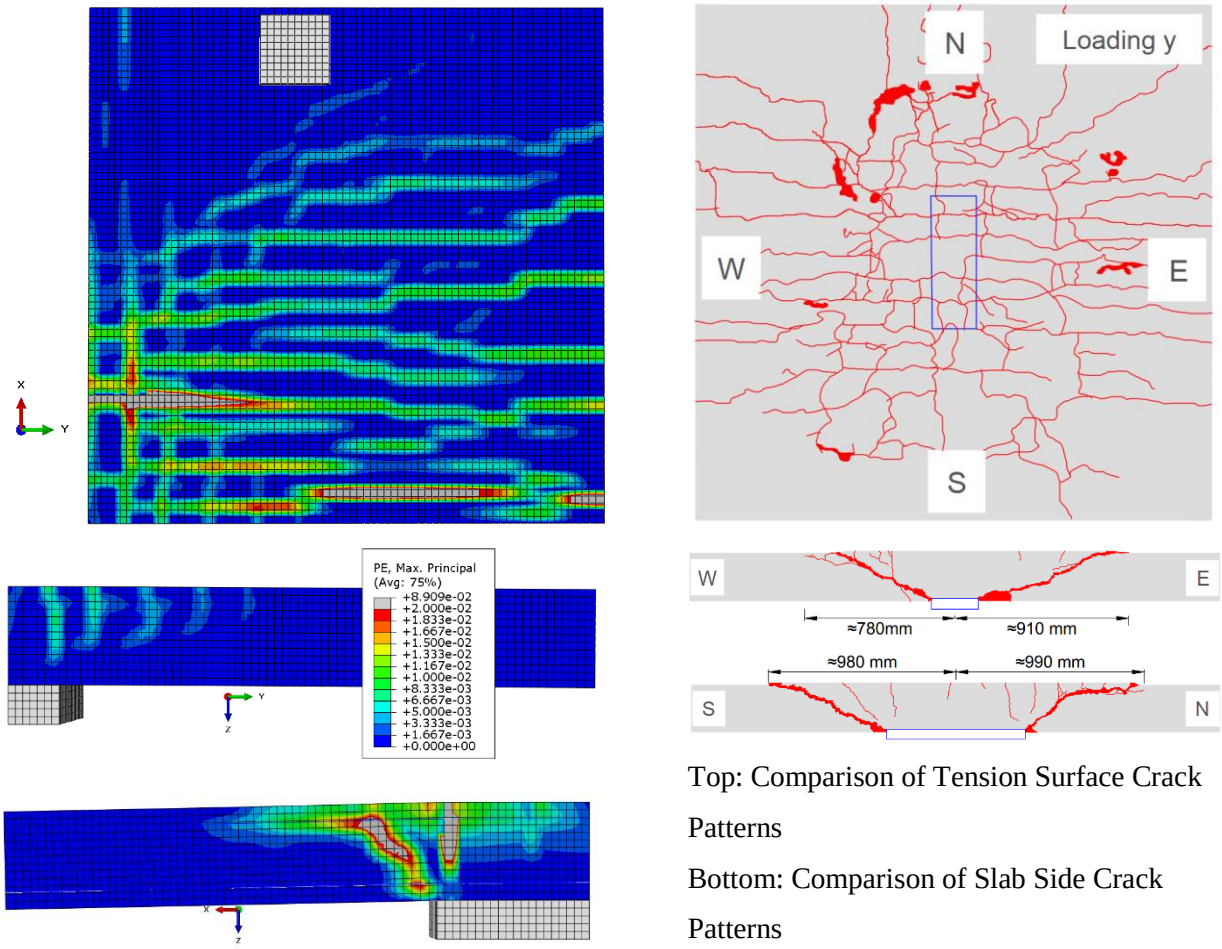

Top: Comparison of Tension Surface Crack Patterns

Bottom: Comparison of Slab Side Crack Patterns

Figure 4-46: Comparison of Predicted and Experimental Crack Pattern, Slab AM02

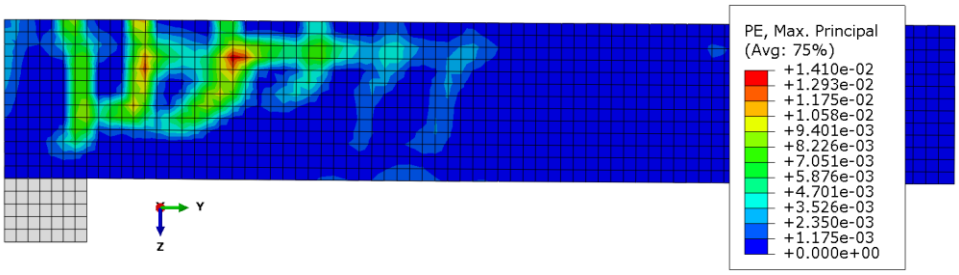

Figure 4-47: Predicted Crack Pattern on Slab Side Post Punching, Slab AM02

The predicted shear stress distribution in the slab around the steel support plate perimeter for slab AM02 is shown in Figure 4-48. The FEA predicted a high concentration of shear stress at the corner and along the short side of the supported area, which was also observed experimentally by Sagaseta et al. (2014). A similar shear stress distribution was predicted for slab AM01.

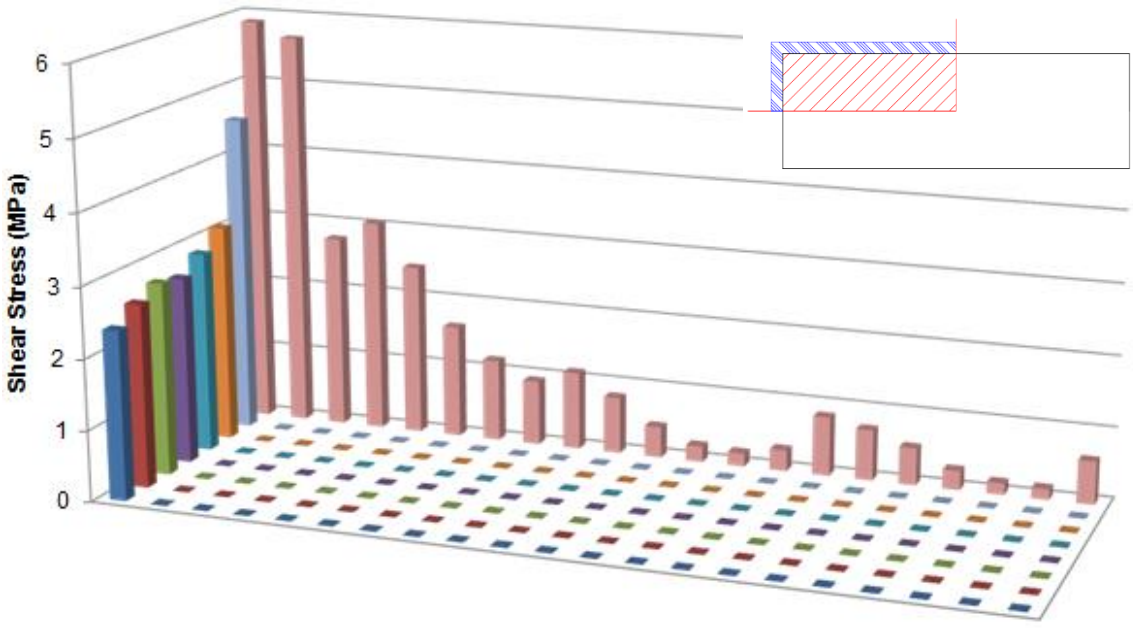

Figure 4-48: Predicted Shear Stress Distribution in Slab Around the Steel Support Plate, AM02

The predicted load-rotation response and experimental results for slab AM03 are provided in Figure 4-49. Unlike the results for slabs AM01 and AM02, the finite element predictions deviated from the experimental response as the load was increased. The capacity predicted by the FEM was 742.1kN, which is approximately 16% lower than the experimental capacity of 883kN.

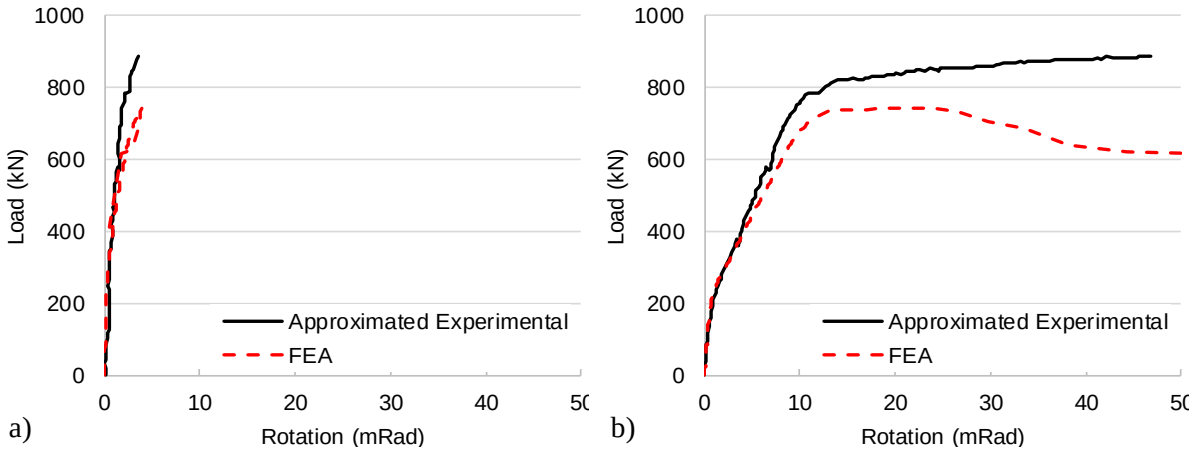

Figure 4-49: Comparison of Predicted Load-Rotation Response and Experimental Data Slab AM03, a) X-direction, b) Y-direction

The finite element predictions showed good correlation with the experimental results in the linear elastic portion and start of the plastic portion of the response. However, at a load of approximately 600kN the finite element model predictions began to deviate from the experimental response. The likely reason for the discrepancy between the finite element predictions and experimental results is that slab AM03 failed in flexure. Of the four slabs in the AM series, slab AM03 was the only one which failed in flexure. The original calibration of the finite element model was conducted considering slab AM04, which failed in punching at a load well below its estimated flexural capacity. As previously discussed, a simplified stress-strain relationship was used for the flexural reinforcement since the FEM was focused on capturing shear failures. The FEM model is able to accurately predict the behaviour of slabs AM01 and AM02 since they also failed in punching before formation of the flexural failure mechanism. However, the model neglects numerous parameters which would contribute to the flexural response such as strain hardening.

The FEM model predicted slab AM03 to fail in one-way shear which does not match the experimental failure mode. In addition to the lack of a detailed stress-strain curve, the predicted behaviour of slab AM03 may be affected by the contact definitions used. Since the contact between the top of the steel support plate and the slab base allowed the slab to lift and rotate, the slab becomes supported on the edge of the steel plate only as the slab rotates. Since the predicted rotations of slab AM03 are much larger than the other slabs in the AM series, it is possible that the contact definition used impact the predicted response.

A comparison of the predicted crack pattern to the experimental crack pattern is shown in Figure 4-50. Since a very high strain magnitude is predicted in the elements very close to the edge of the slab, the maximum contour limit is modified to show the crack pattern. The crack pattern on the tension surface agreed reasonably well with that observed in the experiment as most of the predicted cracks are vertical and perpendicular to the short side of the column. However, more vertical cracks are predicted than observed in the test and the diagonal cracks extending towards the slab corner are not predicted by the FEM. On the slab side parallel to the short side of the column, the model also predicted more cracks than observed experimentally. However, even at later frames no punching cone is formed, reinforcing the conclusion that the model failed in one-way shear.

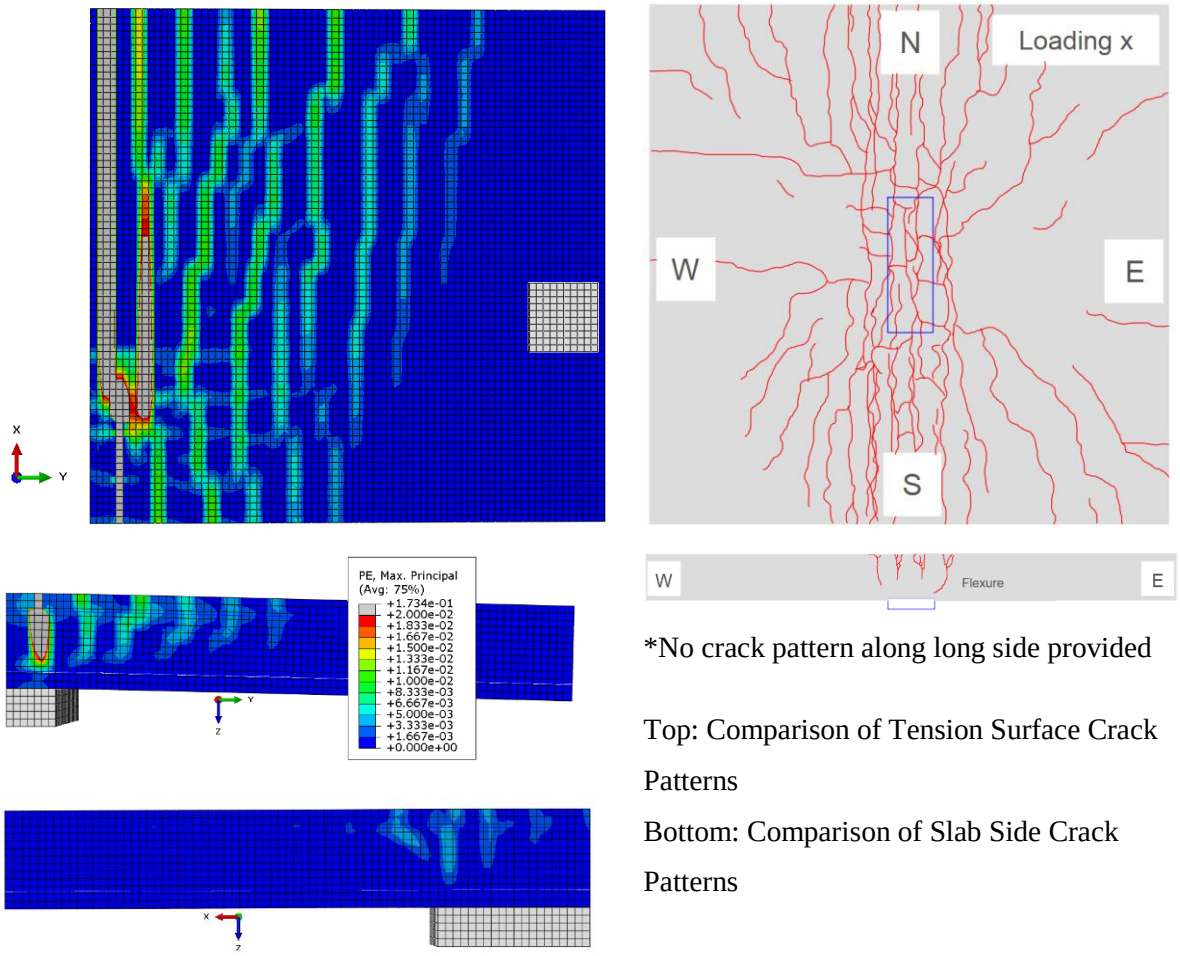

*No crack pattern along long side provided

Top: Comparison of Tension Surface Crack Patterns

Bottom: Comparison of Slab Side Crack Patterns

Figure 4-50: Comparison of Experimental and Predicted Crack Pattern, Slab AM03

The predicted shear stress distribution around the column for slab AM03 is shown in Figure 4-51. Again, there is a concentration of shear stress around the column corner/short side. However, unlike

the models of AM01, AM02 and AM04, the concrete along the short side of the support plate away from the corner is under very low shear stress.

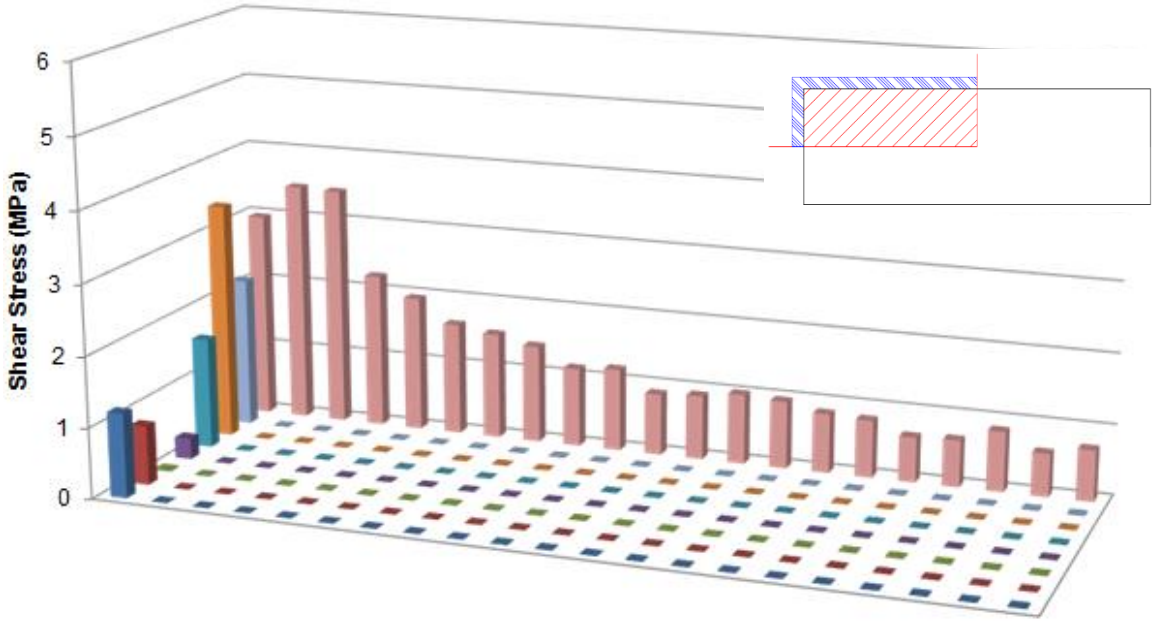

Figure 4-51: Predicted Shear Stress Distribution in Slab Around the Steel Support Plate, AM03

Overall, the FEM predictions correlated well with the experimental results, especially for the slabs which failed in shear. The FEM predicted larger rotations in the direction of the load application which matches the experimental observations. Additionally, the slope of the punching cones on the slab side parallel to the long side of the supported area in slabs AM01 and AM02 are steeper than that in the perpendicular direction, which matches observations by Sagaseta et al. (2014; 2011).

A comparison of the predicted shear stress distribution in the four AM series slabs along the short and long sides of the support plate perimeter at the peak load is shown in Figure 4-52. As expected, the shape of the shear stress distributions for slabs AM01, AM02, and AM04 are similar since all three slabs failed in punching shear. The shear stress distributions for these three specimens showed a high concentration of stress near the corner of the supported area and along the short side compared to the shear stress values along the long side near the center of the supported region. The shear stress at the corner of the supported area at the peak load for each specimen was approximately 6MPa. The shear stress values along the short side of the supported area for slabs AM01 and AM02 are higher than those predicted for slab AM04 which makes sense because the load was applied on the slab edges parallel to the short side of the supported region in the tests of slab AM01 and AM02. The

shape of the shear stress distribution for slab AM03 on the other hand is quite different. The peak shear stress did not occur at the corner of the supported region but occurred at some distance away from it. The peak shear stress along the long and short sides of the supported region occurred at an approximate distance of 50mm and 100mm away from the corner respectively. However, it is interesting that a distance greater than approximately 50mm from the corner of the supported area that the shear stress magnitudes along the long side are similar in all four specimens.

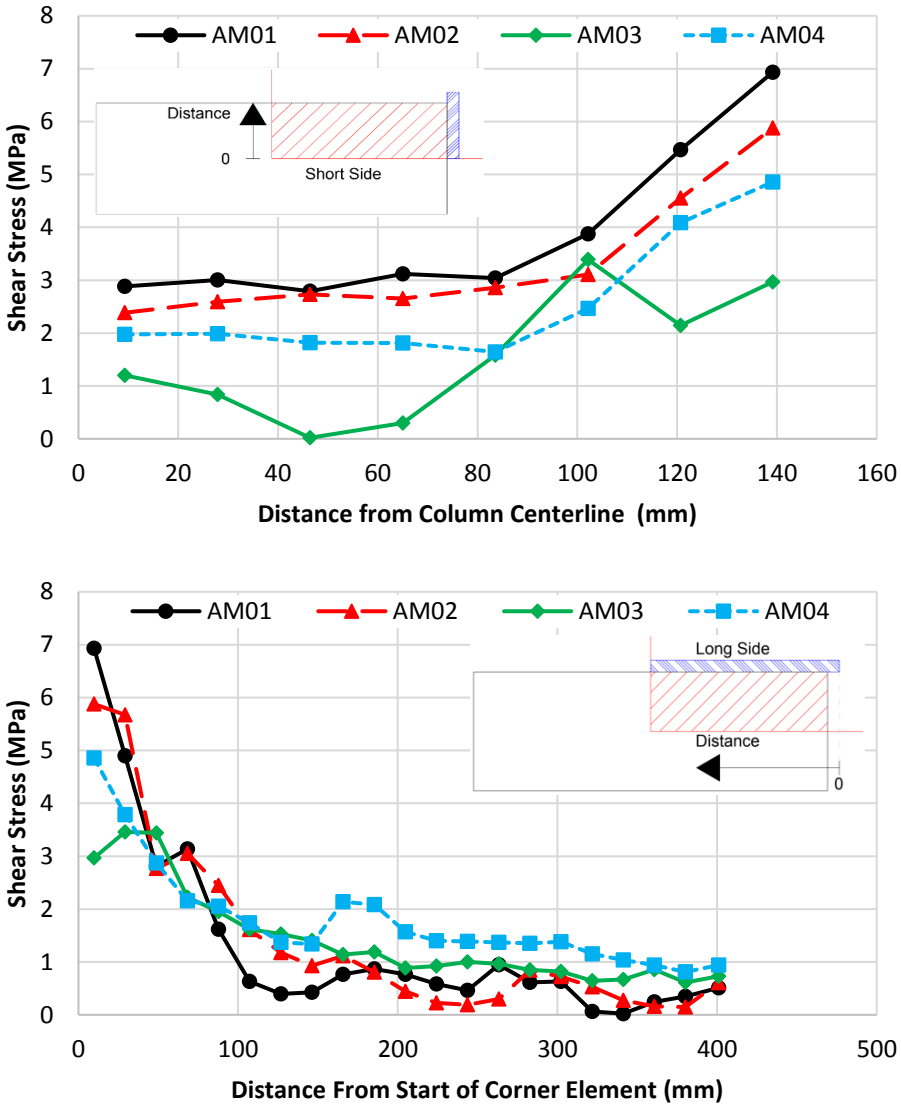

Figure 4-52: Predicted Shear Stress Distributions, AM Series Slabs

4.5.2 Select PT Series Slabs

4.5.2.1 Experimental Program

Sagaseta et al. (2011) tested seven reinforced concrete slabs to study the impact of non-axis symmetric flexural reinforcing layouts on punching shear behaviour. The slabs were 3m square in plan and 250mm thick, which matches the slabs in the AM series (Sagaseta, Muttoni, Fernández Ruiz, & Tassinari, 2011; Sagaseta, Tassinari, Fernández Ruiz, & Muttoni, 2014). Loading was applied through eight steel plates, whose centers were on the radius of contraflexure, and the slabs were supported on central 260mm square steel plates. Three of the seven slabs, PT22, PT31 and PT32 were modelled in ABAQUS to verify that the calibrated model was capable of predicting the behaviour of slabs supported on square columns and with different reinforcing ratios in each direction. A summary of the concrete compressive strength, average effective depth, flexural reinforcement diameter, tensile reinforcing ratio and flexural reinforcement yield strength in both orthogonal directions is provided in Table 4-13. All four slabs also included flexural reinforcement on the compression side of the slab, which consisted of 10mm diameter bars at the same spacing as the reinforcement on the tension side. Two yield strengths, 533MPa and 568MPa, are listed for the 10mm bars, but the specific yield strength for the bars used on the compression side in each slab was not provided.

Table 4-13: Summary of Material Properties for Select PT Slabs (Sagaseta, Muttoni, Fernández Ruiz, & Tassinari, 2011)

Slab	f_c' (MPa)	d_{avg} (mm)	Tensile Flexural Reinforcement		
			Bar diameter x-y (mm)	ρ_x-ρ_y (%)	f_{yx}-f_{yy} (MPa)
PT22	67.0	196	16-16	0.82-0.82	552-552
PT31	66.3	212	20-20	1.48-1.48	540-540
PT32	40.0	215	20-16	1.46-0.75	540-558

As seen in Table 4-13, PT22 and PT31 had symmetric reinforcing ratios, which matches slab AM04. However, these slabs had a much higher concrete compressive strength compared to slab AM04. PT32 was selected for the analysis since the concrete compressive strength was similar to slab AM04, but the flexural reinforcing was non-axis symmetric.

4.5.2.2 Finite Element Modelling

For slabs PT22 and PT31, the finite element model is the same as the AM04 model except that the uniaxial compressive stress-strain relationship by Thorendfeldt, Tomaszewicz and Jensen (1987), which is valid for concrete compressive strengths up 125MPa (MacGregor & Bartlett, 2000), was used in place of the Hognestad parabola, which is only valid for compressive strengths less than or equal to 60MPa. According to Thorendfeldt, Tomaszewicz and Jensen (1987), the uniaxial compressive stress-strain relationship for concrete can be calculated using equation 4.15

$$f_c = \left[\frac{n \times \left(\frac{\varepsilon_c}{\varepsilon_c'}\right)}{n - 1 + \left(\frac{\varepsilon_c}{\varepsilon_c'}\right)^{nk}}\right] f_c' \qquad (4.15),$$

where n is a constant equal to $0.8 + f_c'/17$, f_c' is the concrete compressive strength (MPa), ε_c' is the strain at peak stress calculated using equation 4.16, k is a constant which is equal to 1.0 when the total strain, ε_c, is less than the peak strain and is equal to the maximum of $0.67 + f_c'/62$ or 1.0 when the total strain exceeds the peak strain (MacGregor & Bartlett, 2000).

$$\varepsilon_c' = \frac{f_c'}{E_c}\left(\frac{n}{n-1}\right) \qquad (4.16),$$

where E_c is the initial elastic modulus of concrete which can be approximated as $4500\sqrt{f_c'}$ for normal density concrete (MacGregor & Bartlett, 2000). For slabs PT22 and PT31, $4500\sqrt{f_c'}$ was used for the elastic modulus in the ABAQUS models, compared to the value of $5000\sqrt{f_c'}$ used in the AM04 and PT32 analysis. A comparison of the concrete compression curve derived by Thorendfeldt, Tomaszewicz and Jensen (1987) and the Hognestad Parabola, which was presented in Section 4.3.2.2, is shown in Figure 4-53. As seen in Figure 4-53, the Hognestad Parabola predicts a more gradual post peak drop in capacity compared to the Thorendfeldt, Tomaszewicz and Jensen (1987) model. It is well known that concrete becomes more brittle as the compressive strength is increased, which is why the Hognestad parabola is invalid for concrete strengths exceeding 60MPa.

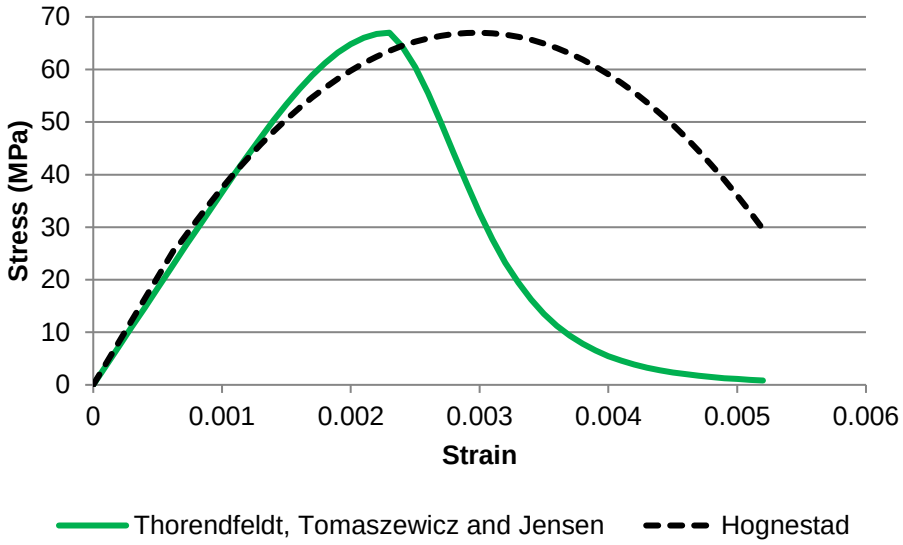

Figure 4-53: Comparison of Uniaxial Compression Curve by Thorendfeldt, Tomaszewicz and Jensen (1987) (MacGregor & Bartlett, 2000) and Hognestad Parabola

The finite element model for PT32 is the same as that for AM04 except that a half model is used instead of a quarter model due to the non-axis symmetric reinforcement layout. Since a half model is used, only one symmetry condition is applied in the model. Therefore, an additional lateral support boundary condition is required since the displacements in the X-direction are no longer restricted by symmetry. This additional lateral support boundary was applied on the base of the steel support plate. The pressure magnitudes are also modified to account for the different experimental capacities of the slabs. 3.7MPa pressure loads were used in the models for slabs PT22 and PT32 a 5.0MPa pressure was used in the PT31 model. The boundary conditions of the PT32 model are shown in Figure 4-54.

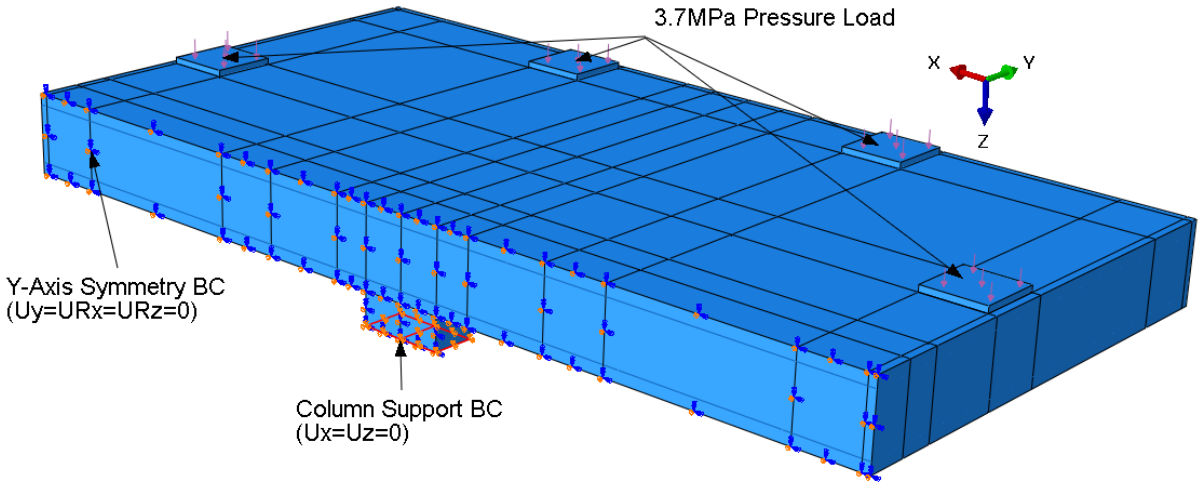

Figure 4-54: PT32 Model Boundary Conditions

As previously discussed, two yield strengths were provided for the 10mm bars by Sagaseta et al. (2011). In the PT slab models, the 10mm bars were assumed to have a yield strength of 568MPa which corresponds to the maximum value provided by Sagaseta et al. (2011). However, this assumed strength was found to have no impact on the final results as the axial stresses in the truss elements used to model the compression side reinforcement were very low (typically <100MPa). Therefore, defining the yield strength as 533MPa or 568MPa would not have any impact on the final results since the elastic modulus was defined as 200000MPa and the steel did not yield.

4.5.2.3 Finite Element Analysis Results

A summary of the predicted load capacity and rotation at failure compared to the experimental results for the selected PT slabs is provided in Table 4-14. The load-rotation curves for PT22, PT31 and PT32 predicted by the FEM and measured experimentally are provided in Figure 4-55.

Table 4-14: Comparison of FEA and Experimental Results, PT Series Slabs

Slab	Experimental			Finite Element Analysis			% Difference		
	Capacity, kN	ψ_x, mRad	ψ_y, mRad	Capacity, kN	ψ_x, mRad	ψ_y, mRad	Capacity	ψ_x	ψ_y
PT22	989	14.4	16.7	908.3	13.82	13.81	-8.2	-4.0	-17.3
PT31	1433	9.5	11.6	1225.0	9.29	9.29	-14.5	-2.2	-19.9
PT32	1157	10	12	961.4	8.93	12.22	-16.9	-10.7	1.9

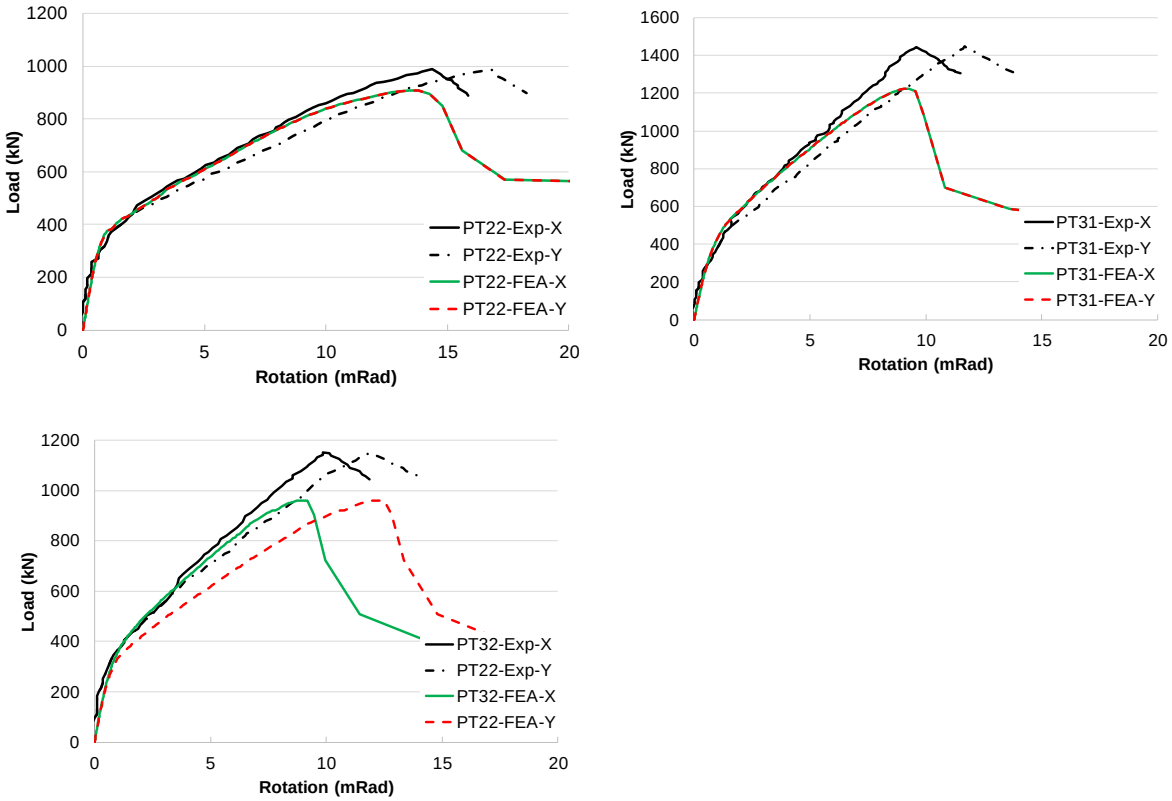

Figure 4-55: Comparison of Predicted and Measured Load-Rotation Plots – PT22, PT31 and PT32

Based on the percent differences in Table 4-14, the load-rotation plots in Figure 4-55 and the results for the AM series slabs discussed in Sections 4.4 and 4.5, it is clear that the calibrated finite element model is able to accurately estimate the load capacity of the six slabs which failed in shear (AM01, AM02, AM04 and all three PT slabs), and is typically conservative compared to the experimental results. The calibrated finite element model was also found to accurately predict the rotations at failure in both orthogonal directions for the investigated slabs. For PT22 and PT31 the FEM underpredicted the experimental rotation in the Y-direction by 17.3% and 19.9% respectively. However, these large errors are because the ABAQUS model is perfectly symmetric, and therefore, it predicts nearly identical responses in both directions. The experimental results on the other hand are slightly non-symmetric, and therefore, the difference between the predicted behaviour is larger. The ABAQUS model is not capable of capturing imperfections unless they are inputted into the model.

The stress distribution around the column perimeter were also analyzed for the three PT slabs. Since similar trends were observed for all three models only the stress distribution for PT22 is discussed. The stress distribution for slab PT22 is shown in Figure 4-56. As observed experimentally by various researchers, including Sherif and Dilger (1996), and Oliveria, Regan and Melo (2004), a concentration of shear stress was predicted at the corner of the supported area due to the 90 degree corners . However, the shear stress in the slab along the plate perimeter away from the corner were found to have approximately the same magnitude, which is expected due to the use of a square column (Vanderbilt, 1972; Filatov, 2017).

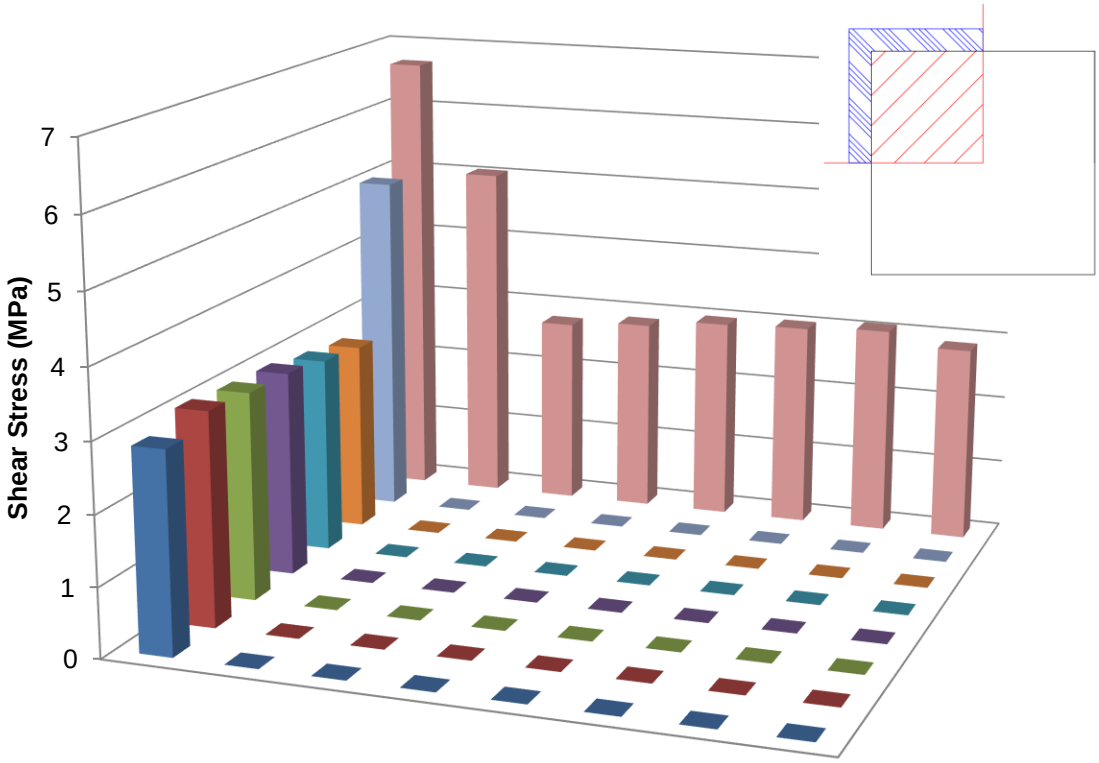

Figure 4-56: Predicted Shear Stress Distribution in the Slab Around the Steel Support Plate, PT22

4.6 Summary of Calibrated Model

A summary of the concrete and steel parameters in the calibrated AM04 model, which was used in the parametric study discussed in the next chapter, are provided in Table 4-15, Table 4-16 and Table 4-17. The specific Hognestad parabola and bilinear tensile stress-crack width relationship for slab

AM04, based on a concrete compressive strength of 44.6MPa, are provided in Figure 4-57 and Figure 4-58 respectively. When calculating the fracture energy, G_f, and the bilinear tensile stress-crack width response f_{ck} was calculated as $f_c' - 1.6\ (MPa)$ (Reineck, Kuchma, Kim, & Marx, 2003) which matches the work of Stoner (2015) and Barrage (2017).

Table 4-15: Summary of Concrete Parameters in Calibrated AM04 and Parametric Study Model

Concrete	
ABAQUS Material Model	Concrete Damaged Plasticity
Compression Model	Hognestad Parabola (see Figure 4-12 on page 84 for equations)
Tension Model	Bilinear tensile stress–crack width
Fracture Energy (G_f)	0.093N/mm (Calculated from Model Code 1990)
Dilation Angle	45°
Eccentricity (ε)	0.1 (ABAQUS Default)
Viscosity (μ)*	1.0×10^{-5} (not used in ABAQUS/Explicit)
σ_{bo}/σ_{co}	1.16 (ABAQUS Default)
K_c	0.667 (ABAQUS Default)
Damage Parameters	Not Included
Element Type	C3D8R
Approximate Element Size	20mm
Modulus of Elasticity (E_c)	33392MPa, Calculated as ($5000\sqrt{f_c'}$)
Poisson's Ratio (ν)	0

Table 4-16: Summary of Load and Support Plate Steel Parameters in Calibrated AM04 and Parametric Study Model

Steel – Load and Support Plates	
Material Model	Linear elastic
Modulus of Elasticity	200000MPa
Poisson's Ratio (ν)	0.3
Element Type	C3D8R
Approximate Element Size	20mm
Contacts	Load Plate and Slab – Cohesive Slab and Support Plate – Hard

Table 4-17: Summary of Flexural Rebar Steel Parameters in Calibrated AM04 and Parametric Study Model

Steel – Flexural Rebar	
Material Model	Linear elastic, perfectly plastic (see Figure 4-24 on page 99)
Modulus of Elasticity	200000MPa
Poisson's Ratio (ν)	0.3
Yield Strength (f_y)	516MPa (16mm bars), 526MPa (12mm bars)
Element Type	T3D2 (embedded in concrete elements)
Approximate Element Size	20mm
Depth to Tension Side Flexural Reinforcement	202mm (measured from compression surface)
Depth to Compression Side Flexural Reinforcement	43.55mm (measured from compression surface, assumed based on bar size and cover to tension side reinforcement)

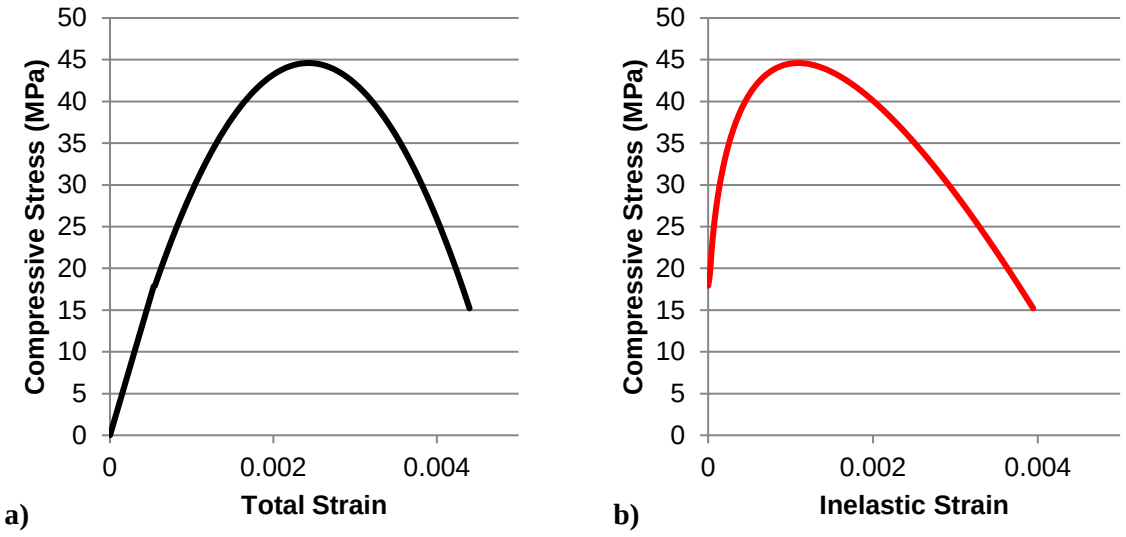

Figure 4-57: Hognestad Parabola used in AM04 and Parametric Study Finite Element Model a) Stress vs Total Strain b) Stress vs Inelastic Strain (Inputted into ABAQUS)

Tensile Stress (MPa)	Crack Width (mm)
2.204	0.0
0.735	0.0341
0*	0.1533

*ABAQUS sets the minimum stress at 10^{-2} times the initial stress

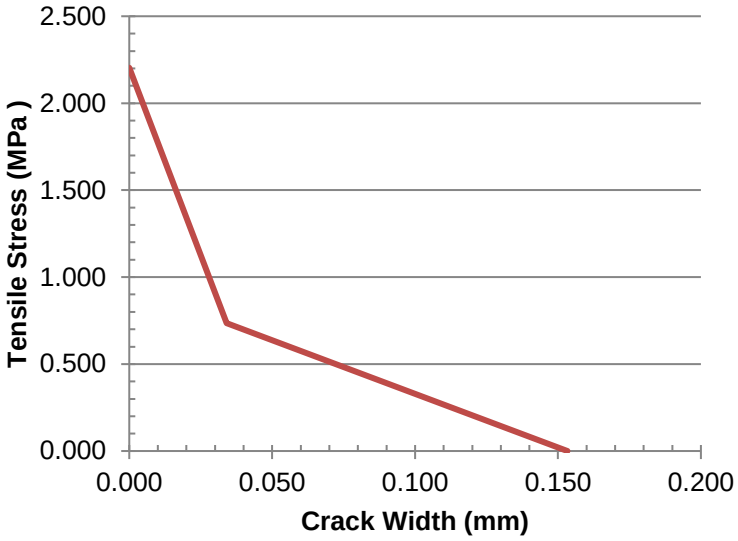

Figure 4-58: Bilinear Tensile Stress-Crack Width Relationship, AM04 and Parametric Study Model

Chapter 5: Parametric Study of Column Rectangularity

In this Chapter, the parametric study of column rectangularity carried out in ABAQUS using the calibrated AM04 model is discussed. Firstly, the methodology used to arrive at the models included in the study will be discussed. Secondly, the results of the parametric study are presented and discussed.

5.1 Parametric Study Setup

Firstly, the impact of column rectangularity predicted by numerous design codes is compared. Next, an overview of the models included in the parametric study and the constraints imposed by the use of the AM04 specimen are discussed.

5.1.1 Comparison of Code Provisions

As outlined in Section 2.5, current and historical design codes differ in how they consider column rectangularity. ACI 318M-14 reduces the nominal shear capacity along the critical perimeter using equations based on the column aspect ratio and the ratio of the critical perimeter length to the effective slab depth. The 2004 edition of Eurocode 2 only accounted for column rectangularity when the slab-column connection was subjected to unbalanced moments. Earlier drafts of EC2 accounted for column rectangularity by considering portions of the critical perimeter to be ineffective in carrying punching shear when the column dimensions exceeded specific values. Model Code 1978 was similar to the drafts of EC2 except that the entire critical perimeter length was assumed to contribute to the shear capacity of the connection, although portions of the critical perimeter were assumed to have a lower shear capacity. Model Code 2010 is similar to the drafts of EC2 where portions of the critical perimeter length are assumed to have zero shear capacity. In Model Code 2010 the maximum critical perimeter length per column side is three times the slab depth.

For each code which accounts for column rectangularity, a reduction factor can be calculated, and compared to those calculated from the other codes, to contrast the impact of column rectangularity in each code. The estimated reduction factors for ACI 318M-14, Model Code 1978 and Model Code 2010 for column aspect ratios between 1 and 10 for multiple ratios of the minimum column dimension to effective slab depth (c_{min}/d) are shown Figure 5-1. These three codes were compared as they form the basis of many codes worldwide and all assume the critical perimeter to be located at d/2 from the column face. Reduction factors for additional c_{min}/d ratios are provided in Appendix C.

The reduction factor for ACI 318M-14 is quite obvious. The general form of the ACI 318M-14 provisions is some constant, denoted α in this thesis, multiplied by the square root of the concrete compressive strength. For a square column, α is equal to 0.33 according to equation 2.6 in Section 2.5.2. If equation 2.7, which is dependent on the column aspect ratio, or equation 2.8, which is dependent on the ratio of critical perimeter length to effective depth govern, α will be less than 0.33. Therefore, the reduction factor for ACI 318M-14 was calculated as α divided by 0.33.

For both investigated Model Codes, a reduction factor with a similar form to that from ACI 318M-14 cannot be derived, since the code equations do not directly include a term to account for column rectangularity or column size. However, both codes require the calculation of the total critical perimeter length, b_1 , and an effective critical perimeter length, b_o . Following the work of Sagaseta et al. (2014), the reduction factor for both Model Codes is taken as b_o/b_1.

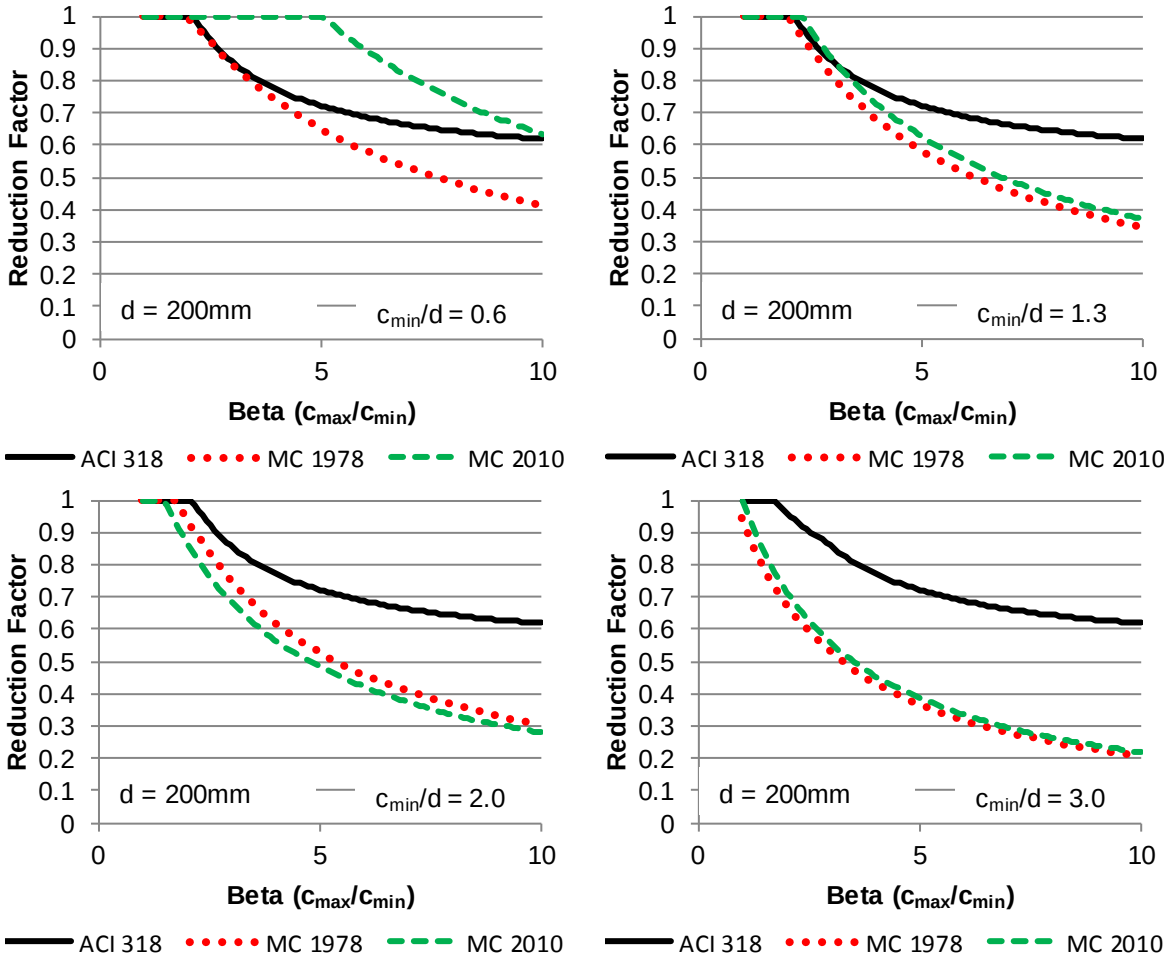

Figure 5-1: Reduction Factors for ACI 318 and Model Code 1978 and 2010 for d =200mm

From Figure 5-1 numerous conclusions are drawn. Firstly, it can be concluded that the impact of column rectangularity in both Model Codes varies depending on the c_{min}/d ratio, whereas the ACI 318M-14 provisions are nearly independent of c_{min}/d. The ACI 318M-14 reduction factors for c_{min}/d ratios less than 2 are identical, and only slight reductions in the reduction factor for column aspect ratios between 1.5 and 3 are observed for a c_{min}/d ratio of 3. Secondly, for c_{min}/d ratios approximately equal to 1, which are common in practice (Sagaseta, Tassinari, Fernández Ruiz, & Muttoni, 2014), the three design codes predict similar reduction factors for column aspect ratios less than or equal to 5. Thirdly, for very low c_{min}/d ratios the reduction factors for Model Code 1978 and ACI 318M-14 are similar for column aspect ratios less than or equal to 5. For these very low c_{min}/d ratios Model Code 2010 predicts that column rectangularity does not have a negative impact on punching capacity until the column aspect ratio is quite large (i.e. >6). This lack of rectangularity impact for low c_{min}/d ratios is because the Model Code 2010 provisions assume that portions of the critical perimeter within 1.5d from the column corner in each direction are effective in resisting punching shear.

5.1.2 Investigated Models and Considered Factors

Based on the design code comparison in the previous section, it was observed that Model Code 1978 and Model Code 2010 do not predict the same impact of column rectangularity for different c_{min}/d ratios, whereas ACI 318M-14 predicts a similar impact for all investigated c_{min}/d ratios. Additionally, the difference between the reduction factors from ACI 318M-14 and the two Model Codes increased as the c_{min}/d ratio increased.

Varying impact of column rectangularity for different c_{min}/d ratios was also observed during the FEM calibration described in Chapter 4. In the SB1 rectangularity study, a very minimal impact of column rectangularity on punching capacity was observed for aspect ratios between 1 and 11. However, since the length of the critical perimeter was kept constant in the SB1 rectangularity study, the c_{min}/d ratio decreased as the column aspect ratio increased. The limited impact of column rectangularity observed agrees well with the Model Code 2010 reduction factor for low c_{min}/d ratios (i.e. 0.6).

The observed impact of column rectangularity was more severe in the Hawkins' slab analysis. In this analysis, the typical c_{min}/d ratio of the slab-column connections was 1.3, with a minimum and maximum value of 0.9 and 2.6 respectively. For a c_{min}/d ratio of 1.3, all three investigated codes predict a significant impact of column rectangularity on punching capacity.

Therefore, based on the code provision comparison and the FEM calibration results, two parameters, the c_{min}/d ratio and the column aspect ratio, were investigated in the parametric study. A summary of the models included in the parametric study is provided in Table 5-1 and a detailed breakdown of the column dimensions and rectangularity values is provided in Appendix D.

Table 5-1: Summary of Models Included in Parametric Study

c_{min}/d ratio					Minimum	Maximum
Desired	Actual	# of studies	Min. β	Max. β	c_{max}/L	c_{max}/L
0.5	0.594	19	1.000	10.000	0.018	0.178
0.75	0.792	15	1.000	8.000	0.024	0.190
1	0.990	12	1.000	6.600	0.030	0.196
1.25	1.287	9	1.000	5.077	0.039	0.196
1.5	1.485	7	1.000	4.000	0.044	0.178
1.75	1.782	6	1.000	3.556	0.053	0.190
2	1.980	5	1.000	3.000	0.059	0.178
3	2.970	3	1.000	2.000	0.089	0.178

As shown in Table 5-1, the desired c_{min}/d ratios do not match the investigated c_{min}/d ratios. Modifications to the desired c_{min}/d ratios were required due to the AM04 geometry and use of 20mm elements. According to the ABAQUS user manual, the aspect ratio of C3D8R elements should be close to 1 for accurate results (Dassault Systemes Simulia Corp., 2012). Therefore, the investigated c_{min}/d ratios were partly chosen to ensure mesh uniformity. For the investigated c_{min}/d ratios, the minimum element side length was 18.5mm. The investigated c_{min}/d ratios are within the range of those included in the ACI 445 punching shear database. For slabs supported on square columns, the minimum, maximum and average c_{min}/d ratios are 0.528, 8.40 and 2.43 respectively. For slabs supported on rectangular columns, the minimum, maximum and average c_{min}/d ratios of the collected tests are 0.94, 4.20 and 2.65 respectively (Ospina, et al., 2015)

The use of partitions in the FEM, as shown in Figure 5-2a, also influenced the c_{min}/d ratios and column rectangularities which were considered in the parametric study. Partitions were used to limit mesh skewing, ensure alignment of the load and support plate meshes with the slab mesh and to ensure elements lied along the ACI critical perimeter. When partitions are used in ABAQUS the meshing algorithm ensures that nodes of the elements are placed along the partition line. However, the use of partitions can also lead to meshing issues (very small elements etc.) if the partitions are spaced at values which are not a multiple of the global mesh size.

In order to extract the shear stress distributions along the ACI critical perimeter partitions were created parallel and perpendicular to the column sides. The first set of partitions were located along the edges of the support plate and extended to the slab edge to ensure the element size along the slab edges matched that in the area above the support plate. The second set of partitions were parallel to the first partitions, and were used to ensure elements lied along the critical perimeter at d/2. For all models, except for the model of AM04, the two sets of partitions were spaced at a distance of 100mm as shown in Figure 5-2a, which is the approximate value of d/2 for slab AM04 (101mm). For the AM04 model, the distance between the partitions was increased to 110mm to avoid meshing issues caused by the partitions for the bottom right load plate.

Since the overall slab size and the load plate locations were kept constant in the models, the bottom right load plate partitions impacted the investigated column dimensions as shown in Figure 5-2c. Column dimensions were chosen to ensure 20mm element side lengths within the load plate partition areas to ensure alignment of the slab mesh and load plate meshes in this area. The column size shown in Figure 5-2c also corresponds to the maximum column height considered in the parametric study.

The minimum column size and maximum column width considered in the parametric study are shown in Figure 5-2b and Figure 5-2d respectively. Due to the overall size of AM04, the maximum column rectangularity and number of studies for each c_{min}/d ratio decreased as the c_{min}/d ratio increased. It was desired to investigate column rectangularities at increments of 0.5, but due to the reasons outlined above the investigated column rectangularities were also adjusted to ensure mesh sizes of approximately 20mm.

Finally, the ratio of the maximum column dimension, c_{max}, to the slab span, L, was considered when selecting column dimensions in the parametric study. As discussed in Section 2.6.3, Simmonds (1970) concluded that reinforced concrete slabs behave as one-way slabs when the c_{max}/L ratio exceeds 0.4 in either orthogonal direction, based on the results of a linear elastic finite difference analysis of a multiple bay slab system. On the basis of linear elastic finite element analysis, Sagaseta et al. (2014) found that reinforced concrete slabs begin to behave as one-way slabs when the c_{max}/L ratio exceeds 0.35. The highest value of c_{max}/L for the parametric studies was found to be approximately 0.2 as shown in Table 5-1, and therefore, one way-behaviour was not expected to govern any of the proposed models. The slab span was estimated as 25 times the slab thickness based on tests by Guandalini, Burdet and Muttoni (2009) which were geometrically similar to AM04.

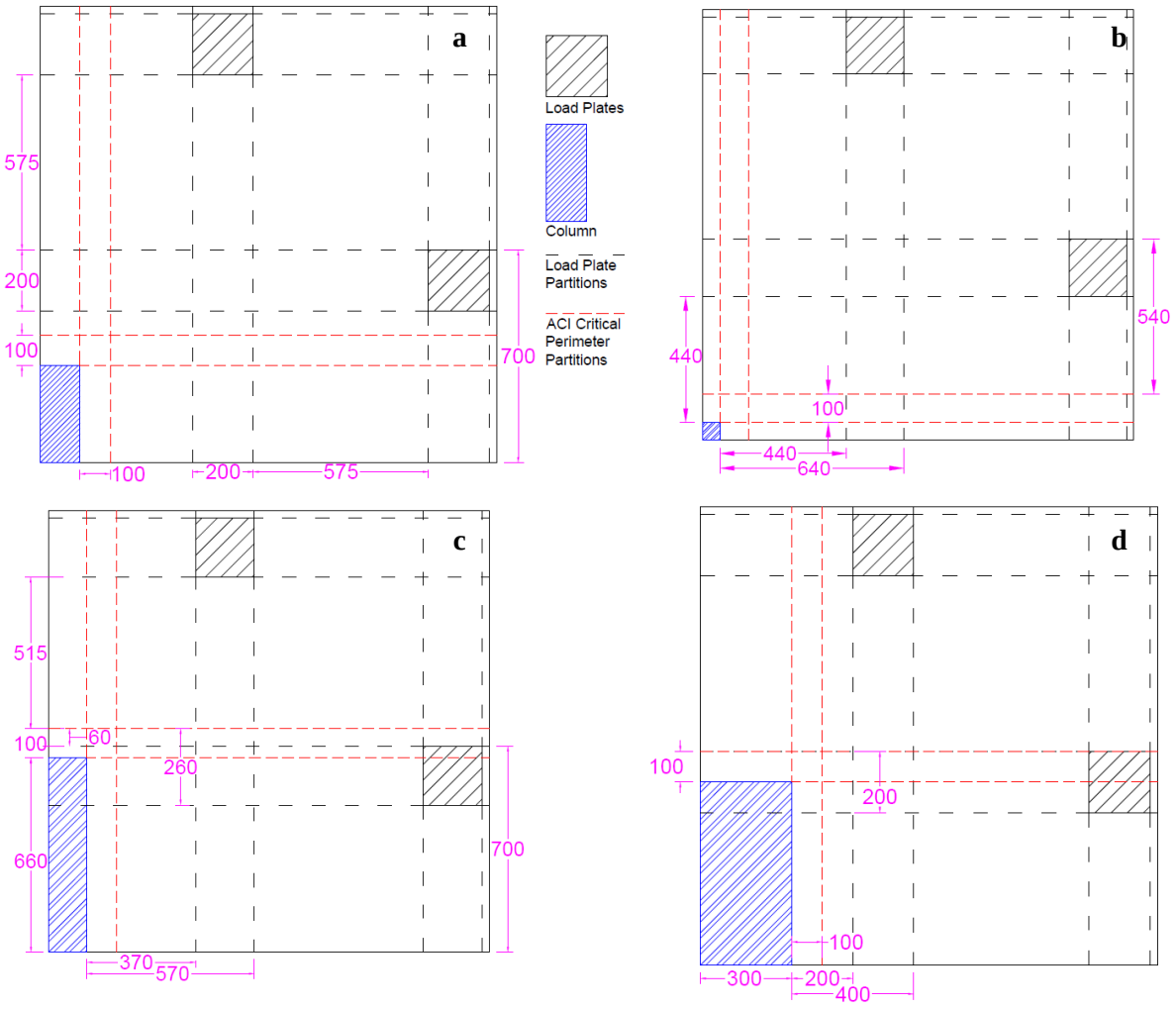

Figure 5-2: Considerations When Selecting Column Dimensions, a) Overall Layout b) Minimum Column Size (60x60mm), c) Maximum Column Height (660mm) d) Maximum Column Width (300mm)

Since the calibrated model for slab AM04, which is summarized in Table 4-15, Table 4-16 and Table 4-17 in Section 4.6, was used in the parametric study, the following parameters were consistent between all models in the parametric study:

- Overall slab dimensions, plan – 3000x3000mm (1500x1500mm quarter model used in FEA)
- Slab thickness – 250mm
- Load Plate Location
- Maximum aggregate size – 16mm
- Concrete compressive strength – 44.6MPa

- Concrete tensile strength – 2.204MPa (approximated as $0.33\sqrt{f_c'}$)
- Average effective depth (tension side) – 202mm
- Average effective depth (compression side) – 43.55mm
- Tension side reinforcement – 16mm diameter bars at 125mm o/c (f_y = 516MPa)
- Compression side reinforcement – 12mm diameter bars at 125mm o/c (f_y = 526MPa)

5.2 Discussion of FEA Results for Each C_{min}/d Ratio

The purpose of this section is to present and discuss the parametric study results specific to each individual c_{min}/d ratio. A discussion of the results for all c_{min}/d ratios is provided in Section 5.3. The results will be presented in the following order:

1. Total shear capacity and load-displacement behaviour predicted by FEA
2. Comparison of punching capacity predicted by FEA and design codes (ACI 318M-14, Eurocode 2 (2004), Model Code 2010, Critical Shear Crack Theory (CSCT))
3. Comparison of nominal shear stress predicted by FEA and design codes along the ACI 318 critical perimeter
4. Analysis of shear stress distributions around the support plate perimeter predicted by FEA
5. Predicted crack patterns

In the following discussion, the X and Y-directions are consistent with the experimental setup of AM04. Therefore, the Y-direction is perpendicular to the short side of the support plate and the X-direction is perpendicular to the long side of the support plate, as shown in Figure 5-3. In this section, the support plate is also referred to as a column or supported area.

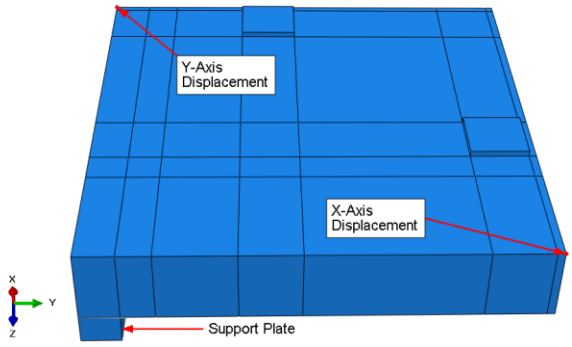

Figure 5-3: Displacement Locations used in Parametric Studies

The displacements reported in this section are the vertical displacements at the locations shown in Figure 5-3. As such, the displacements referred to in the provided tables and plots in the X-direction (Δ_X) and in the Y-direction (Δ_Y) correspond to the vertical displacement of the slab as shown in Figure 5-4.

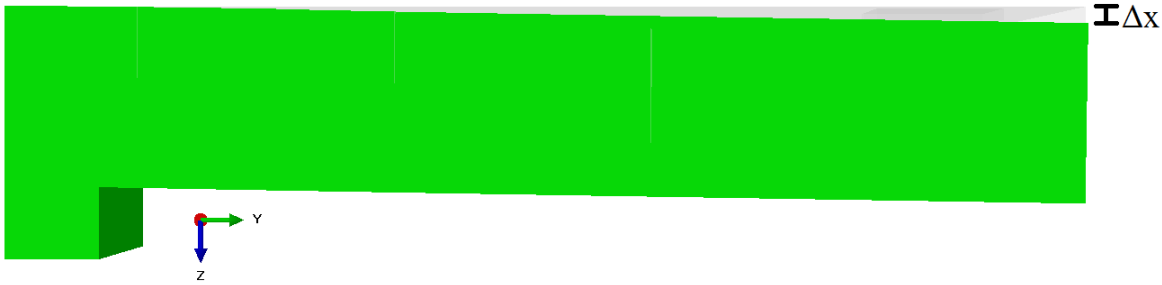

Figure 5-4: Vertical Deflection of Slab Recorded During FEA (X-direction Shown)

For the code predictions discussed in this section the following assumptions were made. The Eurocode 2 (2004) provisions are given in terms on characteristic compressive strength. Following the work of Reineck, Kuchma, Kim and Marx (2003), the characteristic concrete strength was assumed to be equal to the concrete compressive strength, f_c', minus 1.6MPa. The predictions for all other design codes used f_c'. Additionally, the average reinforcing ratio of AM04, 0.75%, was used when computing the punching resistance of all slabs in the parametric study. As with the Hawkins' slab study, the provisions requiring the reinforcing ratio to be calculated over a total width equal to three times the column width plus three times the effective slab depth on each side of the column were neglected to remove the influence of reinforcing ratio on the predictions. For both the Model Code 2010 and the CSCT predictions, the rotations at failure in both orthogonal directions predicted from the FEA were used, instead of the analytical equations to estimate slab rotations. The use a calibrated non-linear finite element analysis to estimate slab rotations corresponded with the LoA IV in Model Code 2010, which is the highest level of approximation available, and in theory should provide the most accurate estimates of shear capacity (Genikomsou A. , 2015). For both the Model Code 2010 and the CSCT predictions, the critical perimeter was divided into X and Y components as discussed in Section 2.5.5, instead of using the maximum rotation from the two orthogonal directions.

The crack patterns for all investigated c_{min}/d ratios and rectangularity values are provided in Appendix F. The crack patterns are not provided in the body of this thesis to allow the reader to easily compare the crack patterns as β is increased.

5.2.1 $C_{min}/d = 0.594$

A summary of the column dimensions, column rectangularity values (β), predicted capacity and predicted deflections at peak load in the X and Y-directions for the models with a c_{min}/d ratio of 0.594 are provided in Table 5-2. The load-displacement plots for the integer values of β are provided in Figure 5-5, and the remaining load-displacement plots can be found in Appendix E. Based on the results provided in Table 5-2 and Figure 5-5, it was observed that the FEM generally predicts a higher shear capacity as the column size, and rectangularity, are increased. This increase in shear capacity is expected since the overall column area, and length of the critical perimeter, are increased as the column rectangularity is increased.

Table 5-2: Summary of FEA Results for $c_{min}/d = 0.594$

c_{min} (mm)	c_{max} (mm)	β	Predicted Capacity (kN)	Δ_X (mm)	Δ_Y (mm)
120	120	1.000	625.6	12.23	12.23
120	200	1.667	674.0	13.27	13.19
120	240	2.000	685.2	13.62	13.47
120	320	2.667	760.1	15.71	15.25
120	360	3.000	794.6	17.13	16.37
120	440	3.667	837.2	17.99	16.80
120	480	4.000	852.2	18.96	17.39
120	560	4.667	876.6	18.67	16.88
120	600	5.000	889.3	18.65	16.58
120	680	5.667	903.4	19.36	16.73
120	720	6.000	902.4	19.69	17.02
120	800	6.667	965.2	21.87	17.59
120	840	7.000	985.1	22.89	17.81
120	920	7.667	993.6	22.43	17.05
120	960	8.000	992.2	21.60	16.16
120	1040	8.667	1014.8	23.12	16.09
120	1080	9.000	1017.2	25.24	15.83
120	1160	9.667	1019.0	24.83	14.62
120	1200	10.000	1022.0	25.83	14.07

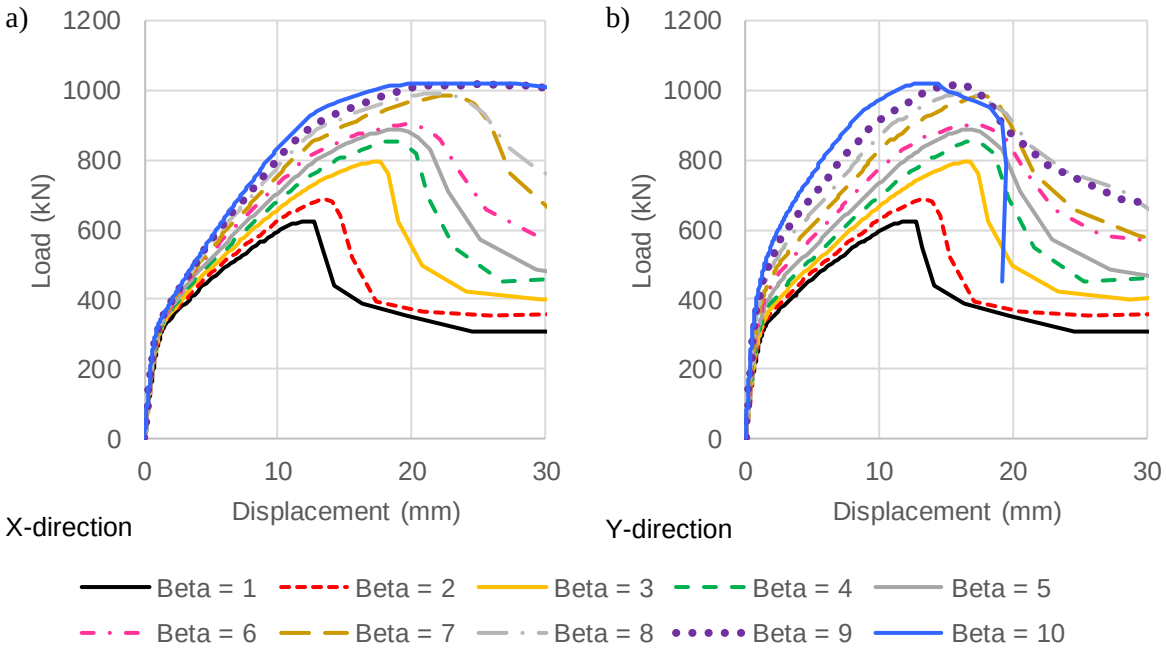

Figure 5-5: Predicted Load-Displacement Response, $c_{min}/d = 0.594$

After analyzing the post failure deflected shapes predicted by the FEM, it was concluded that all the analyzed slabs were predicted to fail due to punching, although the higher rectangularity values (i.e. β>8.667) appeared to be transitioning from punching (two-way shear) behaviour to one-way shear behaviour, as the predicted maximum principal plastic strains, which represent concrete cracking, were beginning to concentrate in a line parallel to the long side of the column. An example of the typical deflected shape associated with punching shear failure is provided in Figure 5-6. It should be noted that the model with a support plate aspect ratio of 10 was predicted to initially fail in punching, before a secondary one-way shear failure was predicted in the next recorded analysis frame. Therefore, this model, which had a maximum support plate dimension of 600mm, was believed to represent the transition point between two-way and one-way shear failure.

Overall, there was no trend in the predicted deflections. For the models with β less than 4.667, the deflections in both orthogonal directions typically increased as the column rectangularity was increased. However, after this point the deflections in both directions stayed approximately constant until β equaled 5. After this point, the deflections in the X-direction typically increased as the rectangularity was increased. The deflections in the Y-direction increased until β equaled 7.667 before decreasing with increasing column rectangularity. It is possible that the deflections in the Y-

direction decreased as β is increased beyond 7.667 because the length of the supported area in this direction approached 40% of the isolated specimen length for these larger support areas.

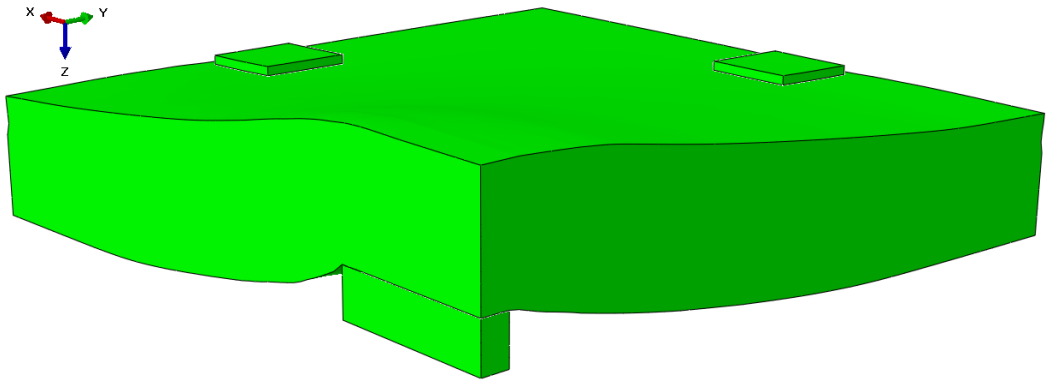

Figure 5-6: Post-Punching Deflected Shape, β = 6, c_{min}/d = 0.594

The predicted stiffness of the slabs in both orthogonal directions increased as the column rectangularity was increased. In both the linear elastic and plastic portions of the slab's response, the stiffness increase in the Y-direction was larger. In the X-direction the change in stiffness in the linear elastic portion of the response was rather small, and although a larger increase in stiffness was observed in the plastic region, the increase in stiffness in the X-direction was still smaller than that observed in the Y-direction. The overall stiffness was also found to be higher in the Y-direction, which matches experimental results by other researchers (Tan & Teng, 2005; Anggadjaja & Teng, 2008; Himawan & Teng, 2014).

As previously mentioned, the FEA results are compared with the code predictions according to design methods and codes used in the United States and Europe, ACI 318M-14, Eurocode 2 (2004), Model Code 2010 and the CSCT. All of these design methods and codes are based on the critical shear perimeter concept, although the shape and location of the critical perimeter is not consistent between them. None of the investigated methods or codes includes a term to directly account for the c_{min}/d ratio.

A comparison of the shear capacity predicted by the FEA to ACI 318M-14 (ACI), Eurocode 2 (2004) (EC2), Model Code 2010 (MC 2010) and the Critical Shear Crack Theory (CSCT) is provided for a subset of the models in Figure 5-7, and for all the models with a c_{min}/d ratio of 0.594 in Figure 5-8 and Table 5-3. An additional bar chart similar to Figure 5-7 is provided in Appendix E for the remaining rectangularity values.

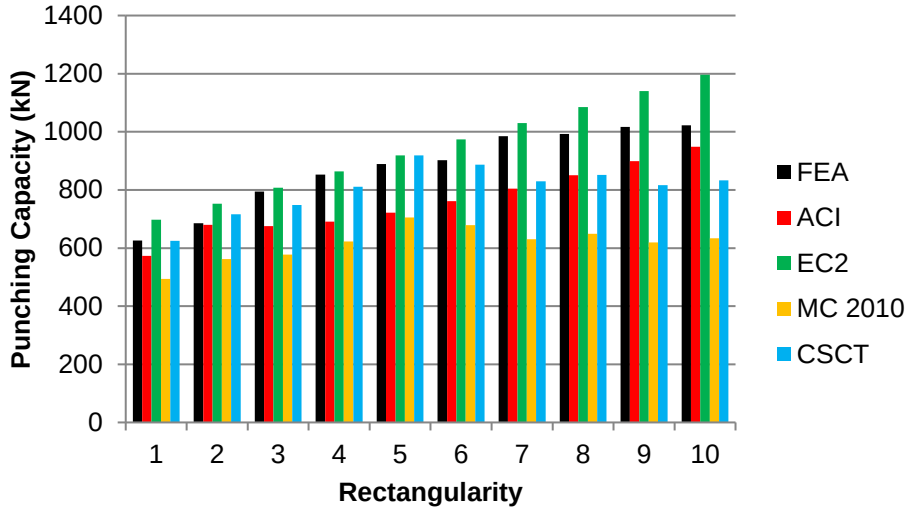

Figure 5-7: Comparison of Shear Capacity Predicted by FEA and Various Design Codes, Integer β Values only, $c_{min}/d = 0.594$

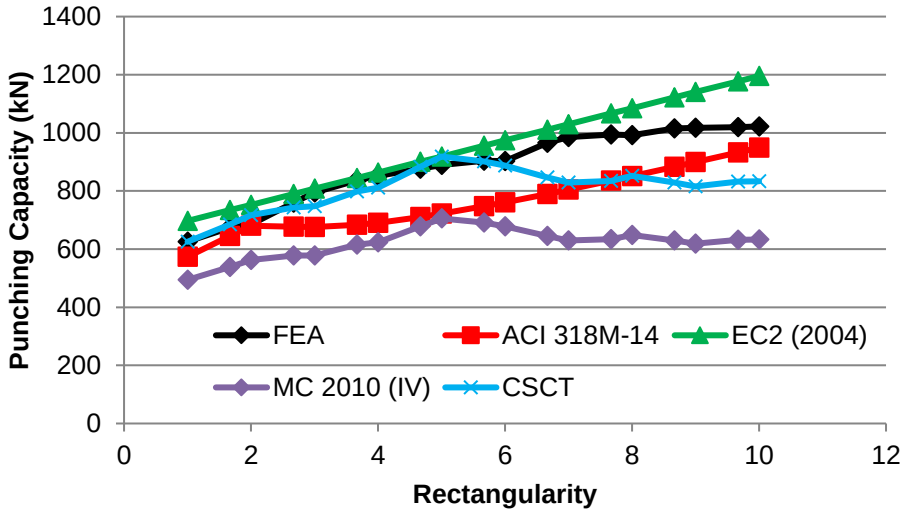

Figure 5-8: Comparison of Shear Capacity Predicted by FEA and Various Design Codes, all Investigated β values, $c_{min}/d = 0.594$

Table 5-3: Comparison of Code Predictions and FEA Results – $c_{min}/d = 0.594$

c_{min} (mm)	c_{max} (mm)	β	FEA Capacity (kN)	V_{FEA}/V_{ACI}	V_{FEA}/V_{EC2}	V_{FEA}/V_{MC2010}	V_{FEA}/V_{CSCT}
120	120	1.000	625.6	1.09	0.90	1.27	1.00
120	200	1.667	674.0	1.05	0.92	1.25	0.98
120	240	2.000	685.2	1.01	0.91	1.22	0.96
120	320	2.667	760.1	1.12	0.96	1.32	1.02
120	360	3.000	794.6	1.18	0.98	1.37	1.06
120	440	3.667	837.2	1.23	0.99	1.36	1.05
120	480	4.000	852.2	1.23	0.99	1.37	1.05
120	560	4.667	876.6	1.23	0.97	1.29	0.99
120	600	5.000	889.3	1.23	0.97	1.26	0.97
120	680	5.667	903.4	1.21	0.95	1.31	1.00
120	720	6.000	902.4	1.19	0.93	1.33	1.02
120	800	6.667	965.2	1.22	0.95	1.50	1.14
120	840	7.000	985.1	1.22	0.96	1.56	1.19
120	920	7.667	993.6	1.19	0.93	1.57	1.19
120	960	8.000	992.2	1.17	0.91	1.53	1.16
120	1040	8.667	1014.8	1.15	0.90	1.61	1.22
120	1080	9.000	1017.2	1.13	0.89	1.64	1.25
120	1160	9.667	1019.0	1.09	0.87	1.61	1.23
120	1200	10.000	1022.0	1.08	0.85	1.61	1.23
			Average	1.16	0.93	1.42	1.09
			COV (%)	6.02	4.33	10.42	9.43

The ACI 318M-14, Model Code 2010 and CSCT provisions are conservative compared to the FEA predictions for a c_{min}/d ratio of 0.594, whereas the Eurocode 2 (2004) provisions are not. Both ACI 318M-14 and EC2 (2004) predict a larger total shear capacity as the column rectangularity is increased. This was expected since the overall column size, and the length of critical perimeter assumed to carry shear in both codes, increased as the column rectangularity is increased. For column aspect ratios less than or equal to 5, the Model Code 2010 and CSCT provisions also predict an increased shear capacity as β increased. For column aspect ratios greater than 5, the capacities predicted by Model Code 2010 and the CSCT are approximately constant; because the effective perimeter length using the 3d method is less than the total critical perimeter length.

On average, the capacity predictions according to ACI 318M-14, EC2 (2004), Model Code 2010 and the CSCT are 16% lower, 7% higher, 42% lower and 9% lower than the capacity predicted by the FEM respectively. The EC2 (2004) predictions were found to be most accurate, but unconservative, for column rectangularity values between 3 and 7 (V_{FEA}/V_{EC2} is between 0.95 and 0.99). For these same rectangularity values, the ACI predictions were found to be the most inaccurate, but

conservative (V_{FEA}/V_{ACI} is between 1.18 and 1.23). The CSCT provisions were the most accurate for rectangularities between 1 and 6 and were generally conservative compared to the FEA results (V_{FEA}/V_{CSCT} is between 0.96 and 1.06). The Model Code 2010 provisions were also found to be most accurate for column aspect ratios between 1 and 6, but were very conservative compared to the FEA results (V_{FEA}/V_{MC2010} is between 1.22 and 1.37). For rectangularities greater than 6 the predictions according to the CSCT and Model Code 2010 became more conservative, whereas the predictions according to ACI 318M-14 and EC2 (2004) generally became less conservative and more unconservative respectively. The EC2 (2004) provisions were found to have the least variation based on the coefficient of variation of the ratio of V_{CODE}/V_{FEA}. None of the investigated specimens were predicted to fail in one-way shear by ACI 318M-14 or EC2 (2004), which matches the FEA results.

In order to compare the impact of column rectangularity predicted by EC2 (2004), Model Code 2010 and the CSCT to the FEA and ACI 318M-14 predictions, a normalized nominal shear stress around the ACI critical perimeter, v_{norm}, was calculated using equation 5.1, which was originally presented as equation 4.3 in Section 4.3.1.

$$v_{norm} = \frac{V_{pre}}{b_{o,ACI} d \sqrt{f_c'}} \tag{5.1}$$

where V_{pre} is the shear capacity predicted by the design code being considered (N), $b_{o,ACI}$ is the length of the ACI 318 critical perimeter (mm), d is the effective slab depth (mm), and f_c' is the concrete compressive strength (MPa).

A comparison of the normalized nominal shear stress predicted by ACI 318M-14, EC2 (2004), Model Code 2010, the CSCT and the finite element model along the ACI critical perimeter located at d/2 from the column perimeter is provided in Figure 5-9. As expected, based on the total capacity estimates, the nominal shear stress predicted by ACI 318M-14 is conservative when compared to the finite element model. However, it should be noted that the finite element model predicts an approximately linear response, compared to the curved response predicted by ACI 318M-14. The difference in these behaviours (linear vs curved) is why the ACI predictions were found to most conservative for the intermediate rectangularity values. For intermediate rectangularity values the ACI predictions predict a steep drop in nominal stress, which becomes asymptotic as the rectangularity increases. For example, between a β value of 2 and 4 the ACI 318 method predicts a drop in nominal shear stress from 2.2 MPa to 1.7MPa. However, between β values of 6 and 8 the ACI 318 method predicts a drop in nominal capacity of 1.51MPa to 1.42MPa. Additionally, the finite

element model predicts an impact of rectangularity for β values between 1 and 2 which is different than the ACI 318 method, which assumes slight rectangularity does not have a negative impact on punching capacity based on the results of Hawkins et al. (1971).

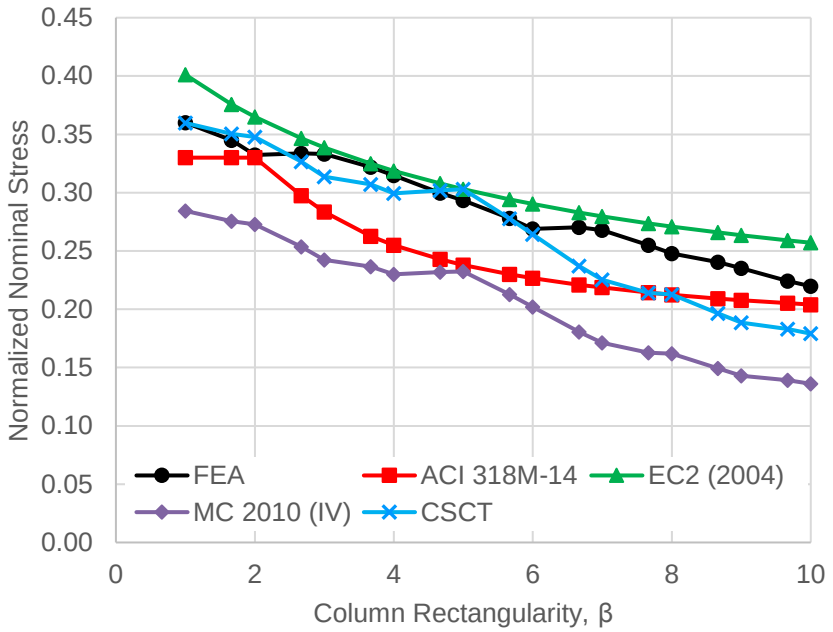

Figure 5-9: Comparison of Nominal Shear Capacity Predicted by FEA and Design Codes, c_{min}/d = 0.594

Overall, the trend of the normalized nominal shear stress predicted by EC2 (2004) is similar to that of the FEM, though the code predictions do deviate for very small (β<2) and very large (β>8.667) aspect ratios. However, as expected based on the capacity comparisons, the normalized nominal shear stress predicted by EC2 (2004) is typically higher than that from the FEM. Again, the EC2 provisions are found to be fairly accurate for rectangularity values between 3 and 7. Unlike ACI 318M-14 the EC2 provisions predict a decrease in the normalized nominal shear stress for rectangularity values between 1 and 2, which matches the FEA results. Like the ACI 318M-14 predictions the impact of column rectangularity in EC2 (2004) is curved, and becomes less severe as β is increased.

The trend of the normalized nominal stress based on the CSCT provisions is also similar to that from the FEA especially for rectangularities between 1 and 6. Unlike the total capacity estimates, which were approximately constant for column aspect ratios greater than 6, the predicted normalized nominal shear stress continues to decrease as β is increased. The nominal shear stress continues to

decrease because the predicted capacity, which is approximately constant, is divided by the length of the ACI 318M-14 perimeter, which increases in length as β is increased. The trend of the normalized nominal shear stress calculated from Model Code 2010 correlated well with the FEA results and is almost identical to the trend of the CSCT predictions. Based on Figure 5-8 and Figure 5-9, it is clear that Model Code 2010 provisions are a very conservative version of the CSCT predictions. As such, for all subsequent c_{min}/d ratios only the trends of the CSCT predictions will be discussed.

The shear stress distributions in the slab around the column perimeter at the peak load calculated from the FEA results for the investigated integer rectangularity values are provided in Figure 5-10. The overall shape of the shear stress distribution was found to be similar for all rectangularity values. For the slab supported on a square steel plate, the shear stress distribution around both sides of the plate was approximately symmetric. For the slabs supported on rectangular plates, a concentration of shear stress was observed at the corner of the supported area and along the short side of the supported area. Along the long side of the support plate, the predicted shear stress decreases in magnitude as the distance from the corner is increased. It is interesting that the shear stress levels at a specific distance from the column corner are similar for all investigated rectangularity values. For example, at a distance of approximately 100mm from the start of the corner element the predicted shear stress level is approximately 2 to 2.5MPa for all models. The shear stress distributions for the remaining rectangularity values are provided in Appendix G and were considered in the trends discussed above.

In all models, the peak shear stress was observed at the corner of the support pate, and the shear stress magnitude generally decreased from the corner to the support plate centerline. The peak shear stress at the peak load level was found to decrease as β was increased from 1 to 6. As β was increased from 6 to 8 the peak stress increased. Once β exceeded 8, the predicted peak shear stress dropped as β was increased. The peak shear stresses for all rectangularity values greater than 1 were between approximately 4.8 and 6.3MPa. The peak stress observed in the square column model was 7.1MPa. The difference between the peak stress values for the square and rectangular columns demonstrates the large impact that rectangularity has on the shear stress distribution.

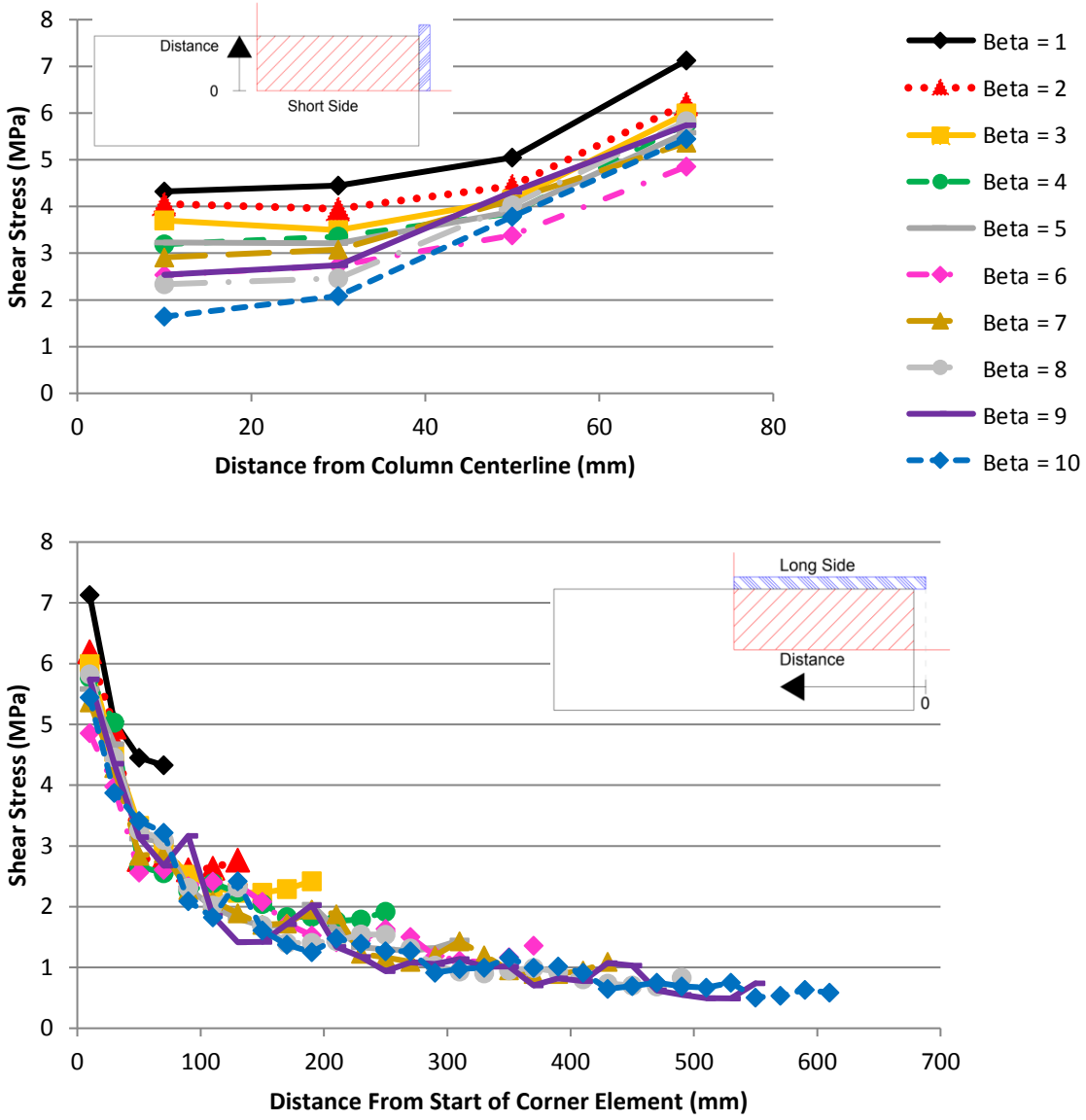

Figure 5-10: Predicted Shear Stress Distribution Around Support Plate Perimeter, $c_{min}/d = 0.594$, Top) Stresses Along Short Side, Bottom) Stresses Along Long Side, Integer β values

The shear stress distributions along the ACI 318 critical perimeter, calculated from the FEA results at the peak load, are shown in Figure 5-11 for the same column rectangularities shown in Figure 5-10. The shear stress distributions for the remaining rectangularities are provided in Appendix G. Unlike the shear stress distribution around the column perimeter, the shear stresses along the ACI 318 critical perimeter do not display a clear trend. As such, only the shear stress distributions around the support

plate perimeter are discussed for the remaining c_{min}/d ratios. The shear stress distributions around the ACI 318 critical perimeter for all c_{min}/d ratios are provided in Appendix G.

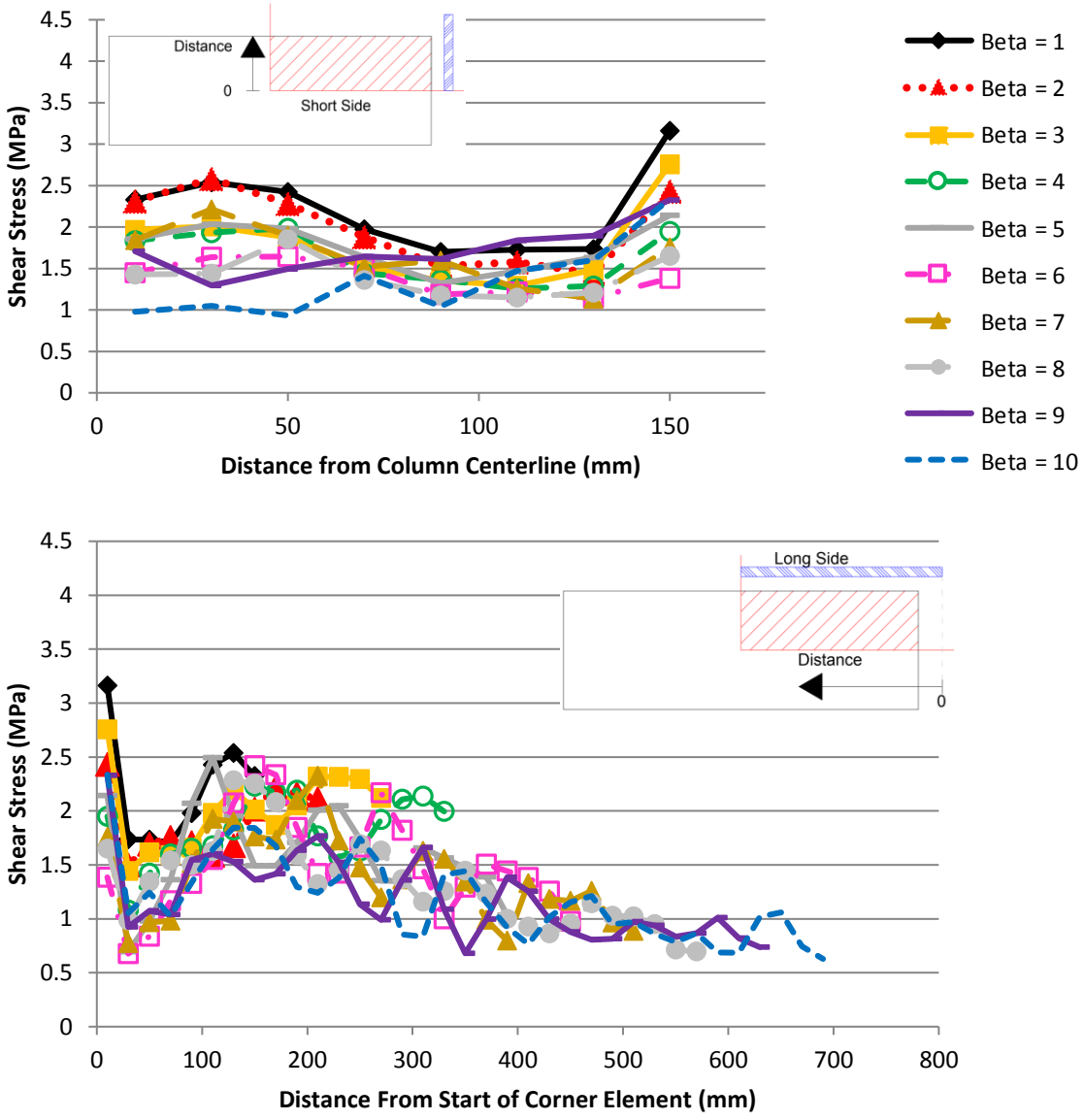

Figure 5-11: Predicted Shear Stress Distribution Around ACI 318 Critical Perimeter, c_{min}/d = 0.594, Top) Stresses Along Short Side, Bottom) Stresses Along Long Side, Integer β values

Analyzing the tension surface crack patterns provided in Appendix F leads to numerous conclusions. Firstly, the predicted crack pattern on the tension surface of the slab for the model supported on a square support plate was approximately uniform. A uniform crack pattern was expected due to the symmetry in loading and support conditions. Secondly, the impact of column

rectangularity on the predicted crack pattern is extremely apparent. Since the support plate size for a c_{min}/d ratio of 0.594 is small the tension surface crack patterns for column rectangularities less than or equal to 2 are approximately uniform. However, for larger β values the crack patterns were significantly influenced by the support area geometry. For example, as the rectangularity of the column was increased, the number of cracks perpendicular to the long and short sides of the column on the slab's tension surface increased. These perpendicular cracks, and the presence of one long crack parallel to the long side of the support plate, which is visible for rectangularities greater than 6.667, demonstrate the increasing influence of one-way shear behaviour on the predicted response. This crack was found to extend across the full slab with for a β value of 8.667. Thirdly, as the rectangularity was increased the number of diagonal cracks, which extended from the corner of the support plate to the corner of the slab, decreased in number, size and length. The cracks on the tension surface also become more focused near the corner of the supported area, and less cracking was predicted near the slab centerlines (symmetry edges in the model).

Analyzing the slab side crack patterns provided in Appendix F also leads to numerous conclusions. When the column rectangularity is low, very clear conical crack patterns are predicted along both slab sides, which matches crack patterns from previous experimental programs and structures which failed in punching. As the rectangularity of the support plate was increased the shape of the predicted crack pattern on the slab side perpendicular to the long side of the supported area became less conical, as shown in Figure 5-12. With increased rectangularity the crack pattern on the slab side perpendicular to the long side of the support plate transitioned from a conical shape, to a reverse Z shape ($\beta>5.667$), which is shown in Figure 5-12, before becoming almost non-existent ($\beta>9$). The change in the slab side crack patterns perpendicular to the long side of the support plate further proves that one-way shear behaviour becomes more dominant as column aspect ratio is increased.

Finally, for very high rectangularity values (i.e. $\beta \geq 7.667$), more significant cracking in the slab above the support plate was predicted. This cracking concentration could be caused by the contact definitions used, or could be due to the extreme difference in the short and long side dimensions for the two lowest c_{min}/d ratios studied (0.594 and 0.792), as this behaviour was not observed for any models with c_{min}/d greater than 0.792.

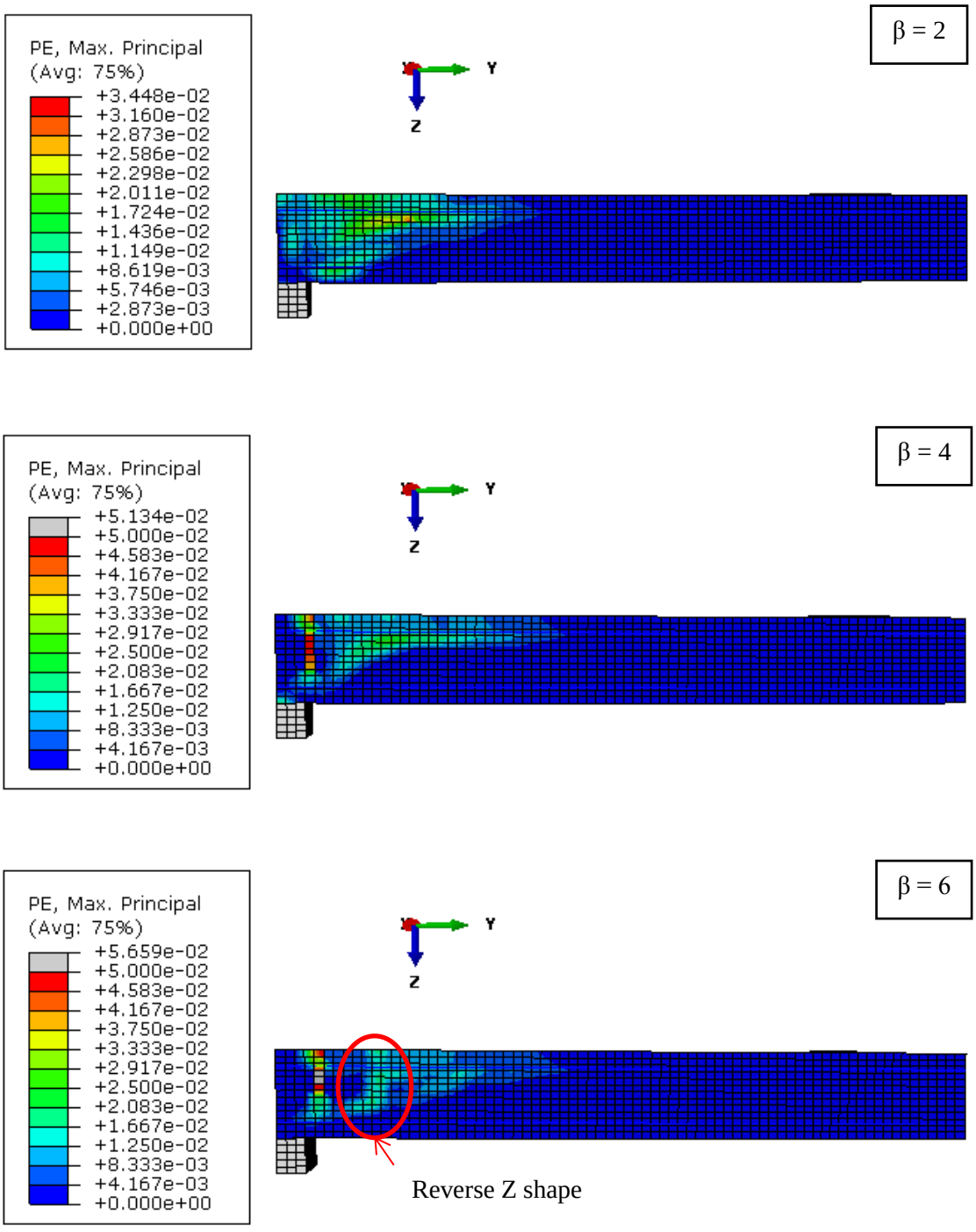

Figure 5-12: Comparison of Slab Side Crack Pattern, Perpendicular to Long Side, c_{min}/d =0.594

5.2.2 $C_{min}/d = 0.792$

A summary of the column dimensions, column rectangularity values, predicted capacity and predicted deflections at peak load in the X and Y-directions for the models with a c_{min}/d ratio of 0.792 are provided in Table 5-4, and the load-displacement plots for integer values of β analyzed are provided in Figure 5-13. The remaining load-displacement plots can be found in Appendix E. As with the results for a c_{min}/d ratio of 0.594, the FEM predicted a higher shear capacity as the column size, and rectangularity, were increased.

Table 5-4: Summary of FEA Results for $c_{min}/d = 0.792$

c_{min} (mm)	c_{max} (mm)	β	Predicted Capacity (kN)	Δ_X (mm)	Δ_Y (mm)
160	160	1.000	700.2	14.02	14.02
160	240	1.500	738.1	14.63	14.53
160	320	2.000	792.2	16.22	15.75
160	400	2.500	844.6	18.24	17.22
160	480	3.000	884.1	19.80	18.18
160	560	3.500	894.6	19.09	17.14
160	640	4.000	916.0	19.25	16.80
160	720	4.500	924.2	19.76	17.03
160	800	5.000	998.1	22.90	18.15
160	880	5.500	1006.7	22.40	16.85
160	960	6.000	1021.9	23.22	16.78
160	1040	6.500	1031.3	24.04	16.31
160	1120	7.000	1032.8	23.91	14.72
160	1200	7.500	1039.4	24.05	13.46
160	1280	8.000	1047.2	20.71	11.52

After analyzing the post-punching deflected shape of all the models with $c_{min}/d=0.792$, it was observed that all slabs with a rectangularity less than 7.5 were predicted to fail in punching. Slabs supported on plates where β exceeded 7.5 were predicted to fail in one-way shear. An example of the typical deflected shape observed for the models which failed in one-way shear is shown in Figure 5-14.

As with the results for $c_{min}/d=0.594$, no overall trends in the predicted deflections were observed. The deflections in both orthogonal directions were found to increase as β was increased when β was less than 3. After β exceeds 3, the deflections in the X-direction (perpendicular to the long side of the support plate) stay approximately constant until β = 4.5. For β greater than 4.5, the deflections in the X-direction typically increase as the column rectangularity is increased, except for when β equaled 8. The deflections in the Y-direction show no clear trend for rectangularities between 3 and 5. For

rectangularities between 5 and 8, the predicted deflection in the Y-direction typically decreased as the column rectangularity increased.

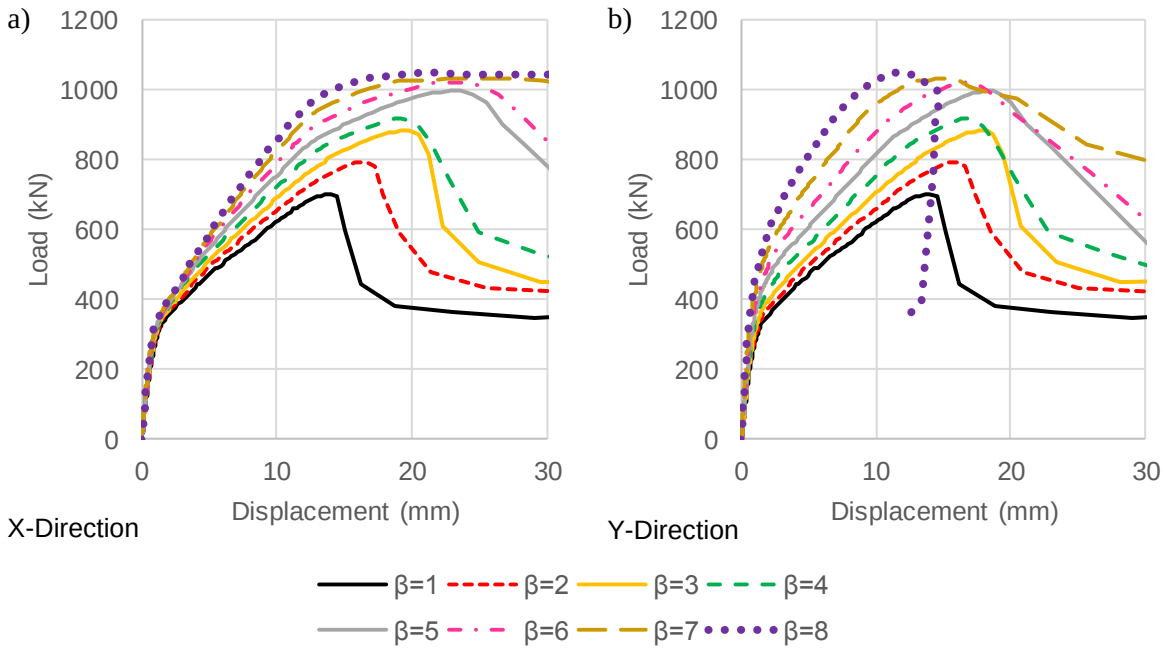

Figure 5-13: Predicted Load-Displacement Response, $c_{min}/d = 0.792$

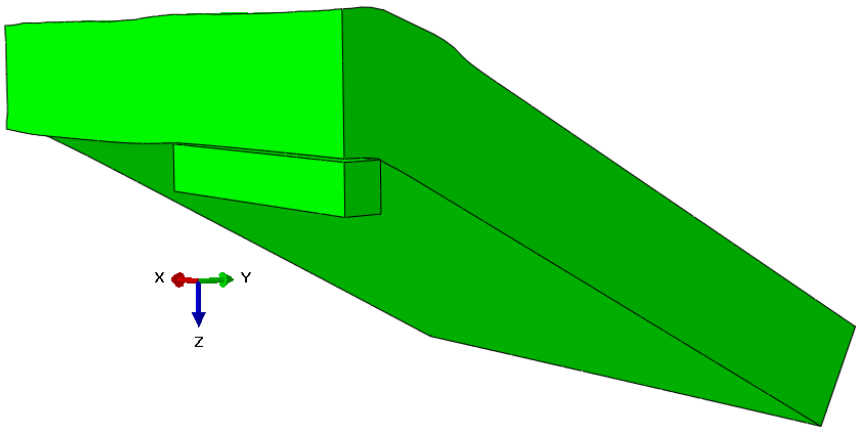

Figure 5-14: Typical One-Way Shear Deflected Shape, Model Shown: β = 8, $c_{min}/d = 0.792$

Consistent with the $c_{min}/d=0.594$ results, the predicted stiffness in both directions was found to increase as the column rectangularity increased. In both the elastic and plastic portion of the response, the stiffness increase was larger in the Y-direction. In the X-direction, the increase in stiffness in the

elastic region was found to be rather small, whereas the change in the plastic region was much larger, but smaller than the change in stiffness observed in the Y-direction.

A comparison of the shear capacity predicted by the FEA to ACI 318M-14 (ACI), Eurocode 2 (2004) (EC2), Model Code 2010 (MC 2010) and the Critical Shear Crack Theory (CSCT) is provided for a subset of the models in Figure 5-15, and for all the models with a c_{min}/d ratio of 0.792 in Figure 5-16 and Table 5-5. An additional bar chart similar to Figure 5-15 is provided in Appendix E for the remaining rectangularity values.

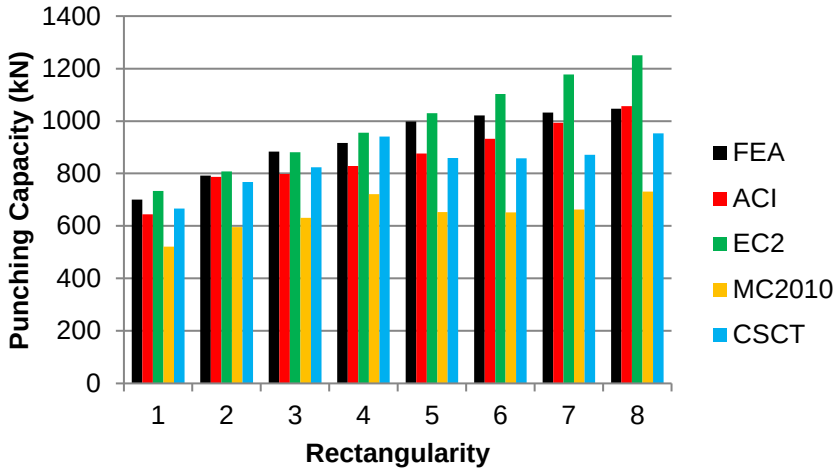

Figure 5-15: Shear Capacity from FEA and Design Codes, Integer β Values, $c_{min}/d=0.792$

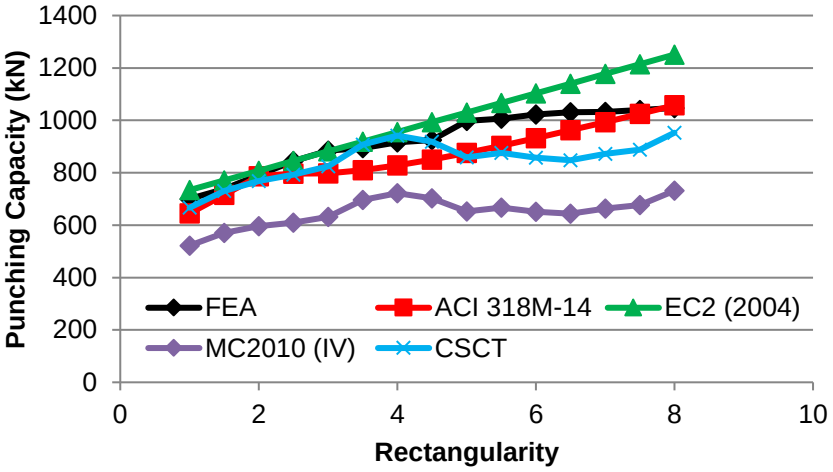

Figure 5-16: Shear Capacity from FEA and Design Codes, All β Values, $c_{min}/d=0.792$

Table 5-5: Comparison of Code Predictions and FEA Results – $c_{min}/d = 0.792$

c_{min} (mm)	c_{max} (mm)	β	FEA Capacity (kN)	V_{FEA}/V_{ACI}	V_{FEA}/V_{EC2}	V_{FEA}/V_{MC2010}	V_{FEA}/V_{CSCT}
160	160	1.000	700.2	1.09	0.95	1.34	1.05
160	240	1.500	738.1	1.03	0.96	1.30	1.01
160	320	2.000	792.2	1.01	0.98	1.33	1.03
160	400	2.500	844.6	1.06	1.00	1.38	1.07
160	480	3.000	884.1	1.11	1.00	1.40	1.07
160	560	3.500	894.6	1.10	0.97	1.28	0.99
160	640	4.000	916.0	1.11	0.96	1.27	0.97
160	720	4.500	924.2	1.09	0.93	1.32	1.01
160	800	5.000	998.1	1.14	0.97	1.53	1.16
160	880	5.500	1006.7	1.11	0.94	1.51	1.15
160	960	6.000	1021.9	1.10	0.93	1.57	1.19
160	1040	6.500	1031.3	1.07	0.90	1.60	1.22
160	1120	7.000	1032.8	1.04	0.88	1.56	1.18
160	1200	7.500	1039.4	1.01	0.86	1.54	1.17
160	1280	8.000	1047.2	0.99	0.84	1.43	1.10
			Average	1.07	0.94	1.42	1.09
			COV (%)	4.17	5.34	8.20	7.51

The ACI 318M-14 provisions were found to be generally conservative for a c_{min}/d ratio of 0.792, as the ratio of V_{FEA}/V_{ACI} exceeds 1 for all investigated models where β is less than 8. The EC2 (2004) provisions on the other hand are typically unconservative as V_{FEA}/V_{EC2} is less than 1 for all models, except for the models where β equaled 2.5 and 3, where V_{FEA}/V_{EC2} equals 1.0. As with the results for $c_{min}/d=0.594$, both ACI 318M-14 and EC2 (2004) predict a larger total shear capacity as the column rectangularity is increased. For column aspect ratios less than or equal to 4, the Model Code 2010 and CSCT provisions also predict an increased shear capacity as β increased. For column aspect ratios greater than 4, the capacities predicted by Model Code 2010 and the CSCT are approximately constant; because the effective perimeter length using the 3d method is less than the total critical perimeter length.

On average, the capacity predictions according to ACI 318M-14, EC2 (2004), Model Code 2010 and the CSCT are 7% lower, 6% higher, 42% lower and 9% lower than the capacity predicted by the FEM respectively. The EC2 (2004) predictions were found to be most accurate, but typically slightly unconservative, for column rectangularity values between 1 and 5 (V_{FEA}/V_{EC2} is between 0.93 and 1.0). For all investigated rectangularity values, the ACI predictions were found to be accurate and typically conservative (V_{FEA}/ V_{ACI} is between 0.99 and 1.14). The CSCT provisions were the most

accurate for rectagularities between 1 and 4.5 and were generally conservative compared to the FEA results (V_{FEA}/V_{CSCT} is between 0.97 and 1.07). For rectangularities greater than 4.5, the predictions according to the CSCT and Model Code 2010 became more conservative, whereas the predictions according to ACI 318M-14 and EC2 (2004) generally became less conservative and more unconservative respectively. The ACI 318M-14 provisions were found to have smallest variation based on the coefficient of variation of the ratio of V_{CODE}/V_{FEA}. None of the investigated specimens were predicted to fail in one-way shear by ACI 318M-14 or EC2 (2004). The FEM on the other hand, predicted one-way shear failures for slabs supported on plates with aspect ratios greater than or equal to 7.5 ($c_{max} \geq 1200$mm).

A comparison of the normalized nominal shear stress predicted by ACI 318M-14, EC2 (2004), Model Code 2010, the CSCT and the finite element model at the ACI critical perimeter located at d/2 from the column perimeter is provided in Figure 5-17. As expected, based on the total capacity estimates, the nominal shear stress predicted by ACI 318M-14 is generally conservative when compared to the finite element model. However, the finite element model still predicts an approximately linear decrease in nominal shear capacity with increasing rectangularity, whereas a curved relationship is used in ACI 318. The ACI predictions for a c_{min}/d ratio of 0.792 and 0.594 are identical, and as such, the changes in nominal stress for specific rectangularity values discussed in the Section 5.2.1 are applicable. The ACI 318 method predicts that the impact of column rectangularity becomes less significant as the rectangularity value becomes very large (i.e. $\beta > 5$), but this does not match the FEA results. Again, the finite element method predicts a reduction in the nominal shear stress for slightly rectangular columns (i.e $1 < \beta \leq 2$).

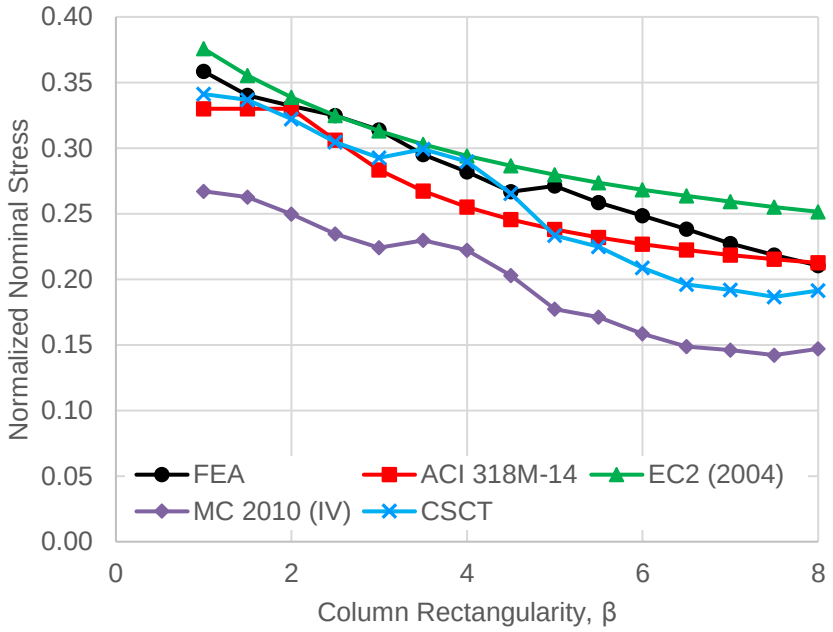

Figure 5-17: Comparison of Nominal Shear Capacity Predicted by FEA and Design Codes, c_{min}/d = 0.792

Overall, the trend of the normalized nominal shear stress predicted by EC2 (2004) is similar to that of the FEM. As expected, based on the capacity comparisons, the normalized nominal shear stress predicted by EC2 (2004) is typically higher than that from the FEM, and begins to deviate from the trend of the FEA results for β values greater than or equal to 6.5. The EC2 (2004) provisions are found to be fairly accurate for rectangularity values between 1 and 5. Unlike ACI 318M-14, the EC2 (2004) provisions predict a decrease in the normalized nominal stress for rectangularity values between 1 and 2, which matches the FEA results.

The trend of the normalized nominal stress based on the CSCT provisions is also similar to that from the FEA especially for rectangularities between 1 and 4.5. Unlike the total capacity estimates, which were approximately constant for column aspect ratios greater than 4.5, the predicted normalized nominal shear stress continues to decrease as β is increased. The nominal shear stress continues to decrease because the predicted capacity, which is approximately constant, is divided by the length of the ACI 318M-14 perimeter, which increases in length as β is increased.

The shear stress distribution calculated from the FEM results at the peak load level for the integer rectangularity values with c_{min}/d=0.792 are shown in Figure 5-18, and the distributions for the non-

integer rectangularity values are provided in in Appendix G. Again, the overall shape of the predicted shear stress distribution along both sides of the support plate was found to be similar for all investigated rectangularity values. As with the results for a c_{min}/d ratio of 0.594, the shear stresses were found to concentrate around the corner and short side of the support plate. Again, the magnitude of the shear stress along the long side at an equivalent distance from the corner of the support plate was found to be similar in all models.

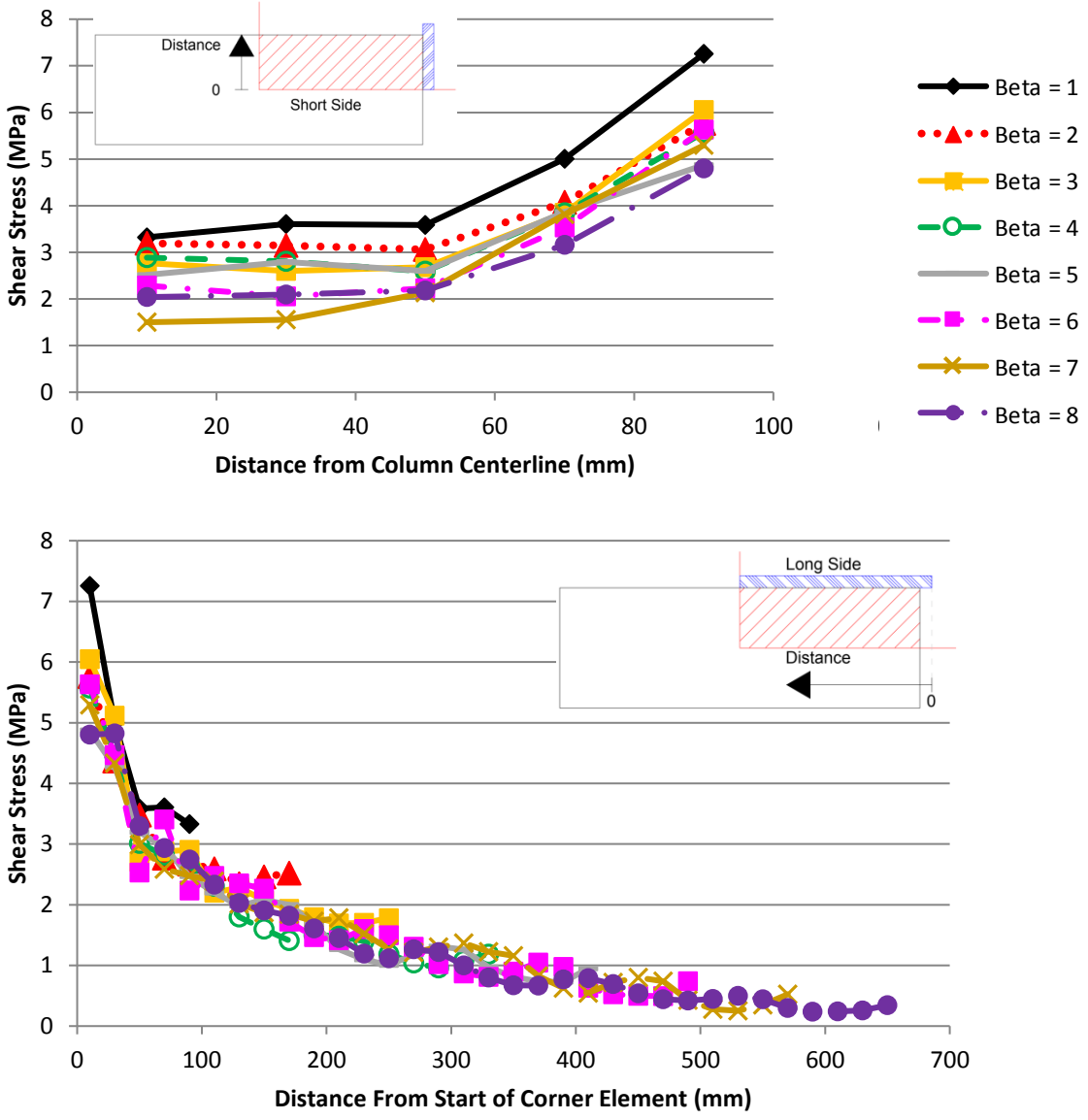

Figure 5-18: Predicted Shear Stress Distribution Around Support Plate Perimeter, c_{min}/d = 0.792, Top) Stresses Along Short Side, Bottom) Stresses Along Long Side

As was observed in the $c_{min}/d=0.594$ models, the maximum shear stress occurred at the corner of the supported area and the magnitude of the shear stresses decreased as the distance from the corner increased. Overall, there was no clear trend in the predicted maximum shear stress at the support plate corner as the rectangularity was increased. The magnitude of the maximum shear stress was found to be between approximately 4.8MPa and 6.3MPa for all models where β is greater than 1, which matched the results of the models with $c_{min}/d=0.594$. The peak stress for the model supported on a square steel plate was approximately 7.3MPa, which is slightly higher than the 7.1MPa observed for the square column with a c_{min}/d ratio of 0.594. Again, the maximum shear stress for the square support area is larger than that observed for rectangular support areas, showing that column rectangularity does have a large impact on the shear stress distribution.

The trends in the predicted crack patterns for a c_{min}/d ratio of 0.792 are very similar to those observed for the $c_{min}/d=0.594$ models. As the column rectangularity increased, the amount of diagonal cracking on the tension surface of the slab decreased. Very few diagonal cracks are predicted for the models where β is greater than or equal to 7.5. The trend of the crack patterns on the slab sides are also similar. For low rectangularity values, typical conical shapes are observed. As β is increased beyond 4.5, the conical shape on the slab side perpendicular to the long side of the support plate becomes very thin, before transitioning into a reverse z shape, similar to that shown in Figure 5-12. The punching cones on the slab side perpendicular to the long side of the support plate were found to be nearly non-existent for models with β greater than 7. The punching cones for a c_{min}/d ratio of 0.594 were found to become non-existent when β was greater than or equal to 9. Therefore, the maximum rectangularity before the punching cones become nearly non-existent, which coincides with the transition from two-way shear behaviour to one-way shear behaviour, decreased as the c_{min}/d ratio was increased. However, it should be noted that the column length in the quarter model for β equal to 9 and $c_{min}/d=0.594$ is 540mm ($c_{max}=1080$mm) and for β equal to 7 and $c_{min}/d=0.792$ is 560mm ($c_{max}=1120$mm). Therefore, even though the rectangularity value where the punching cones become non-existent decreased as c_{min}/d increased, the maximum column dimension when this behaviour occurred is similar. Furthermore, the presence of one long crack extending across the entire slab width parallel to the long side of the column was first observed when β equaled 6.5 when $c_{min}/d=0.792$, which again is lower than the value observed for $c_{min}/d=0.594$ ($\beta = 8.667$). However, the column length in the quarter model in both cases is 520mm ($c_{max}=1040$mm), which shows that the overall column length, and not just the support aspect ratio, may be important in the shear behaviour of reinforced concrete slabs.

Finally, when β was greater than or equal to 6.5, the predicted crack patterns on the slab sides show a large concentration of cracks in the slab directly above the supported area. Similar behaviour was observed in the models where c_{min}/d equaled 0.594 when β exceeded 7.667. The column length in the quarter model where this behaviour was first observed is 520mm (c_{max}=1040mm) and 460mm (c_{max}=920mm) for a c_{min}/d ratio of 0.792 and 0.594 respectively. This tendency was not observed in any other c_{min}/d ratios.

5.2.3 $C_{min}/d = 0.990$

A summary of the column dimensions, column rectangularity values, predicted capacity and predicted deflections at peak load in the X and Y-directions for the models with a c_{min}/d ratio of 0.990 are provided in Table 5-6, and the load-displacement plots for integer values of β are provided in Figure 5-19. The remaining load-displacement plots can be found in Appendix E. As with the results for c_{min}/d ratios of 0.594 and 0.792, the FEM predicted a higher shear capacity as the column size, and rectangularity, were increased.

Table 5-6: Summary of FEA Results for $c_{min}/d = 0.990$

c_{min} (mm)	c_{max} (mm)	B	Predicted Capacity (kN)	Δ_X (mm)	Δ_Y (mm)
200	200	1.000	758.6	14.97	14.97
200	320	1.600	830.6	16.98	16.56
200	400	2.000	879.6	18.89	17.95
200	520	2.600	917.8	19.79	18.02
200	600	3.000	930.3	19.29	17.07
200	720	3.600	932.4	19.45	16.80
200	800	4.000	990.8	21.30	17.15
200	920	4.600	1037.8	25.19	17.97
200	1000	5.000	1024.1	22.69	16.46
200	1120	5.600	1057.0	29.20	15.15
200	1200	6.000	1060.6	29.01	13.49
200	1320	6.600	1058.2	26.33	11.04

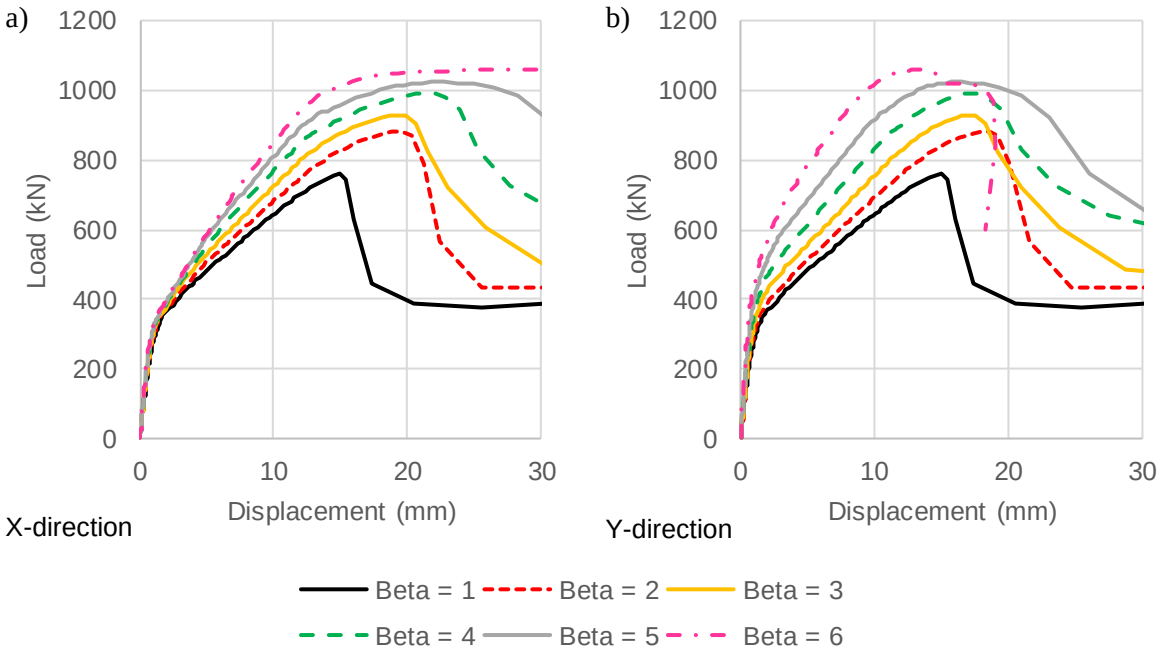

Figure 5-19: Predicted Load-Displacement Response, $c_{min}/d = 0.990$

After analyzing the post failure deflected shape of all the finite element models, it was concluded that all models with a column aspect ratio less than 6 were predicted to fail via the punching mode. Models with higher column aspect ratios were predicted to fail in one-way shear.

The trend in the deflection results is consistent with those discussed for the previously investigated c_{min}/d ratios. For lower values of rectangularity, the predicted deflections increase as the rectangularity is increased. For intermediate β values the deflections stay approximately constant. As the rectangularity is further increased, the deflections in the X-direction typically increase and the deflections in the Y-direction decrease. The trends in stiffness are also consistent with those observed for the previous two c_{min}/d ratios, and therefore, are not discussed here.

A comparison of the shear capacity predicted by the FEA to ACI 318M-14 (ACI), Eurocode 2 (2004) (EC2), Model Code 2010 (MC 2010) and the Critical Shear Crack Theory (CSCT) is provided for a subset of the models in Figure 5-20, and for all the models with a c_{min}/d ratio of 0.990 in Figure 5-21 and Table 5-7. An additional bar chart similar to Figure 5-20 is provided in Appendix E for the remaining rectangularity values.

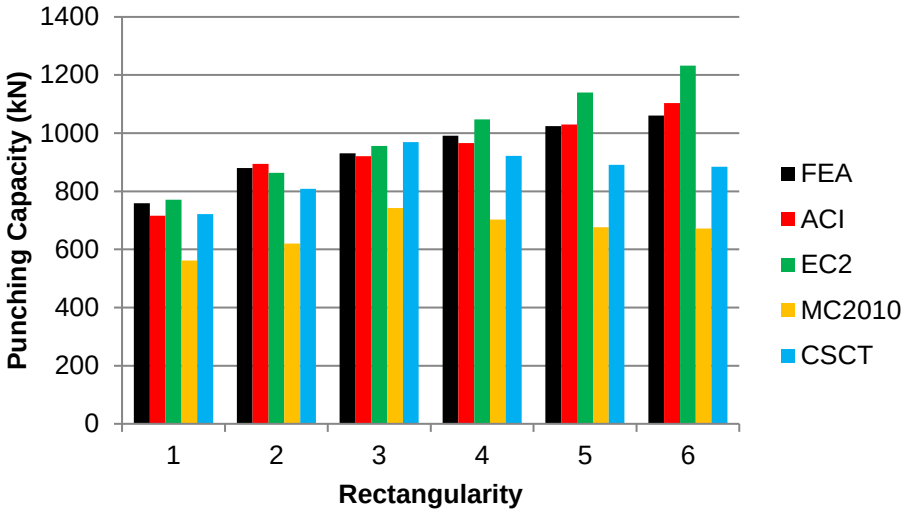

Figure 5-20: Shear Capacity from FEA and Design Codes, Integer β Values, $c_{min}/d=0.990$

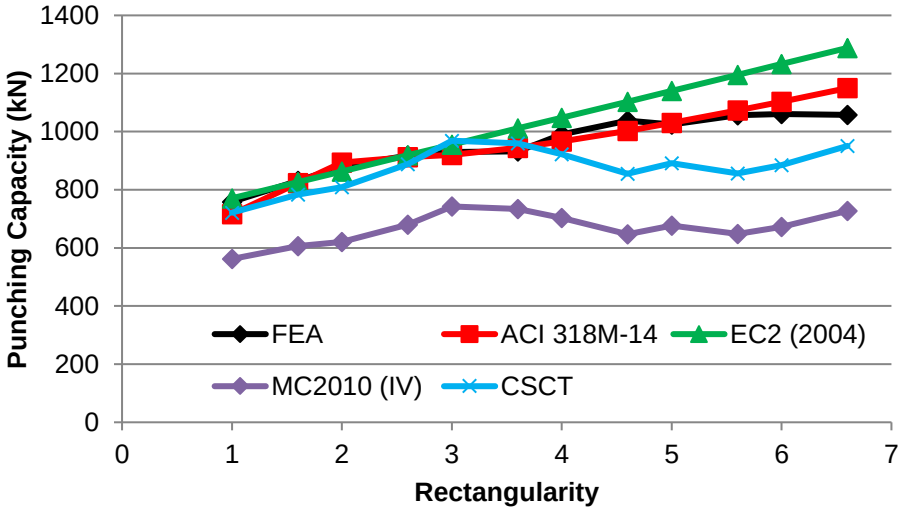

Figure 5-21: Shear Capacity from FEA and Design Codes, All β Values, $c_{min}/d=0.990$

Table 5-7: Comparison of Code Predictions and FEA Results – $c_{min}/d = 0.990$

c_{min} (mm)	c_{max} (mm)	β	FEA Capacity (kN)	V_{FEA}/V_{ACI}	V_{FEA}/V_{EC2}	V_{FEA}/V_{MC2010}	V_{FEA}/V_{CSCT}
200	200	1.000	758.6	1.06	0.98	1.35	1.05
200	320	1.600	830.6	1.01	1.01	1.37	1.06
200	400	2.000	879.6	0.98	1.02	1.42	1.09
200	520	2.600	917.8	1.01	1.00	1.35	1.03
200	600	3.000	930.3	1.01	0.97	1.25	0.96
200	720	3.600	932.4	0.99	0.92	1.27	0.97
200	800	4.000	990.8	1.03	0.95	1.41	1.07
200	920	4.600	1037.8	1.03	0.94	1.60	1.21
200	1000	5.000	1024.1	0.99	0.90	1.51	1.15
200	1120	5.600	1057.0	0.98	0.88	1.63	1.23
200	1200	6.000	1060.6	0.96	0.86	1.58	1.20
200	1320	6.600	1058.2	0.92	0.82	1.46	1.11
			Average	1.00	0.94	1.43	1.10
			COV (%)	3.60	6.64	8.75	8.17

For a c_{min}/d ratio of 0.990, the ACI 318M-14 provisions were found to be typically slightly conservative, as the ratio of V_{FEA}/V_{ACI} is near 1 for all investigated models. However, it is clear that as the c_{min}/d ratio increases, the ACI318M-14 provisions become less conservative. As with the previous two c_{min}/d ratios, the EC2 (2004) provisions are typically unconservative, as V_{FEA}/V_{EC2} is less than 1 for most of the investigated rectangularities. As with the results for c_{min}/d=0.594 and 0.792, both ACI 318M-14 and EC2 (2004) predict a larger total shear capacity as the column rectangularity is increased. For column aspect ratios less than or equal to 3.6 the Model Code 2010 and the CSCT provisions also predict an increased shear capacity as β increased. For column aspect ratios greater than 3.6, the capacities predicted by Model Code 2010 and the CSCT are approximately constant; this is because the effective perimeter length using the 3d method is less than the total critical perimeter length for β greater than 3.

On average, the capacity predictions according to ACI 318M-14, EC2 (2004), Model Code 2010 and the CSCT are 0% lower, 6% higher, 43% lower and 10% lower than the capacity predicted by the FEM respectively. The EC2 (2004) predictions were found to be most accurate, and typically slightly conservative, for column rectangularity values between 1 and 3 (V_{FEA}/V_{EC2} is between 0.97 and 1.02). For all investigated rectangularity values less than 6.6, the ACI predictions were found to be accurate and typically conservative (V_{FEA}/V_{ACI} is between 0.96 and 1.06). The CSCT provisions were conservative for all investigated rectangularity values other than 3 and 3.6 and were most accurate for

rectagularities between 1 and 4 (V_{FEA}/V_{CSCT} is between 0.96 and 1.09). For rectangularities greater than 4.6, the predictions according to the CSCT and Model Code 2010 became more conservative whereas the predictions according to ACI 318M-14 and EC2 (2004) generally became more unconservative. As with the c_{min}/d=0.792 results, the ACI 318M-14 provisions were found to have the smallest variation based on the coefficient of variation of the ratio of V_{CODE}/V_{FEA}. None of the investigated specimens were predicted to fail in one-way shear by ACI 318M-14 or EC2 (2004), which differs from the FEM, which predicted one-way shear failures for slabs supported on plates with aspect ratios greater than or equal to 6 ($c_{max}\geq$1200mm).

A comparison of the normalized nominal shear stress predicted by ACI 318M-14, EC2 (2004), Model Code 2010, the CSCT and the finite element model at the ACI critical perimeter located at d/2 from the column perimeter is provided in Figure 5-22. As expected, based on the total capacity estimates, the nominal shear stress predicted by ACI 318M-14 shows good correlation with the FEA results for rectangularity values between 1.6 and 6. As with the previous c_{min}/d ratios, the finite element model predicts an approximately linear relationship between nominal shear capacity and column rectangularity, which differs from ACI 318. Again, the finite element method predicts a reduction in the nominal shear stress for slightly rectangular columns (i.e $1<\beta\leq2$).

The trend of the normalized nominal shear stress predicted by EC2 (2004) is similar to that of the FEM for rectangularities less than 3. For rectangularities greater than 3, the nominal shear stress predicted by EC2 (2004) is higher than that predicted from the FEA. As with the previous c_{min}/d ratios, the EC2 (2004) provisions predict a decrease in the normalized nominal stress for rectangularity values between 1 and 2, which matches the FEA results.

The trend of the normalized nominal stress based on the CSCT provisions is similar to that from the FEA for rectangularities less than 3.6 and conservative for rectangularities greater than 3.6. Unlike the results for the previous c_{min}/d ratios, the nominal stresses do not continually decrease as β is increased. For column rectangularities greater than or equal to 5.6, the nominal stress predicted by the CSCT (and MC 2010) are approximately constant.

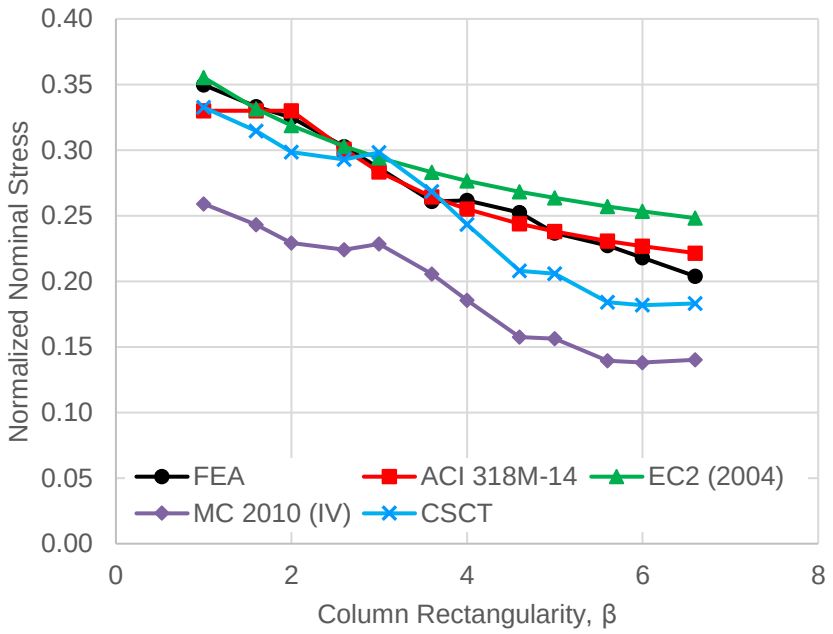

Figure 5-22: Comparison of Nominal Shear Capacity Predicted by FEA and Design Codes, c_{min}/d = 0.990

The shear stress distribution around the support plate perimeter at the peak load calculated from the FEA results for the integer rectangularity values are shown in Figure 5-23, and the shear stress distributions for the non-integer rectangularity values are provided in Appendix G. As with the previously investigated c_{min}/d ratios, the overall shape of the shear stress distribution along the long and short sides of the support plate is similar for all investigated models. The maximum shear stress occurs at the corner of the supported area and decreases as the distance from the corner increases. The calculated peak shear stress for all models with a c_{min}/d ratio of 0.990, except for the slab supported on a square plate, are between 4.5 and 6.3MPa. This peak shear stress range is similar to that observed in the two previously discussed c_{min}/d ratios, but the minimum peak stress is slightly lower (4.5MPa vs 4.8MPa). The peak shear stress for the slab supported on a square plate is 8.5MPa, once again showing the large impact of column rectangularity on the shear stress distribution around the perimeter of the supported area. The peak shear stress for a square support plate and a c_{min}/d ratio of 0.990 is higher than that observed in the previous two c_{min}/d ratios (8.5MPa vs approximately 7MPa).

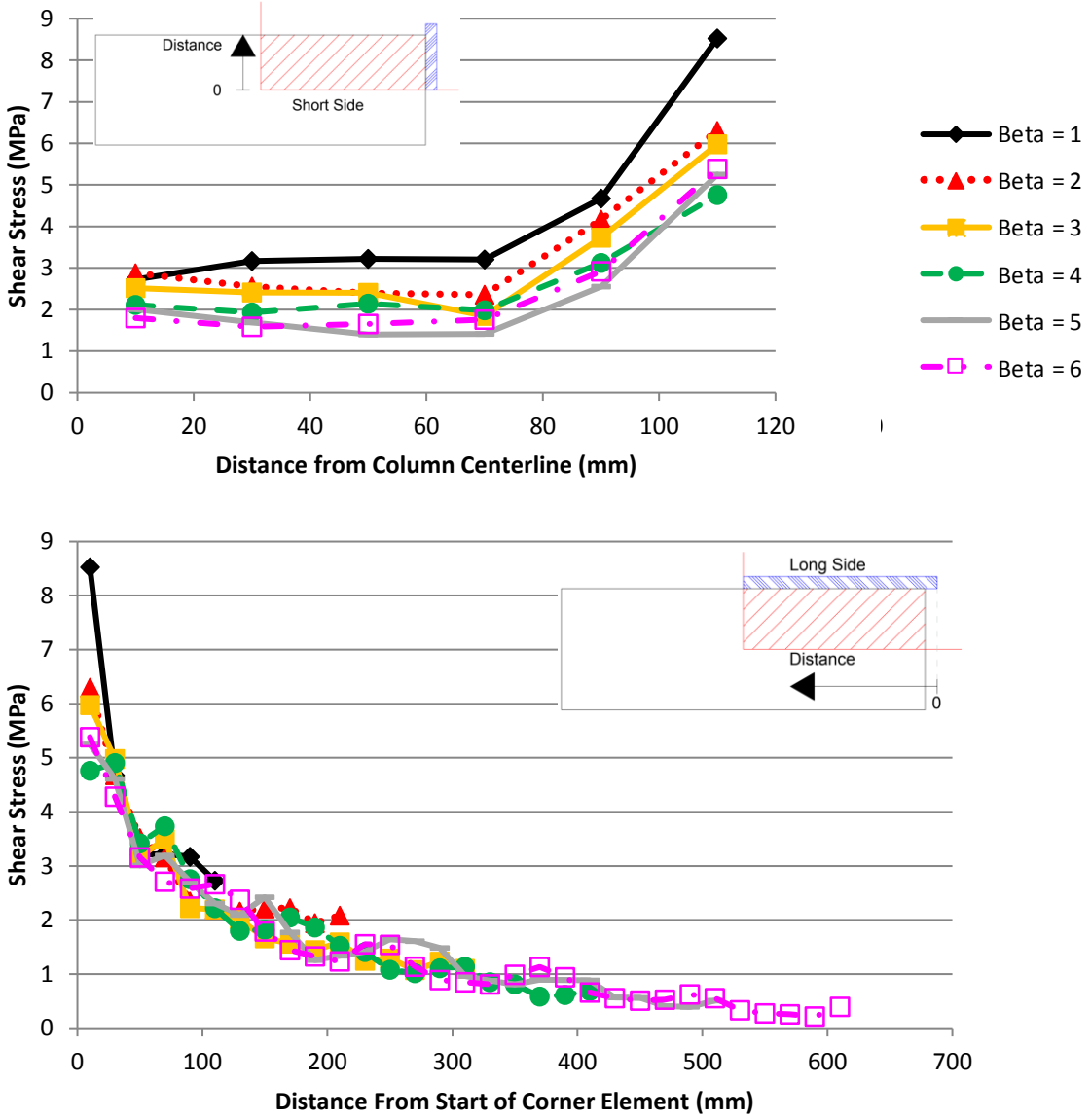

Figure 5-23: Predicted Shear Stress Distribution Around Support Plate Perimeter, c_{min}/d = 0.990, Top) Stresses Along Short Side, Bottom) Stresses Along Long Side

The trends observed in the predicted crack patterns for a c_{min}/d ratio of 0.990 are very similar to those observed in the previous two c_{min}/d ratios. As the support rectangularity was increased, the amount of diagonal cracking on the tension side decreased. Very few diagonal cracks are predicted for models where β exceeds 6. Similar behaviour was observed in the two previous c_{min}/d ratios at higher rectangularities but similar column lengths. The shape of the crack patterns along the slab sides also display similar behaviour to that observed for c_{min}/d ratios of 0.594 and 0.792. For low

rectangularities, the slab side crack patterns have a distinct conical shape, but as β is increased beyond 3.6 the conical shape on the slab side perpendicular to the long side of the column thins and becomes a reverse Z shape, similar to that shown in Figure 5-12. For rectangularities greater than 6, the punching cones on the slab side perpendicular to the long side of the support plate become almost non-existent, which is at a lower rectangularity, but similar column length compared to the other two c_{min}/d ratios. Unlike the two previously investigated c_{min}/d ratios, where only one conical crack was observed on the slab sides, a second crack was observed on the slab side perpendicular to the short side of the support plate. This second crack forms below the other conical crack and extends from the mid-depth of the slab to the compression surface of the slab near the support. The long crack on the tension surface of the slab was observed in models where β exceeds 4.6, which is at lower rectangularity value than for the two previous c_{min}/d ratios, and also a smaller column length (920mm vs 1040mm). Finally, the impact of column rectangularity on the crack patterns is very apparent as the crack pattern for the model with β equal to 1.5 was noticeably non-symmetric, and a noticeable increase in the amount of cracking perpendicular to the sides of the supported area was observed.

5.2.4 C_{min}/d = 1.287

A summary of the column dimensions, column rectangularity values (β), predicted capacity and predicted deflections at the peak load in the X and Y-directions for the models with a c_{min}/d ratio of 1.287 are provided in Table 5-8. The load-displacement plots for the investigated models are provided in Figure 5-24. Again, the FEM predicted a higher capacity as the column size, and rectangularity, were increased. This increase in total shear capacity is expected since the overall column area, and length of the critical perimeter increased as β increased. One outlier exists, which corresponds to model where β equals 2.462, which has a lower predicted capacity than the model where β equals 2.

Table 5-8: Summary of FEA Results for c_{min}/d = 1.287

c_{min} (mm)	c_{max} (mm)	β	Predicted Capacity (kN)	Δ_X (mm)	Δ_Y (mm)
260	260	1.000	824.2	16.52	16.48
260	390	1.500	921.9	19.89	19.23
260	520	2.000	987.7	22.21	20.17
260	640	2.462	976.3	19.39	17.03
260	780	3.000	997.7	21.80	18.20
260	920	3.538	1050.2	20.89	15.51
260	1040	4.000	1059.7	22.69	15.99
260	1160	4.462	1092.4	34.32	13.82
260	1320	5.077	1089.8	37.65	11.15

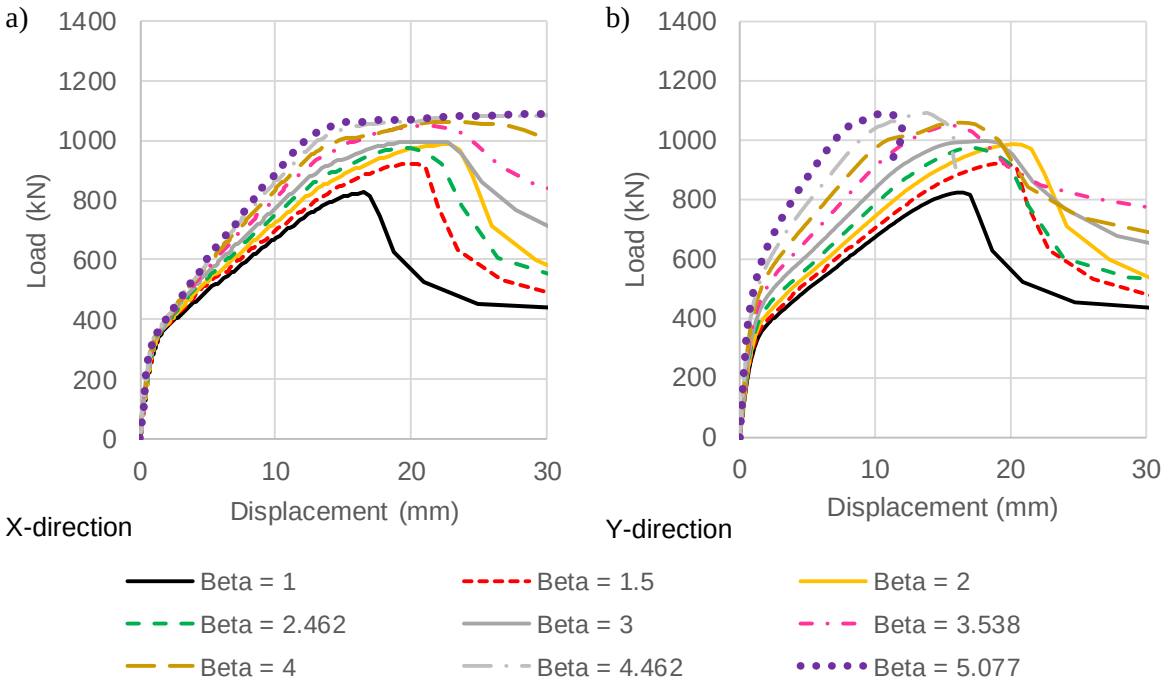

Figure 5-24: Predicted Load-Displacement Response, $c_{min}/d = 1.287$

After analyzing the post failure deflected shape of all the finite element models, it was concluded that all models with a rectangularity less than 4.462 were predicted to fail via the punching mode. Models with higher rectangularities were predicted to fail in one-way shear.

The predicted deflections show no clear trend. For the intermediate rectangularity values (β=2.462–4) there is no trend in the predicted deflections with increased column rectangularity. However, when one-way behaviour began to dominate (β≥4.462), the deflections in the X-direction increased and the deflections in the Y-direction decreased as the column rectangularity was increased.

The trends in stiffness are also consistent with the previous models, and therefore, they are not discussed in detail in this section. The reader is recommended to review the conclusions provided in the $c_{min}/d = 0.792$ and 0.594 subsections.

A comparison of the shear capacity predicted by the FEA to ACI 318M-14 (ACI), Eurocode 2 (2004) (EC2), Model Code 2010 (MC 2010) and the Critical Shear Crack Theory (CSCT) for all the models with a c_{min}/d ratio of 1.287 are provided in Figure 5-25, Figure 5-26 and Table 5-9.

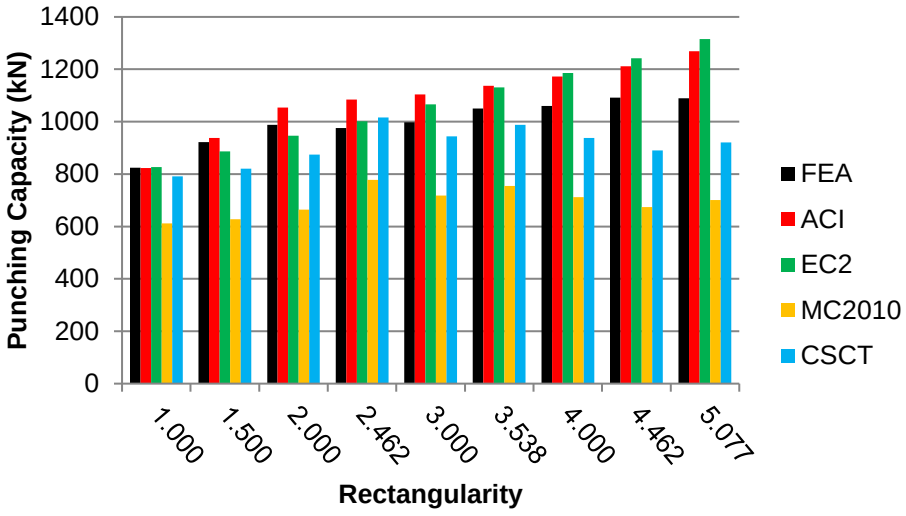

Figure 5-25: Shear Capacity from FEA and Design Codes, All β Values, $c_{min}/d=1.287$, Bar Chart

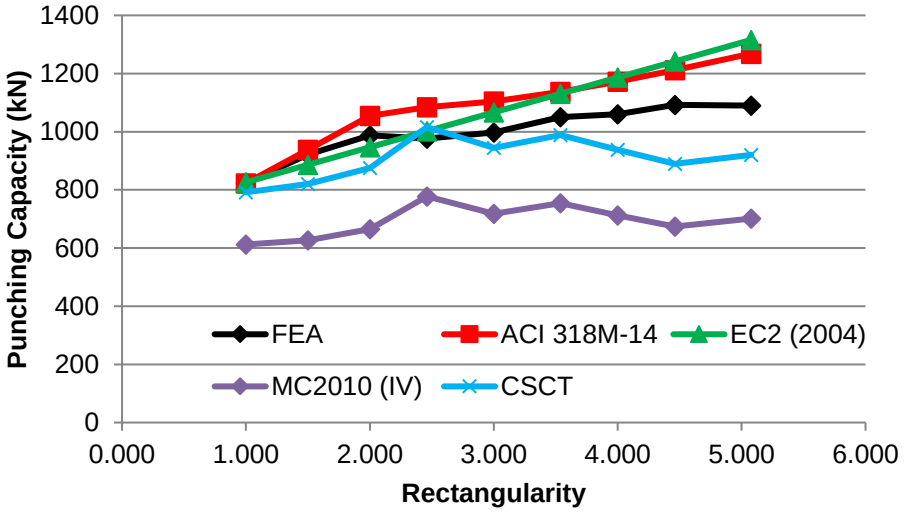

Figure 5-26: Shear Capacity from FEA and Design Codes, All β Values, $c_{min}/d=1.287$

Table 5-9: Comparison of Code Predictions and FEA Results – $c_{min}/d = 1.287$

c_{min} (mm)	c_{max} (mm)	β	FEA Capacity (kN)	V_{FEA}/V_{ACI}	V_{FEA}/V_{EC2}	V_{FEA}/V_{MC2010}	V_{FEA}/V_{CSCT}
260	260	1.000	824.2	1.00	1.00	1.35	1.04
260	390	1.500	921.9	0.98	1.04	1.47	1.12
260	520	2.000	987.7	0.94	1.04	1.49	1.13
260	640	2.462	976.3	0.90	0.97	1.26	0.96
260	780	3.000	997.7	0.90	0.94	1.39	1.06
260	920	3.538	1050.2	0.92	0.93	1.39	1.06
260	1040	4.000	1059.7	0.90	0.89	1.49	1.13
260	1160	4.462	1092.4	0.90	0.88	1.62	1.23
260	1320	5.077	1089.8	0.86	0.83	1.55	1.18
			Average	0.92	0.95	1.44	1.10
			COV (%)	4.80	7.78	7.67	7.28

For a c_{min}/d ratio of 1.287, the ACI 318M-14 and EC2 (2004) provisions were found to be typically unconservative, as the ratio of V_{FEA}/V_{ACI} and V_{FEA}/V_{EC2} are below 0.95 for most of the investigated models. As discussed for the previous c_{min}/d ratios, both ACI 318M-14 and EC2 (2004) predict a larger total shear capacity as the column rectangularity is increased. For column aspect ratios less than or equal to 2.462, the Model Code 2010 and CSCT provisions also predict an increased shear capacity as β increased. For column aspect ratios greater than 2.462, the capacities predicted by Model Code 2010 and the CSCT are approximately constant; this is because the effective perimeter length using the 3d method is less than the total critical perimeter length for rectangularities greater than or equal to 2.462.

On average, the capacity predictions according to ACI 318M-14, EC2 (2004), Model Code 2010 and the CSCT are 8% higher, 5% higher, 44% lower and 10% lower than the capacity predicted by the FEM respectively. The EC2 (2004) predictions were found to be most accurate, and typically slightly conservative, for column rectangularity values between 1 and 2.462 (V_{FEA}/V_{EC2} is between 0.97 and 1.04). The ACI 318 provisions on the other hand were only accurate for rectangularity values of 1 and 1.5. The CSCT provisions were conservative for all investigated rectangularity values other than 2.462, and were fairly accurate for all rectangularity values investigated (V_{FEA}/V_{CSCT} is between 0.96 and 1.23). For rectangularities greater than 4, the predictions according to the CSCT and Model Code 2010 became more conservative, whereas the predictions according to ACI 318M-14 and EC2 (2004) generally became more unconservative. As with the c_{min}/d=0.792 and 0.990 results, the ACI 318M-14 provisions were found to have lowest variation based on the coefficient of

variation of the ratio of V_{CODE}/V_{FEA}. None of the investigated specimens were predicted to fail in one-way shear by ACI 318M-14 or EC2 (2004) which differs from the FEM, which predicted one-way shear failures for slabs supported on plates with aspect ratios greater than or equal to 4.462.

A comparison of the normalized nominal shear stress predicted by ACI 318M-14, EC2 (2004), Model Code 2010, the CSCT and the finite element model at the ACI critical perimeter located at d/2 from the column perimeter is provided in Figure 5-27. As expected, based on the total capacity estimates, the nominal shear stress predicted by ACI 318M-14 is higher than that calculated from the FEA results for all rectangularities greater than 1. Again, the finite element model predicts an approximately linear relationship between nominal shear capacity and column rectangularity, which differs from ACI 318. However, the rate of change predicted by the ACI 318M-14 provisions and the FEA is similar for column rectangularities greater than 2. Therefore, a potential way to improve the accuracy of the ACI 318M-14 provisions is to include a decrease in nominal shear capacity for column rectangularities less than 2, as predicted by the FEA, and adjust the current provisions to account for this change. However, assuming the linear trend of the FEA results continues for higher rectangularity values it is observed that the difference between the FEA results and the ACI method would grow quite rapidly as the current ACI provisions approach an asymptote as β is increased.

The trend of the normalized nominal shear stress predicted by EC2 (2004) is similar to that predicted by the FEM for rectangularities less than or equal to 2.462. For rectangularities greater than 2.462, the nominal shear stress predicted by EC2 is higher than that predicted from the FEA and the difference between the EC2 and FEA predictions becomes larger as β increases.

The trend of the normalized nominal stress based on the CSCT provisions is similar to that from the FEA for all rectangularities other than β equal to 2.462. Consistent with the $c_{min}/d = 0.594$ and 0.792 results, the predicted normalized nominal shear stress decreases as β is increased and does not approach a constant value, as was observed for a c_{min}/d ratio of 0.990.

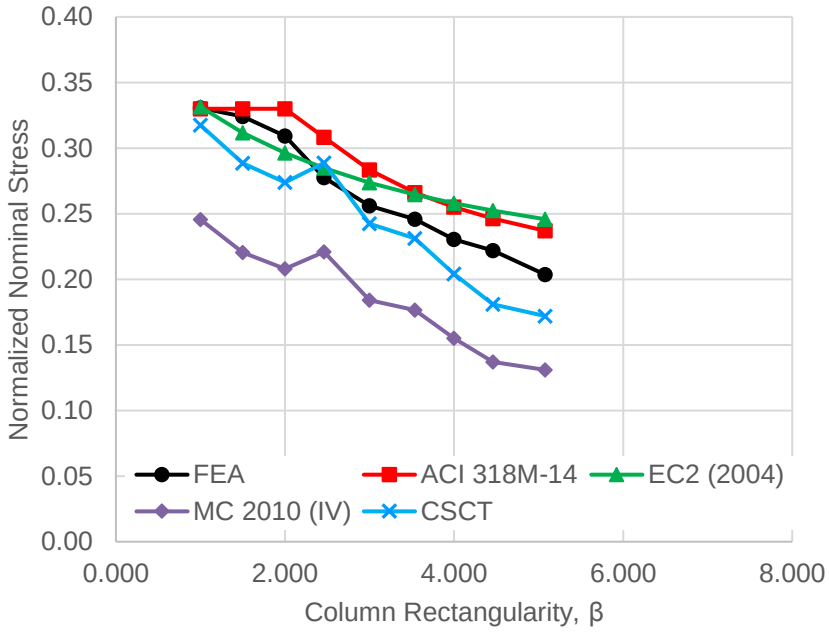

Figure 5-27: Comparison of Nominal Shear Capacity Predicted by FEA and Design Codes, c_{min}/d = 1.287

The shear stress distributions around the column perimeter calculated from the FEA for the nine investigated rectangularity values are shown in Figure 5-28. The overall shape of the predicted shear stress distributions around the column perimeter is similar for all the investigated rectangularity values as was observed for the previous c_{min}/d ratios. The trends in the predicted shear stress levels along the long side of the support plate are less consistent than those for the previous c_{min}/d ratios and appear to be dependent on the slab rebar. The increased shear stress magnitude observed at a distance of approximately 150mm from the column corner corresponds to the approximate location of the flexural reinforcement on the compression and tension faces of the slab. Due to the assumption of perfect bond, the forces in the model may concentrate around the rebar due to the higher stiffness of the steel rebar compared to the concrete elements. If the peak shear stress from the investigated models with c_{min}/d = 1.287 are plotted together, the calculated peak stresses for all models, including the square support area, are between approximately 4.8 and 5.9MPa. This stress range is similar to that observed in the previously discussed c_{min}/d ratios. However, the maximum peak stress is lower (5.9MPa vs 6.3MPa) and the peak stress for the square support area is not significantly higher than all the other investigated rectangularity values, which differs from the previously investigated c_{min}/d ratios.

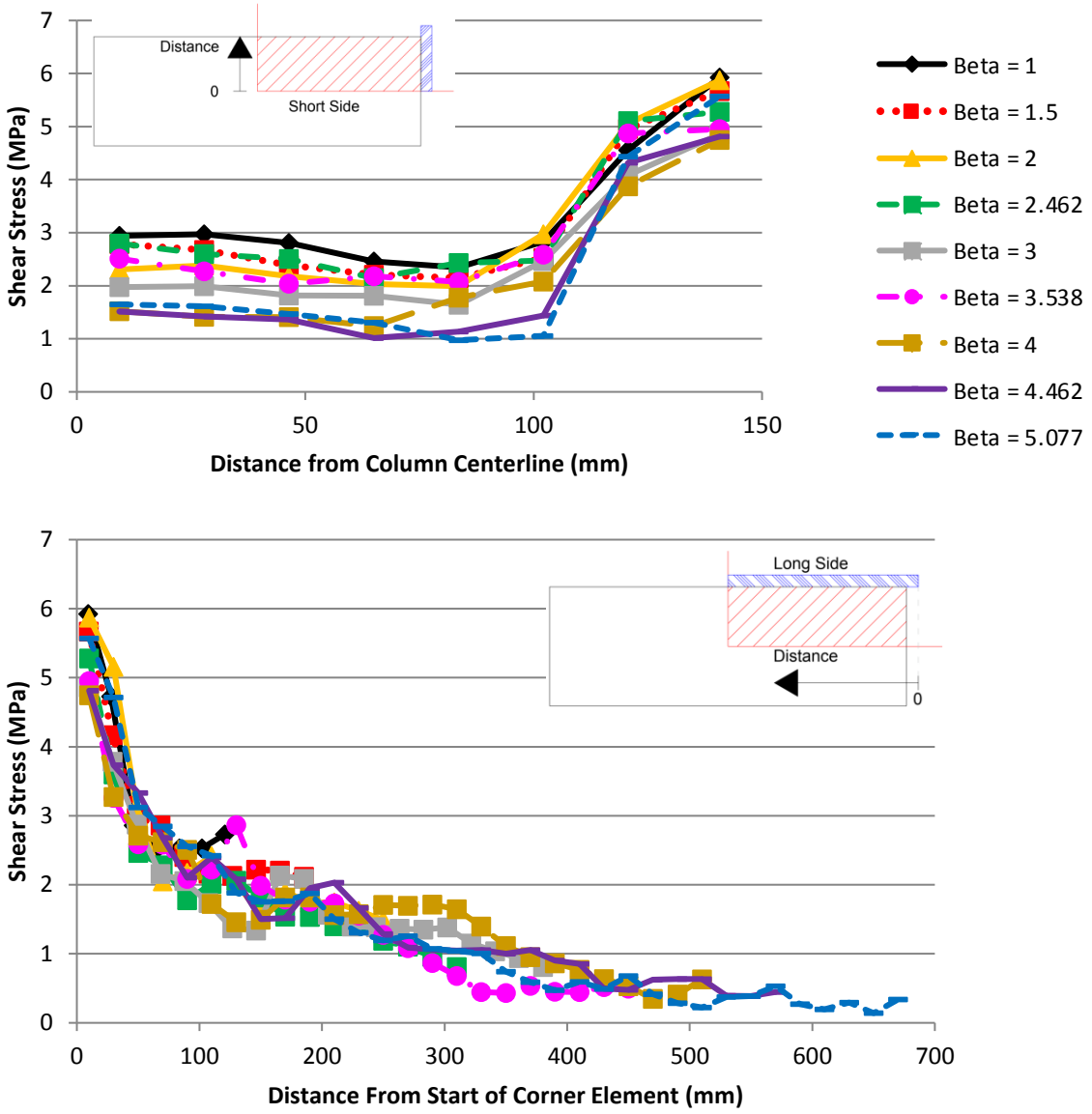

Figure 5-28: Predicted Shear Stress Distribution Around Support Plate Perimeter, $c_{min}/d = 1.287$, Top) Stresses Along Short Side, Bottom) Stresses Along Long Side

The trends observed in the crack patterns for the $c_{min}/d=1.287$ models are very similar to those discussed for the previous c_{min}/d ratios. As the rectangularity was increased beyond 1, the amount of diagonal cracking on the tension side decreased. Along with this decrease in diagonal cracking, an increased amount of cracking perpendicular to the sides of the supported area was observed as β was increased. Additionally, it was observed that the cracks concentrated near the corner of the supported area as β was increased. The shape of the failure cones along the sides of the slab was also similar to

that observed in the previously discussed models. At low rectangularity values, a conical crack which extends from the tension surface of the slab to the compression surface was observed. As the rectangularity was increased, the plastic strain magnitudes predicted along the slab sides perpendicular to both sides of the support plate decreased denoting a reduced amount of cracking. Along the slab side perpendicular to the long side of the support plate, the conical crack shape transitions into a reverse z shape ($\beta = 2.462$), before becoming almost non-existent at a β value of 4.462. The lack of clear punching cones on slab side perpendicular to the long side of the supported area was expected since a crack extending across the entire slab width, and parallel to the long side of the support plate, which is assumed to be associated with one-way shear, began to appear at a β value of 4. Finally, as observed in the $c_{min}/d=0.990$ models, a second crack, extending from the mid-depth of the slab to the compression surface of the slab near the support, was predicted below the top conical crack along the slab side perpendicular to the short side of the supported area in all models.

5.2.5 $C_{min}/d = 1.485$

A summary of the column dimensions, column rectangularity values (β), predicted capacity and predicted deflections at peak load in the X and Y-directions for the models with a c_{min}/d ratio of 1.485 are provided in Table 5-10, and the load-displacement plots are provided in Figure 5-29. Once again, the FEM predicted a higher total capacity as the column size, and rectangularity, were increased. This increase in total shear capacity was expected since the overall column area, and length of the critical perimeter were increased with increasing column rectangularity.

Table 5-10: Summary of FEA Results for $c_{min}/d = 1.485$

c_{min} (mm)	c_{max} (mm)	β	Predicted Capacity (kN)	Δ_X (mm)	Δ_Y (mm)
300	300	1.000	846.8	16.17	16.14
300	450	1.500	964.4	20.82	19.91
300	600	2.000	998.1	21.20	18.92
300	760	2.533	1043.5	21.28	17.62
300	920	3.067	1070.3	20.36	15.37
300	1040	3.467	1090.2	25.28	16.35
300	1200	4.000	1110.7	33.57	12.65

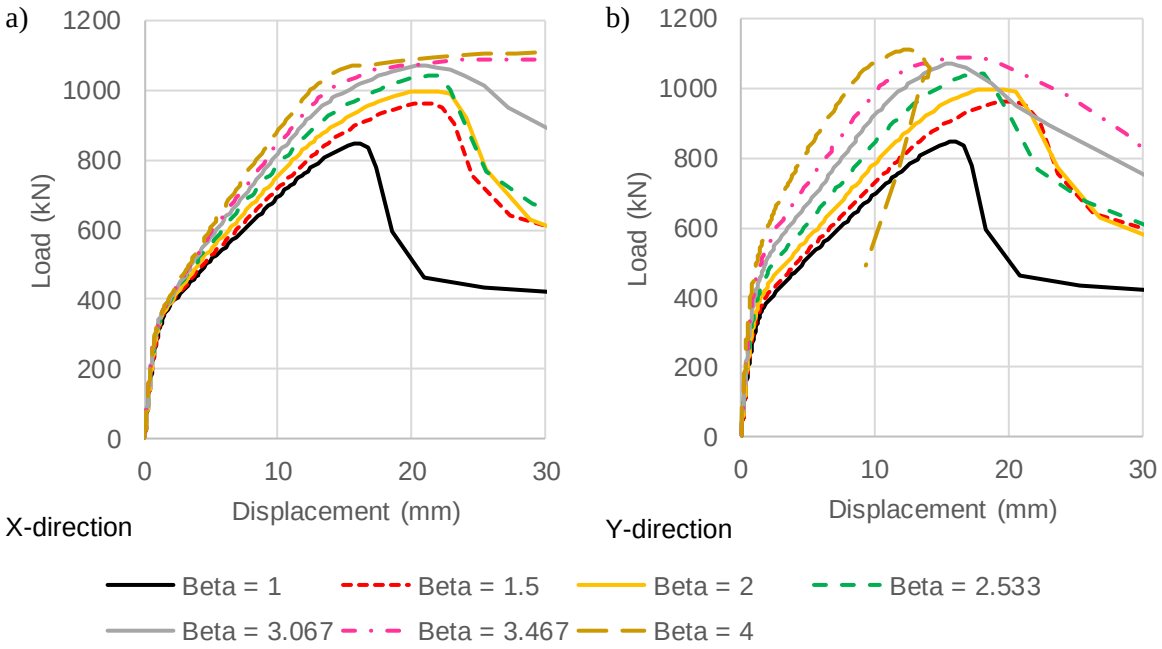

Figure 5-29: Predicted Load-Displacement Response, $c_{min}/d = 1.485$

From analysis of the post failure deflected shape of all models, it was found that all models where β was less than 4 were predicted to fail in punching shear. The model where β equaled 4 was predicted to fail in one-way shear.

Generally, the deflections in the X-direction increased as the column rectangularity was increased, with the model where β equaled 3.067 being the exception. The deflections in the Y-direction generally decreased as the support plate rectangularity was increased with the exceptions being the models where β equaled 1 or 3.467.

The trends in stiffness were consistent with the previous c_{min}/d ratios, and therefore, they are not discussed in detail in this section. Detailed discussions are provided in Section 5.2.1 and 5.2.2.

A comparison of the shear capacity predicted by the FEA to ACI 318M-14 (ACI), Eurocode 2 (2004) (EC2), Model Code 2010 (MC 2010) and the Critical Shear Crack Theory (CSCT) for all the models with a c_{min}/d ratio of 1.485 are provided in Figure 5-30, Figure 5-31 and Table 5-11.

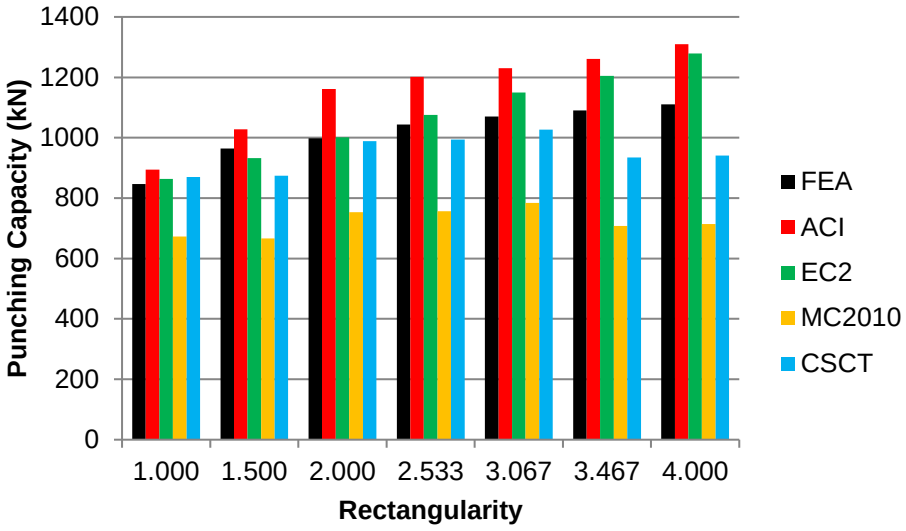

Figure 5-30: Shear Capacity from FEA and Design Codes, All β Values, $c_{min}/d=1.485$, Bar Chart

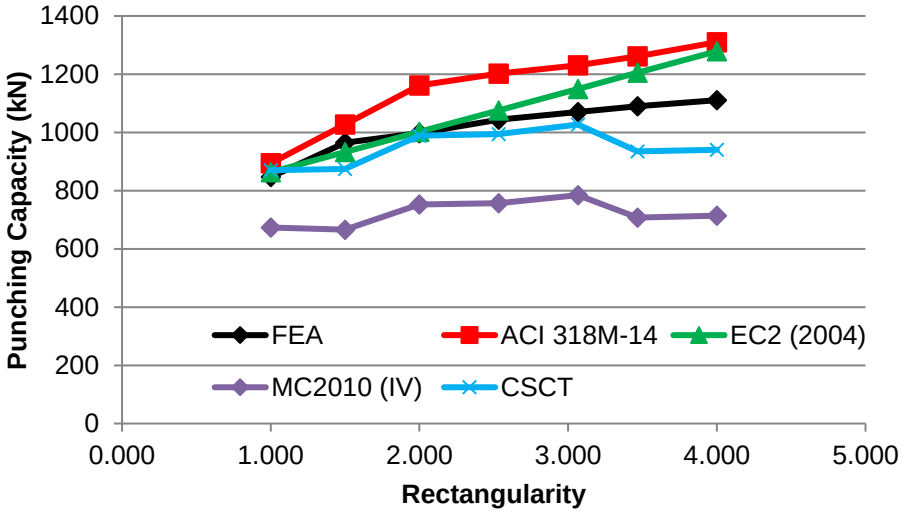

Figure 5-31: Shear Capacity from FEA and Design Codes, All β Values, $c_{min}/d=1.485$

Table 5-11: Comparison of Code Predictions and FEA Results – $c_{min}/d = 1.485$

c_{min} (mm)	c_{max} (mm)	β	FEA Capacity (kN)	V_{FEA}/V_{ACI}	V_{FEA}/V_{EC2}	V_{FEA}/V_{MC2010}	V_{FEA}/V_{CSCT}
300	300	1.000	846.8	0.95	0.98	1.26	0.97
300	450	1.500	964.4	0.94	1.03	1.45	1.10
300	600	2.000	998.1	0.86	1.00	1.33	1.01
300	760	2.533	1043.5	0.87	0.97	1.38	1.05
300	920	3.067	1070.3	0.87	0.93	1.36	1.04
300	1040	3.467	1090.2	0.86	0.90	1.54	1.17
300	1200	4.000	1110.7	0.85	0.87	1.55	1.18
			Average	0.89	0.96	1.41	1.08
			COV (%)	4.54	5.96	7.82	7.29

For a c_{min}/d ratio of 1.485, the ACI 318M-14 and EC2 (2004) provisions were found to be typically unconservative, as the ratio of V_{FEA}/V_{ACI} and V_{FEA}/V_{EC2} are below 0.95 and 0.97 respectively, for most of the investigated models. As with all previous c_{min}/d ratios, both ACI 318M-14 and EC2 (2004) predict a larger total shear capacity as the column rectangularity is increased. For the investigated models, the ACI provisions typically predict a capacity higher than that predicted by both the FEA and EC2 (2004). As the rectangularity was increased, the difference between the ACI 318 and EC2 (2004) predictions became smaller, and at a β value of 5 the predicted capacities from both codes were nearly identical.

For column aspect ratios less than or equal to 3.067, the Model Code 2010 and CSCT provisions also predict an increased shear capacity as β increased. For column aspect ratios greater than 3.067, the capacities predicted by Model Code 2010 and the CSCT are approximately constant; this constant capacity is primarily due to the fact that the effective perimeter length using the 3d method is less than the total critical perimeter length for β greater than or equal to 2.533.

On average, the capacity predictions according to ACI 318M-14, EC2 (2004), Model Code 2010 and the CSCT are 11% higher, 4% higher, 41% lower and 8% lower than the capacity predicted by the FEM respectively. However, it should be noted that as the c_{min}/d ratio is increased, the average V_{FEA}/V_{ACI} is decreasing and the average V_{FEA}/V_{EC2} is increasing. Therefore, the ACI 318M-14 provisions are becoming less conservative/more unconservative as the c_{min}/d ratio increases and the EC2 (2004) provisions are becoming less unconservative.

The EC2 (2004) predictions were found to be most accurate for column rectangularity values between 1 and 2.533 (V_{FEA}/V_{EC2} is between 0.97 and 1.03). The ACI 318 provisions on the other hand

were only accurate for rectangularity values of 1 and 1.5. The CSCT provisions were conservative for all investigated column aspect ratios other than 1, and were fairly accurate for all rectangularity values investigated (V_{FEA}/V_{CSCT} is between 0.97 and 1.18). As with the previous c_{min}/d ratios, the CSCT and Model Code 2010 predictions are most conservative for the largest column rectangularity values ($\beta \geq 3.467$) and the ACI318M-14 and EC2 (2004) predictions are the most unconservative. As with the c_{min}/d=0.792, 0.990 and 1.287 results, the ACI 318M-14 provisions were found to have the smallest variation based on the coefficient of variation of the ratio of V_{CODE}/V_{FEA}. None of the investigated specimens were predicted to fail in one-way shear by ACI 318M-14 or EC2 (2004), which differs from the FEM, which predicted one-way shear failures for slabs supported on plates with aspect ratios greater than or equal to 4 ($c_{max} \geq 1200$mm).

A comparison of the normalized nominal shear stress predicted by ACI 318M-14, EC2 (2004), Model Code 2010, the CSCT and the finite element model at the ACI critical perimeter located at d/2 from the column perimeter is provided in Figure 5-32. As expected, based on the total capacity estimates, the nominal shear stress predicted by ACI 318M-14 is always higher than that predicted by the finite element model for all rectangularities greater than 1, which leads to ACI overpredicting the punching capacity. Again, the finite element model predicts an approximately linear relationship between nominal shear capacity and column rectangularity, which differs from ACI 318. As was observed for a c_{min}/d ratio of 1.287, the rate of change of nominal shear stress vs column rectangularity for the FEA and ACI 318M-14 provisions are similar when β is greater than 2. However, the lack of impact for column rectangularity values less than 2 assumed in ACI 318M-14 has a significant impact on the difference observed between the two methods.

The trend of the normalized nominal shear stress predicted by EC2 (2004) is similar to that of the FEM for rectangularities less than or equal to 2.462. For rectangularities greater than 2.462, the nominal shear stress predicted by EC2 (2004) is higher than that predicted from the FEA and the difference between the EC2 (2004) and FEA predictions becomes larger as β increases.

The trend of the normalized nominal stress based on the CSCT provisions is similar to that from the FEA for all rectangularities other than β equal to 2.462. As was observed for c_{min}/d ratios of 0.594, 0.792 and 1.287, the normalized nominal shear stress predicted by the CSCT does not approach a constant value and decreases as β is increased.

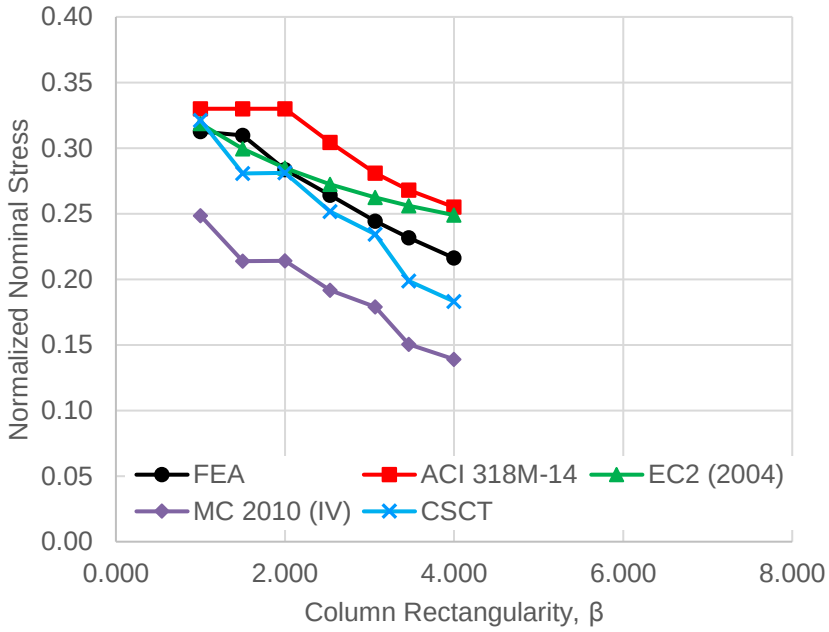

Figure 5-32: Comparison of Nominal Shear Capacity Predicted by FEA and Design Codes, c_{min}/d = 1.485

The shear stress distributions around the column perimeter at the peak load level calculated from the FEA for the seven rectangularity values investigated are shown in Figure 5-33. Overall, the shape of the predicted shear stress distributions around the column perimeter was similar for all investigated rectangularity values as was observed for the previous c_{min}/d ratios. The peak shear stress for all models where β exceeds 1 are between approximately 4.3 and 5.5MPa. This stress range is similar to, but lower than, that observed in the previous discussed c_{min}/d ratios. This decrease in the achievable peak shear stress confirms that both the aspect ratio of the support area and the ratio of the minimum dimension to the slab depth (i.e. relative size) impact the overall behaviour. Again, the finite element model is predicting a higher achievable peak shear stress at the corner of the square support area which matches the results for the lower c_{min}/d ratios other than c_{min}/d = 1.287. The magnitude of the predicted corner stress for the slab supported on a square steel plate is equal to approximately 6.4MPa

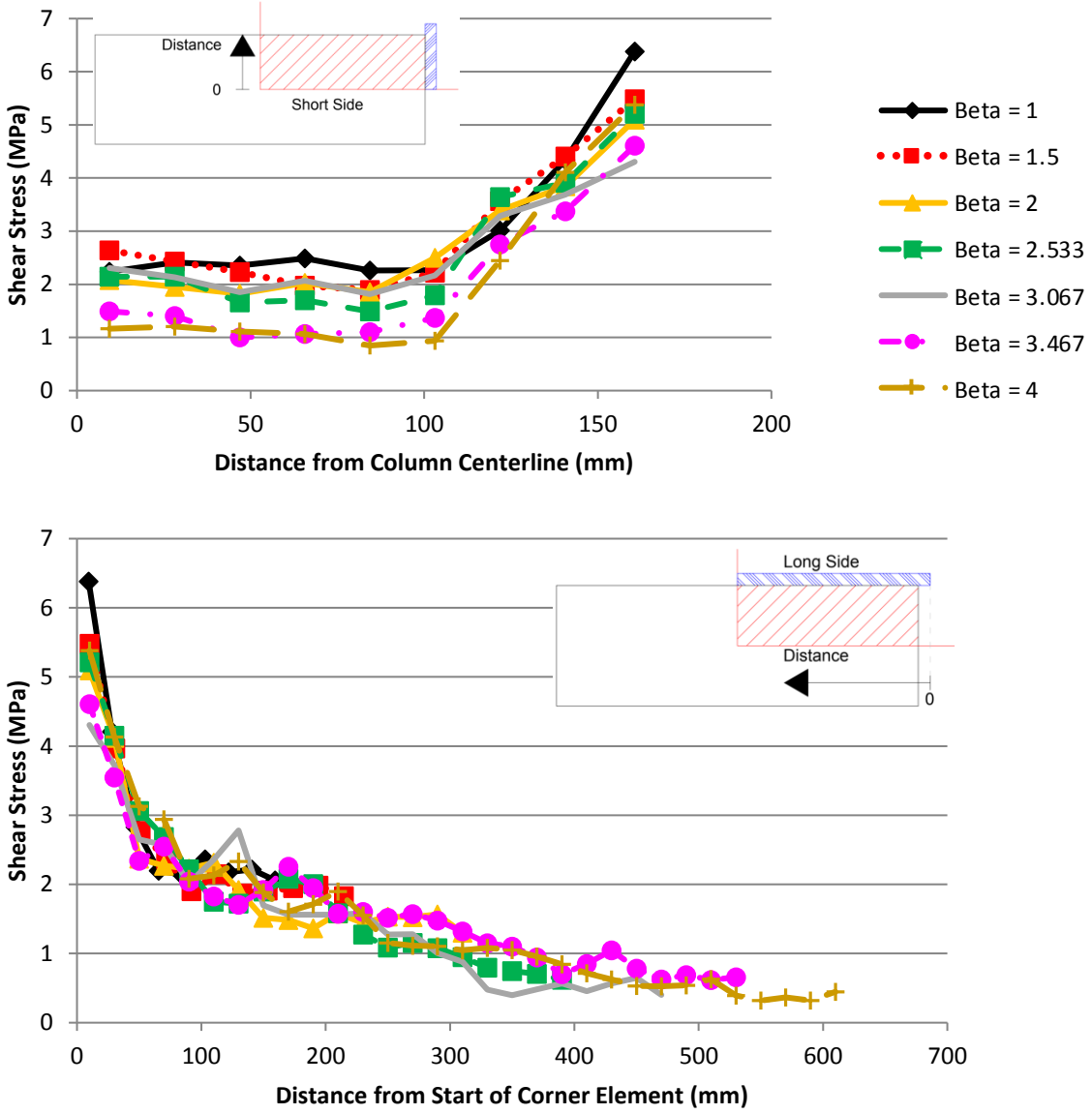

Figure 5-33: Predicted Shear Stress Distribution Around Support Plate Perimeter, $c_{min}/d = 1.485$, Top) Stresses Along Short Side, Bottom) Stresses Along Long Side

The trends in observed in the crack patterns for the $c_{min}/d=1.485$ models are very similar to those observed for the previous c_{min}/d ratios. As the rectangularity was increased beyond 1, the amount of diagonal cracking on the tension side decreased. Along with this decrease in diagonal cracking, an increased amount of cracking perpendicular to the sides of the supported area were observed as β was increased. Additionally, it was observed that the cracks concentrated near the corner of the supported area as β was increased. The shape of the failure cones along the sides of the slab was also similar to

that observed in the previously discussed models. At low rectangularity values, a conical crack extending from the tension surface of the slab to the compression surface was observed. As the rectangularity was increased, the plastic strain magnitudes predicted along the slab sides perpendicular to both sides of the support plate decreased, which denotes less cracking. Along the slab side perpendicular to the long side of the support plate, the conical shape transitions into a reverse z shape, before becoming almost non-existent at a β value of 4. The lack of clear punching cones on both sides of the supported area for larger β values was expected since a one-way shear crack which is parallel to the long side of the support plate, and extends across the slab width, was observed for all models where β exceeded 3.467. Finally, as observed in the c_{min}/d=0.990 and 1.287 models, a second crack starting at the mid-depth of the slab and extending to the compression surface near the support was observed on the slab side perpendicular to the short side of the supported area. This second crack forms below the top conical crack.

5.2.6 C_{min}/d = 1.782

A summary of the column dimensions, column rectangularity values (β), predicted capacity and predicted deflections at peak load in the X and Y-directions for the models with a c_{min}/d ratio of 1.782 are provided in Table 5-12 and the load-displacement plots are provided in Figure 5-34. As with the previously discussed c_{min}/d ratios, the FEM predicted a higher total capacity as the column size, and rectangularity, were increased.

Table 5-12: Summary of FEA Results for c_{min}/d = 1.782

c_{min} (mm)	c_{max} (mm)	β	Predicted Capacity (kN)	Δ_X (mm)	Δ_Y (mm)
360	360	1.000	988.1	22.43	22.44
360	540	1.500	1026.2	21.81	20.30
360	720	2.000	1082.5	23.66	19.95
360	920	2.556	1126.4	26.35	17.33
360	1080	3.000	1142.6	30.70	14.77
360	1280	3.556	1146.9	34.22	11.49

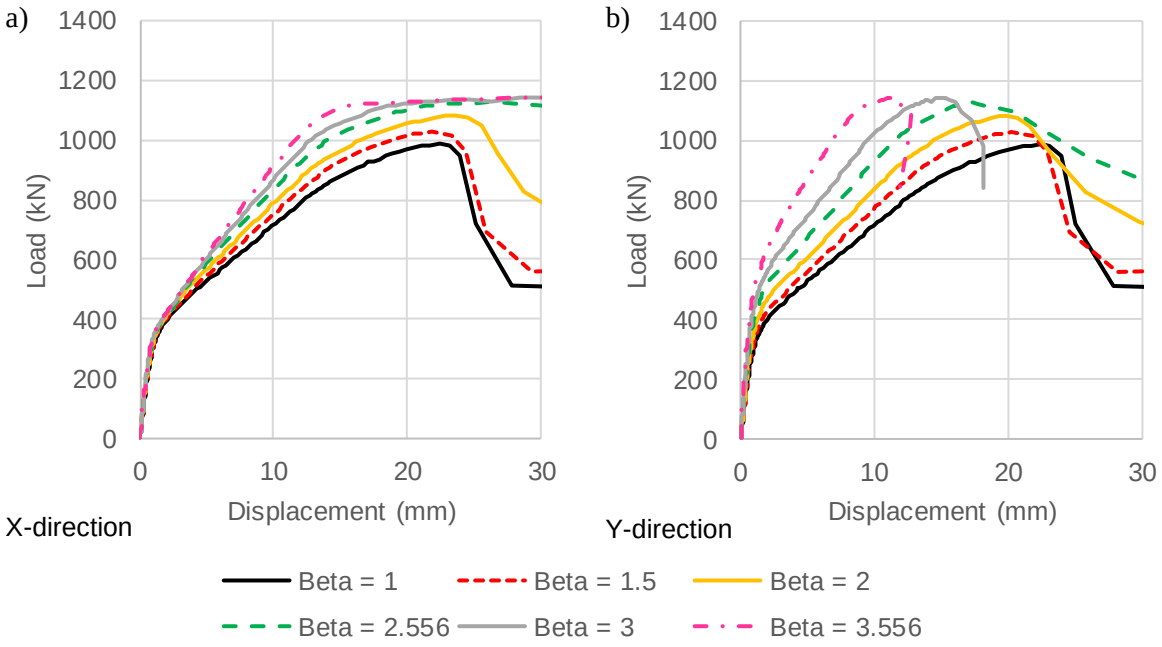

Figure 5-34: Predicted Load-Displacement Response, $c_{min}/d = 1.782$

Based on the post failure deflected shape, all models with a support plate rectangularity less than 3 were predicted to fail in punching shear. The models where β was greater than or equal to 3 were predicted to fail in one-way shear.

Generally, the deflections in the X-direction were found to increase as the column rectangularity increased, with the model where β equaled 1.5 being the exception. The deflections in the Y-direction decreased as the rectangularity increased.

The trends in stiffness were consistent with the previous c_{min}/d ratios, and therefore, they are not discussed in detail in this section.

A comparison of the shear capacity predicted by the FEA to ACI 318M-14 (ACI), Eurocode 2 (2004) (EC2), Model Code 2010 (MC 2010) and the Critical Shear Crack Theory (CSCT) for all the models with a c_{min}/d ratio of 1.782 are provided in Figure 5-35, Figure 5-36 and Table 5-13.

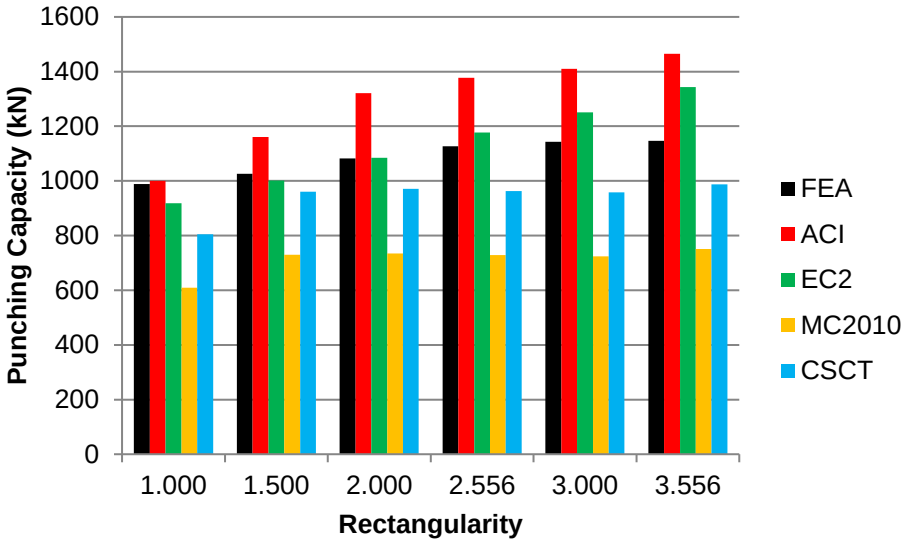

Figure 5-35: Shear Capacity from FEA and Design Codes, All β Values, $c_{min}/d=1.782$, Bar Chart

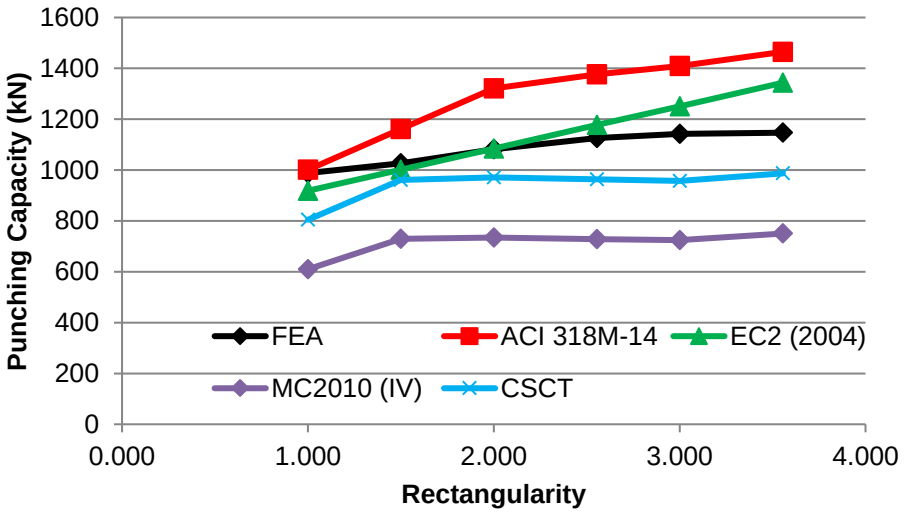

Figure 5-36: Shear Capacity from FEA and Design Codes, All β Values, $c_{min}/d=1.782$

Table 5-13: Comparison of Code Predictions and FEA Results – $c_{min}/d = 1.782$

c_{min} (mm)	c_{max} (mm)	β	FEA Capacity (kN)	V_{FEA}/V_{ACI}	V_{FEA}/V_{EC2}	V_{FEA}/V_{MC2010}	V_{FEA}/V_{CSCT}
360	360	1.000	988.1	0.99	1.08	1.62	1.23
360	540	1.500	1026.2	0.88	1.02	1.41	1.07
360	720	2.000	1082.5	0.82	1.00	1.47	1.11
360	920	2.556	1126.4	0.82	0.96	1.55	1.17
360	1080	3.000	1142.6	0.81	0.91	1.58	1.19
360	1280	3.556	1146.9	0.78	0.85	1.53	1.16
			Average	0.85	0.97	1.53	1.16
			COV (%)	8.80	8.22	5.00	4.95

For a c_{min}/d ratio of 1.782, the ACI 318M-14 and EC2 (2004) provisions were typically found to be unconservative, as the ratio of V_{FEA}/V_{ACI} and V_{FEA}/V_{EC2} are below 0.88 and 0.96 respectively for most of the investigated models. However, it should be noted that the EC2 (2004) predictions are conservative for column aspect ratios less than or equal to 2. For the investigated rectangularities the ACI provisions were found to predict the highest capacity. As with all previous c_{min}/d ratios, both ACI 318M-14 and EC2 (2004) predict a larger total shear capacity as the column rectangularity is increased. None of the investigated specimens were predicted to fail in one-way shear by ACI 318M-14 or EC2 (2004), which differs from the FEM which predicted one-way shear failures for slabs supported on plates with aspect ratios greater than or equal 3.0 ($c_{max} \geq 1080$mm).

For column aspect ratios greater than or equal to 1.5, the Model Code 2010 and CSCT provisions predict an approximately constant capacity as β increased. For column aspect ratios greater than or equal to 2.556, the FEM results also plateau at a constant capacity.

On average, the capacity predictions according to ACI 318M-14, EC2 (2004), Model Code 2010 and the CSCT are 15% higher, 3% higher, 53% lower and 16% lower than the capacity predicted by the FEM respectively. As noted in Section 5.2.5, the ACI 318M-14 provisions are becoming more unconservative and the EC2 provisions are becoming less unconservative as the c_{min}/d ratio is increased.

The EC2 (2004) predictions were found to be most accurate for column rectangularity values between 1 and 2.556 (V_{FEA}/V_{EC2} is between 0.96 and 1.08). The ACI 318 provisions on the other hand were only accurate for a rectangularity value of 1. The CSCT provisions were conservative for all investigated column aspect ratios other than 1, and were fairly accurate for all rectangularity values investigated (V_{FEA}/V_{CSCT} is between 1.07 and 1.23). Unlike the previous c_{min}/d ratios, the CSCT

predictions were found to have the least variability based on the coefficient of variation of V_{CODE}/V_{FEA}. This reduced variability compared to the previous c_{min}/d ratios is likely due to the fact that fewer rectangularities were investigated, and the predicted capacities for most of the models were similar due to the use of an effective critical perimeter length according to the 3d method in Model Code 2010.

A comparison of the normalized nominal shear stress predicted by ACI 318M-14, EC2 (2004), Model Code 2010, the CSCT and the finite element model at the ACI critical perimeter located at d/2 from the column perimeter is provided in Figure 5-37. As expected, based on the total capacity estimates, the nominal shear stress predicted by ACI 318M-14 is higher than that predicted by the finite element model, which leads to ACI overpredicting the punching capacity. Additionally, the assumption of zero impact for rectangularity values less than 2 is leading to increased error, as the finite element model is predicting a significant impact of column rectangularity for rectangularity values between 1 and 2.

The impact of column rectangularity predicted by EC2 (2004) is less severe than that predicted by the FEM. For rectangularities greater than 2.556, the nominal shear stress predicted by EC2 is higher than that predicted from the FEA and the difference between the EC2 and FEA predictions becomes larger as β increases.

The trend of the normalized nominal stress based on the CSCT provisions is similar to that from the FEA for all rectangularities other than β equal to 1. As was observed for c_{min}/d ratios of 0.594, 0.792, 1.287 and 1.485, the normalized nominal shear stress predicted by the CSCT does not approach a constant value and decreases as β is increased.

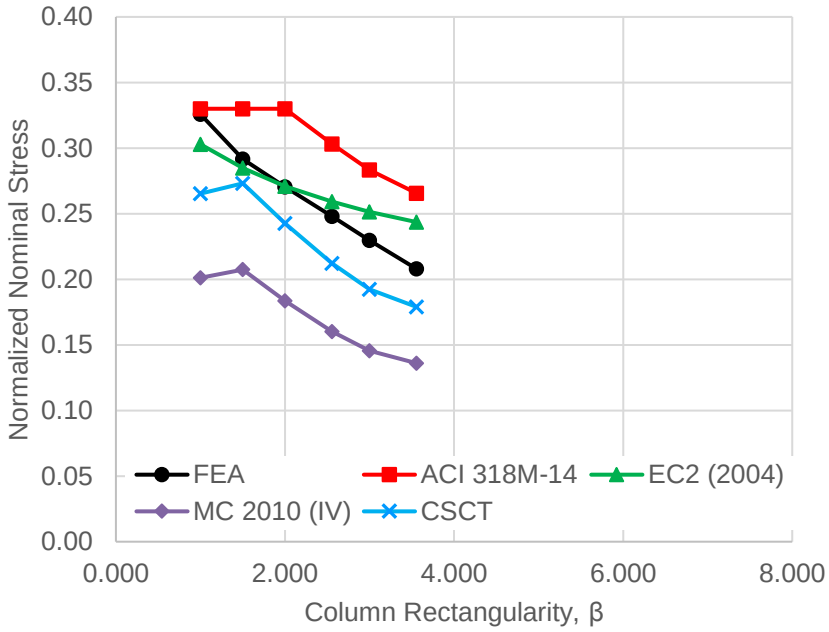

Figure 5-37: Comparison of Nominal Shear Capacity Predicted by FEA and Design Codes, c_{min}/d = 1.782

The shear stress distributions in the slab around the support plate perimeter at the peak load level calculated from the FEA results for the six rectangularity values investigated are shown in Figure 5-38. The overall shape of the predicted shear stress distributions around the column perimeter was similar for all investigated rectangularity values, which is consistent with the results from the other c_{min}/d ratios.

If the peak shear stresses from the six models are plotted together the calculated peak stress for all models including the square support area, are between approximately 5.2 and 6.2MPa. This stress range is higher than that observed for the c_{min}/d = 1.485 results. However, this stress range is similar to that observed for the lower c_{min}/d ratios.

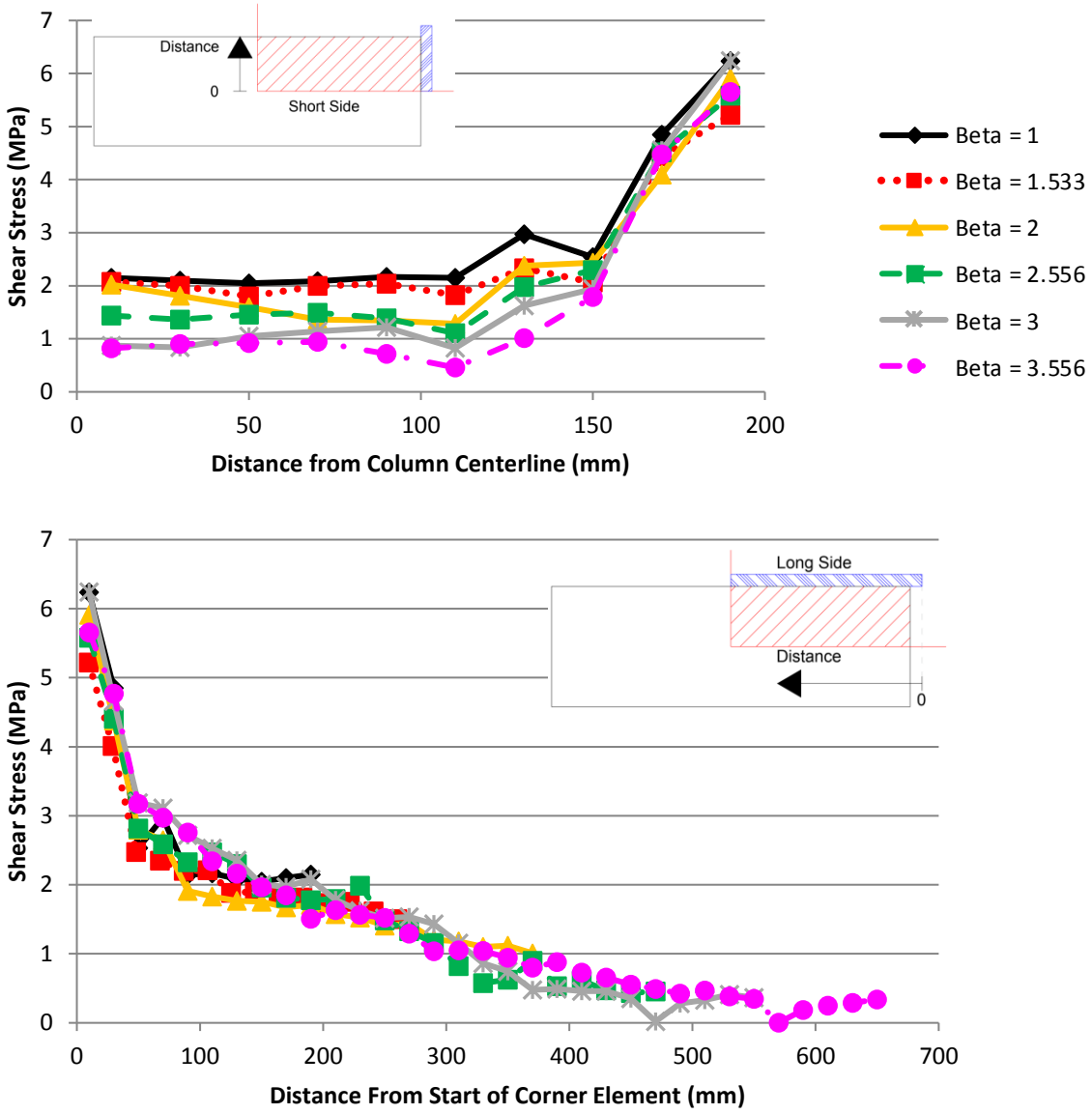

Figure 5-38: Predicted Shear Stress Distribution Around Support Plate Perimeter, c_{min}/d = 1.782, Top) Stresses Along Short Side, Bottom) Stresses Along Long Side

The trends in observed in the crack patterns for the c_{min}/d=1.782 models are very similar to those discussed for the previous c_{min}/d ratios. As the rectangularity was increased beyond 1, the amount of diagonal cracking predicted on the tension side decreased. Along with the decrease in diagonal cracking, an increased amount of cracking perpendicular to the sides of the supported area were predicted as β was increased. Additionally, the cracks concentrated near the corner of the supported area as β was increased. The shape of the failure cones along the sides of the slab was also similar to

that observed in the previously discussed models. At low rectangularity values, a conical crack extending from the tension surface of the slab to compression surface was predicted. As the rectangularity increased, the plastic strain magnitudes predicted along both the long and short sides decreased, which denotes less cracking. Along the slab side perpendicular to the long side of the steel plate, the conical shape transitions into a reverse z shape, before becoming almost non-existent at a β value of 3, which is a lower rectangularity but similar column length at which similar behaviour was observed for the lower c_{min}/d ratios. The lack of clear punching cones on both sides of the supported area was expected since a one-way shear crack extending across the slab width parallel to the long side of the steel plate began to appear at a β value of 2.5. Again, this one-way shear crack appeared at a lower rectangularity value when compared to the previous c_{min}/d ratios, but the overall column length was similar. Finally, as observed in the models with a c_{min}/d ratio greater than or equal to 0.990, a second crack starting at the mid-depth of the slab and extending to the compression surface of the slab near the support was observed on the slab side perpendicular to the short side of the supported area in all models. This second crack forms below the top conical crack.

5.2.7 C_{min}/d = 1.980

A summary of the column dimensions, column rectangularity values (β), predicted capacity and predicted deflections at peak load in the X and Y-directions for the models with a c_{min}/d ratio of 1.980 are provided in Table 5-14 and the load-displacement plots are provided in Figure 5-39. As with the previously discussed c_{min}/d ratios, the FEM predicted a higher total capacity as the column size, and rectangularity, were increased.

Table 5-14: Summary of FEA Results for c_{min}/d = 1.980

c_{min} (mm)	c_{max} (mm)	β	Predicted Capacity (kN)	Δ_X (mm)	Δ_Y (mm)
400	400	1.000	1025.0	23.20	23.20
400	600	1.500	1078.8	23.36	21.17
400	800	2.000	1134.9	23.96	19.00
400	1000	2.500	1162.9	32.79	17.08
400	1200	3.000	1178.9	30.21	12.75

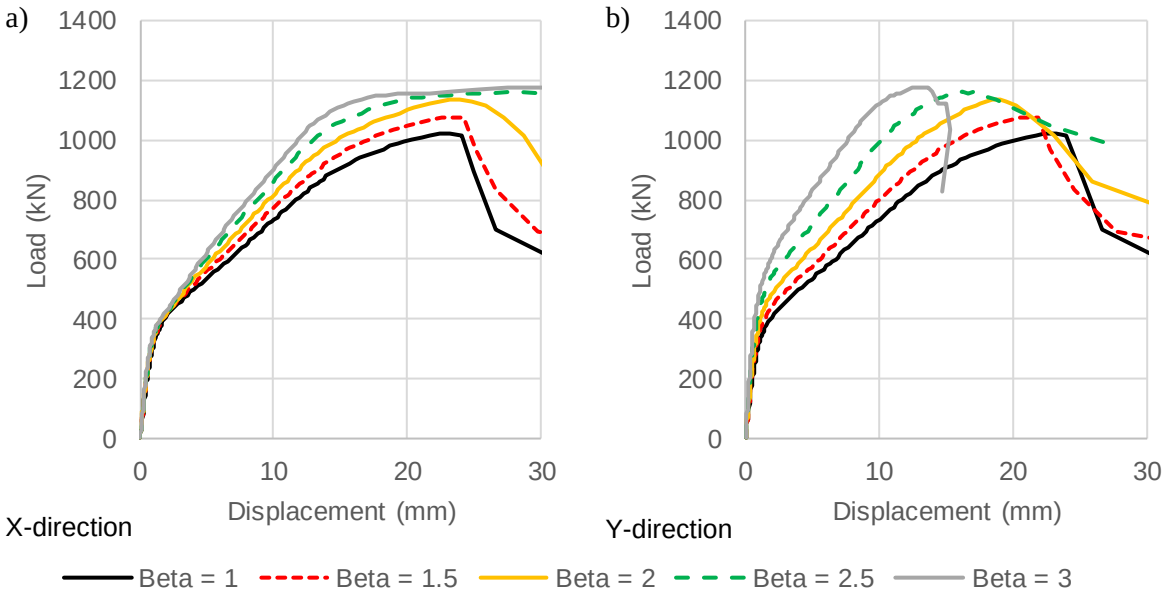

Figure 5-39: Predicted Load-Displacement Response, $c_{min}/d = 1.980$

The FEM model predicted all slabs to fail in punching shear, except for the slab where β equaled 3. The slab where β equaled 3 was predicted to fail in one-way shear.

Generally, the deflections in the X-direction increased as the column rectangularity increased, with the model where β equaled 3.0 being the exception. The deflections in the Y-direction decreased as the rectangularity increased.

The trends in stiffness are consistent with the previous models, and therefore, they are not discussed in detail in this section.

A comparison of the shear capacity predicted by the FEA to ACI 318M-14 (ACI), Eurocode 2 (2004) (EC2), Model Code 2010 (MC 2010) and the Critical Shear Crack Theory (CSCT) for all the models with a c_{min}/d ratio of 1.980 are provided in Figure 5-40, Figure 5-41 and Table 5-15.

For the investigated slabs with a c_{min}/d ratio of 1.980, the ACI 318M-14 provisions were found to be unconservative and the EC2 (2004) provisions were found to be typically conservative. However, it should be noted that the EC2 (2004) predictions are unconservative for column aspect ratios greater than or equal to 2.5. For the investigated aspect ratios, the ACI provisions predict the highest capacity. As with all previous c_{min}/d ratios, the EC2 (2004) provisions predict a larger total shear capacity as the column rectangularity is increased. The ACI provisions on the other hand predicted an increase in capacity with increasing rectangularity for rectangularity values less than 2.5. For column

rectangularities greater than or equal to 2.5 with a c_{min}/d ratio of 1.980 the one-way shear capacity predicted from ACI 318M-14 governs leading to a constant shear capacity with increasing rectangularity. None of the investigated specimens were predicted to fail in one-way shear by EC2 (2004). The FEA model predicted that one-way shear behaviour begins to govern at a column rectangularity of 3 (c_{max}=1200mm) and at a load value of 1178.9 kN. Based on the work of Regan and Rezai-Jorabi (1988), it is expected that the one-way shear capacity predicted by the FEA would be less than that predicted from ACI 318M-14 (1486kN) since the ACI equation assumes the slab to be under uniformly distributed loading.

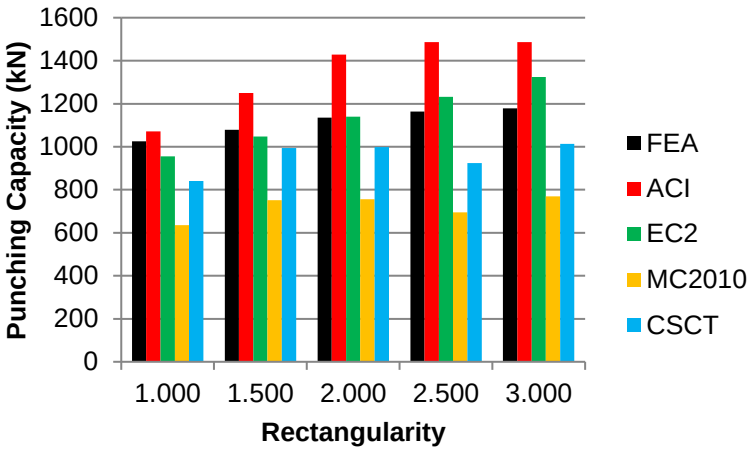

Figure 5-40: Shear Capacity from FEA and Design Codes, All β Values, c_{min}/d=1.980, Bar Chart

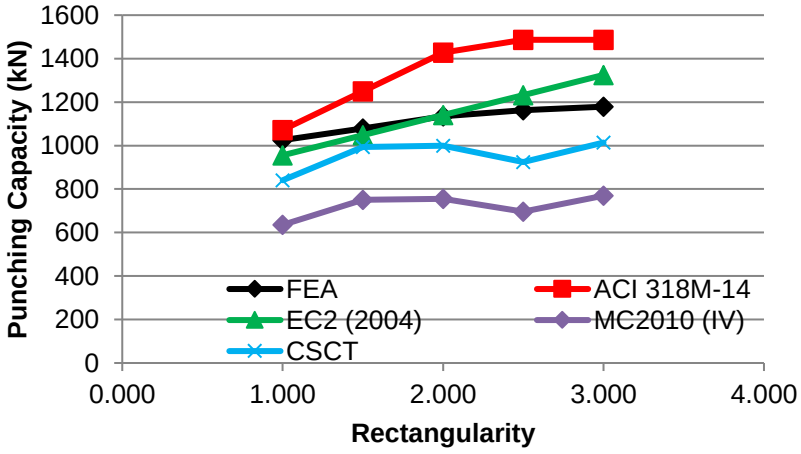

Figure 5-41: Shear Capacity from FEA and Design Codes, All β Values, c_{min}/d=1.980

For column aspect ratios greater than or equal to 1.5, the Model Code 2010 and CSCT provisions predict an approximately constant capacity as β increased. As seen in Figure 5-40 and Figure 5-41, the FEM predictions begin to plateau for column rectangularities greater than or equal to 2.

Table 5-15: Comparison of Code Predictions and FEA Results – $c_{min}/d = 1.980$

c_{min} (mm)	c_{max} (mm)	β	FEA Capacity (kN)	V_{FEA}/V_{ACI}	V_{FEA}/V_{EC2}	V_{FEA}/V_{MC2010}	V_{FEA}/V_{CSCT}
400	400	1.000	1025.0	0.96	1.07	1.61	1.22
400	600	1.500	1078.8	0.86	1.03	1.44	1.09
400	800	2.000	1134.9	0.79	1.00	1.50	1.14
400	1000	2.500	1162.9	0.78*	0.94	1.67	1.26
400	1200	3.000	1178.9	0.79*	0.89	1.53	1.16
			Average	0.84	0.99	1.55	1.17
			COV (%)	8.77	7.27	5.97	5.78

*Governed by one-way shear capacity

On average, the capacity predictions according to ACI 318M-14, EC2 (2004), Model Code 2010 and the CSCT are 16% higher, 1% higher, 55% lower and 17% lower than the capacity predicted by the FEM respectively. As noted in Section 5.2.5, the ACI 318M-14 provisions are becoming more unconservative and the EC2 (2004) provisions are becoming less unconservative as the c_{min}/d ratio is increased.

The EC2 (2004) predictions were found to be most accurate for column rectangularity values between 1 and 2.5 (V_{FEA}/V_{EC2} is between 1.00 and 1.07). The ACI 318 provisions on the other hand are unconservative for all investigated rectangularity values with a maximum V_{FEA}/V_{ACI} value of 0.96 for a square support area. The CSCT provisions were conservative for all investigated column aspect ratios other than 1 and were fairly accurate for all rectangularity values investigated (V_{FEA}/V_{CSCT} is between 1.09 and 1.26). Similar to the results for a c_{min}/d ratio of 1.982, the CSCT predictions were found to have the least variability based on the coefficient of variation of V_{CODE}/V_{FEA}. Again, the reduced variability of the CSCT predictions is because fewer rectangularities were studied, and the predicted capacities for most of the models were similar due to the use of an effective critical perimeter length according to the 3d method in Model Code 2010.

A comparison of the normalized nominal shear stress predicted by ACI 318M-14, EC2 (2004), Model Code 2010, the CSCT and the finite element model at the ACI critical perimeter located at d/2 from the column perimeter is provided in Figure 5-42. As expected, based on the total capacity estimates, the nominal shear stress predicted by ACI 318M-14 is higher than that predicted by the

finite element model, which leads to ACI overpredicting the punching capacity. Additionally, the assumption of zero impact for rectangularity values less than 2 is leading to increased error, as the finite element model is predicting a significant impact of column rectangularity for rectangularity values between 1 and 2.

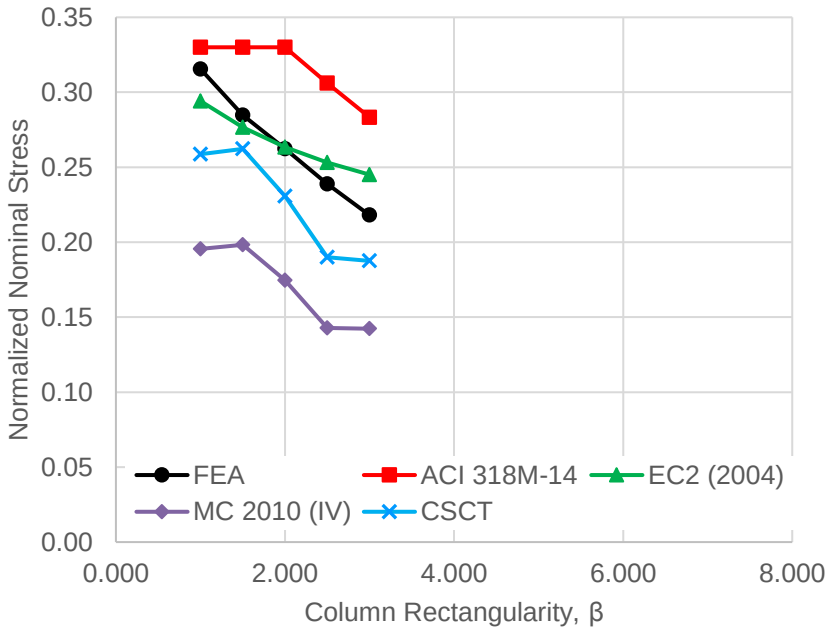

Figure 5-42: Comparison of Nominal Shear Capacity Predicted by FEA and Design Codes, c_{min}/d = 1.980

The impact of column rectangularity predicted by EC2 (2004) is less severe than that predicted by the FEM. For rectangularities greater than 2, the nominal shear stress predicted by EC2 (2004) is higher than that predicted from the FEA and the difference between the EC2 (2004) and FEA predictions becomes larger as β increases.

The trend of the normalized nominal stress based on the CSCT provisions is similar to that from the FEA for rectangularities between 1.5 and 2.5. However, for column rectangularities between 1 and 1.5 and 2.5 and 3, the normalized nominal shear stress is constant.

The shear stress distributions around the column perimeter at the peak load level calculated from the FEA results for the five investigated rectangularity values are shown in Figure 5-43. As with the previous c_{min}/d ratios, the overall shape of the predicted shear stress distributions around the support plate perimeter was similar for all investigated rectangularity values. The peak shear stress occurred

at the corner of the supported area, and the shear stress magnitude dropped as the distance from this corner increased.

If the peak shear stress in the slab at the plate corner are plotted together, the calculated peak stress for all models, including the square support area, are between approximately 5.0 and 5.9MPa. This stress range is similar to that observed in the $c_{min}/d = 1.782$ results.

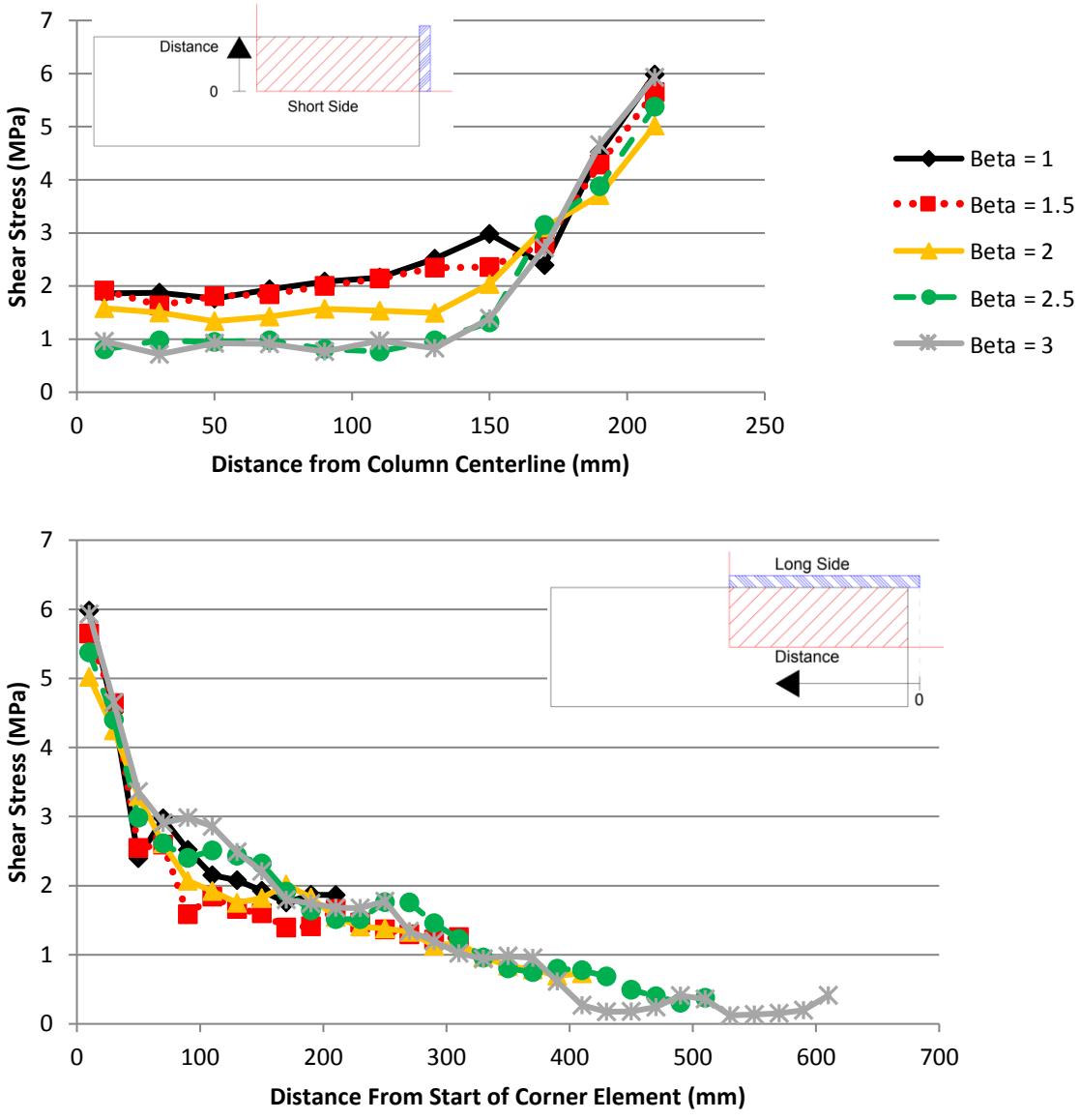

Figure 5-43: Predicted Shear Stress Distribution Around Support Plate Perimeter, $c_{min}/d = 1.980$, Top) Stresses Along Short Side, Bottom) Stresses Along Long Side

The trends in observed in the crack patterns for the $c_{min}/d = 1.980$ models are very similar to those observed for previously discussed c_{min}/d ratios. As the rectangularity was increased beyond 1, the amount of diagonal cracking on the tension side decreased. Along with the decreased diagonal cracking, the amount of cracking perpendicular to the sides of the supported area increased as β was increased. The cracks also concentrated near the corner of the supported area as β was increased. The shape of the failure cones along the sides of the slab is similar to that observed in the previously discussed models. At low rectangularity values, a conical crack extending from the compression portion of the slab to the tension side was predicted. As the rectangularity was increased, the plastic strain magnitudes predicted along both the long and short sides decreased. Along the slab side perpendicular to the long side of the support, the conical shape transitioned into a reverse z shape, before becoming almost non-existent at a β value of 3, which matches the rectangularity value where similar behaviour was observed for a c_{min}/d ratio of 1.782. The lack of clear punching cones on both sides of the supported area corresponded with the development of a one-way shear crack on the tension surface of the slab when β was greater than or equal to 2. As with the previous c_{min}/d ratios, the one-way shear crack appeared at a lower rectangularity value but a similar overall column length. Finally, as observed in the models with a c_{min}/d ratio greater than or equal to 0.990, a second crack starting at the mid-depth of the slab and extending to the compression surface of the slab near the support was observed on the slab side perpendicular to the short side of the supported area in some of the models. This second crack forms below the top conical crack and was observed for models where β equaled 1.5, 2 and 2.5.

5.2.8 $C_{min}/d = 2.970$

A summary of the column dimensions, column rectangularity values (β), predicted capacity and predicted deflections at peak load in the X and Y-directions for the models with a c_{min}/d ratio of 2.970 are provided in Table 5-16, and the load-displacement plots are provided in Figure 5-44. As with the previously discussed c_{min}/d ratios, the FEM predicted a higher total capacity as the column size, and rectangularity, were increased.

Table 5-16: Summary of FEA Results for $c_{min}/d = 2.970$

c_{min} (mm)	c_{max} (mm)	β	Predicted Capacity (kN)	Δ_X (mm)	Δ_Y (mm)
600	600	1.000	1200.8	24.87	24.87
600	920	1.533	1285.9	25.97	18.81
600	1200	2.000	1336.6	35.23	14.62

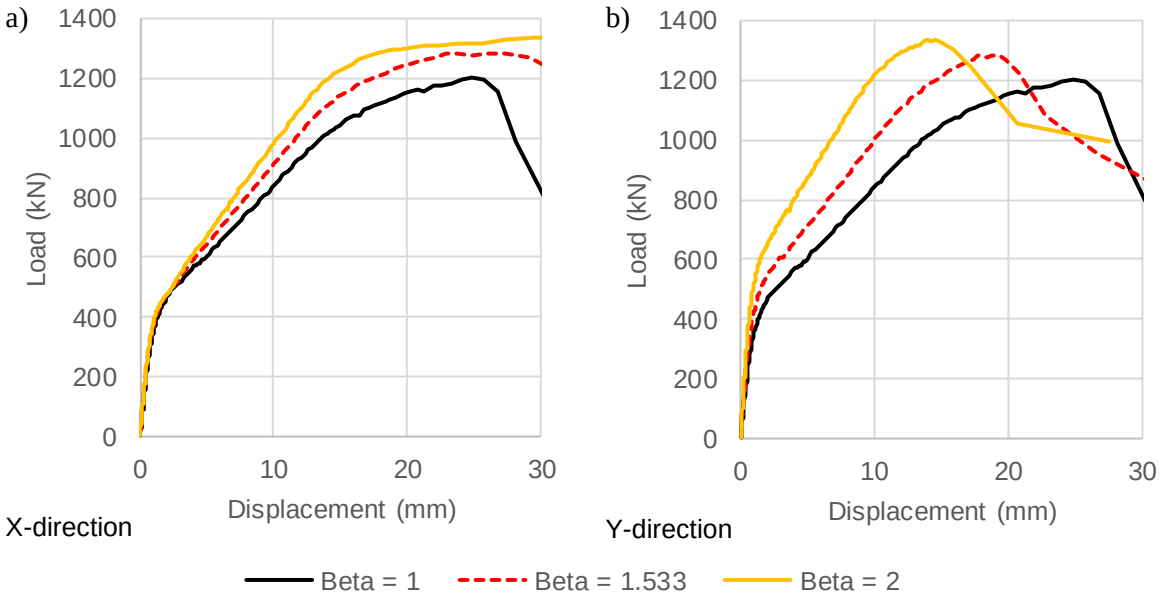

Figure 5-44: Predicted Load-Displacement Response, c_{min}/d = 2.970

All models with a c_{min}/d ratio of 2.970 were predicted to fail via the punching mode. It should be noted that the behaviour of the model where c_{min}/d and β equaled 2.970 and 2 respectively was similar to that observed in the model where c_{min}/d and β equaled 0.594 and 10 respectively. In both these models, an initial punching failure was predicted by the FEA before a secondary one-way shear failure. For the model where c_{min}/d and β equaled 2.970 and 2 respectively this secondary one-way failure did not occur instantaneously after punching, which differs from the model where c_{min}/d and β equaled 0.594 and 10 respectively.

The deflections in the X-direction increased and the deflections in the Y-direction decreased as the column rectangularity increased.

The trends in stiffness are also consistent with the previous models, and therefore, they are not discussed in detail in this section

A comparison of the shear capacity predicted by the FEA to ACI 318M-14 (ACI), Eurocode 2 (2004) (EC2), Model Code 2010 (MC 2010) and the Critical Shear Crack Theory (CSCT) for all the models with a c_{min}/d ratio of 1.980 are provided in Figure 5-45, Figure 5-46 and Table 5-17.

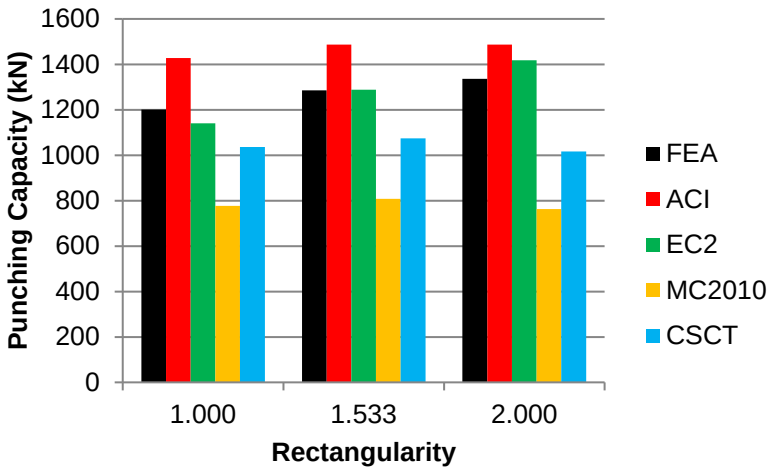

Figure 5-45: Shear Capacity from FEA and Design Codes, All β Values, c_{min}/d=2.970, Bar Chart

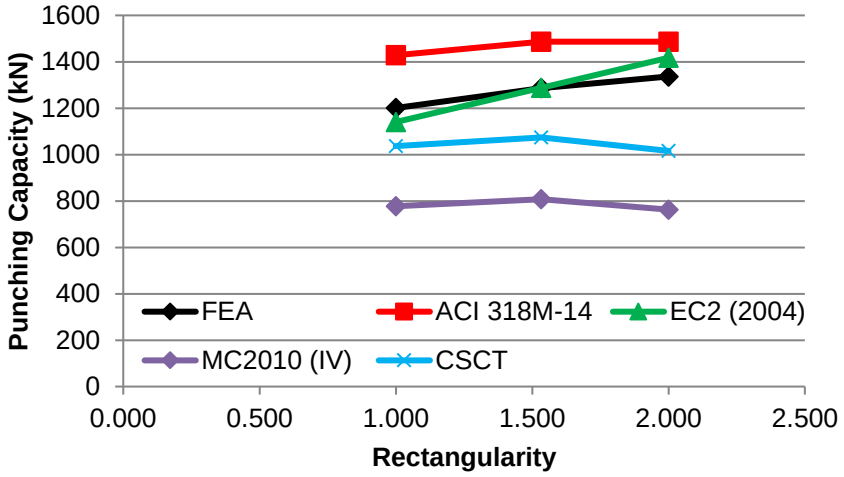

Figure 5-46: Shear Capacity from FEA and Design Codes, All β Values, c_{min}/d=2.970

For a c_{min}/d ratio of 2.970, the ACI 318M-14 provisions were found to be unconservative and the EC2 (2004) provisions were found to be typically conservative for the investigated models. However, it should be noted that the EC2 (2004) predictions are unconservative for the largest investigated column aspect ratio (β=2). Consistent with the results for all c_{min}/d ratios greater than or equal to 1.485, the ACI provisions predict the highest capacity compared to the FEA and the other design codes. As with all previous c_{min}/d ratios, the EC2 (2004) provisions predict a larger total shear capacity as the column rectangularity is increased and all models are predicted to fail in punching shear, which is consistent with the FEA results. The ACI provisions on the other hand predicted an

increase in capacity with increasing rectangularity for rectangularity values less than 1.533. For column rectangularities greater than or equal to 1.533 with a c_{min}/d ratio of 2.970, the one-way shear capacity predicted from ACI 318M-14 governs leading to a constant shear capacity with increasing rectangularity.

Table 5-17: Comparison of Code Predictions and FEA Results – $c_{min}/d = 2.970$

c_{min} (mm)	c_{max} (mm)	β	FEA Capacity (kN)	V_{FEA}/V_{ACI}	V_{FEA}/V_{EC2}	V_{FEA}/V_{MC2010}	V_{FEA}/V_{CSCT}
600	600	1.000	1200.8	0.84	1.05	1.55	1.16
600	920	1.533	1285.9	0.86*	1.00	1.59	1.20
600	1200	2.000	1336.6	0.90*	0.94	1.75	1.32
			Average	0.87	1.00	1.63	1.22
			COV (%)	3.37	5.51	6.66	6.69

*Governed by one-way shear capacity

For the investigated column rectangularities, the Model Code 2010 and CSCT provisions predict an approximately constant capacity as β increased. The FEM predicted capacities on the other hand do not plateau for the investigated column rectangularities.

On average, the capacity predictions according to ACI 318M-14, EC2 (2004), Model Code 2010 and the CSCT are 13% higher, 0% higher, 63% lower and 22% lower than the capacity predicted by the FEM respectively. As noted in Section 5.2.5 and 5.2.7, the ACI 318M-14 provisions are becoming more unconservative and the EC2 provisions are becoming less unconservative as the c_{min}/d ratio is increased. The CSCT and Model Code 2010 predictions become more conservative as the c_{min}/d ratio is increased.

The EC2 (2004) predictions were found to be most accurate of the considered design codes for a c_{min}/d ratio of 2.970 (V_{FEA}/V_{EC2} is between 0.94 and 1.05). The ACI 318 provisions on the other hand are unconservative for all investigated rectangularity values with a maximum V_{FEA}/V_{ACI} value of 0.90 for a rectangularity of 2, which is governed by one-way shear capacity. The CSCT provisions were conservative for all investigated column aspect ratios and became more conservative as the column aspect ratio was increased (V_{FEA}/V_{CSCT} is between 1.16 and 1.32). For a c_{min}/d ratio of 2.970 the ACI 318M-14 predictions were found to have the least variability based on the coefficient of variation of V_{CODE}/V_{FEA} because two of the three aspect ratios studied were governed by one-way shear capacity.

A comparison of the normalized nominal shear stress predicted by ACI 318M-14, EC2 (2004), Model Code 2010, the CSCT and the finite element model at the ACI critical perimeter located at d/2

from the column perimeter is provided in Figure 5-47. As expected the nominal shear stress predicted by ACI 318M-14 is much higher than that predicted by the finite element model, which leads to ACI 318 overpredicting the shear punching capacity.

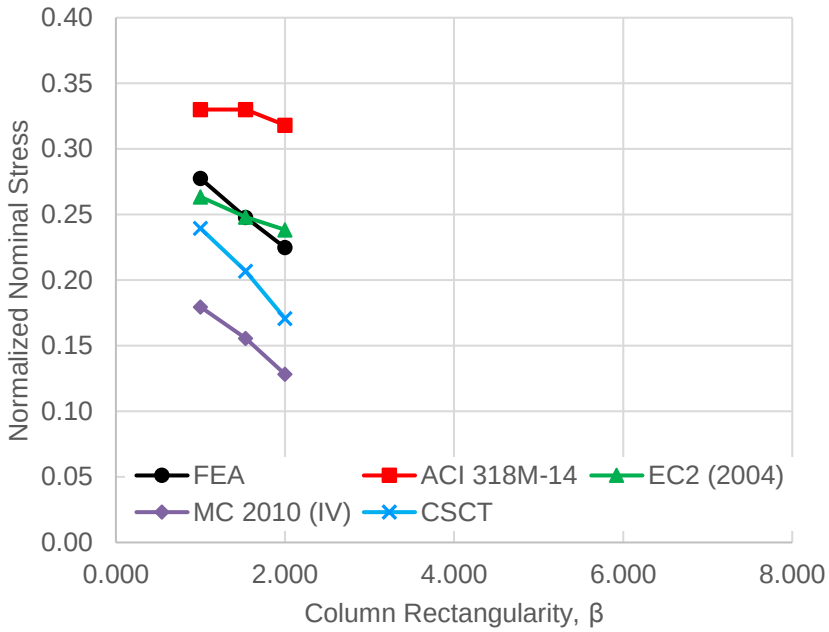

Figure 5-47: Comparison of Nominal Shear Capacity Predicted by FEA and Design Codes, c_{min}/d = 2.970

The impact of column rectangularity predicted by EC2 (2004) and the CSCT are similar to that predicted by the FEM for the rectangularities studied. However, the nominal capacities predicted by the CSCT are quite conservative compared to EC2 (2004) and the FEM.

The shear stress distributions around the column perimeter at the peak load level calculated from the FEA results for the three rectangularity values investigated are shown in Figure 5-48. As with all previously discussed c_{min}/d ratios, the overall shape of the predicted shear stress distributions around the column perimeter is similar for all investigated rectangularity values. The calculated peak shear stress occurred at the corner of the supported area, and the shear stress level dropped as the distance from the corner increased. From the short side stress distributions, it was observed that the peak shear stress at the column corner (at the peak load level) decreased as β increased. Unlike the results for the lower c_{min}/d ratios, the shear stresses along the short side of the support plate are quite low. As discussed previously, experimental results have shown that shear stresses typically concentrate

around the short side of the column. However, in the three stress distributions shown in Figure 5-48, this concentration is not observed as the shear stresses magnitude decreases significantly after the first few elements. It is possible that this lack of shear stress concentration is due to the overall column size, or influence of one-way shear behaviour, but further investigation is required.

The calculated peak stress for all models with a c_{min}/d ratio of 2.970 are between approximately 5.3 and 6.0MPa. This stress range similar to that observed in the c_{min}/d = 1.782 and 1.980 results.

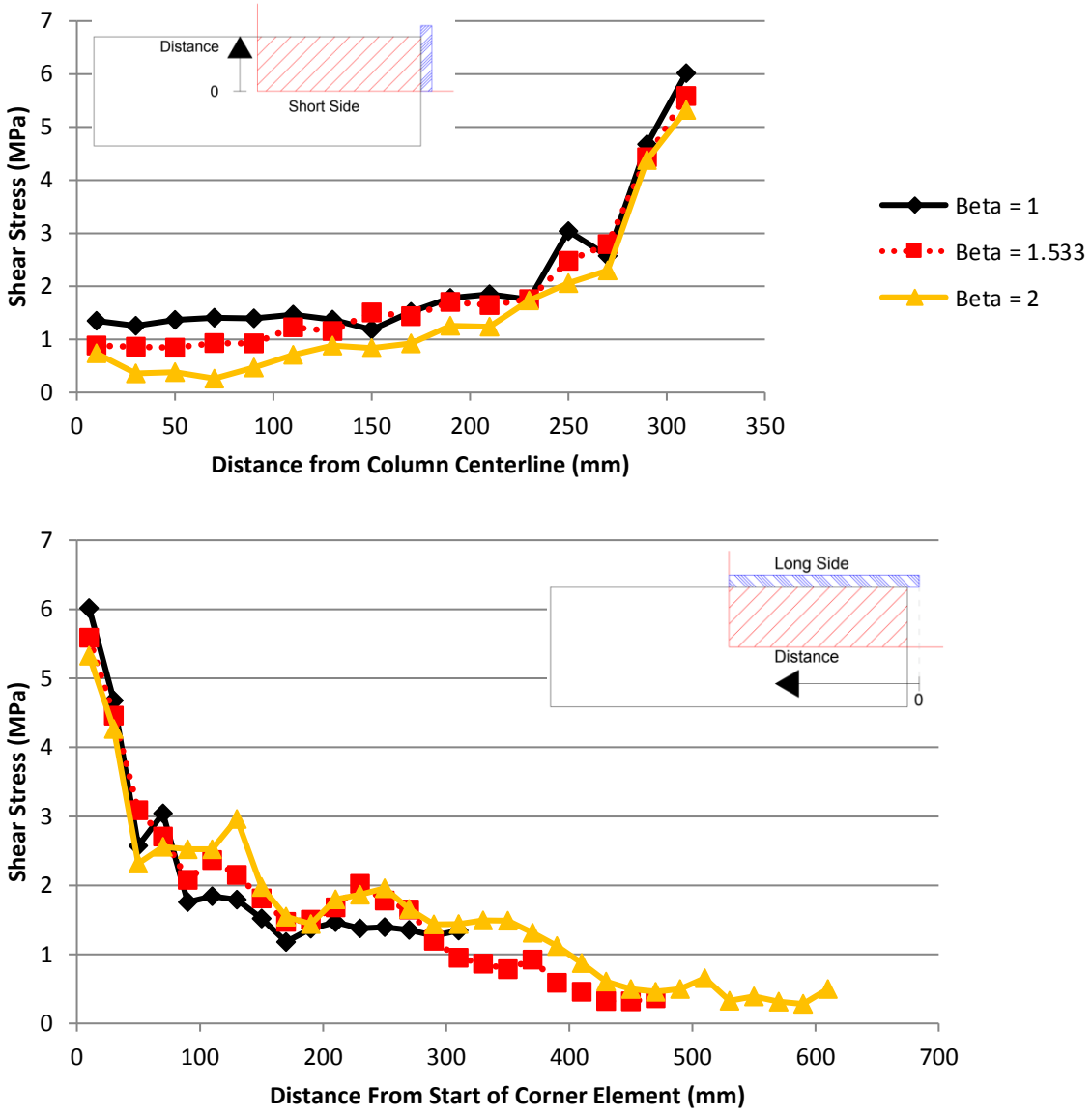

Figure 5-48: Predicted Shear Stress Distribution Around Support Plate Perimeter, c_{min}/d = 2.970, Top) Stresses Along Short Side, Bottom) Stresses Along Long Side

The trends observed in the crack patterns for the $c_{min}/d = 2.970$ models are very similar to those observed for the previous c_{min}/d ratios. As the rectangularity was increased beyond 1, the amount of diagonal cracking predicted on the tension side decreased. Along with the decrease in diagonal cracking an increased amount of cracking perpendicular to the sides of the supported area were observed as β was increased. Additionally, it was observed that the predicted cracks concentrated near the corner of the supported area as β was increased. The trends in the failure cones along the slab sides are consistent with those observed for the previously discussed c_{min}/d ratios. However, the crack pattern on the slab side perpendicular to the long side of the support plate quickly transitioned from conical to a reverse z shape. In the model where β equaled 1.5, the reverse z shape is visible inside the punching cone, and in the model where β equaled 2, only the reverse z portion of the crack is fairly noticeable. Again, as the rectangularity was increased the plastic strain magnitudes predicted along both the long and short sides decreased, which was consistent with all previous model results. Unlike the results for c_{min}/d ratios greater than or equal to 0.990, a second crack below the top conical crack, starting at the slab mid-depth and extending towards the compression surface of the slab near the support, was not observed on the slab side perpendicular to the short side of the supported area.

5.3 Discussion of FEA Results for All C_{min}/d Ratios

In this section, results considering all eight investigated c_{min}/d ratios simultaneously are discussed. In Section 5.3.1, a comparison of the impact of column rectangularity predicted by the FEM and the four investigated design methods is provided. In Section 5.3.2, a further discussion of the predicted shear stress distributions in the slab around the support plate perimeter is provided.

5.3.1 Code Comparisons

The primary aim of the parametric study was to determine if the impact of column rectangularity is dependent on the ratio of minimum column dimension, c_{min}, to the effective slab depth d. This parameter was investigated due to differences seen in current and historical design code provisions as discussed in Section 5.1.1.

In this section, a comparison of the FEA results and code predictions for all investigated c_{min}/d ratios is provided. Firstly, a comparison of the nominal shear stress predicted by ACI 318M-14 and the FEM is presented. Secondly, the impact of column rectangularity predicted for each c_{min}/d ratio according to EC2 (2004), Model Code 2010 (LoA IV) and the CSCT is discussed. These three design methods are not directly compared to the FEA results as detailed discussions are provided throughout

Section 5.2. Thirdly, the change in nominal shear stress for constant rectangularity values, but varying c_{min}/d ratios, predicted by the FEA and the four design methods are compared. Fourthly, the overall trends of the code predictions compared to the FEA results for all c_{min}/d ratios are discussed. Finally, a summary of the models predicted to fail in one-way shear is provided.

5.3.1.1 Comparison of Nominal Shear Capacity Predicted by FEM and ACI 318M-14

A comparison of the normalized nominal shear stress along the ACI 318 critical perimeter predicted by the FEM and ACI 318M-14 is shown in Figure 5-49. Unlike the FEA results, which demonstrated that the impact of column rectangularity is highly dependent on the c_{min}/d ratio, the ACI 318M-14 predictions are largely independent of the c_{min}/d ratio. As shown in Figure 5-49, the nominal shear stress capacity predicted by ACI 318M-14 for column aspect ratios between 1.5 and 3 for a c_{min}/d ratio of 2.970 is slightly lower than that predicted for the smaller c_{min}/d ratios. For all other rectangularity values, the ACI 318 predictions are identical for the eight investigated c_{min}/d ratios.

Furthermore, the FEA predictions display an approximately linear decrease in nominal shear capacity as the support aspect ratio increases. The slope of a trendline fit to the FEA predictions shown in Figure 5-49, for each c_{min}/d ratio, became steeper as the c_{min}/d ratio increased, as shown in Table 5-18. Therefore, the FEM predicted a more severe impact of column rectangularity as the c_{min}/d ratio was increased. Unlike the FEA predictions, the ACI 318M-14 predictions are curved and assume that moderate column rectangularity ($\beta \leq 2$) has no effect on nominal shear stress capacity. The FEA predictions on the other hand show that even moderate column rectangularity has a negative impact on nominal shear stress capacity. The trendlines referenced in Table 5-18 are provided in Appendix J.

Table 5-18: Slope of Trendline Fit to Nominal Shear Stress vs β Plot for each c_{min}/d ratio

c_{min}/d	β_{max}	Trendline Slope (Punching Capacity vs β)	R^2 of Trendline
0.594	10	-0.0154	0.9884
0.792	8	-0.0208	0.9891
0.990	6.6	-0.0262	0.9819
1.287	5.077	-0.0331	0.9778
1.485	4	-0.0346	0.9858
1.782	3.556	-0.0447	0.9892
1.980	3	-0.0482	0.9946
2.970	2	-0.0528	0.9987

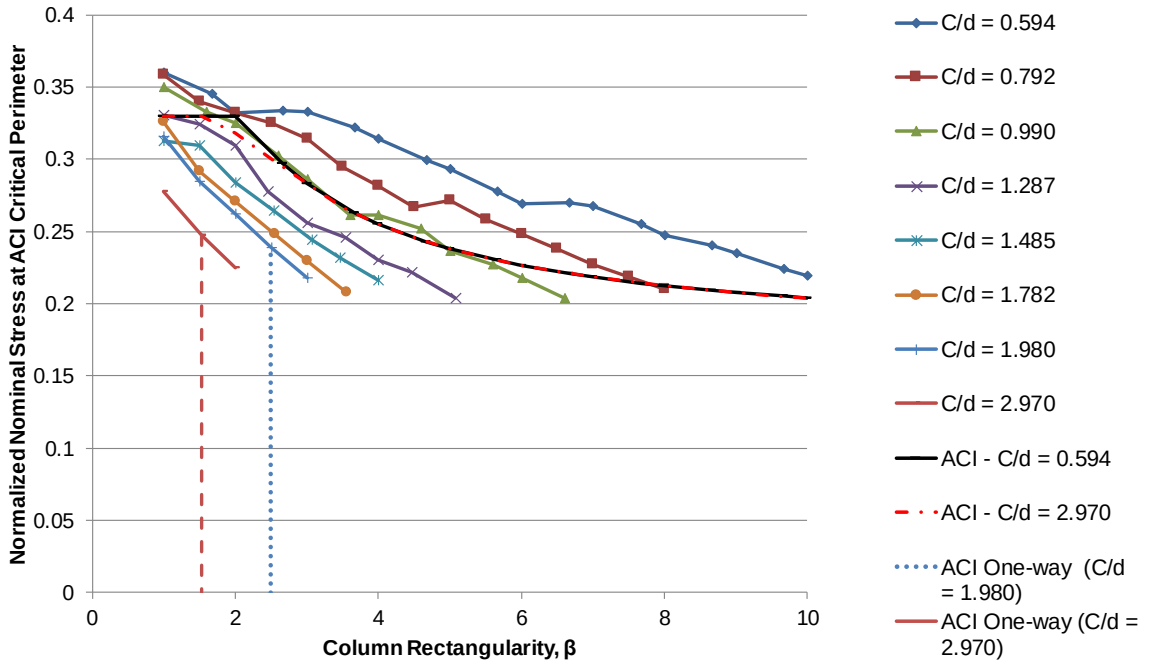

Figure 5-49: Comparison of Nominal Shear Stress Around ACI 318 Critical Perimeter Predicted by ACI 318M-14 and FEA, all c_{min}/d ratios

The nominal shear capacity predicted by ACI 318M-14 is generally conservative compared to the FEA results for all investigated rectangularity values for the two smallest c_{min}/d ratios, 0.594 and 0.792. Additionally, the nominal capacity predicted by ACI 318M-14 and the FEM for a c_{min}/d ratio of 0.990 are very close until a rectangularity of 5. As β is increased beyond 5, the ACI predictions become unconservative compared to the FEA results. For a c_{min}/d ratio of 1.287, the nominal stress predicted by ACI 318M-14 is higher than that from the FEA, though the values are similar. For all other investigated c_{min}/d ratios, the difference between the nominal capacity predicted by ACI 318M-14 and the FEA grows as the c_{min}/d ratio is increased. It should be noted that the nominal shear stress capacities calculated according to ACI 318M-14 shown in Figure 5-49 do not account for one-way shear. For c_{min}/d ratios of 1.980 and 2.970, and an average effective slab depth of 202mm, the ACI 318M-14 provisions predict one-way shear capacity to govern for investigated column aspect ratios greater than or equal to 2.5 and 1.533 respectively.

5.3.1.2 Discussion of Nominal Shear Capacity Predicted by EC2 (2004), Model Code 2010 and the CSCT

As discussed in Section 5.2.1, a normalized nominal shear stress was used to compare the impact of column rectangularity predicted by EC2 (2004), Model Code 2010 and the CSCT to the FEA and ACI 318M-14 predictions. In this section, the overall trends of each code are analyzed. Detailed comparisons of the code predictions to the FEA results are provided in Section 5.2.

The predicted nominal shear stress around the ACI 318 critical perimeter for Eurocode 2 (2004) is shown in Figure 5-50. The predicted nominal shear stress according to ACI 318 for the investigated c_{min}/d ratios less than or equal to 1.980 are also provided in Figure 5-50. As previously stated, the ACI 318M-14 predictions for the largest c_{min}/d ratio of 2.970 are nearly the same as those for the lower c_{min}/d ratios. Therefore, the nominal shear stress according to the ACI 318M-14 for a c_{min}/d ratio of 2.970 was removed from Figure 5-50 for clarity. The impact of one-way shear according to ACI 318M-14 is also neglected in Figure 5-50, as it only governed the predictions when β exceeded 2.5 or 1.533 for c_{min}/d ratios of 1.980 and 2.970 respectively. It should also be noted that unlike the ACI 318M-14 predictions, none of the investigated slab-column connections were predicted to be governed by one-way shear by EC2 (2004).

Even though the EC2 (2004) provisions do not include a term to directly account for column rectangularity the nominal punching capacity around the ACI 318 critical perimeter decreased as the column rectangularity increased. Additionally, the nominal shear stress for the same rectangularity value significantly decreases as the c_{min}/d ratio increases, which differs from the current ACI 318M-14 provisions (2014), where a minimal difference in the nominal stress for different c_{min}/d ratios is predicted. Also, unlike the ACI 318M-14, which predicts a constant nominal stress for rectangularity values between 1 and 2, the nominal shear stress predicted by EC2 (2004) decreases for β values between 1 and 2, which matches the FEA results. As discussed for each individual c_{min}/d ratio in Section 5.2, the impact of rectangularity predicted by the EC2 provisions is very similar to that predicted by the FEA, though the EC2 provisions are typically slightly unconservative.

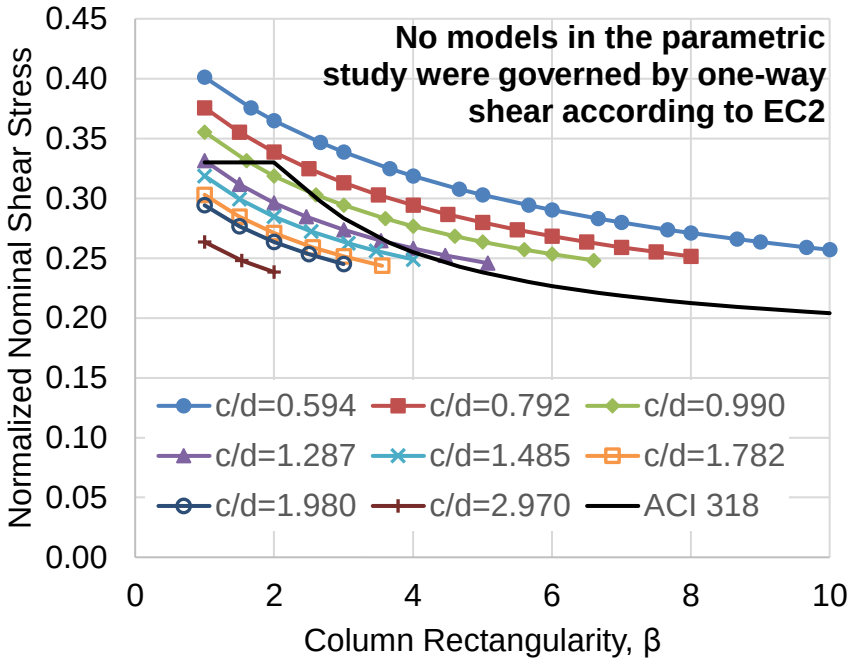

Figure 5-50: Predicted Nominal Shear Stress Capacity Along ACI 318 Critical Perimeter vs Rectangularity for all Investigated c_{min}/d ratios, EC2 (2004)

The predicted nominal shear stress around the ACI 318 critical perimeter according to the CSCT and Model Code 2010 (LoA IV) provisions, which are derived from the CSCT (Muttoni & Fernández Ruiz, 2012; Muttoni, Fernández Ruiz, Bentz, Foster, & Sigrist, 2013; Ricker & Siburg, 2016; Soares & Vollum, 2015), are shown in Figure 5-51. As with Figure 5-50, the ACI 318M-14 predictions for c_{min}/d ratios less than or equal to 1.980, neglecting the impact of one-way shear, are provided for comparison.

As with the FEA and EC2 (2004) predictions, the impact of column rectangularity predicted by Model Code 2010 and the CSCT are dependent on the c_{min}/d ratio. Additionally, for the majority of the investigated c_{min}/d ratios, both Model Code 2010 and the CSCT predict a decrease in the nominal shear stress capacity along the ACI 318 critical perimeter for columns with aspect ratios between 1 and 2. As mentioned in Section 5.2.1, the trend of the Model Code 2010 and CSCT predictions are identical, but the Model Code 2010 provisions, even at the highest level of approximation, are much more conservative.

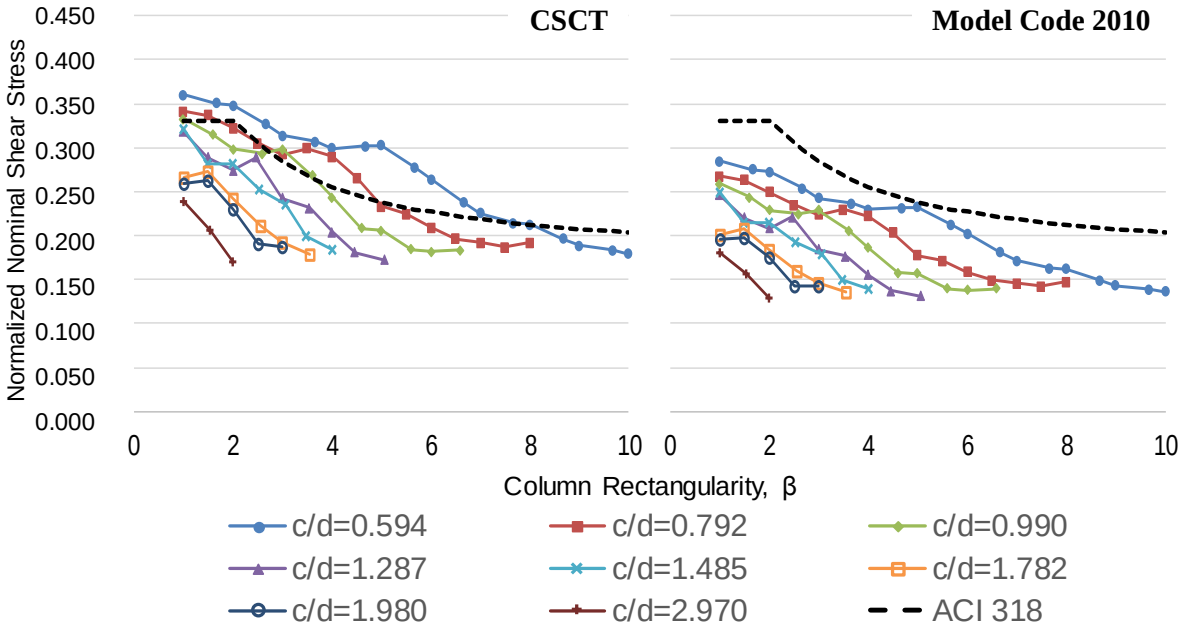

Figure 5-51: Predicted Nominal Shear Stress Capacity Along ACI 318 Critical Perimeter vs Rectangularity for all Investigated c_{min}/d ratios, Left: CSCT, Right: Model Code 2010

5.3.1.3 Comparison of Predicted Nominal Stress for Constant β Values and Varying c_{min}/d Ratios

A comparison of the nominal shear stress capacity along the ACI critical perimeter calculated from the FEA results, ACI 318M-14, EC2 (2004), Model Code 2010 (LoA IV) and the CSCT provisions for consistent rectangularity values between 1 and 5 and varying c_{min}/d ratios are provided in Figure 5-52.

The current ACI 318 provisions typically predict a constant nominal shear stress capacity along the critical perimeter for each individual rectangularity considered since the provisions are independent of the c_{min}/d ratio and are primarily based on the column aspect ratio. It should be noted that the ACI 318 provisions predict a slight change in nominal shear stress capacity when the column aspect ratio equals 2 since the equation based on d/b_o governs over the equation based on the column aspect ratio for a c_{min}/d ratio of 2.970. It should be noted that when β exceeds a value of 2.5 for a c_{min}/d ratio of 1.980 or a value of 1.533 for a c_{min}/d ratio of 2.970, the one-way shear capacity predicted by ACI 318 governs compared to the punching capacity. This lower one-way shear capacity is not accounted for in the plots in Figure 5-52. The ACI 318 predictions are found to be unconservative when compared to the FEA predictions for many of the c_{min}/d ratios investigated.

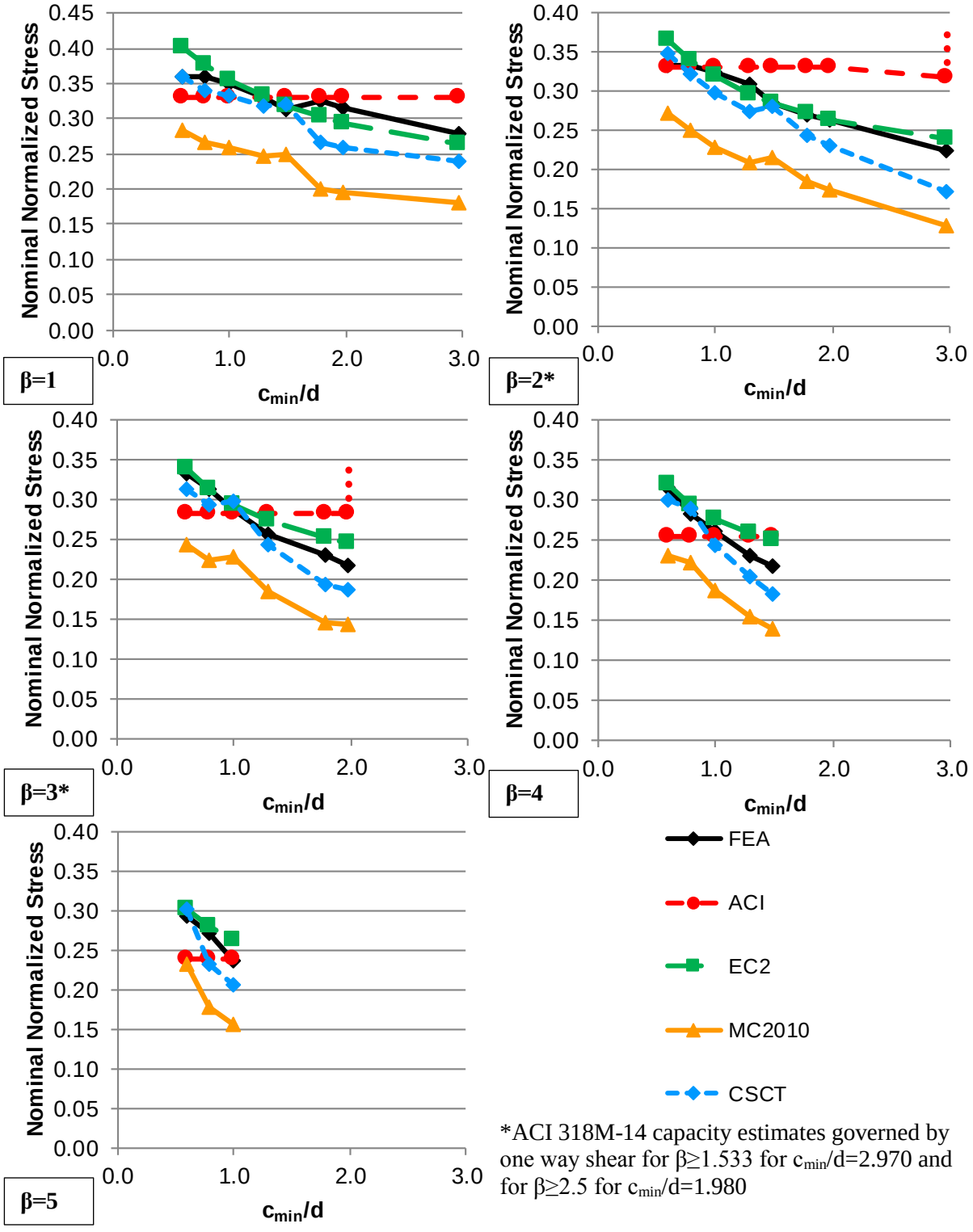

Figure 5-52: Comparison of Normalized Nominal Shear Stress Along ACI 318 Critical Perimeter Predicted by FEA and Codes for Varying c_{min}/d Ratios and Consistent Rectangularities, 1≤β≤5

Unlike the ACI provisions, which predict a constant normalized nominal shear stress capacity for most of the c_{min}/d ratios, both the FEA results and predictions according to EC2 (2004), Model Code 2010 (LoA IV) and the CSCT predict a reduction in the normalized nominal stress for a constant β value and increasing c_{min}/d ratio.

The EC2 (2004) provisions predict a similar reduction in nominal stress when compared to the FEA results. When considering the results for square columns or slightly elongated columns (β=2), the EC2 (2004) provisions predict normalized nominal stresses at the ACI critical perimeter which are very close to those predicted by the FEA results. However, the EC2 (2004) provisions are found to be slightly unconservative compared to the FEA results for the very small c_{min}/d ratios (0.594 and 0.792). The EC2 (2004) provisions are also found to be slightly unconservative compared to the FEA results for all c_{min}/d ratios for the larger column aspect ratios (β = 4 and 5).

Overall, the CSCT predictions correlate very well with the finite element predictions for all β and c_{min}/d ratios included in Figure 5-52. Typically, the CSCT predictions are conservative compared to the FEA results with a few predictions that are slightly higher. The Model Code 2010 predictions, according to LoA IV, are very conservative compared to the FEA results for all β and c_{min}/d ratios included in Figure 5-52. Theoretically, LoA IV predictions should be the least conservative (Muttoni & Fernández Ruiz, 2012; Genikomsou A. , 2015), which demonstrates that although Model Code 2010 captures the overall impact of column rectangularity well, it is extremely conservative.

Based on the comparison of the FEA results and the code predictions presented in Figure 5-52, it is concluded that the punching provisions according to EC2 (2004), Model Code 2010 and the CSCT better capture the predicted impact of column rectangularity compared to ACI 318M-14. As previously stated, EC2 (2004) was based on Model Code 1990 (European Concrete Platform ASBL, 2008), and the punching provisions in Model Code 1990 were primarily based on experimental results (Muttoni & Fernández Ruiz, 2012). On the other hand, the punching provisions in Model Code 2010 are mechanically based on the CSCT (Muttoni & Fernández Ruiz, 2012; Muttoni, Fernández Ruiz, Bentz, Foster, & Sigrist, 2013; Ricker & Siburg, 2016; Soares & Vollum, 2015) so the positive correlation with the FEA results observed for both codes is not caused by the codes sharing a similar basis. The predictions according to EC2 (2004), Model Code 2010 and the CSCT prove that the column aspect ratio and ratio of the critical perimeter length to the effective slab depth considered in ACI 318M-14 are not the only important parameters when estimating the punching capacity of slab-rectangular column connections.

5.3.1.4 Summary of Code Predictions vs FEA Predictions

Table 5-19 summarizes the results for the average ratio of the FEA to code predicted shear capacity discussed in Section 5.2 for each individual c_{min}/d ratio. The coefficient of variation of V_{CODE}/V_{FEA} for each code for each c_{min}/d ratio is also included in Table 5-19.

Table 5-19: Comparison of Code Predicted Capacity to Capacity Predicted by FEA

			V_{FEA}/V_{ACI}		V_{FEA}/V_{EC2}		$V_{FEA}/_{MC2010}$		V_{FEA}/V_{CSCT}	
c_{min}/d	β_{max}	# of Models	Average	COV (%)	Average	COV (%)	Average	COV (%)	Average	COV (%)
0.594	10.0	19	1.16	6.02	0.93	4.33	1.42	10.42	1.09	9.43
0.792	8.0	15	1.07	4.17	0.94	5.34	1.42	8.20	1.09	7.51
0.990	6.6	12	1.00	3.60	0.94	6.64	1.43	8.75	1.10	8.17
1.287	5.077	9	0.92	4.80	0.95	7.78	1.44	7.67	1.10	7.28
1.485	4.0	7	0.89	4.54	0.96	5.96	1.41	7.82	1.08	7.29
1.782	3.556	6	0.85	8.80	0.97	8.22	1.53	5.00	1.16	4.95
1.980	3.0	5	0.84	8.77	0.99	7.27	1.55	5.97	1.17	5.78
2.970	2.0	3	0.87	3.37	1.00	5.51	1.63	6.66	1.22	6.69

In general, the ACI 318M-14 provisions become less conservative compared to the FEA results as the c_{min}/d ratio is increased and are generally unconservative for c_{min}/d ratios larger than 1. Generally, the EC2 (2004) provisions were unconservative compared to the FEA results but improved in accuracy as the c_{min}/d ratio increased. The EC2 (2004) provisions were typically more accurate than the ACI 318M-14 predictions with a minimum ratio of the finite element estimated capacity to the code predicted capacity of 0.93 for EC2 (2004) and 0.84 for ACI 318. The EC2 (2004) provisions may be more accurate since the design equations account for size effect and flexural reinforcement ratio, whereas ACI 318 does not. Additionally, the shear stresses along the critical perimeter located at 2d from the column face used in the EC2 (2004) provisions have been found to be approximately uniform even for rectangular columns (Oliveira, Regan, & Melo, 2004). As such, the EC2 (2004) predictions are likely less impacted by column rectangularity. The predictions according to Model Code 2010 (LoA IV) were the most conservative, with a minimum ratio of the finite element predicted capacity to the code predicted capacity of 1.41. In general, the Model Code 2010 predictions became more conservative as the c_{min}/d ratio increased. This occurred since the rotations predicted by the FEM typically increased as the c_{min}/d ratio increased. Since the punching provisions

in Model Code 2010 are derived from the CSCT (Muttoni & Fernández Ruiz, 2012; Muttoni, Fernández Ruiz, Bentz, Foster, & Sigrist, 2013; Ricker & Siburg, 2016; Soares & Vollum, 2015), larger rotations lead to smaller punching capacities. Typically, the CSCT predictions were slightly conservative compared to the FEA results and became more conservative as the c_{min}/d increased.

Finally, the observation of one-way shear failures predicted by the FEA should be discussed. As discussed in Section 5.1.2, one-way shear failures were not expected to govern any of the slabs included in the parametric study as the ratio of the column (support plate) dimensions, c, to the estimated slab span, L, measured from column centerline to centerline, were much less than 0.4 or 0.35. One-way behaviour was found to govern at c/L ratios greater than or equal to 0.4 or 0.35 by Simmonds (1970) and Sagaseta et al. (2014) respectively. These c/L ratios were determined through finite differences using a quarter model of a full slab system (Simmonds, 1970) and through linear elastic FEA on a full slab system (Sagaseta et al., 2014) subjected to uniformly distributed loading.

The models by Simmonds (1970) and Sagaseta et al. (2014) differ from the quarter models used in the parametric study. The quarter models used in the parametric study are based on an isolated slab-column connection which was tested in a laboratory. These isolated slab-column specimens are sized to approximate the extent of the negative moment region around the column in a full slab system, which is known as the radius of contraflexure. This radius of contraflexure is typically assumed to be located at 0.22L from the center of the supported area. Additionally, slab AM04, which was the baseline of the parametric study, was loaded via discrete point loads at the radius of contraflexure. Regan and Rezai-Jorabi (1988) showed that the one-way shear capacity of slabs subjected to concentrated loads is less than that for slabs under uniformly distributed load. It has also been proven that the behaviour of an isolated slab-column connection specimen is different than that of a slab-column connection in a continuous slab due to the lack of membrane action and other confining effects (Alam, Amanat, & Seraj, 2009; Mowrer & Vanderbilt, 1967; Genikomsou & Polak, 2017a). Therefore, it is possible that one-way shear behaviour is governing at a lower c/L ratio, if the length of the full system is considered, due to the differences in the specimen (isolated versus continuous) and the loading (uniformly distributed versus discrete point loads).

The models predicted to fail in one-way shear and the corresponding c_{max}/L ratios, considering the length of the isolated specimen and the column in the quarter model, are provided in Table 5-20. From Table 5-20, it is clear that one-way shear behavior is predicted to govern for a consistent column length and c_{max}/L ratio across the investigated c_{min}/d ratios. The minimum and maximum

lengths of the support plate in the quarter models predicted to fail in one-way shear were 540mm and 600mm respectively, which correspond to c_{max}/L ratios of 0.36 and 0.40. Therefore, the c/L ratios where one-way shear behaviour was predicted to govern for the isolated slab-column specimens subjected to concentrated loads are similar to the c/L ratios where one-way shear behavior was found to govern for continuous concrete slabs subjected to uniformly distributed loads.

Table 5-20: Summary of Models Predicted to Fail in one-way Shear

C_{min}/d	β	$C_{min}/2$ [(a)]	$C_{max}/2$ [(a)]	$C_{max}/L_{1/4\ model}$ [(b)]
0.594 [(c)]	10	60	600	0.40
0.792	7.5	80	600	0.40
0.990	6	100	600	0.40
1.287	4.462	130	580	0.39
1.485	4	150	600	0.40
1.782	3	180	540	0.36
1.980	3	200	600	0.40
2.970 [(d)]	-	-	-	-

[(a)] Half dimensions used in quarter model due to symmetry
[(b)] Length of quarter model = 3000mm/2 = 1500mm
[(c)] Simultaneous two-way and one-way shear failure predicted for β = 10 model
[(d)] One-way shear failure not found to govern for c_{min}/d = 2.970 results. β = 2 model experienced secondary one-way shear failure model

5.3.2 Slab Shear Stress Distribution Discussion

In this section, the predicted shear stress distributions in the slab around the support plate perimeter and the peak shear stress in the slab at the corner of the support plate are analyzed at different load levels. In Section 5.3.2.1, shear stress distributions around the support plate perimeter at 30% and 90% of the peak load level are presented. In Section 5.3.2.2, the peak shear stresses calculated at the corner of the support plate at 30%, 90% and 100% of the peak load are discussed. Firstly, the calculated peak stresses for constant β values and varying c_{min}/d ratios are presented. Secondly, the peak stresses for all β values and c_{min}/d ratios in the parametric study are analyzed.

5.3.2.1 Shear Stress Distribution Along the Perimeter of the Supported Area vs. Load Level

As discussed in Section 2.6.3, most of the previous FEA of reinforced concrete slabs supported on rectangular columns has been focused on estimating the linear elastic shear stress distribution around

the column or critical perimeter. Using NLFEA, it is possible to estimate the shear stress distribution around the column or critical perimeter during the non-linear portion of the response. Since no trends in the predicted shear stress distribution at the critical perimeter at d/2 from the column face were observed, only the shear stress distributions around the column perimeter are analyzed in this section. Three load levels were considered in the analysis, 30% of the peak load, 90% of the peak load and the peak load. 30% of the peak load was selected as it represented the approximate end of the linear elastic region on the load-displacement curves for each slab in the parametric study. 90% of the peak load was used to analyze the behaviour of the slab before failure, and to determine if stress redistribution was occurring as the slab-column connection approached failure. In this section, the shear stress distributions at all three load levels around the support plate for specific slab-column connections are presented and discussed. Shear stress distributions in the slab around the support plate for all models in the parametric study at 30% and 90% of the peak load are provided in Appendix H. The distributions in Appendix H are similar in format to those presented in Section 5.2.

For each c_{min}/d ratio the stress distribution for three rectangularities at 30%, 90% and 100% of the peak load were plotted together to investigate the overall shape of the shear stress distribution around the support plate, and to determine if any stress redistribution occurred. The three rectangularities selected corresponded to the square support plate, maximum rectangularity in each c_{min}/d ratio and an intermediate rectangularity, which was typically selected to be near the median rectangularity in each c_{min}/d ratio. A summary of the models considered is provided in Table 5-21. The shear stress distributions for the three models with a c_{min}/d ratio of 1.287 are provided in Figure 5-53 and the remaining distributions are provided in Appendix I.

Table 5-21: Column Aspect Ratios Considered in the Stress Distribution vs. Load Level Analysis

c_{min}/d	Rectangularities (β) Investigated		
0.594	1	5	10
0.792	1	4.5	8
0.990	1	4	6.6
1.287	1	3	5.077
1.485	1	2.533	4
1.782	1	2	3.566
1.980	1	2	3
2.970	1	1.533	2

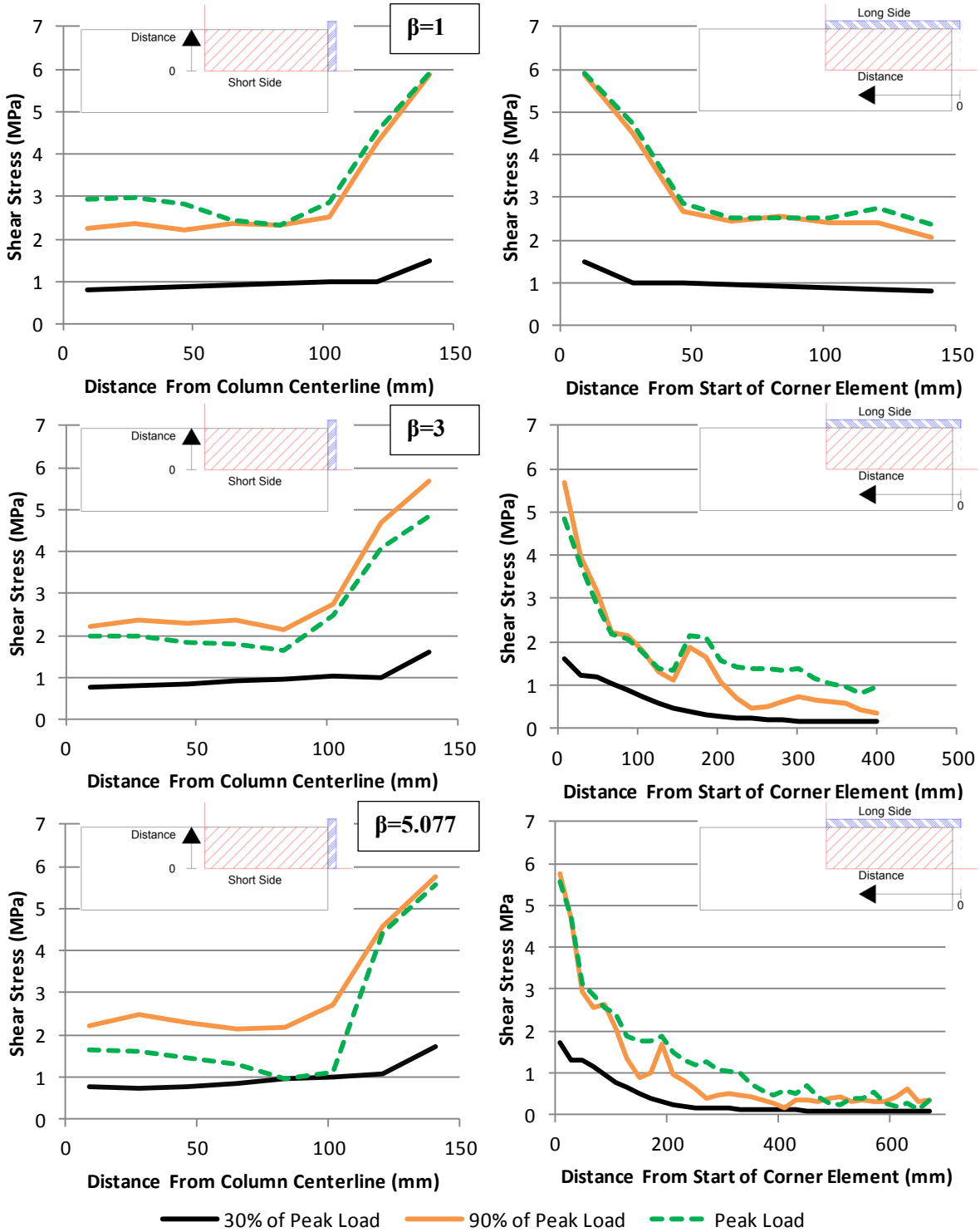

Figure 5-53: Shear Stress Distribution Along Support at Different Load Levels, $c_{min}/d=1.287$

From Figure 5-53, and the stress distributions provided in Appendix I, two conclusions can be drawn. Firstly, the overall shape of the stress distribution changes throughout the course of the analysis for all investigated c_{min}/d ratios and β values. In the linear elastic region, the impact of column rectangularity is extremely clear, as a concentration of shear stress at the corner of the support plate and along the short side of the plate was observed for all investigated slab-column connections. For connections with c_{min}/d ratios less than or equal to 1.485, the shear stresses along the short side of the column are fairly uniform and have magnitudes which are similar to those at the corner of the supported area. For slab-column connections with c_{min}/d ratios greater than 1.485, the shear stresses become more concentrated near the corner of the supported area and the shear stress magnitude along the short side is less uniform, but still typically higher than that near the centerline of the long side of the supported area.

Secondly, for most of the slab-rectangular column connections in Table 5-21, a shear stress redistribution between 90% and 100% of peak load was observed. For all the investigated models which have elongated columns and c_{min}/d ratios less than or equal to 1.485, a clear redistribution of stress from the short side of the supported area to the long side is observed after 90% of the peak load is applied. In most of the investigated slab-rectangular column connections, the shear stress levels along the short side of the supported area dropped after 90% of the peak load had been reached and the stresses along the long side, typically towards the centerline of the supported area, increased after this point. Therefore, shear failures of slab-column connections are initiated by failure of the slab concrete along the short side of the supported area. The concrete along the long side of the column is temporarily able to redistribute and sustain these stresses, before failure occurs when the long side is no longer able to carry the additional load. Stress redistribution was also observed for the three largest c_{min}/d ratios, 1.782, 1.980 and 2.970, but some different behaviour compared to the results for the lower c_{min}/d ratios was observed. For example, the stress distribution for the model with a square supported area and a c_{min}/d ratio of 1.782 displayed an increase in stress at all element lines except for at the column corner, which differs from the results for the lower c_{min}/d ratios discussed on the following page. For the c_{min}/d ratio of 1.782, the other two rectangularity values also show some discrepancy from the trend. For example, for the slab-column connections with an aspect ratio of 2 or 3.556, the stresses away from the corner were found to redistribute, but the stresses at the column corner continued to increase after 90% of the peak load was reached. Similar discrepancies were observed in the investigated stress distributions for c_{min}/d ratios of 1.980 and 2.970.

For the models supported on square plates with a c_{min}/d ratio less than 1.485, a redistribution of stress from one side of the column to the other was not observed. For the models which are supported on square plates, the predicted shear stress at every line of elements increased as the load increased towards the peak load. The lack of stress redistribution may be due to a lack of a "weak" side since the model is symmetric. Therefore, for the models supported on square columns, failure is initiated when the slab on both sides of the supported area reaches its maximum shear capacity. This lack of stress redistribution is also likely why the peak stresses at the column perimeter, which occurred at the column corners for models supported on square columns, are typically higher than those for the slabs supported on elongated columns.

5.3.2.2 Peak Shear Stress in the Slab at the Corner of the Supported Area

The maximum shear stress in the slab at 30% of the peak load for each model, which was found to occur at the column of the support plate in all models, for the rectangularity values between 1 and 5, for each c_{min}/d ratio, is provided in Figure 5-54. There is no clear trend in the predicted shear stress at the support plate corner, but all the calculated stresses fall within a small stress range (1.36-1.96MPa), even though the investigated load level for each model is not the same. Unlike the peak shear stresses calculated at higher load levels, the peak shear stress for slabs supported on square columns do not exceed those for slabs supported on elongated columns.

The maximum shear stress calculated for each model at 30% of the peak load level for all the investigated rectangularity values and c_{min}/d ratios are provided in Figure 5-55. Unlike the data in Figure 5-54, which displayed no clear trend between the peak stress and the c_{min}/d ratio, the data in Figure 5-55 show a clear trend between the column rectangularity and the peak stress level. For most of the models in the parametric study, it is clear that as the column rectangularity was increased the peak stress at the column corner increased. This peak shear stress increase shows that a large portion of the stress in the linear elastic and initial plastic portions of the slabs response is carried by the concrete near the corner of the supported area.

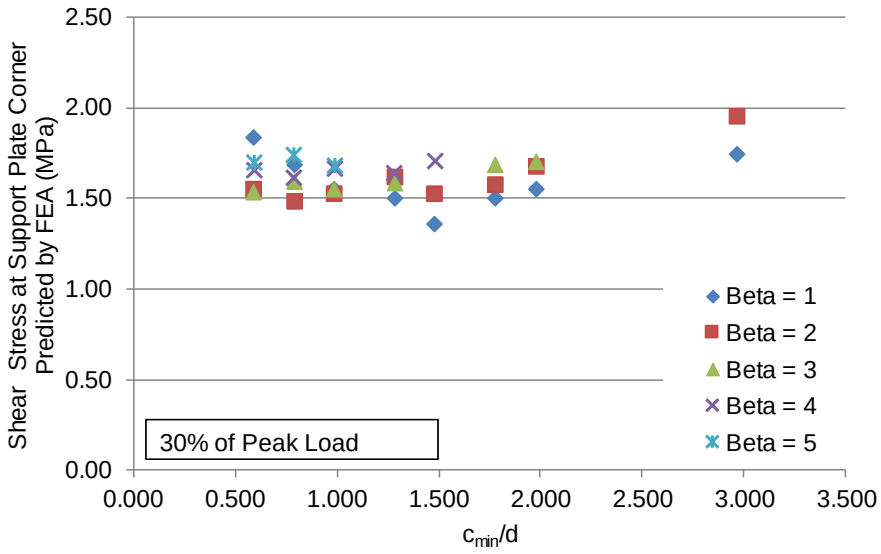

Figure 5-54: Comparison of Shear Stress at Column Corner, 30% of Peak Load, 1≤β≤5

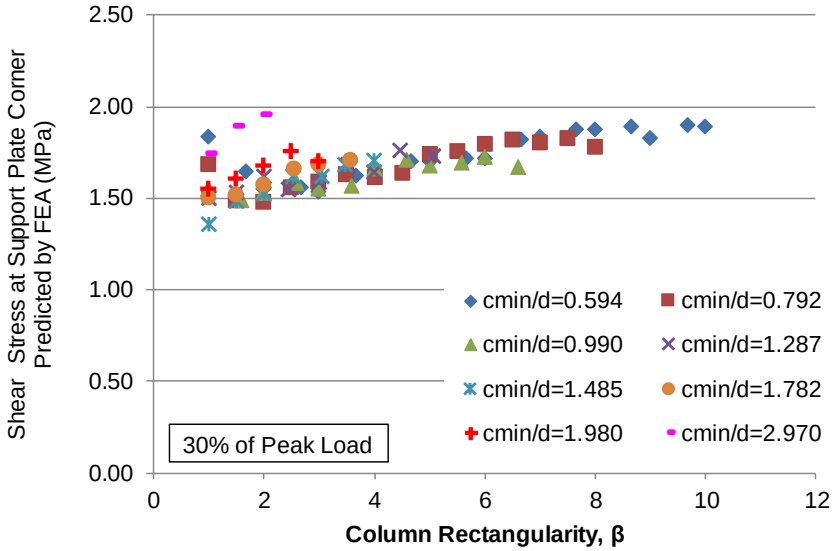

Figure 5-55: Peak Shear Stresses at Column Corner Predicted by FEA, 30% of Peak Load, All β

The maximum predicted shear stress at 90% of the peak load for each c_{min}/d ratio for the rectangularity values between 1 and 5 are provided in Figure 5-56. As with the results at 30% of the peak load level, no consistent trend between the c_{min}/d ratio and peak stress was observed. However, unlike the results for 30% of the peak load, the peak shear stress for slabs supported on square columns exceeds the peak shear stress for slabs supported on elongated columns.

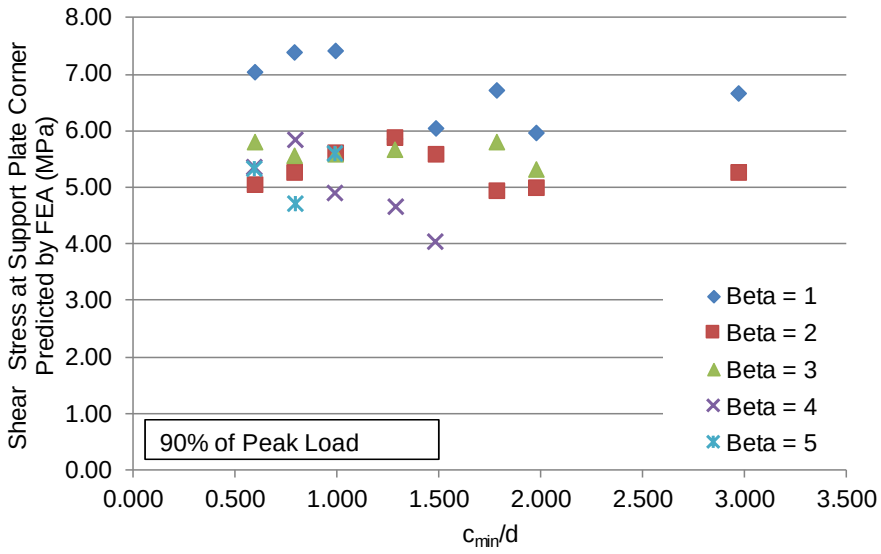

Figure 5-56: Comparison of Shear Stress at Column Corner, 90% of Peak Load, 1≤β≤5

A comparison of the peak stress versus column rectangularity for each c_{min}/d ratio at 90% of the peak load is provided in Figure 5-57. Unlike the results at 30% of the peak load, no clear trend between the column rectangularity and peak stress was observed. The calculated peak stresses fall within the range of approximately 4MPa to 7MPa, with the majority of the models having a peak stress between 5 to 6MPa. This small band of peak stress values suggests that punching shear and one-way shear failures are triggered when the stress at the column corner exceeds a value of 5MPa.

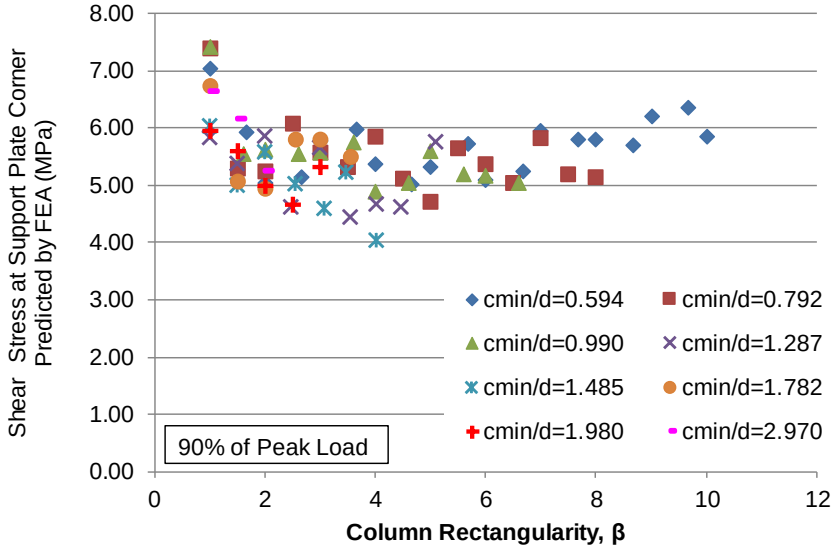

Figure 5-57: Peak Shear Stresses at Column Corner Predicted by FEA, 90% of Peak Load, All β

The maximum predicted shear stress at the peak load level for each c_{min}/d ratio for the rectangularity values between 1 and 5 are provided in Figure 5-58. As with the results at 30% and 90% of the peak load level, no consistent trend between the peak stress at the corner of the support plate and the c_{min}/d ratio was observed. However, unlike the results for 30% of the peak load, and similar to the results at 90% of the peak load level, the peak stress for slabs supported on square columns typically exceeded the peak stress for slabs supported on elongated columns.

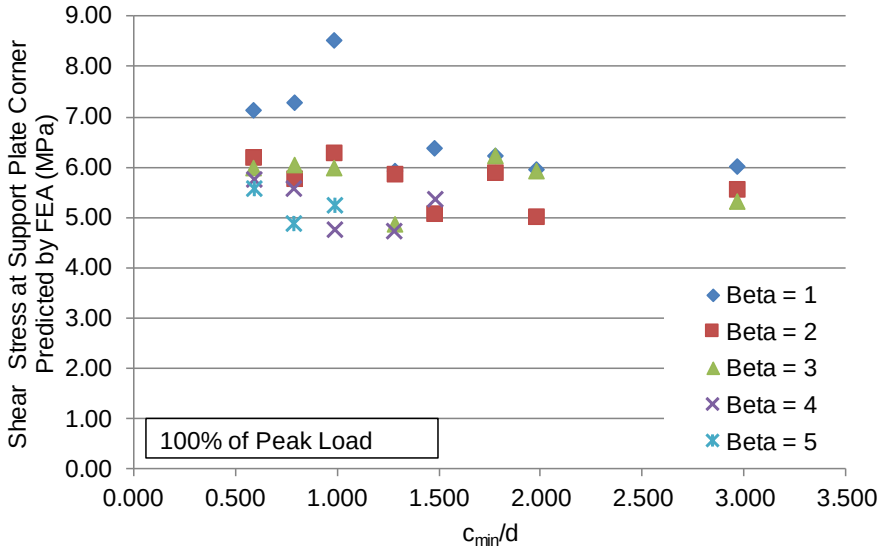

Figure 5-58: Comparison of Shear Stress at Column Corner, Peak Load, 1≤β≤5

A comparison of the peak stress for all 77 models in the parametric study at the peak load is provided in Figure 5-59. Unlike the results for 90% of the peak load, there appears to be a relationship between the column aspect ratio and the peak stress. The observed trend is opposite to that observed for the 30% of peak load results. At 30% of the peak load, the peak shear stress typically increased as the column rectangularity was increased for each c_{min}/d ratio. At the peak load level, the peak shear stress typically decreased as the column rectangularity was increased within each c_{min}/d ratio. Some of the predicted shear stress values do not match this trend, but overall the peak shear stress decreased towards a single value as the column rectangularity was increased for each c_{min}/d ratio. Additionally, most of the calculated peak shear stresses are within the range of 5 and 7MPa, which matches the results at 90% of the peak load. Some lower values do exist, but none of the calculated peak stresses are below 4MPa. Finally, the only stresses which exceed 7MPa are for

square columns which is likely due to the lack of stress redistribution observed for slabs supported on square support plates.

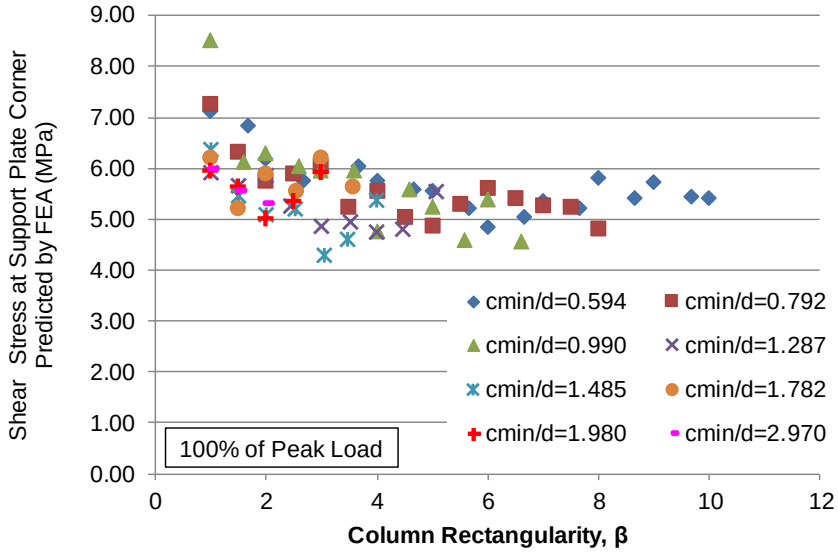

Figure 5-59: Peak Shear Stresses at Column Corner Predicted by FEA, Peak Load, All β

Chapter 6: Conclusions and Future Work

In this chapter, the conclusions of the capability study and finite element calibration presented in Chapter 4 and the parametric study presented in Chapter 5 are provided. A summary of the work conducted in this thesis and recommendations for future work are also provided.

6.1 Summary

Even though the empirical database for punching shear of reinforced concrete slabs supported on columns is large, it cannot address all parameters which impact punching shear. Additionally, most of the empirical data is for slabs supported on square or circular columns, and experimental tests of slabs supported on rectangular columns subjected to concentric loads are limited. Nonlinear finite element models, properly calibrated based on experimental results, can provide a cost-effective way to study parameters which are difficult to evaluate experimentally, or are not adequately accounted for in the existing experimental database. The capability of the commercial finite element software ABAQUS to accurately capture the punching shear behaviour of reinforced concrete slabs supported on square columns using the "Concrete Damaged Plasticity" model was proven by Genikomsou (2015).

The work presented in this thesis was undertaken to investigate the impact of column rectangularity on the punching shear behaviour of reinforced concrete slabs supported on rectangular columns using a nonlinear finite element model based on the "Concrete Damaged Plasticity" model available in ABAQUS. First, modified versions of the model presented by Genikomsou (2015) were used to model hypothetical and experimentally tested slab-column connections to verify ABAQUS' ability to accurately capture the impact on column rectangularity. The overall trends of the finite element model results correlated well with design code predictions and experimental results, but the punching capacities and deflections at failure were typically underpredicted by approximately 20%. Therefore, the finite element model was recalibrated considering seven experimental slab-column specimens. Four of the seven slabs, tested by Sagaseta et al. (2014), were supported on rectangular steel plates, with an aspect ratio of three, and were subjected to different loading layouts. The remaining three slabs, tested by Sagaseta et al. (2011), were supported on square steel plates and loaded in two-way action. The slabs supported on square steel plates also had different reinforcing ratios and concrete compressive strengths compared to the slabs supported on rectangular steel plates.

The calibrated model was then used to investigate the impact of two parameters, the support aspect ratio, β, and the ratio of the minimum column dimension, c_{min}, to the effective slab depth, d, on the

punching shear behaviour of isolated slab-column connections. These two parameters were selected for the parametric study based on a comparison of the reduction factors for column rectangularity calculated from various design codes and the finite element analysis results from the capability study.

6.2 Capability Study and Finite Element Model Calibration

Chapter 4 presented three studies which were used to verify ABAQUS' capability to capture the impact of column rectangularity on the punching shear behaviour of reinforced concrete slabs. The first of these studies was conducted considering one slab supported on square column, tested by Adetifa and Polak (2005), and five hypothetical slab column specimens with consistent critical perimeter lengths according to ACI 318M-14, but increasing column rectangularity. In the second study, the nine slabs tested by Hawkins, Fallsen and Hinojosa (1971) were modelled. In the third study, one slab supported on a rectangular steel plate with an aspect ratio of three was modelled. This slab was used to calibrate the finite element model used in the parametric study. The calibration was verified by modelling three additional slabs supported on rectangular steel plates (Sagaseta, Tassinari, Fernández Ruiz, & Muttoni, 2014) and three slabs supported on square steel plates (Sagaseta, Muttoni, Fernández Ruiz, & Tassinari, 2011). The following conclusions were made from these studies:

- ABAQUS predicts an impact of column rectangularity which agrees with current design code provisions and published experimental results. ABAQUS is also capable of capturing the impact of different load arrangements and reinforcing ratios on the punching shear behaviour of reinforced concrete slabs supported on square or rectangular columns. The analysis results from ABAQUS simulations can also be used to analyze the shear stress distribution in the slab around the column/support perimeter or any chosen critical perimeter. However, if C3D8R elements are used to mesh the slab only perimeters with 90° corners should be analyzed.
- Nonlinear finite element models must be calibrated based on experimental results since modelling choices including the boundary conditions, assumed concrete fracture energy, dilation angle (if the "Concrete Damaged Plasticity" model is used) and mesh size effect the predicted crack pattern and load-deflection response.
- A recalibration of the finite element model parameters is required for each experimental setup considered.

- Force driven loads should be used in ABAQUS when applying equivalent loads over discrete loading areas. If displacement boundary conditions are used the force distribution over the loaded areas will not be uniform. If force driven loads are used, quasi-static analysis in ABAQUS/Explicit is required to observe a peak capacity in the load-deflection curve. If a static analysis in ABAQUS/Standard is conducted, the load will continue to ramp until the end of the analysis.
- The rotation of isolated slab-column specimens subjected to concentrated loads can be approximated using a linear approximation based on the slab deflections at the end of the supported area and the slab edge.
- For slabs which fail in punching before reaching their flexural capacity, the slab reinforcement crossing the column boundary or near the column typically yields before punching.
- For a constant critical perimeter length, the impact of column rectangularity diminishes as the c_{min}/d ratio is decreased. Eurocode 2 (2004) does not predict column rectangularity to have any impact for slab-column connections subjected to concentric vertical loads if the total critical perimeter length is constant.

6.3 Parametric Study

A parametric study using the calibrated AM04 model was conducted to evaluate the impact of the aspect ratio of the supported area and to investigate if the impact of column rectangularity on punching shear behaviour is dependent on the ratio of the minimum column dimension, c_{min}, to the effective slab depth, d. From the results of 77 finite element simulations, the following conclusions were made:

- The impact of column rectangularity on punching shear capacity of slab-column connections was found to not only be dependent on the column aspect ratio. The impact of column rectangularity on the total capacity, and nominal shear capacity along the ACI 318M-14 critical perimeter predicted by the FEM, which was approximately linear for the investigated aspect ratios within each c_{min}/d ratio, was found to become more severe as the c_{min}/d ratio increased. Even though the punching provisions in Eurocode 2 (2004), Model Code 2010 and those derived from the Critical Shear Crack Theory (CSCT) are not explicitly functions of the c_{min}/d ratio, these three design methods predict a more severe

impact of column rectangularity as the c_{min}/d ratio is increased. ACI 318M-14, on the other hand does not predict a significant change in the impact of column rectangularity as the c_{min}/d ratio is increased.

- ACI 318M-14 and Eurocode 2 (2004) are most accurate for column aspect ratios between 1 and 5. The ACI provisions were found to be most accurate for c_{min}/d ratios less than approximately 1.3 and the Eurocode 2 (2004) provisions were found to be most accurate for c_{min}/d ratios greater than 1.3.
- The assumption that minimal column rectangularity ($1<\beta\leq2$) has no impact on punching capacity in ACI 318M-14 does not match the FEM results or the predictions according to Eurocode 2 (2004), Model Code 2010 or the CSCT. This assumption makes the ACI 318 provisions unconservative for c_{min}/d ratios greater than 1.3.
- The Model Code 2010 provisions and capacity predictions according to the CSCT, using the 3d method from Model Code 2010 to calculate the effective critical perimeter length, and the maximum slab rotation in each orthogonal direction calculated from the NLFEA, typically predict an impact of column rectangularity which agrees with the FEA results. Generally, the CSCT predictions were found to be conservative compared to the FEA results and the Model Code 2010 predictions were found to be extremely conservative even at the highest level of approximation (level IV). The Model Code 2010 provisions were found to be a very conservative adaptation of the CSCT provisions.
- The stiffness of the slab-column connection in both orthogonal directions was found to increase with increasing column rectangularity. This increase was found to be larger in the direction perpendicular to the short side of the column, which was predicted to be the stiffer direction by the FEM. A higher stiffness in the direction perpendicular to the short side of the column was observed experimentally by Tan and Teng (2005), Anggadjaja and Teng (2008) and Himawan and Teng (2014).
- The impact of column rectangularity on the crack pattern of the slabs was consistent for all investigated c_{min}/d ratios. As the column rectangularity is increased, the predicted crack patterns became non-uniform on the tension side and slab sides. On the tension side, the amount of diagonal cracking decreases and the amount of cracking perpendicular to the long and short sides of the supported area increases. The cracks also tend to concentrate

near the corner of the supported area. The predicted punching cones on the slab sides also become thinner as the column rectangularity is increased. Along the slab side perpendicular to the long side of the supported area the punching cone becomes smaller in size, and eventually non-existent, as the column rectangularity is increased. The disappearance of the punching cone on the slab side perpendicular to the long side of the supported area coincides with the formation of a one-way shear crack across the entire slab width parallel to the long side of the supported area on the tension surface of the slab. This one-way shear crack is predicted to occur at lower column rectangularities, but similar column lengths as the c_{min}/d ratio is increased. One-way shear failures were predicted by the FEM when the column length was equal to 35-40% of the isolated specimen length.

- The shear stresses in the slab around the perimeter of the support plate calculated from the FEA results were found to concentrate near the corner and along the short side of the support plate, which matches previous experimental and FEA results (Al-Yousif & Regan, 2003; Teng, Cheong, Kuang, & Geng, 2004; Oliveira, Regan, & Melo, 2004; Anggadjaja & Teng, 2008; Borges, Melo, & Gomes, 2013; Himawan & Teng, 2014; Shu, Belletti, Muttoni, Scolari, & Plos, 2017). As the c_{min}/d ratio increased, the concentration of shear stresses in the slab at the corner of the supported area was found to increase and the concentration of shear stresses along the short side of the supported area was found to decrease. The maximum shear stress in the slab was predicted to occur at the corner of the supported area. Also, the shape of the shear stress distribution around the support plate perimeter was found to change with load level, and a redistribution of stress from the portion of the slab along the short side of the supported area to the portion of the slab along the long side of the support plate was found to occur before failure.
- No clear trends were observed in the calculated stress distribution at the ACI 318M-14 critical perimeter located at d/2 from the column face.

6.4 Recommendations for Future Work

The calibrated finite element model presented in this thesis has been found to be robust for analyses of reinforced concrete slabs failing in shear under different load conditions. However, as discussed in Section 4.5.1, the current model is not capable of accurately capturing flexural failures due to the simplified stress-strain curve used for the reinforcing steel. Therefore, a more detailed stress-strain

curve for the reinforcing steel should be added to the model and the model's ability to accurately model reinforced concrete slabs failing in flexure should be verified by analyzing slabs such as AM03 tested by Sagaseta et al. (2014). Assuming the steel stress-strain curve is updated, and the model is found to accurately capture flexural failures, the model can then be used to conduct various parametric studies similar to the calibrated model presented by Genikomsou (2015). If the stress-strain curve is not updated, the model can still be used to conduct parametric studies but the stresses in the flexural reinforcing will have to be carefully analyzed to ensure the simplified stress-strain curve is not impacting the results.

The effect of unbalanced moments in one or both orthogonal directions on the punching shear behaviour of slab-rectangular column connections should be evaluated. As discussed in Chapter 2, some experimental work has been conducted on this subject, but the current experimental database is quite small, and the column rectangularities investigated are limited. If damage parameters are incorporated into the concrete modelling, the impact of cyclic loads could also be analyzed.

The effect of openings on the shear capacity and shear stress distribution in the slab around the column and critical perimeters can also be evaluated using the calibrated finite element model. As with unbalanced moments, limited experimental work has been conducted in this area for slabs supported on rectangular columns. The optimal opening size and layout and adequacy of current code provisions can be analyzed using the calibrated finite element model.

Following the modelling recommendations of Genikomsou (2015), the calibrated finite element model can also be used to evaluate the impact of shear reinforcement on the punching shear behaviour of slab-rectangular column connections. The impact of radial or orthogonal shear reinforcing layouts, and different shear reinforcement types can be analyzed. The impact of shear reinforcing layout and spacing on the failure modes and load-deflection capacity can be evaluated.

The impact of compressive membrane forces, which exist in continuous slab specimens (Alam, Amanat, & Seraj, 2009; Mowrer & Vanderbilt, 1967; Genikomsou & Polak, 2017a), on the punching shear capacity of slab-rectangular column connections can also be evaluated using the calibrated model. Modified isolated slab-column connections, similar to those proposed by Genikomsou (2015), or continuous models can be used with the calibrated model parameters to evaluate the impact of compressive membrane forces on the shear stress distributions, the punching capacity and connection stiffness in both orthogonal directions.

The calibrated finite element model can also be extended to evaluate the punching shear behaviour of slabs supported partially supported on long walls. It is common for slabs to be partially supported on shear walls, but this design scenario is not discussed in ACI 318M-14 or EC2 (2004). Model Code 2010 recommends a critical perimeter which can be used to evaluate punching capacity around the end of the wall, but no reference to the experimental or analytical research leading to this assumed critical perimeter is provided. The calibrated finite element model can be used to evaluate the portion of the wall perimeter or critical perimeter which is effective in resisting punching shear and the results can be used to draft code provisions. The tributary area of the wall can also be evaluated using a finite element model of a continuous slab system.

Finally, it is recommended that some of the slabs modelled in this thesis be tested experimentally to validate the finite element results. It is recommended that some of the hypothetical connections from the SB1 rectangularity study be tested to verify that impact of column rectangularity decreases with decreasing c_{min}/d ratios. It is also recommended that some of the models which were predicted to fail in one-way shear be tested to verify that isolated specimens where the column length is equal to approximately 40% of the specimen length fail in one-way shear. It would also be beneficial to model and test slabs with the same c_{min}/d ratios and column rectangularities as those included in the parametric study. It is recommended that some of these slabs be larger than AM04 so the impact of the location of the load plates on the finite element results can be verified.

Letters of Copyright

The letters/agreements granting permission to reproduce figures from previously published literature are provided on the following pages.

American Concrete Institute

Always advancing

Graeme Milligan
University of Waterloo
200 University Avenue West
Waterloo, ON, N2L 3G1
CANADA

June 29, 2018

Subject: Use of ACI Copyrighted Material

Your request to:

___X___ Use information/figures/tables indicated below. Please credit American Concrete Institute, author(s) and publication.

___X___ Reprint the information described in the quantity indicated. Please add a note to the reprint similar to: *Authorized reprint from (publication) (issue/volume/year as appropriate.)*

_____ Payment of Right-to-Reprint fee of ($0) is required.

Permission is granted to reference and reprint *Figure 1 Curved Compression Strut* from *May–June 1992 ACI Structural Journal, Vol. 89 No. 3, Title No. 89-S32 "Bond Model for Concentric Punching Shear"*

Figure 4 Assembly of load-resisting struts from *May–June 1987 ACI Structural Journal, Vol. 84 No. 3, Title No. 84-S27 "Bond Model for Concentric Punching Shear"*

Figure 4 Correlation between opening of critical shear crack, thickness of slab, and rotation Ψ from *July–August 2008 ACI Structural Journal, Vol. 105 No. 4, Title No. 105-S42 "Punching Shear Strength of Reinforced Concrete Slabs Without Transverse Reinforcement"*

Signed: Angela Matthews Date: 29 June 2018

Angela Matthews
Editor, Publishing Services
Angela.Matthews@Concrete.org

American Concrete Institute

Always advancing

Graeme Milligan
University of Waterloo
200 University Avenue West
Waterloo, ON, N2L 3G1
CANADA

July 9, 2018

Subject: Use of ACI Copyrighted Material

Your request to:

__X__ Use information/figures/tables indicated below. Please credit American Concrete Institute, author(s) and publication.

__X__ Reprint the information described in the quantity indicated. Please add a note to the reprint similar to: *Authorized reprint from (publication) (issue/volume/year as appropriate.)*

_____ Payment of Right-to-Reprint fee of ($0) is required.

Permission is granted to reference and reprint:

Figure 4 Assembly of load-resisting struts from *May–June 1987 ACI Structural Journal, Vol. 84 No. 3, Title No. 84-S27 "Ultimate Strength of Slab-Column Connections"*

Figure 9 Typical Punching Shear Failure from *Sept–Oct 2008 ACI Structural Journal, Vol. 105 No. 5, Title No. 105-S50 "Edge-Column Slab Connections under Gravity and Lateral Loading"*

Signed: Angela Matthews Date: 9 July 2018

Angela Matthews
Editor, Publishing Services
Angela.Matthews@Concrete.org

Copyright Clearance Center

Confirmation Number: 11726840
Order Date: 06/27/2018

Customer Information

Customer: Graeme Milligan
Account Number: 3001303611
Organization: University of Waterloo
Email: gjmillig@uwaterloo.ca
Phone: +1 (519) 888-4567
Payment Method: Invoice

This is not an invoice

Order Details

Proceedings

Billing Status: **N/A**

Order detail ID:	71267492
ISSN:	1753-7789
Publication Type:	Journal
Volume:	
Issue:	
Start page:	
Publisher:	Institution of Civil Engineers
Author/Editor:	Institution of Civil Engineers (Great Britain)

Permission Status: **Granted**

Permission type: Republish or display content
Type of use: Republish in a thesis/dissertation
Order License Id: 4377270380743

Requestor type	Academic institution
Format	Print, Electronic
Portion	chart/graph/table/figure
Number of charts/graphs/tables/figures	1
The requesting person/organization	Graeme Jacob Milligan
Title or numeric reference of the portion(s)	Fig. 3
Title of the article or chapter the portion is from	PREDICTING THE PUNCHING STRENGTH OF CONVENTIONAL SLAB-COLUMN SPECIMENS
Editor of portion(s)	N/A
Author of portion(s)	G.I.B Rankin, A.E. Long
Volume of serial or monograph	82
Issue, if republishing an article from a serial	2
Page range of portion	327-346
Publication date of portion	1987 (online 2015)
Rights for	Main product
Duration of use	Life of current edition
Creation of copies for the disabled	no
With minor editing privileges	no

For distribution to	Worldwide
In the following language(s)	Original language of publication
With incidental promotional use	no
Lifetime unit quantity of new product	Up to 499
Title	Nonlinear Finite Element Analysis of Punching Shear of Reinforced Concrete Slabs Supported on Rectangular Columns
Instructor name	n/a
Institution name	n/a
Expected presentation date	Aug 2018

Note: This item was invoiced separately through our **RightsLink service.** More info **$ 0.00**

Total order items: 1 **Order Total: $0.00**

Copyright Clearance Center

Confirmation Number: 11726840

Special Rightsholder Terms & Conditions

The following terms & conditions apply to the specific publication under which they are listed

Proceedings
Permission type: Republish or display content
Type of use: Republish in a thesis/dissertation

TERMS AND CONDITIONS

The following terms are individual to this publisher:

None

Other Terms and Conditions:

STANDARD TERMS AND CONDITIONS

1. Description of Service; Defined Terms. This Republication License enables the User to obtain licenses for republication of one or more copyrighted works as described in detail on the relevant Order Confirmation (the "Work(s)"). Copyright Clearance Center, Inc. ("CCC") grants licenses through the Service on behalf of the rightsholder identified on the Order Confirmation (the "Rightsholder"). "Republication", as used herein, generally means the inclusion of a Work, in whole or in part, in a new work or works, also as described on the Order Confirmation. "User", as used herein, means the person or entity making such republication.

2. The terms set forth in the relevant Order Confirmation, and any terms set by the Rightsholder with respect to a particular Work, govern the terms of use of Works in connection with the Service. By using the Service, the person transacting for a republication license on behalf of the User represents and warrants that he/she/it (a) has been duly authorized by the User to accept, and hereby does accept, all such terms and conditions on behalf of User, and (b) shall inform User of all such terms and conditions. In the event such person is a "freelancer" or other third party independent of User and CCC, such party shall be deemed jointly a "User" for purposes of these terms and conditions. In any event, User shall be deemed to have accepted and agreed to all such terms and conditions if User republishes the Work in any fashion.

3. Scope of License; Limitations and Obligations.

3.1 All Works and all rights therein, including copyright rights, remain the sole and exclusive property of the Rightsholder. The license created by the exchange of an Order Confirmation (and/or any invoice) and payment by User of the full amount set forth on that document includes only those rights expressly set forth in the Order Confirmation and in these terms and conditions, and conveys no other rights in the Work(s) to User. All rights not expressly granted are hereby reserved.

3.2 General Payment Terms: You may pay by credit card or through an account with us payable at the end of the month. If you and we agree that you may establish a standing account with CCC, then the following terms apply: Remit Payment to: Copyright Clearance Center, 29118 Network Place, Chicago, IL 60673-1291. Payments Due: Invoices are payable upon their delivery to you (or upon our notice to you that they are available to you for downloading). After 30 days, outstanding amounts will be subject to a service charge of 1-1/2% per month or, if less, the maximum rate allowed by applicable law. Unless otherwise specifically set forth in the Order Confirmation or in a separate written agreement signed by CCC, invoices are due and payable on "net 30" terms. While User may exercise the rights licensed immediately upon issuance of the Order Confirmation, the license is automatically revoked and is null and void, as if it had never been issued, if complete payment for the license is not received on a timely basis either from User directly or through a payment agent, such as a credit card company.

3.3 Unless otherwise provided in the Order Confirmation, any grant of rights to User (i) is "one-time" (including the editions and product family specified in the license), (ii) is non-exclusive and non-transferable and (iii) is subject to any and all limitations and restrictions (such as, but not limited to, limitations on duration of use or circulation) included in the Order Confirmation or invoice and/or in these terms and conditions. Upon completion of the licensed use, User shall either secure a new permission for further use of the Work(s) or immediately cease any new use of the Work(s) and shall render inaccessible (such as by deleting or by removing or severing links or other locators) any further copies of the Work (except for copies printed on paper in accordance with this license and still in User's stock at the end of such period).

3.4 In the event that the material for which a republication license is sought includes third party materials (such as photographs, illustrations, graphs, inserts and similar materials) which are identified in such material as having been used

by permission, User is responsible for identifying, and seeking separate licenses (under this Service or otherwise) for, any of such third party materials; without a separate license, such third party materials may not be used.

3.5 Use of proper copyright notice for a Work is required as a condition of any license granted under the Service. Unless otherwise provided in the Order Confirmation, a proper copyright notice will read substantially as follows: "Republished with permission of [Rightsholder's name], from [Work's title, author, volume, edition number and year of copyright]; permission conveyed through Copyright Clearance Center, Inc. " Such notice must be provided in a reasonably legible font size and must be placed either immediately adjacent to the Work as used (for example, as part of a by-line or footnote but not as a separate electronic link) or in the place where substantially all other credits or notices for the new work containing the republished Work are located. Failure to include the required notice results in loss to the Rightsholder and CCC, and the User shall be liable to pay liquidated damages for each such failure equal to twice the use fee specified in the Order Confirmation, in addition to the use fee itself and any other fees and charges specified.

3.6 User may only make alterations to the Work if and as expressly set forth in the Order Confirmation. No Work may be used in any way that is defamatory, violates the rights of third parties (including such third parties' rights of copyright, privacy, publicity, or other tangible or intangible property), or is otherwise illegal, sexually explicit or obscene. In addition, User may not conjoin a Work with any other material that may result in damage to the reputation of the Rightsholder. User agrees to inform CCC if it becomes aware of any infringement of any rights in a Work and to cooperate with any reasonable request of CCC or the Rightsholder in connection therewith.

4. Indemnity. User hereby indemnifies and agrees to defend the Rightsholder and CCC, and their respective employees and directors, against all claims, liability, damages, costs and expenses, including legal fees and expenses, arising out of any use of a Work beyond the scope of the rights granted herein, or any use of a Work which has been altered in any unauthorized way by User, including claims of defamation or infringement of rights of copyright, publicity, privacy or other tangible or intangible property.

5. Limitation of Liability. UNDER NO CIRCUMSTANCES WILL CCC OR THE RIGHTSHOLDER BE LIABLE FOR ANY DIRECT, INDIRECT, CONSEQUENTIAL OR INCIDENTAL DAMAGES (INCLUDING WITHOUT LIMITATION DAMAGES FOR LOSS OF BUSINESS PROFITS OR INFORMATION, OR FOR BUSINESS INTERRUPTION) ARISING OUT OF THE USE OR INABILITY TO USE A WORK, EVEN IF ONE OF THEM HAS BEEN ADVISED OF THE POSSIBILITY OF SUCH DAMAGES. In any event, the total liability of the Rightsholder and CCC (including their respective employees and directors) shall not exceed the total amount actually paid by User for this license. User assumes full liability for the actions and omissions of its principals, employees, agents, affiliates, successors and assigns.

6. Limited Warranties. THE WORK(S) AND RIGHT(S) ARE PROVIDED "AS IS". CCC HAS THE RIGHT TO GRANT TO USER THE RIGHTS GRANTED IN THE ORDER CONFIRMATION DOCUMENT. CCC AND THE RIGHTSHOLDER DISCLAIM ALL OTHER WARRANTIES RELATING TO THE WORK(S) AND RIGHT(S), EITHER EXPRESS OR IMPLIED, INCLUDING WITHOUT LIMITATION IMPLIED WARRANTIES OF MERCHANTABILITY OR FITNESS FOR A PARTICULAR PURPOSE. ADDITIONAL RIGHTS MAY BE REQUIRED TO USE ILLUSTRATIONS, GRAPHS, PHOTOGRAPHS, ABSTRACTS, INSERTS OR OTHER PORTIONS OF THE WORK (AS OPPOSED TO THE ENTIRE WORK) IN A MANNER CONTEMPLATED BY USER; USER UNDERSTANDS AND AGREES THAT NEITHER CCC NOR THE RIGHTSHOLDER MAY HAVE SUCH ADDITIONAL RIGHTS TO GRANT.

7. Effect of Breach. Any failure by User to pay any amount when due, or any use by User of a Work beyond the scope of the license set forth in the Order Confirmation and/or these terms and conditions, shall be a material breach of the license created by the Order Confirmation and these terms and conditions. Any breach not cured within 30 days of written notice thereof shall result in immediate termination of such license without further notice. Any unauthorized (but licensable) use of a Work that is terminated immediately upon notice thereof may be liquidated by payment of the Rightsholder's ordinary license price therefor; any unauthorized (and unlicensable) use that is not terminated immediately for any reason (including, for example, because materials containing the Work cannot reasonably be recalled) will be subject to all remedies available at law or in equity, but in no event to a payment of less than three times the Rightsholder's ordinary license price for the most closely analogous licensable use plus Rightsholder's and/or CCC's costs and expenses incurred in collecting such payment.

8. **Miscellaneous.**

8.1 User acknowledges that CCC may, from time to time, make changes or additions to the Service or to these terms and conditions, and CCC reserves the right to send notice to the User by electronic mail or otherwise for the purposes of notifying User of such changes or additions; provided that any such changes or additions shall not apply to permissions already secured and paid for.

8.2 Use of User-related information collected through the Service is governed by CCC's privacy policy, available online here: http://www.copyright.com/content/cc3/en/tools/footer/privacypolicy.html.

8.3 The licensing transaction described in the Order Confirmation is personal to User. Therefore, User may not assign or transfer to any other person (whether a natural person or an organization of any kind) the license created by the Order Confirmation and these terms and conditions or any rights granted hereunder; provided, however, that User may assign such license in its entirety on written notice to CCC in the event of a transfer of all or substantially all of User's rights in the new material which includes the Work(s) licensed under this Service.

8.4 No amendment or waiver of any terms is binding unless set forth in writing and signed by the parties. The Rightsholder and CCC hereby object to any terms contained in any writing prepared by the User or its principals, employees, agents or affiliates and purporting to govern or otherwise relate to the licensing transaction described in the Order Confirmation, which terms are in any way inconsistent with any terms set forth in the Order Confirmation and/or in these terms and conditions or CCC's standard operating procedures, whether such writing is prepared prior to, simultaneously with or subsequent to the Order Confirmation, and whether such writing appears on a copy of the Order Confirmation or in a separate instrument.

8.5 The licensing transaction described in the Order Confirmation document shall be governed by and construed under the law of the State of New York, USA, without regard to the principles thereof of conflicts of law. Any case, controversy, suit, action, or proceeding arising out of, in connection with, or related to such licensing transaction shall be brought, at CCC's sole discretion, in any federal or state court located in the County of New York, State of New York, USA, or in any federal or state court whose geographical jurisdiction covers the location of the Rightsholder set forth in the Order Confirmation. The parties expressly submit to the personal jurisdiction and venue of each such federal or state court.If you have any comments or questions about the Service or Copyright Clearance Center, please contact us at 978-750-8400 or send an e-mail to info@copyright.com.

v 1.1

Close

INTRODUCTION

1. The publisher for this copyrighted material is Elsevier. By clicking "accept" in connection with completing this licensing transaction, you agree that the following terms and conditions apply to this transaction (along with the Billing and Payment terms and conditions established by Copyright Clearance Center, Inc. ("CCC"), at the time that you opened your Rightslink account and that are available at any time at http://myaccount.copyright.com).

GENERAL TERMS

2. Elsevier hereby grants you permission to reproduce the aforementioned material subject to the terms and conditions indicated.
3. Acknowledgement: If any part of the material to be used (for example, figures) has appeared in our publication with credit or acknowledgement to another source, permission must also be sought from that source. If such permission is not obtained then that material may not be included in your publication/copies. Suitable acknowledgement to the source must be made, either as a footnote or in a reference list at the end of your publication, as follows:
"Reprinted from Publication title, Vol /edition number, Author(s), Title of article / title of chapter, Pages No., Copyright (Year), with permission from Elsevier [OR APPLICABLE SOCIETY COPYRIGHT OWNER]." Also Lancet special credit - "Reprinted from The Lancet, Vol. number, Author(s), Title of article, Pages No., Copyright (Year), with permission from Elsevier."
4. Reproduction of this material is confined to the purpose and/or media for which permission is hereby given.
5. Altering/Modifying Material: Not Permitted. However figures and illustrations may be altered/adapted minimally to serve your work. Any other abbreviations, additions, deletions and/or any other alterations shall be made only with prior written authorization of Elsevier Ltd. (Please contact Elsevier at permissions@elsevier.com). No modifications can be made to any Lancet figures/tables and they must be reproduced in full.
6. If the permission fee for the requested use of our material is waived in this instance, please be advised that your future requests for Elsevier materials may attract a fee.
7. Reservation of Rights: Publisher reserves all rights not specifically granted in the combination of (i) the license details provided by you and accepted in the course of this licensing transaction, (ii) these terms and conditions and (iii) CCC's Billing and Payment terms and conditions.
8. License Contingent Upon Payment: While you may exercise the rights licensed immediately upon issuance of the license at the end of the licensing process for the transaction, provided that you have disclosed complete and accurate details of your proposed use, no license is finally effective unless and until full payment is received from you (either by publisher or by CCC) as provided in CCC's Billing and Payment terms and conditions. If full payment is not received on a timely basis, then any license preliminarily granted shall be deemed automatically revoked and shall be void as if never granted. Further, in the event that you breach any of these terms and conditions or any of CCC's Billing and Payment terms and conditions, the license is automatically revoked and shall be void as if never granted. Use of materials as described in a revoked license, as well as any use of the materials beyond the scope of an unrevoked license, may constitute copyright infringement and publisher reserves the right to take any and all action to protect its copyright in the materials.
9. Warranties: Publisher makes no representations or warranties with respect to the licensed material.
10. Indemnity: You hereby indemnify and agree to hold harmless publisher and CCC, and their respective officers, directors, employees and agents, from and against any and all claims arising out of your use of the licensed material other than as specifically authorized pursuant to this license.
11. No Transfer of License: This license is personal to you and may not be sublicensed, assigned, or transferred by you to any other person without publisher's written permission.

12. No Amendment Except in Writing: This license may not be amended except in a writing signed by both parties (or, in the case of publisher, by CCC on publisher's behalf).
13. Objection to Contrary Terms: Publisher hereby objects to any terms contained in any purchase order, acknowledgment, check endorsement or other writing prepared by you, which terms are inconsistent with these terms and conditions or CCC's Billing and Payment terms and conditions. These terms and conditions, together with CCC's Billing and Payment terms and conditions (which are incorporated herein), comprise the entire agreement between you and publisher (and CCC) concerning this licensing transaction. In the event of any conflict between your obligations established by these terms and conditions and those established by CCC's Billing and Payment terms and conditions, these terms and conditions shall control.
14. Revocation: Elsevier or Copyright Clearance Center may deny the permissions described in this License at their sole discretion, for any reason or no reason, with a full refund payable to you. Notice of such denial will be made using the contact information provided by you. Failure to receive such notice will not alter or invalidate the denial. In no event will Elsevier or Copyright Clearance Center be responsible or liable for any costs, expenses or damage incurred by you as a result of a denial of your permission request, other than a refund of the amount(s) paid by you to Elsevier and/or Copyright Clearance Center for denied permissions.

LIMITED LICENSE

The following terms and conditions apply only to specific license types:
15. **Translation**: This permission is granted for non-exclusive world **English** rights only unless your license was granted for translation rights. If you licensed translation rights you may only translate this content into the languages you requested. A professional translator must perform all translations and reproduce the content word for word preserving the integrity of the article.
16. **Posting licensed content on any Website**: The following terms and conditions apply as follows: Licensing material from an Elsevier journal: All content posted to the web site must maintain the copyright information line on the bottom of each image; A hyper-text must be included to the Homepage of the journal from which you are licensing at http://www.sciencedirect.com/science/journal/xxxxx or the Elsevier homepage for books at http://www.elsevier.com; Central Storage: This license does not include permission for a scanned version of the material to be stored in a central repository such as that provided by Heron/XanEdu.
Licensing material from an Elsevier book: A hyper-text link must be included to the Elsevier homepage at http://www.elsevier.com . All content posted to the web site must maintain the copyright information line on the bottom of each image.

Posting licensed content on Electronic reserve: In addition to the above the following clauses are applicable: The web site must be password-protected and made available only to bona fide students registered on a relevant course. This permission is granted for 1 year only. You may obtain a new license for future website posting.
17. **For journal authors:** the following clauses are applicable in addition to the above:
Preprints:
A preprint is an author's own write-up of research results and analysis, it has not been peer-reviewed, nor has it had any other value added to it by a publisher (such as formatting, copyright, technical enhancement etc.).
Authors can share their preprints anywhere at any time. Preprints should not be added to or enhanced in any way in order to appear more like, or to substitute for, the final versions of articles however authors can update their preprints on arXiv or RePEc with their Accepted Author Manuscript (see below).
If accepted for publication, we encourage authors to link from the preprint to their formal publication via its DOI. Millions of researchers have access to the formal publications on ScienceDirect, and so links will help users to find, access, cite and use the best available

version. Please note that Cell Press, The Lancet and some society-owned have different preprint policies. Information on these policies is available on the journal homepage.
Accepted Author Manuscripts: An accepted author manuscript is the manuscript of an article that has been accepted for publication and which typically includes author-incorporated changes suggested during submission, peer review and editor-author communications.
Authors can share their accepted author manuscript:

- immediately
    - via their non-commercial person homepage or blog
    - by updating a preprint in arXiv or RePEc with the accepted manuscript
    - via their research institute or institutional repository for internal institutional uses or as part of an invitation-only research collaboration work-group
    - directly by providing copies to their students or to research collaborators for their personal use
    - for private scholarly sharing as part of an invitation-only work group on commercial sites with which Elsevier has an agreement
- After the embargo period
    - via non-commercial hosting platforms such as their institutional repository
    - via commercial sites with which Elsevier has an agreement

In all cases accepted manuscripts should:

- link to the formal publication via its DOI
- bear a CC-BY-NC-ND license - this is easy to do
- if aggregated with other manuscripts, for example in a repository or other site, be shared in alignment with our hosting policy not be added to or enhanced in any way to appear more like, or to substitute for, the published journal article.

Published journal article (JPA): A published journal article (PJA) is the definitive final record of published research that appears or will appear in the journal and embodies all value-adding publishing activities including peer review co-ordination, copy-editing, formatting, (if relevant) pagination and online enrichment.
Policies for sharing publishing journal articles differ for subscription and gold open access articles:
Subscription Articles: If you are an author, please share a link to your article rather than the full-text. Millions of researchers have access to the formal publications on ScienceDirect, and so links will help your users to find, access, cite, and use the best available version.
Theses and dissertations which contain embedded PJAs as part of the formal submission can be posted publicly by the awarding institution with DOI links back to the formal publications on ScienceDirect.
If you are affiliated with a library that subscribes to ScienceDirect you have additional private sharing rights for others' research accessed under that agreement. This includes use for classroom teaching and internal training at the institution (including use in course packs and courseware programs), and inclusion of the article for grant funding purposes.
Gold Open Access Articles: May be shared according to the author-selected end-user license and should contain a CrossMark logo, the end user license, and a DOI link to the formal publication on ScienceDirect.
Please refer to Elsevier's posting policy for further information.
18. **For book authors** the following clauses are applicable in addition to the above:
Authors are permitted to place a brief summary of their work online only. You are not allowed to download and post the published electronic version of your chapter, nor may you scan the printed edition to create an electronic version. **Posting to a repository:** Authors are permitted to post a summary of their chapter only in their institution's repository.

19. **Thesis/Dissertation**: If your license is for use in a thesis/dissertation your thesis may be submitted to your institution in either print or electronic form. Should your thesis be published commercially, please reapply for permission. These requirements include permission for the Library and Archives of Canada to supply single copies, on demand, of the complete thesis and include permission for Proquest/UMI to supply single copies, on demand, of the complete thesis. Should your thesis be published commercially, please reapply for permission. Theses and dissertations which contain embedded PJAs as part of the formal submission can be posted publicly by the awarding institution with DOI links back to the formal publications on ScienceDirect.

Elsevier Open Access Terms and Conditions

You can publish open access with Elsevier in hundreds of open access journals or in nearly 2000 established subscription journals that support open access publishing. Permitted third party re-use of these open access articles is defined by the author's choice of Creative Commons user license. See our open access license policy for more information.

Terms & Conditions applicable to all Open Access articles published with Elsevier:

Any reuse of the article must not represent the author as endorsing the adaptation of the article nor should the article be modified in such a way as to damage the author's honour or reputation. If any changes have been made, such changes must be clearly indicated.

The author(s) must be appropriately credited and we ask that you include the end user license and a DOI link to the formal publication on ScienceDirect.

If any part of the material to be used (for example, figures) has appeared in our publication with credit or acknowledgement to another source it is the responsibility of the user to ensure their reuse complies with the terms and conditions determined by the rights holder.

Additional Terms & Conditions applicable to each Creative Commons user license:

CC BY: The CC-BY license allows users to copy, to create extracts, abstracts and new works from the Article, to alter and revise the Article and to make commercial use of the Article (including reuse and/or resale of the Article by commercial entities), provided the user gives appropriate credit (with a link to the formal publication through the relevant DOI), provides a link to the license, indicates if changes were made and the licensor is not represented as endorsing the use made of the work. The full details of the license are available at http://creativecommons.org/licenses/by/4.0.

CC BY NC SA: The CC BY-NC-SA license allows users to copy, to create extracts, abstracts and new works from the Article, to alter and revise the Article, provided this is not done for commercial purposes, and that the user gives appropriate credit (with a link to the formal publication through the relevant DOI), provides a link to the license, indicates if changes were made and the licensor is not represented as endorsing the use made of the work. Further, any new works must be made available on the same conditions. The full details of the license are available at http://creativecommons.org/licenses/by-nc-sa/4.0.

CC BY NC ND: The CC BY-NC-ND license allows users to copy and distribute the Article, provided this is not done for commercial purposes and further does not permit distribution of the Article if it is changed or edited in any way, and provided the user gives appropriate credit (with a link to the formal publication through the relevant DOI), provides a link to the license, and that the licensor is not represented as endorsing the use made of the work. The full details of the license are available at http://creativecommons.org/licenses/by-nc-nd/4.0.

Any commercial reuse of Open Access articles published with a CC BY NC SA or CC BY NC ND license requires permission from Elsevier and will be subject to a fee.

Commercial reuse includes:

- Associating advertising with the full text of the Article
- Charging fees for document delivery or access
- Article aggregation
- Systematic distribution via e-mail lists or share buttons

Posting or linking by commercial companies for use by customers of those companies.

20. **Other Conditions**:

v1.9

PERMISSIONS <permissions@asce.org> 7/3/2018, 12:10 PM

RE: Requesting Copyright Permissions to Reproduce Figures from ASCE Publications for use in a Master's Thesis

To Graeme Milligan <graememilligan_3@sympatico.ca>

Dear Graeme,
Hi. We actually don't hold the copyright on that image. It is referenced "Turner, C. A. P. (1905b) *Engineering News*, October 12, 383–384 (letter)."

But based on the publication date (1905) that should be in the public domain.

Sorry we couldn't be more help.

Sincerely,
Leslie Connelly
Senior Marketing Coordinator
American Society of Civil Engineers
1801 Alexander Bell Drive
Reston, VA 20191

PERMISSIONS@asce.org

703-295-6169
Internet: www.asce.org/pubs | www.ascelibrary.org | http://ascelibrary.org/page/rightsrequests

From: Graeme Milligan <graememilligan_3@sympatico.ca>
Sent: Tuesday, July 03, 2018 11:14 AM
To: PERMISSIONS <permissions@asce.org>
Subject: Requesting Copyright Permissions to Reproduce Figures from ASCE Publications for use in a Master's Thesis

Good morning,

I am a graduate student at the University of Waterloo currently working on my Master's thesis. In my literature review I would like to use a portion of Figure 6 from "Contributions of C. A. P. Turner to Development of Reinforced Concrete Flat Slabs 1905–1909" (Journal of Structural Engineering, Volume 128, Issue 10 October 2002) and was wondering about the procedure/who to contact to acquire the permission to reproduce this figure. My thesis would be published in the institutional repository at the University of Waterloo (Waterloo, Ontario, Canada). I have attached the portion of Figure 6 I wish to reproduce.

If any additional information is required please let me know. Thank you in advance for your time.

Kind Regards,
Graeme Milligan
MASc Candidate, University of Waterloo

Corinne Bottollier <webmaster@fib-international.org> 7/4/2018, 9:45 AM

Re: FIB | The International Federation for Structural Concrete: Requesting Copyright Permissions to Reproduce Figures from CEB Bulletins for use in a Master's Thesis

To Graeme Milligan <gjmillig@uwaterloo.ca>

Dear Graeme,

Thank you for your interest in the *fib*.

We are happy that you can use the Figure 3.8 from CEB Bulletin 168. We allow you to use it without any inconvenience on our side. We do not have records to have the full rights for the figure. Figure 3.8 is a drawing that I presume has been developed by the task group, then we think that you can use them with the proper reference to the CEB Bulletin 168 as per below:

> Figure 3.8:
> Reproduced from CEB Bulletin 168: - Punching Shear in Reinforced Concrete a state of art report by P.E. Regan and M.W. Braestrup (January 1985) with permission from the International Federation for Structural Concrete (*fib*).

Please let me know if there is anything else that you would need from us.

Meanwhile, I invite you to check our website (https://www.fib-international.org). Do not hesitate to visit the Membership page (https://www.fib-international.org/membership.html) to check all the benefits you could get if you wish to become a *fib* member,

Best regards,

Corinne

Best Regards,

Webmaster

fib A *B*ridge between *R*esearch and *P*ractice
International Federation for Structural Concrete

publications@fib-international.org
+41 21 693 2749
www.fib-international.org

> On 3 Jul 2018, at 17:05, FIB | The International Federation for Structural Concrete <webmaster@fib-international.org> wrote:
>
> This is an enquiry email via https://www.fib-international.org/ from:
> Graeme Milligan <gjmillig@uwaterloo.ca>

Hi,
I am a graduate student at the University of Waterloo currently working on my Master's thesis. In my literature review I would like to use Figure 3.8 from CEB Bulletin 168 - Punching Shear in Reinforced Concrete a state of art report by P.E. Regan and M.W. Braestrup (January 1985) and was wondering about the procedure/who to contact to acquire the permission to reproduce this figure. My thesis would be published in the institutional repository at the University of Waterloo (Waterloo, Ontario, Canada).
If you require any additional information please let me know. Thank you in advance for your time.
Kind Regards,
Graeme Milligan
MASc Candidate, University of Waterloo

Aikaterini Genikomsou <aikaterini.genikomsou@queensu.ca> 7/10/2018, 10:21 AM

RE: Permission to Reproduce Figures From Your Thesis

To Graeme Milligan <graememilligan_3@sympatico.ca>

Hi Graeme,

Yes can. You have my permission.
Wishing you good luck with the thesis.

All the best,
Katerina

From: Graeme Milligan [graememilligan_3@sympatico.ca]
Sent: Tuesday, July 10, 2018 5:18 PM
To: Aikaterini Genikomsou <aikaterini.genikomsou@queensu.ca>
Subject: Permission to Reproduce Figures From Your Thesis

Hi Katerina,

I hope all is well with you in Kingston.

Currently, I am working on completing my Master's thesis with the plan to graduate this term and return to UW in the fall to begin work on a PhD with Professor Polak.

In my thesis I was hoping to reproduce some of your figures when I summarize the work you completed. After speaking with the copyright librarian at UW (Lauren Byl) I was informed that I needed to request permission from you to reproduce the figures and to check that the figures were not reproduced from someone else (as I would need to request permission from them).

I have attached the three figures I wish to reproduce. At your earliest convenience could you let me know if you are the copyright owner of the attached images (or the publication where you took them from). Assuming you are the copyright owner please let me know if I can reproduce the figures in my thesis.

Best Regards,

Graeme

Rosa Lönneborg via RT <ask-kthb@kth.se> 7/5/2018, 6:40 AM

[kth.se #2721220] Requesting Copyright Permissions to Reproduce Figures From Transactions of the Royal Institute of Technology

To gjmillig@uwaterloo.ca

Hi Graeme,

When it comes to newer publications we normally ask the author of permission, but since this is published in 1960 KTH gives a general permission to reproduce parts of the material as long as it is in line with good research practice. So it is ok for you to reproduce the figures as long as you properly cite the source.

Kind regards,
Rosa Lönneborg
KTH Library

On Wed Jul 04 16:37:24 2018, gjmillig@uwaterloo.ca wrote:

> Fråga till: Huvudbiblioteket
> Från: Graeme Milligan,
> gjmillig@uwaterloo.ca
>
> Fråga
> Hi,
> I am a graduate student at the University of Waterloo currently working on my Master's thesis. In my literature review I would like to use Figure 31a,b and c from "Punching of Concrete Slabs Without Shear Reinforcement" (1960) by Kinnunen and Nylander and was wondering about the procedure/who to contact to acquire the permission to reproduce this figure. My thesis would be published in the institutional repository at the University of Waterloo (Waterloo, Ontario, Canada).
>
> If you require any additional information please let me know. Thank you in advance for your time.
>
> Kind Regards,
> Graeme Milligan
> MASc Candidate, University of Waterloo

Kaitlin Beer <kbeer@cement.org> 7/24/2018, 12:51 PM

RE: Requesting Copyright Permissions to Reproduce Figures from PCA Publications for use in a Master's Thesis

To Graeme Milligan <graememilligan_3@sympatico.ca>

Hi Graeme,

That looks great to me! Have a great day and again good luck wrapping up your thesis!

Best wishes,

Kaitlin Beer
Library Information Specialist
Portland Cement Association
5420 Old Orchard Road
Skokie, IL 60077
847.972.9176 (office)
kbeer@cement.org

PCA Since 1916
America's Cement Manufacturers™

From: Graeme Milligan [graememilligan_3@sympatico.ca]
Sent: Monday, July 23, 2018 10:13 AM
To: Beer, Kaitlin <kbeer@cement.org>
Subject: RE: Requesting Copyright Permissions to Reproduce Figures from PCA Publications for use in a Master's Thesis

Hi Kaitlin,

Thank you for providing me with the permission to reproduce Figure 2 from the Journal of the PCA Research and Development Laboratories, Vol.6, no. 1, 1964. Based on conversations with the copyright librarian here at the University of Waterloo your previous email is all I require for my thesis.

I have captioned the figure as shown below citing the original article and attributing the figure to the PCA as you recommended. If any changes need to be made please let me know.

Tensile Stress-Strain Curve for Reinforcing Bars Manufactured to Various ASTM Standards (Pfister & Hognestad, 1964), Adapted from the Journal of the PCA Research and Development Laboratories, Volume 6, No. 1 (1964), Reproduced with Permission

Kind Regards,

Graeme Milligan

---------- Original Message ----------
From: "Beer, Kaitlin" <kbeer@cement.org>
Date: July 20, 2018 at 4:54 PM

Hello Graeme,

Thank you for your request. You are more than welcome to reproduce figure 2 from the *Journal of the PCA Research and Development Laboratories,* Vol. 6, no. 1, 1965. Would you like a written permission form or will this email suffice? Please be sure to cite and attribute the figure to the Portland Cement Association. If you need anything else please let me know and good luck wrapping up your thesis.

Best wishes,

Kaitlin Beer
Library Information Specialist
Portland Cement Association
5420 Old Orchard Road
Skokie, IL 60077
847.972.9176 (office)
kbeer@cement.org

PCA Since 1916
America's Cement Manufacturers™

From: Graeme Milligan [graememilligan_3@sympatico.ca]
Sent: Tuesday, July 17, 2018 2:35 PM
To: Beer, Kaitlin <kbeer@cement.org>
Subject: Re: Requesting Copyright Permissions to Reproduce Figures from PCA Publications for use in a Master's Thesis

Hi Kaitlin,

I just wanted to follow up on my July 3rd request to reproduce figures from a PCA publication. As mentioned in my previous email, I hope to reproduce a stress-strain curve for deformed reinforcing bars manufactured according to ASTM A432. As I plan to submit my thesis in August I am hoping to acquire all copyright permissions sometime this month.

Best Regards,

Graeme Milligan

> ---------- Original Message ----------
> From: Graeme Milligan <graememilligan_3@sympatico.ca>
> Date: July 3, 2018 at 12:03 PM

Good Morning Kaitlin,

I am a graduate student at the University of Waterloo currently working on my Master's thesis. In my thesis I would like to reproduce the first graph in Figure 2 from "High Strength Bars as Concrete Reinforcement Part 6. Fatigue Tests" (Journal of the PCA Research and Development Laboratories, Volume 6, #1, January 1964). Lauren Byl from the University of Waterloo recommended I contact you in regards to getting permissions to reproduce this figure.

My thesis would be published in the institutional repository at the University of Waterloo (Waterloo, Ontario, Canada).

If any additional information is required please let me know. Thank you in advance for your time.

Kind Regards,
Graeme Milligan
MASc Candidate, University of Waterloo

- image001.png (13 KB)

Canada Permissions <canadapermissions@pearson.com> 7/26/2018, 3:50 AM

Re: Fwd: Permission Request Form Submission - CANADA

To Graeme Milligan <graememilligan_3@sympatico.ca>

Dear Graeme

Our ref: **564**

Thank you for your e-mail and the confirmation furnished.

I am pleased to be able to grant permission for you to use figures 13.2 and 13.35 of our publication, Reinforced Concrete: Mechanism and Design Canadian Edition by James G MacGregor and F Michael Bartlett in your Masters thesis: Nonlinear Finite Element Analysis of Punching Shear of Reinforced Concrete Slabs on Rectangular Columns which will be published by the University of Waterloo in August 2019.
Permission is granted free of charge, subject to acknowledgement to author/title and ourselves as publishers.
Permission does not extend to material that has been acknowledged to another source.
Acknowledgement: Title, author, Pearson Education Limited and Copyright line as it appears in our publication.
This permission is for Canada, non-exclusive print and electronic rights in the English language. Electronic content must appear on an access controlled website.

I thank you and trust you find the above to be in order.

Kind regards

Gaynor Thomas

On Fri, Jul 20, 2018 at 4:29 PM, Graeme Milligan <graememilligan_3@sympatico.ca> wrote:

> Hi Gaynor,
>
> Thanks for the follow up.
>
> Yes, please proceed to grant permission for the two figures as mentioned in your previous email.
>
> I just have one question about obtaining permission for Figure 13.36. I see that this photo is courtesy of Dr. James. MacGregor. As you mentioned this content belongs to the author and I would need to contact him. However, I believe Dr. MacGregor passed away in 2015. In cases such as these is it possible to obtain permissions?
>
> Thanks for any insight you can provide.
>
> Cheers,
>
> Graeme Milligan
>
> > ---------- Original Message ----------
> > From: "Permissions, Canada" <canadapermissions@pearson.com>
> > Date: July 20, 2018 at 1:47 AM
> >
> > Dear Graeme
> >
> > Our ref: **564**
> >
> > Thank you very much for the additional information furnished.
> >
> > Yes, there are usually separate Credits pages, but this is not the case with every title.
> >
> > I note that the the figure 13.36 is accredited to the author. Usually when a credit line like this appears, the content belongs to the author in his personal capacity. In this regard, you will have to reach out to the author directly to obtain permission.
> >
> > I can proceed to grant permission for the use of the other two figures. Please confirm this is how you wish to proceed.
> >
> > I thank you and look forward to hearing from you.
> >
> > Kind regards
> >
> > Gaynor Thomas
> >
> > On Tue, Jul 17, 2018 at 9:27 PM, Graeme Milligan < graememilligan_3@sympatico.ca> wrote:
> >
> > > Hi Gaynor,
> > >
> > > I just wanted to confirm you received the additional information from ISBN 013101403X I sent last Monday (July 9). If so, is there any update on my request? (Reference # 564).
> > >
> > > Best Regards,
> > >
> > > Graeme Milligan
> > >
> > > > ---------- Original Message ----------
> > > > From: Graeme Milligan < graememilligan_3@sympatico.ca >

Date: July 9, 2018 at 12:31 PM

Good Afternoon Gaynor,

Please find copies of Figures 13-2, 13-35 and 13-36 and the acknowledgement page from ISBN 013101403X attached. I was unable to locate a credits page. Is it typically separate from the acknowledgements?

I plan to reproduce the content in my Master's thesis submitted to the University of Waterloo which will be published this August 2018. My thesis will be made available in print and electronic formats in the library at the University of Waterloo.

Details of my thesis are as follows:

Thesis Title: Nonlinear Finite Element Analysis of Punching Shear of Reinforced Concrete Slabs Supported on Rectangular Columns

Author: Graeme Milligan

Let me know if anything else is required.

Best Regards,

Graeme

---------- Original Message ----------
From: "Permissions, Canada" < canadapermissions@pearson.com >
Date: July 9, 2018 at 5:21 AM

Dear Graeme

Our ref: **564**

I acknowledge receipt of your request, which you submitted via the online form.

Please be advised that your request is currently receiving our attention. In order for us to process your request further, please furnish:

- your publication details i.e. the title, author, edition number, print run and your publication date;
- copies of the content (figures 13.2, 13.35 and 13.36), scanned directly from the source title i.e. ISBN: 013101403X;
- copies of the Credits and Acknowledgement pages, scanned directly from the source title i.e. ISBN: 013101403X;
- formats requested i.e. print/electronic

Once the above is received, I will be in a position to process your request further.

Kind regards

Gaynor Thomas

---------- Forwarded message ----------
From: **Permission-Request-Form@pearson.com** < Permission-Request-Form@pearson.com>
Date: Sat, Jul 7, 2018 at 7:56 PM
Subject: Permission Request Form Submission - CANADA
To: canadapermissions@pearson.com

```
Book Title: Reinforced Concrete: Mechanics and Design
Edition: First Canadian Edition
Author: James G. MacGregor and F. Michael Bartlett
ISBN: 0-13-101403-X
URL:
Ancillary Title:
Edition:
Author:
ISBN:
URL:
Type of Use: other
Requested Material: Figure 13-2 page 578, Figure 13-35 and Figure 13-
36 page 617
Select the intentional uses for the material: Republication
Number of copies/units that will be reproduced, if any:
Will the textbook be adopted and students required to purchase the text or product for the course?: No
URL where the content will appear: https://uwspace.uwaterloo.ca/
Number of users who will access material: Unknown
Type of users who will have access: Academics
Access to the information be restricted and password protected: No
If yes, explain how:
```

Downloading, printing, and copying will be restricted: No
If yes, explain how:
Educator/Contact Name: Graeme Jacob Milligan
School/Company: University of Waterloo
Address: 200 University Avenue West
City: Waterloo
Province: Ontario
Postal Code: N2L 3G1
Email: gjmillig@uwaterloo.ca
Fax:

--
Global Innovations & Services
Pearson Canada
4th Floor, Auto Atlantic
Corner Hertzog Boulevard and Heerengracht

Cape Town, 8001
South Africa
E: permissions@pearson.com

Learn more at za.pearson.com

--
Global Innovations & Services
Pearson Canada
4th Floor, Auto Atlantic
Corner Hertzog Boulevard and Heerengracht

Cape Town, 8001
South Africa
E: permissions@pearson.com

Learn more at za.pearson.com

--
Global Innovations & Services
Pearson Canada
4th Floor, Auto Atlantic
Corner Hertzog Boulevard and Heerengracht
Cape Town, 8001
South Africa
E: permissions@pearson.com

Learn more at za.pearson.com

Bibliography

ACI Committee 318. (1956). *Building Code Requirements for Reinforced Concrete (ACI 318-56).* Detroit, Michigan: American Concrete Institute.

ACI Committee 318. (1963). *Building Code Requirements for Reinforced Concrete (ACI 318-63).* Detroit, Michigan: American Concrete Institute.

ACI Committee 318. (1965). *Special Publication 10 Commentary on Building Code Requirements for Reinforced Concrete (ACI 318-63).* Detroit, Michigan: American Concrete Institute.

ACI Committee 318. (2014). *Building Code Requirements for Structural Concrete (ACI 318M-14) and Commentary (ACI 318RM-14).* Farmington Hills, MI: American Concrete Institute.

ACI Committee 501. (1936). *Building Regulations for Reinforced Concrete (A.C.I. 501-36T).* American Concrete Institute.

ACI Committee E-1. (1927). *Tentative Building Regulations for the Use of Reinforced Concrete (E-1A-27T).* American Concrete Institute.

Adetifa, B., & Polak, M. (2005). Retrofit of Interior Slab connections for punching using shear bolts. *ACI Structural Journal, 102*(2), 268-274.

Alam, A. J., & Amanat, K. M. (2012). Finite Element Simulation on Punching Shear Behaviour of Reinforced Concrete Slabs. *ISRN Civil Engineering, 2012*, 1-9.

Alam, A. J., & Amanat, K. M. (2014). Investigation on punching shear behaviour of multi-panel flat slab. *International Journal of Structural Engineering, 5*(3), 189-206.

Alam, A. J., & Amanat, K. M. (2015). Effect of column size on punching shear behaviour of multi panel RC flat plate. *International Journal of Structural Engineering, 6*(3), 280-302.

Alam, A. J., Amanat, K., & Seraj, S. M. (2009). An Experimental Study on Punching Shear Behavior of Concrete Slabs. *Advances in Structural Engineering, 12*(2), 257-265.

Alexander, S. D., & Simmonds, S. H. (1987). Ultimate Strength of Slab-Column Connections. *ACI Structural Journal, 84*(3), 255-261.

Alexander, S. D., & Simmonds, S. H. (1992). Bond model for concentric punching shear. *ACI Structural Journal, 89*(3), 325-334.

Ali Mirza, S., & MacGregor, J. G. (1979). Variability of Mechanical Properties of Reinforcing Bars. *Journal of the Structural Division, 105*(5), 921-937.

Al-Yousif, A. T., & Regan, P. E. (2003). Punching Resistance of RC slabs supported by large/or elongated columns. *Structural Engineer, 81*(5), 30-34.

American Concrete Institute. (1920). *Standard Specification No. 23 Standard Building Regulations for the Use of Reinforced Concrete.* American Concrete Institute.

Anggadjaja, E., & Teng, S. (2008). Edge-Column Slab Connections under Gravity and Lateral Loading. *ACI Structural Journal, 105*(5), 541-551.

ASCE-ACI Committee 426. (1974). The shear strength of reinforced concrete members - slabs. *Journal of the Structural Divison, 100*(8), 1543-1591.

ASTM International. (1965). *1965 Book of ASTM Standards - Part 4 Structural Steel; Concrete Reinforcing Steel; Boiler and Pressure Vessel Plates; Steel Rails, Wheels, and Tires; Bearing Steel; Steel Forgings; Ferrous Filler Metal; Ferro-Alloys.* Philadelphia: American Society for Testing and Materials.

Barrage, R. (2017). *Finite Element Modelling of FRP Reinforced Concrete Beams and Comparative Analysis of Current Strength Prediction Models.* Masters Thesis, University of Waterloo, Waterloo, Ontario, Canada.

Bédard, C., & Kotsovos, M. D. (1985). Application of NLFEA to concrete structures. *Journal of Structural Engineering, 111*(12), 2691-2707.

Belletti, B., Pimentel, M., Scolari, M., & Walraven, J. C. (2015). Safety assessment of punching shear failure according to the level of approximation approach. *Structural Concrete, 16*(3), 366-380.

Birkle, G., & Dilger, W. H. (2008). Influence of Slab Thickness on Punching Shear Strength. *ACI Structural Journal, 105*(2), 180-188.

Bompa, D. V., & Onet, T. (2016). Punching shear strength of RC flat slabs at interior connections to columns. *Magazine of Concrete Research, 68*(1), 24-42.

Borges, L. L., Melo, G. S., & Gomes, R. B. (2013). Punching shear of reinforced concrete flat plates with openings. *ACI Structural Journal, 110*(4), 547-556.

Chen, W. (1982). *Plasticity in Reinforced Concrete.* New York: McGraw Hill.

Chen, W.-F., & Han, D. (1988). *Plasticity for Structural Engineers.* New York: Springer-Verlag.

Comité Euro-International Du Béton. (1978). CEB-FIP Model Code for Concrete Structures. In *Bulletin D'Information N. 124/125-E* (Vol. II). Paris: Comité Euro-International Du Béton.

Comite Euro-International Du Beton. (1980). *Bulletin D'Information 137 Complement to CEB-FIp Model Code 1978 Final Draft English Version.* Paris: Comite Euro-International Du Beton.

Comité Euro-International du Béton. (1993). *CEB-FIP Model Code 1990: Design Code.* London: Thomas Telford.

Committee of Laws and Ordinances. (1908). *Requirements for Reinforced Concrete or Concrete-Steel Constructed Buildings Recommended by the National Board of Fire Underwriters.* National Association of Cement Users .

Cornelissen, H., Hordijk, D., & Reinhardt, H. (1986). Experimental determination of crack softening characteristics of normalweight and lightweight concrete. *HERON, 31*(2), 45-56.

Dassault Systemes Simulia Corp. (2012). *ABAQUS Analysis User's Manual 6.12-3.* Providence, RI, USA.

Eder, M. A., Vollum, R. L., Elghazouli, A. Y., & Abdel-Fattah, T. (2010). Modelling and experimental assessment of punching shear in flat slabs with shearheads. *Engineering Structures, 32*(12), 3911-3924.

Einpaul, J., Bujnak, J., Fenández Ruiz, M., & Muttoni, A. (2016). Study on influence of column size and slab slenderness on punching strength. *ACI Structural Journal, 113*(1), 135-146.

Elstner, R. C., & Hognestad, E. (1956). Shearing Strength of Reinforced Concrete Slabs. *Journal Proceedings, 53*(7), 29-58.

Eom, T.-S., Song, J.-W., Song, J.-K., Kang, G.-S., Yoon, J.-K., & Kang, S.-M. (2017). Punching-shear behavior of slabs with bar truss shear reinforcement on rectangular columns. *Engineering Structures, 134*, 390-399.

Erdogan, H., Binici, B., & Ozcebe, G. (2011). Effect of column rectangularity on CFRP-strengthened RC flat plates. *Magazine of Concrete Research, 63*(7), 511-525.

European Comittee for Standardization (CEN). (1993). *ENV 1992-1-1: 1991 Eurocode 2 Design of Concrete Structures - Part 1: General Rules and Rules for Buldings (English Language Version).* London, UK: British Standard Insitute.

European Commitee For Standardization. (2004). *Eurocode 2: Design of concrete structures - Part 1-1: General Rules and Rules for Buildings.* Brussels, Belgium.

European Concrete Platform ASBL. (2008). *Eurocode 2 Commentary.*

fédération internationale du béton (fib). (2013). *fib Model Code for Concrete Structures 2010.* Lausanne, Switzerland.

Fernández Ruiz, M., & Muttoni, A. (2009). Applications of critical shear crack theory to punching of reinforced concrete slabs with transverse reinforcement. *ACI Structural Journal, 106*(4), 485-494.

FIB. (2001). Punching of structural concrete slabs. *fib Bulletin 12*.

FIB. (2010). *fib Bulletin 52: Structural Concrete Textbook on behaviour, design and performance* (2 ed., Vol. 2). Lausanne, Switzerland: International federation for structural concrete (fib).

Filatov, V. (2017). Experimental investigation of stress-strain conditions in punching zone of flat slabs. *MATEC Web of Sciences. 117.* EDP Sciences. doi:10.1051/matecconf/201711700045

Filatov, V. (2018). Evaluation of punching shear strength of flat slabs supported on rectangular columns. *E3S Web of Conferences. 33*, p. 02007. EDP Sciences.

Filatov, V., & Bubnov, E. (2016). Experimental Investigation of the Deformability of Reinforced Concrete Slabs under Punching. *MATEC Web of Conferences. 86.* EDP Sciences. doi:10.1051/matecconf/20168601007

Fürst, A., & Marti, P. (1997). Robert Maillart's Design Approach for Flat Slabs. *Journal of Structural Engineering, 123*(8), 1102-1110.

Gardner, N. J. (2011). Verification of punching shear provisions for reinforced concrete flat slabs. *ACI Structural Journal, 108*(5), 572-580.

Gardner, N. J., & Shao, X.-y. (1996). Punching Shear of Continuous Flat Reinforced Concrete Slabs. *ACI Structural Journal, 96*(2), 218-228.

Gardner, N., Huh, J., & Chung, L. (2002). Lessons from the Sampoong department store collapse. *Cement and Concrete Composites, 24*(6), 523-529.

Gasparini, D. A. (2002). Contributions of C.A.P. Turner to development of reinforced concrete flat slabs 1905-1909. *Journal of Structural Engineering, 128*(10), 1243-1252.

Genikomsou, A. (2015). *Nonlinear finite element analysis of punching shear of reinforced concrete slab-column connections.* PhD Thesis, University of Waterloo, Waterloo, Ontario, Canada.

Genikomsou, A. S., & Polak, M. (2015). Finite element analysis of punching shear of concrete slabs using damaged plasticity model in ABAQUS. *Engineering Structures, 98*, 38-48.

Genikomsou, A. S., & Polak, M. (2016). Finite-element analysis of reinforced concrete slabs with punching shear reinforcement. *Journal of Structural Engineering, 142*(12), 04016129.

Genikomsou, A. S., & Polak, M. (2017a). 3D finite element investigation of the compressive membrane action effect in reinforced concrete flat slabs. *Engineering Structures, 136*, 233-244.

Genikomsou, A. S., & Polak, M. (2017b). Effect of Openings on Punching Shear Strength of Reinforced Concrete Slabs—Finite Element Investigation. *ACI Structural Journal, 114*(5), 1249-1262.

Genikomsou, A., & Polak, M. A. (2017c). Finite element simulation of concrete slabs with various placement and amount of shear bolts. *Procedia Engineering, 193*, 313-320.

González-Vidosa, F., Kotsovos, M. D., & Pavlovic, M. N. (1988). Symmetrical Punching of Reinforced Concrete Slabs: An Analytical Investigation Based on Nonlinear Finite Element Modeling. *ACI Structural Journal, 85*(3), 241-250.

Guan, H., & Polak, M. (2007). Finite element studies of reinforced concrete slab – edge column connections with openings. *Canadian Journal of Civil Engineering, 34*(8), 952-965.

Guandalini, S., Burdet, O. L., & Muttoni, A. (2009). Punching Tests of Slabs with Low Reinforcement Ratios. *ACI Structural Journal, 106*(1), 87-95.

Habibi, F., Redl, E., Egberts, M., Cook, W. D., & Mitchell, D. (2012). Assessment of CSA A23.3 structural integrity requirements for two-way slabs. *Canadian Journal of Civil Engineering, 39*(4), 351-361.

Hallgren, M., & Bjerke, M. (2002). Non-linear finite element analyses of punching shear failure of column footings. *Cement & Concrete Composites, 24*(6), 491-496.

Hamberg, C. L., & Vavrinek, R. (1993). Shoelace Algorithm. *IMSA Math Journal, 2*(1), 3-7.

Hanif, H. U., Ibrahim, Z., Jameel, M., Ghaedi, K., & Aslam, M. (2016). A new approach to estimate damage in concrete beams using non-linearity. *Construction and Building Materials, 124*, 1080-1089.

Hany, N. F., Hantouche, E. G., & Harajli, M. H. (2016). Finite element modeling of FRP-confined concrete using modified concrete damaged plasticity. *Engineering Structures, 125*, 1-14.

Hartley, G. A., & El Kafrawy, M. F. (1984). Elongated columns and column offsets in reinforced concrete building frames. *Canadian Journal of Civil Engineering, 11*(1), 8-18.

Hawkins, N. M., Fallsen, H. B., & Hinojosa, R. C. (1971). Influence of Column Rectangularity on the Behavior of Flat Plate Structures. *ACI Special Publication, 30*, 127-146.

Himawan, A., & Teng, S. (2014). Cyclic Behaviour of Post-Tensioned Slab-Rectangular Column Connections. *ACI Structural Journal, 111*(1), 177-188.

Inácio, M. M., Almeida, A. F., Faria, D. M., Lúcio, V. J., & Ramos, A. P. (2015). Punching of high strength concrete flat slabs without shear reinforcement. *Engineering Structures, 103*, 275-284.

Johnson, R. P. (2009). Eurocodes, 1970-2010: why 40 years? *Proceedings of the Institution of Civil Engineers-Structures and Buildings, 162*(6), 371-379.

Kinnunen, S., & Nylander, H. (1960). Punching of concrete slabs without shear reinforcement. *Transactions of the Royal Institute of Technology, Stockholm, Sweden, 158*, 112.

Kueres, D., Siburg, C., Herbrand, M., Classen, M., & Hegger, J. (2017). Uniform design method for punching shear in flat slabs and column bases. *Engineering Structures, 136*, 149-164.

Kupfer, H., Hilsdorf, H. K., & Rüsch, H. (1969). Behavior of Concrete Under Biaxial Stresses. *Journal Proceedings, 66*(8), 656-666.

Lantsoght, E. O., van der Veen, C., Walraven, J. C., & de Boer, A. (2015). Transition from one-way to two-way shear in slabs under concentrated loads. *Magazine of Concrete Research, 67*(17), 909-922.

Lee, J., & Fenves, G. L. (1998a). Plastic-damage model for cyclic loading of concrete structures. *Journal of engineering mechanics, 124*(8), 892-900.

Lee, J., & Fenves, G. L. (1998b). A plastic-damage concrete model for earthquake analysis of dams. *Earthquake Engineering & Structural Dynamics, 27*(9), 937-956.

Lips, S., Fernández Ruiz, M., & Muttoni, A. (2012). Experimental investigation on punching strength and deformation capacity of shear-reinforced slabs. *ACI Structural Journal, 109*(6), 889-900.

MacGregor, J. G., & Bartlett, F. (2000). *Reinforced Concrete Mechanics and Design - First Canadian Edition.* Toronto: Pearson Education Canada Inc.

Mahmoud, A. M. (2015). Finite element implementation of punching shear behaviours in shear-reinforced flat slabs. *Ain Shams Engineering Journal, 6*(3), 735-754.

Marzouk, H., & Hussein, A. (1991). Punching shear analysis of reinforced high-strength concrete slabs. *Canadian Journal of Civil Engineering, 18*(6), 594-963.

Masterson, D. M., & Long, A. E. (1974). The Punching Strength of Slabs, A Flexural Approach Using Finite Elements. *ACI Special Publication 42*, 767-768.

Megally, S., & Ghali, A. (2000). Punching of Concrete Slabs Due to Column Moment Transfer. *Journal of Structural Engineering, 126*(2), 180-189.

Menétrey, P. (1996). Analytical computation of the punching strength of reinforced concrete. *ACI Structural Journal, 93*(5), 503-511.

Menétrey, P., Walther, R., Zimmermann, T., Willam, K. J., & Regan, P. E. (1997). Simulation of punching failure in reinforced-concrete structures. *Journal of Structural Engineering, 123*(5), 652-659.

Mitchell, D., Cook, W., & Dilger, W. (2005). Effects of size, geometry and material properties on punching shear resistance. *ACI Special Publication 232*, 39-56.

Moe, J. (1961). *Shearing strength of reinforced concrete slabs and footings under concentrated loads.* Skokie, Illinois: Portland Cement Association.

Moreno, C. L., & Sarmento, A. M. (2013). Punching shear analysis of slab-column connections. *Engineering Computations, 30*(6), 802-814.

Mowrer, R. D., & Vanderbilt, M. D. (1967). Shear strength of lightweight aggregate reinforced concrete flat plates. *Journal Proceedings, 64*(11), 722-729.

Muttoni, A. (2008). Punching shear strength of reinforced concrete slabs without transverse reinforcement. *ACI Structural Journal, 105*(4), 440-450.

Muttoni, A., & Fernández Ruiz, M. (2008). Shear strength of members without transverse reinforcement as function of critical shear crack width. *ACI Structural Journal, 105*(2), 163-172.

Muttoni, A., & Fernández Ruiz, M. (2012). The levels-of-approximation approach in MC 2010: application to punching shear provisions. *Structural Concrete, 13*(1), 32-41.

Muttoni, A., & Schwartz, J. (1991). behaviour of beams and punching in slabs without shear reinforcement. *IABSE Colloquium, 62*, 703-708.

Muttoni, A., Fernández Ruiz, M., Bentz, E., Foster, S., & Sigrist, V. (2013). Background to fib Model Code 2010 shear provisions - Part II: Punching shear. *Structural Concrete, 14*(3), 204-214.

Navarro, M., Ivorra, S., & Varona, F. B. (2016). Parametric computational analysis for punching shear in RC slabs. *Engineering Structures, 165*, 254-263.

Oliveira, D. C., Gomes, R. B., & Melo, G. S. (2014). Punching shear in reinforced concrete flat slabs with hole adjacent to the column and moment transfer. *Ibracon Structures and Materials Journal, 7*(3), 414-467.

Oliveira, D. R., Regan, P. E., & Melo, G. S. (2004). Punching resistance of RC slabs with rectangular columns. *Magazine of Concrete Research, 56*(3), 123-138.

Ospina, C. E., Birkle, G., Widianto, Y., Fernando, S. R., Fernando, S., Catlin, A. C., & Pujol, S. (2015). NEES: ACI 445 Punching Shear Collected Databank. Retrieved from https://datacenterhub.org/resources/256

Paiva, O. S., Ferreira, M. P., Oliveira, D. C., Lima Neto, A. F., & Teixeira, M. R. (2015). Influence of the column rectangularity index and of the boundary conditions in the punching resistance of slab-column connections. *Ibracon Structures and Materials Journal, 8*(3), 260-295.

Park, R., & Gamble, W. (1980). *Reinforced Concrete slabs.* Toronto: John Wiley & Sons Inc.

Petersson, E. (1981). *Crack Growth and Development of Fracture Zones in Plain Concrete and Similar Materials.* Doctoral Dissertation, Lund Institute of Technology, Lund, Sweden.

Pfister, J. F., & Hognestad, E. (1964). High Strength Bars as Concrete Reinforcement Part 6. Fatigue Tests. *Journal of the PCA Research and Development Laboratories, 6*(1), 65-84.

Plos, M., Shu, J., Zandi, K., & Lundgren, K. (2017). A multi-level structural assessment strategy for reinforced concrete bridge deck slabs. *Structure and Infrastructure Engineering, 13*(2), 223-241.

Polak, M. A. (1998). Modeling Punching Shear of Reinforced Concrete Slabs Using Layered Finite Elements. *ACI Structural Journal, 95*(1), 71-80.

Rankin, G., & Long, A. (1987). Predicting the punching strength of conventional slab-column specimens. *Proceedings of the Institution of Civil Engineers (London), 82*(1), 327-346.

Regan, P. E. (1986). Symmetric punching of reinforced concrete slabs. *Magazine of Concrete Research, 38*(136), 115-128.

Regan, P. E., & Rezai-Jorabi, H. (1988). Shear Resistance of One-Way Slabs under Concentrated Loads. *ACI Structural Journal, 85*(2), 150-157.

Regan, P., & Braestrup, M. (1985). *Punching Shear in Reinforced Concrete - Bulletin D'Information 168.* Lausanne: Comite Euro International Du Beton.

Reineck, K.-H., Kuchma, D. A., Kim, K., & Marx, S. (2003). Shear Database for Reinforced Concrete Members Without Shear Reinforcement. *ACI Structural Journal, 100*(2), 240-249.

Ricker, M., & Siburg, C. (2016). Punching shear strength of flat slabs - critical review of Eurocode 2 and fib Model Code 2010 design provisions. *Structural Concrete, 17*(3), 457-468.

Sagaseta, J., Muttoni, A., Fernández Ruiz, M., & Tassinari, L. (2011). Non-axis-symmetrical punching shear around internal columns of RC slabs without transverse reinforcement. *Magazine of Concrete Research, 63*(6), 441-457. doi:10.1680/macr.10.00098

Sagaseta, J., Tassinari, L., Fernández Ruiz, M., & Muttoni, A. (2014). Punching of flat slabs supported on rectangular columns. *Engineering Structures, 77*, 17-33. doi:10.1016/j.engstruct.2014.07.007

Shehata, A., & Regan, P. E. (1989). Punching in R.C. slabs. *Journal of Structural Engineering, 115*(7), 1726-1740.

Sherif, A. G., & Dilger, W. H. (1996). Critical review of the CSA A23.3-94 punching shear strength provisions for interior columns. *Canadian Journal of Civil Engineering, 23*(5), 998-1011.

Sherif, A., Emara, M. B., Ibrahim, A. H., & Magd, S. A. (2005). Effect of the Column Dimensions on the Punching Shear Strength of Edge Column-Slab Connections. *ACI Special Publication 232* , 175-192.

Shu, J. (2017). *Structural Analysis Methods for the Assessment of Reinforced Concrete Slabs.* Doctoral Thesis, Chalmers University of Technology, Göteborg, Sweden.

Shu, J., Belletti, B., Muttoni, A., Scolari, M., & Plos, M. (2017). Internal force distribution in RC slabs subjected to punching shear. *Engineering Structures, 153*, 766-781.

Shu, J., Fall, D., Plos, M., Zandi, K., & Lundgren, K. (2015). Development of modelling strategies for two-way RC slabs. *Engineering Structures, 101*, 439-449.

Shu, J., Plos, M., Zandi, K., Johansson, M., & Nilenius, F. (2016). Prediction of punching behaviour of RC slabs using continuum non-linear FE analysis. *Engineering Structures, 125*, 15-25.

Simmonds, S. H. (1970). Flat Slabs Supported On Columns Elongated in Plan. *Journal Proceedings, 67*(12), 967-976.

Soares, L., & Vollum, R. (2015). Comparison of punching shear requirements in BS 8110, EC2 and MC2010. *Magazine of Concrete Research, 67*(24), 1315-1328.

Sozen, M. A., & Siess, C. P. (1963). Investigation of multiple-panel reinforced concrete floor slabs design methods - their evolution and comparison. *Journal of the American Concrete Institute, 60*(8), 999-1028.

Stoner, J. G. (2015). *Finite Element Modelling of GFRP Reinforced Concrete Beams.* Masters Thesis, University of Waterloo, Waterloo, Ontario, Canada.

Tan, Y., & Teng, S. (2005). Interior Slab-Rectangular Column Connections Under Biaxial Lateral Loadings. *ACI Special Publication 232*, 147-174.

Teng, S., Chanthabouala, K., Lim, D. T., & Hidayat, R. (2018). Punching Shear Strength of Slabs and Influence of Low Reinforcement Ratio. *ACI Structural Journal, 115*(1), 139-150.

Teng, S., Cheong, H. K., Kuang, K. L., & Geng, J. Z. (2004). Punching Shear Strength of Slabs with Openings and Supported on Rectangular Columns. *ACI Structural Journal, 101*(5), 678-687.

The Concrete Centre, part of the MPA. (n.d.). *Background to Eurocode 2*. Retrieved from https://www.concretecentre.com/Concrete-Design/Design-Codes/Eurocode-2/Background-to-Eurocode-2.aspx

Theodorakopoulos, D., & Swamy, R. (2002). Ultimate punching shear strength analysis of slab-column connections. *Cement and Concrete Composites, 24*(6), 509-521.

Turner, C.A.P. (1905, October 12). Engineering News. *(letter),* 383-384.

Ugural, A. C., & Fenster, S. K. (2012). *Advanced Mechanics and Materials of Applied Elasticity* (Fifth Edition ed.). Westford, Massachusetts: Pearson Education Inc.

Vanderbilt, M. D. (1972). Shear Strength of Continuous Plates. *Journal of the Structural Division, 98*(5), 961-973.

Vaz Rodrigues, R., Fernández Ruiz, M., & Muttoni, A. (2008). Shear strength of R/C bridge cantilever slabs. *Engineering Structures, 30*(11), 3024-3033.

Walraven, J., & Bigaj, A. (2011). The 2010 fib model code for concrete structures: a new approach to structural engineering. *Structural Concrete, 12*(3), 139-147.

Winkler, K., & Stangenberg, F. (2008). Numerical analysis of punching shear failure of reinforced concrete slabs. *Abaqus Users' Conference*.

Wosatko, A., Pamin, J., & Polak, M. (2015). Application of damage-plasticity models in finite element analysis of punching shear. *Computers and Structures, 151*, 73-85.

Wu, J., Li, J., & Faria, R. (2006). An energy release rate-based plastic-damage model for concrete. *International Journal of Solids and Structures, 43*(3-4), 583-612.

Yamada, T., Nanni, A., & Endo, K. (1992). Punching Shear Resistance of Flat Slabs: Influence of Reinforcement Type and Ratio. *ACI Structural Journal, 88*(4), 555-563.

Yu, T., Teng, J., Wong, Y., & Dong, S. (2010). Finite element modeling of confined concrete-II: Plastic-damage model. *Engineering Structures, 32*(3), 680-691.

Appendix A

Estimation of Slab Rotations – Linear Approximation Verification

In this appendix, the procedure used to estimate the slab rotations from the finite element results is outlined. The deflected shape of select slabs as the load is increased in the finite element analysis are provided and compared to the linear approximation used.

The predicted deflection profiles in each orthogonal direction along the symmetry faces for all slabs analyzed in this thesis, other than the slabs in the SB1 analysis which were supported at the slab edge, were found to be approximately linear between the end of the supported area (column stub or steel plate) and the unsupported edge of the slab throughout the analysis until punching or one-way shear failure occurred. Therefore, the slab rotations in each orthogonal direction were estimated using equations $A1$ and $A2$, where Δ_i, s_i and c_i are the vertical deflection at the slab edge predicted by the FEA, half length of the isolated specimen and half of the column dimension in each orthogonal direction respectively. The small angle approximation $\tan\theta \cong \theta$ was used in all models.

$$\psi_x = \frac{\Delta_x}{s_x - c_x} \tag{A1}$$

$$\psi_y = \frac{\Delta_y}{s_y - c_y} \tag{A2}$$

For the Hawkins' slabs $s_x = s_y = 1066.8mm$ $(7')$ and for the AM and PT series slabs $s_x = s_y = 1500mm$.

A comparison of this linear approximation to the predicted deflected profile for slabs 1 and 7 from the Hawkins' slab analysis and for slab AM04 (calibrated model) are shown in Figure A-1, Figure A-2, and Figure A-3 respectively. Slab 1 and 7 were loaded in one-way and two-way action respectively. In all investigated cases, the linear approximation was found to correlate well with the predicted deflected profile until approximately 90% of the peak load. Between 90% of the peak load and the peak load, the deviation between the linear approximation and the actual deflection profile increased. However, the linear approximation has a similar slope to the deflected profile near the supported region which is the region of interest. Therefore, the linear approximation was used to estimate all slab rotations in this thesis.

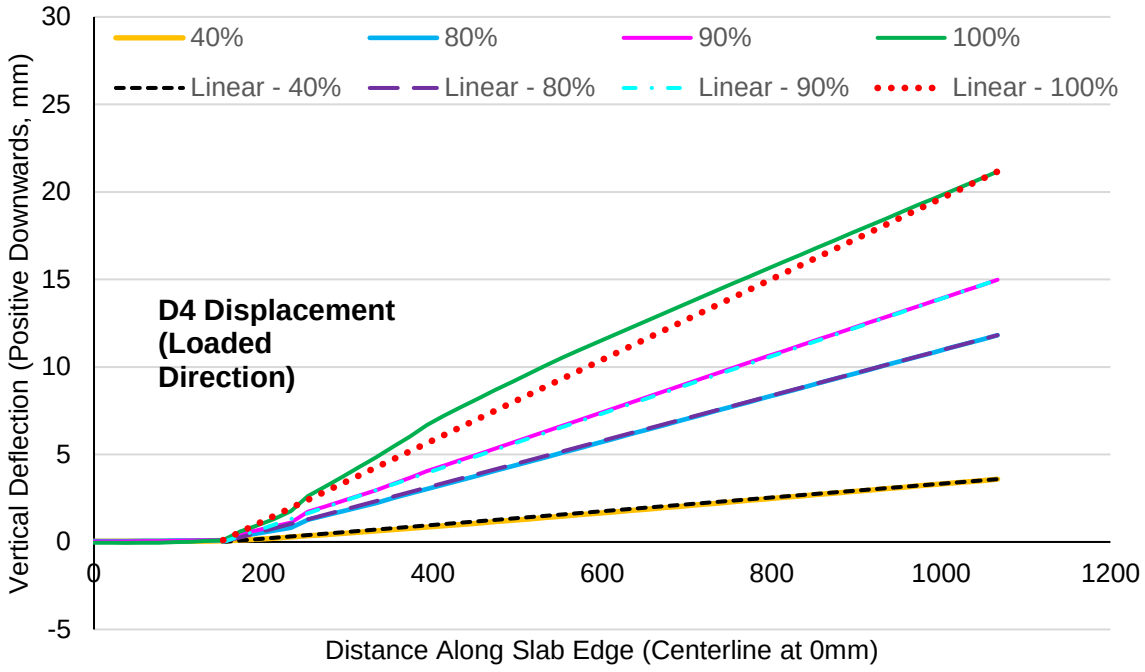

a)

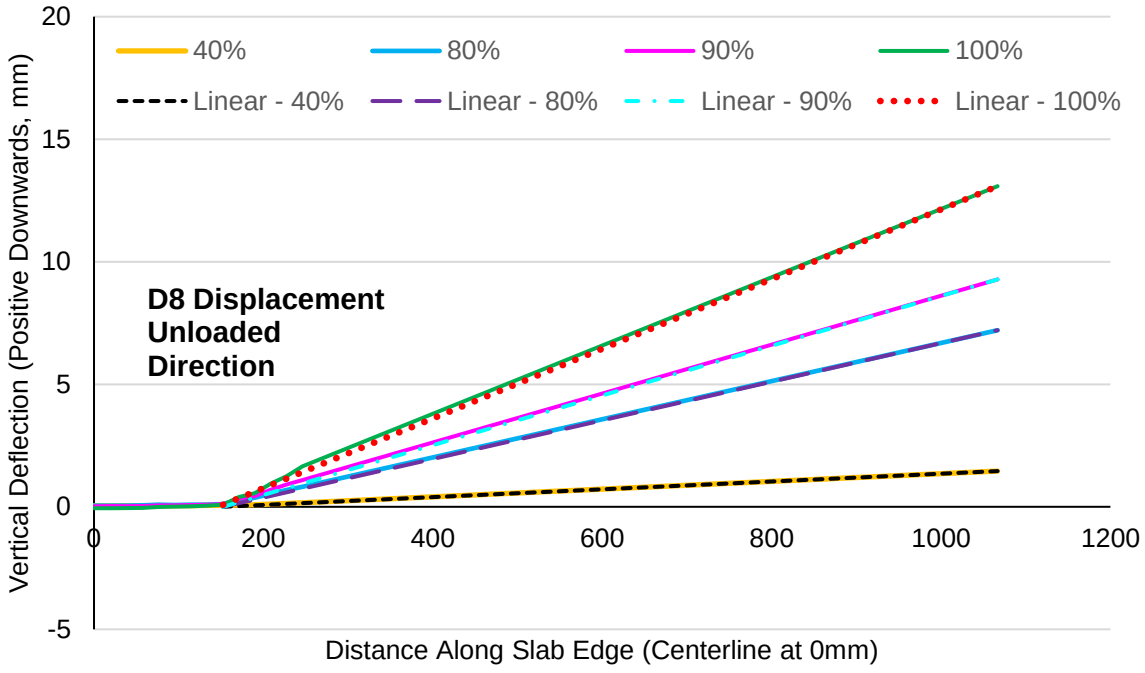

b)

Figure A-1: Predicted Deflection Profile – Slab 1 from Hawkins, Fallsen and Hinojosa (1971)

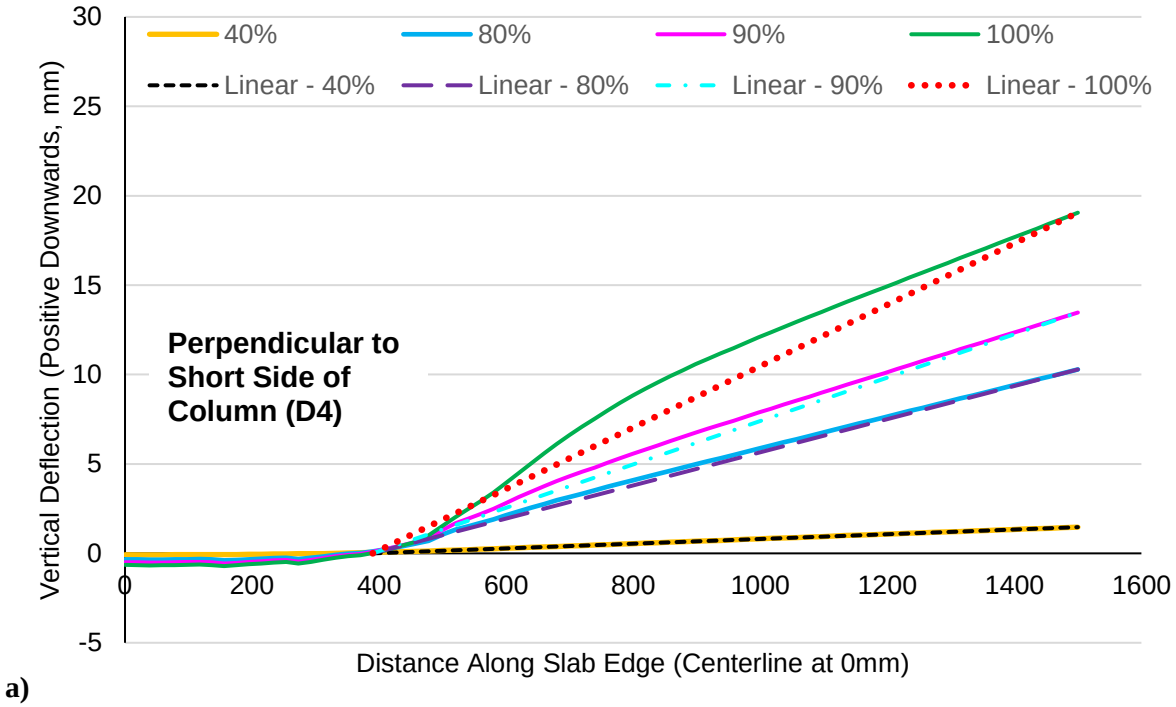

a)

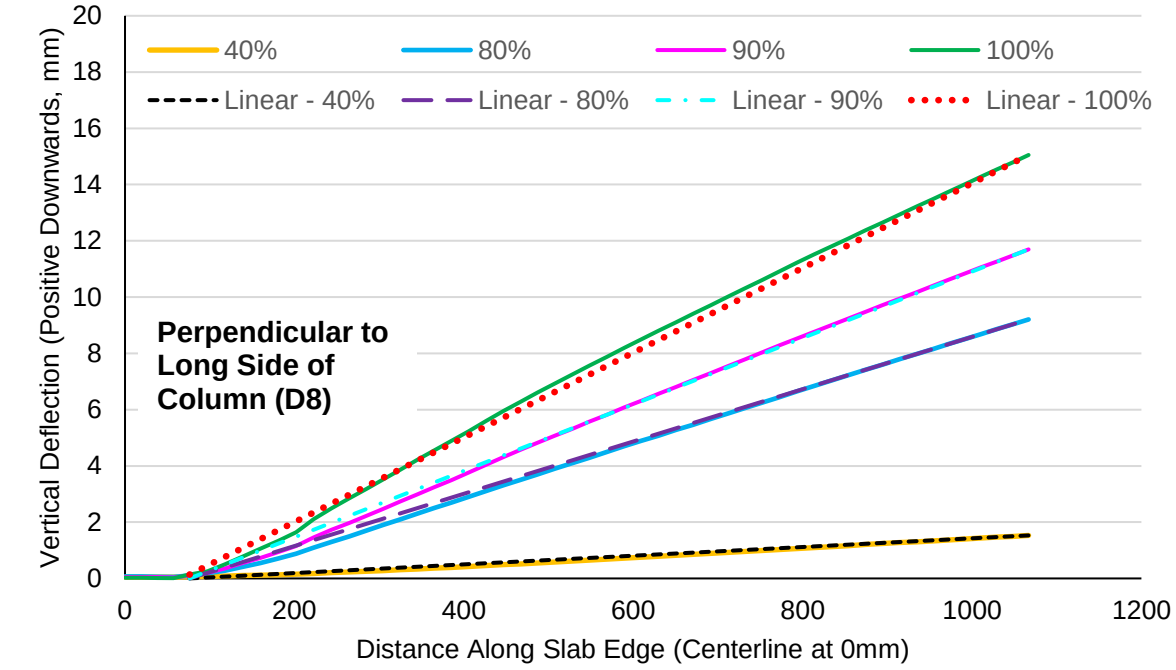

b)

Figure A-2: Predicted Deflection Profile – Slab 7 from Hawkins, Fallsen and Hinojosa (1971)

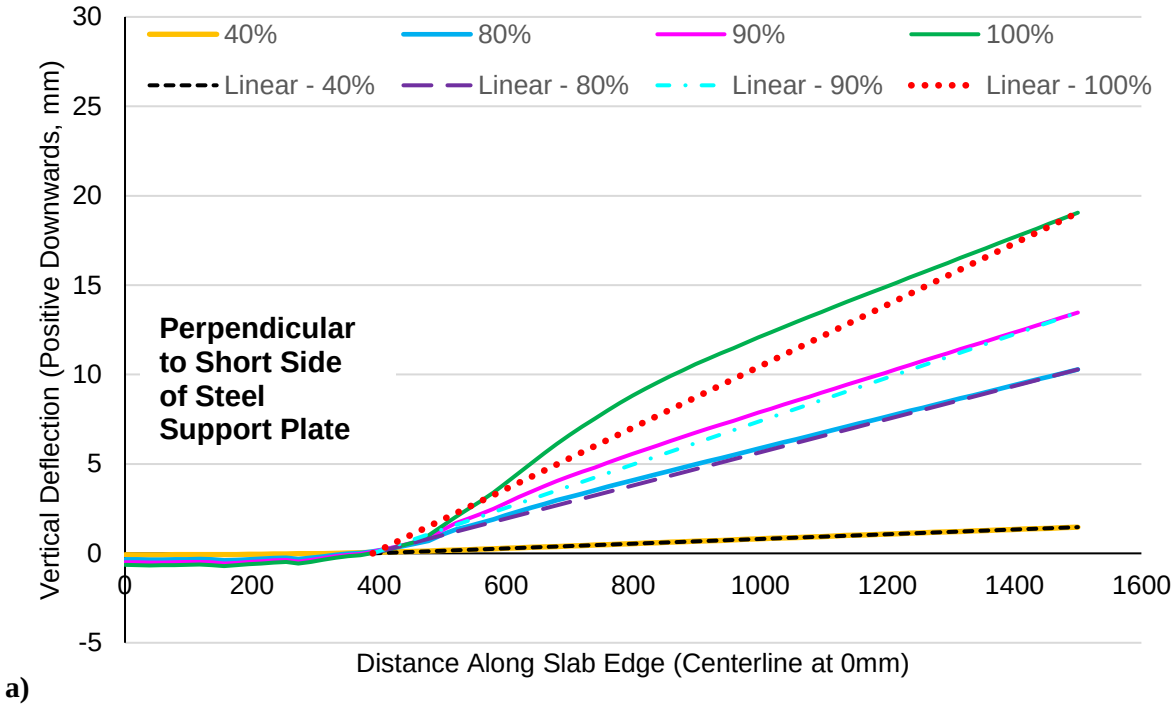

a)

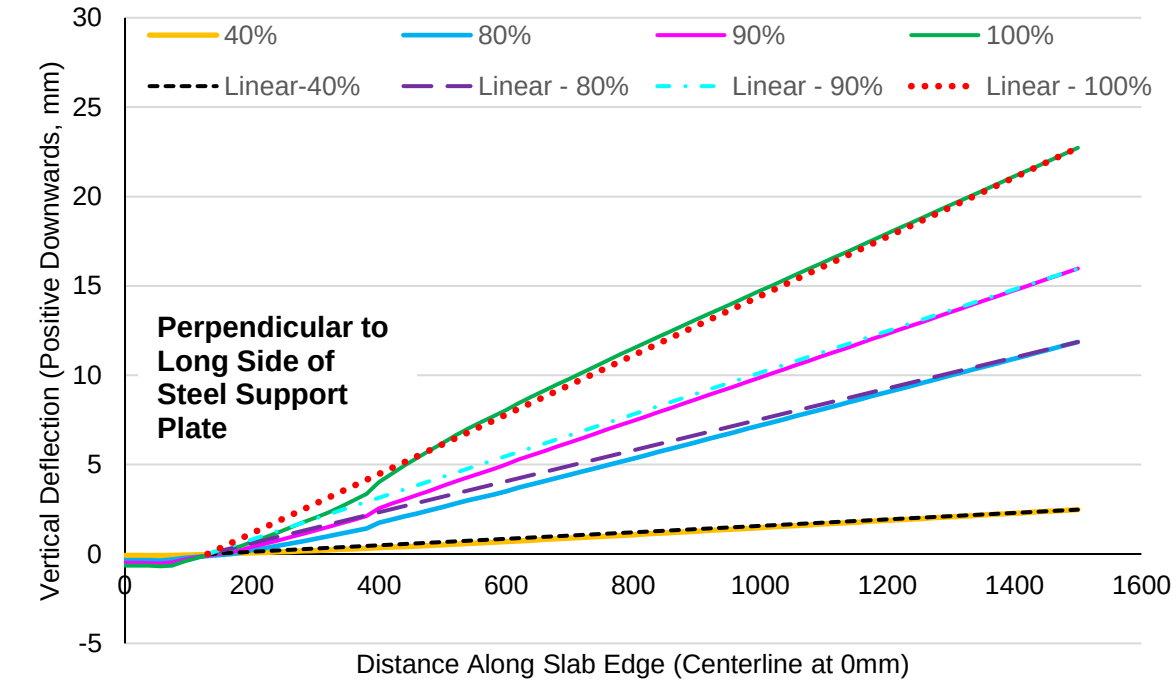

b)

Figure A-3: Predicted Deflection Profile – Slab AM04 from Sagaseta et al. (2014)

Appendix B

Shear Stress Distribution Calculation Methodology

In this appendix, the methodology used to calculate the shear stress distributions in the slab around the column perimeter and the ACI critical perimeter is discussed. Python 2.7 was used to post-process the ABAQUS results and export the results to Microsoft Excel for plotting.

For reference, a top view of the quarter model for the AM series (AM04 is shown) and the parametric study models is provided in Figure B-1. In the ABAQUS model, the X-axis is parallel to the long side of the steel plate and the Y-axis is parallel to the short side of the steel plate, which is opposite of the experimental setup. However, the experimental convention was used when referring to the stress distributions and the load-rotation or load-deflection responses in this thesis. Therefore, the Y-direction was parallel to the long side of the steel plate and the X-direction was parallel to the short side of the steel plate.

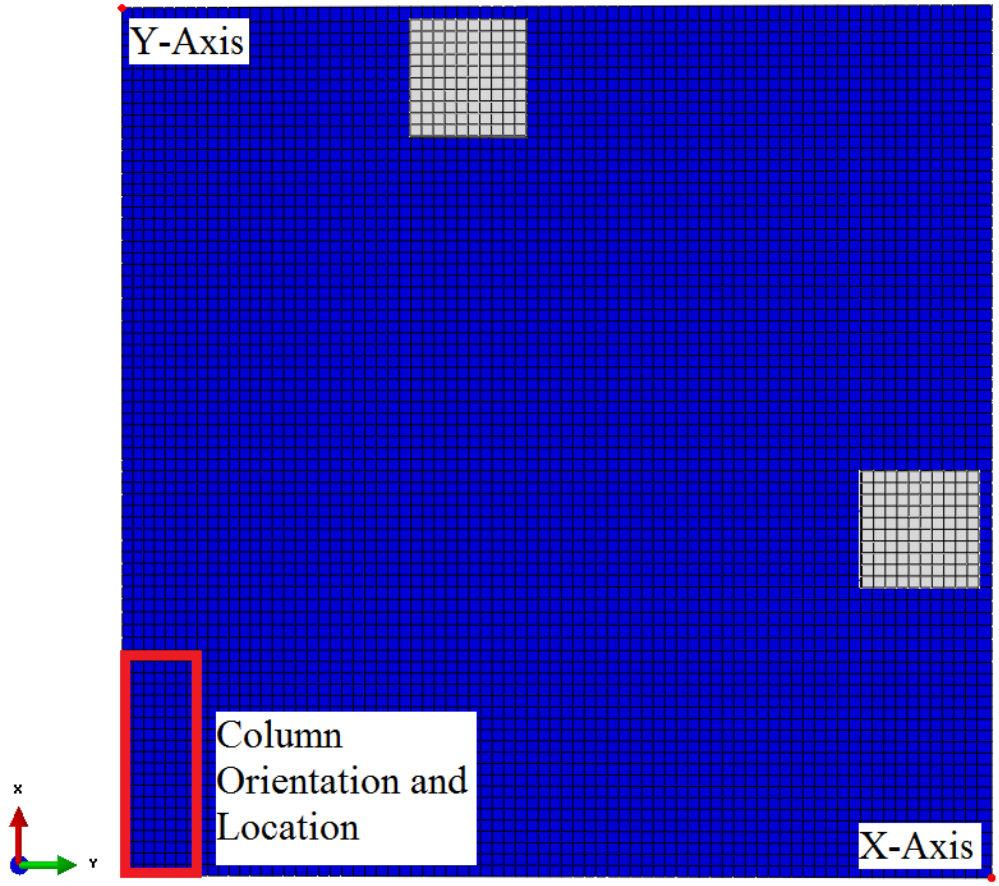

Figure B-1: Overview of AM04 Quarter Model

The location of the elements considered in the calculation of the shear stress distribution in the slab around the perimeter of the steel support plate ("column") and the ACI 318 critical perimeter are shown in Figure B-2. The elements parallel to the short side of the supported area were denoted "Parallel to X" or "Parallel to X ACI." The elements parallel to the long side of the supported area were denoted "Parallel to Y" or "Parallel to Y ACI." In all models, the support plate/column

perimeter elements were located along the outer edge of the supported area as shown in Figure B-2. In all models except for the AM04 model, the ACI critical perimeter elements were located at a distance of 100mm from the outer edge of the supported area. Since the elements only have one integration point, located at the element centroid, the stress values used are calculated at a distance of 90mm away from the edge of the supported area, which is slightly less than d/2 (101mm). In the AM04 model the ACI critical perimeter elements were located at 110mm from the edge of the supported area, and therefore, the integration points are approximately located 100mm from the edge of the supported area. However, the distance of 110mm was not used for all models because it led to meshing issues due to the use of a 20mm global mesh size. For the elements parallel to the short side of the supported area shear stress S13 was recorded during the analysis. For the elements parallel to the long side of the supported area shear stress S23 was recorded.

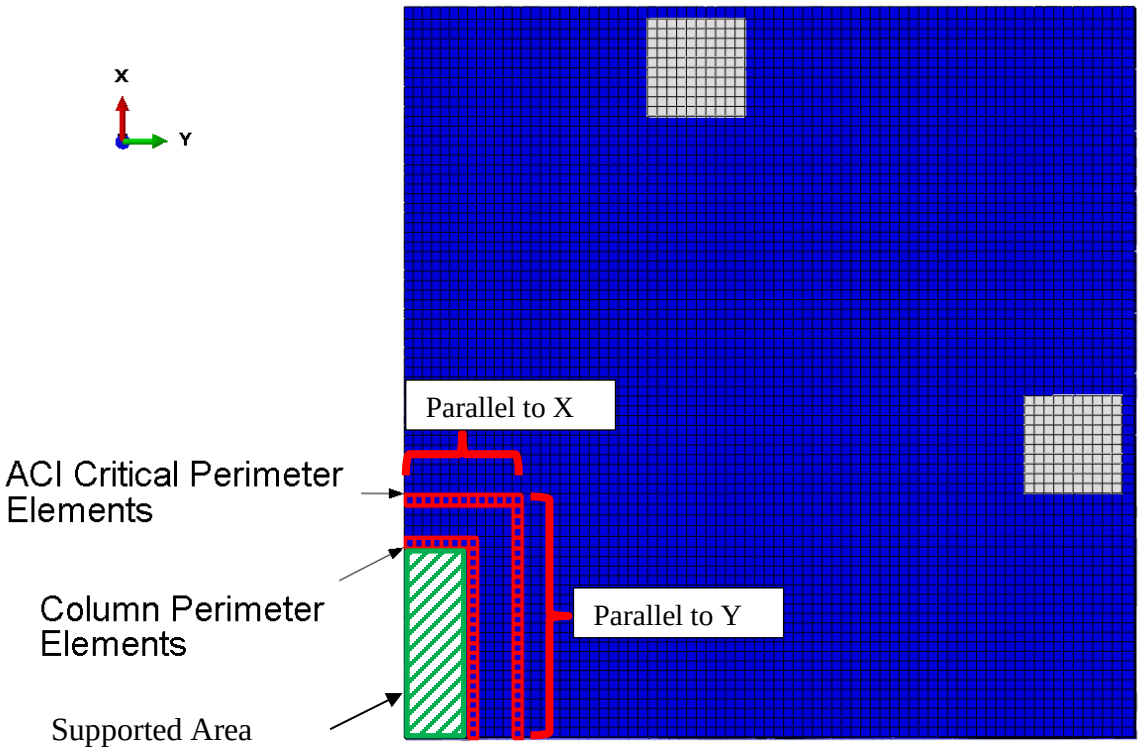

Figure B-2: Top View of Elements Considered in Shear Stress Distribution Calculations

A side view of slab showing the elements considered when calculating the shear stress distribution is shown in Figure B-3. As previously discussed, the elements along the perimeter of the supported area were located along the outer edge of the support plate. All elements through the slab depth were included when calculating the shear stress distribution.

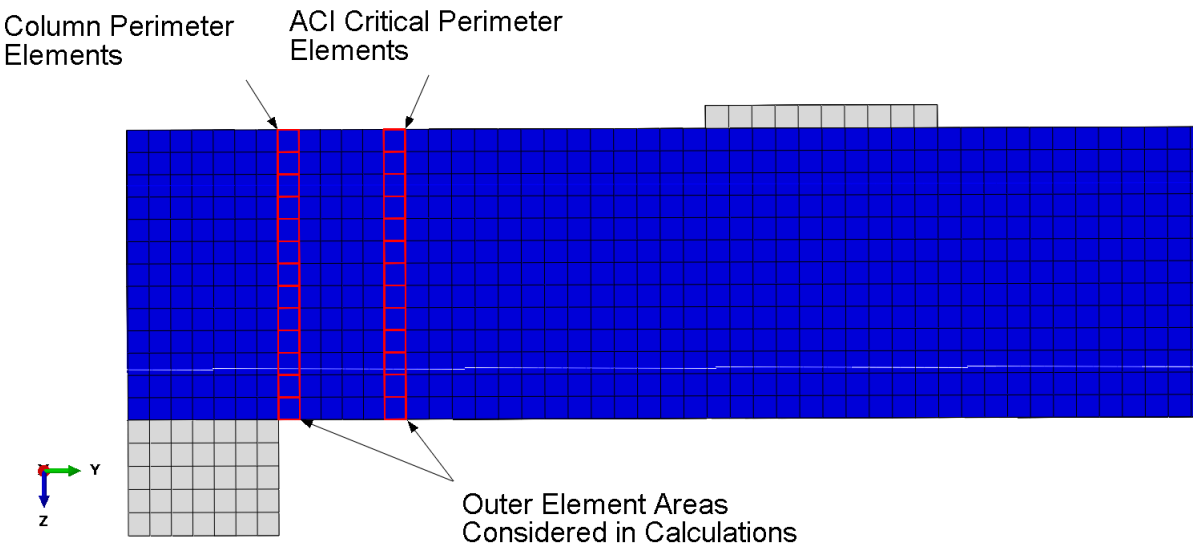

Figure B-3: Side View of Elements Considered in Stress Distribution Calculations

Since the element area is not a variable which can be extracted from ABAQUS it must be calculated using the deformed nodal coordinates of each element. As noted in Figure B-3, the outer element face area was used instead of the inner face area or average face area. Only using the area of the outer element face was found to have a minimal impact on the predicted shear stress distribution but greatly increased the computational efficiency of the Python post processing code.

The Shoelace algorithm, provided in equation $B1$, was used to calculate the outer element face area from the four deformed nodal coordinates at each step during the analysis. The area of a closed polygon with four non-intersecting sides was calculated according to equation $B2$.

$$A = \frac{1}{2}\left|(x_1y_2 + x_2y_3 + \cdots + x_ny_1) - (x_2y_1 + x_3y_2 + \cdots + x_1y_n)\right| \qquad (B1)$$

$$A = \frac{1}{2}\left|(x_1y_2 + x_2y_3 + x_3y_4 + x_4y_1) - (x_2y_1 + x_3y_2 + x_4y_1 + x_1y_4)\right| \qquad (B2)$$

where x_i and y_i are the nodal coordinates of each node of the polygon (1-n) in a Cartesian plane and the nodes are numbered in a counterclockwise or clockwise direction (Hamberg & Vavrinek, 1993).

Using the element area and shear stress at the element integration point, the shear force acting on each element was calculated as shown in Figure B-4. The total shear stress on each column of elements was then calculated as the total force in the column of elements divided by the total area.

This process was repeated for each column of elements along the support plate and critical perimeter. As shown in Figure B-2, the elements considered in each direction intersect at the corner of the supported area or the critical perimeter. Therefore, the procedure outlined above was implemented twice for the corner elements considering the S13 and S23 stresses and the results were summed.

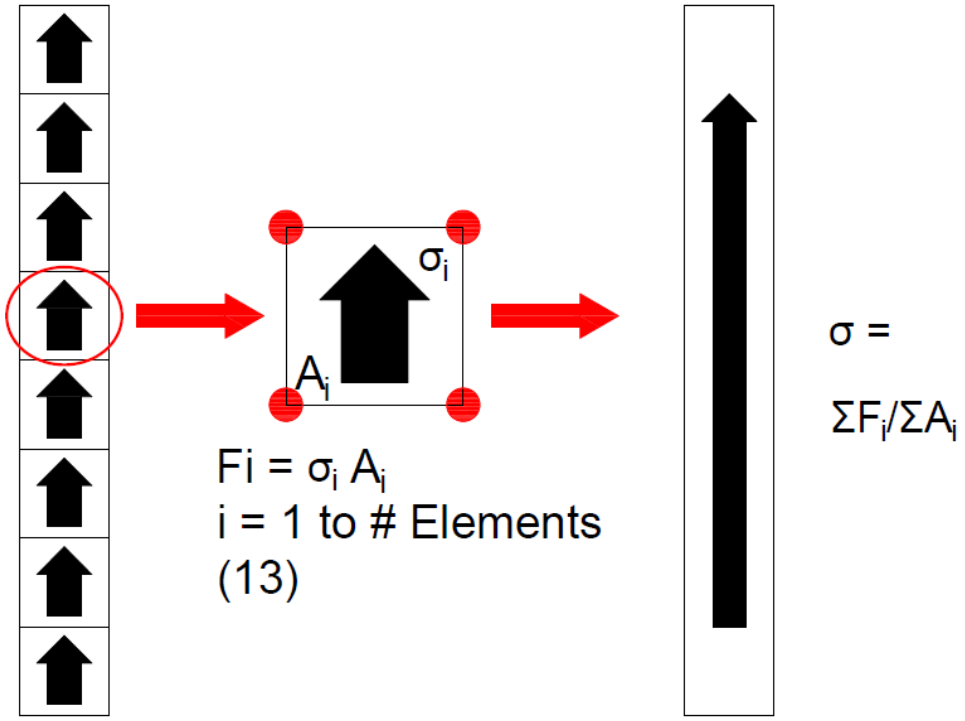

Figure B-4: Procedure to Calculate Total Stress on a Column of Elements

Appendix C

Code Reduction Factor Comparisons for Additional c_{min}/d Ratios

In this appendix, punching shear reduction factors from ACI 318M-14, Model Code 1978 and Model Code 2010 for additional c_{min}/d ratios not included in Section 5.1.1 are provided. In Section 5.1.1, the reduction factors for c_{min}/d ratios of 0.6, 1.3, 2 and 3 were provided. In this appendix, the reduction factors for c_{min}/d ratios of 0.8, 1.0, 1.5, 1.8 and 4 are provided. These additional c_{min}/d ratios were considered in the discussion included in Section 5.1.1.

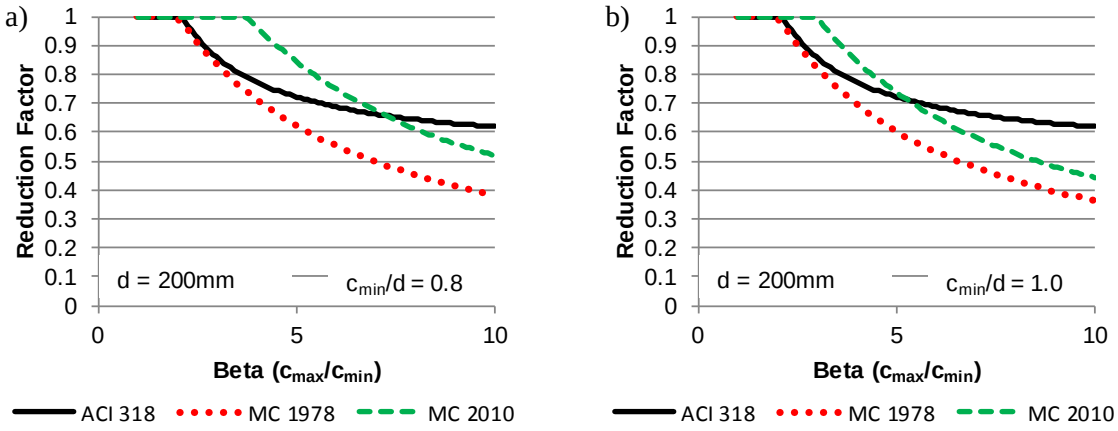

Figure C-1: Reduction Factors for ACI 318M-14, Model Code 1978 and Model Code 2010, Left: c_{min}/d = 0.8, Right c_{min}/d = 1.0, d = 200mm

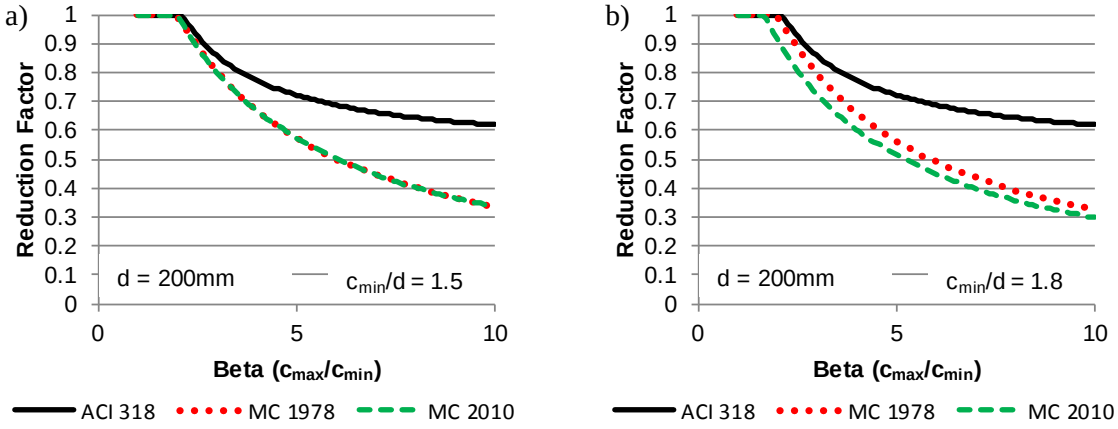

Figure C-2: Reduction Factors for ACI 318M-14, Model Code 1978 and Model Code 2010, Left: c_{min}/d = 1.5, Right c_{min}/d = 1.8, d = 200mm

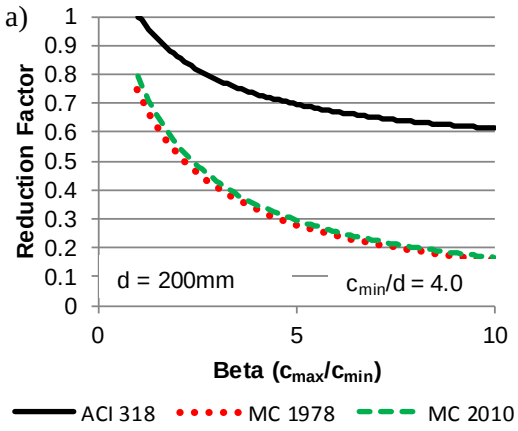

Figure C-3: Reduction Factors for ACI 318M-14, Model Code 1978 and Model Code 2010, c_{min}/d = 4.0, d = 200mm

Appendix D
Summary of Models Included in Parametric Study

In this appendix, a summary of the 77 models in the parametric study is provided. The full column dimensions, column aspect ratios and column dimensions in each quarter model are summarized in the following table for each of the eight c_{min}/d ratios. All other parameters are constant for each model and are summarized in Section 5.1.2.

Final Parametric Matrix					
c_{min}/d	c_{min}	c_{max}	β	$c_{min}/2$	$c_{max}/2$
	120	120	1	60	60
	120	200	1.667	60	100
	120	240	2	60	120
	120	320	2.667	60	160
	120	360	3	60	180
	120	440	3.667	60	220
	120	480	4	60	240
	120	560	4.667	60	280
	120	600	5	60	300
0.594	120	680	5.667	60	340
	120	720	6	60	360
	120	800	6.667	60	400
	120	840	7	60	420
	120	920	7.667	60	460
	120	960	8	60	480
	120	1040	8.667	60	520
	120	1080	9	60	540
	120	1160	9.667	60	580
	120	1200	10	60	600
	160	160	1	80	80
	160	240	1.5	80	120
	160	320	2	80	160
	160	400	2.5	80	200
	160	480	3	80	240
	160	560	3.5	80	280
	160	640	4	80	320
0.792	160	720	4.5	80	360
	160	800	5	80	400
	160	880	5.5	80	440
	160	960	6	80	480
	160	1040	6.5	80	520
	160	1120	7	80	560
	160	1200	7.5	80	600
	160	1280	8	80	640

c_{min}/d	c_{min}	c_{max}	β	$c_{min}/2$	$c_{max}/2$
0.990	200	200	1	100	100
	200	320	1.6	100	160
	200	400	2	100	200
	200	520	2.6	100	260
	200	600	3	100	300
	200	720	3.6	100	360
	200	800	4	100	400
	200	920	4.6	100	460
	200	1000	5	100	500
	200	1120	5.6	100	560
	200	1200	6	100	600
	200	1320	6.6	100	660
1.287	260	260	1.0	130	130
	260	390	1.5	130	195
	260	520	2.0	130	260
	260	640	2.462	130	320
	260	780	3.0	130	390
	260	920	3.538	130	460
	260	1040	4.0	130	520
	260	1160	4.462	130	580
	260	1320	5.077	130	660
1.485	300	300	1.0	150	150
	300	450	1.5	150	225
	300	600	2.0	150	300
	300	760	2.533	150	380
	300	920	3.067	150	460
	300	1040	3.467	150	520
	300	1200	4.00	150	600
1.782	360	360	1.000	180	180
	360	540	1.500	180	270
	360	720	2.000	180	360
	360	920	2.556	180	460
	360	1080	3.000	180	540
	360	1280	3.556	180	640

c_{min}/d	c_{min}	c_{max}	β	$c_{min}/2$	$c_{max}/2$
1.980	400	400	1.000	200	200
	400	600	1.500	200	300
	400	800	2.000	200	400
	400	1000	2.500	200	500
	400	1200	3.000	200	600
2.970	600	600	1.000	300	300
	600	920	1.533	300	460
	600	1200	2.000	300	600

Appendix E
Additional Load-Displacement Plots and Code Comparison Bar Charts

In this appendix, additional load-displacement plots and bar charts of shear capacity vs rectangularity not included in Section 5.2 are provided. These additional figures are for c_{min}/d ratios of 0.594, 0.792 and 0.990 and were not included in the main document for clarity. These additional load-displacement responses and shear capacity predictions were considered in the trends discussed in Section 5.2.

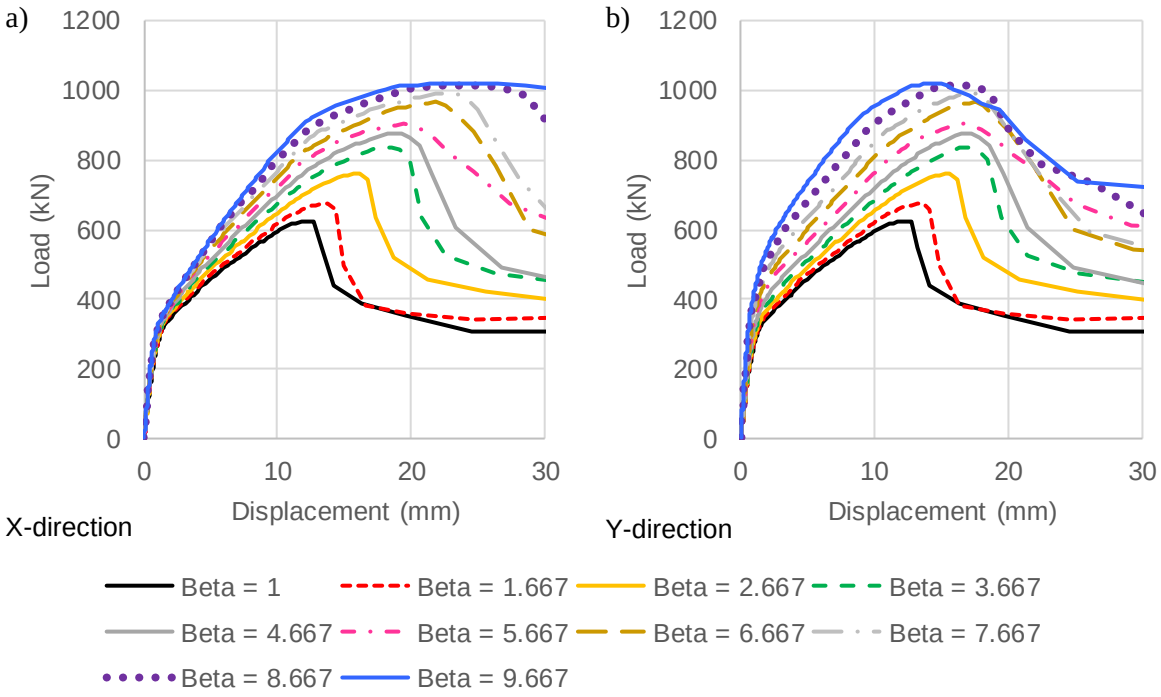

Figure E-1: Additional Load-Deflection Plots for $c_{min}/d = 0.594$, Non-integer β values

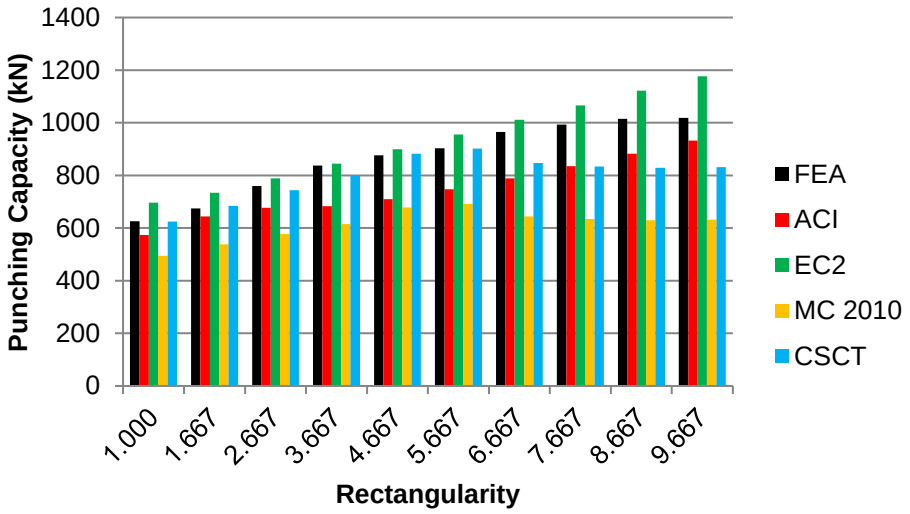

Figure E-2: Capacity Predicted by FEA and Various Design Codes, $c_{min}/d = 0.594$, Non-integer β values

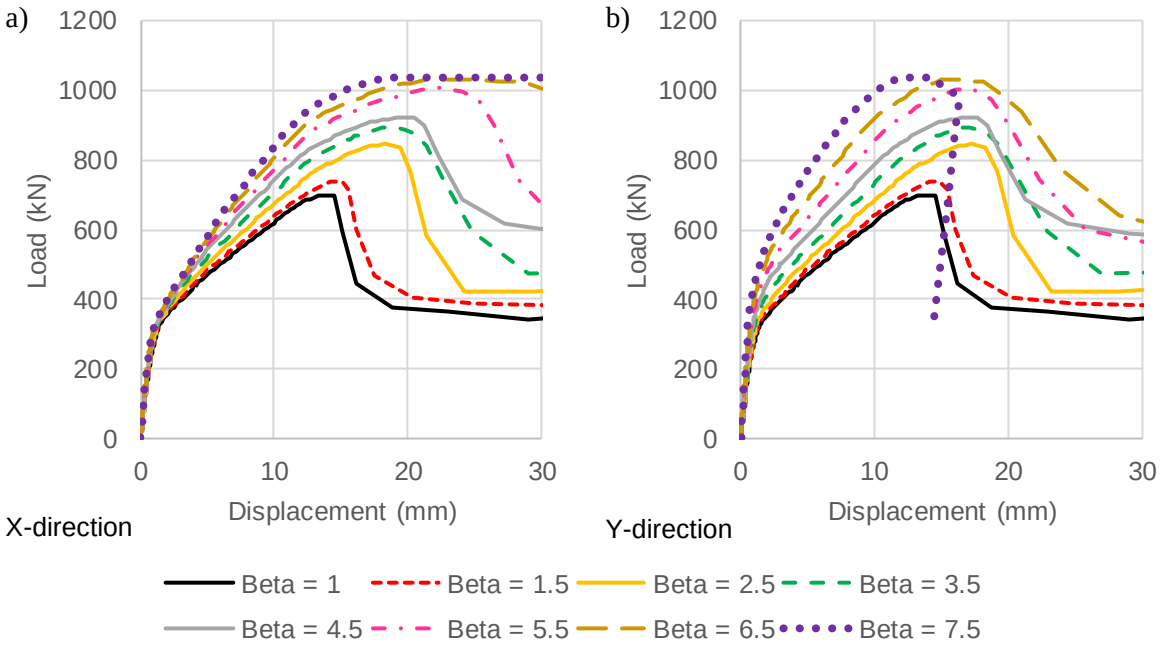

Figure E-3: Additional Load-Deflection Plots for c_{min}/d = 0.792, Non-integer β values

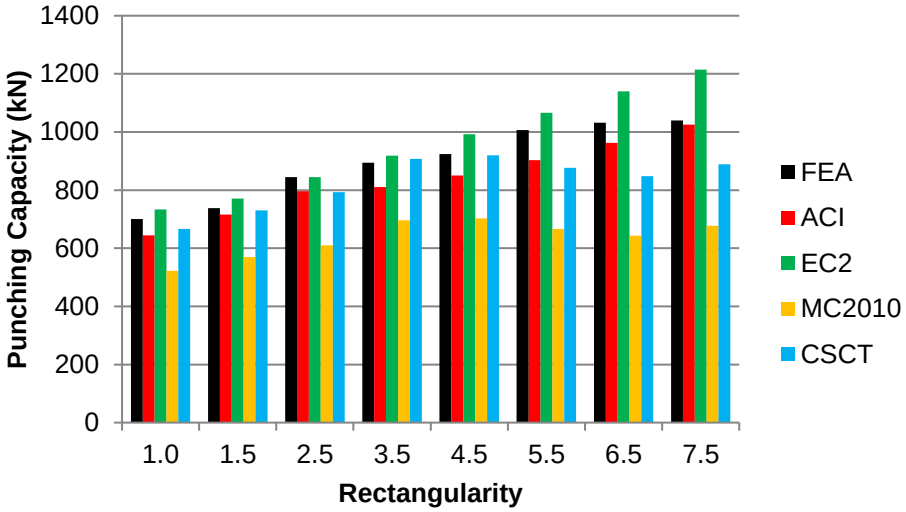

Figure E-4: Capacity Predicted by FEA and Various Design Codes, c_{min}/d = 0.792, Non-integer β values

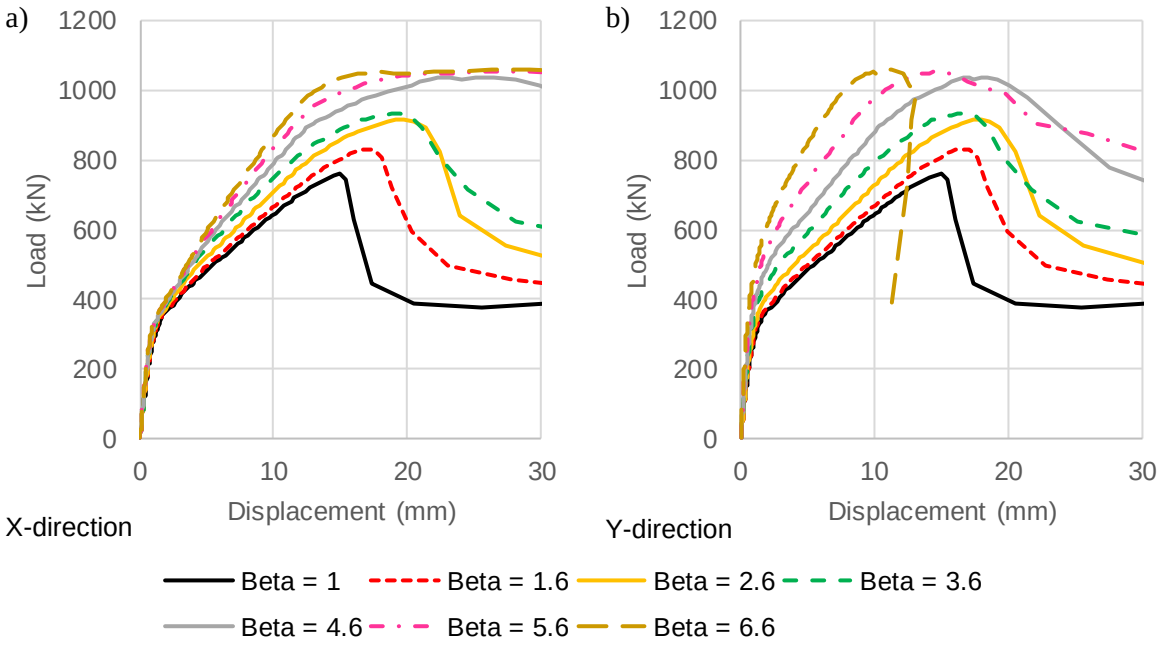

Figure E-5: Additional Load-Deflection Plots for c_{min}/d = 0.990, Non-integer β values

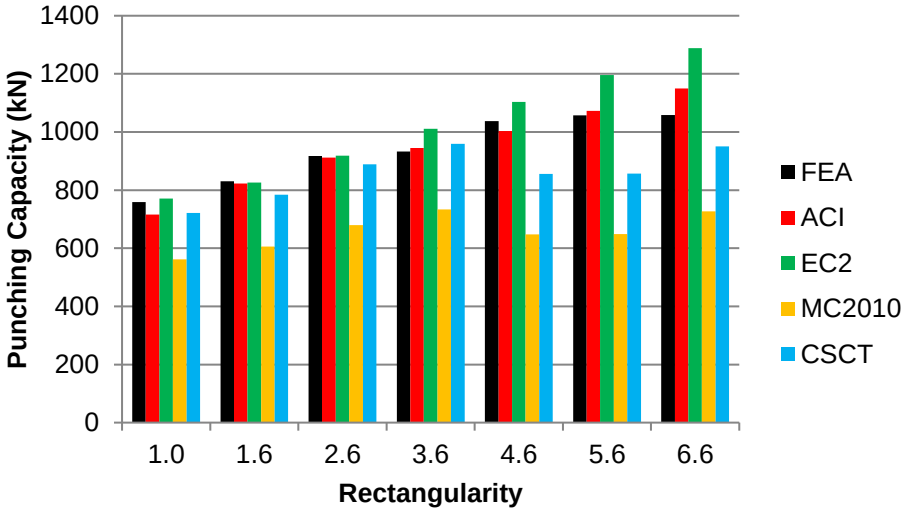

Figure E-6: Capacity Predicted by FEA and Various Design Codes, c_{min}/d = 0.990, Non-integer β values

Appendix F

Predicted Crack Patterns – Parametric Study Models

The predicted crack patterns for each investigated c_{min}/d ratio are provided in this appendix in order of increasing column rectangularity. The crack patterns on the tension surface of the slab, and the sides of the quarter model along the long and short sides of the steel support plate are provided.

The crack patterns are visualized in ABAQUS through the contour plots of the maximum principal plastic strain. In most of the provided contour plots, the maximum plastic strain magnitude has been set to a value of 0.05. This maximum limit was set so that the contour lines shown in each crack pattern represent the same magnitude. Any portions of the slab predicted to have a higher maximum principal plastic strain are shown in grey. The steel support and load plates are white as the material definition of these parts was linear elastic, and as such, no plastic strain is possible. In a few of the models with low c_{min}/d ratios, the maximum principal plastic strain magnitude predicted by ABAQUS was much lower than 0.05. In these contour plots the maximum plastic strain was set to the default value chosen by ABAQUS. These contour plots are labelled as using the default contour limits for clarity.

$c_{min}/d = 0.594$

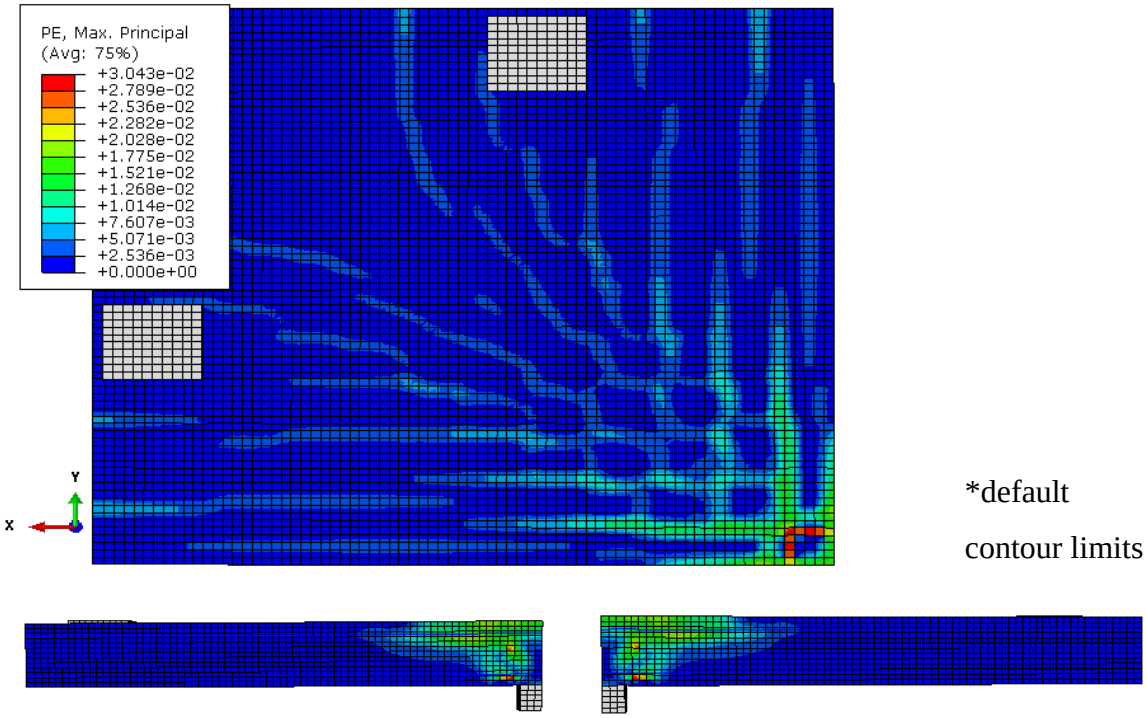

Figure F-1: β = 1 Crack Pattern, Bottom Left: Long Side, Bottom Right: Short Side

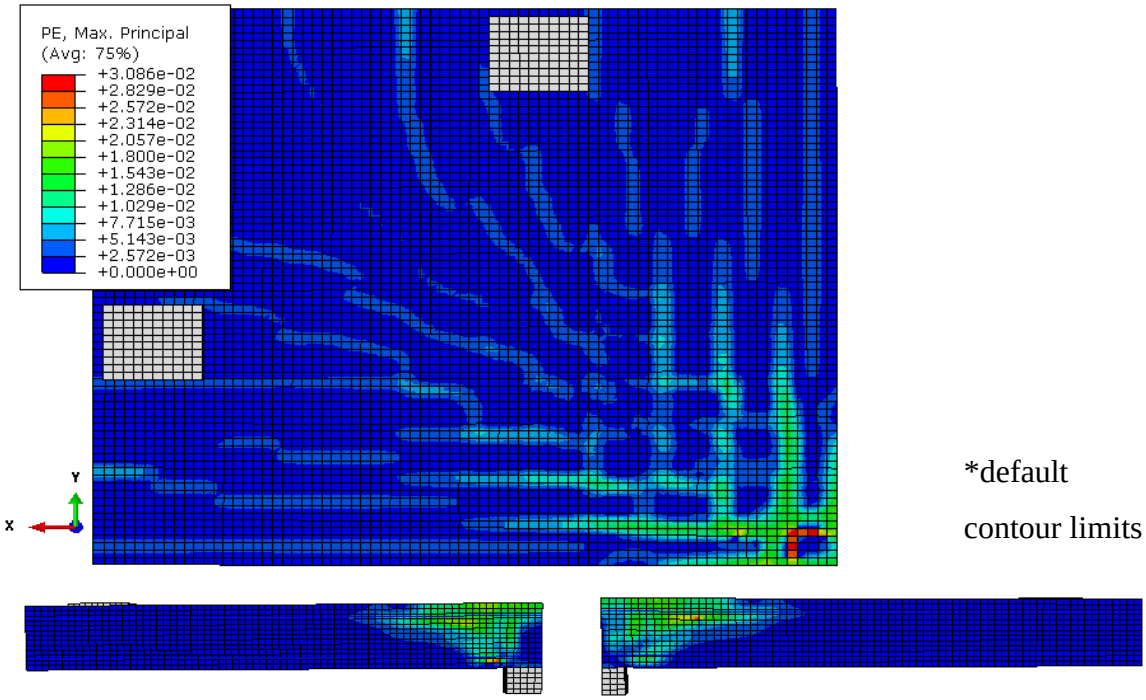

Figure F-2: β = 1.667 Crack Pattern, Bottom Left: Long Side, Bottom Right: Short Side

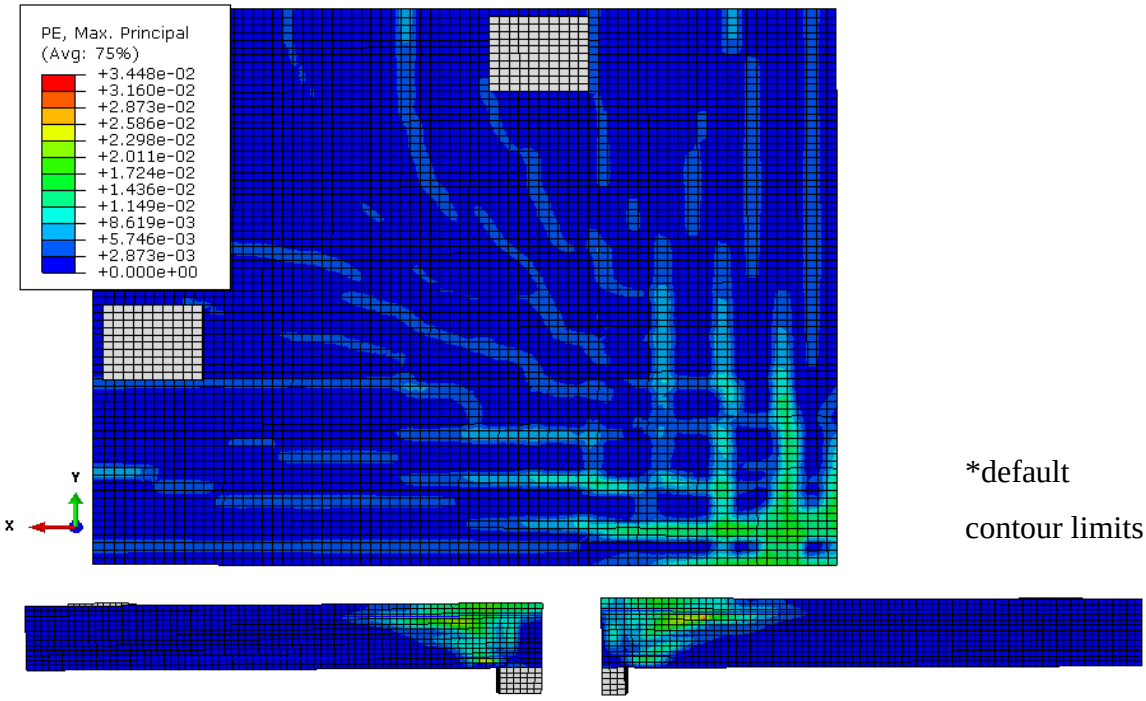

Figure F-3: β = 2 Crack Pattern, Bottom Left: Long Side, Bottom Right: Short Side

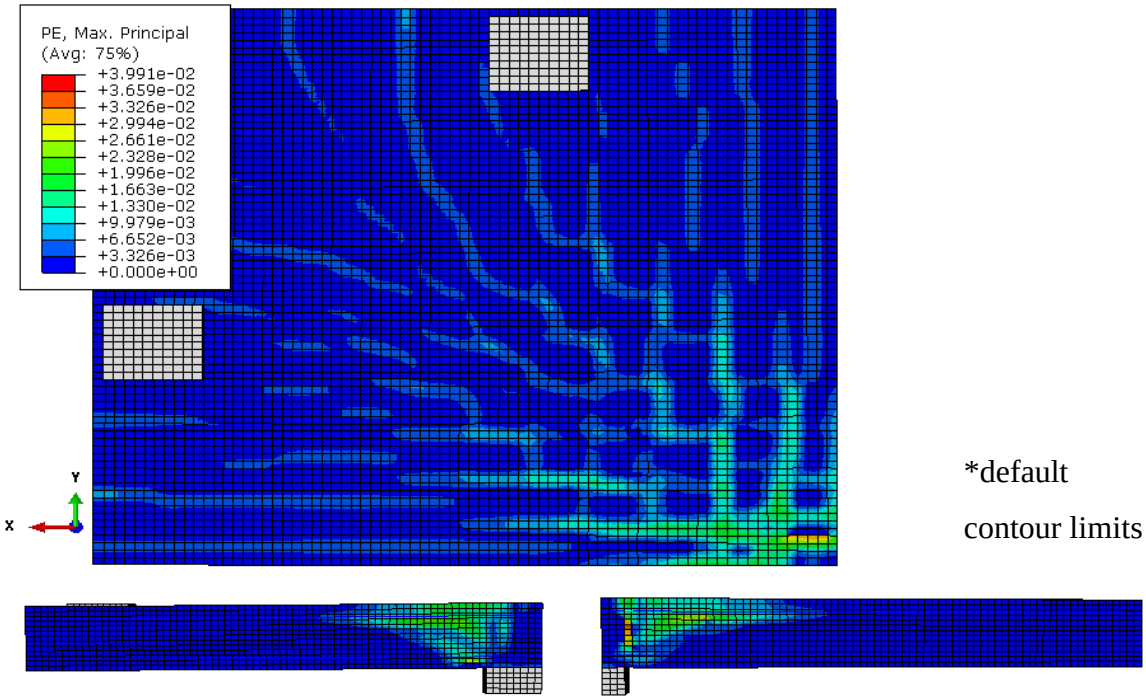

*default contour limits

Figure F-4: β = 2.667 Crack Pattern, Bottom Left: Long Side, Bottom Right: Short Side

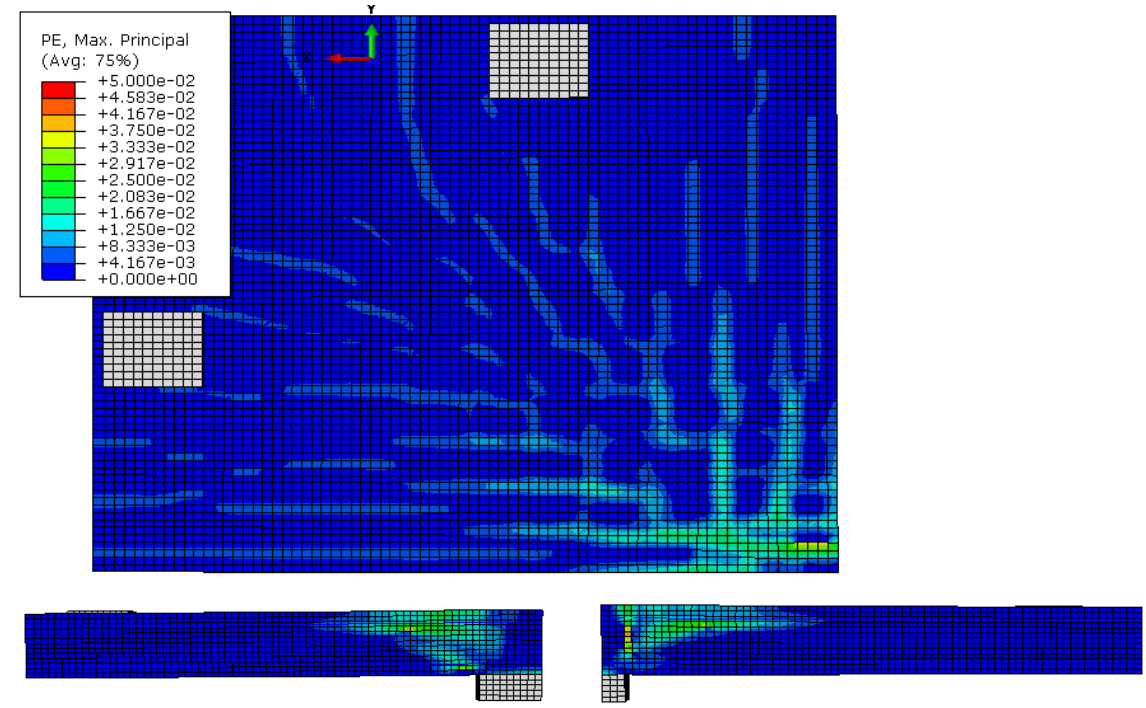

Figure F-5: β = 3 Crack Pattern, Bottom Left: Long Side, Bottom Right: Short Side

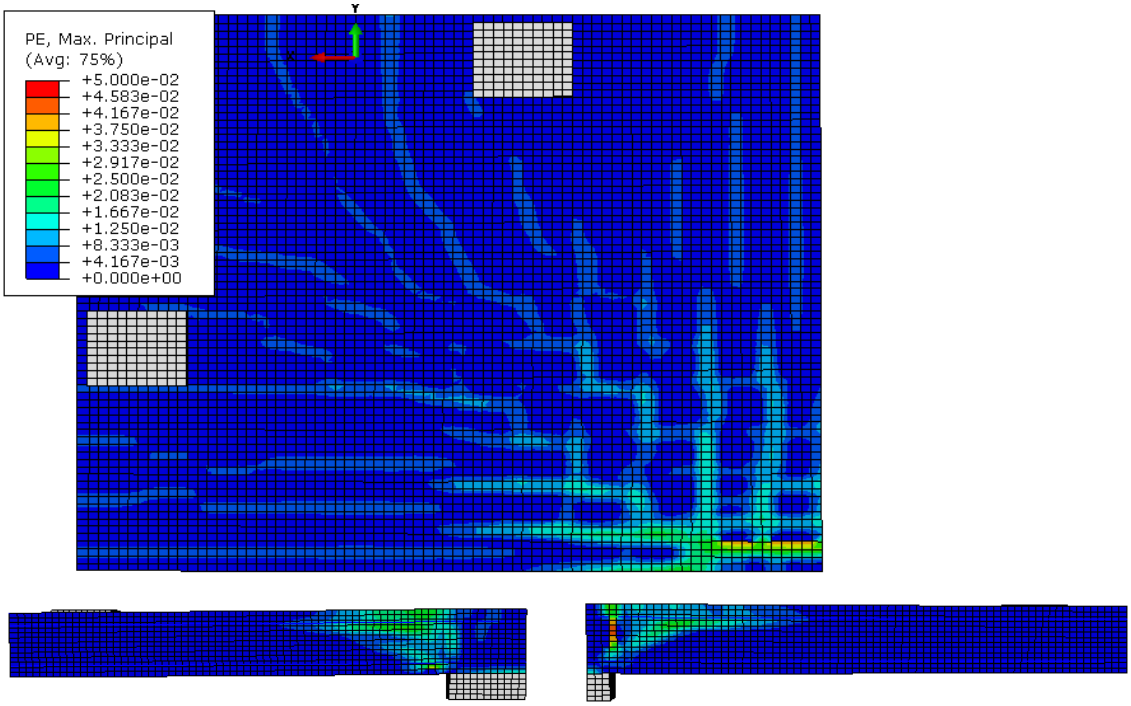

Figure F-6: β = 3.667 Crack Pattern, Bottom Left: Long Side, Bottom Right: Short Side

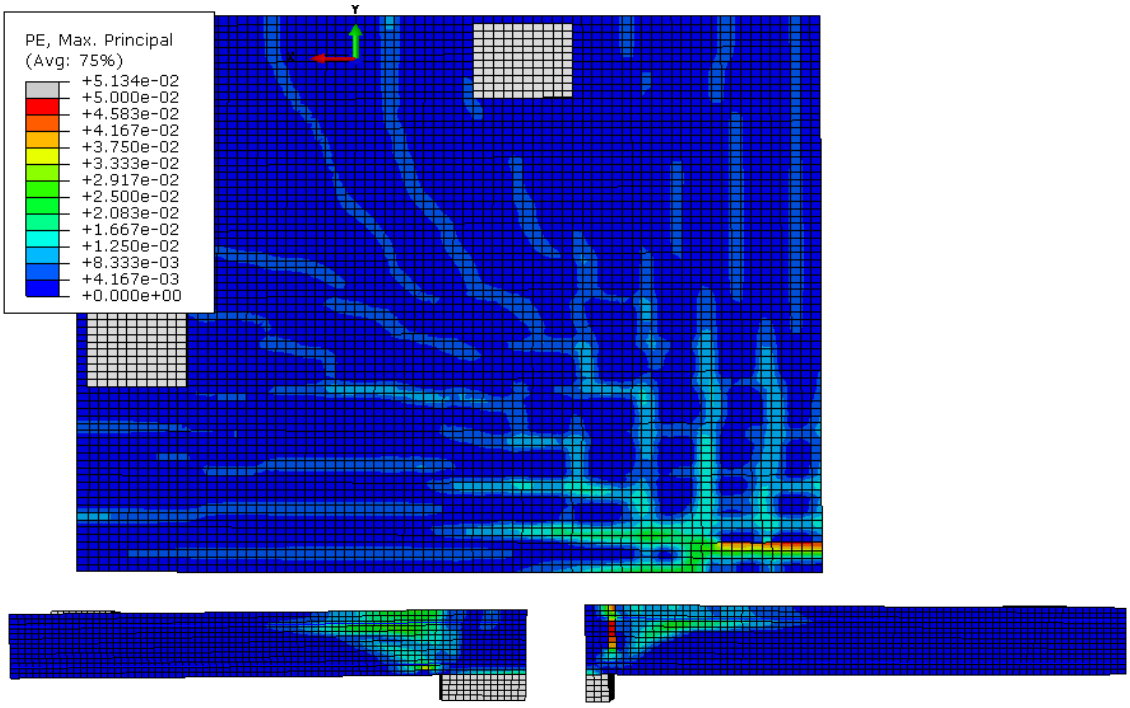

Figure F-7: β = 4 Crack Pattern, Bottom Left: Long Side, Bottom Right: Short Side

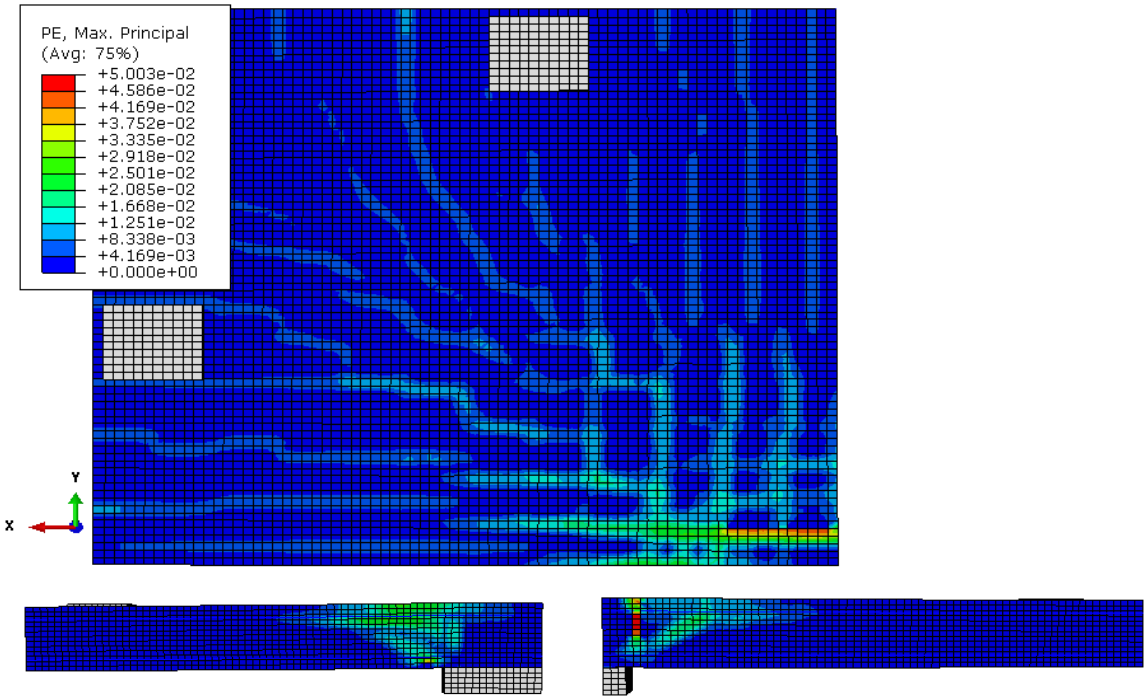

Figure F-8: β = 4.667 Crack Pattern, Bottom Left: Long Side, Bottom Right: Short Side

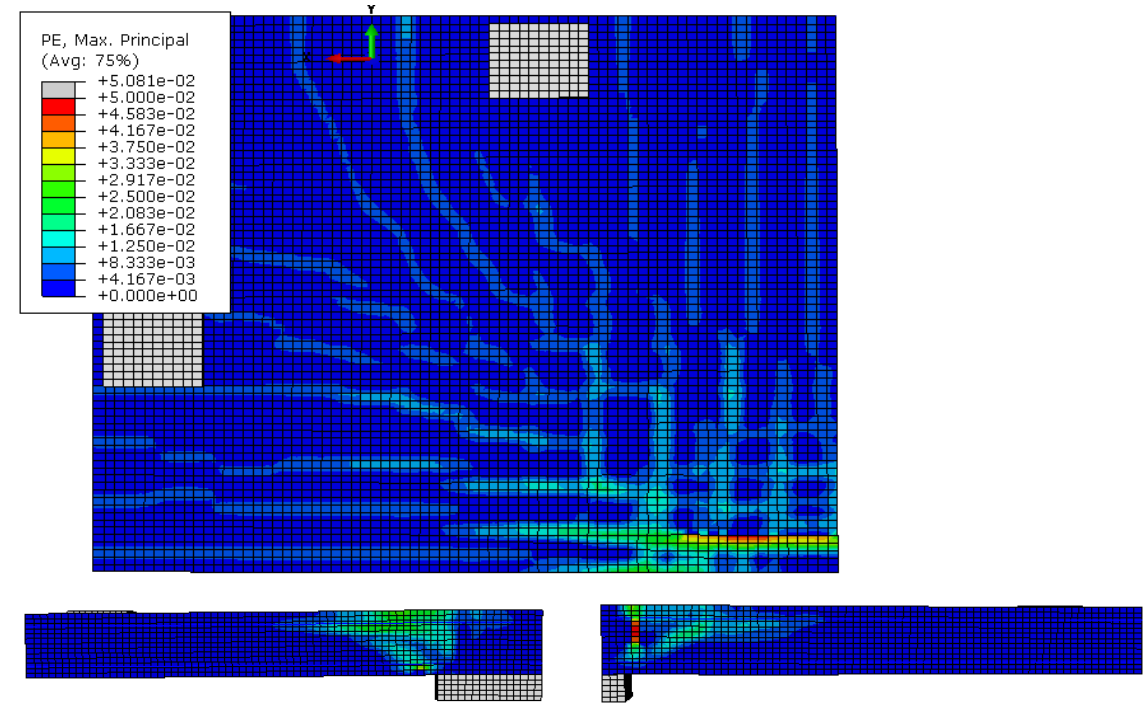

Figure F-9: β = 5 Crack Pattern, Bottom Left: Long Side, Bottom Right: Short Side

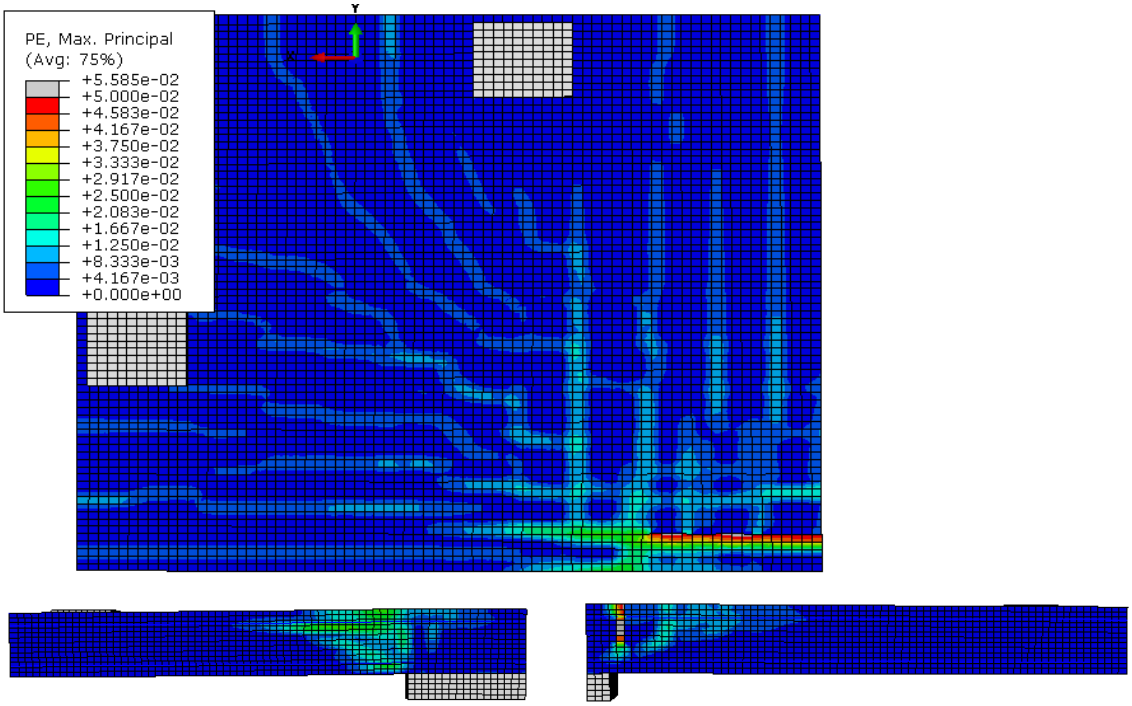

Figure F-10: β = 5.667 Crack Pattern, Bottom Left: Long Side, Bottom Right: Short Side

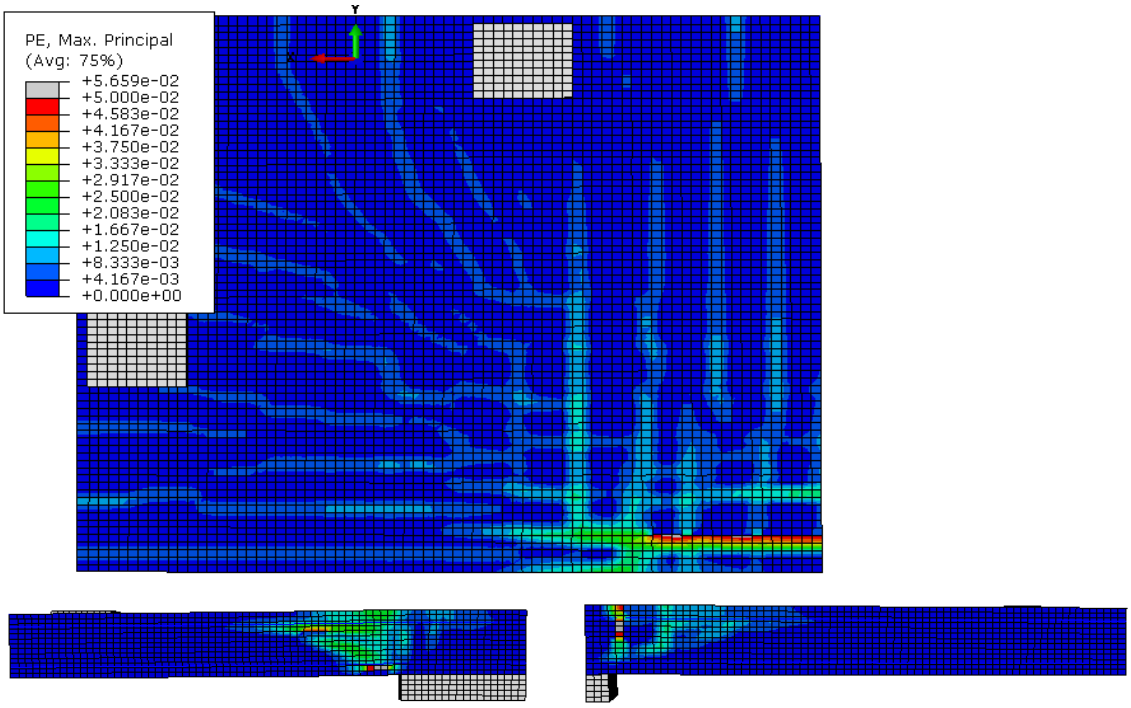

Figure F-11: β = 6 Crack Pattern, Bottom Left: Long Side, Bottom Right: Short Side

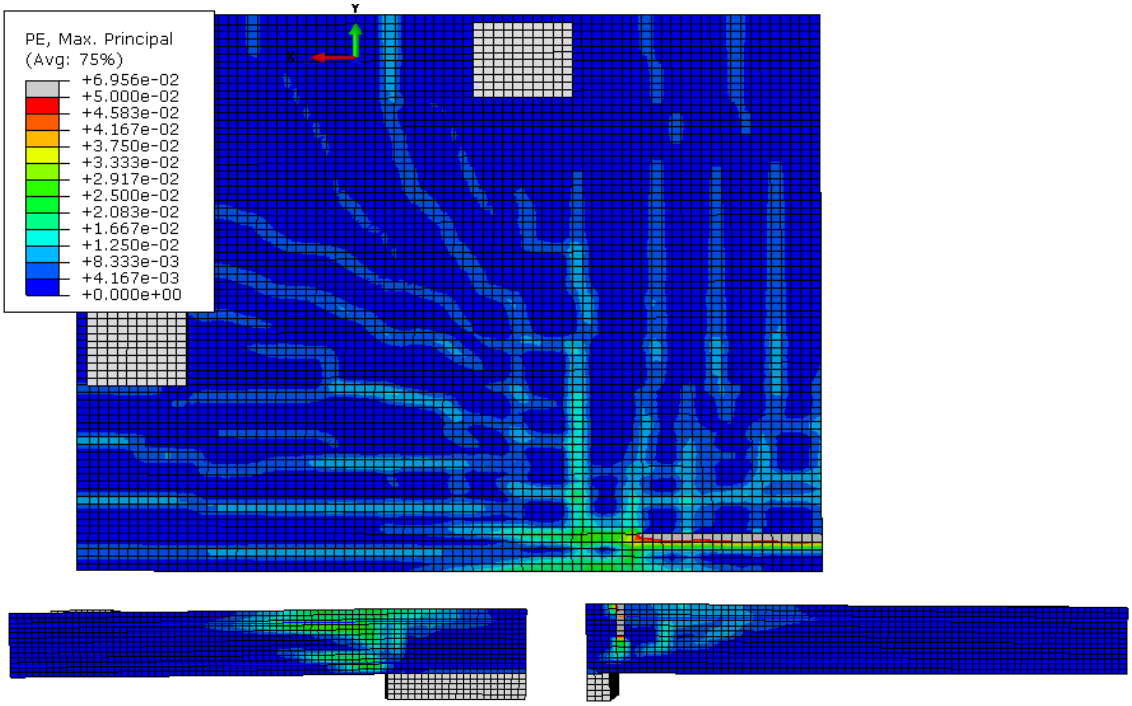

Figure F-12: β = 6.667 Crack Pattern, Bottom Left: Long Side, Bottom Right: Short Side

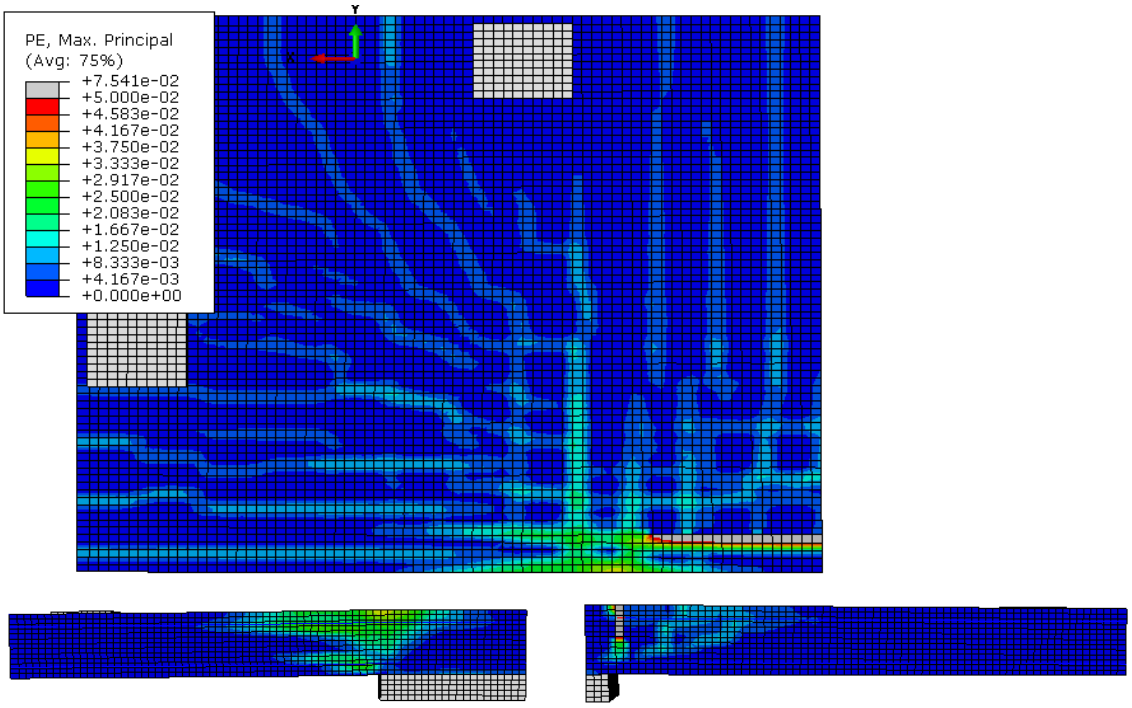

Figure F-13: β = 7 Crack Pattern, Bottom Left: Long Side, Bottom Right: Short Side

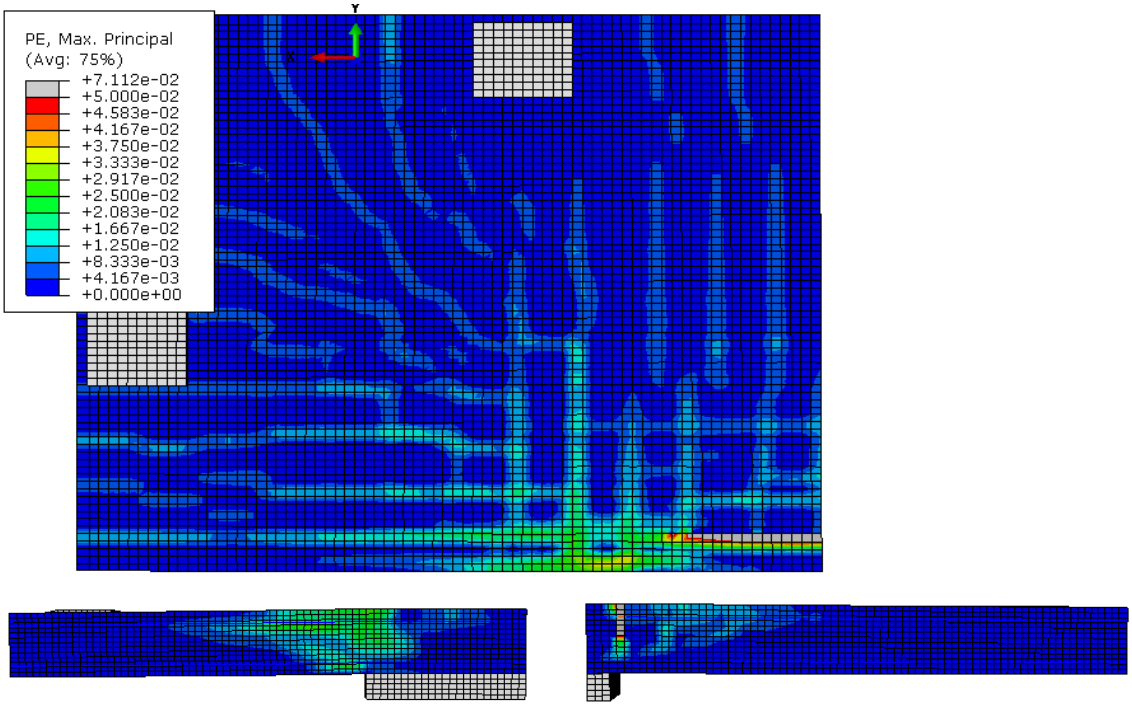

Figure F-14: β = 7.667 Crack Pattern, Bottom Left: Long Side, Bottom Right: Short Side

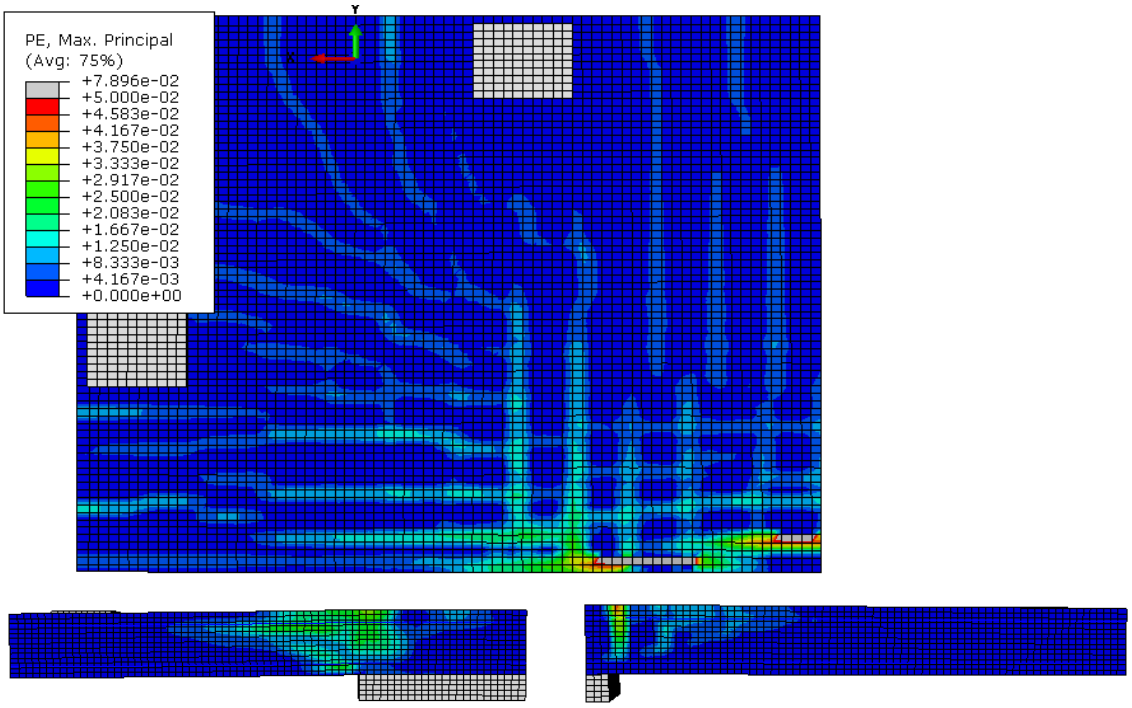

Figure F-15: β = 8 Crack Pattern, Bottom Left: Long Side, Bottom Right: Short Side

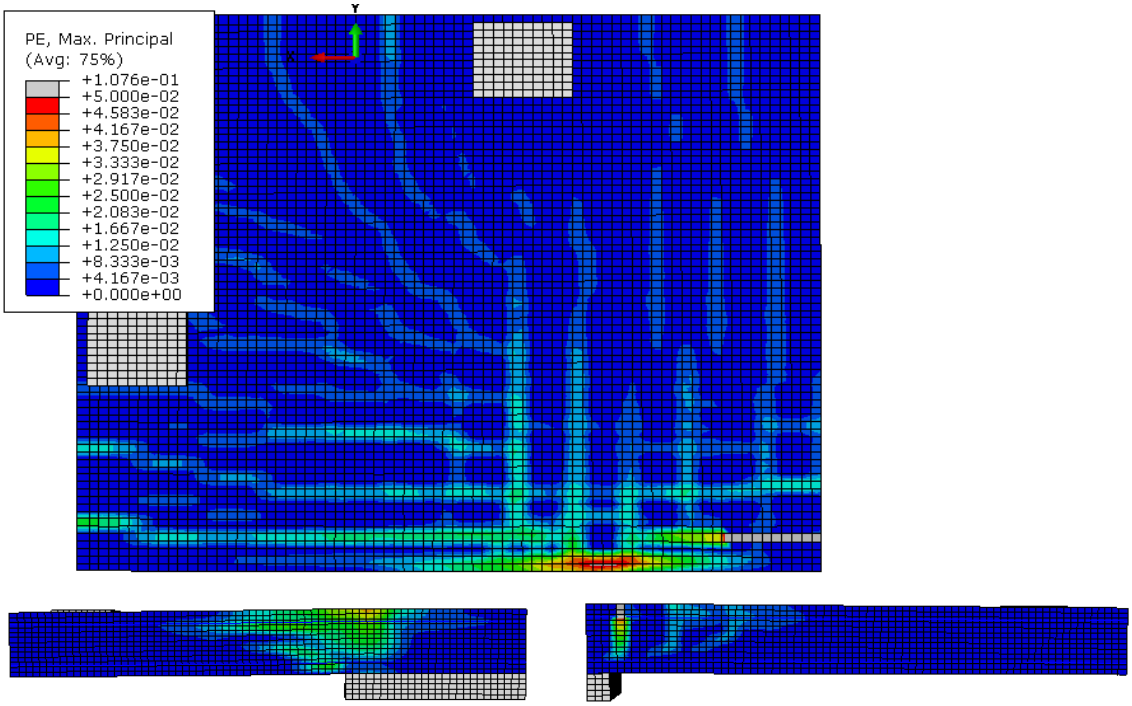

Figure F-16: β = 8.667 Crack Pattern, Bottom Left: Long Side, Bottom Right: Short Side

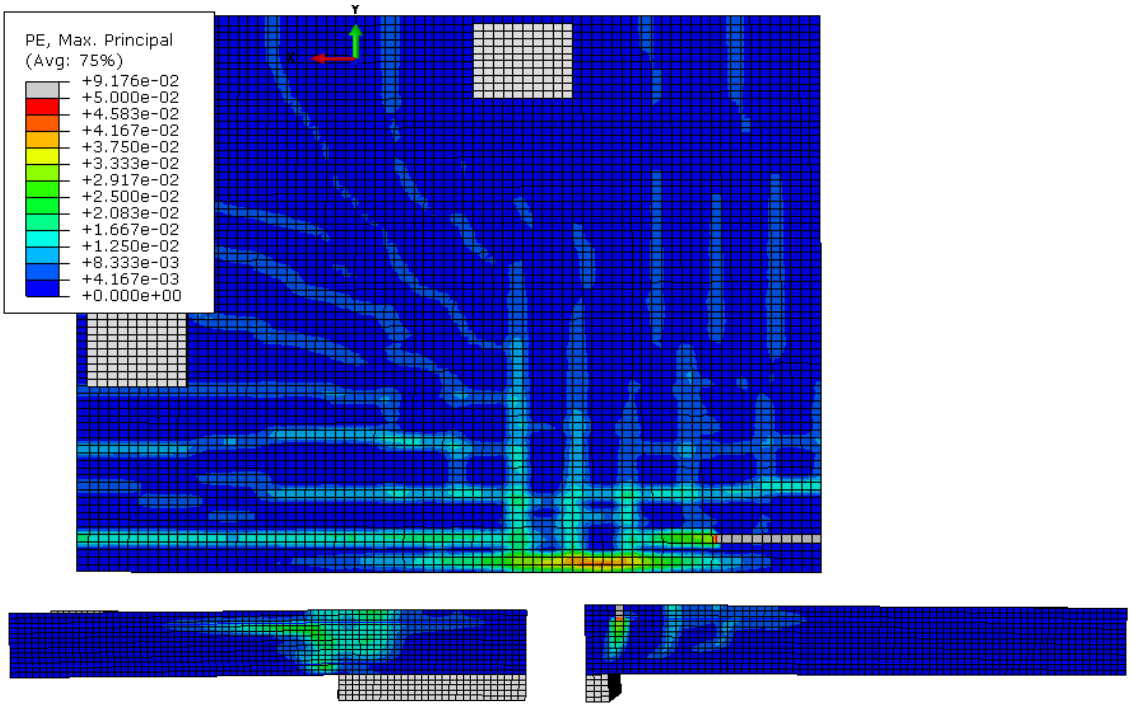

Figure F-17: β = 9 Crack Pattern, Bottom Left: Long Side, Bottom Right: Short Side

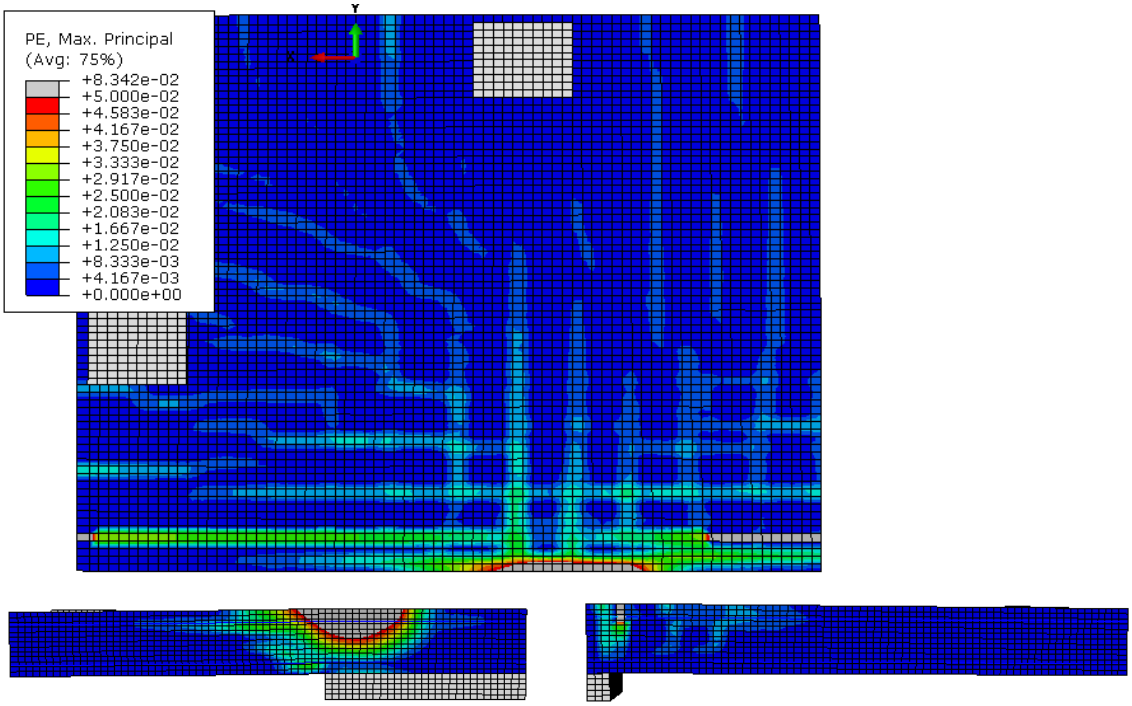

Figure F-18: β = 9.667 Crack Pattern, Bottom Left: Long Side, Bottom Right: Short Side

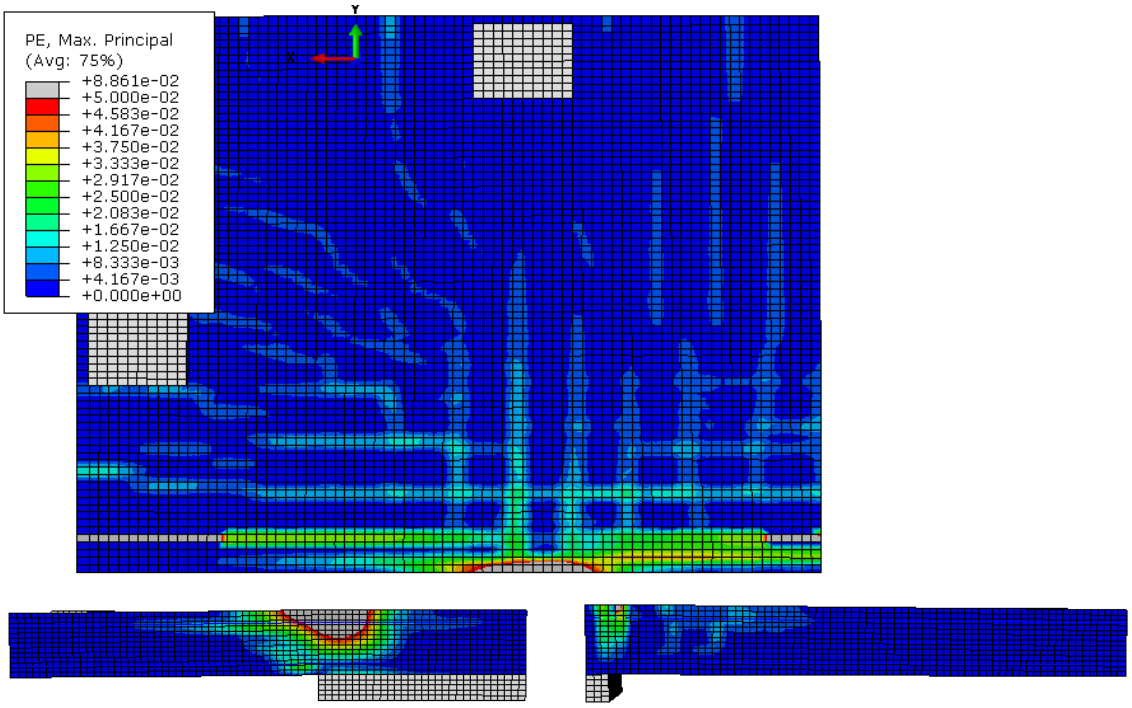

Figure F-19: β = 10 Crack Pattern, Bottom Left: Long Side, Bottom Right: Short Side

$c_{min}/d = 0.792$

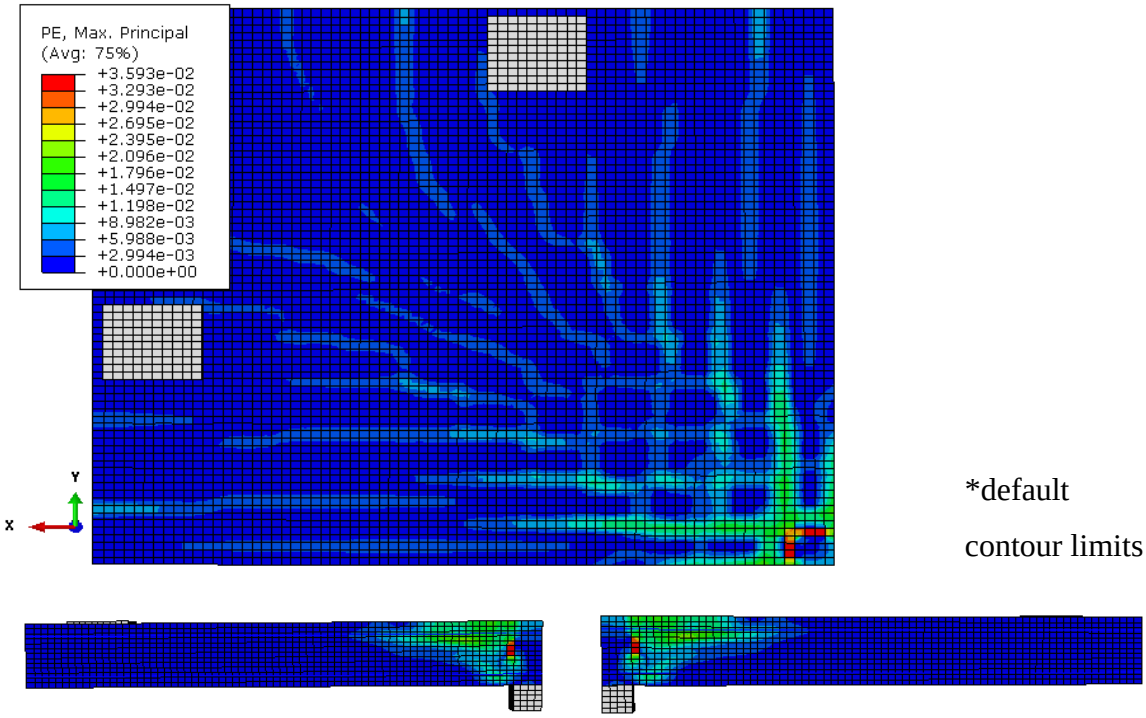

Figure F-20: β = 1 Crack Pattern, Bottom Left: Long Side, Bottom Right: Short Side

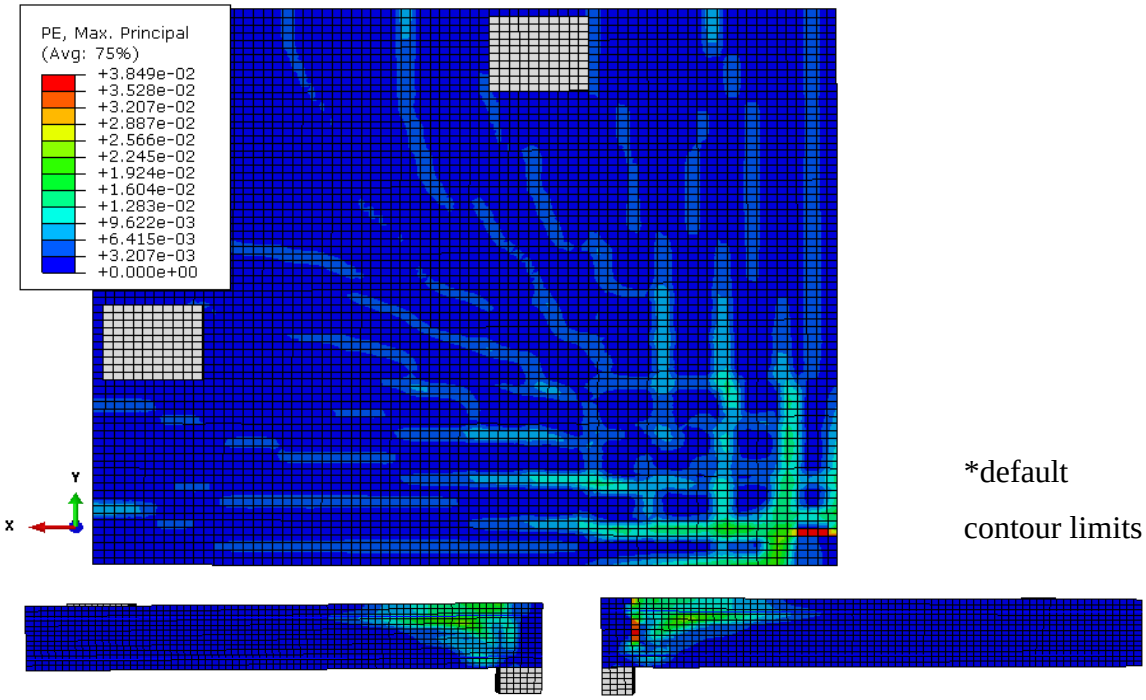

Figure F-21: β = 1.5 Crack Pattern, Bottom Left: Long Side, Bottom Right: Short Side

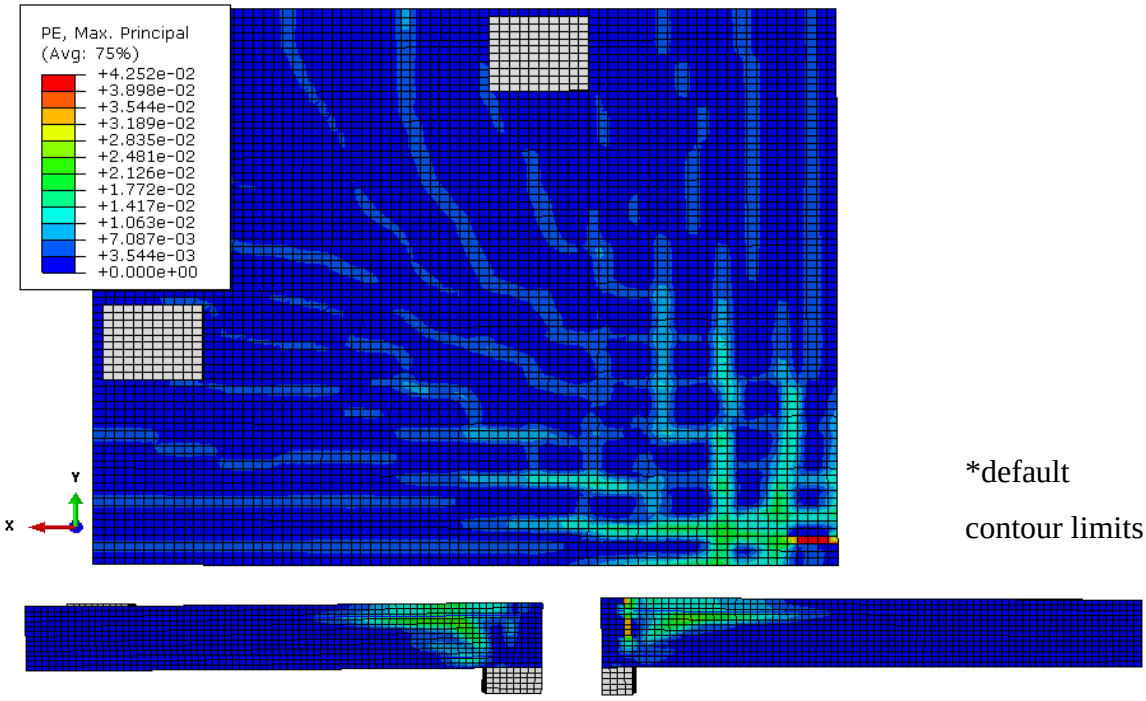

Figure F-22: β = 2 Crack Pattern, Bottom Left: Long Side, Bottom Right: Short Side

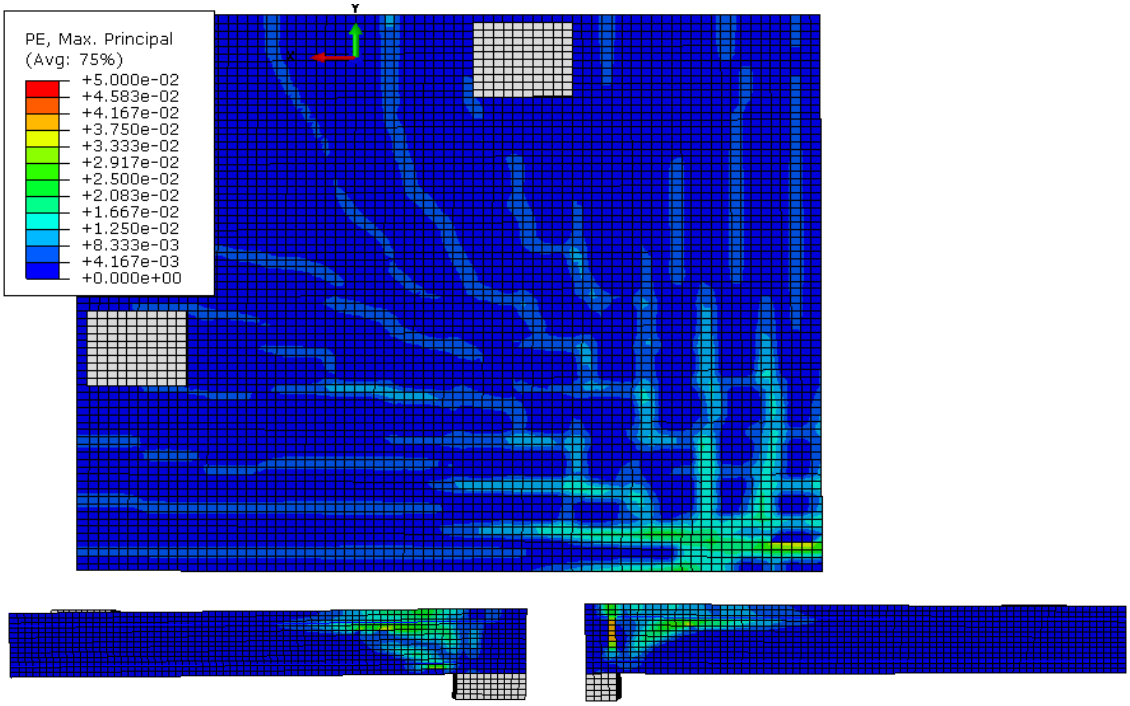

Figure F-23: β = 2.5 Crack Pattern, Bottom Left: Long Side, Bottom Right: Short Side

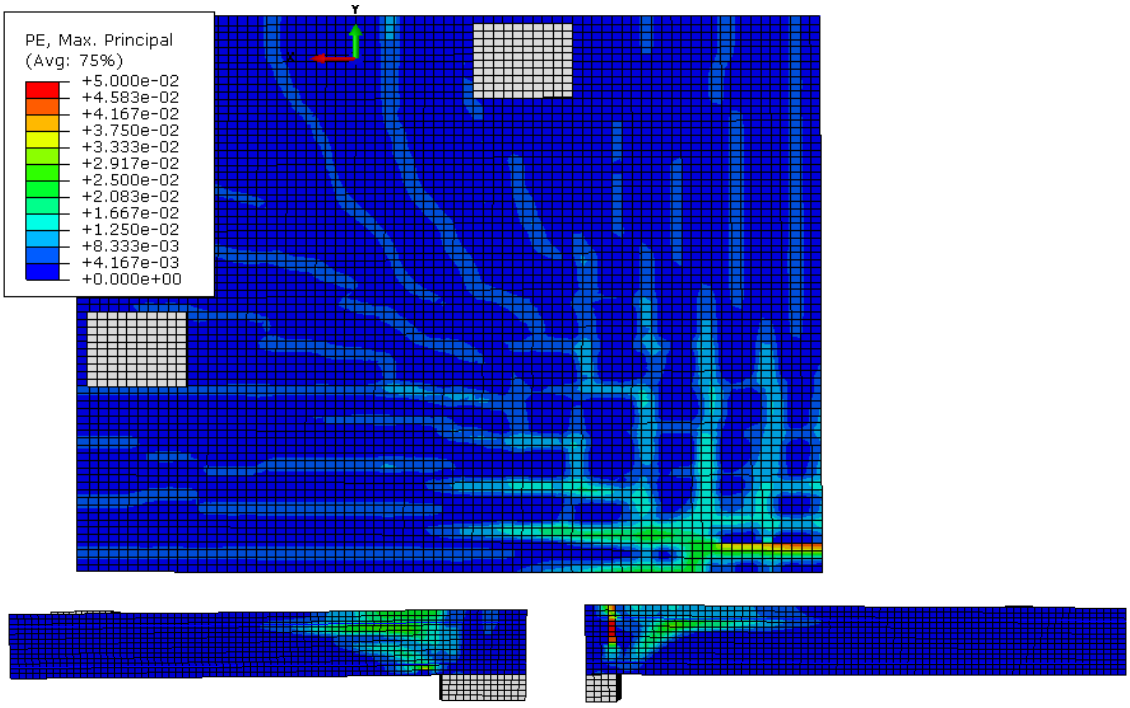

Figure F-24: β = 3 Crack Pattern, Bottom Left: Long Side, Bottom Right: Short Side

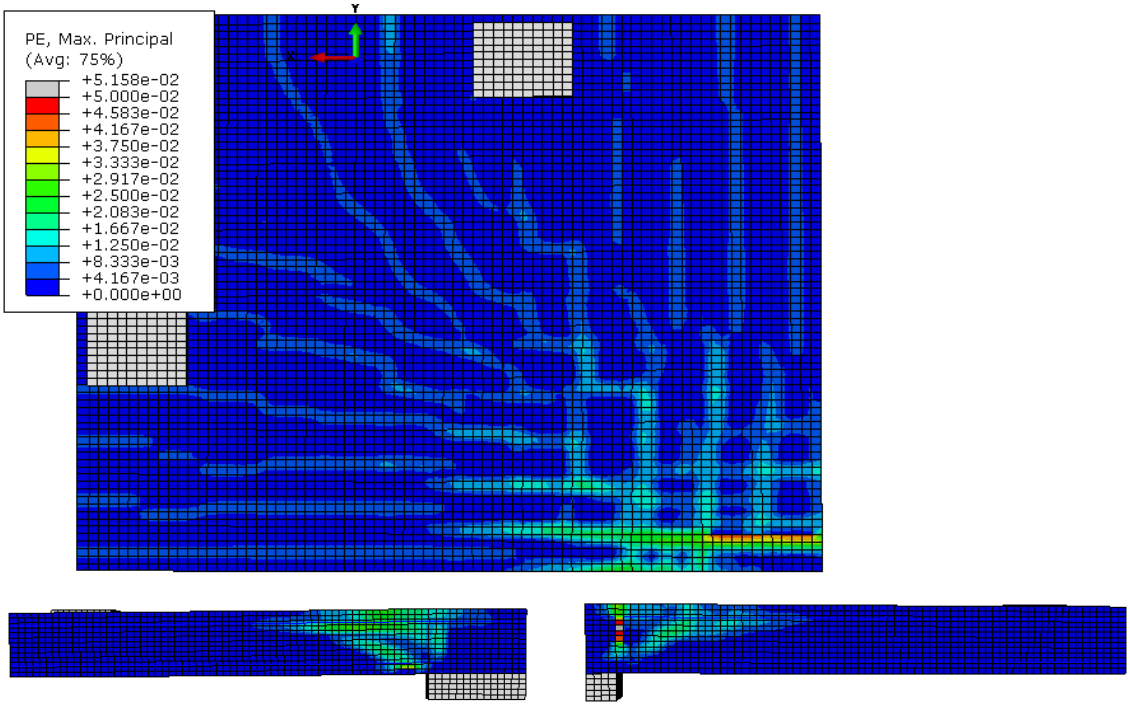

Figure F-25: β = 3.5 Crack Pattern, Bottom Left: Long Side, Bottom Right: Short Side

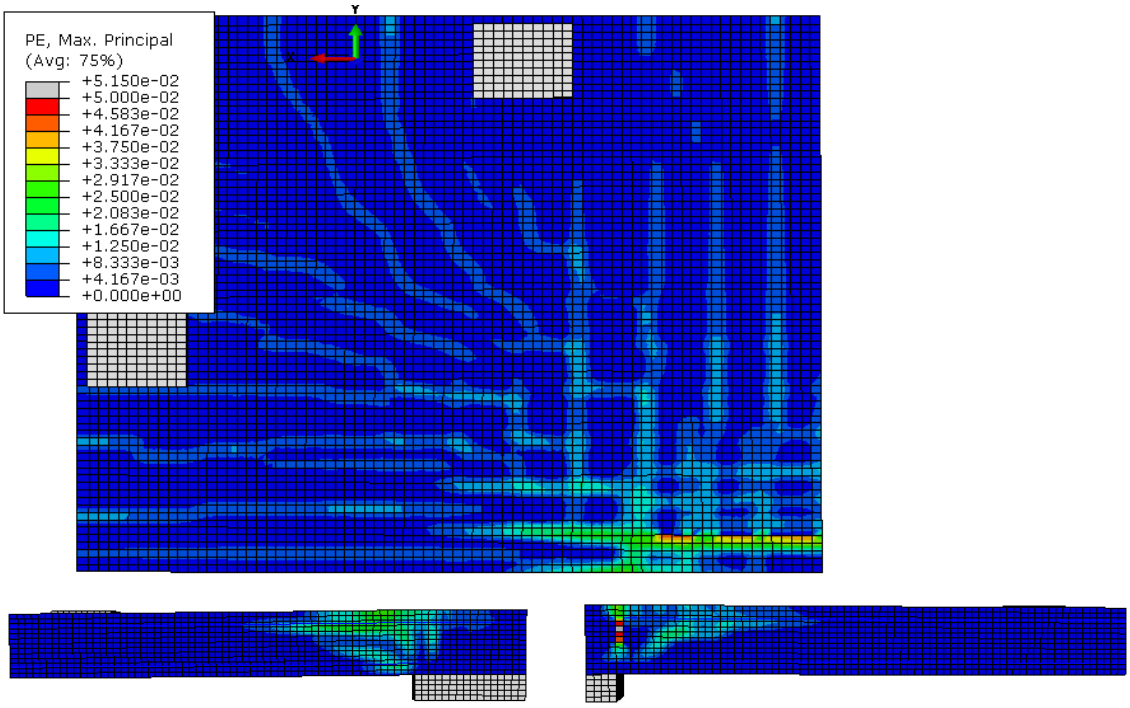

Figure F-26: β = 4 Crack Pattern, Bottom Left: Long Side, Bottom Right: Short Side

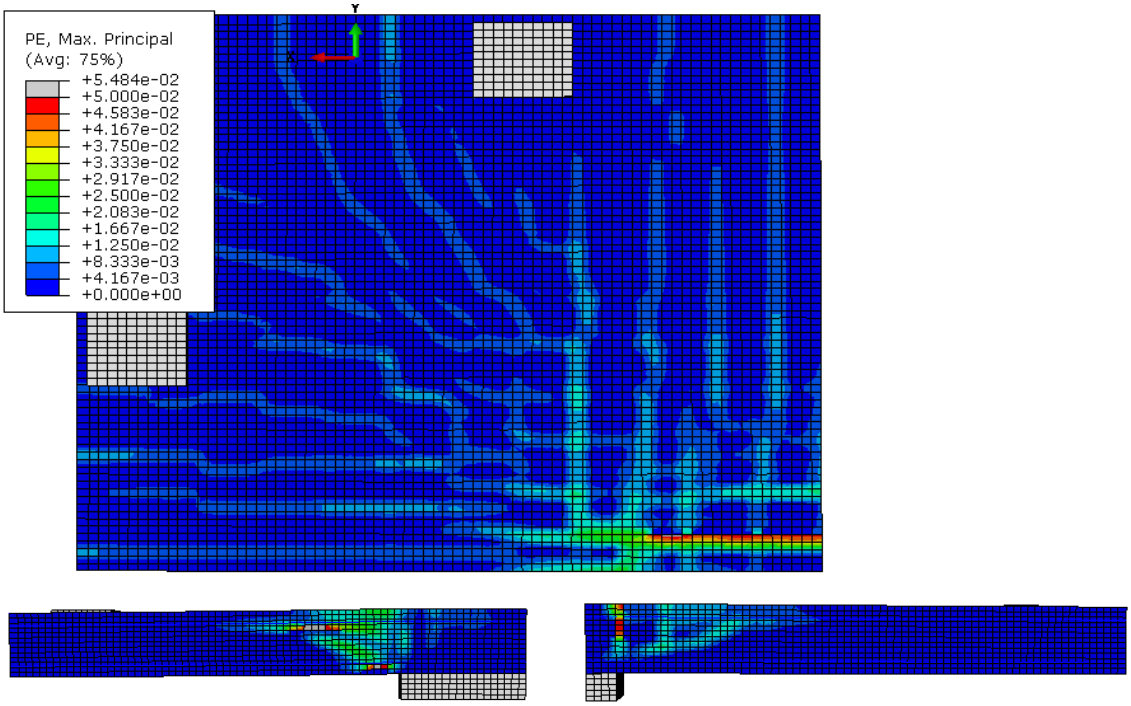

Figure F-27: β = 4.5 Crack Pattern, Bottom Left: Long Side, Bottom Right: Short Side

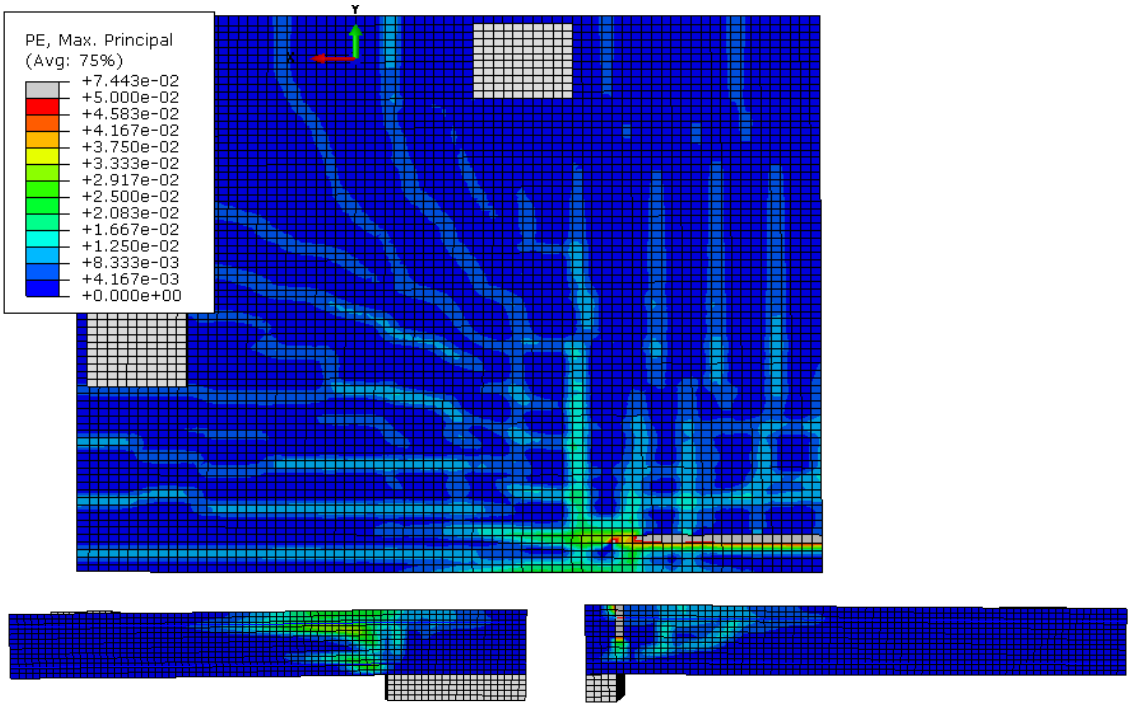

Figure F-28: β = 5 Crack Pattern, Bottom Left: Long Side, Bottom Right: Short Side

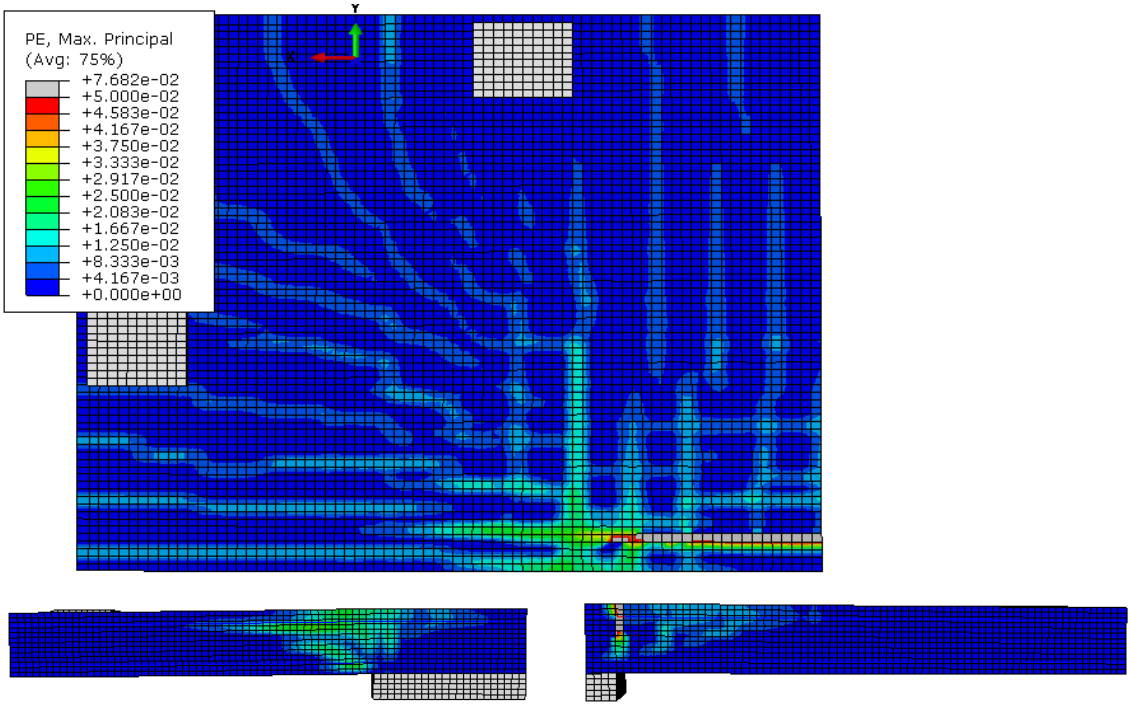

Figure F-29: β = 5.5 Crack Pattern, Bottom Left: Long Side, Bottom Right: Short Side

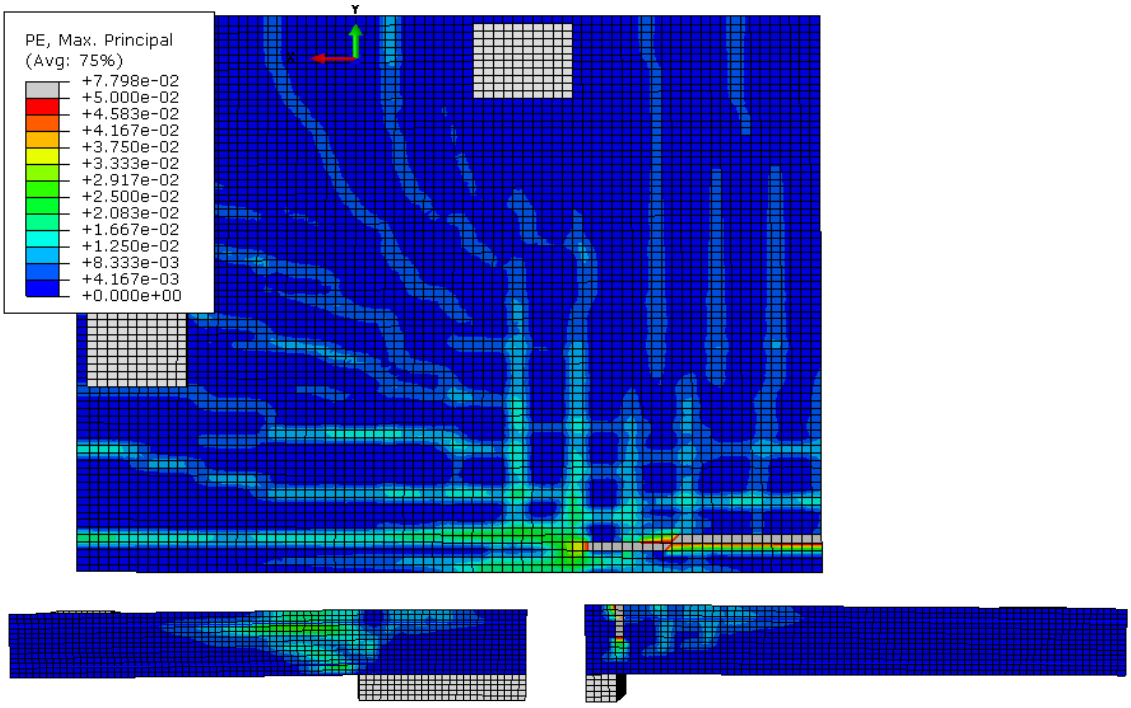

Figure F-30: β = 6 Crack Pattern, Bottom Left: Long Side, Bottom Right: Short Side

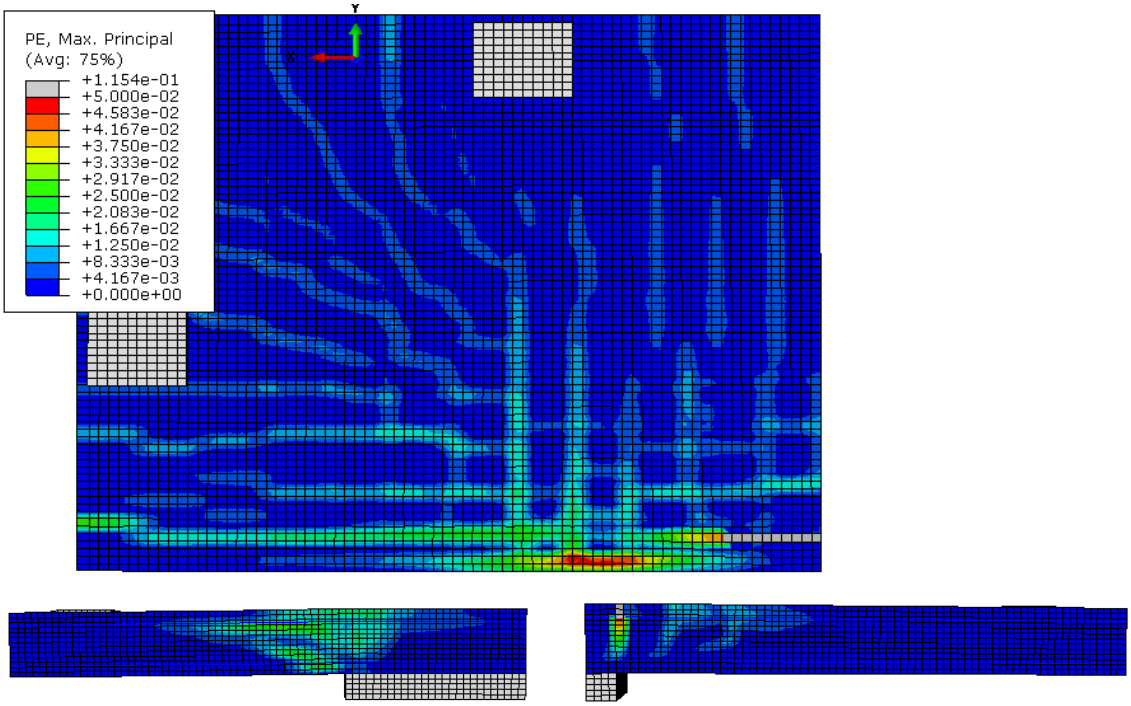

Figure F-31: β = 6.5 Crack Pattern, Bottom Left: Long Side, Bottom Right: Short Side

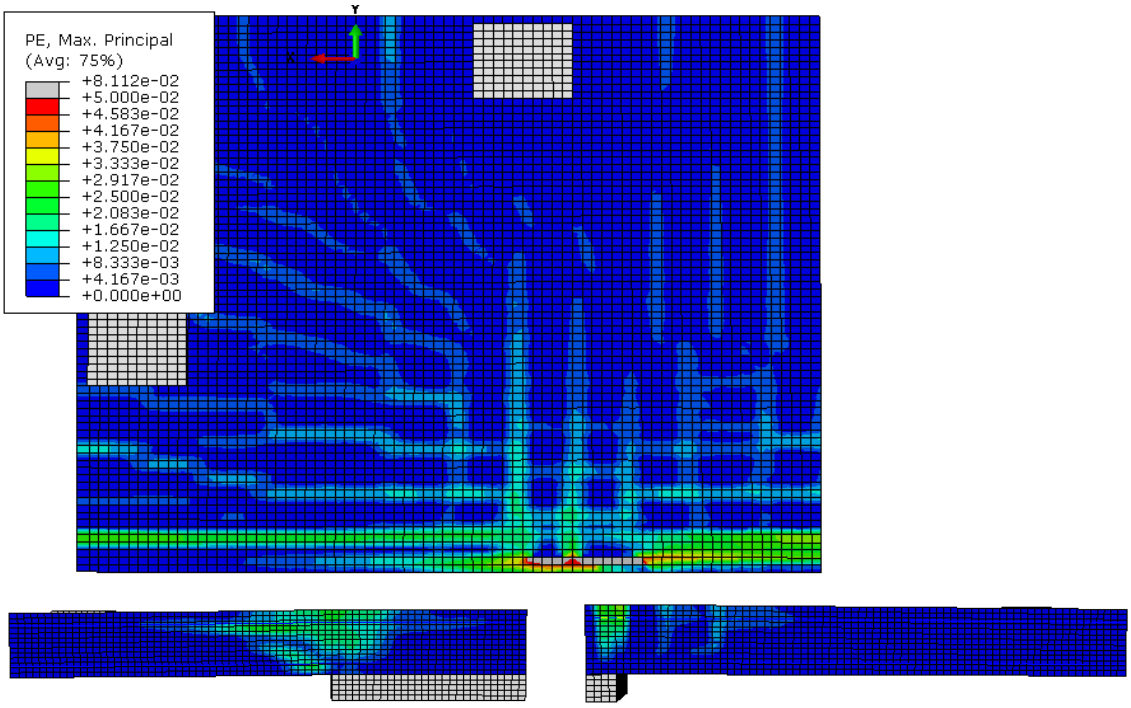

Figure F-32: β = 7 Crack Pattern, Bottom Left: Long Side, Bottom Right: Short Side

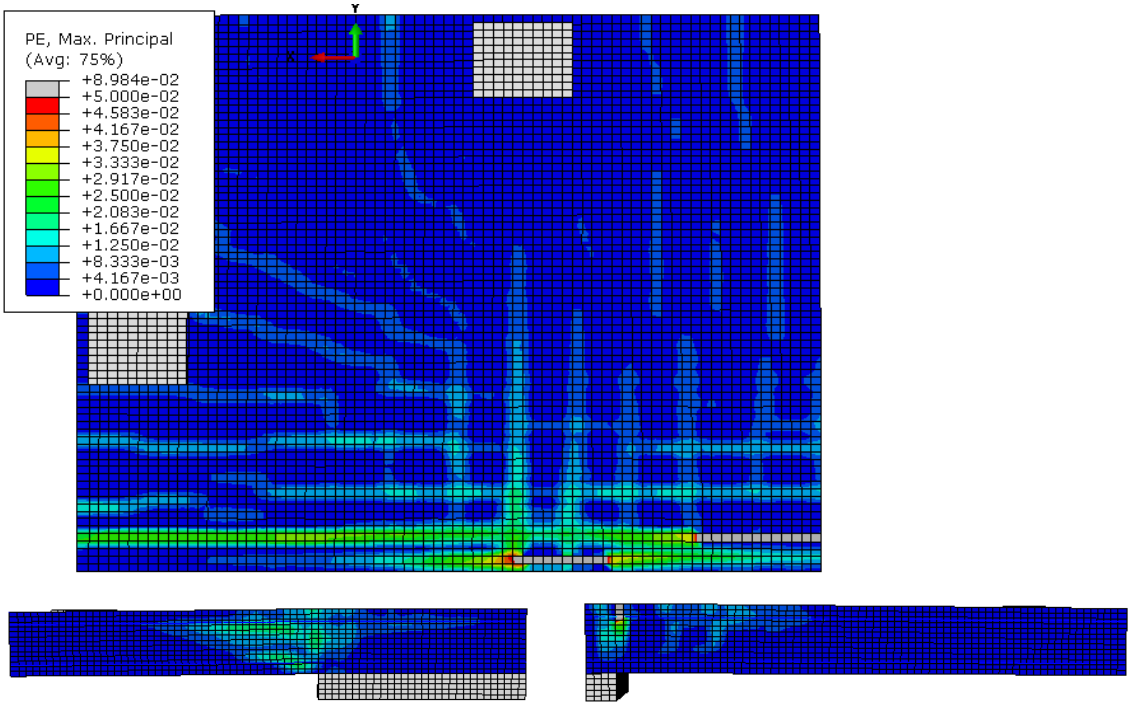

Figure F-33: β = 7.5 Crack Pattern, Bottom Left: Long Side, Bottom Right: Short Side

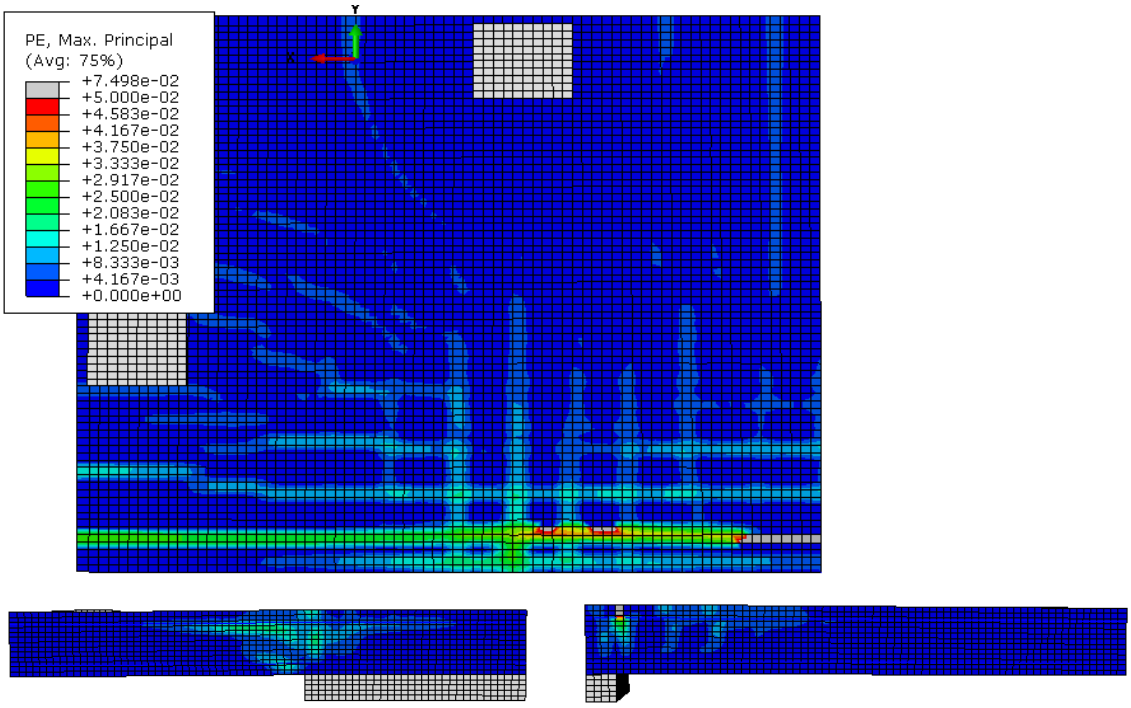

Figure F-34: β = 8 Crack Pattern, Bottom Left: Long Side, Bottom Right: Short Side

$c_{min}/d = 0.990$

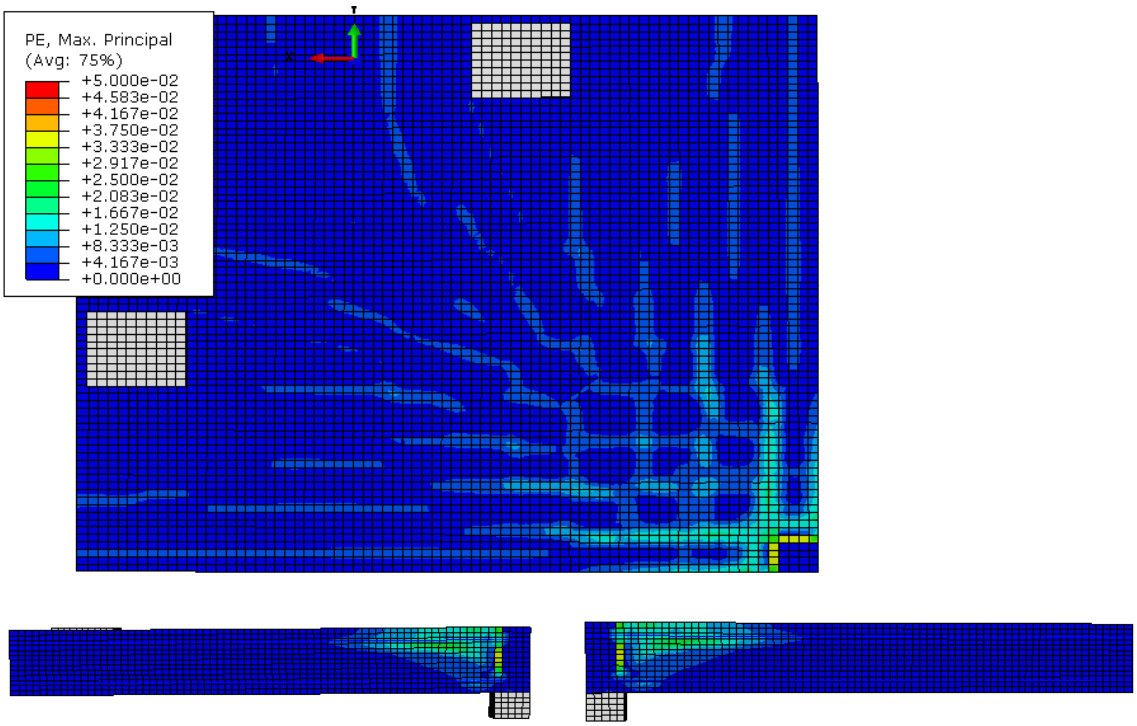

Figure F-35: β = 1 Crack Pattern, Bottom Left: Long Side, Bottom Right: Short Side

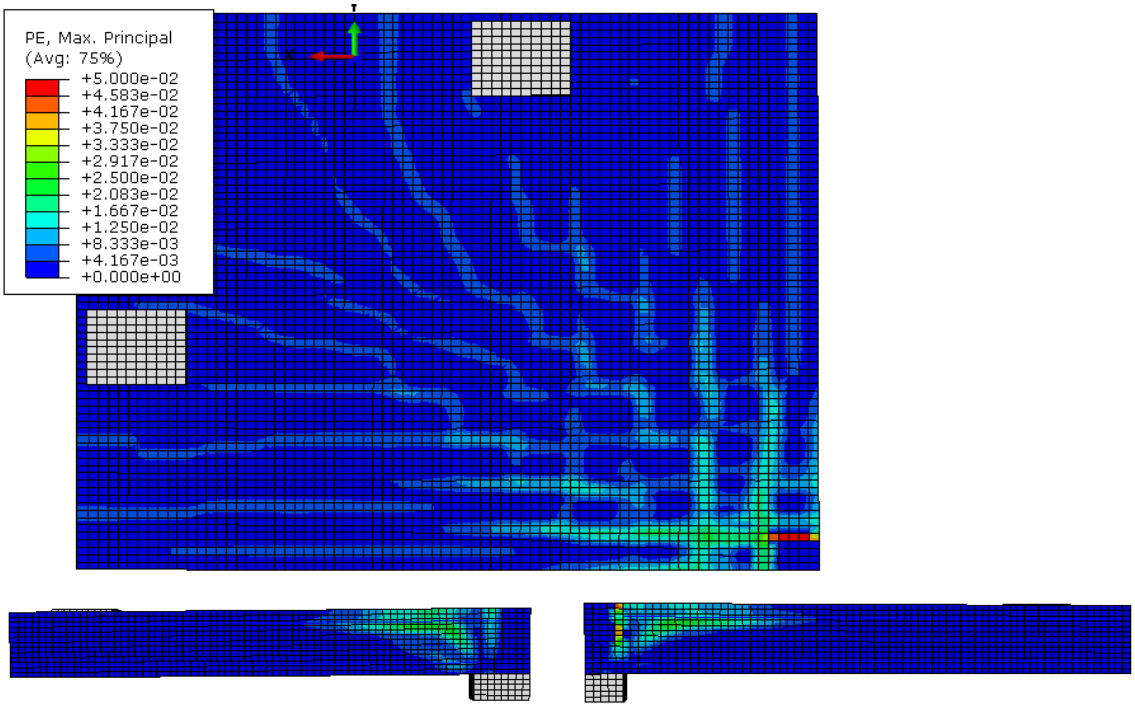

Figure F-36: β = 1.6 Crack Pattern, Bottom Left: Long Side, Bottom Right: Short Side

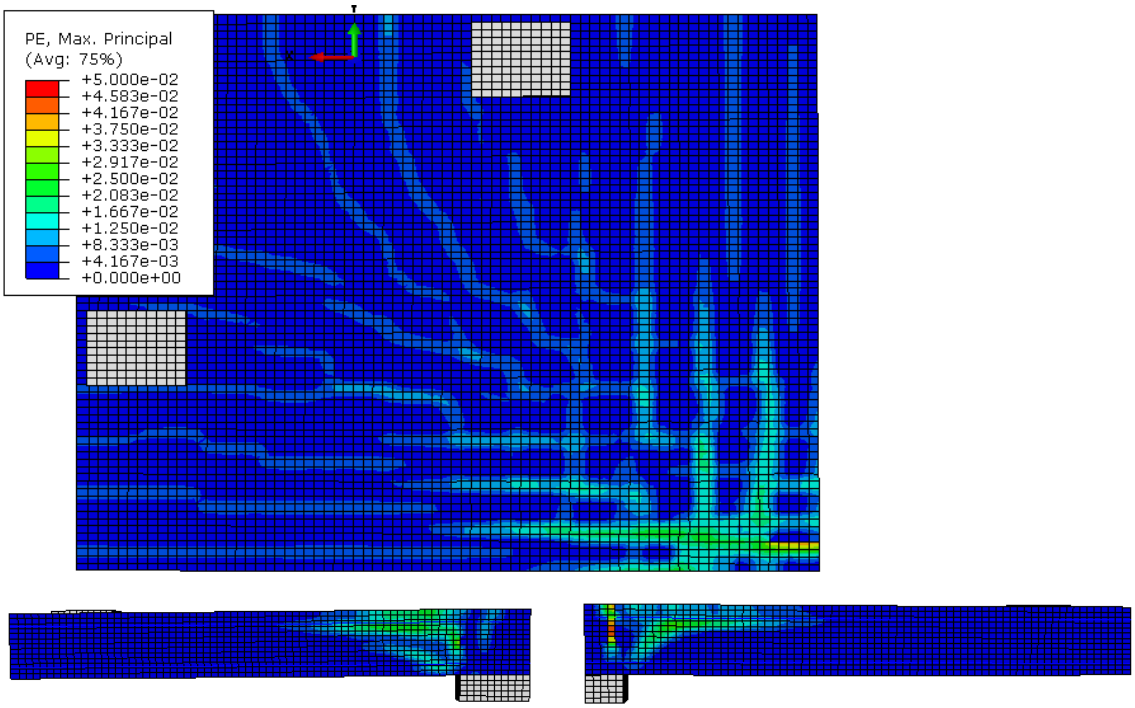

Figure F-37: β = 2 Crack Pattern, Bottom Left: Long Side, Bottom Right: Short Side

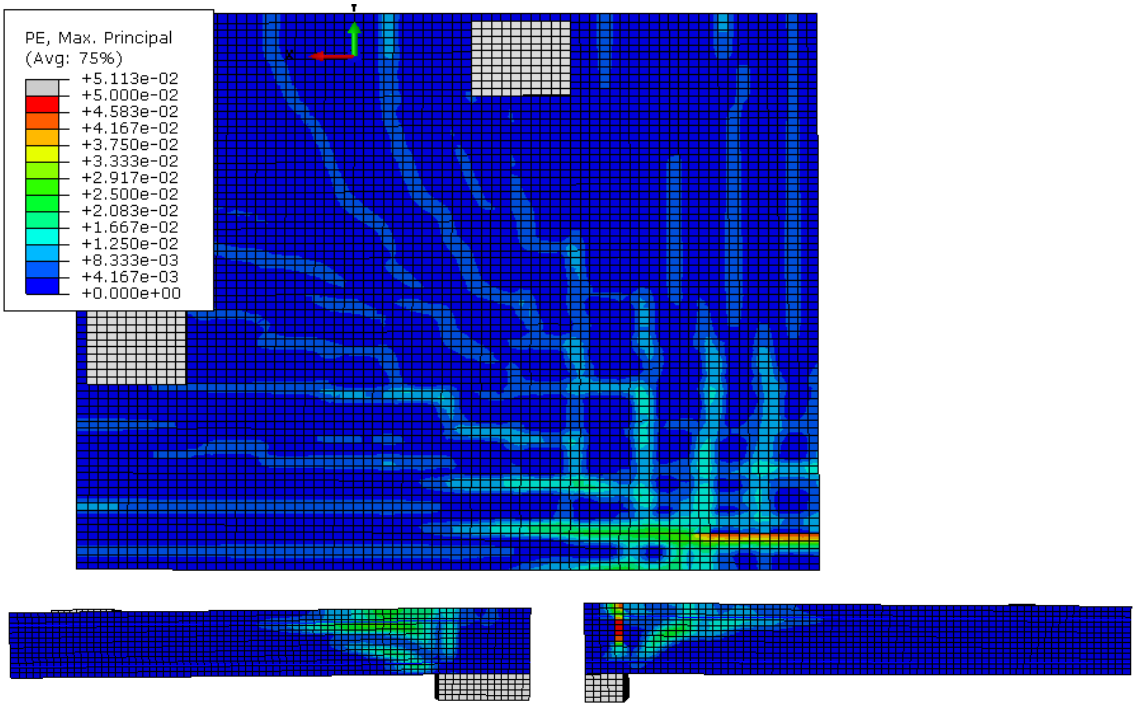

Figure F-38: β = 2.6 Crack Pattern, Bottom Left: Long Side, Bottom Right: Short Side

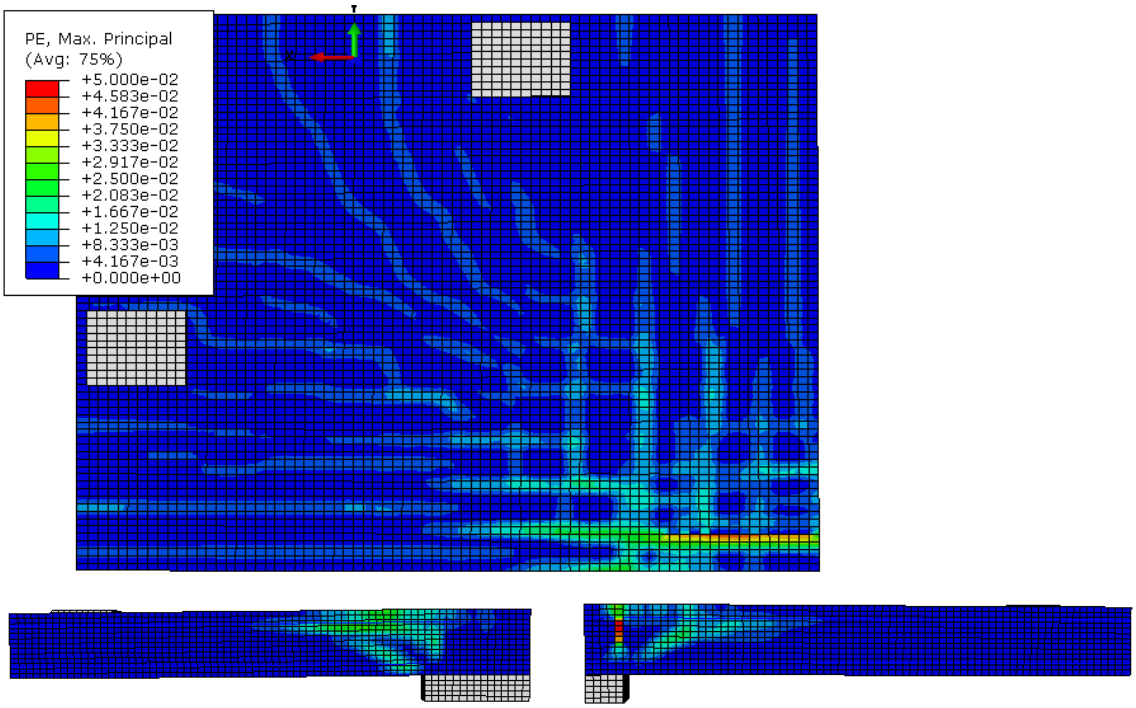

Figure F-39: β = 3 Crack Pattern, Bottom Left: Long Side, Bottom Right: Short Side

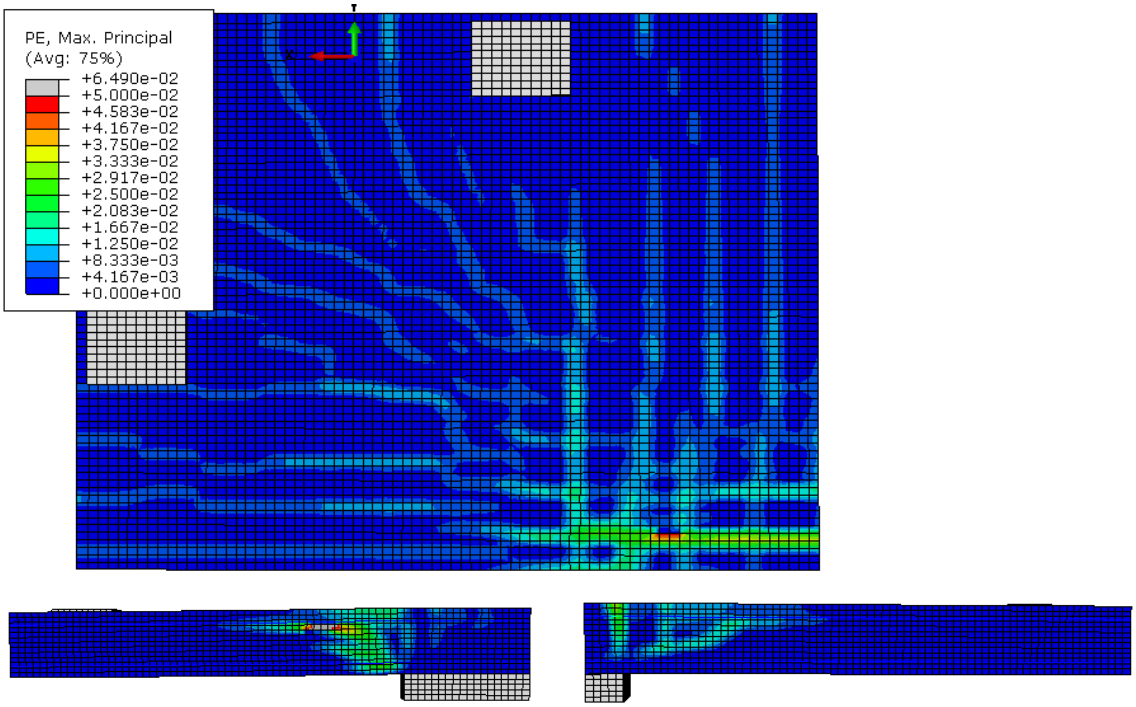

Figure F-40: β = 3.6 Crack Pattern, Bottom Left: Long Side, Bottom Right: Short Side

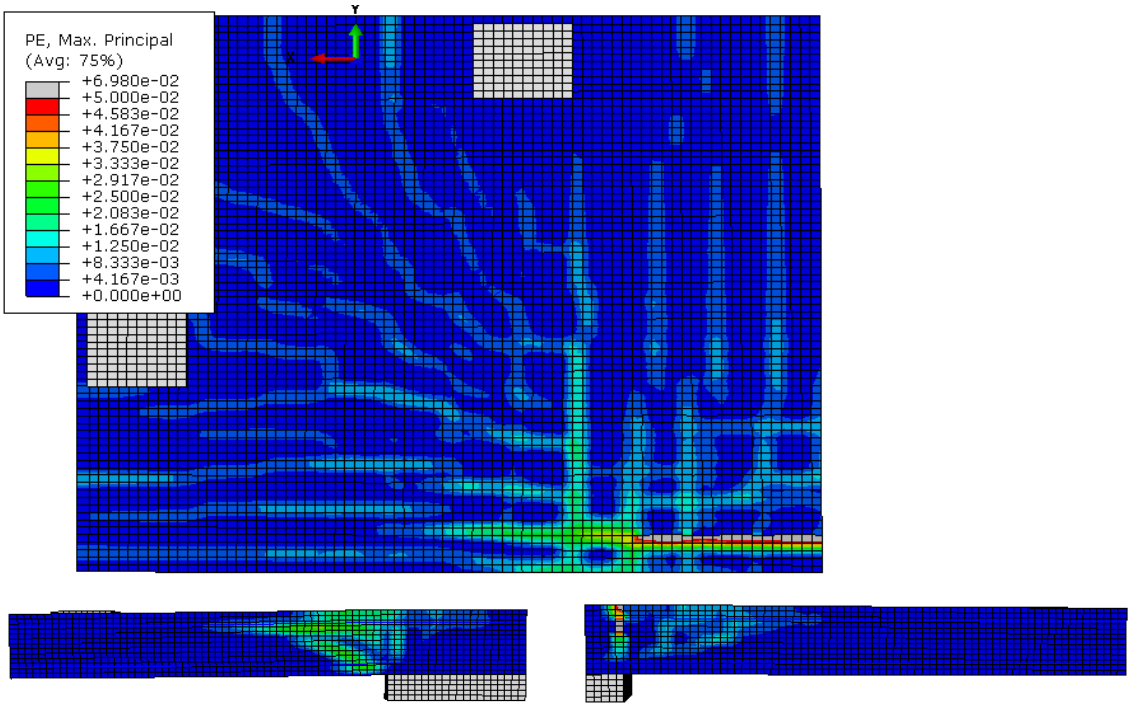

Figure F-41: β = 4 Crack Pattern, Bottom Left: Long Side, Bottom Right: Short Side

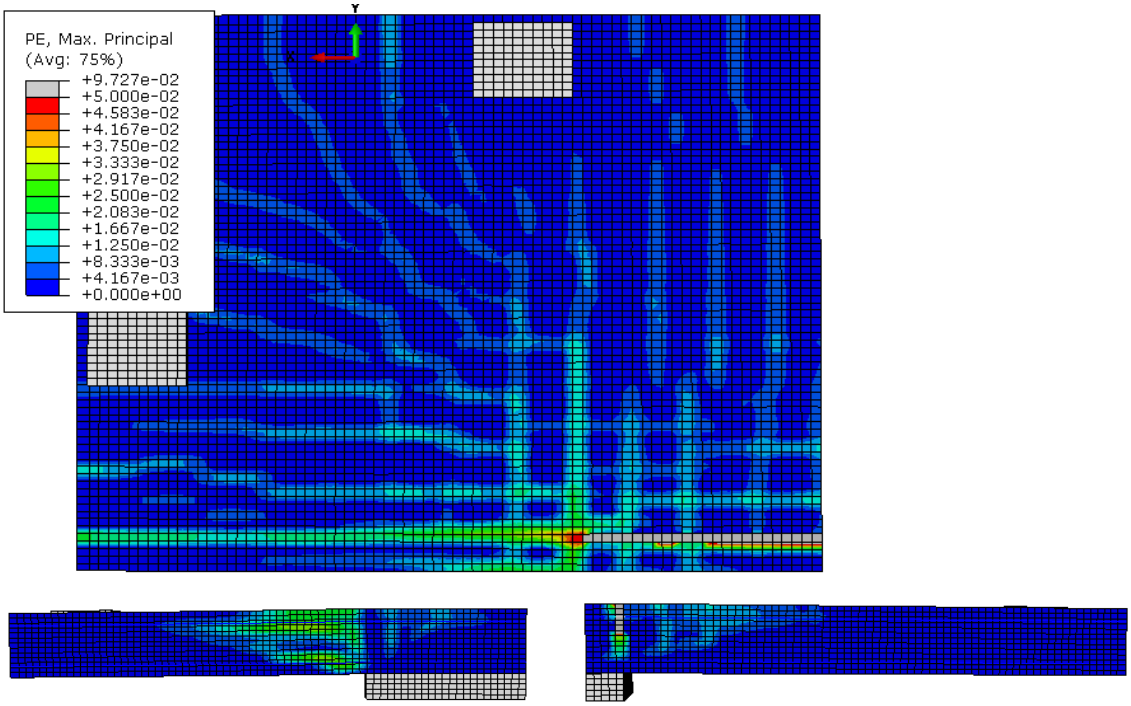

Figure F-42: β = 4.6 Crack Pattern, Bottom Left: Long Side, Bottom Right: Short Side

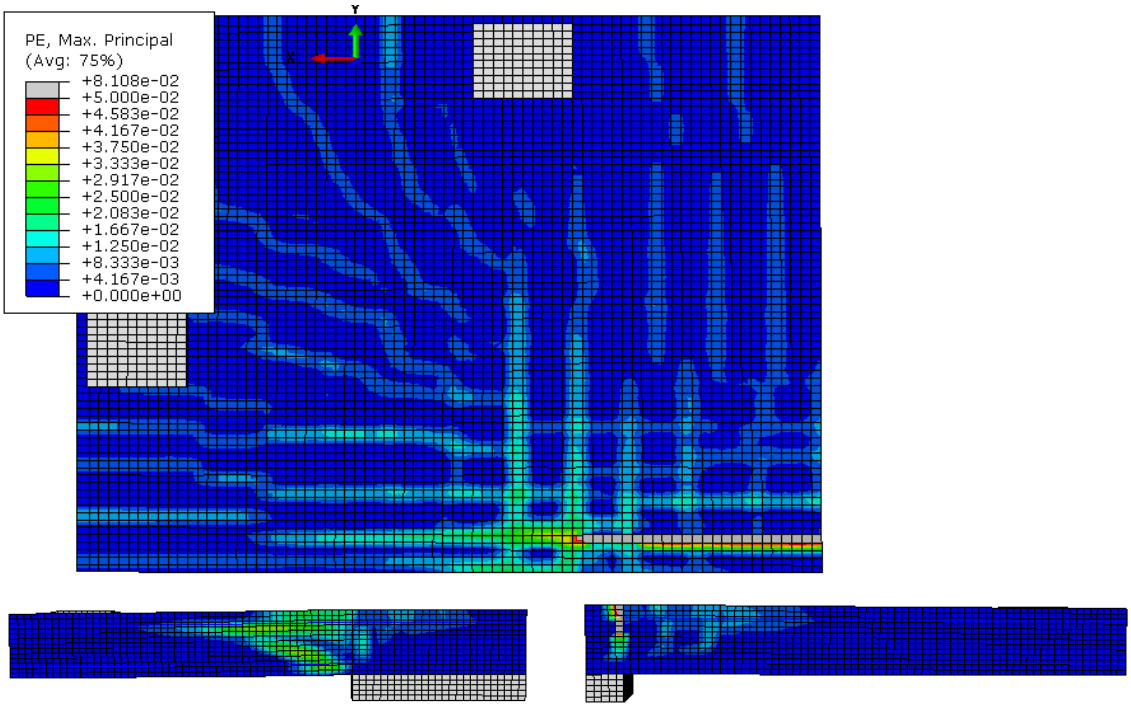

Figure F-43: β = 5 Crack Pattern, Bottom Left: Long Side, Bottom Right: Short Side

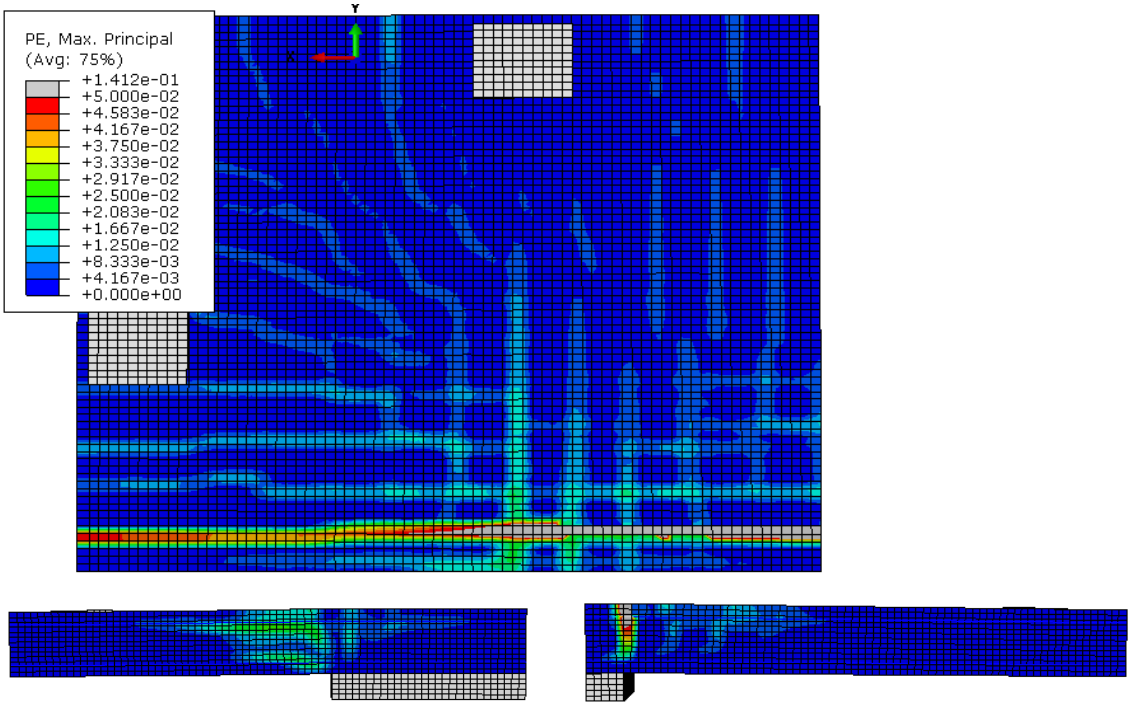

Figure F-44: β = 5.6 Crack Pattern, Bottom Left: Long Side, Bottom Right: Short Side

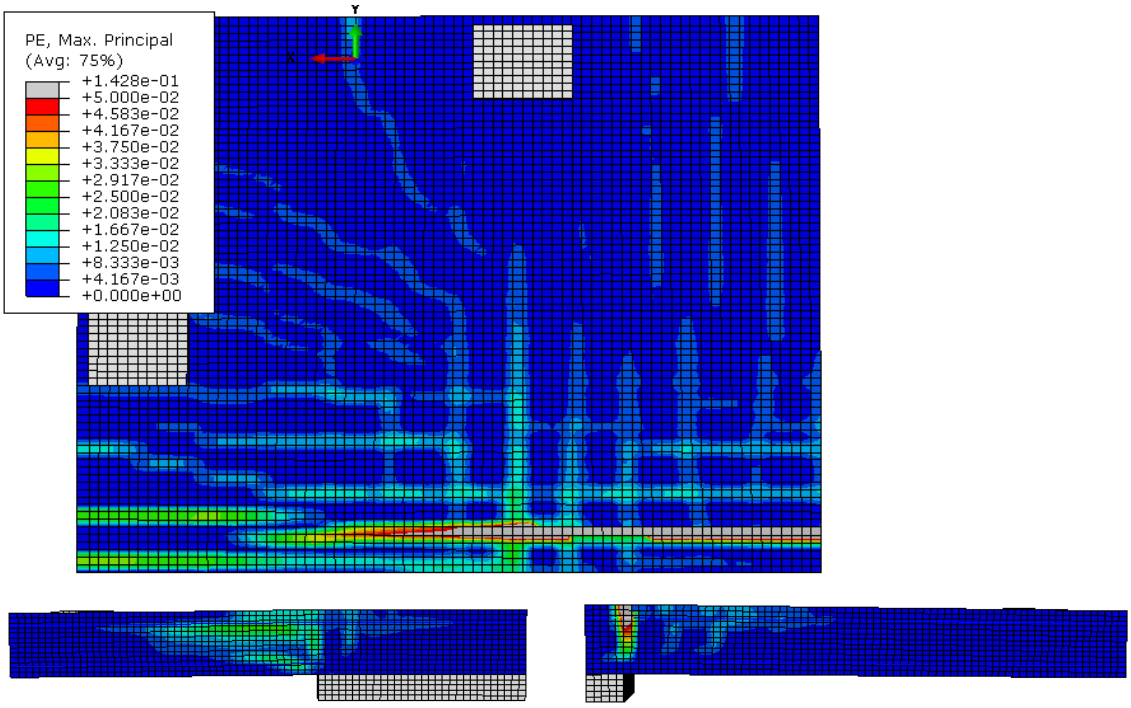

Figure F-45: β = 6 Crack Pattern, Bottom Left: Long Side, Bottom Right: Short Side

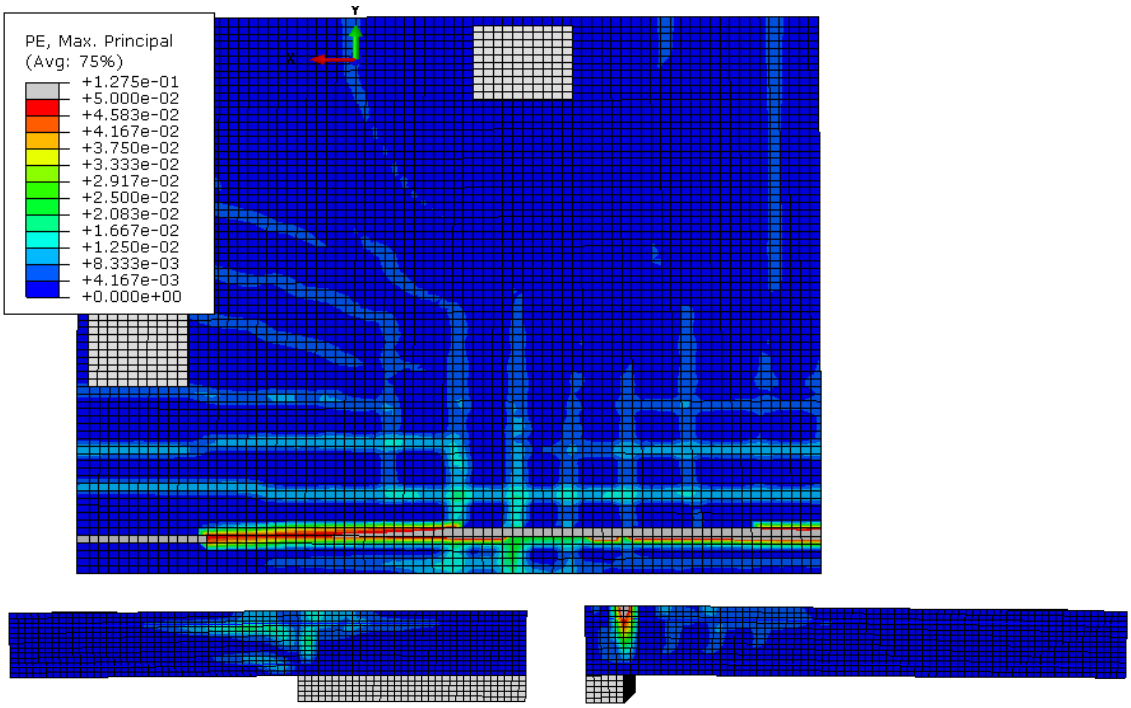

Figure F-46: β = 6.6 Crack Pattern, Bottom Left: Long Side, Bottom Right: Short Side

$c_{min}/d = 1.287$

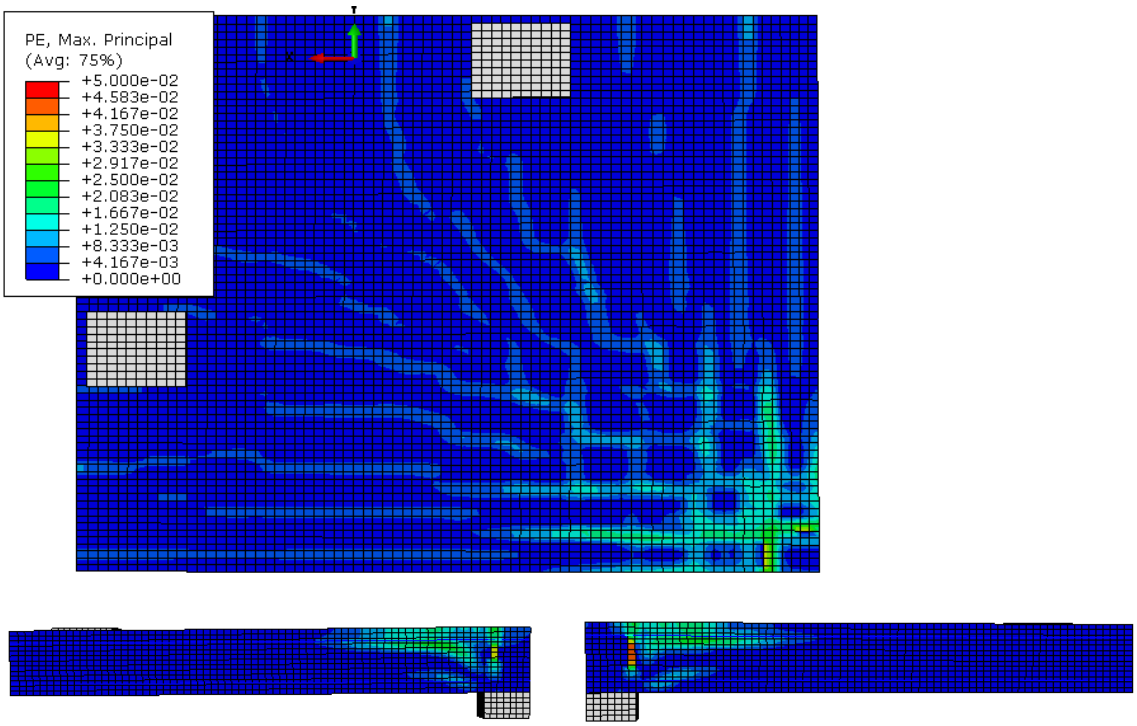

Figure F-47: β = 1 Crack Pattern, Bottom Left: Long Side, Bottom Right: Short Side

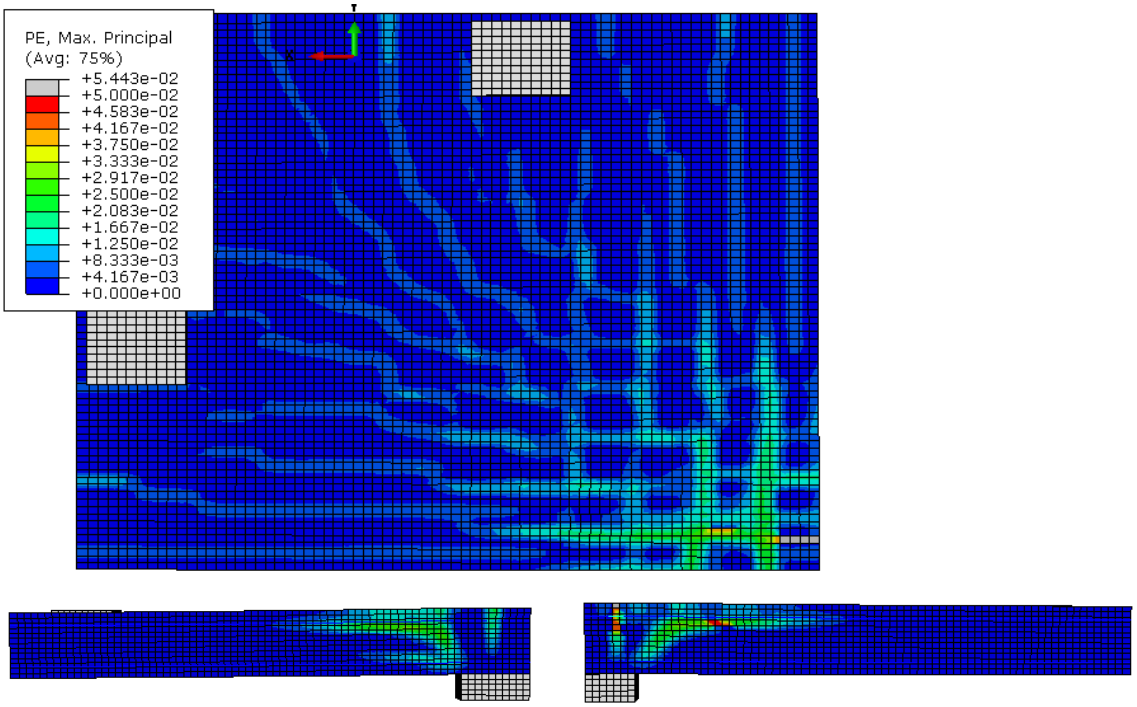

Figure F-48: β = 1.5 Crack Pattern, Bottom Left: Long Side, Bottom Right: Short Side

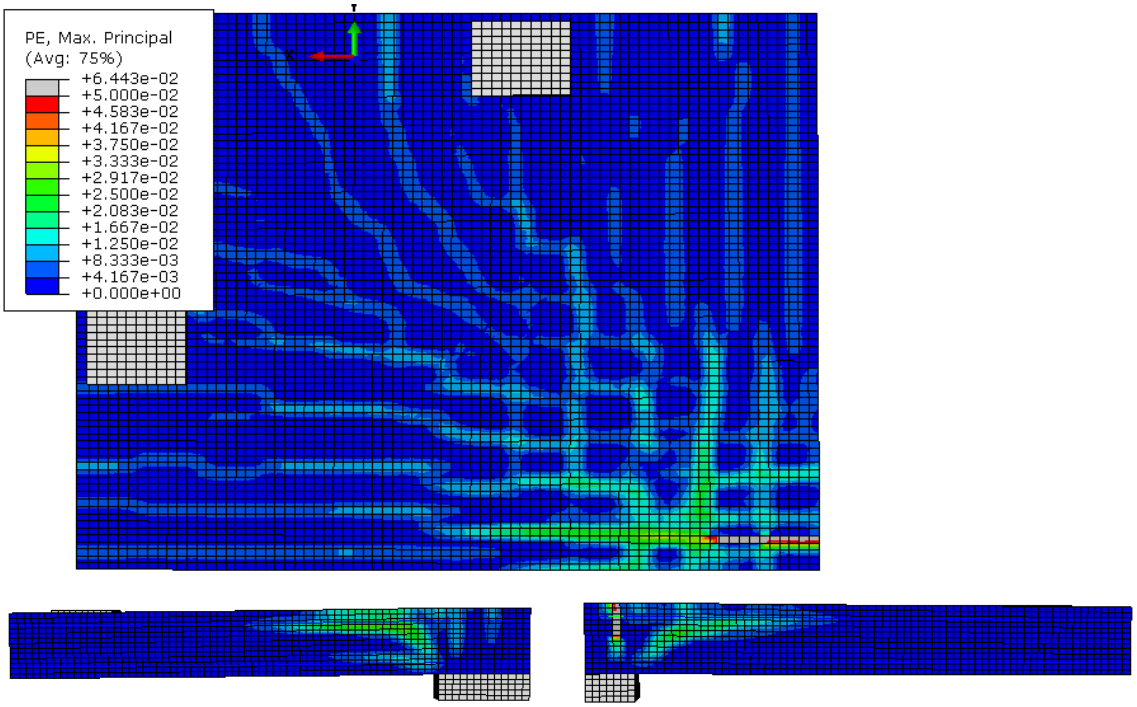

Figure F-49: β = 2 Crack Pattern, Bottom Left: Long Side, Bottom Right: Short Side

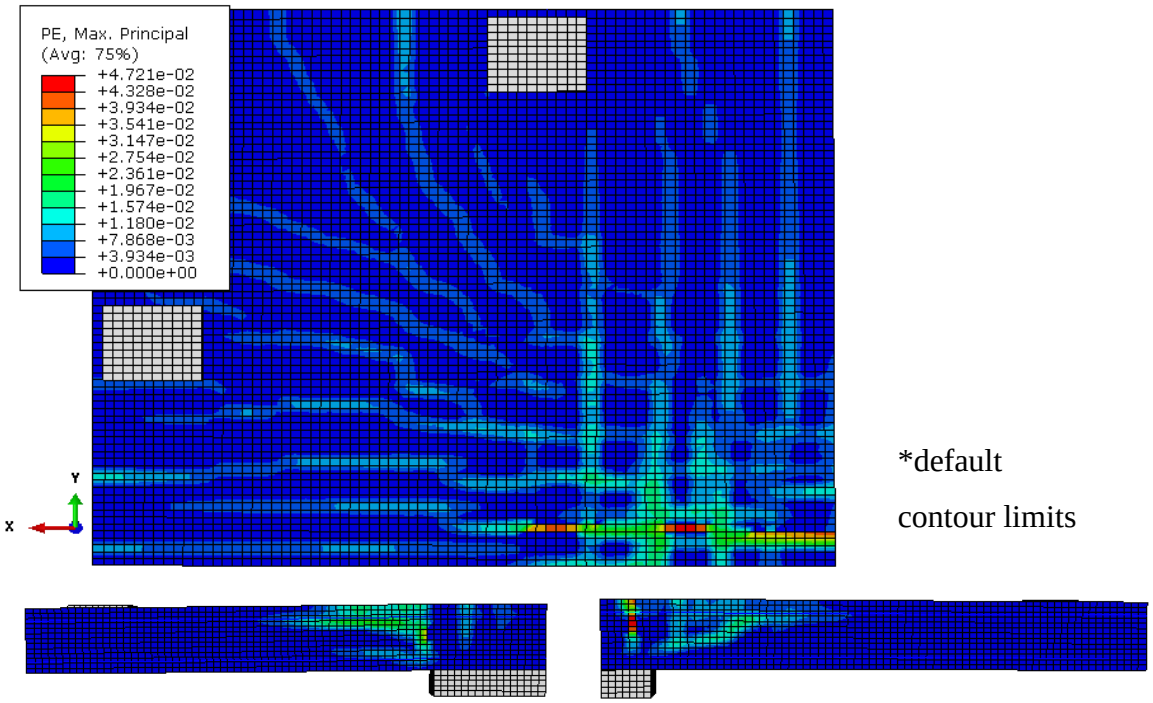

Figure F-50: β = 2.462 Crack Pattern, Bottom Left: Long Side, Bottom Right: Short Side

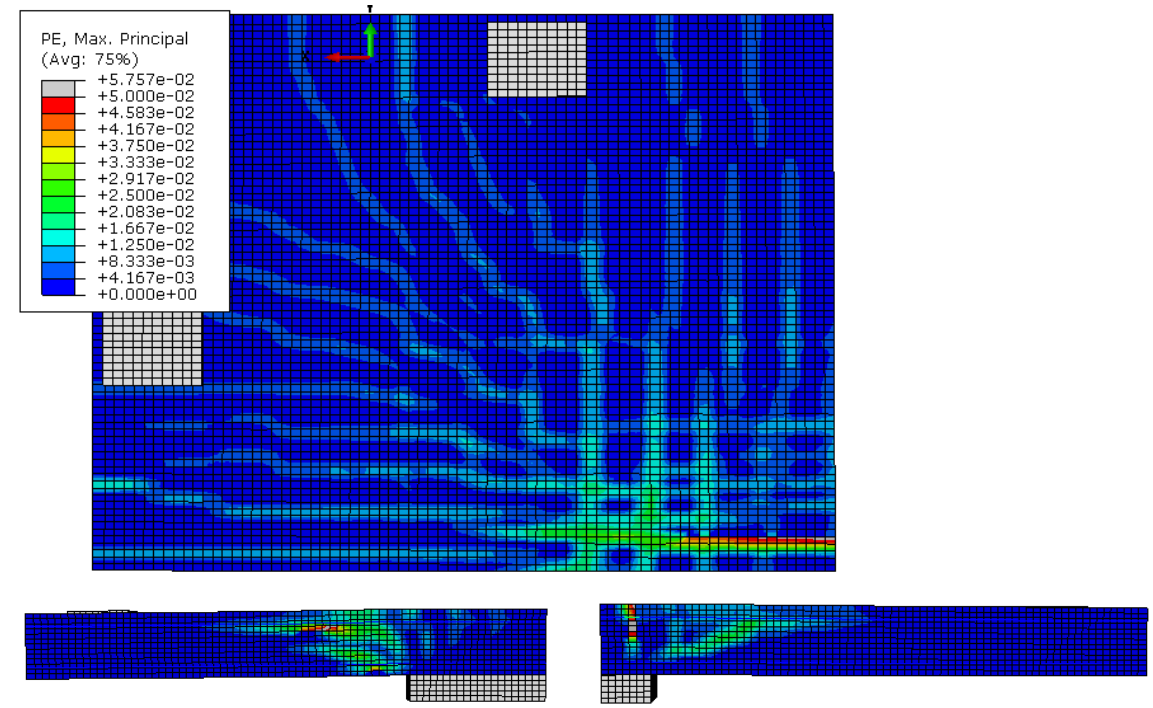

Figure F-51: β = 3 Crack Pattern, Bottom Left: Long Side, Bottom Right: Short Side

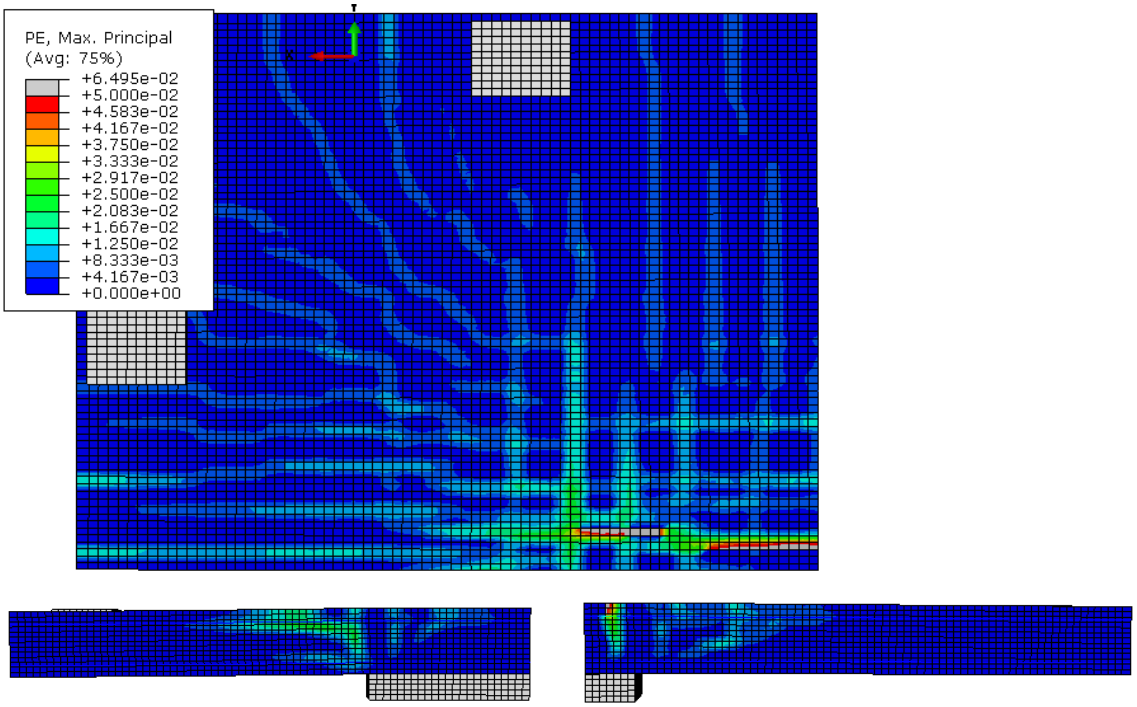

Figure F-52: β = 3.467 Crack Pattern, Bottom Left: Long Side, Bottom Right: Short Side

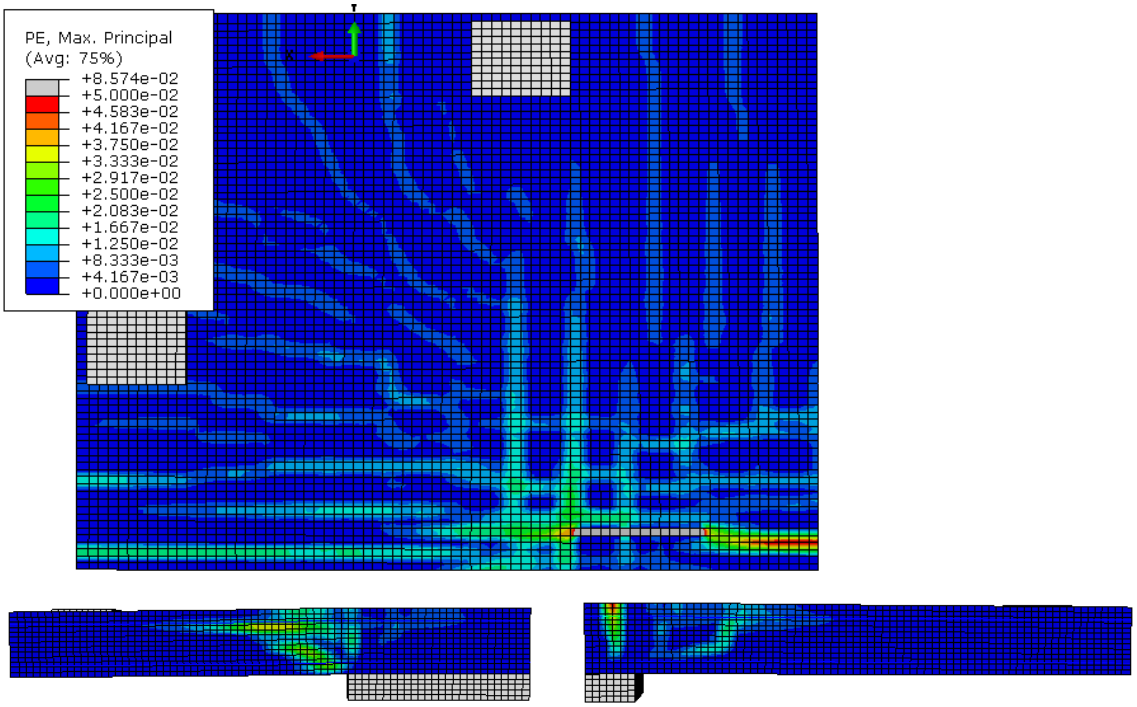

Figure F-53: β = 4 Crack Pattern, Bottom Left: Long Side, Bottom Right: Short Side

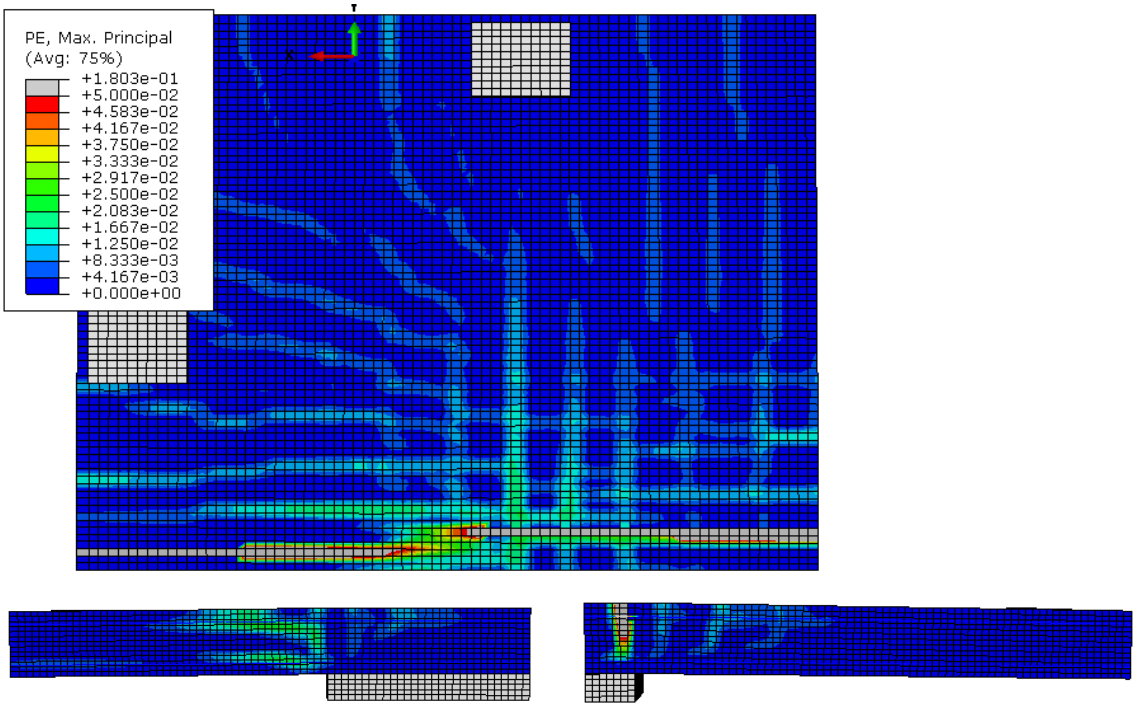

Figure F-54: β = 4.462 Crack Pattern, Bottom Left: Long Side, Bottom Right: Short Side

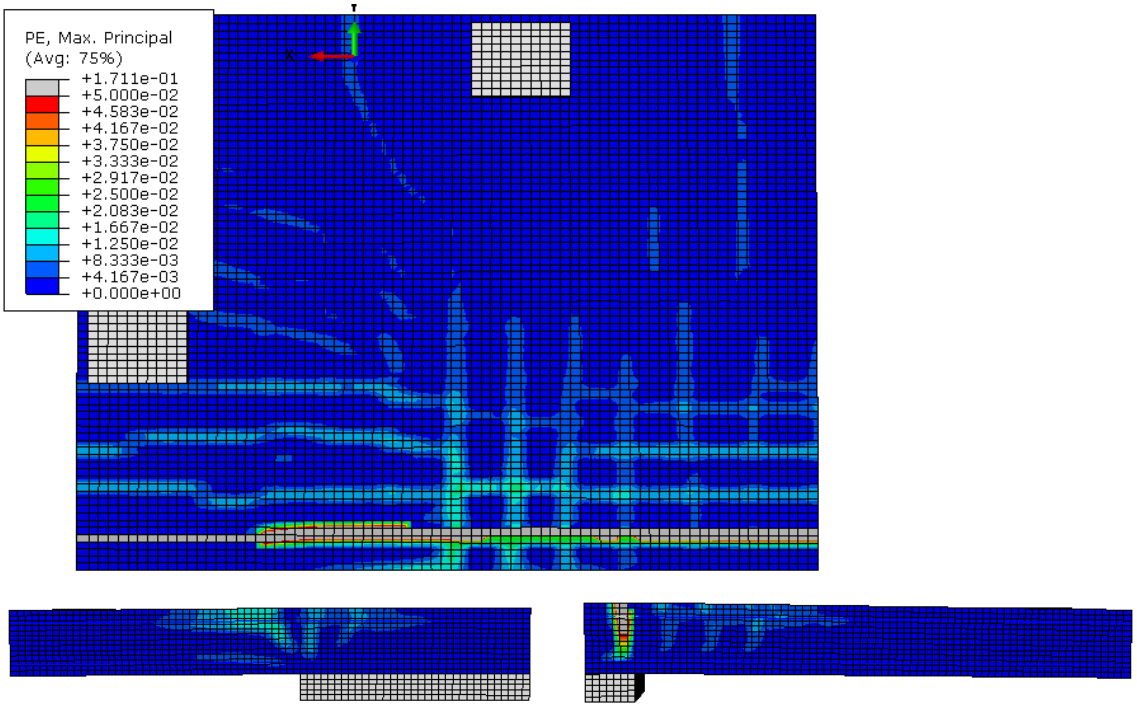

Figure F-55: β = 5.077 Crack Pattern, Bottom Left: Long Side, Bottom Right: Short Side

$c_{min}/d = 1.485$

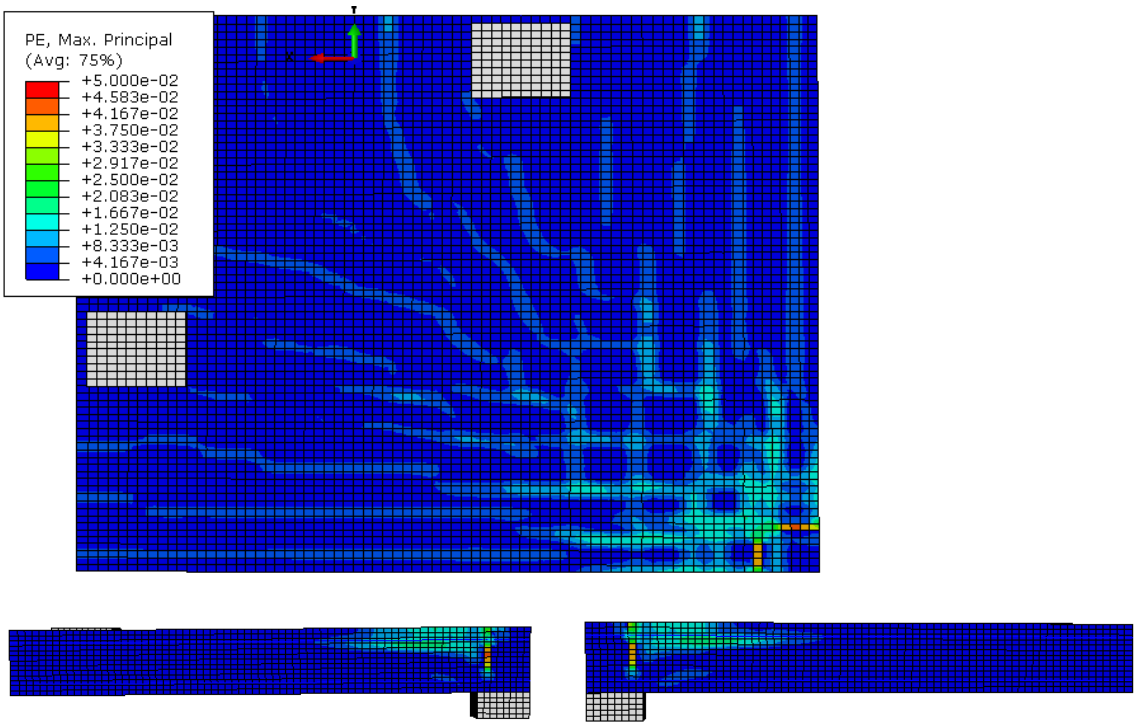

Figure F-56: β = 1 Crack Pattern, Bottom Left: Long Side, Bottom Right: Short Side

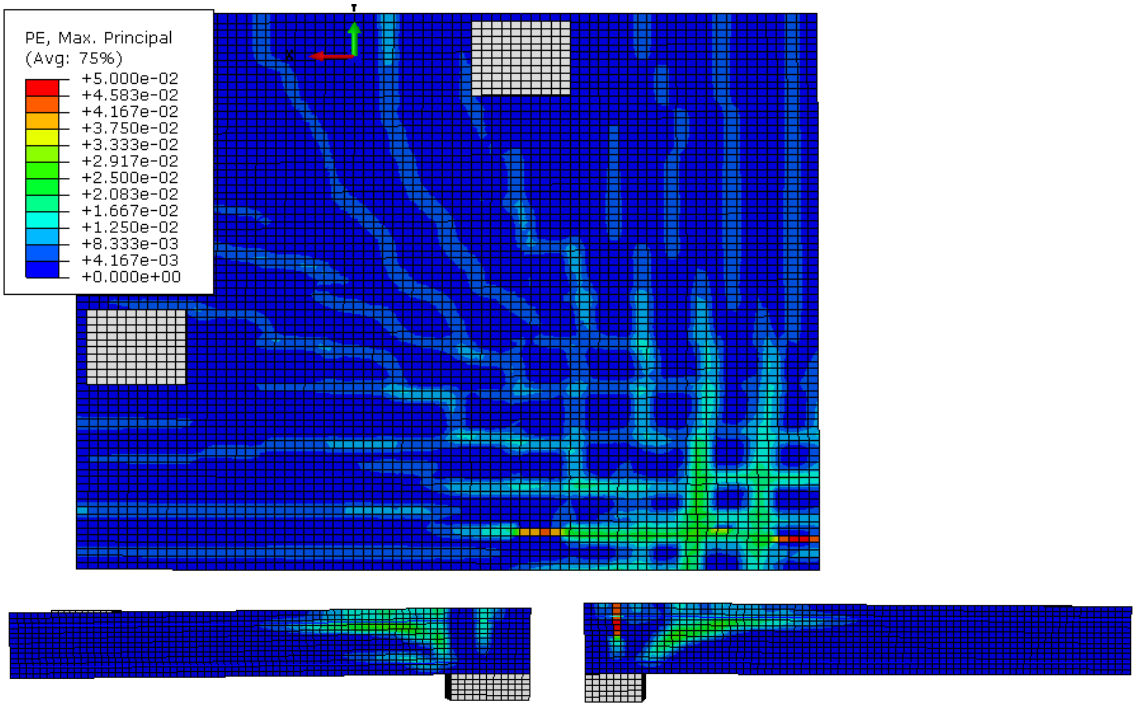

Figure F-57: β = 1.5 Crack Pattern, Bottom Left: Long Side, Bottom Right: Short Side

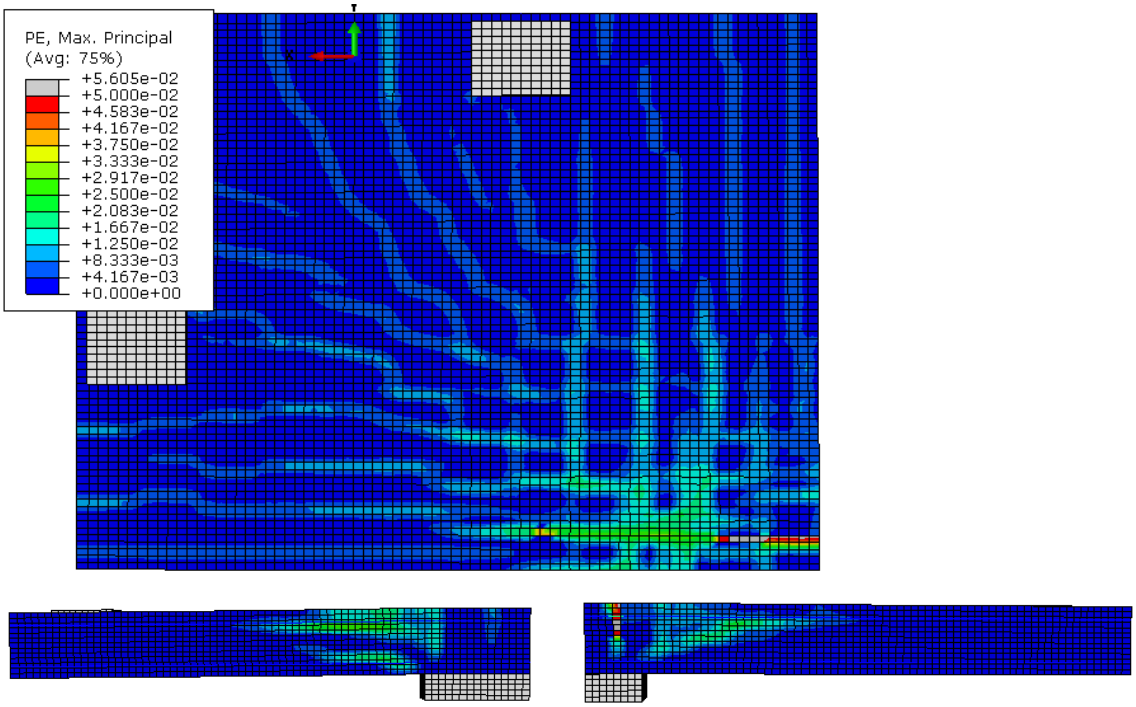

Figure F-58: β = 2 Crack Pattern, Bottom Left: Long Side, Bottom Right: Short Side

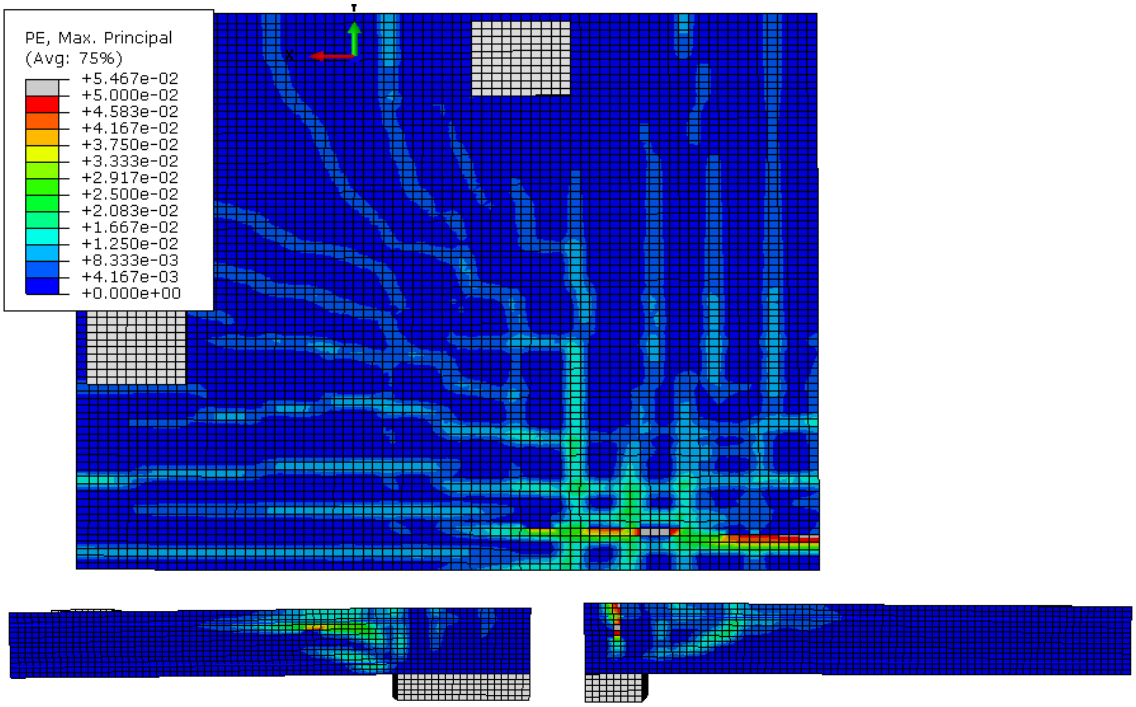

Figure F-59: β = 2.533 Crack Pattern, Bottom Left: Long Side, Bottom Right: Short Side

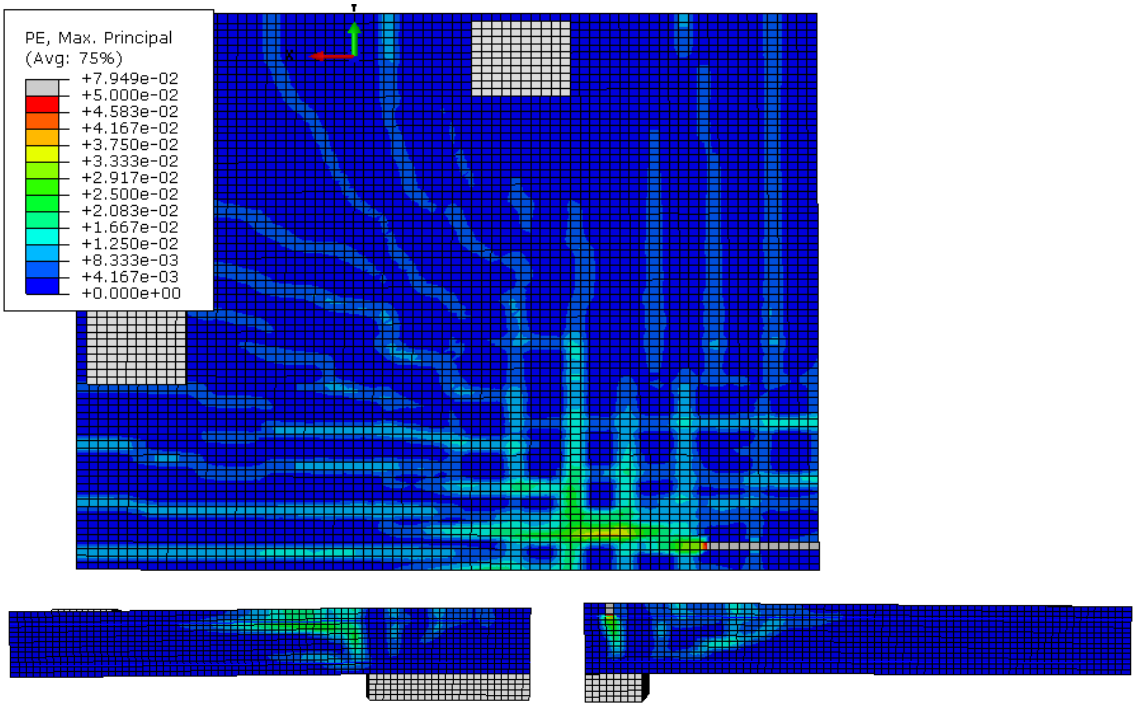

Figure F-60: β = 3.067 Crack Pattern, Bottom Left: Long Side, Bottom Right: Short Side

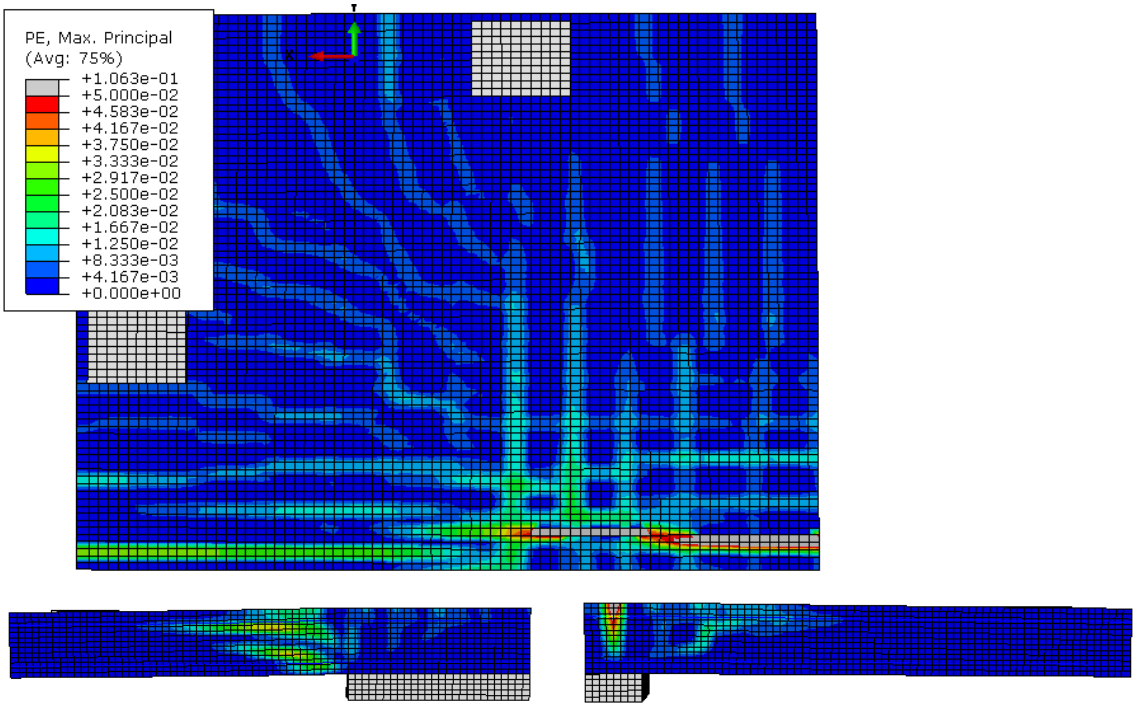

Figure F-61: β = 3.467 Crack Pattern, Bottom Left: Long Side, Bottom Right: Short Side

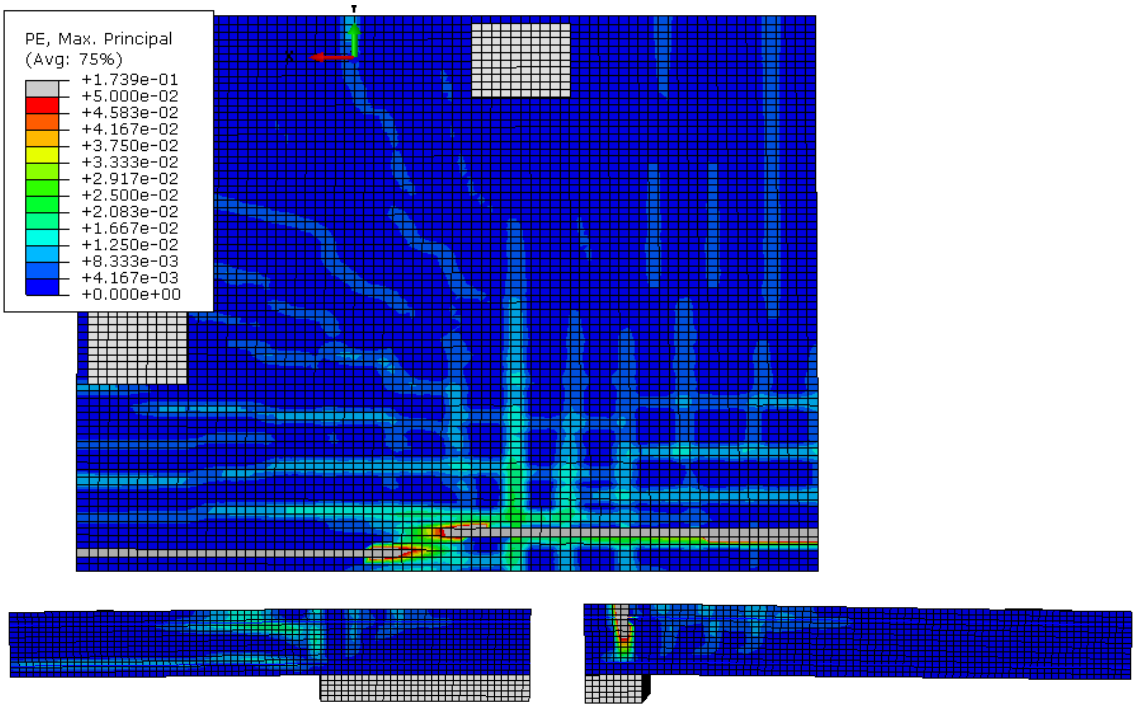

Figure F-62: β = 4 Crack Pattern, Bottom Left: Long Side, Bottom Right: Short Side

$c_{min}/d = 1.782$

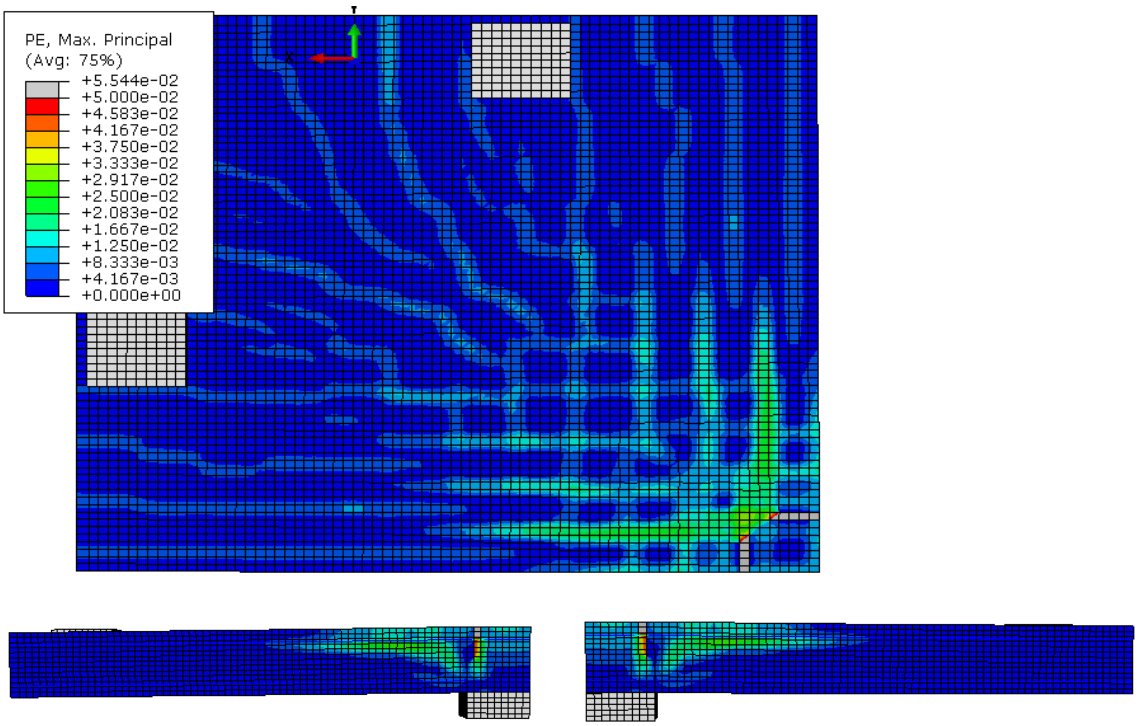

Figure F-63: β = 1 Crack Pattern, Bottom Left: Long Side, Bottom Right: Short Side

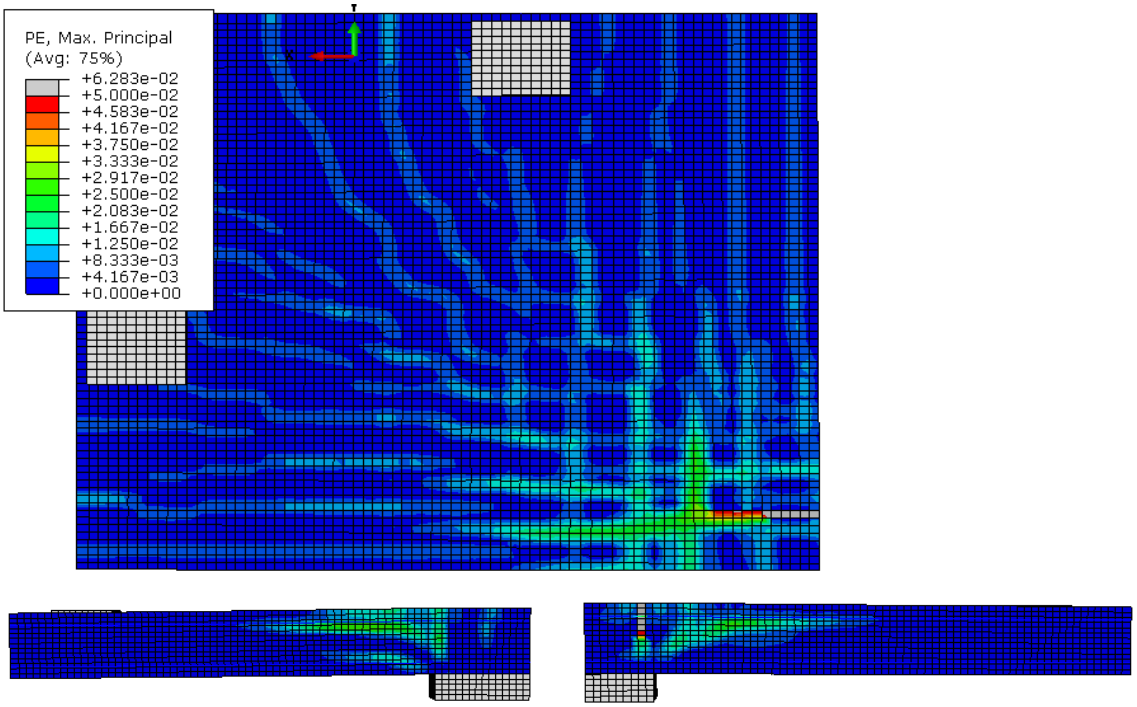

Figure F-64: β = 1.5 Crack Pattern, Bottom Left: Long Side, Bottom Right: Short Side

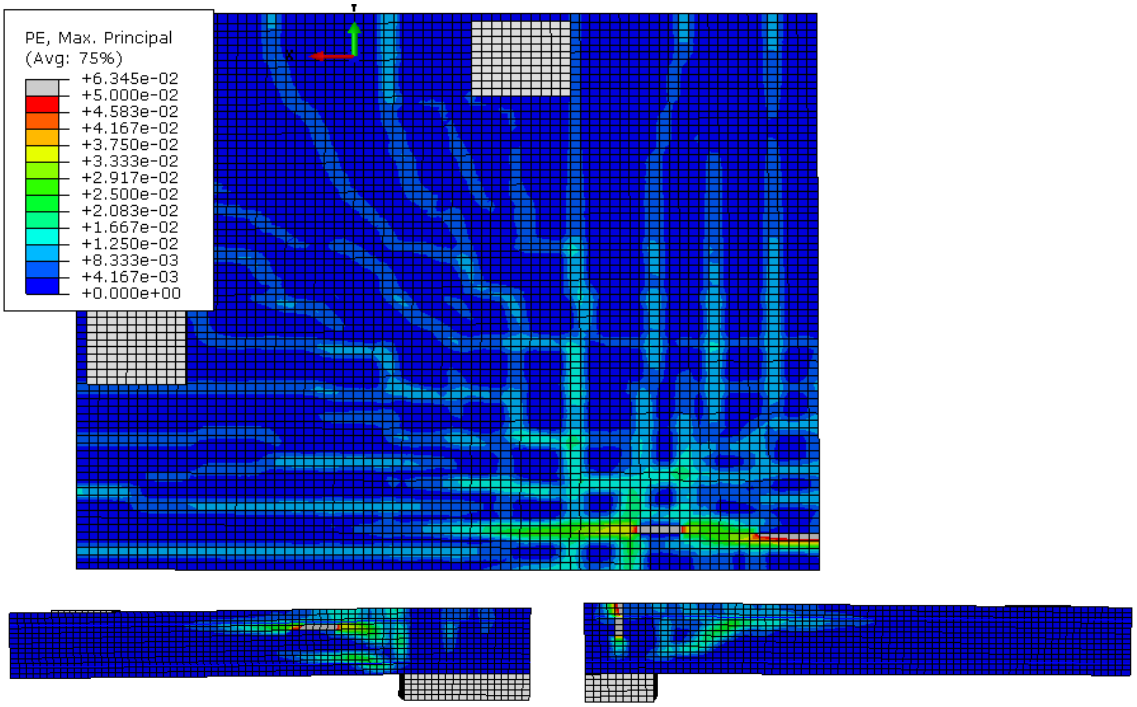

Figure F-65: β = 2 Crack Pattern, Bottom Left: Long Side, Bottom Right: Short Side

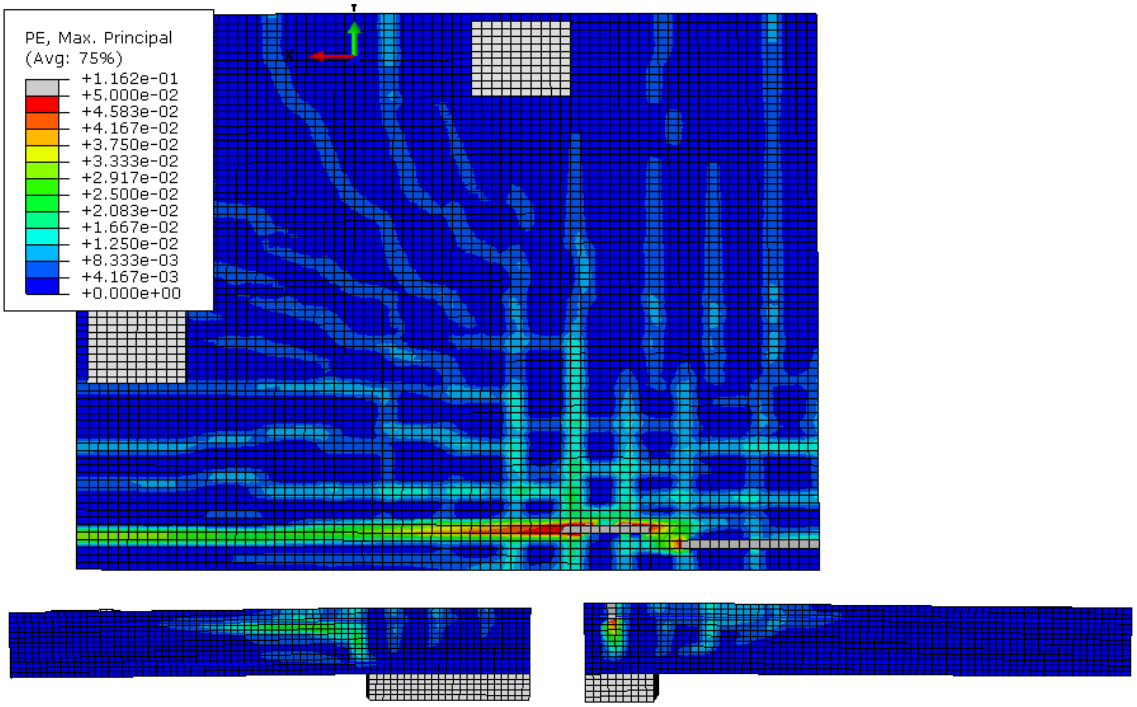

Figure F-66: β = 2.556 Crack Pattern, Bottom Left: Long Side, Bottom Right: Short Side

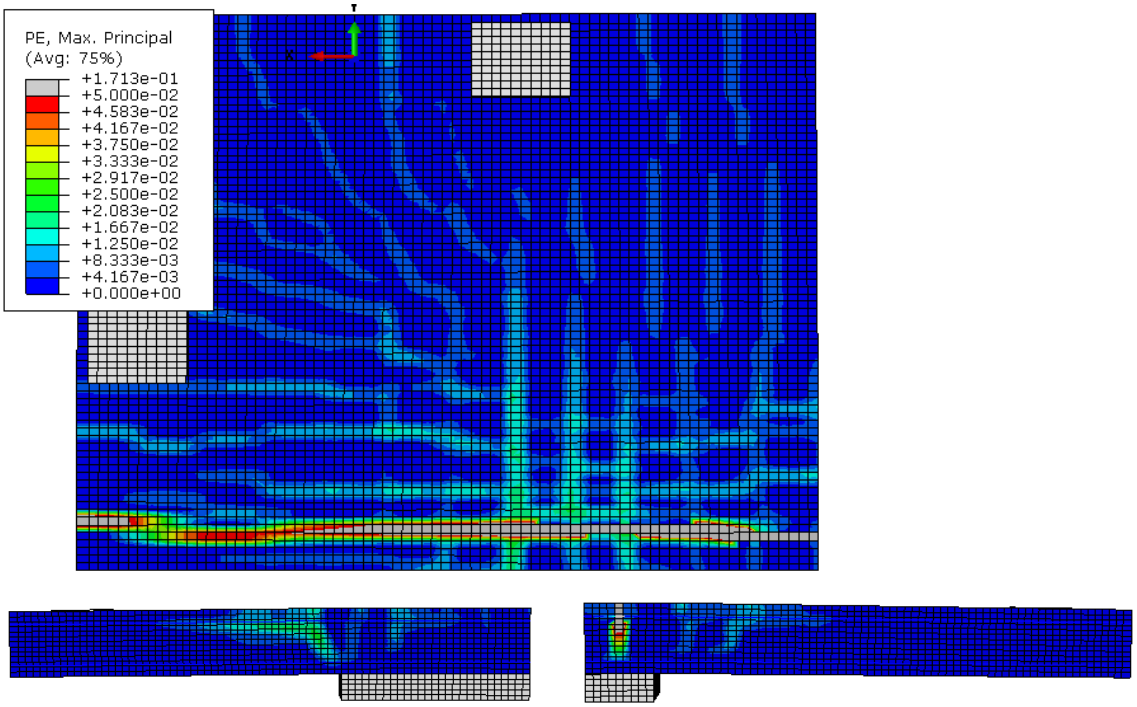

Figure F-67: β = 3 Crack Pattern, Bottom Left: Long Side, Bottom Right: Short Side

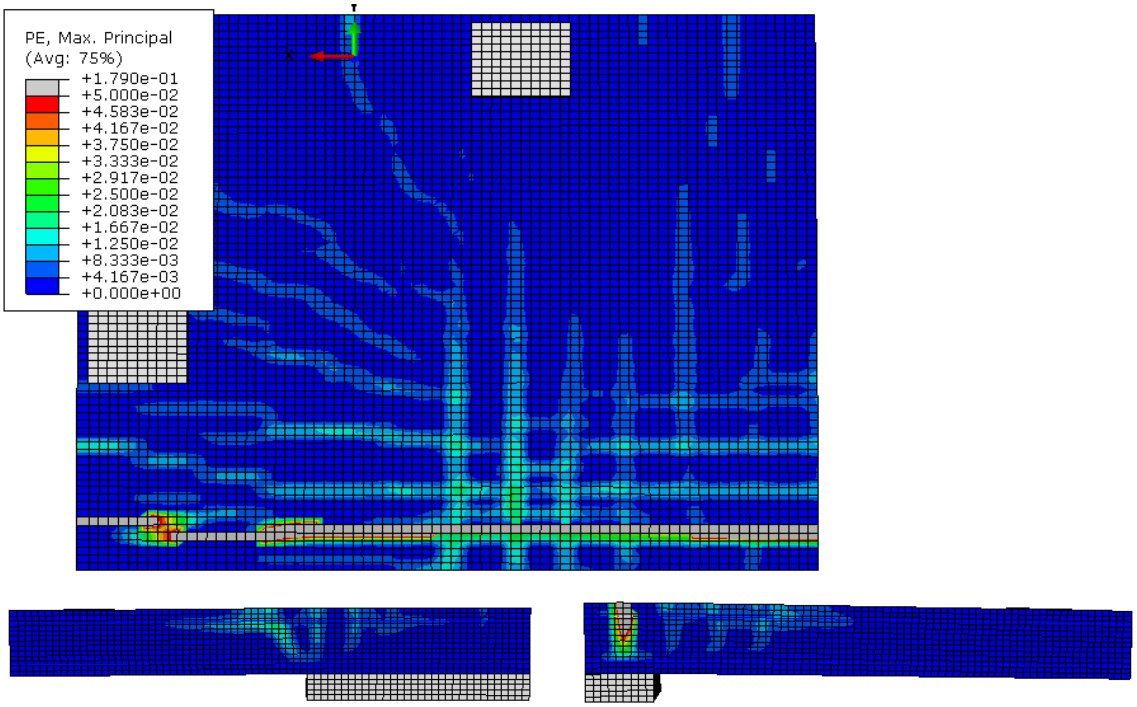

Figure F-68: β = 3.556 Crack Pattern, Bottom Left: Long Side, Bottom Right: Short Side

$c_{min}/d = 1.980$

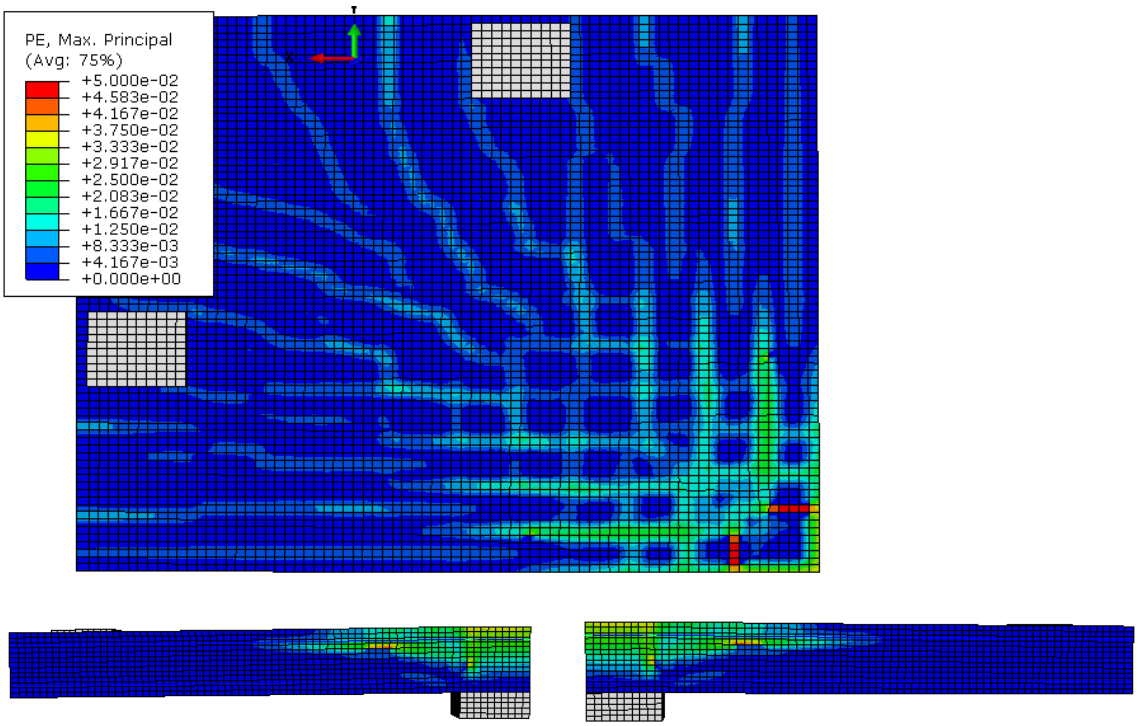

Figure F-69: β = 1 Crack Pattern, Bottom Left: Long Side, Bottom Right: Short Side

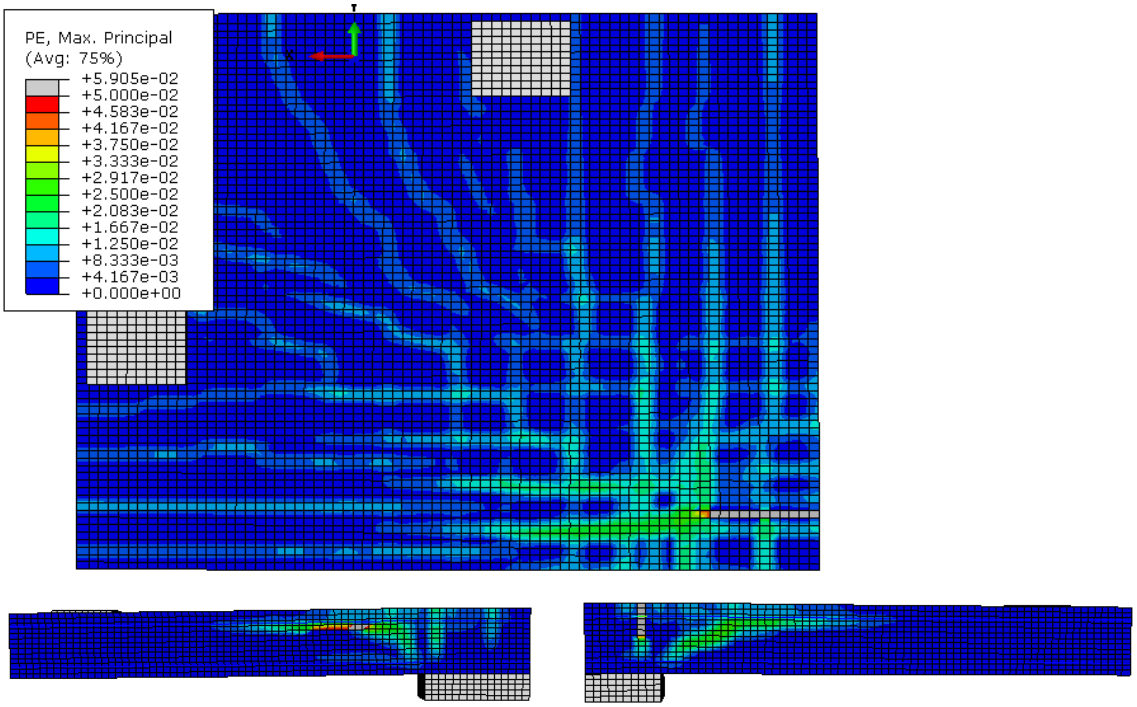

Figure F-70: β = 1.5 Crack Pattern, Bottom Left: Long Side, Bottom Right: Short Side

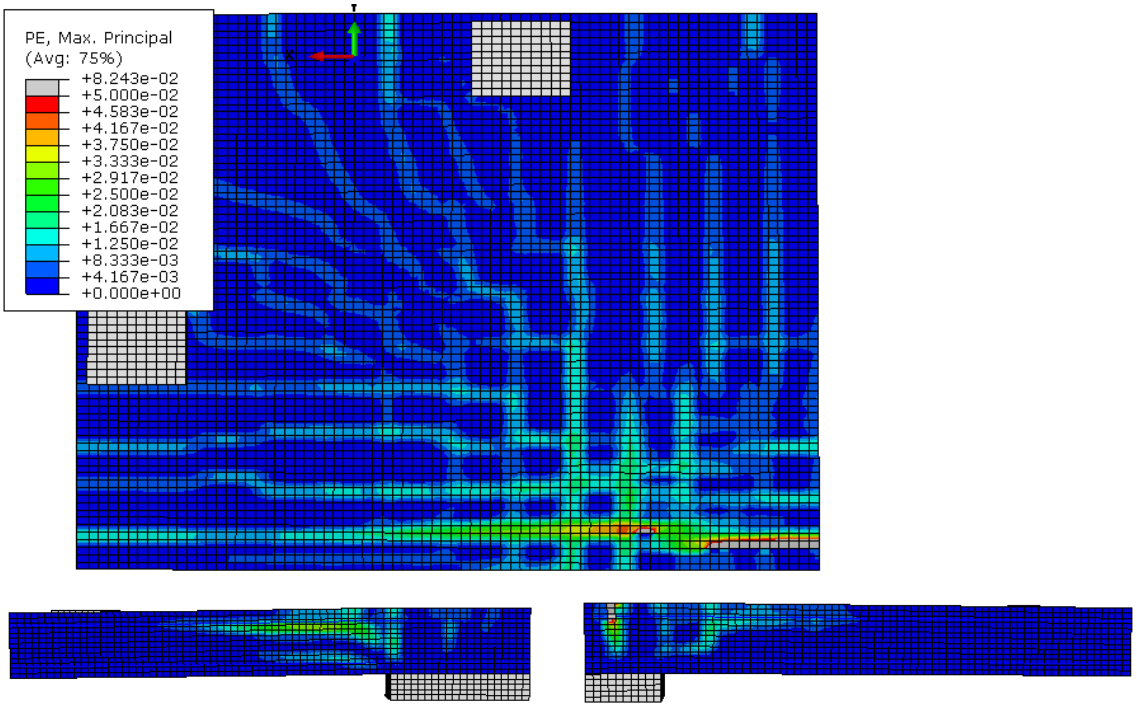

Figure F-71: β = 2 Crack Pattern, Bottom Left: Long Side, Bottom Right: Short Side

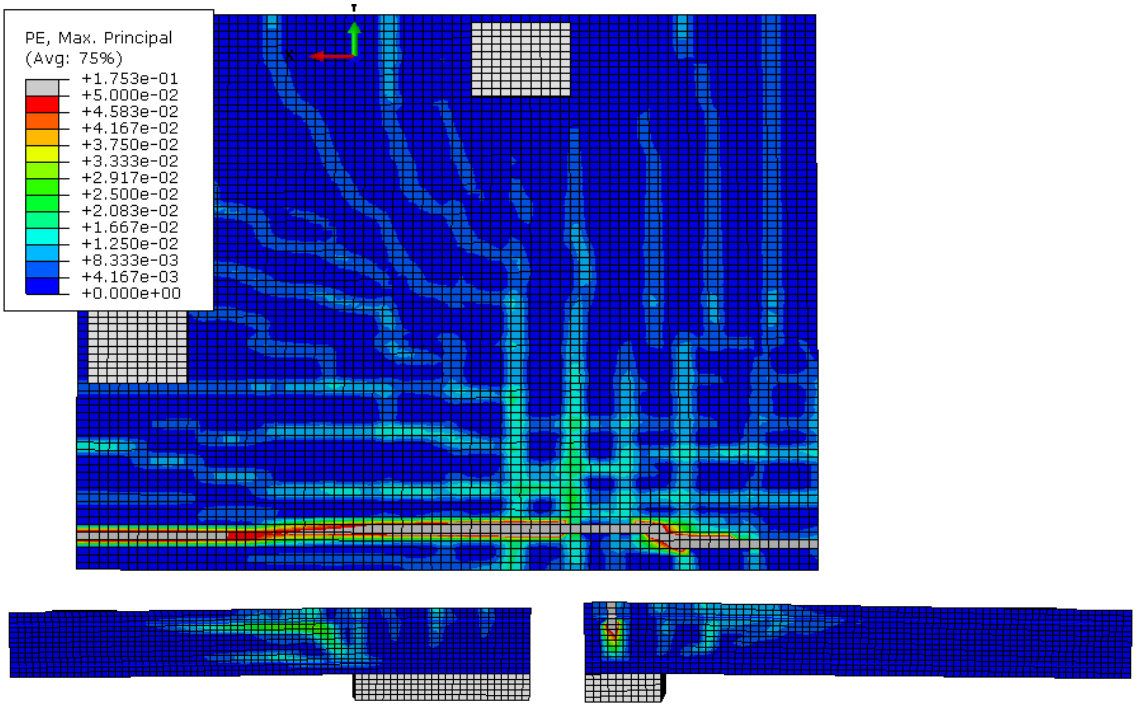

Figure F-72: β = 2.5 Crack Pattern, Bottom Left: Long Side, Bottom Right: Short Side

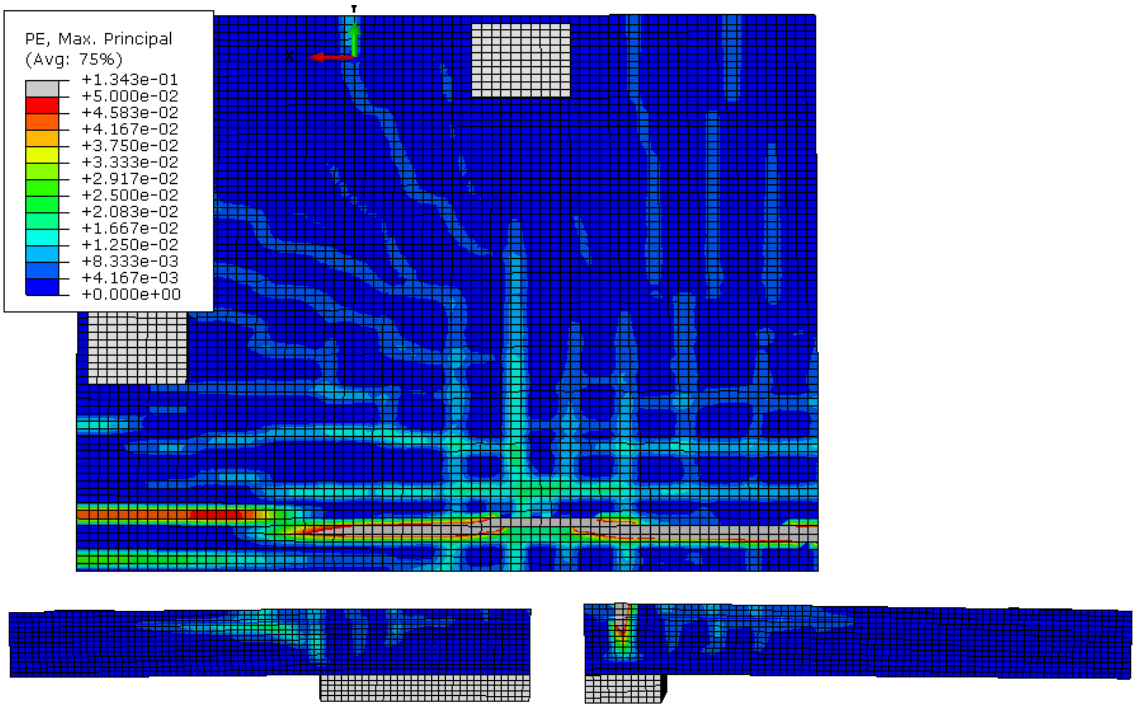

Figure F-73: β = 3 Crack Pattern, Bottom Left: Long Side, Bottom Right: Short Side

$c_{min}/d = 2.970$

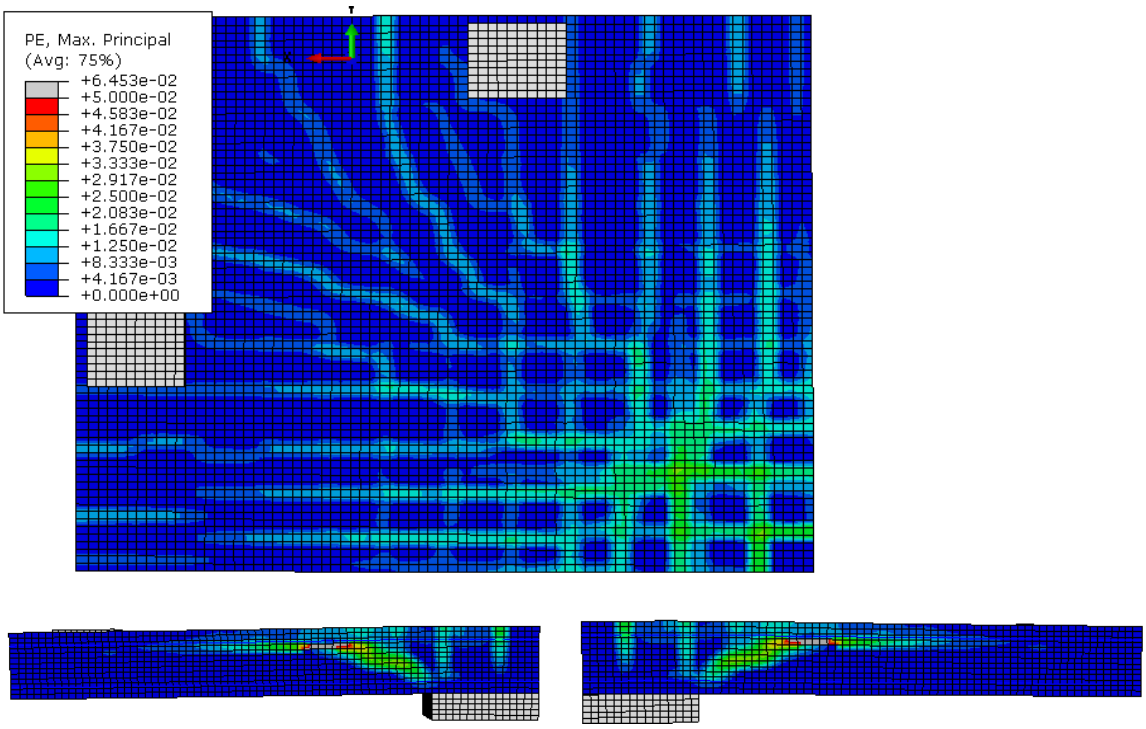

Figure F-74: β = 1 Crack Pattern, Bottom Left: Long Side, Bottom Right: Short Side

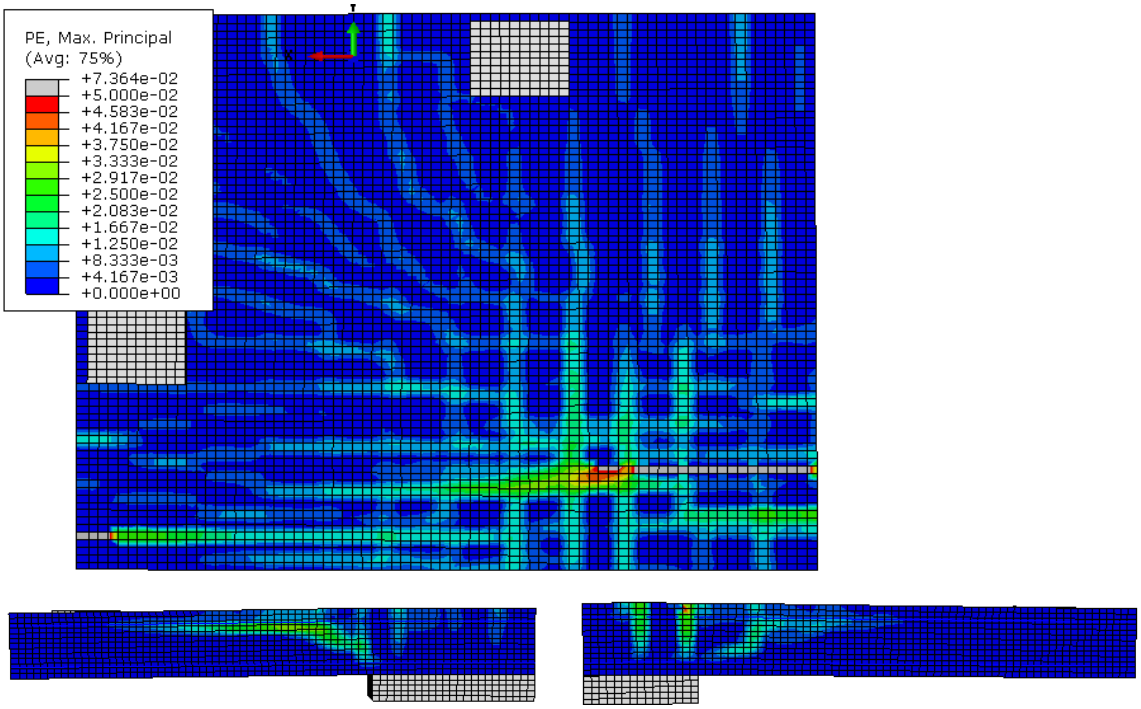

Figure F-75: β = 1.533 Crack Pattern, Bottom Left: Long Side, Bottom Right: Short Side

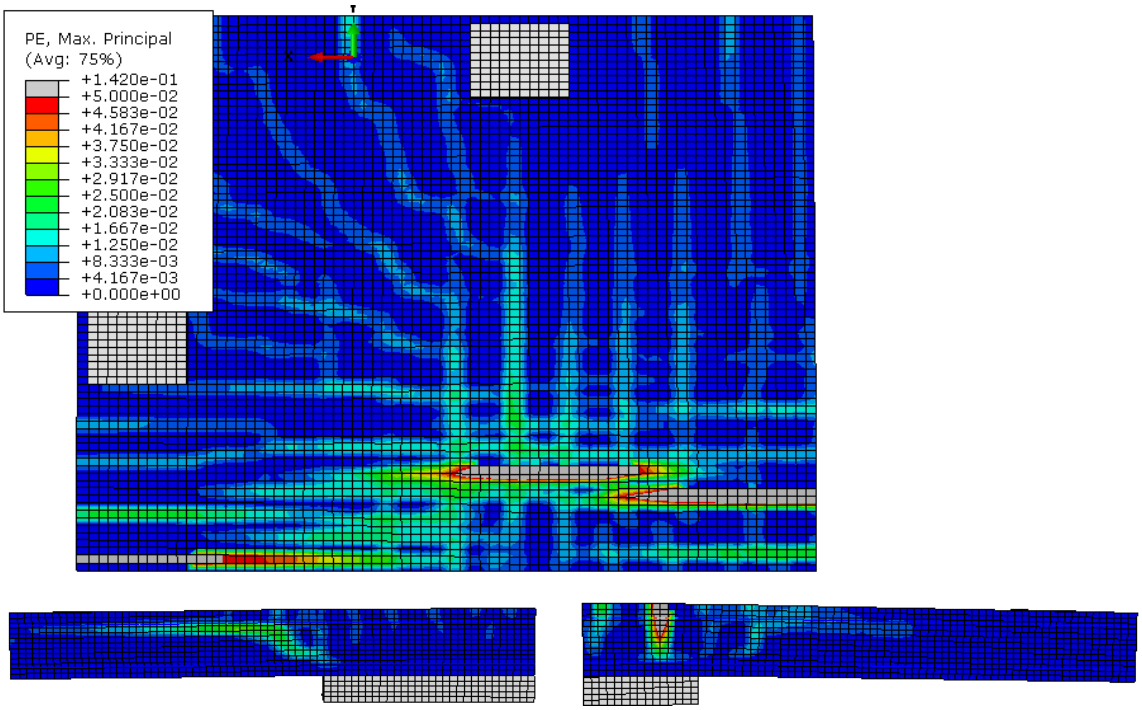

Figure F-76: β = 2 Crack Pattern, Bottom Left: Long Side, Bottom Right: Short Side

Appendix G
Additional Peak Load Shear Stress Distributions

In this appendix, additional shear stress distributions in the slab around the perimeter of the steel support plate and at the ACI critical perimeter at the peak load level predicted in each model not shown in Section 5.2 are provided.

As with the load-displacement plots for the three lowest c_{min}/d ratios (0.594, 0.792 and 0.990) the stress distributions provided in Section 5.2 at both the support plate and critical perimeter do not include the results for all the investigated models. Once again, these models were removed for clarity, but were considered in the discussed trends. The stress distributions for these remaining models are provided in this appendix.

Also provided in this appendix are the predicted stress distributions at the ACI critical perimeter for all eight c_{min}/d ratios. As discussed in Section 5.2.1, no clear trends were observed in the peak stress values around the ACI critical perimeter, but they are included for completeness.

$c_{min}/d = 0.594$

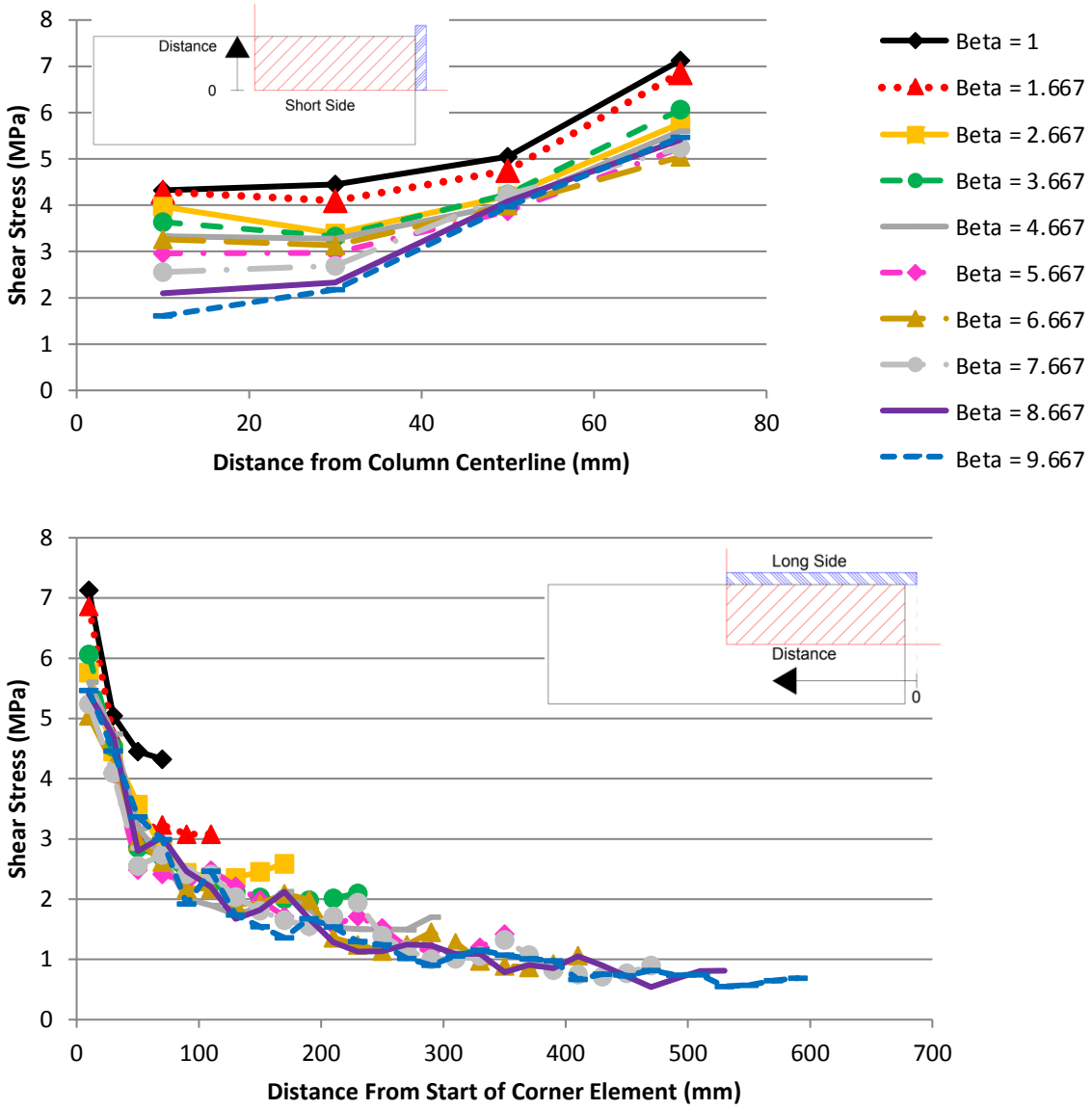

Figure G-1: Predicted Shear Stress Distribution Around Support Plate Perimeter, $c_{min}/d = 0.594$, Top) Stresses Along Short Side, Bottom) Stresses Along Long Side, Non-integer β

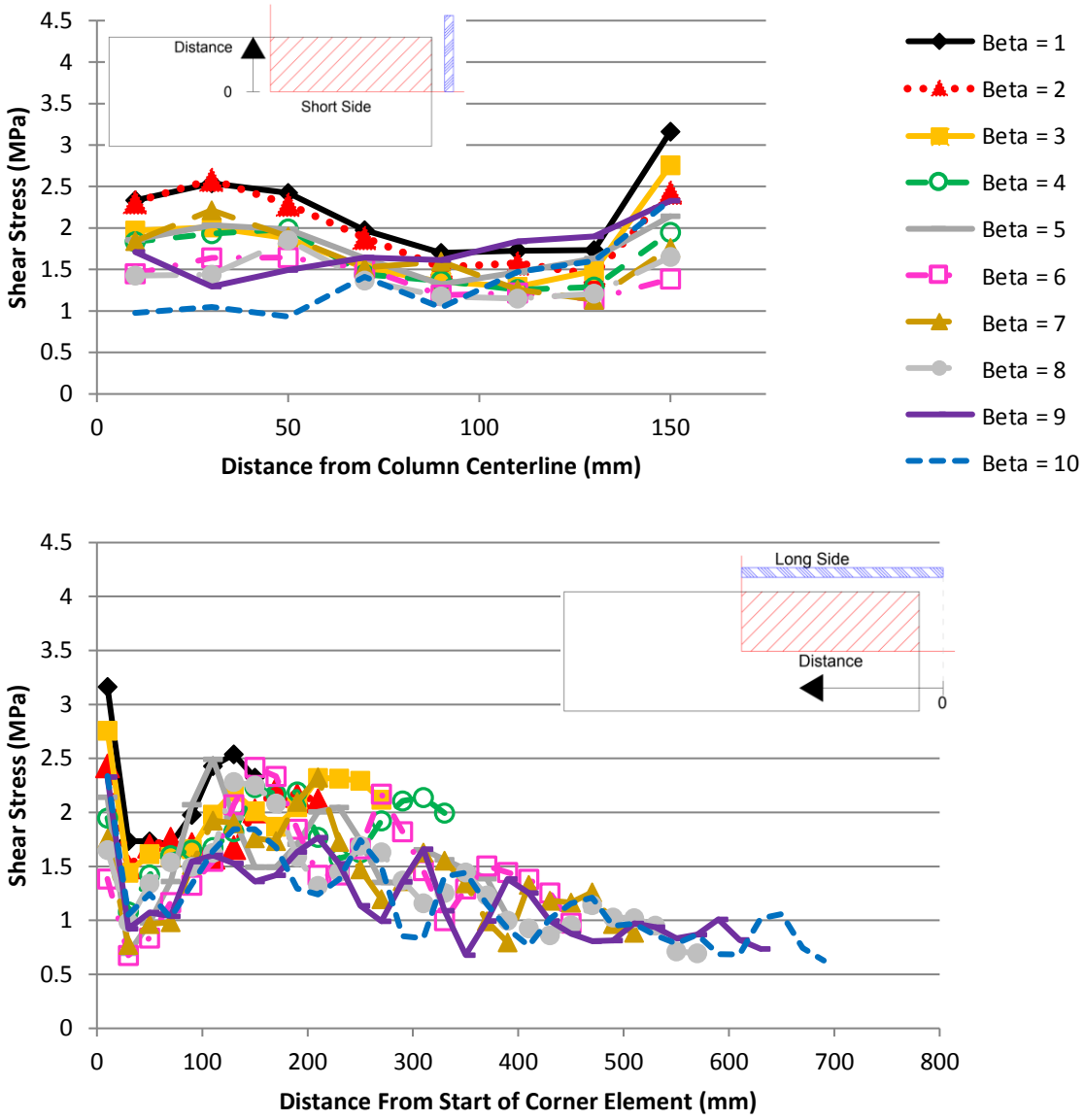

Figure G-2: Predicted Shear Stress Distribution Around ACI Critical Perimeter, $c_{min}/d = 0.594$, Top) Stresses Along Short Side, Bottom) Stresses Along Long Side, Integer β

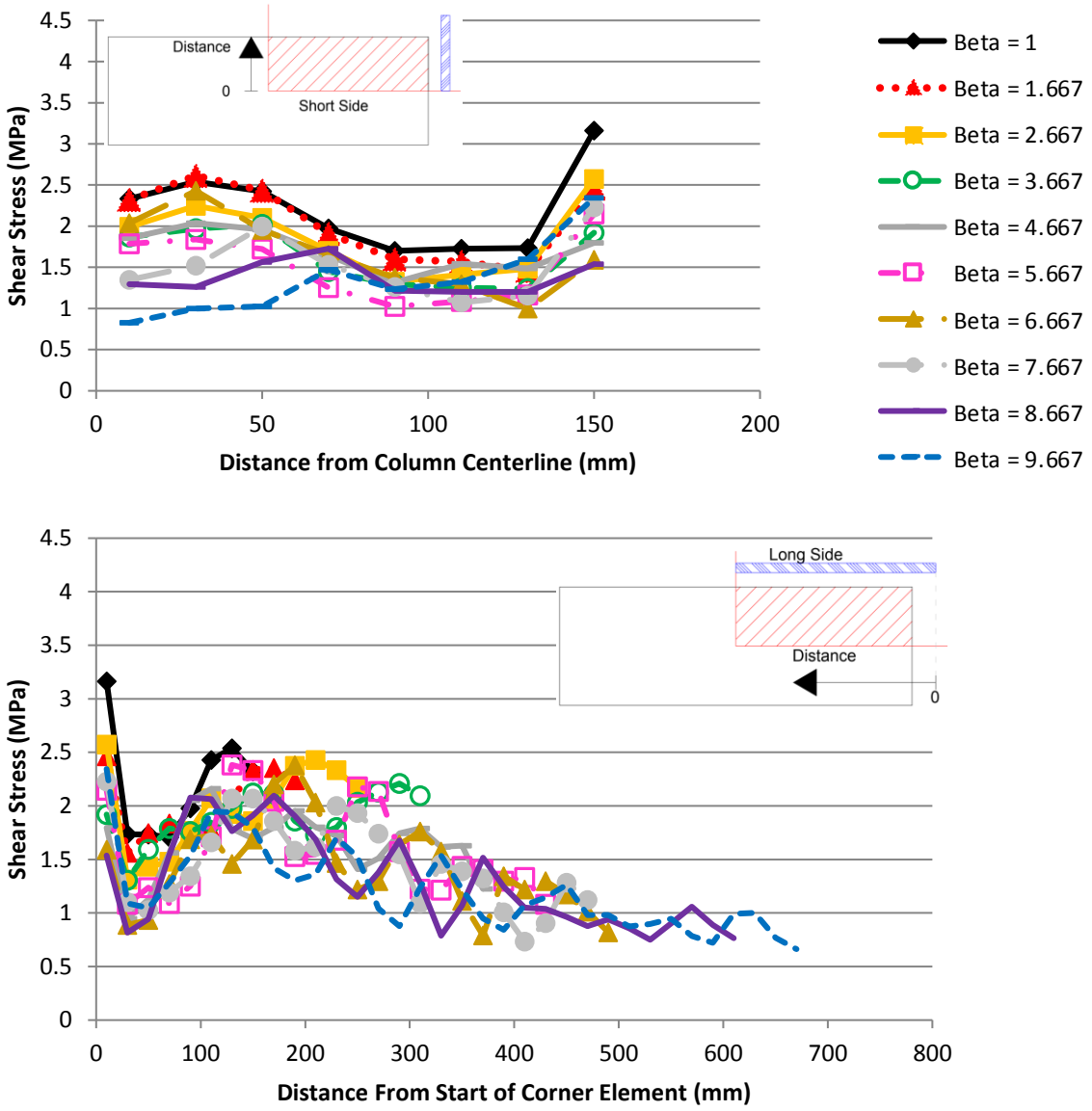

Figure G-3: Predicted Shear Stress Distribution Around ACI Critical Perimeter, $c_{min}/d = 0.594$, Top) Stresses Along Short Side, Bottom) Stresses Along Long Side, Non-Integer β

$c_{min}/d = 0.792$

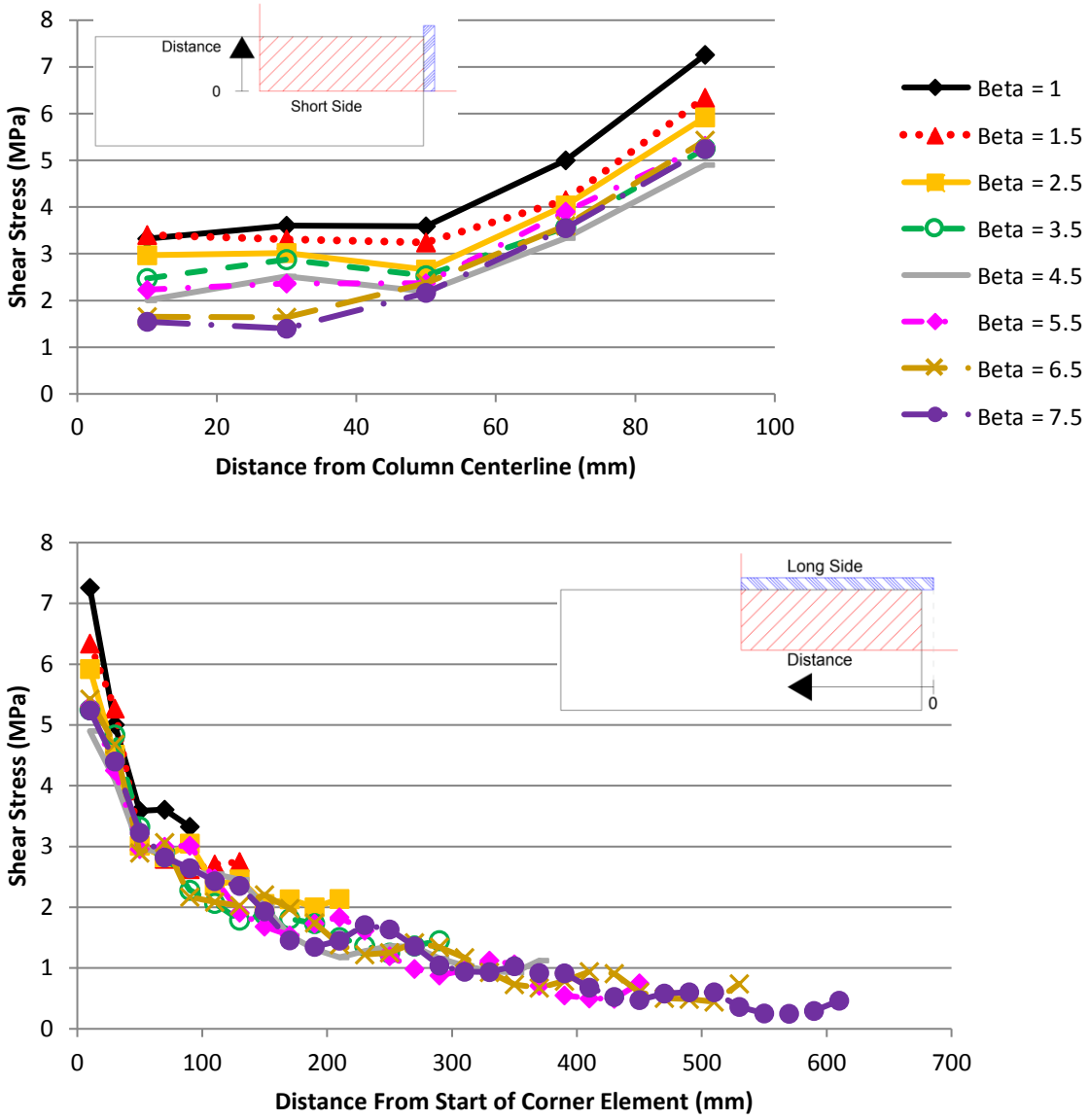

Figure G-4: Predicted Shear Stress Distribution Around Support Plate Perimeter, $c_{min}/d = 0.792$, Top) Stresses Along Short Side, Bottom) Stresses Along Long Side, Non-integer β

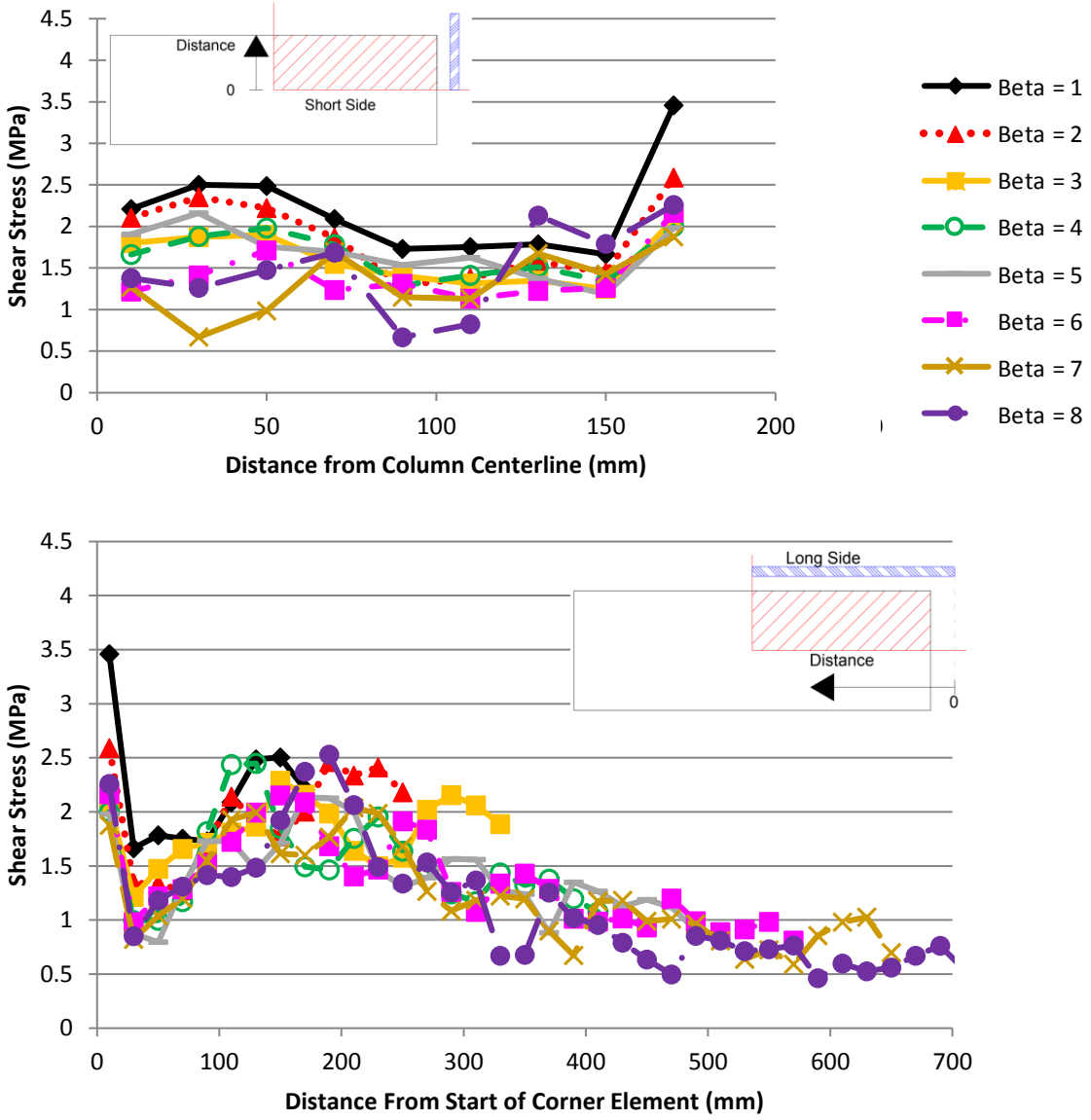

Figure G-5: Predicted Shear Stress Distribution Around ACI Critical Perimeter, $c_{min}/d = 0.792$, Top) Stresses Along Short Side, Bottom) Stresses Along Long Side, Integer β

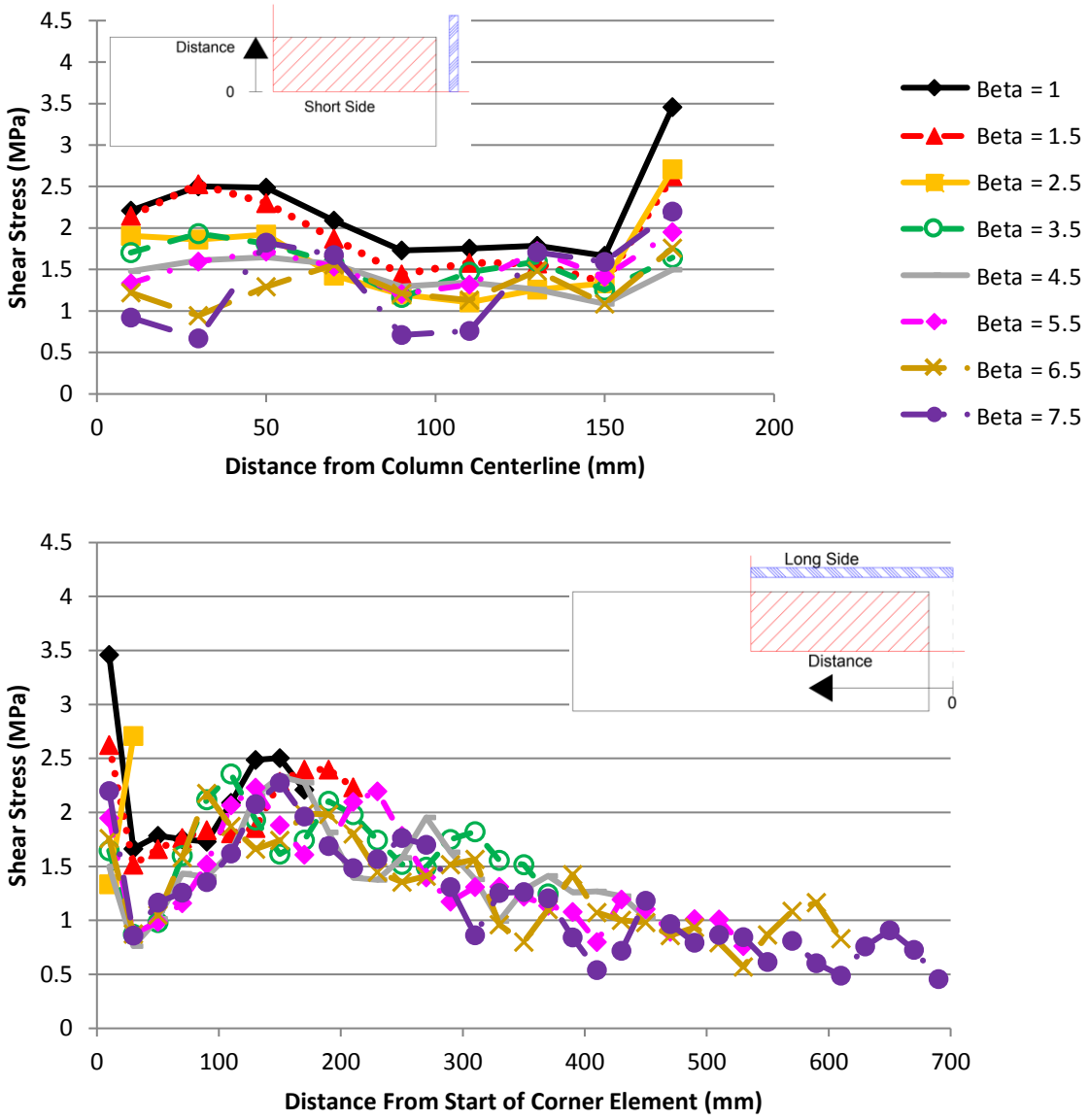

Figure G-6: Predicted Shear Stress Distribution Around ACI Critical Perimeter, $c_{min}/d = 0.792$, Top) Stresses Along Short Side, Bottom) Stresses Along Long Side, Non-Integer β

$c_{min}/d = 0.990$

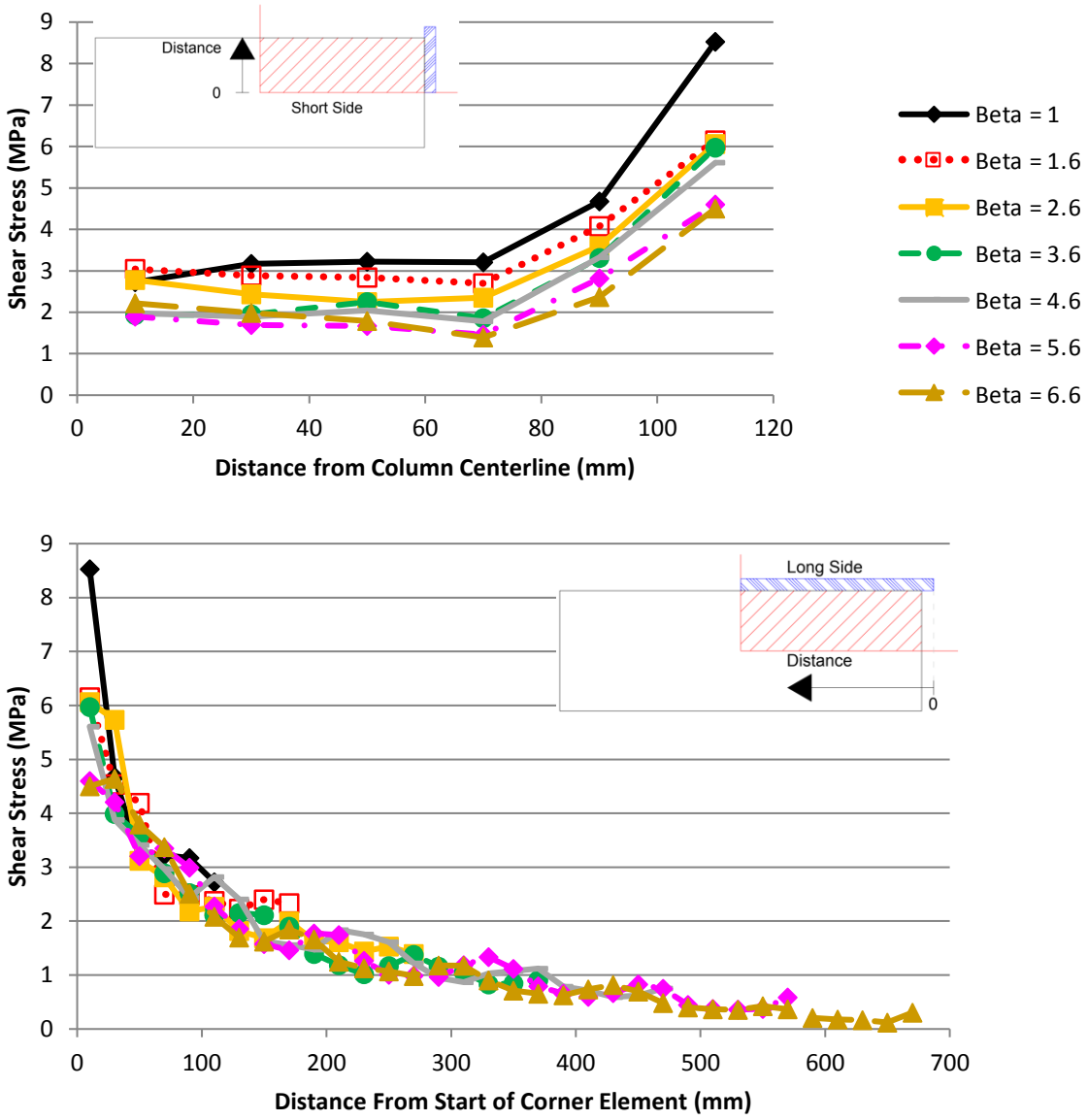

Figure G-7: Predicted Shear Stress Distribution Around Support Plate Perimeter, $c_{min}/d = 0.990$, Top) Stresses Along Short Side, Bottom) Stresses Along Long Side, Non-integer β

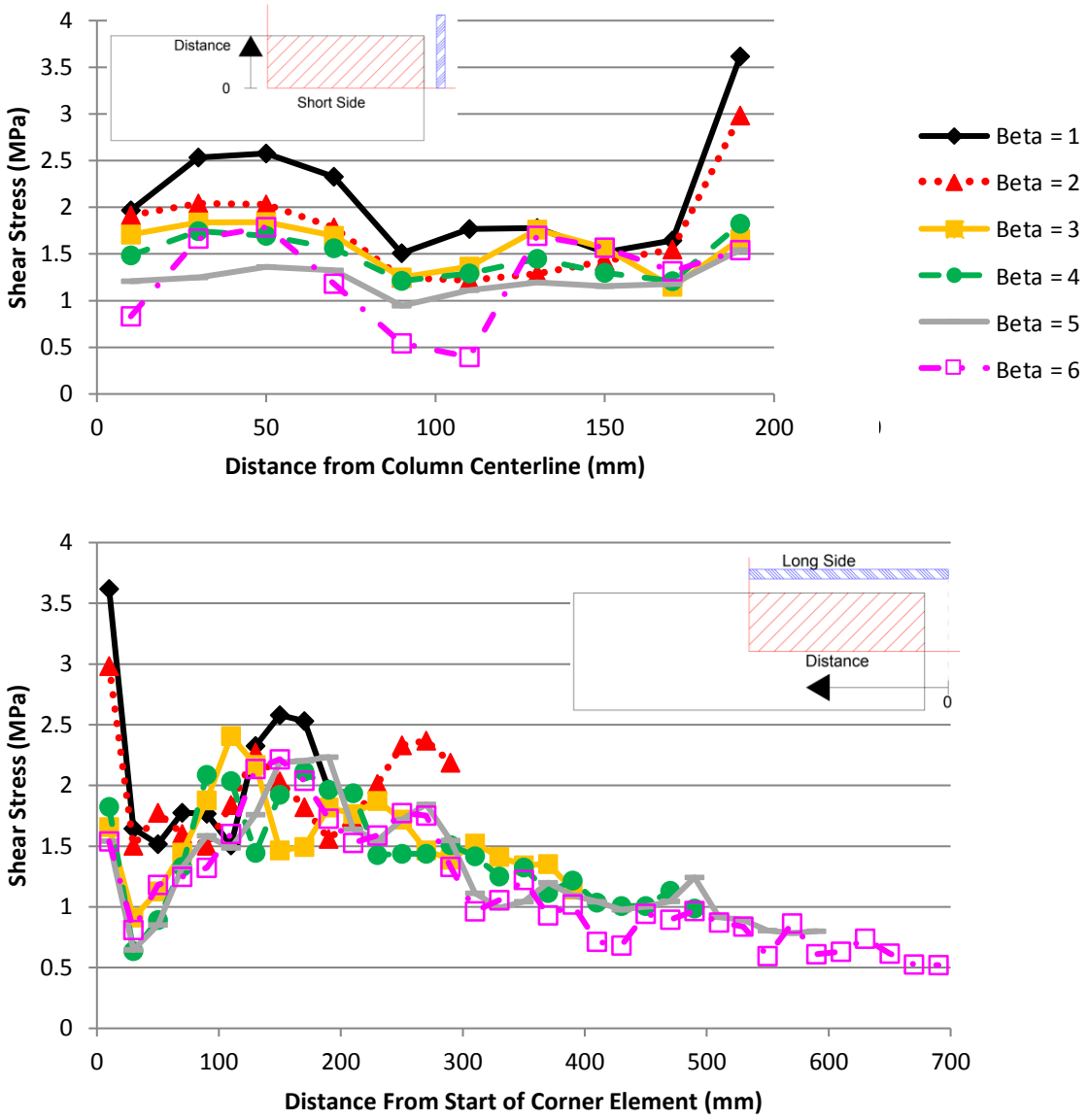

Figure G-8: Predicted Shear Stress Distribution Around ACI Critical Perimeter, $c_{min}/d = 0.990$, Top) Stresses Along Short Side, Bottom) Stresses Along Long Side, Integer β

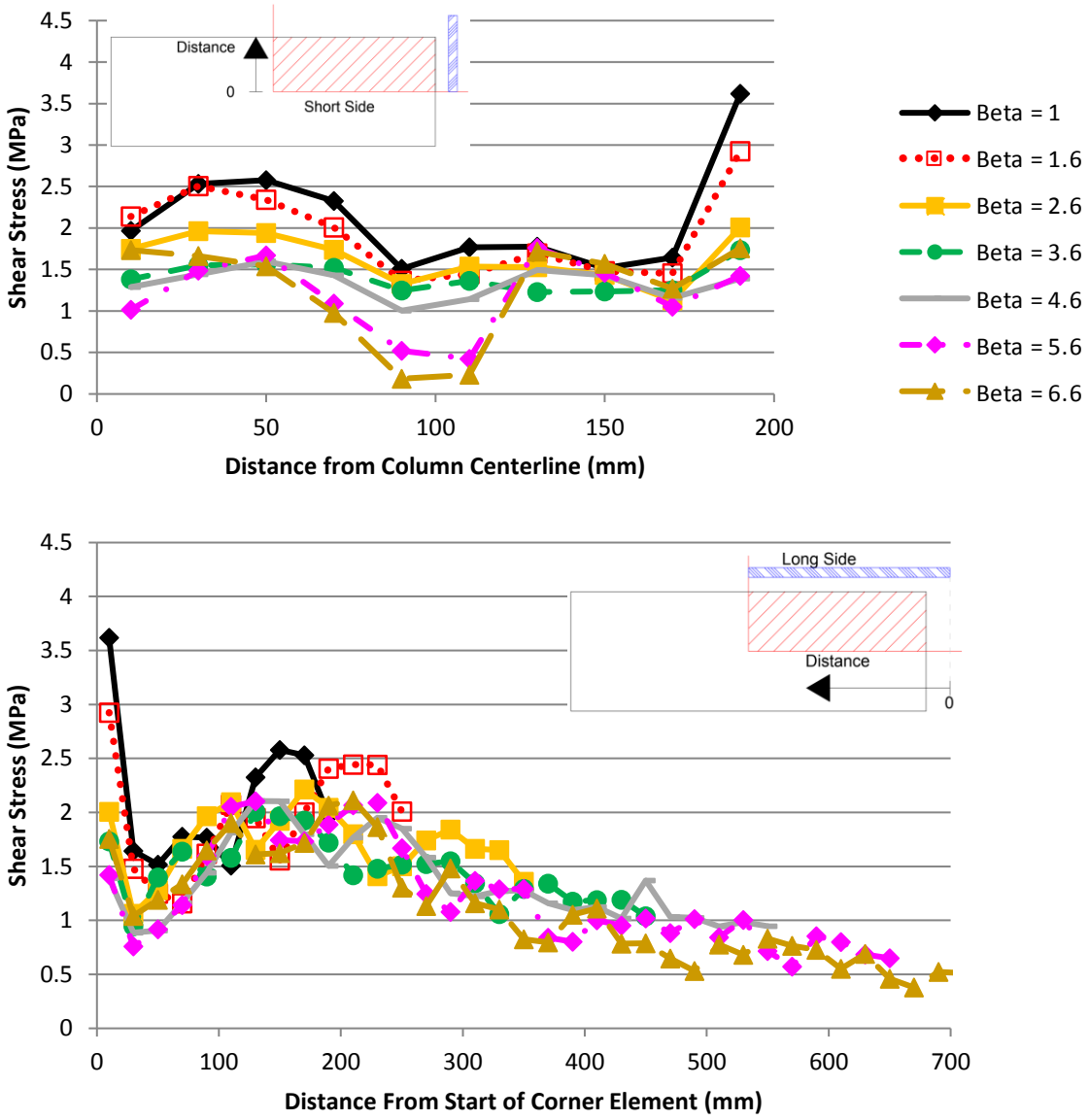

Figure G-9: Predicted Shear Stress Distribution Around ACI Critical Perimeter, $c_{min}/d = 0.990$, Top) Stresses Along Short Side, Bottom) Stresses Along Long Side, Non-Integer β

$c_{min}/d = 1.287$

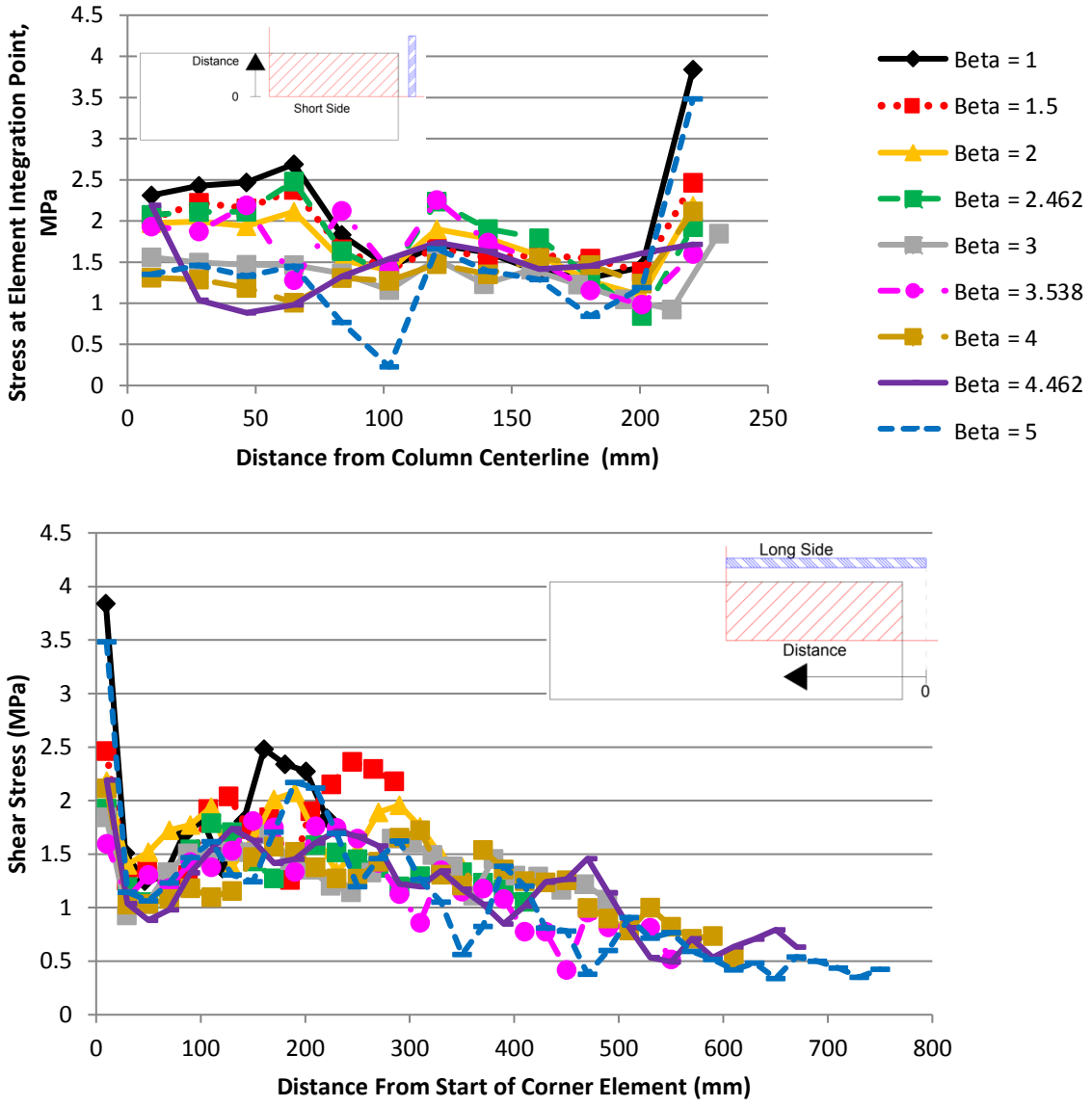

Figure G-10: Predicted Shear Stress Distribution Around ACI Critical Perimeter, $c_{min}/d = 1.287$, Top) Stresses Along Short Side, Bottom) Stresses Along Long Side

$c_{min}/d = 1.485$

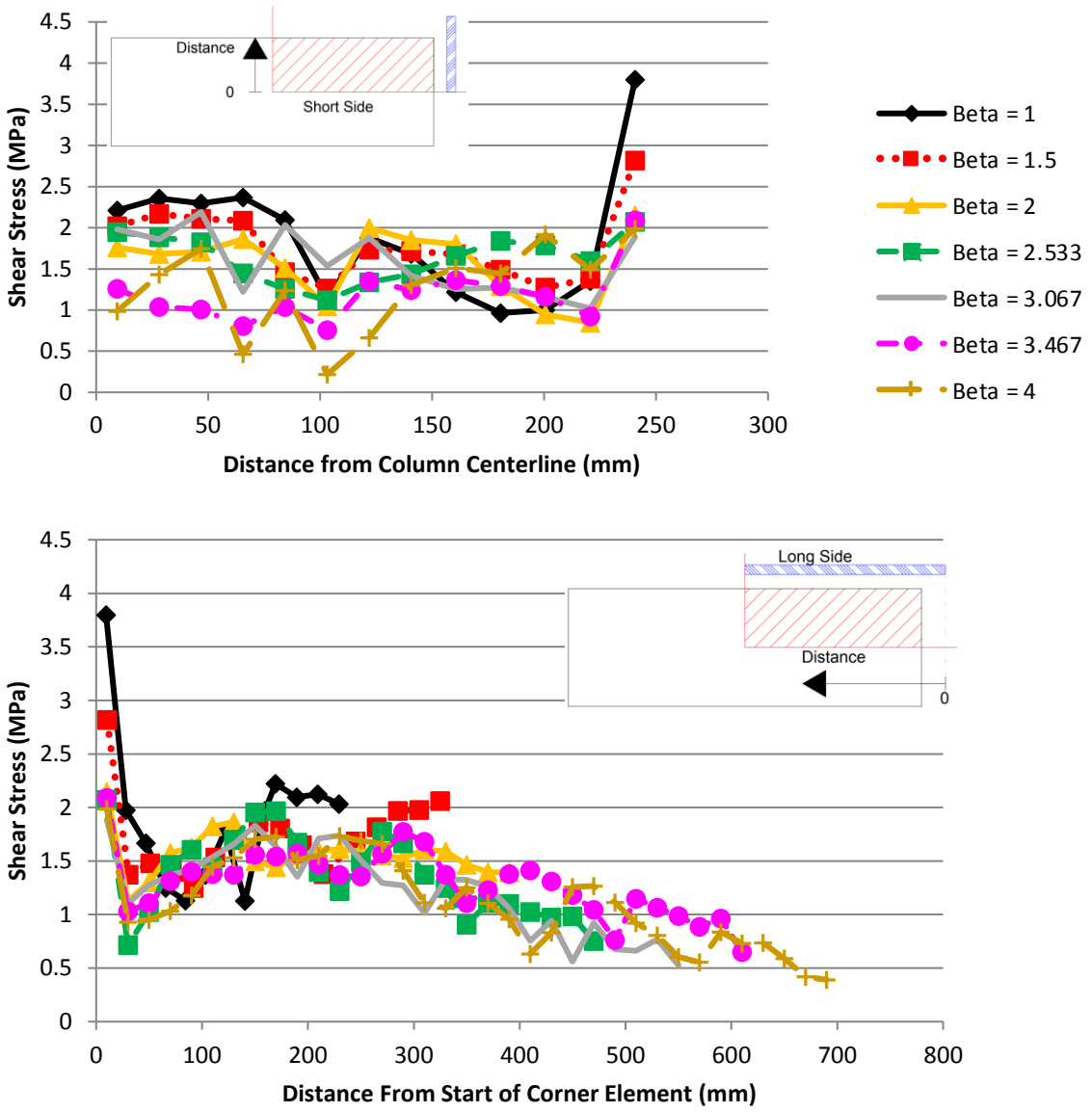

Figure G-11: Predicted Shear Stress Distribution Around ACI Critical Perimeter, $c_{min}/d = 1.485$, Top) Stresses Along Short Side, Bottom) Stresses Along Long Side

$c_{min}/d = 1.782$

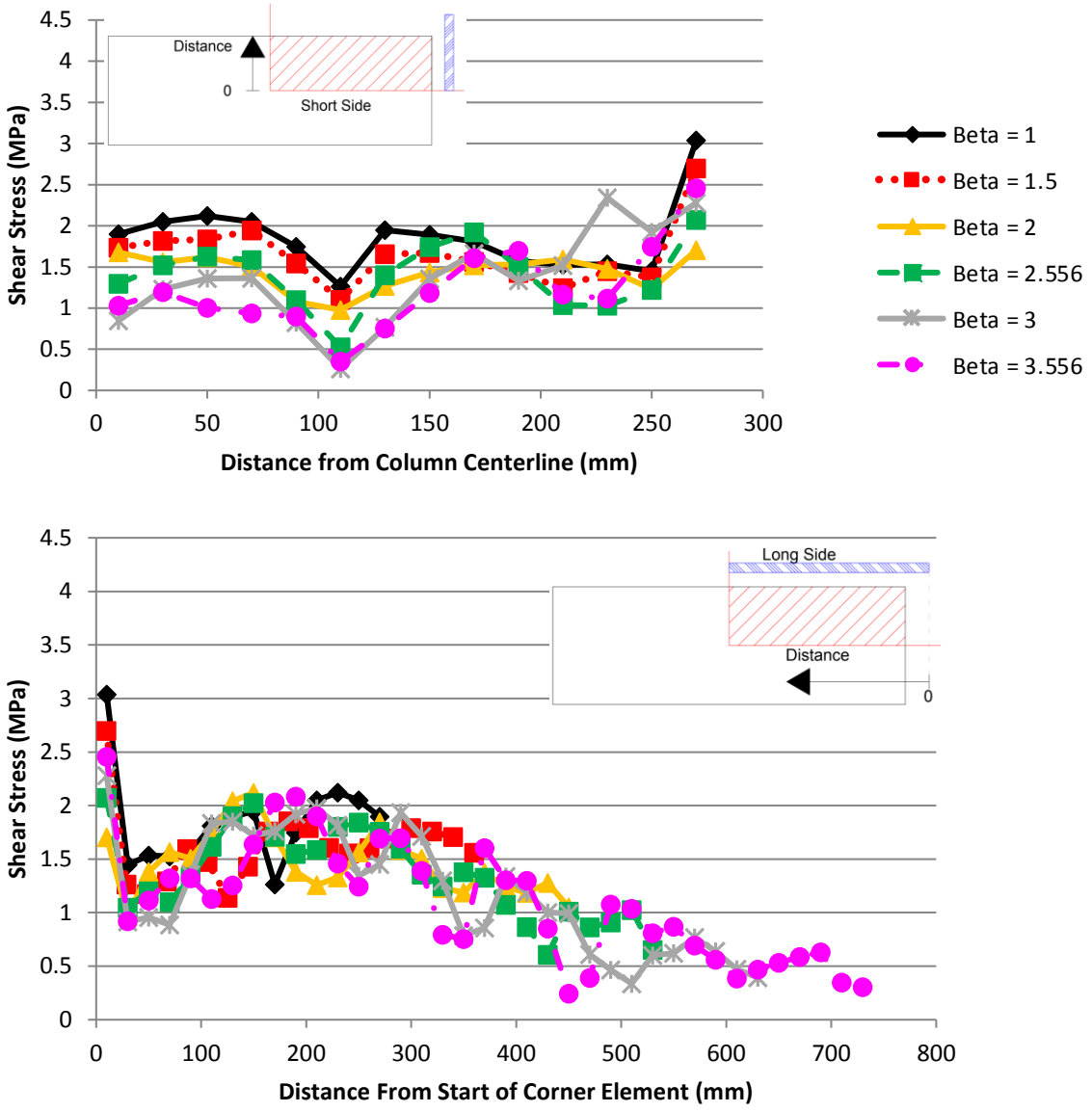

Figure G-12: Predicted Shear Stress Distribution Around ACI Critical Perimeter, $c_{min}/d = 1.782$, Top) Stresses Along Short Side, Bottom) Stresses Along Long Side

c_{min}/d = 1.980

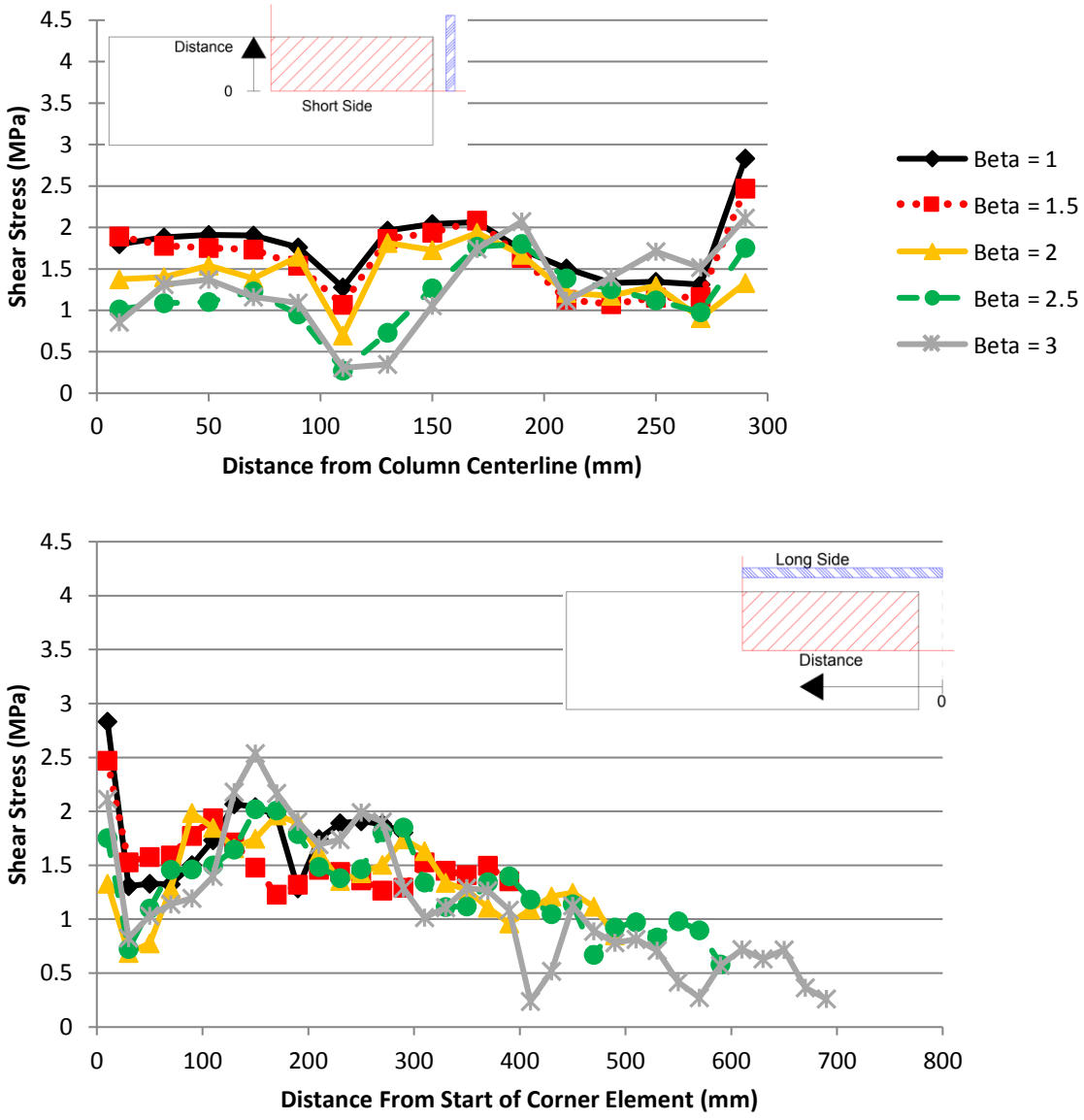

Figure G-13: Predicted Shear Stress Distribution Around ACI Critical Perimeter, c_{min}/d = 1.980, Top) Stresses Along Short Side, Bottom) Stresses Along Long Side

$c_{min}/d = 2.970$

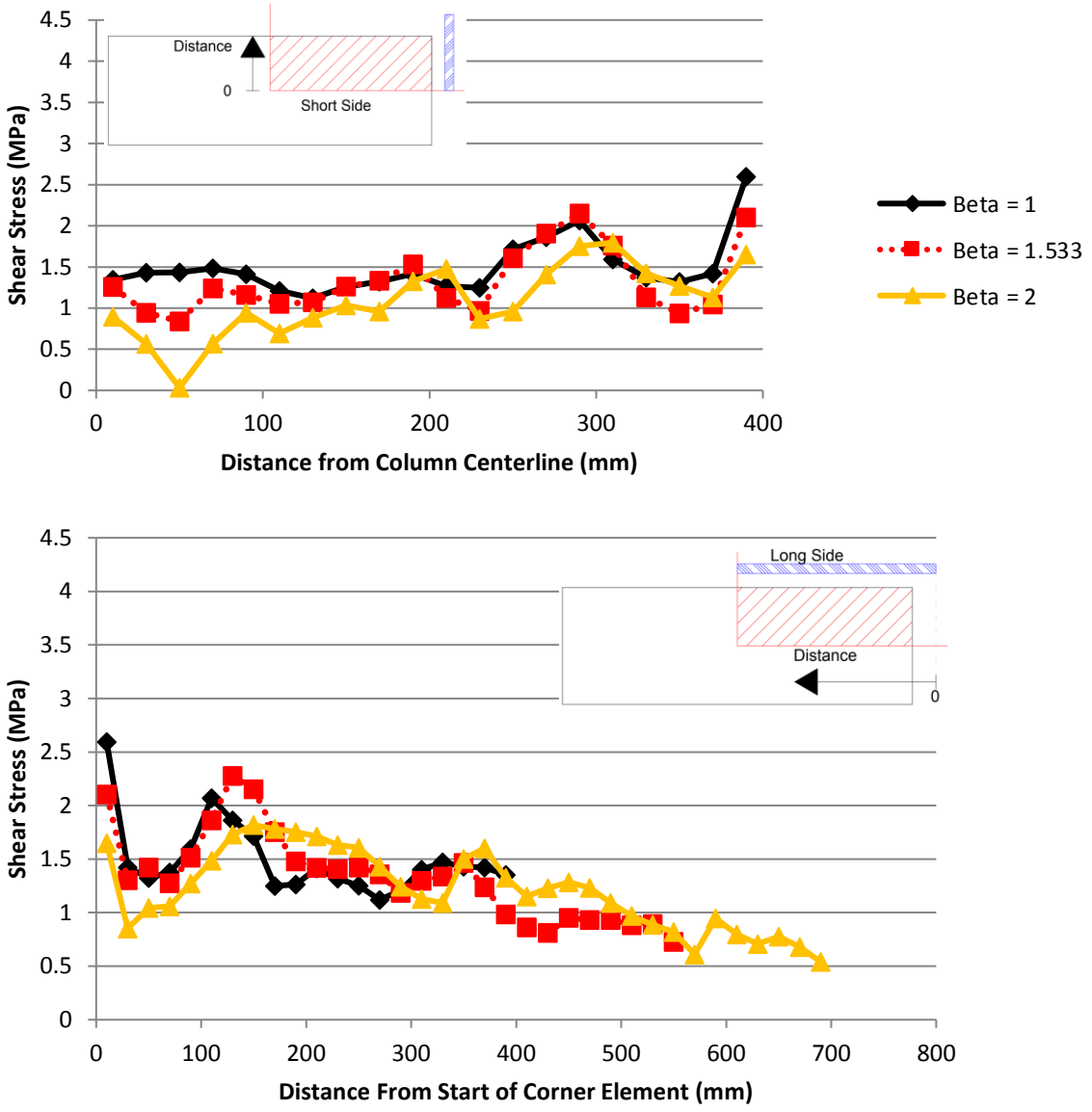

Figure G-14: Predicted Shear Stress Distribution Around ACI Critical Perimeter, $c_{min}/d = 2.970$, Top) Stresses Along Short Side, Bottom) Stresses Along Long Side

Appendix H

Shear Stress Distributions – 30% and 90% of Peak Load

As discussed in Section 5.3.2.1, the shape of the predicted shear stress distribution in the slab around the support plate perimeter was found to change throughout the analysis. In this appendix, the shear stress distributions around the support plate perimeter at 30% and 90% of the peak load for each model are provided for each c_{min}/d ratio.

$c_{min}/d = 0.594$

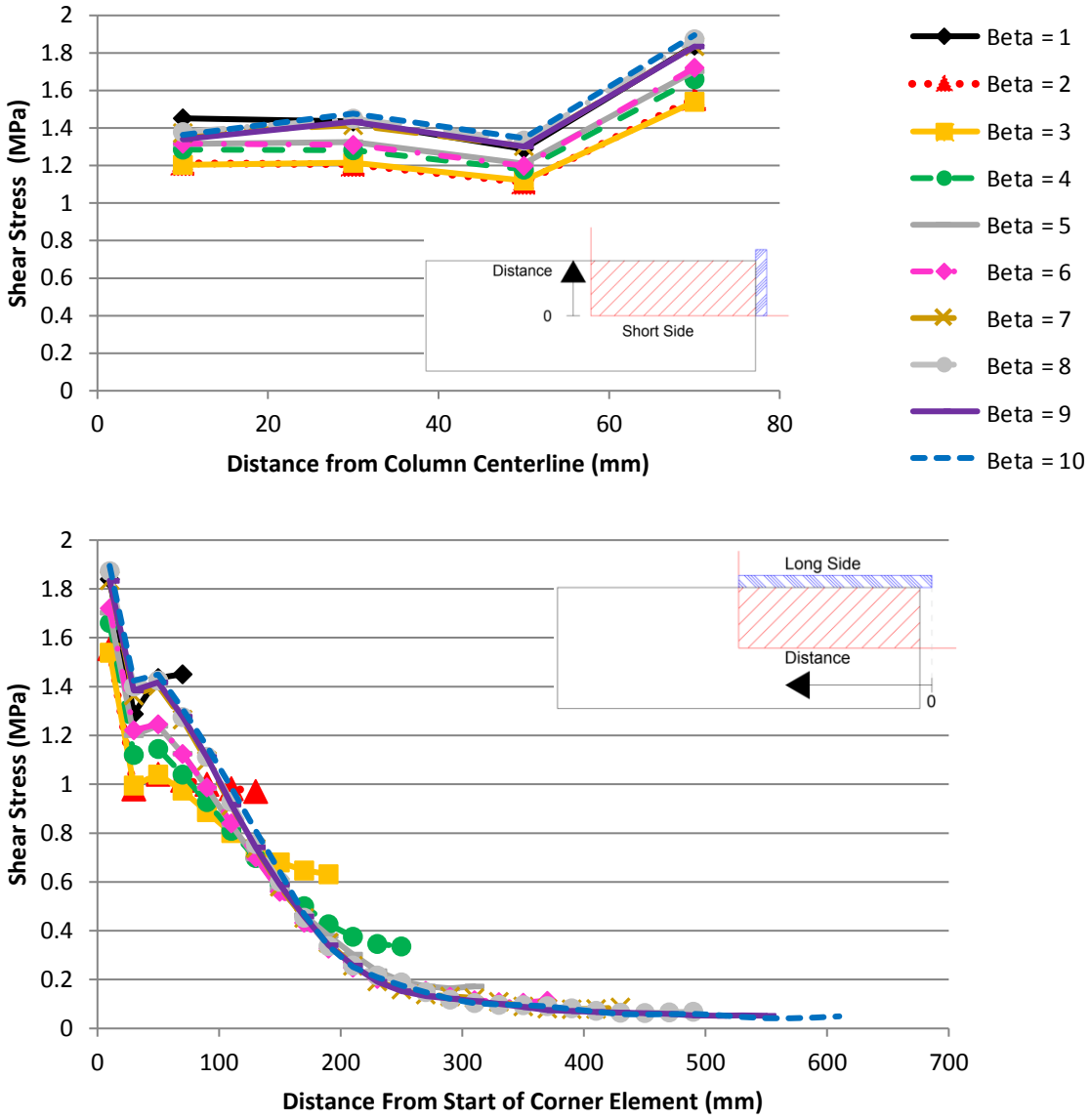

Figure H-1: Predicted Shear Stress Distribution Around Support Plate Perimeter, $c_{min}/d = 0.594$, Top) Stresses Along Short Side, Bottom) Stresses Along Long Side, Integer β, 30% of Peak Load

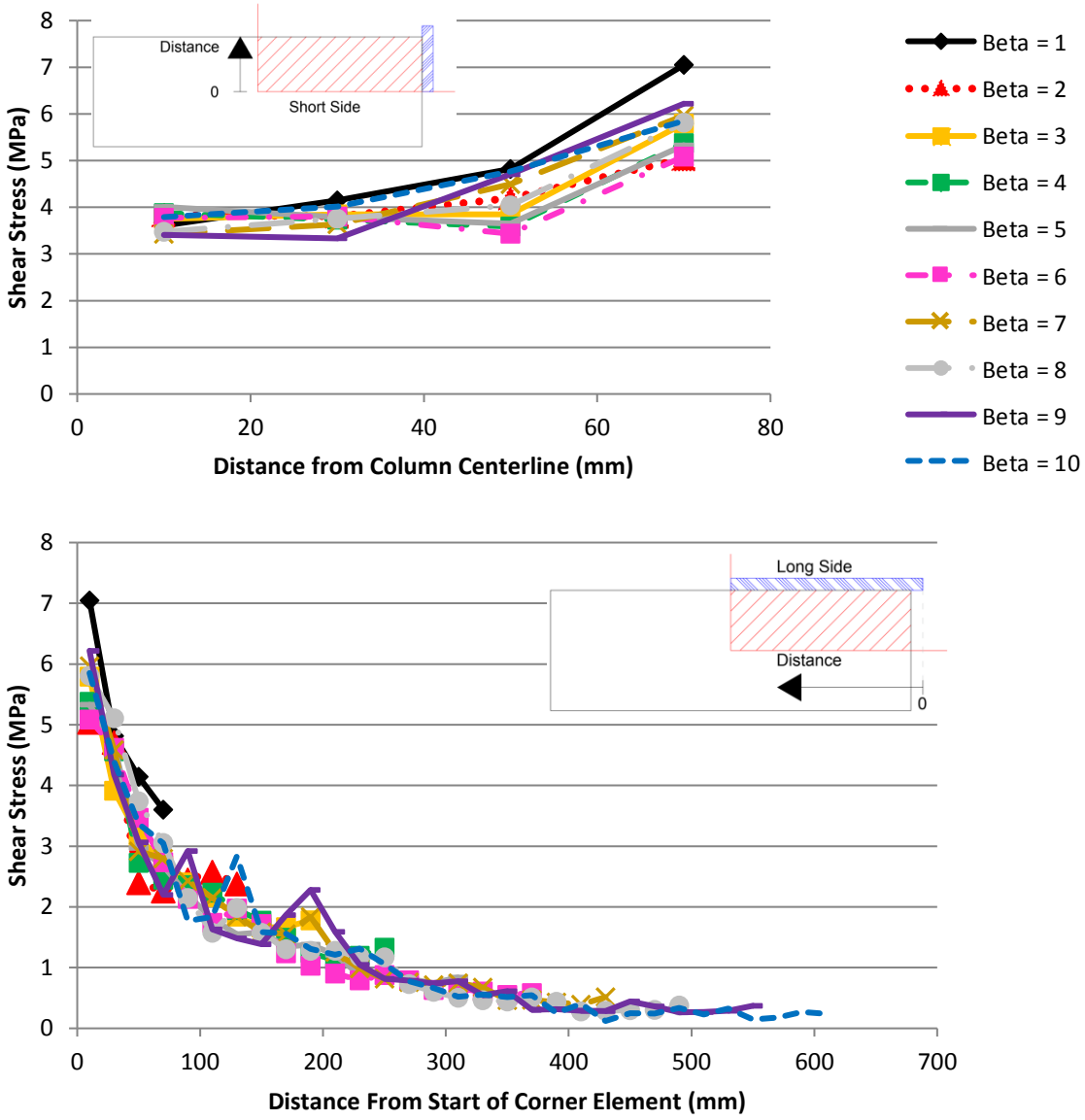

Figure H-2: Predicted Shear Stress Distribution Around Support Plate Perimeter, $c_{min}/d = 0.594$, Top) Stresses Along Short Side, Bottom) Stresses Along Long Side, Integer β, 90% of Peak Load

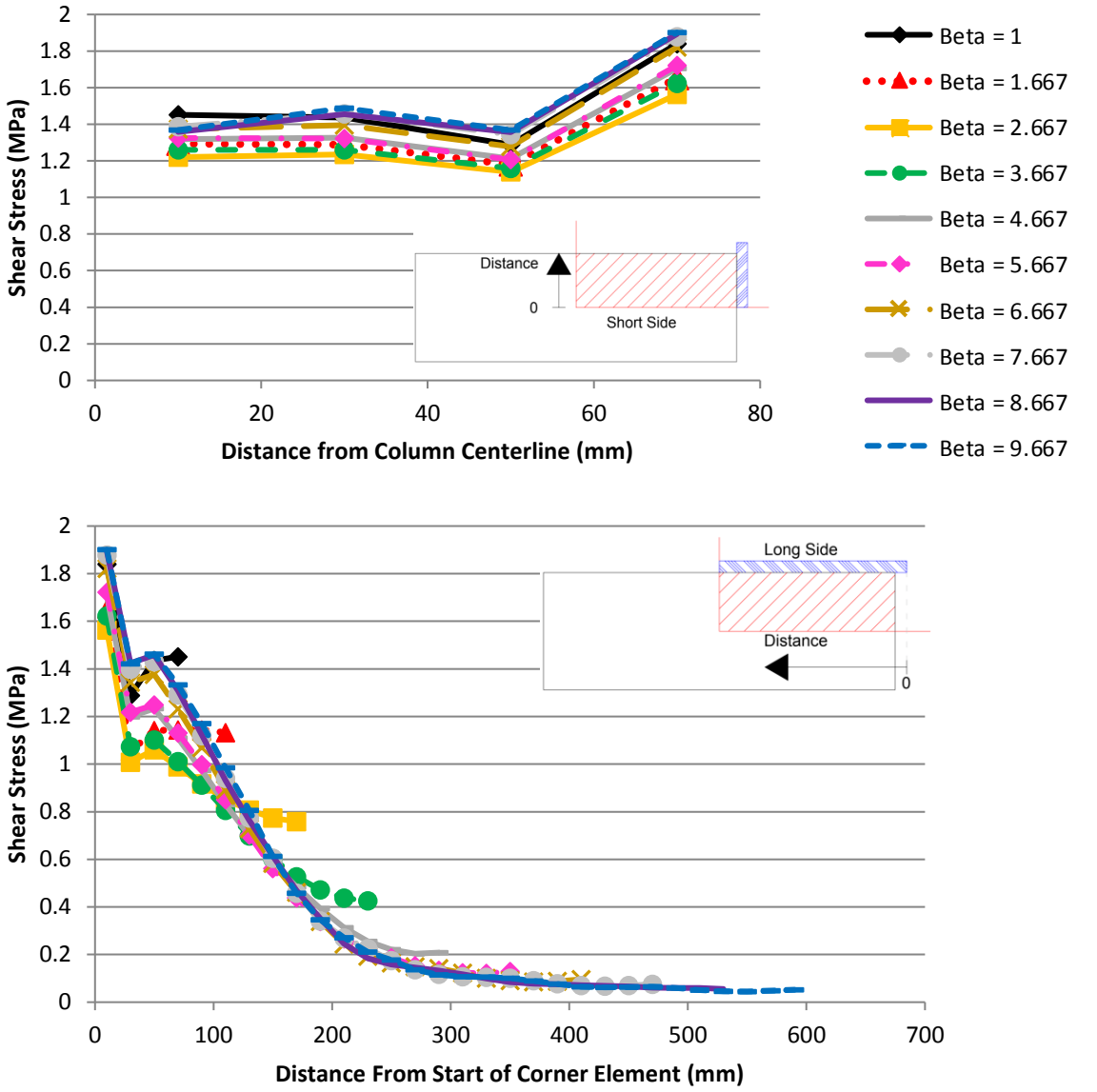

Figure H-3: Predicted Shear Stress Distribution Around Support Plate Perimeter, $c_{min}/d = 0.594$, Top) Stresses Along Short Side, Bottom) Stresses Along Long Side, Non-integer β, 30% of Peak Load

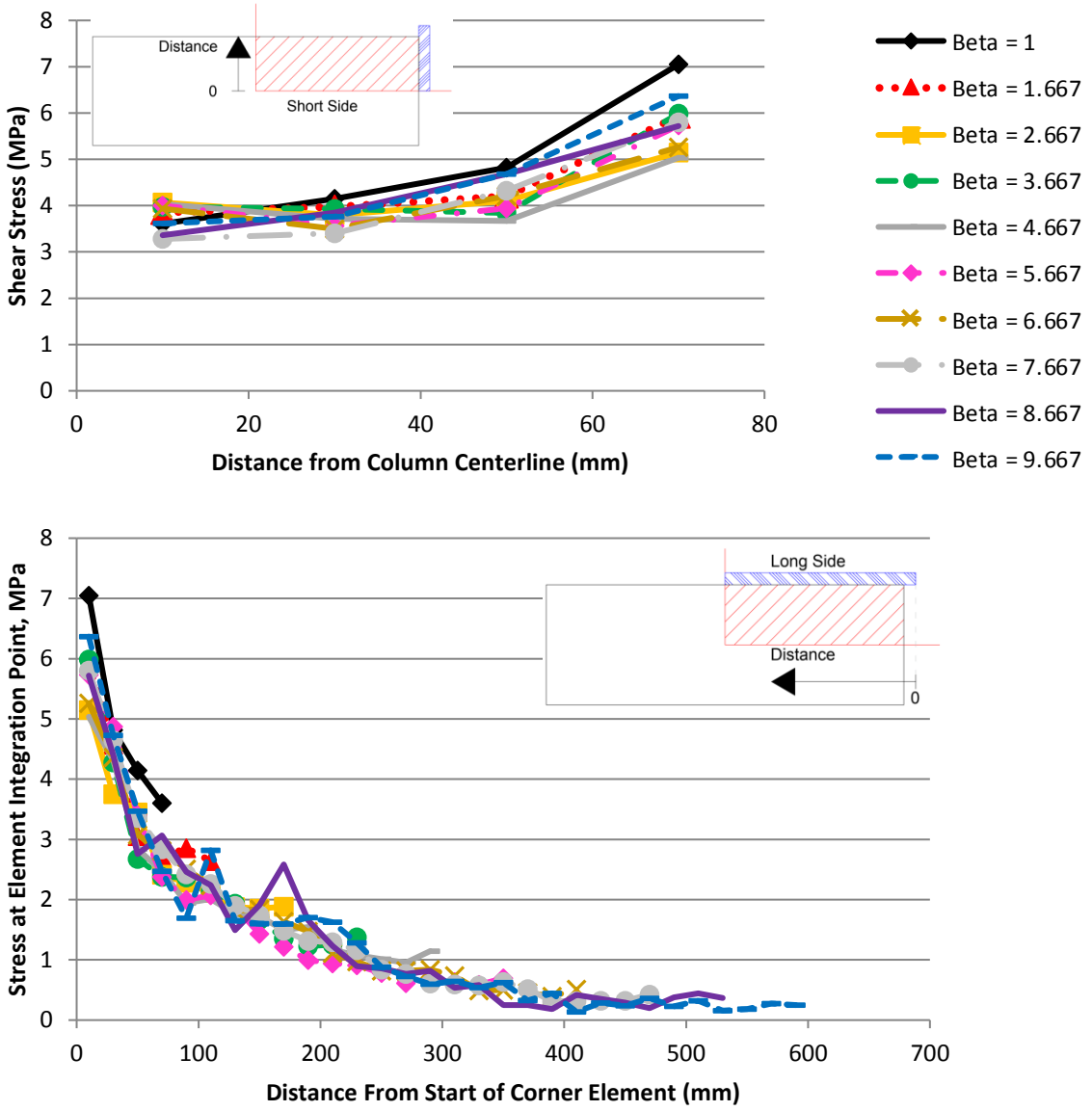

Figure H-4: Predicted Shear Stress Distribution Around Support Plate Perimeter, $c_{min}/d = 0.594$, Top) Stresses Along Short Side, Bottom) Stresses Along Long Side, Non-integer β, 90% of Peak Load

$c_{min}/d = 0.792$

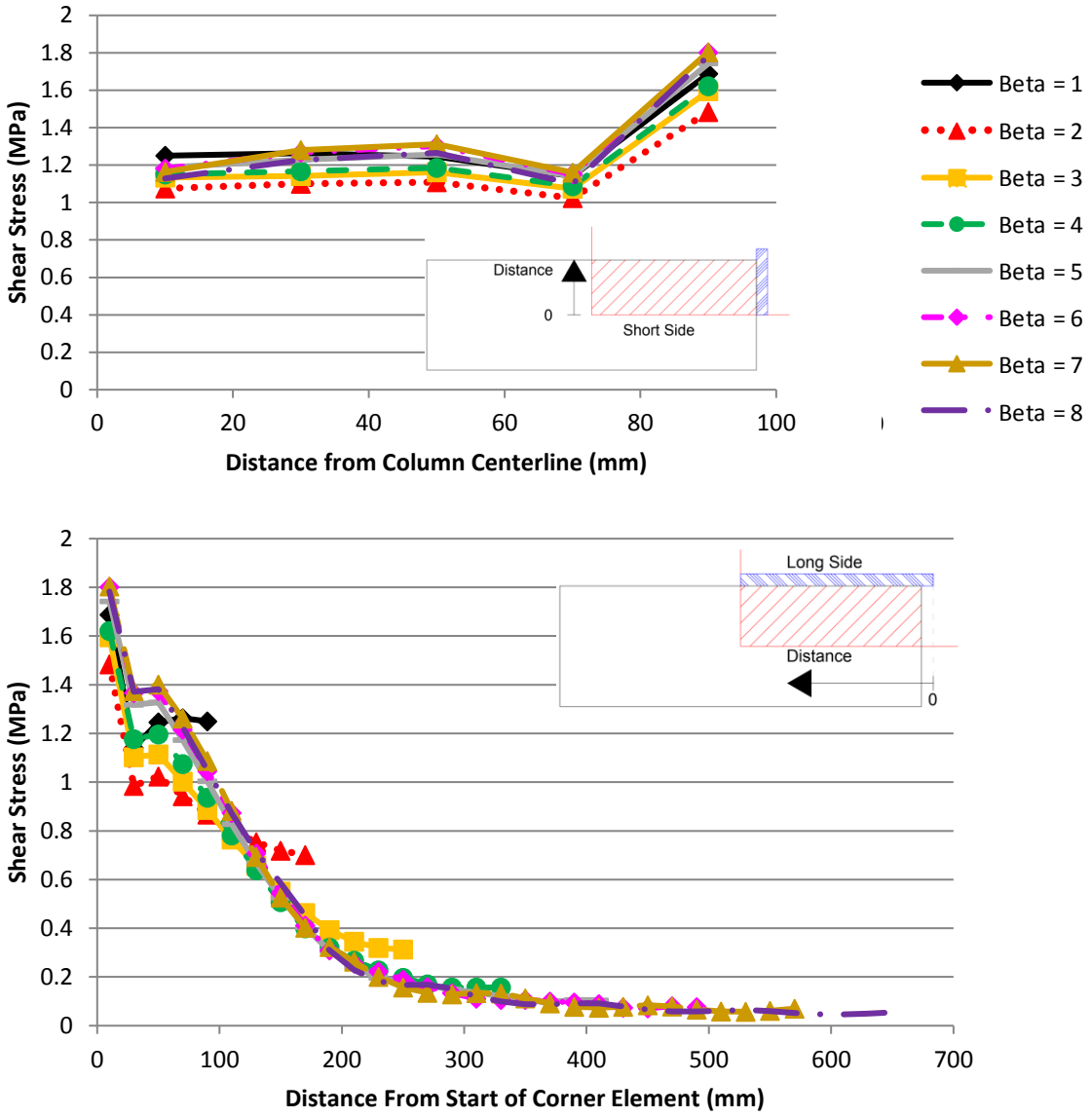

Figure H-5: Predicted Shear Stress Distribution Around Support Plate Perimeter, $c_{min}/d = 0.792$, Top) Stresses Along Short Side, Bottom) Stresses Along Long Side, Integer β, 30% of Peak Load

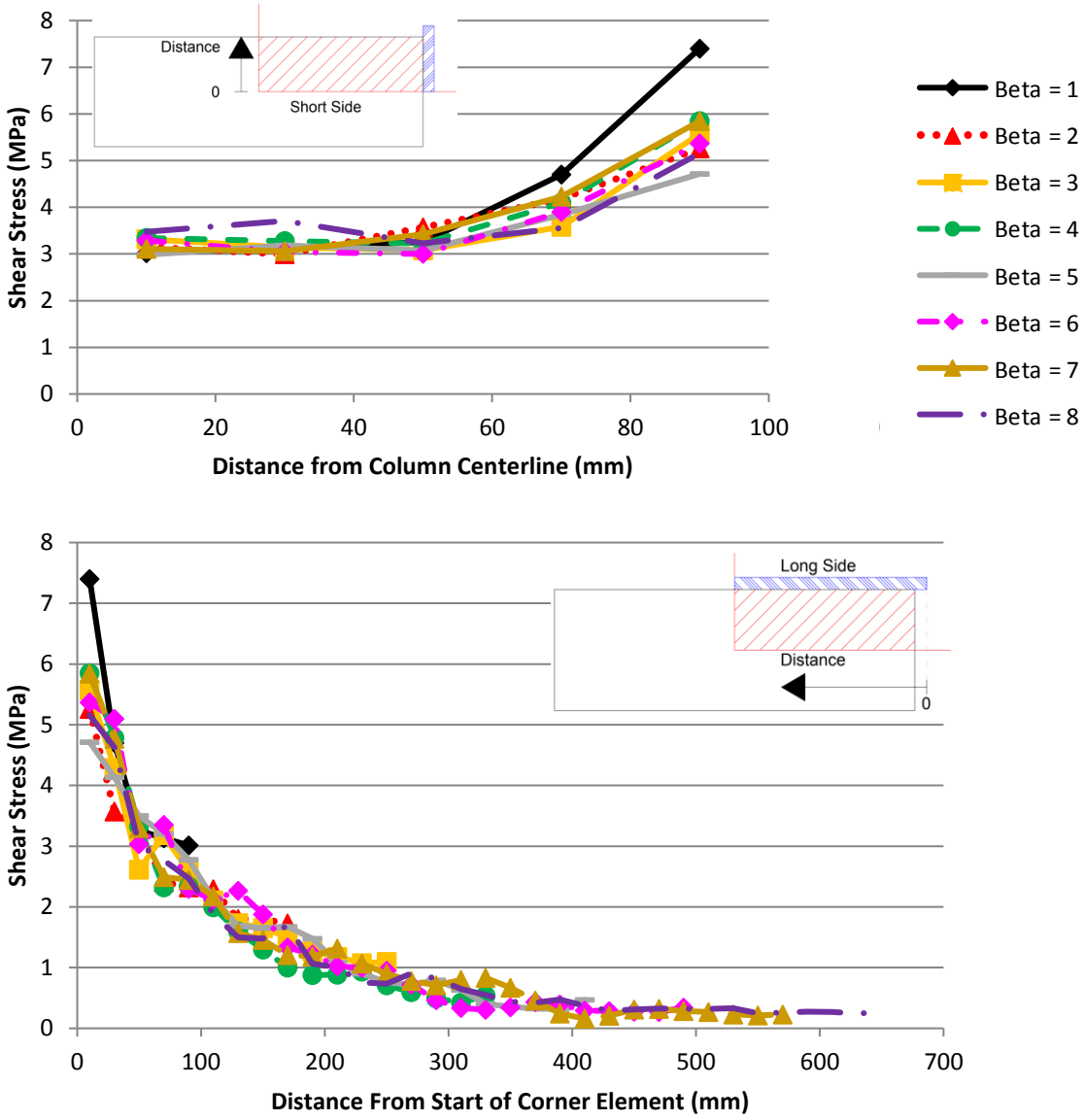

Figure H-6: Predicted Shear Stress Distribution Around Support Plate Perimeter, $c_{min}/d = 0.792$, Top) Stresses Along Short Side, Bottom) Stresses Along Long Side, Integer β, 90% of Peak Load

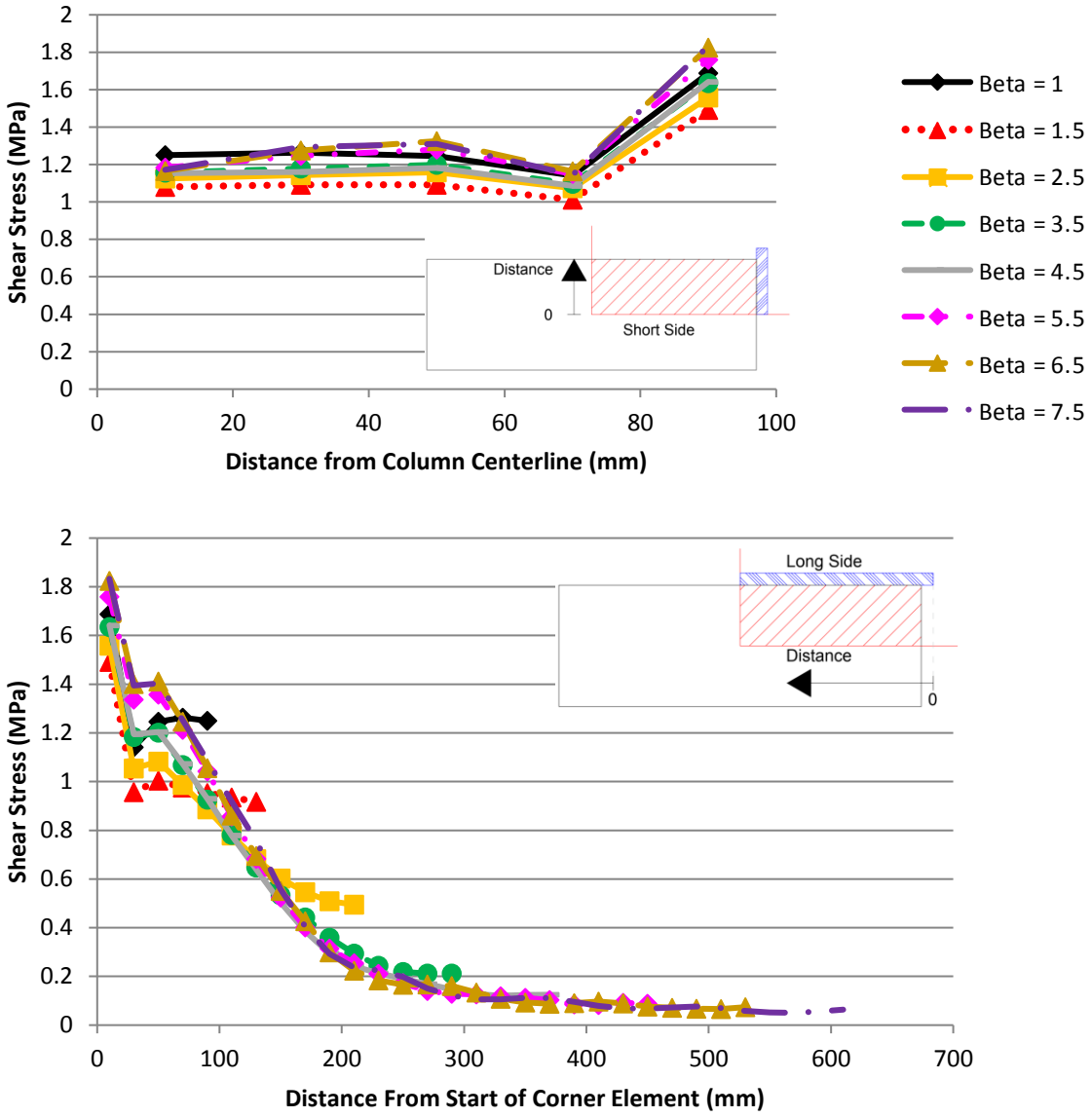

Figure H-7: Predicted Shear Stress Distribution Around Support Plate Perimeter, $c_{min}/d = 0.792$, Top) Stresses Along Short Side, Bottom) Stresses Along Long Side, Non-integer β, 30% of Peak Load

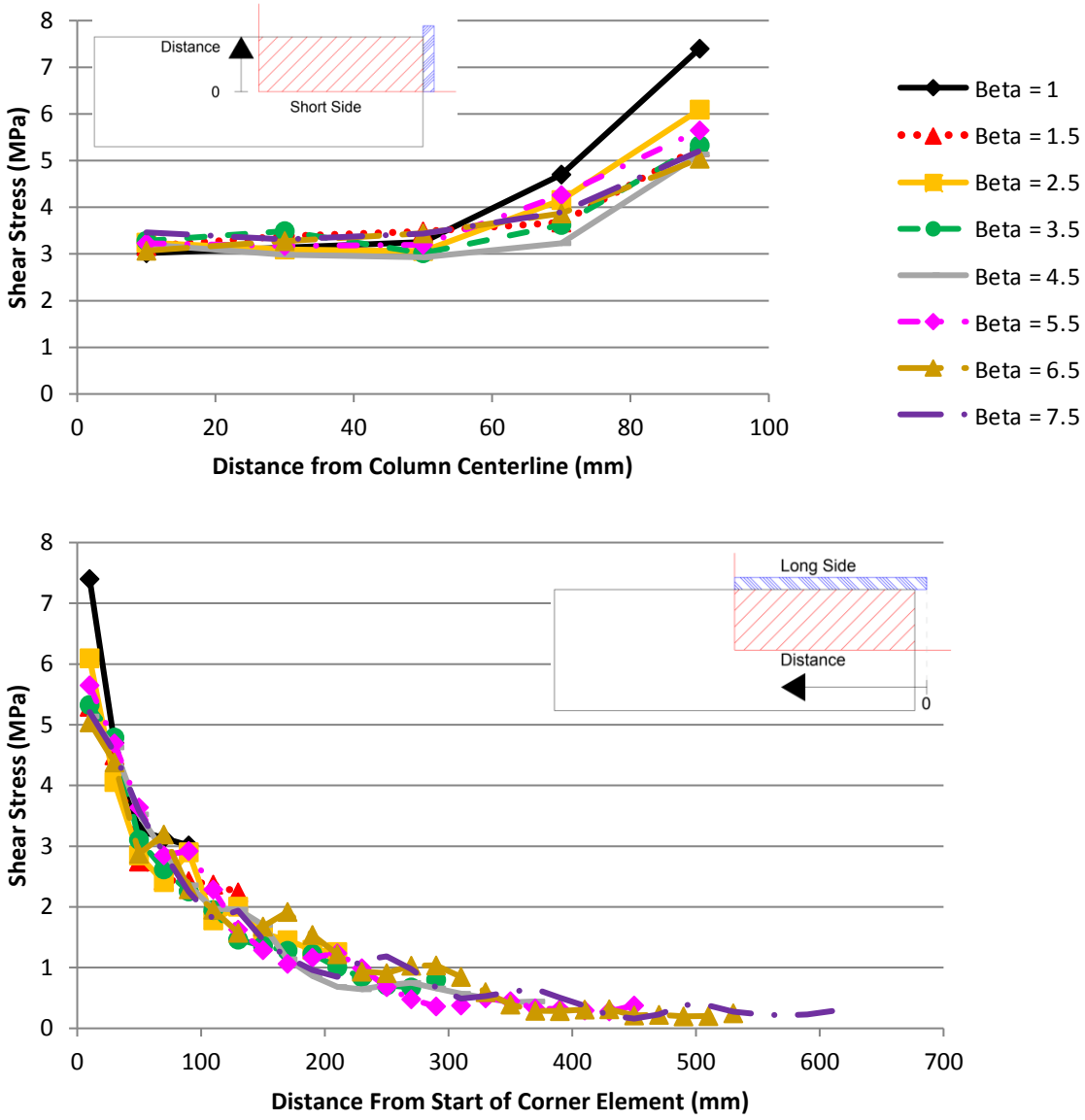

Figure H-8: Predicted Shear Stress Distribution Around Support Plate Perimeter, $c_{min}/d = 0.792$, Top) Stresses Along Short Side, Bottom) Stresses Along Long Side, Non-integer β, 90% of Peak Load

$c_{min}/d = 0.990$

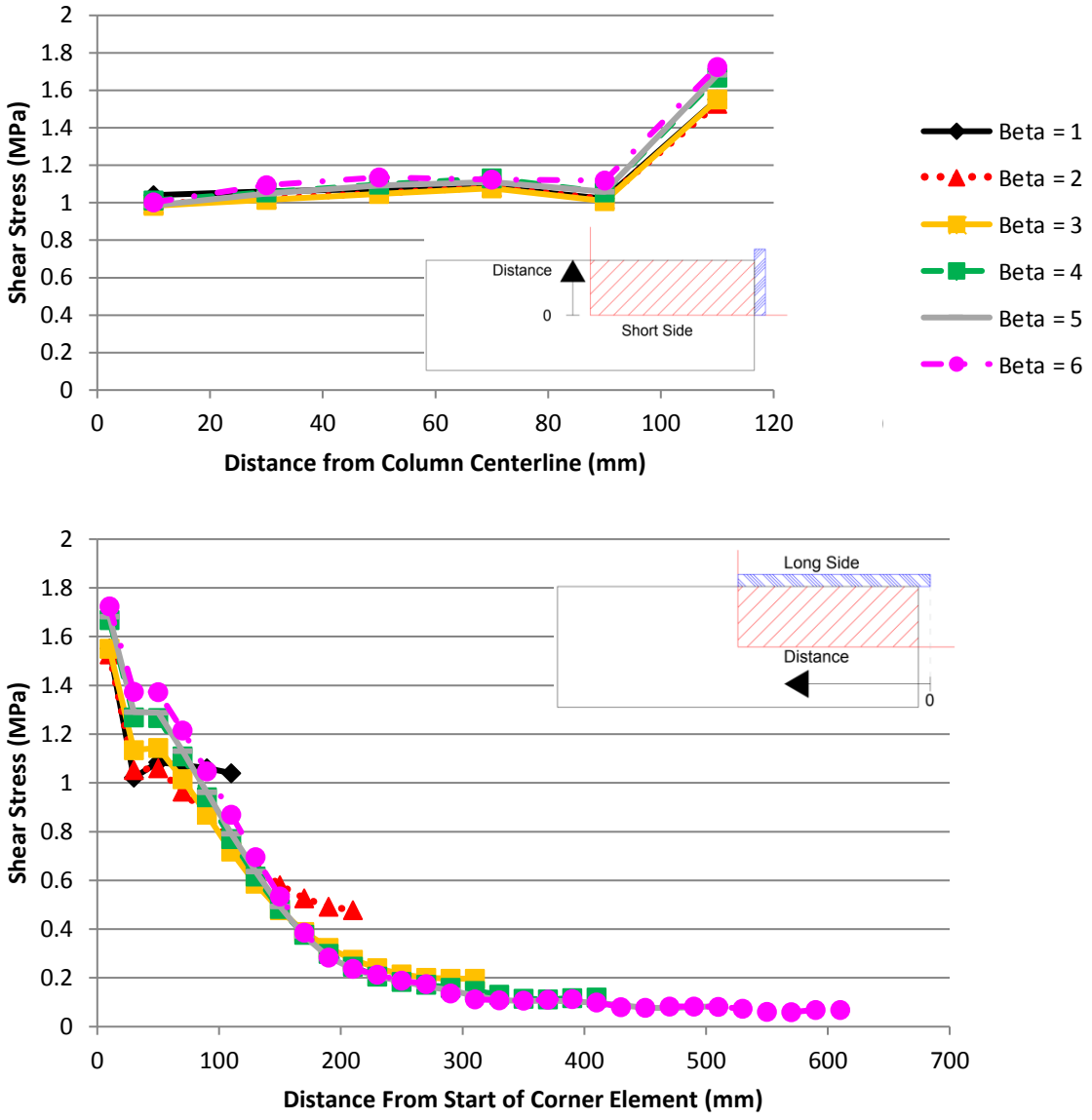

Figure H-9: Predicted Shear Stress Distribution Around Support Plate Perimeter, $c_{min}/d = 0.990$, Top) Stresses Along Short Side, Bottom) Stresses Along Long Side, Integer β, 30% of Peak Load

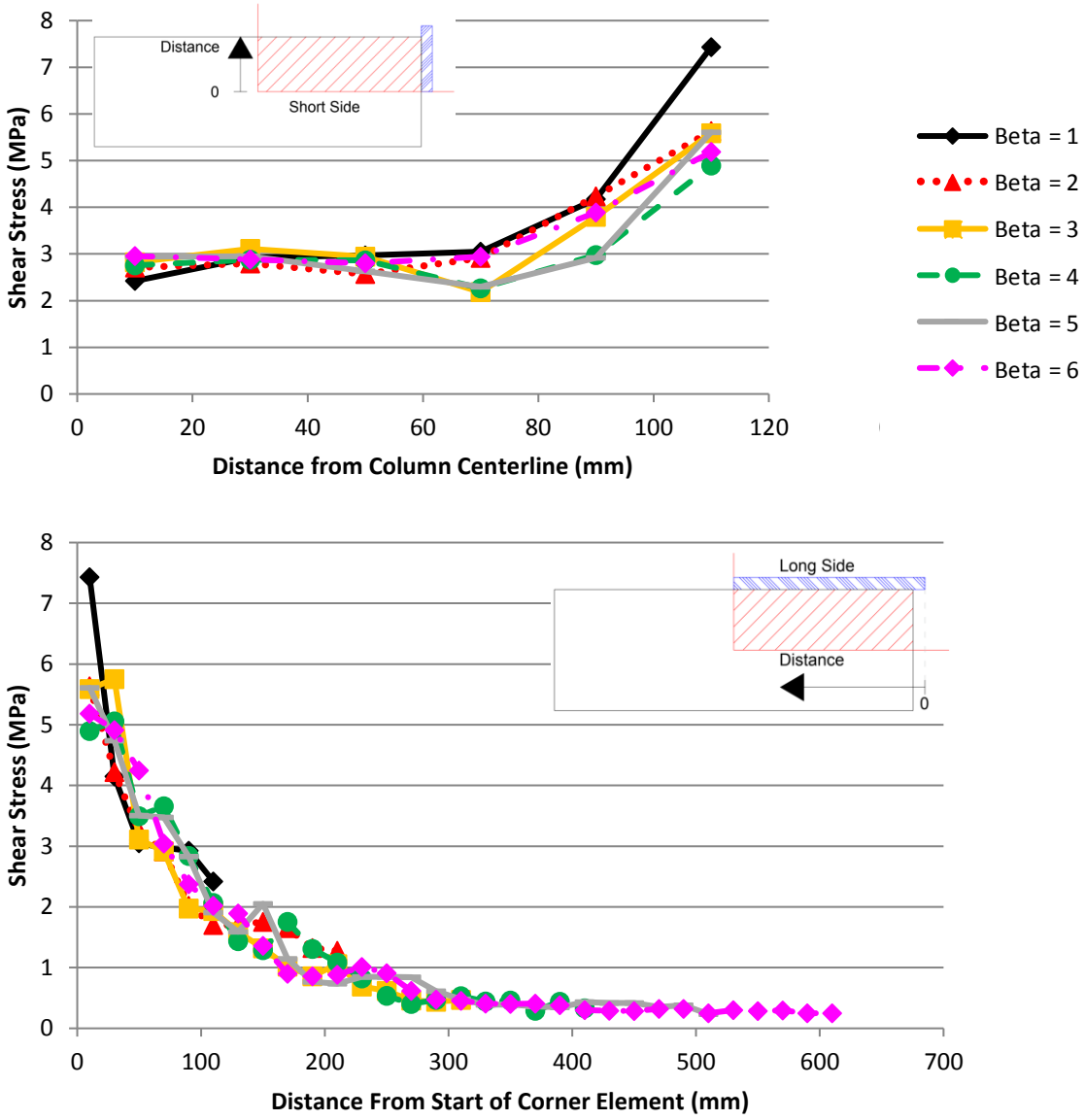

Figure H-10: Predicted Shear Stress Distribution Around Support Plate Perimeter, $c_{min}/d = 0.990$, Top) Stresses Along Short Side, Bottom) Stresses Along Long Side, Integer β, 90% of Peak Load

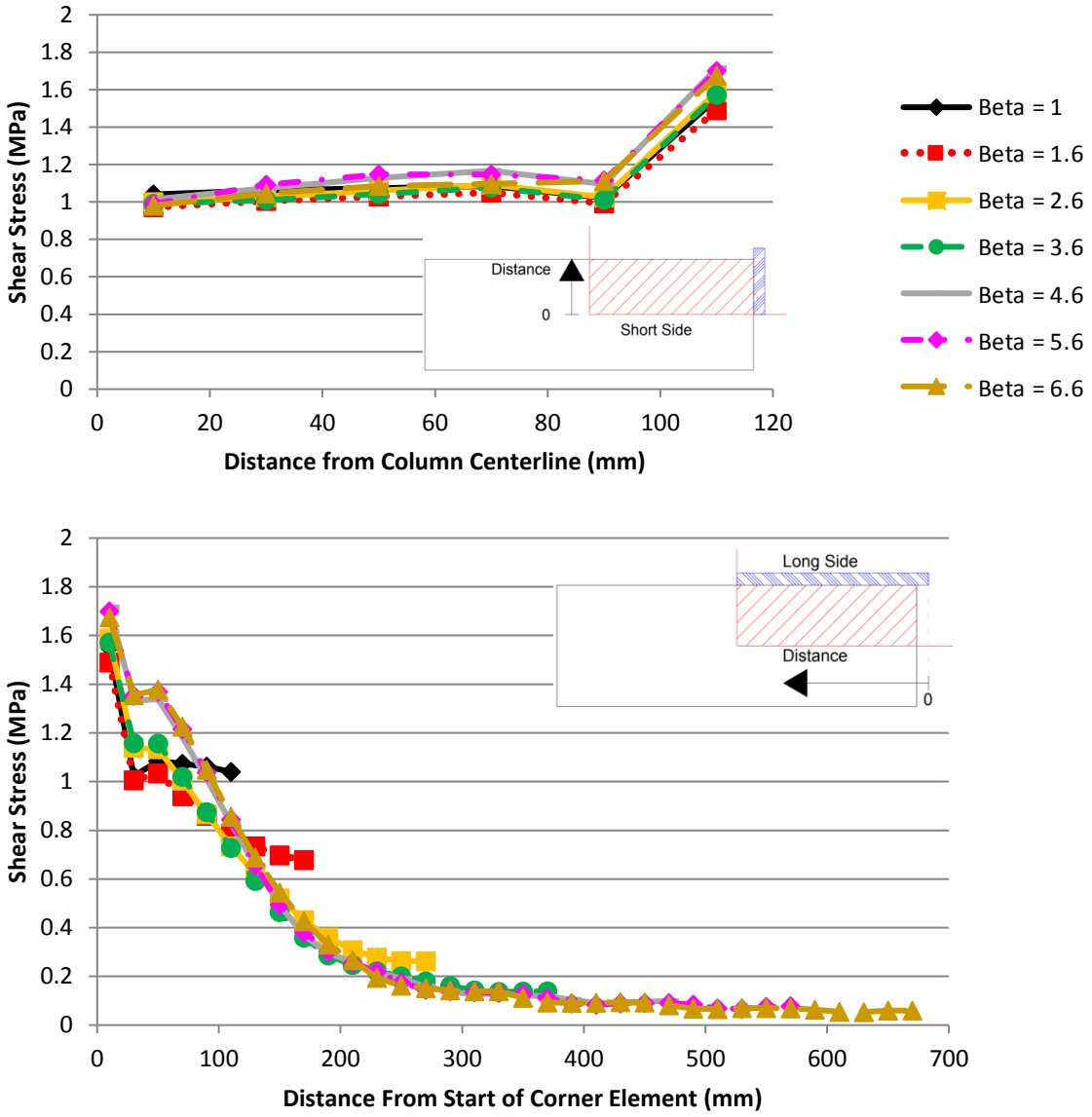

Figure H-11: Predicted Shear Stress Distribution Around Support Plate Perimeter, $c_{min}/d = 0.990$, Top) Stresses Along Short Side, Bottom) Stresses Along Long Side, Non-integer β, 30% of Peak Load

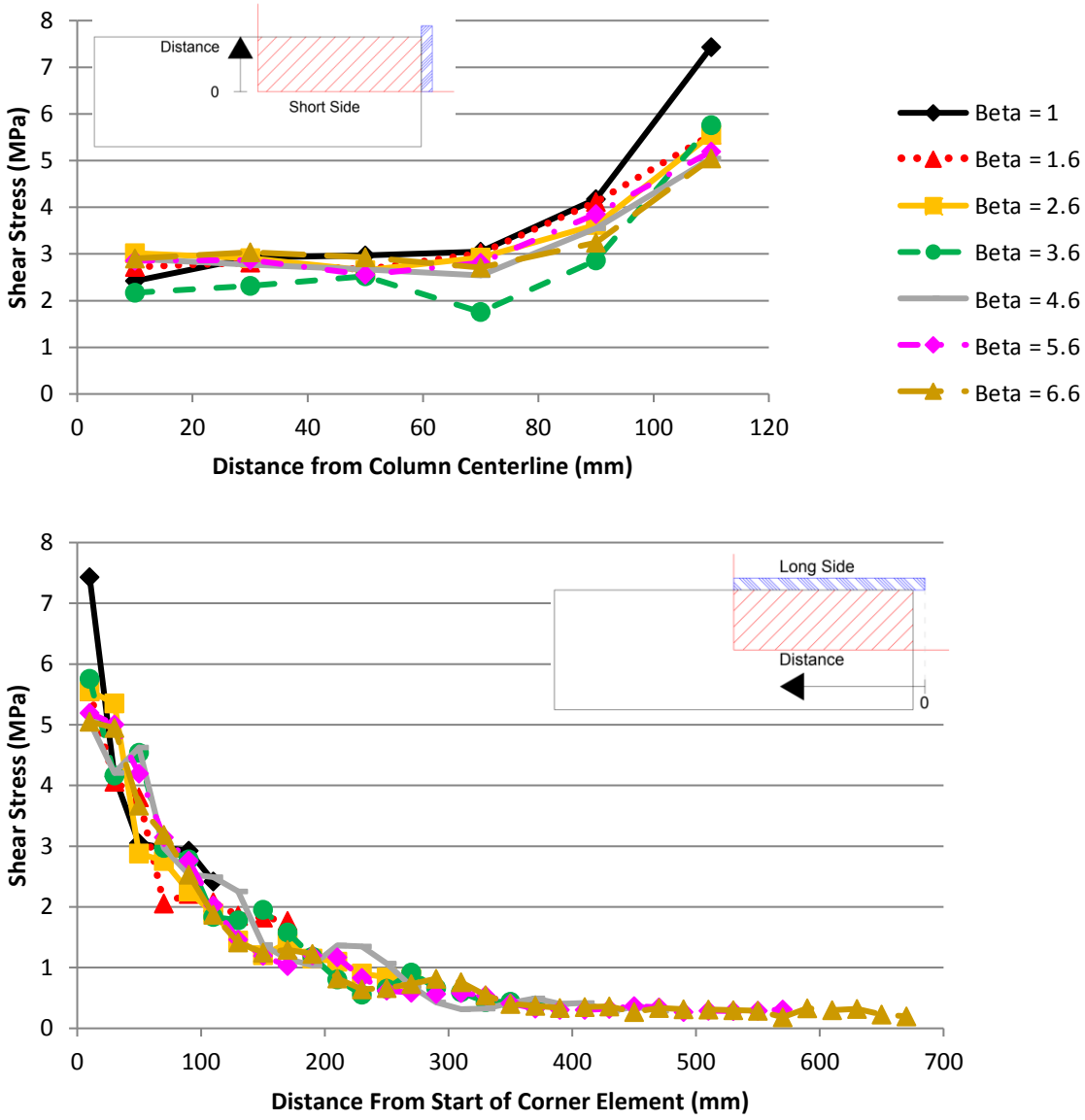

Figure H-12: Predicted Shear Stress Distribution Around Support Plate Perimeter, $c_{min}/d = 0.990$, Top) Stresses Along Short Side, Bottom) Stresses Along Long Side, Non-integer β, 90% of Peak Load

$c_{min}/d = 1.287$

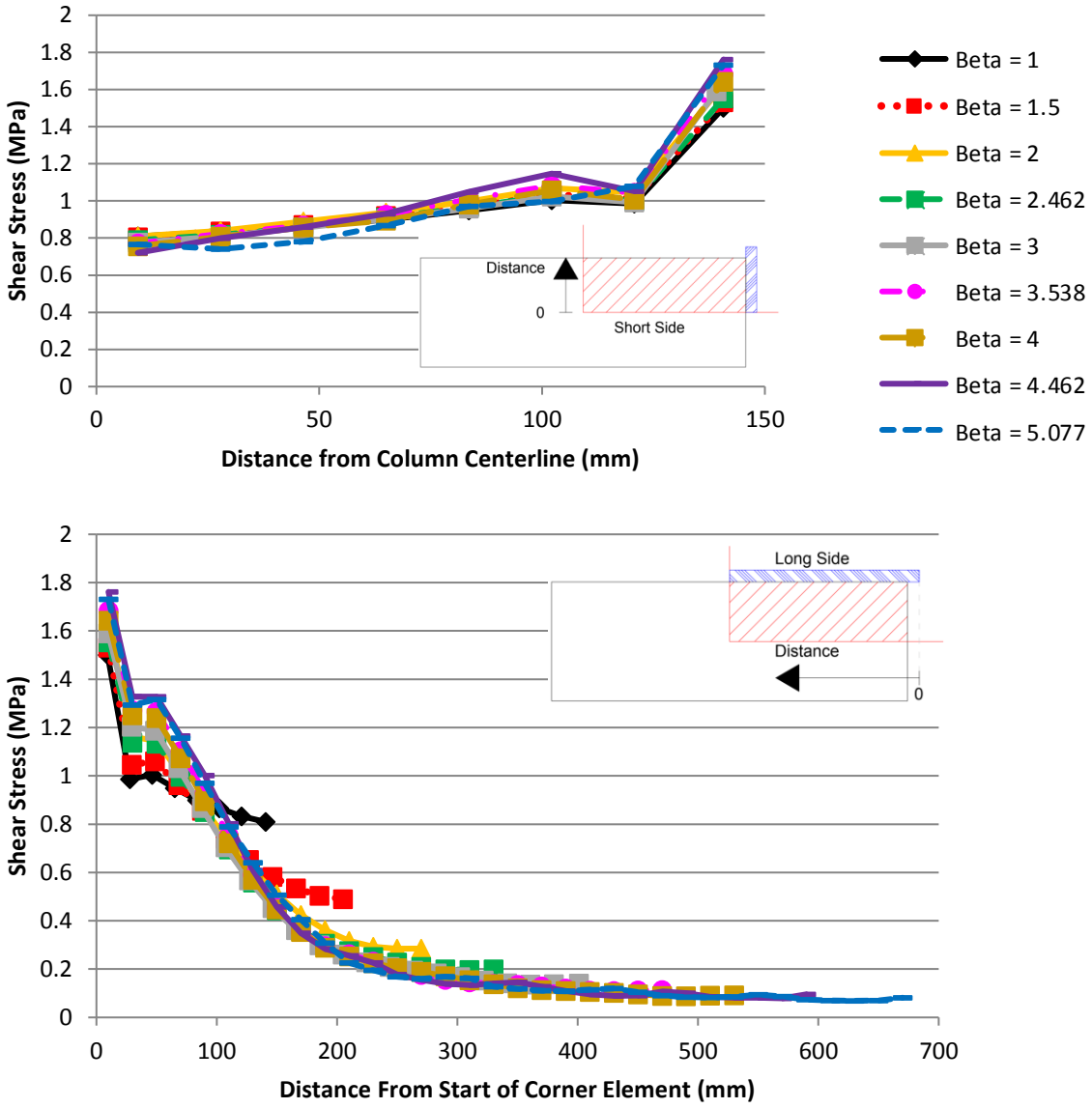

Figure H-13: Predicted Shear Stress Distribution Around Support Plate Perimeter, $c_{min}/d = 1.287$, Top) Stresses Along Short Side, Bottom) Stresses Along Long Side, 30% of Peak Load

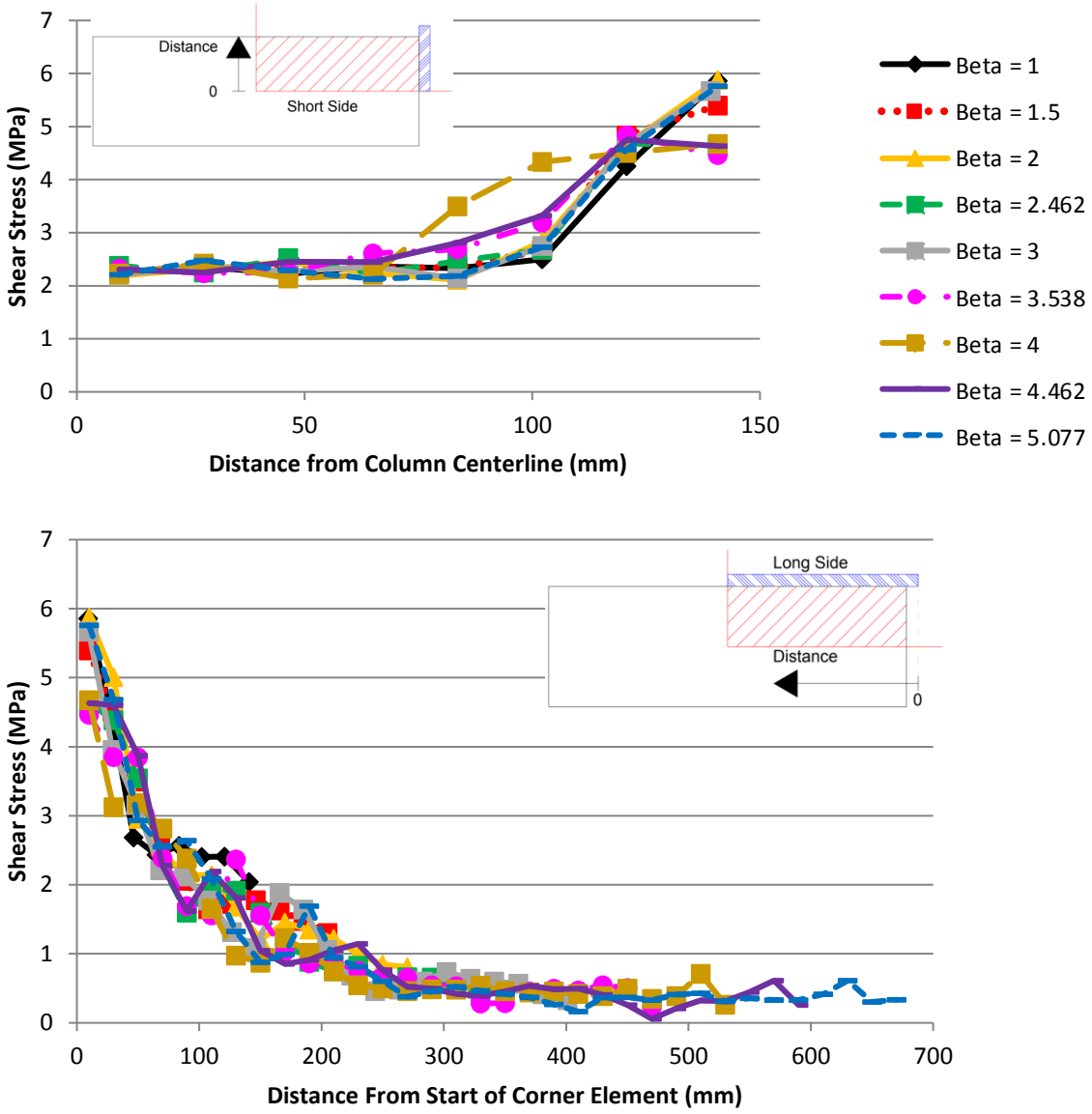

Figure H-14: Predicted Shear Stress Distribution Around Support Plate Perimeter, $c_{min}/d = 1.287$, Top) Stresses Along Short Side, Bottom) Stresses Along Long Side, 90% of Peak Load

$c_{min}/d = 1.485$

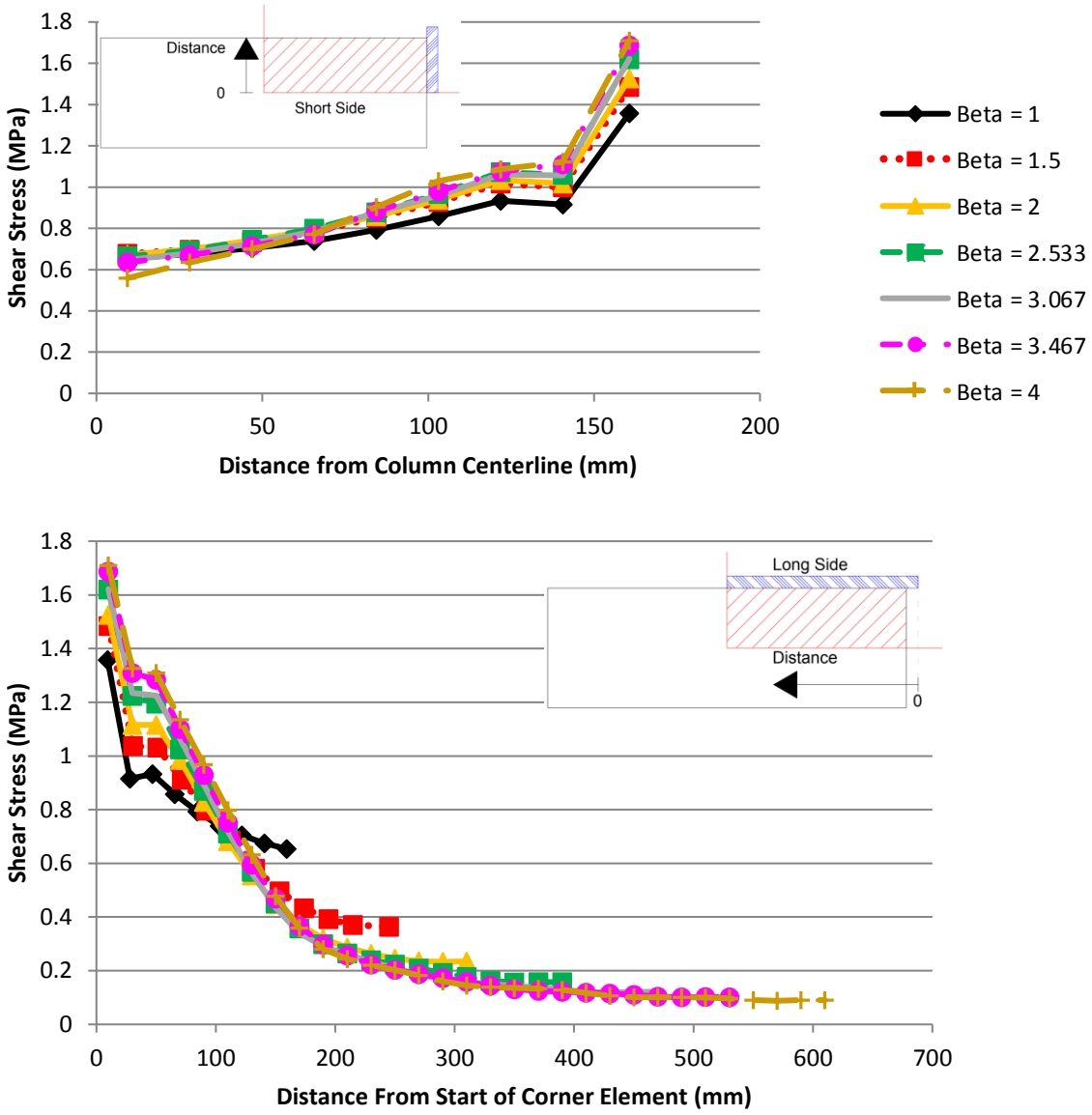

Figure H-15: Predicted Shear Stress Distribution Around Support Plate Perimeter, $c_{min}/d = 1.485$, Top) Stresses Along Short Side, Bottom) Stresses Along Long Side, 30% of Peak Load

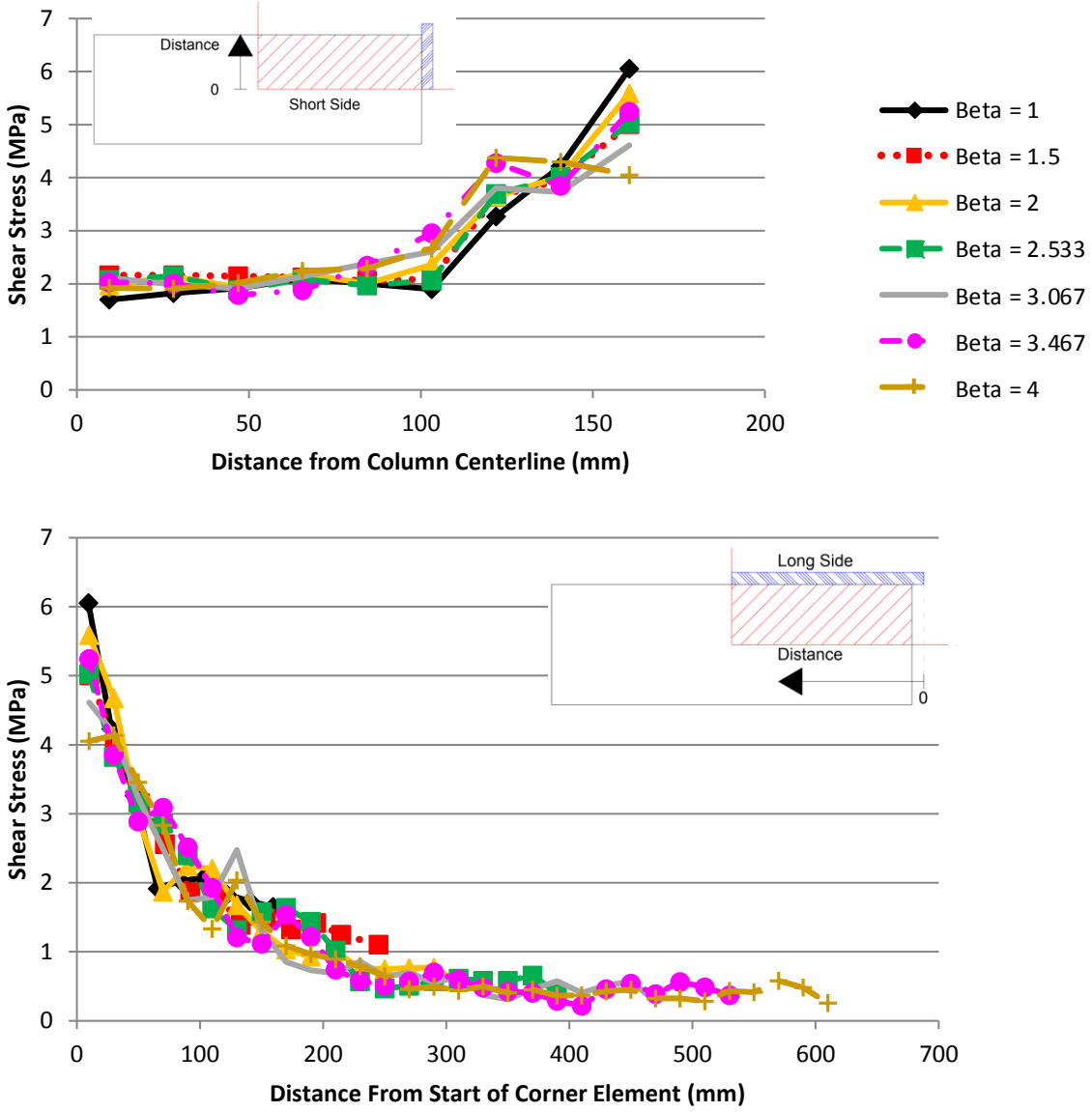

Figure H-16: Predicted Shear Stress Distribution Around Support Plate Perimeter, $c_{min}/d = 1.485$, Top) Stresses Along Short Side, Bottom) Stresses Along Long Side, 90% of Peak Load

$c_{min}/d = 1.782$

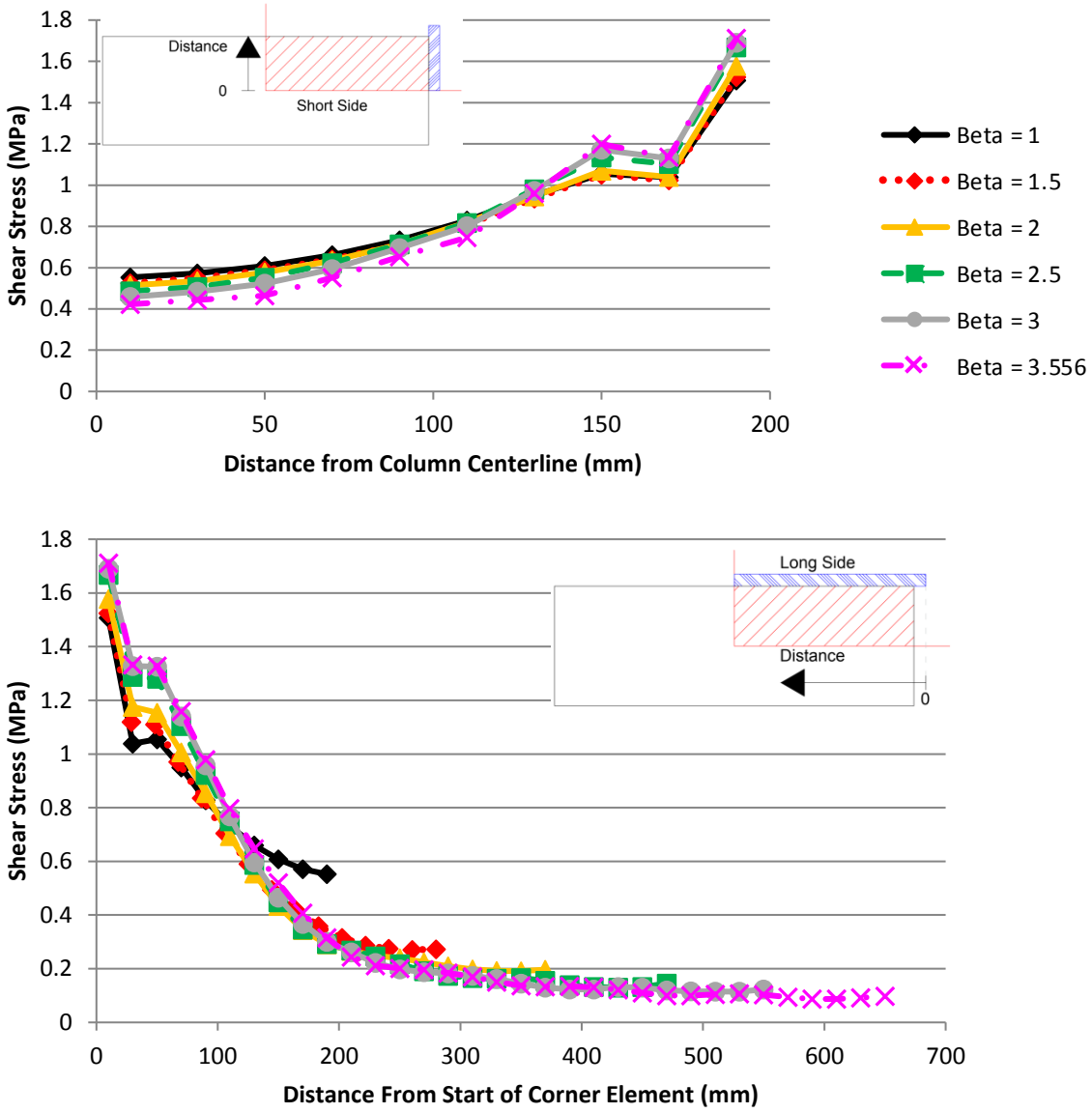

Figure H-17: Predicted Shear Stress Distribution Around Support Plate Perimeter, $c_{min}/d = 1.782$, Top) Stresses Along Short Side, Bottom) Stresses Along Long Side, 30% of Peak Load

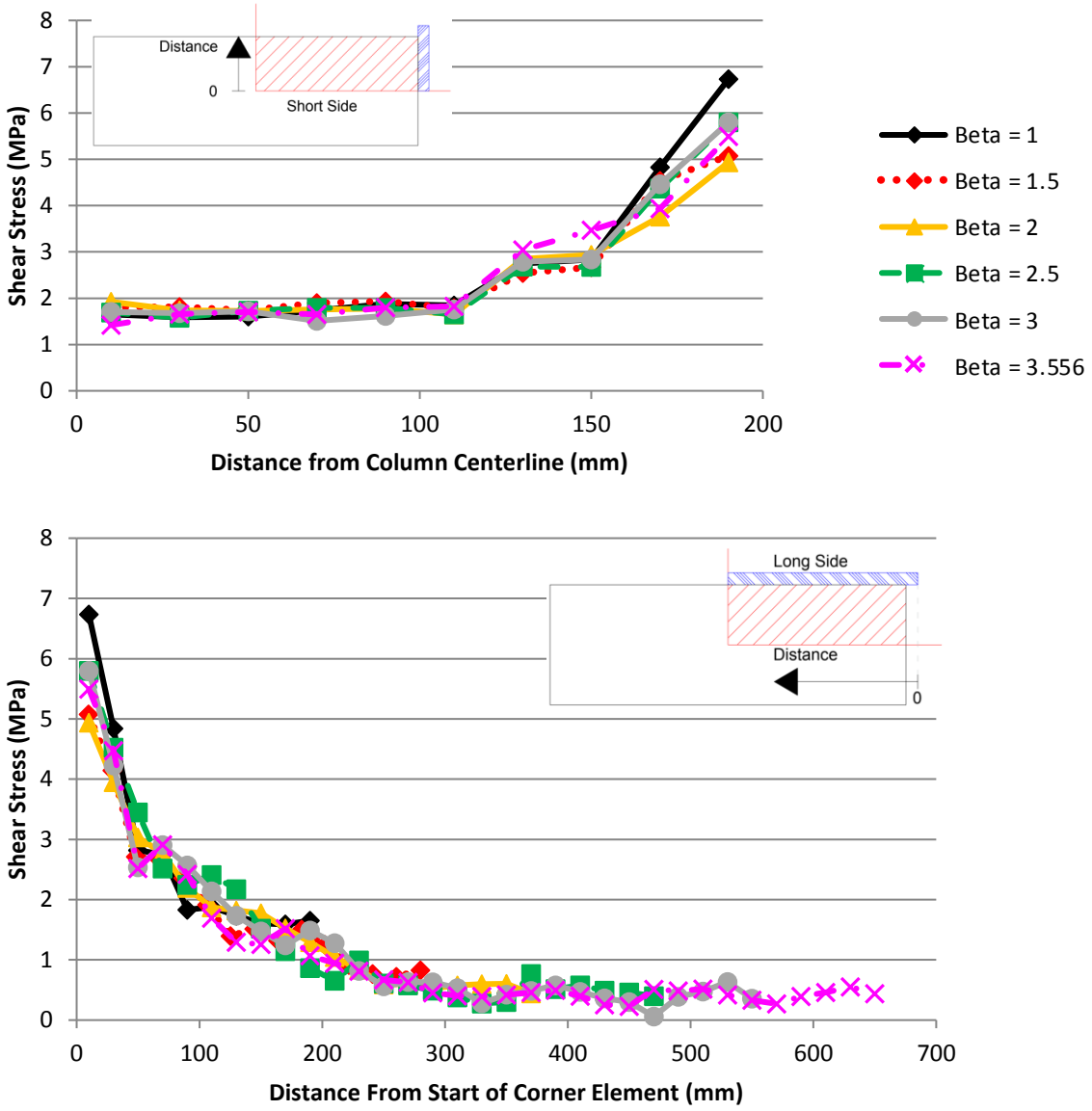

Figure H-18: Predicted Shear Stress Distribution Around Support Plate Perimeter, $c_{min}/d = 1.782$, Top) Stresses Along Short Side, Bottom) Stresses Along Long Side, 90% of Peak Load

$c_{min}/d = 1.980$

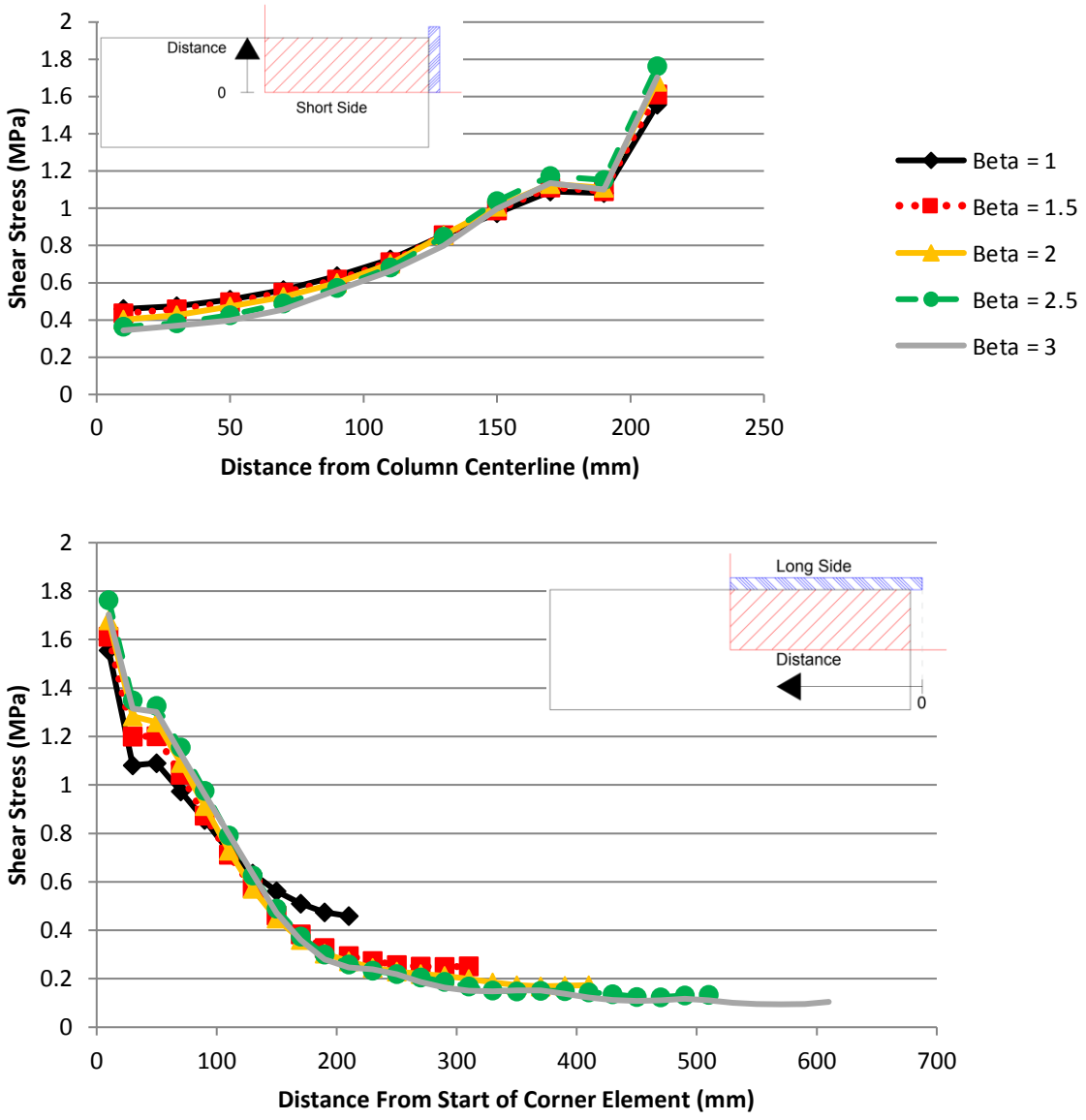

Figure H-19: Predicted Shear Stress Distribution Around Support Plate Perimeter, $c_{min}/d = 1.980$, Top) Stresses Along Short Side, Bottom) Stresses Along Long Side, 30% of Peak Load

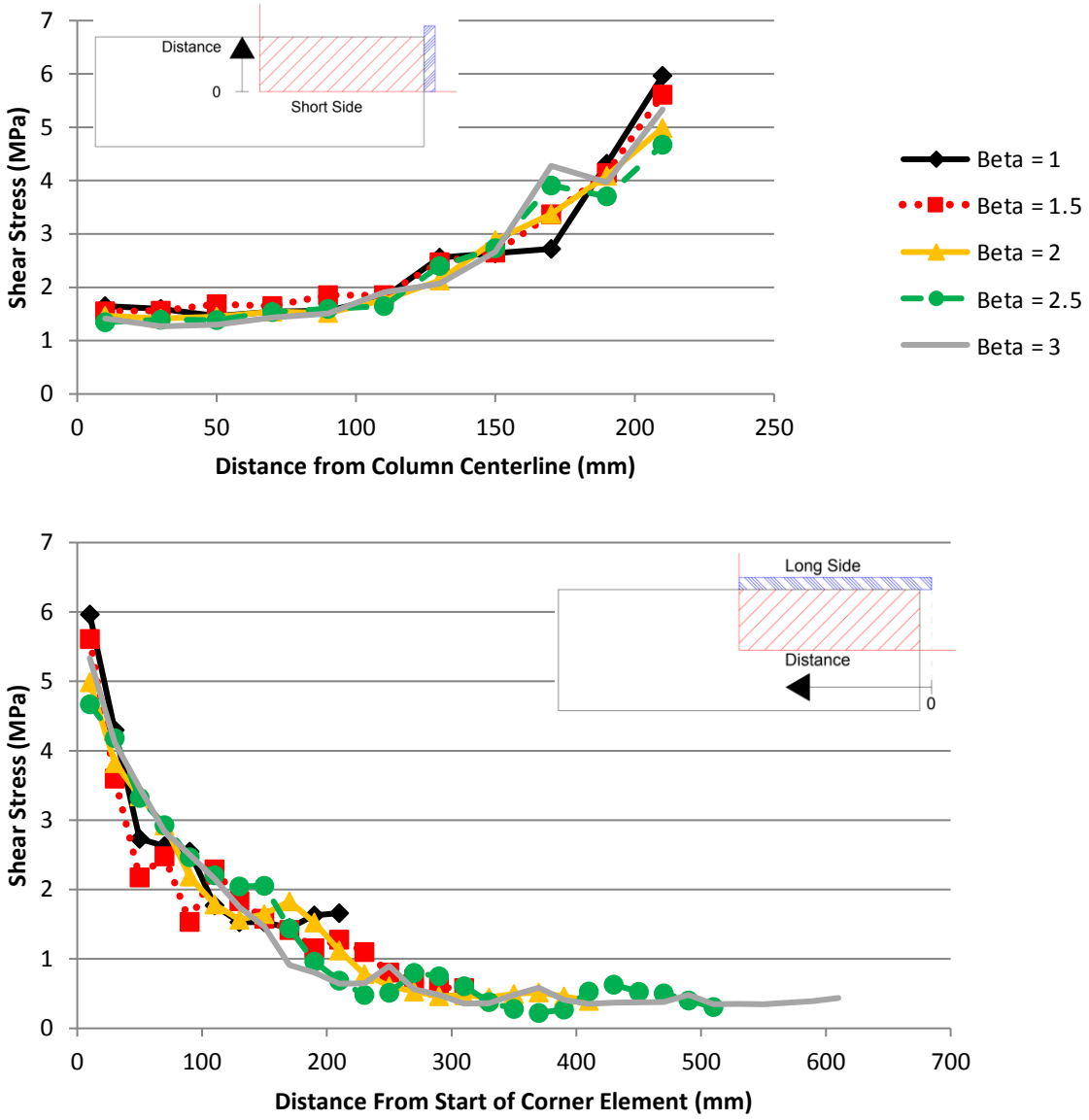

Figure H-20: Predicted Shear Stress Distribution Around Support Plate Perimeter, $c_{min}/d = 1.980$, Top) Stresses Along Short Side, Bottom) Stresses Along Long Side, 90% of Peak Load

$c_{min}/d = 2.970$

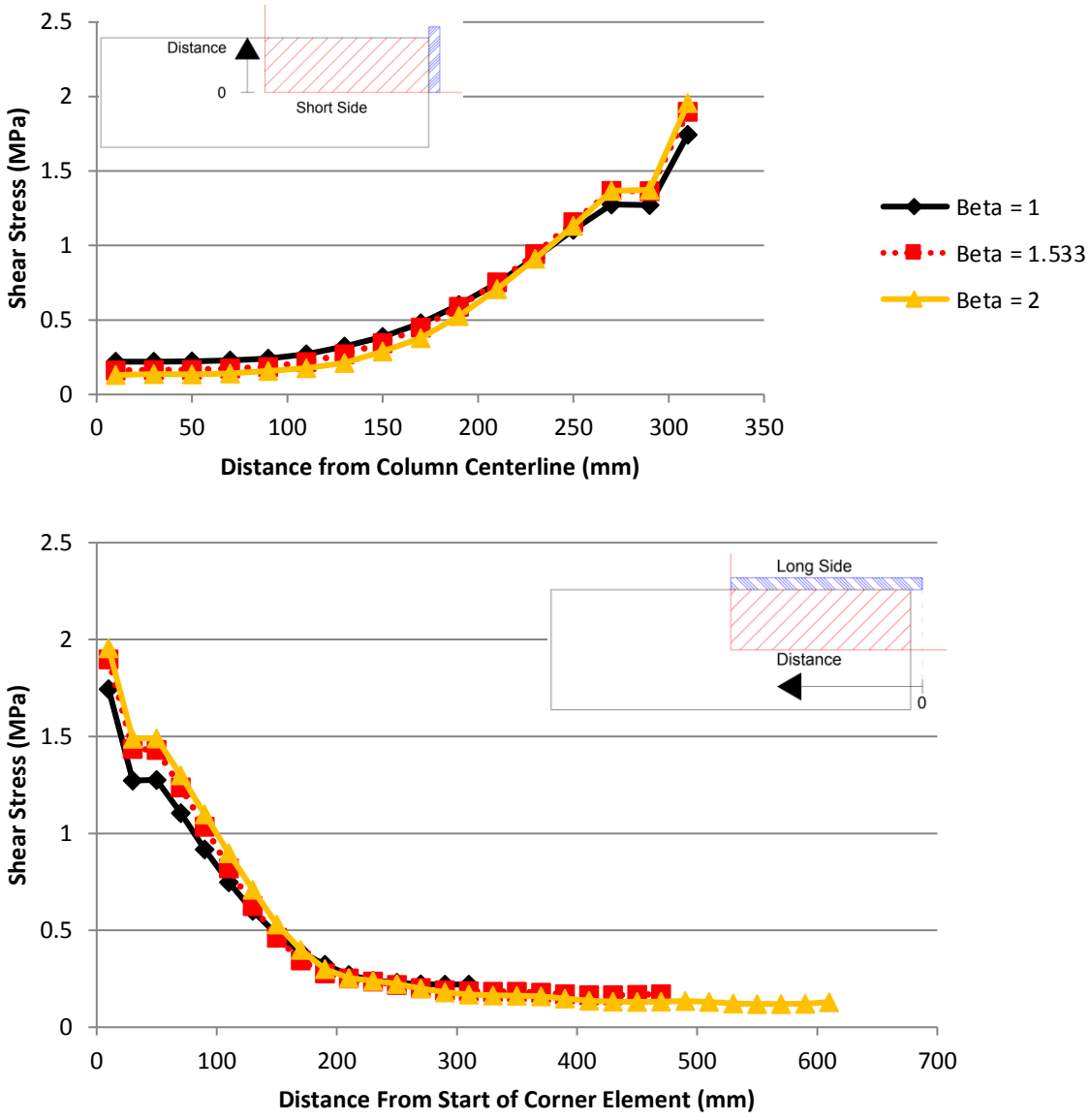

Figure H-21: Predicted Shear Stress Distribution Around Support Plate Perimeter, $c_{min}/d = 2.970$, Top) Stresses Along Short Side, Bottom) Stresses Along Long Side, 30% of Peak Load

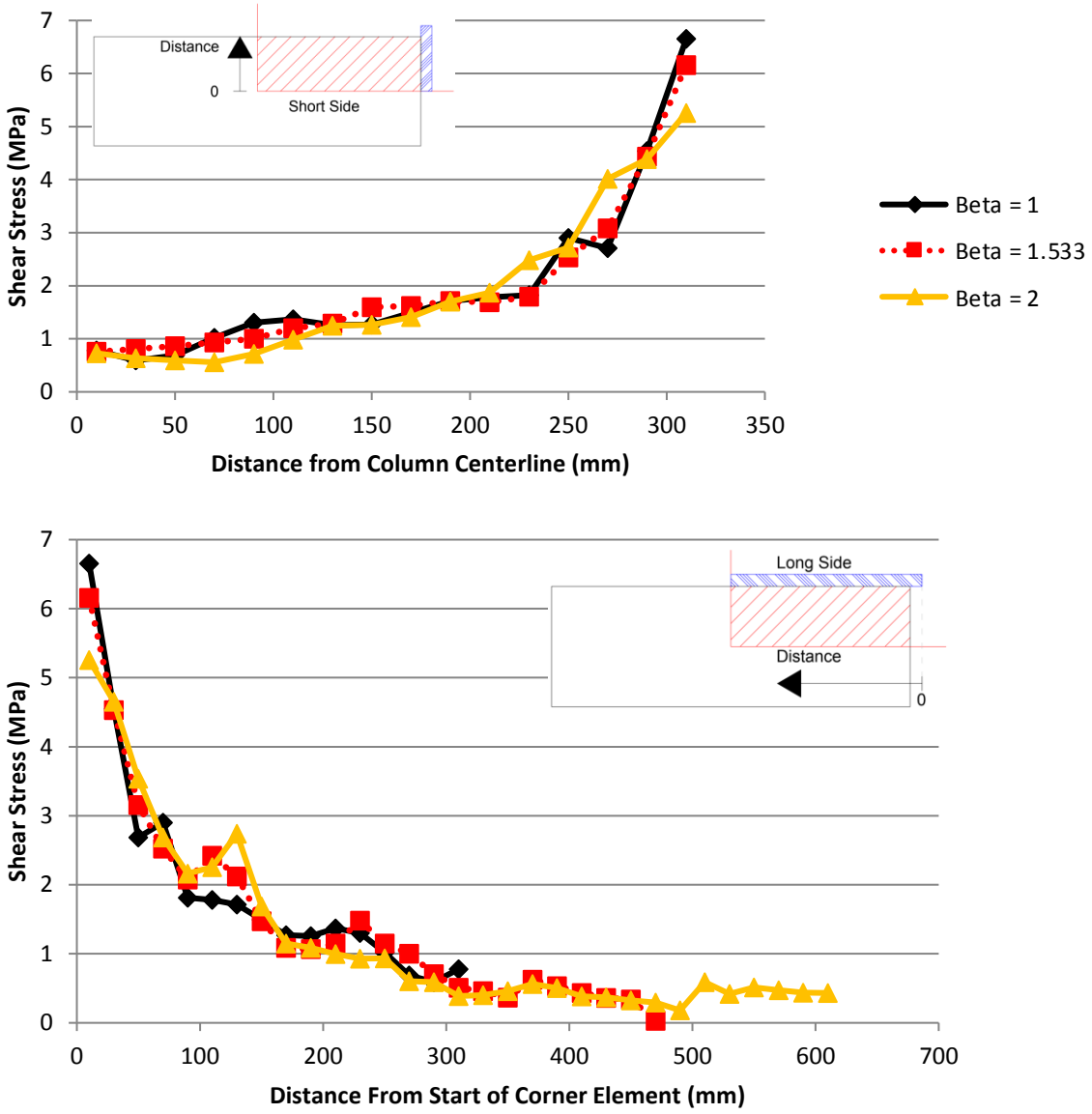

Figure H-22: Predicted Shear Stress Distribution Around Support Plate Perimeter, $c_{min}/d = 2.970$, Top) Stresses Along Short Side, Bottom) Stresses Along Long Side, 90% of Peak Load

Appendix I

Shear Stress Distributions at 30%, 90% and 100% of Peak Load for Select Models

In this appendix, the shear stress distributions in the slab around the support plate perimeter for the remaining models considered in the stress distribution study discussed in Section 5.3.2.1 for the remaining c_{min}/d ratios are provided.

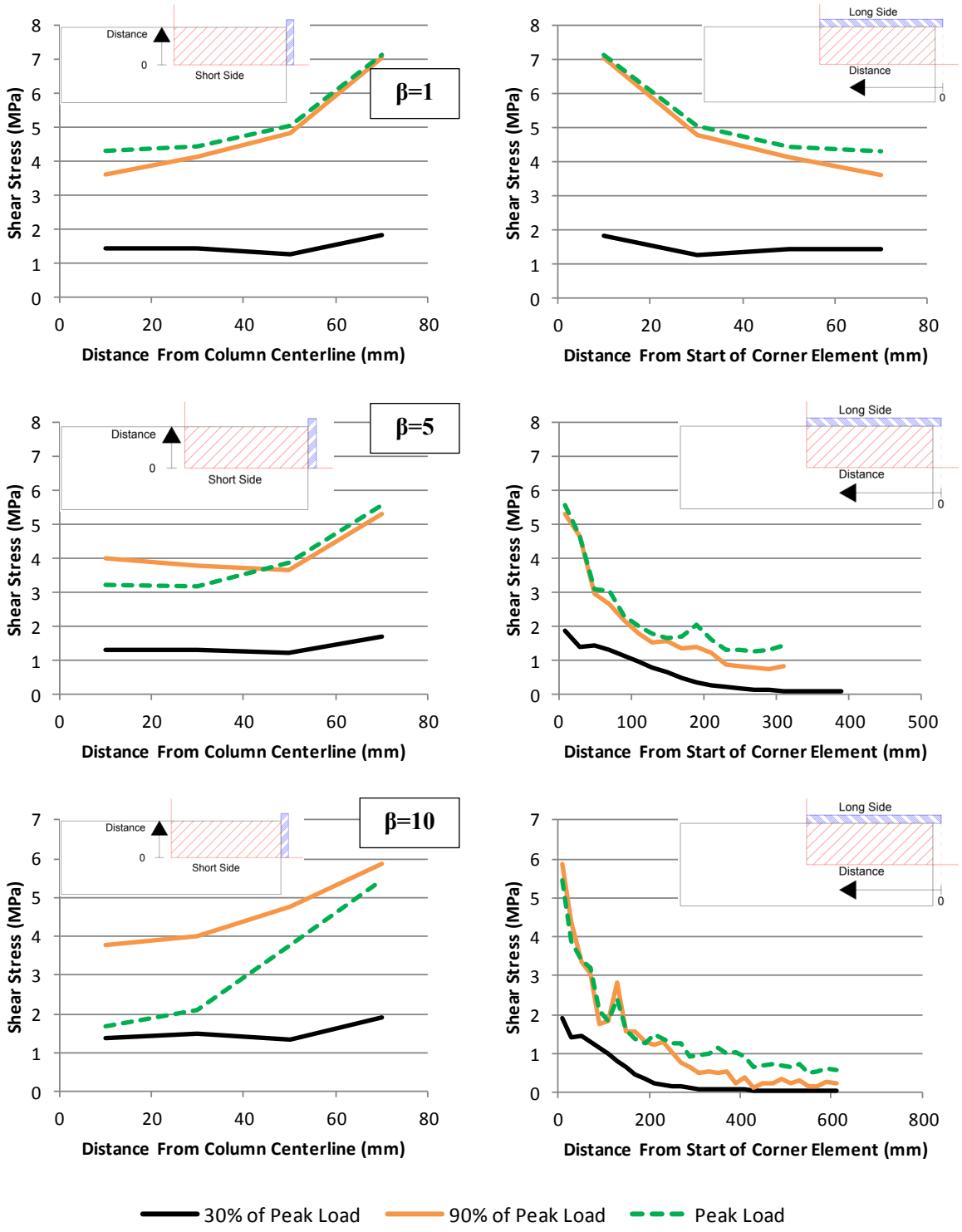

Figure I-1: Shear Stress Distributions in the Slab Around the Support Plate Perimeter at 30%, 90% and 100% of Peak Load for Selected β Values, $c_{min}/d = 0.594$

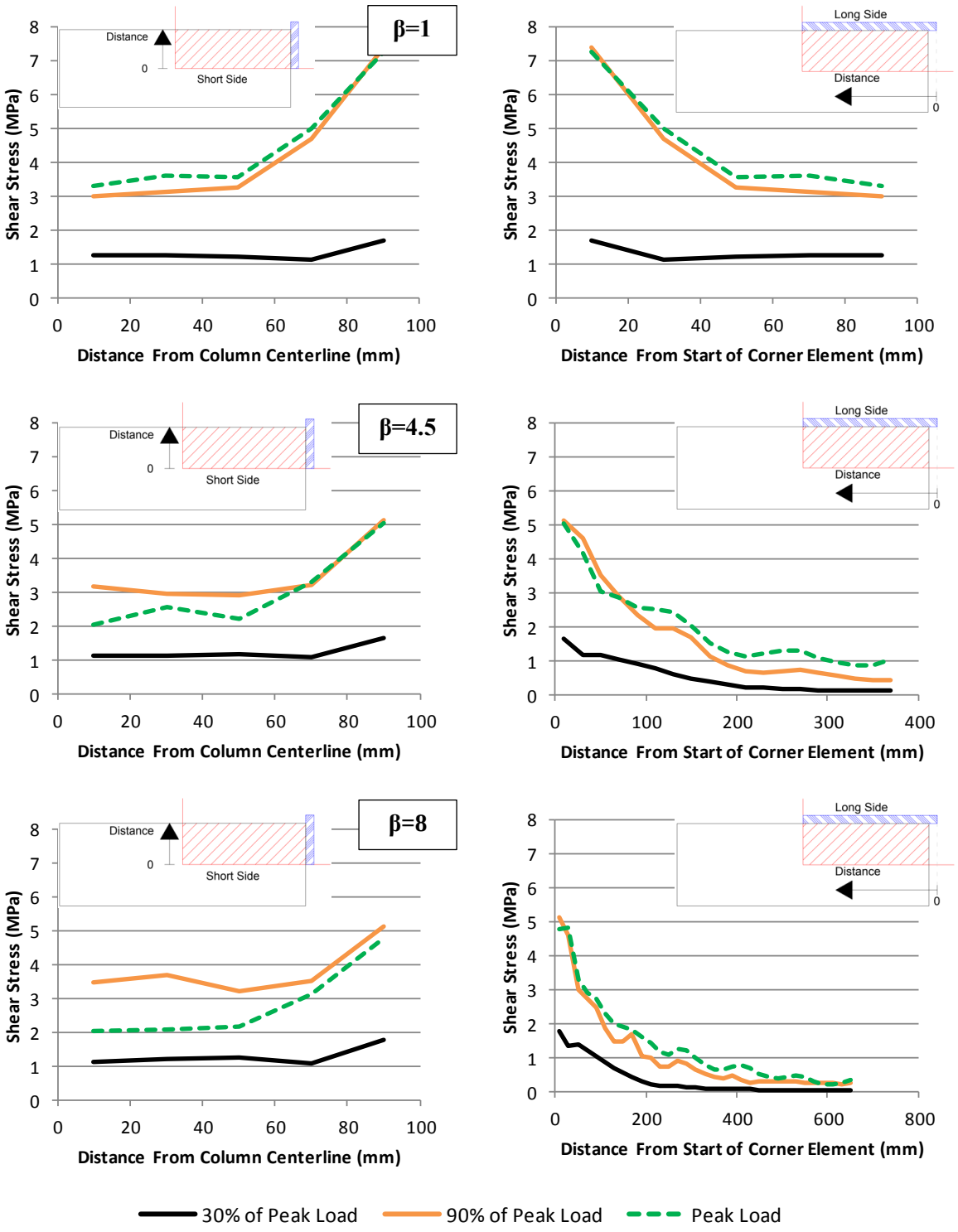

Figure I-2: Shear Stress Distributions in the Slab Around the Support Plate Perimeter at 30%, 90% and 100% of Peak Load for Selected β Values, $c_{min}/d = 0.792$

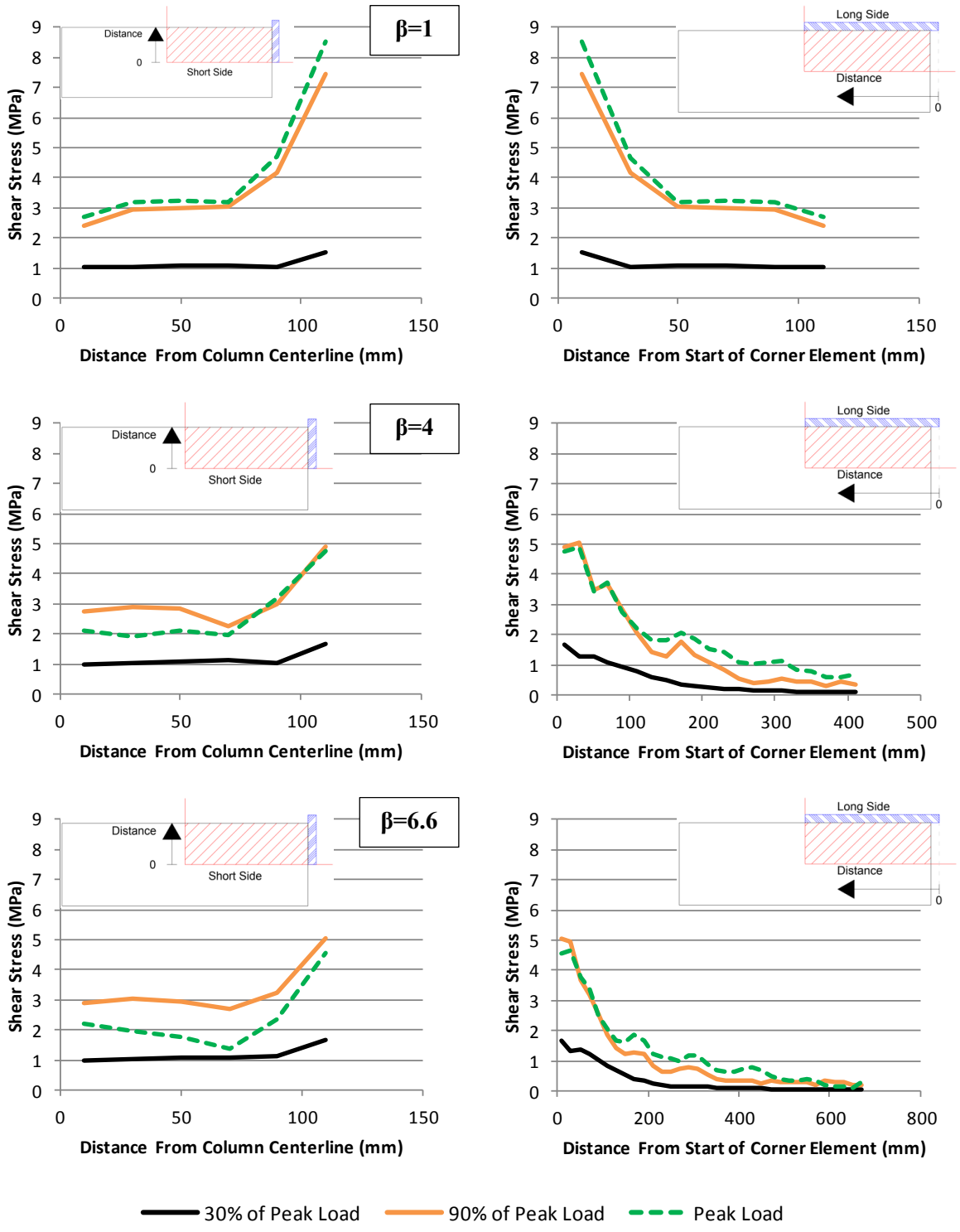

Figure I-3: Shear Stress Distributions in the Slab Around the Support Plate Perimeter at 30%, 90% and 100% of Peak Load for Selected β Values, $c_{min}/d = 0.990$

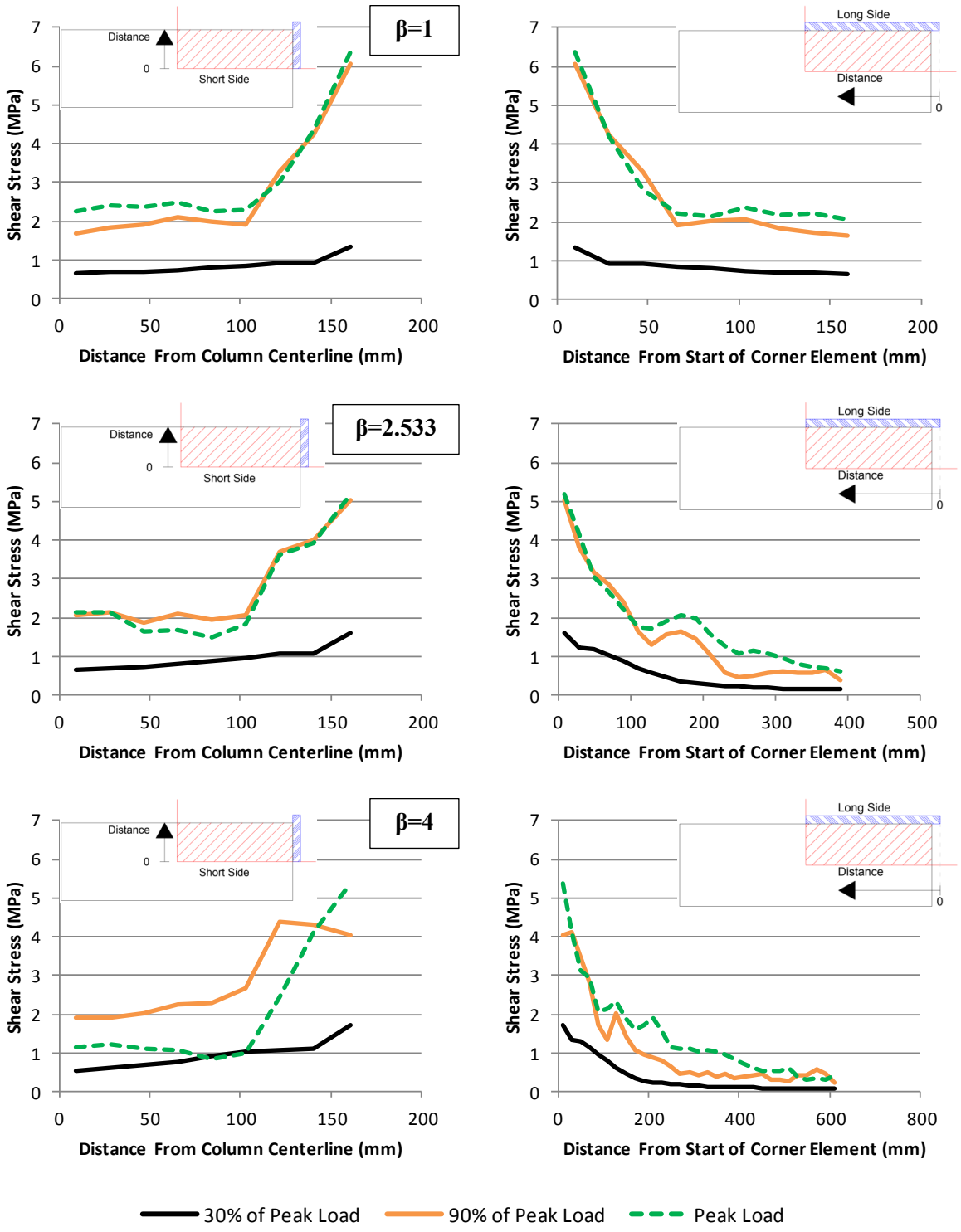

Figure I-4: Shear Stress Distributions in the Slab Around the Support Plate Perimeter at 30%, 90% and 100% of Peak Load for Selected β Values, $c_{min}/d = 1.485$

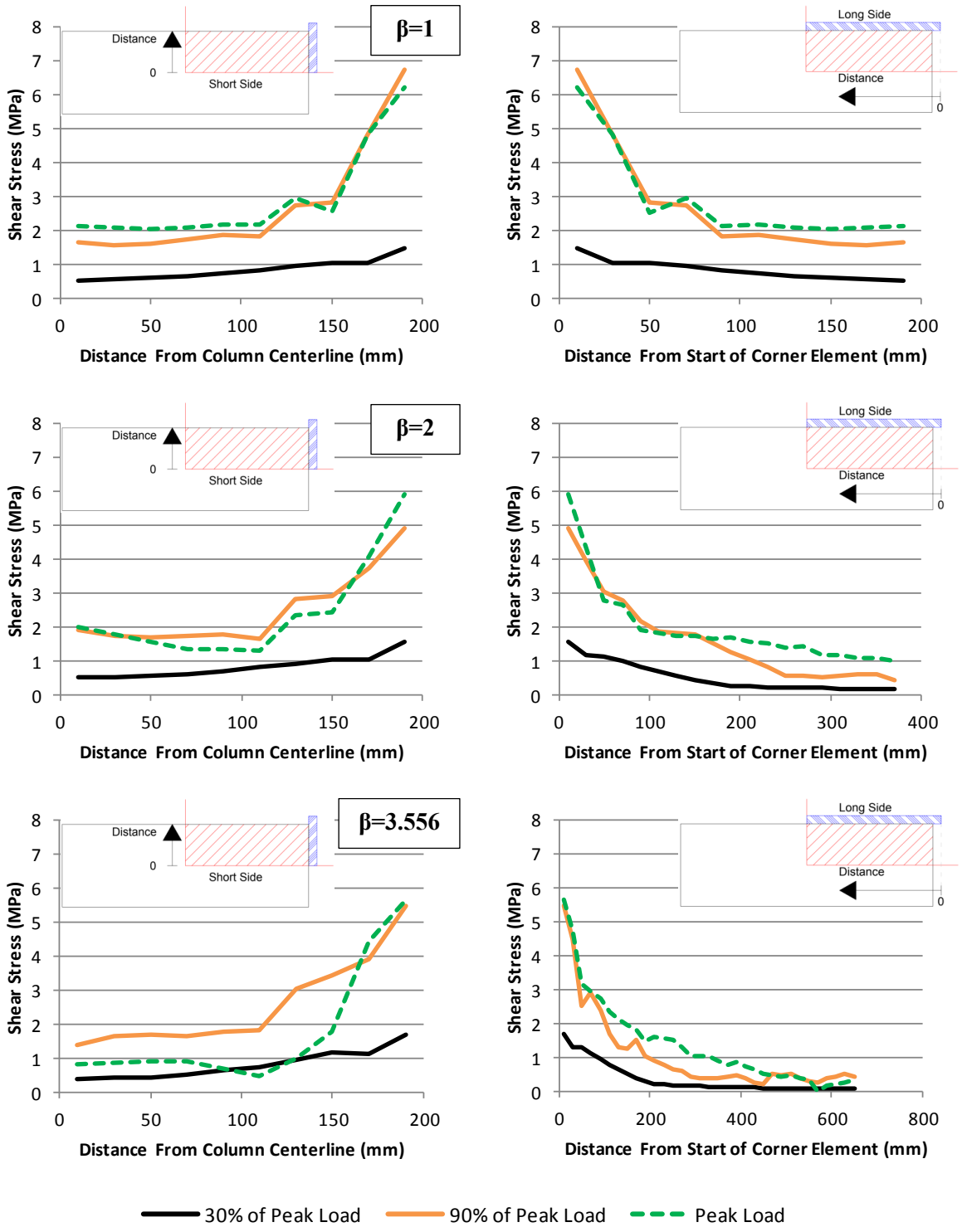

Figure I-5: Shear Stress Distributions in the Slab Around the Support Plate Perimeter at 30%, 90% and 100% of Peak Load for Selected β Values, $c_{min}/d = 1.782$

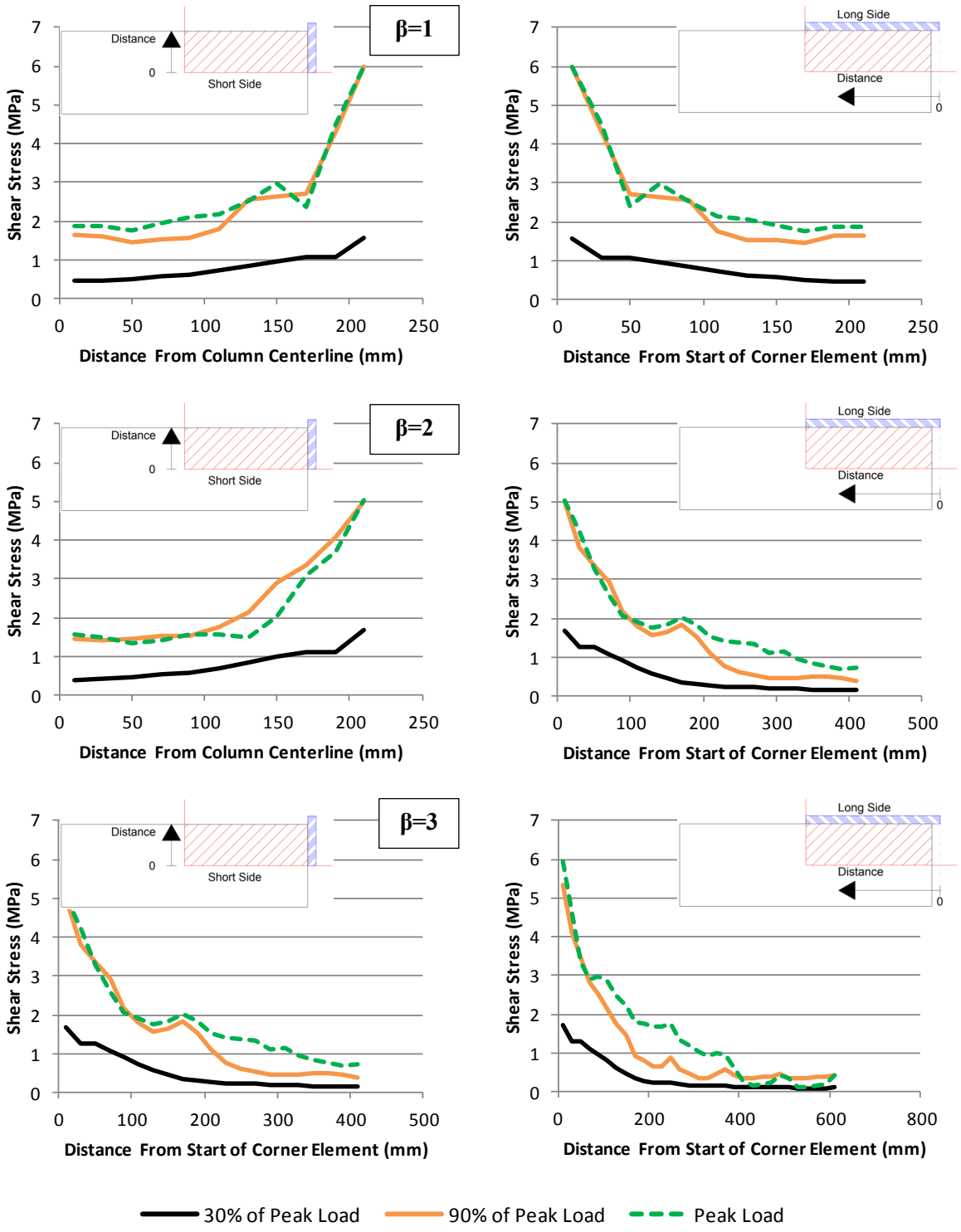

Figure I-6: Shear Stress Distributions in the Slab Around the Support Plate Perimeter at 30%, 90% and 100% of Peak Load for Selected β Values, $c_{min}/d = 1.980$

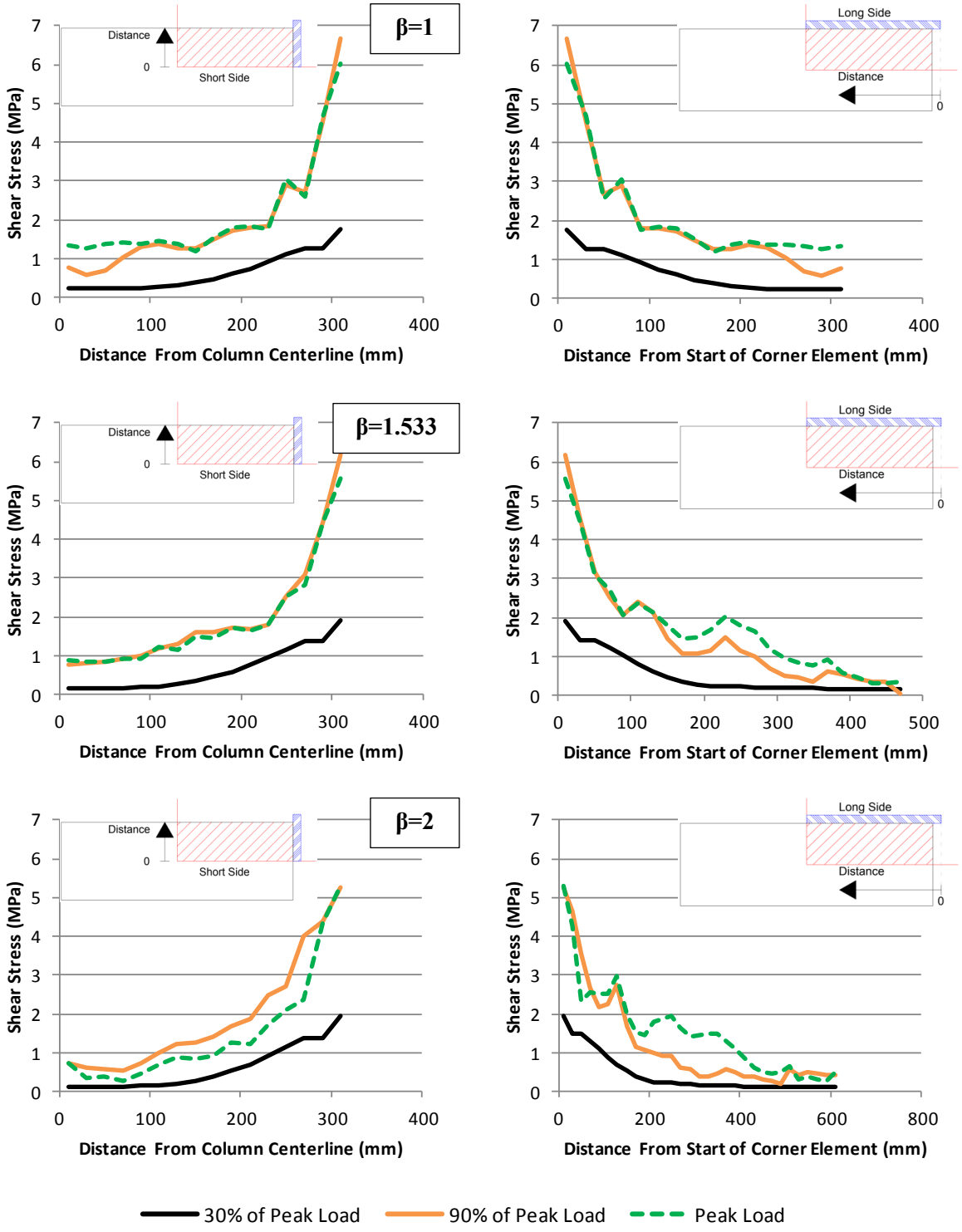

Figure I-7: Shear Stress Distributions in the Slab Around the Support Plate Perimeter at 30%, 90% and 100% of Peak Load for Selected β Values, c_{min}/d = 2.970

Appendix J
Trendlines Plots Referenced in Table 5-18

In this appendix, the trendlines of the FEM predicted normalized nominal shear stress capacity along the ACI critical perimeter versus column rectangularity referenced in Table 5-18 in Section 5.3.1.1 are provided. The trendlines demonstrate that the reduction in normalized nominal shear capacity along the ACI 318 critical perimeter predicted by the FEM is approximately linear, and becomes more severe as the c_{min}/d ratio increases. The plots provided in this appendix, and referenced in Table 5-18, include all models considered in the parametric study, including those which were predicted to fail in one-way shear by the FEM.

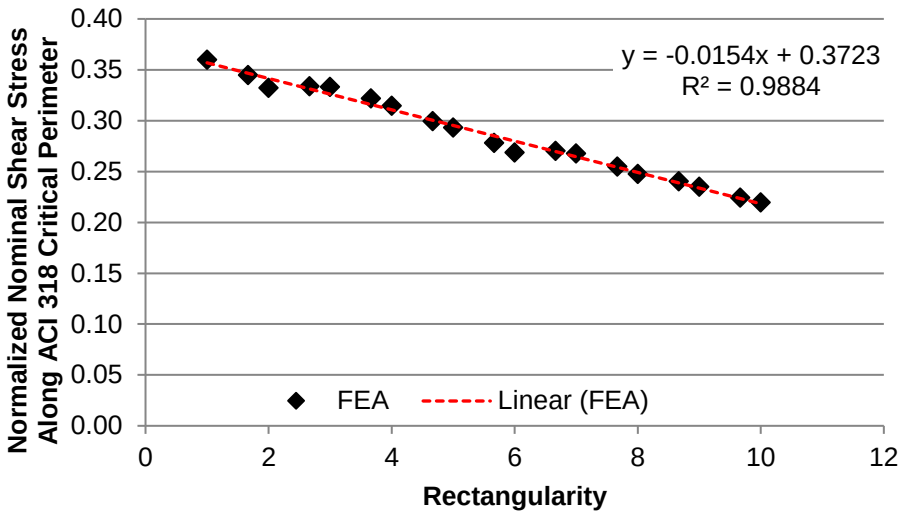

Figure J-1: Normalized Nominal Shear Stress Along ACI 318 Critical Perimeter Versus Column Rectangularity, $c_{min}/d = 0.594$

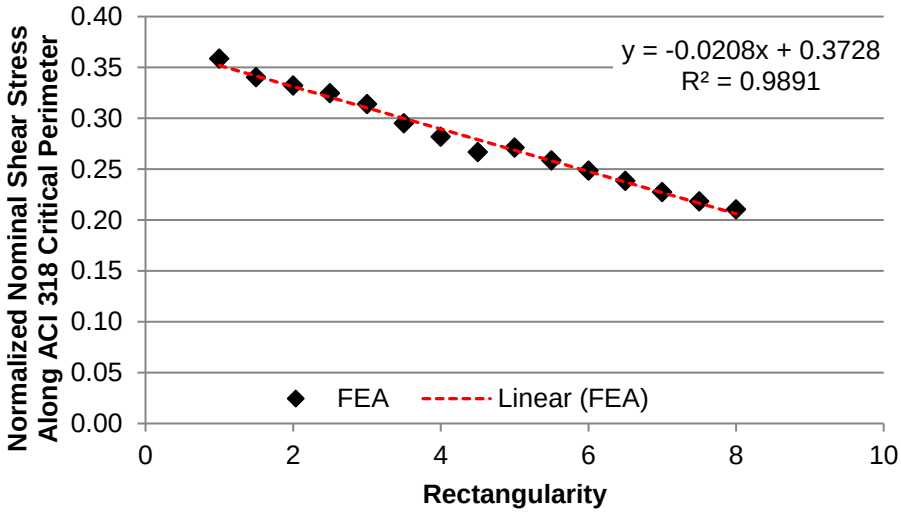

Figure J-2: Normalized Nominal Shear Stress Capacity Along ACI 318 Critical Perimeter Versus Column Rectangularity, $c_{min}/d = 0.792$

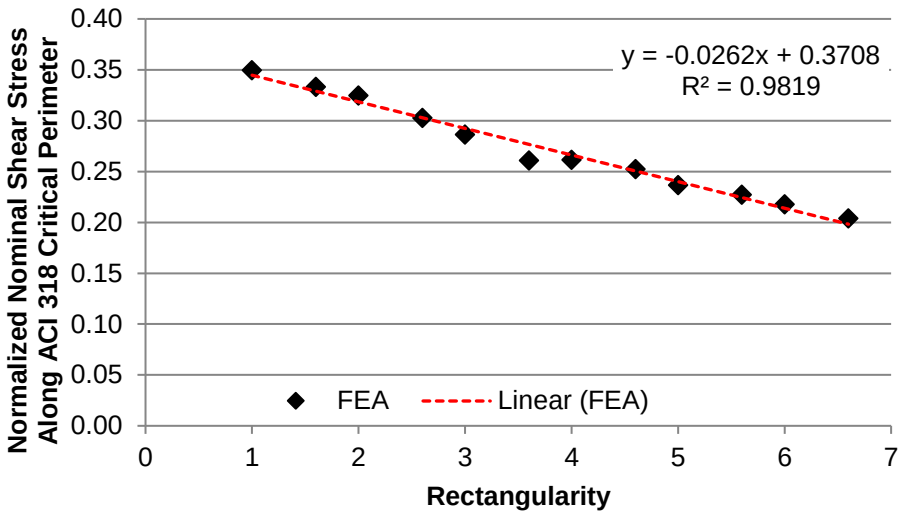

Figure J-3: Normalized Nominal Shear Stress Capacity Along ACI 318 Critical Perimeter Versus Column Rectangularity, $c_{min}/d = 0.990$

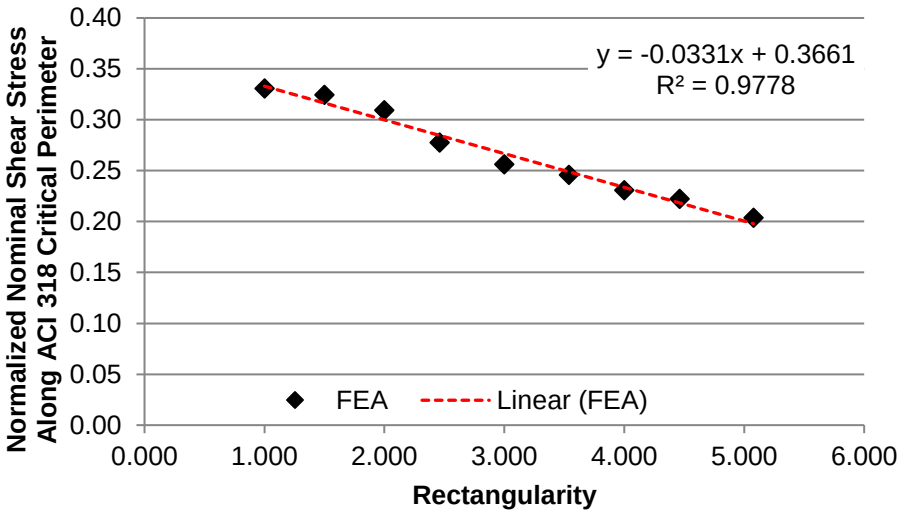

Figure J-4: Normalized Nominal Shear Stress Along Capacity ACI 318 Critical Perimeter Versus Column Rectangularity, $c_{min}/d = 1.287$

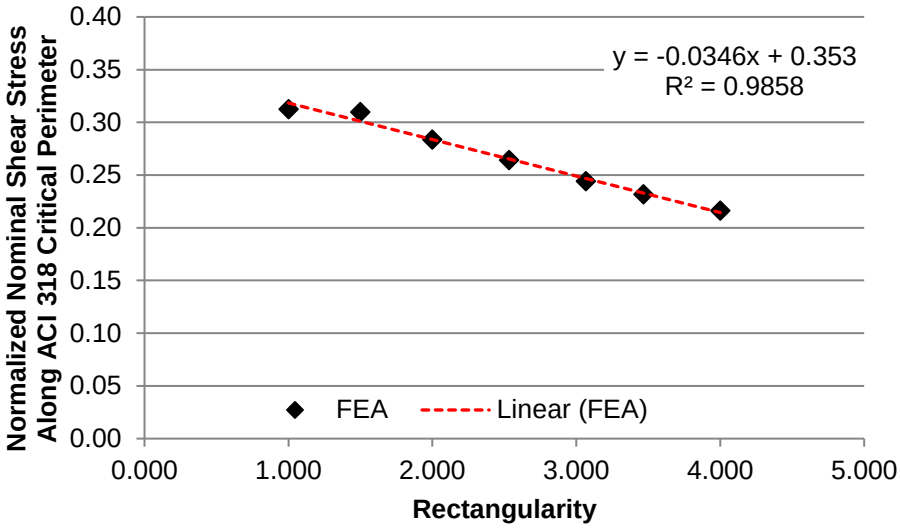

Figure J-5: Normalized Nominal Shear Stress Capacity Along ACI 318 Critical Perimeter Versus Column Rectangularity, $c_{min}/d = 1.485$

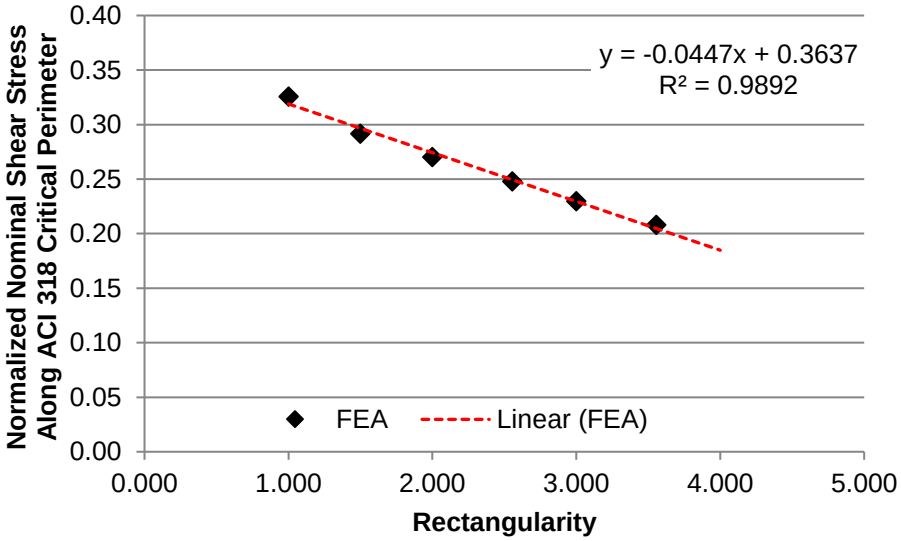

Figure J-6: Normalized Nominal Shear Stress Capacity Along ACI 318 Critical Perimeter Versus Column Rectangularity, $c_{min}/d = 1.782$

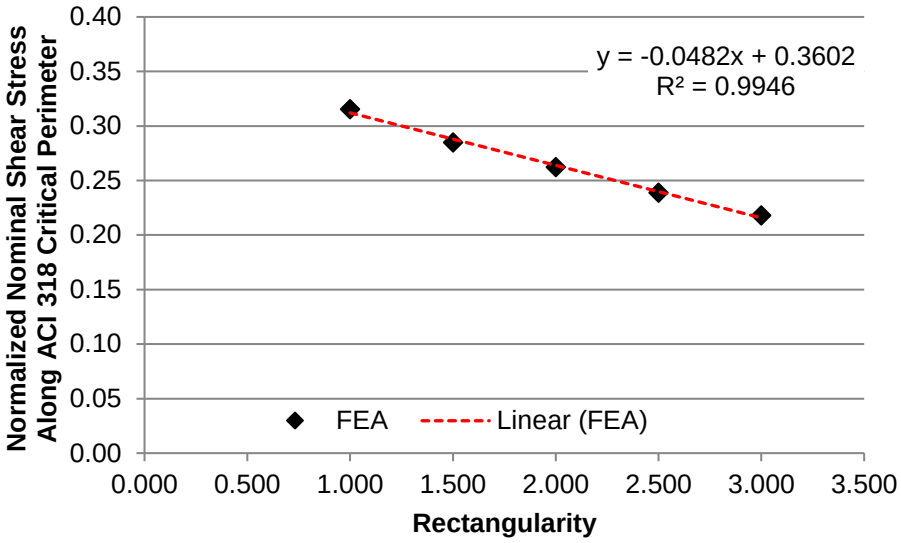

Figure J-7: Normalized Nominal Shear Stress Capacity Along ACI 318 Critical Perimeter Versus Column Rectangularity, c_{min}/d = 1.980

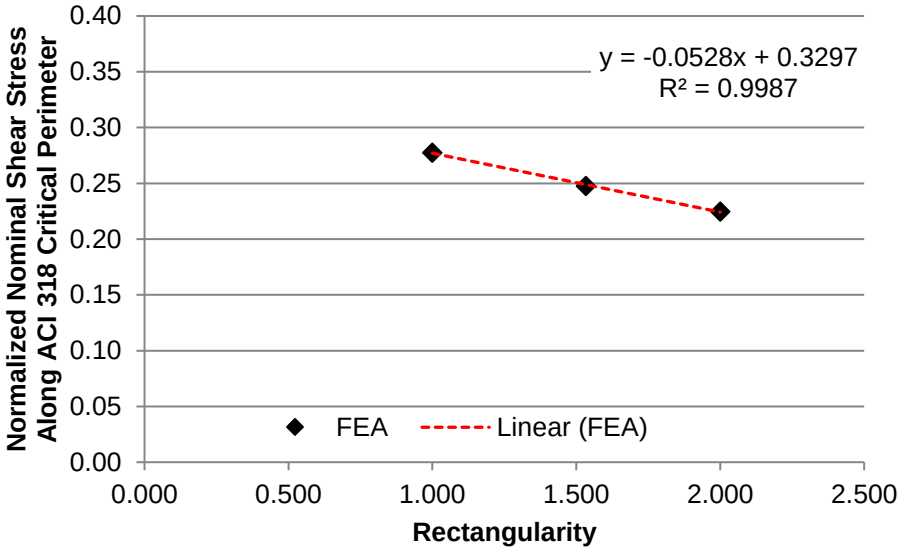

Figure J-8: Normalized Nominal Shear Stress Capacity Along ACI 318 Critical Perimeter Versus Column Rectangularity, c_{min}/d = 2.970